

# Geologic Studies in Alaska by the U.S. Geological Survey, 1995

Julie A. Dumoulin and John E. Gray, Editors

---

U.S. GEOLOGICAL SURVEY PROFESSIONAL PAPER 1574



UNITED STATES GOVERNMENT PRINTING OFFICE, WASHINGTON: 1997

**U.S. DEPARTMENT OF THE INTERIOR**

**BRUCE BABBITT, Secretary**

**U.S. GEOLOGICAL SURVEY**

**Gordon P. Eaton, Director**

For sale by  
U.S. Geological Survey  
Information Services  
Box 25286  
Denver Federal Center  
Denver, CO 80225

Any use of trade, product, or firm names in this publication is for descriptive purposes only and does not imply endorsement by the **U.S.** Government.

**COVER PHOTO:** Aerial view looking north across the Malaspina Glacier toward Mount Saint Elias (elevation 5,489 m), the third highest peak on the North American continent. Uplifted marine strata of Neogene age form the Samovar Hills in the foreground. Topographic relief in this area is dramatic (more than 4,800 vertical meters across less than 21 horizontal kilometers) and demonstrates rapid Neogene uplift and denudation (see article by **O'Sullivan** and others). Photograph by Austin Post.

# CONTENTS

Introduction	
Julie A. Dumoulin and John E. Gray .....	1

## ENVIRONMENT AND CLIMATE

Hydrogeochemistry of mine-drainage waters associated with low-sulfide, gold-quartz veins in Alaska	
Richard J. <b>Goldfarb</b> , Cliff D. Taylor, Allen L. <b>Meier</b> , William M. <b>d'Angelo</b> , and Richard M. O'Leary .....	3
Environmental geochemical study of the Nabesna gold skarn and Kennecott strata-bound copper deposits, Alaska	
Robert G. Eppinger, Stephen J. Sutley, and John B. <b>McHugh</b> .....	19
Mercury in the terrestrial environment, Kuskokwim Mountains region, southwestern Alaska	
Elizabeth A. Bailey and John E. Gray .....	41
Distinguishing between natural geologic and anthropogenic trace element sources, Denali National Park and Preserve	
Larry P. <b>Gough</b> and James G. Crock .....	57
Preliminary evaluation of emergent postglacial shorelines, Naknek and Iliamna Lakes, southwestern Alaska	
Darrell S. Kaufman and Karen B. <b>Stilwell</b> .....	73

## HAZARDS AND RELATED STUDIES

Geodetic studies in the Novarupta area, Katmai National Park, Alaska, <b>1990</b> to <b>1995</b>	
Jack W. <b>Kleinman</b> , Eugene Y. <b>Iwatsubo</b> , John A. Power, and Elliot T. <b>Endo</b> .....	83
The "Twin Peaks fault": not a tectonic or seismogenic structure	
Peter J. Haeussler and Robert S. Anderson .....	93

## RESOURCES

Silver-lead-zinc mineral occurrences in the Howard Pass quadrangle, Brooks Range, Alaska	
Karen D. <b>Kelley</b> , Cliff D. Taylor, and Barrett A. Cieutat .....	101
Areas favorable for metallic mineral resources and newly discovered mineral occurrences in the Buckstock Mountains area, southwestern Alaska	
John E. Gray and Peter M. Theodorakos .....	111
Paleocene molybdenum mineralization in the eastern Coast batholith, Taku River region, and new age constraints on batholith evolution	
Lance D. Miller, Richard J. Goldfarb, Lawrence W. Snee, William C. <b>McClelland</b> , and Paul D. <b>Klipfel</b> .....	125

RESOURCES—*Continued*

- Tidal influence on deposition and quality of coals in the Miocene Tyonek Formation, Beluga coal field, upper Cook Inlet, Alaska  
Romeo M. Flores, Gary D. Stricker, and Robert B. Stiles ..... 137

## GEOLOGIC FRAMEWORK

- Tectono-geophysical domains of interior Alaska as interpreted from new gravity and aeromagnetic data compilations  
Richard W. **Saltus**, John F. Meyer, Jr., David F. Barnes, and Robert L. Morin ..... 157
- Provenance of the Carboniferous Nuka Formation, Brooks Range, Alaska: a multicomponent isotope provenance study with implications for age of cryptic crystalline basement  
Thomas E. Moore, Sidney Hemming, and Warren D. Sharp ..... 173
- Comparison of conodont and calcareous microfossil biostratigraphy and lithostratigraphy of the Lisburne Group (Carboniferous), Sadlerochit Mountains, northeast Brooks Range, Alaska  
Anita G. Harris, Paul L. Brenckle, John F. Baesemann, Andrea P. **Krumhardt**, and Paul D. Gruzlovic ..... 195
- Lower Mississippian (Kinderhookian) biostratigraphy and lithostratigraphy of the western Endicott Mountains, Brooks Range, Alaska  
Charles G. Mull, Anita G. Hams, and John L. Carter ..... 221
- Kinderhookian (Lower Mississippian) calcareous rocks of the Howard Pass quadrangle, west-central Brooks Range  
Julie A. Dumoulin and Anita G. Harris ..... 243
- Late Middle Cambrian trilobites of Siberian aspect from the Farewell terrane, southwestern Alaska  
James M. St. John and Loren E. Babcock ..... 269
- Apatite fission-track thermotectonic history of crystalline rocks in the northern Saint Elias Mountains, Alaska  
Paul B. **O'Sullivan**, George **Plafker**, and John M. Murphy ..... 283
- Paleomagnetic results from Devonian and Permian rocks at Saginaw Bay, Kuiu Island, southeastern Alaska  
Sherman Gromme and John W. **Hillhouse** ..... 295
- Description and regional setting of the Silver Bay segment of the Sitka fault zone, southeastern Alaska, and evidence for possible sinistral separation  
David A. Brew ..... 307

## BIBLIOGRAPHIES

- U.S. Geological Survey reports on Alaska released in 1995  
John P. **Galloway** and Susan Toussaint ..... 317
- Reports about Alaska in non-USGS publications released in 1995 that include USGS authors  
John P. **Galloway** and Susan Toussaint ..... 323

# CONTRIBUTORS TO THIS PROFESSIONAL PAPER

## **Anchorage**

U.S. Geological Survey  
4200 University Drive  
Anchorage, Alaska 99508-4667

*Bailey, Elizabeth A.*  
*Dumoulin, Julie A.*  
*Haeussler, Peter J.*  
*Power, John A.*

## **Denver**

U.S. Geological Survey **MS-**  
Box 25046 Denver Federal Center  
Denver, Colorado 80225-0046

*Crock, James G., MS 973*  
*Eppinger, Robert G., MS 973*  
*Flores, Romeo M., MS 939*  
*Goldfarb, Richard J., MS 973*  
*Gough, Larry P., MS 973*  
*Gray, John E., MS 973*  
*Kelley, Karen D., MS 973*  
***McHugh, John B., MS 973***  
*Meier, Allen L., MS 973*  
***O'Leary, Richard M., MS 973***  
***Saltus, Richard W., MS 964***  
*Snee, Lawrence W., MS 913*  
*Stricker, Gary D., MS 939*  
*Sutley, Stephen J., MS 973*  
*Taylor, Cliff D., MS 973*  
*Theodorakos, Peter M., MS 973*

## **Menlo Park**

U.S. Geological Survey **MS-**  
345 Middlefield Road  
**Menlo Park, California 94025-3591**

*Barnes, David F., MS 989*  
*Brew, David A., MS 904*  
*Galloway, John P., MS 904*  
*Gromme, Sherman, MS 937*  
*Hillhouse, John W., MS 975*  
*Morin, Robert L., MS 989*  
*Moore, Thomas E., MS 904*  
***Plafker, George; MS 904***  
*Toussaint, Susan, MS 955*

## **Ocala**

U.S. Geological Survey  
Water Resources Division  
4500 SW 40th Avenue  
Ocala, Florida 34474-5731

*d'Angelo, William M., MS 973*

## **Reston**

U.S. Geological Survey  
National Center, **MS-**  
12201 Sunrise Valley Drive  
**Reston, Virginia 20192**

*Harris, Anita G., MS 926*

## **Vancouver**

U.S. Geological Survey  
Cascades Volcano Observatory  
5400 **MacArthur** Boulevard  
Vancouver, Washington 98661

*Endo, Elliot T.*  
*Iwatsubo, Eugene Y.*  
*Kleinman, Jack W. (deceased)*

## **Others**

*Anderson, Robert S.*  
Earth Sciences  
University of California  
Santa **Cruz**, California 95064

*Babcock, Loren E.*  
*St. John, James M.*  
Department of Geological Sciences  
**Orton Hall**  
The Ohio State University  
155 South Oval Mall  
Columbus, Ohio 43210-1397

***Baesemann, John F.***  
*Brenckle, Paul L.*  
Amoco Corporation  
Exploration and Production Technology Group  
P.O. Box 3092  
Houston, Texas 77253

*Carter, John L.*

Carnegie Museum of Natural History  
**4400** Forbes Avenue  
 Pittsburgh, Pennsylvania **15213**

*Cieutat, Barrett A.*

ERM Southwest  
**3501** North Causeway Boulevard, Suite **200**  
 Metairie, Louisiana **70002**

*Gruzlovic, Paul D.*

Delta Environmental Consultants, Inc.  
**5401** West Kennedy Boulevard, Suite **400**  
 Tampa, Florida **33609**

*Hemming, Sidney*

Lamont-Doherty Earth Observatory  
 Route 9W  
 Palisades, New York **10964**

*Kaufman, Darrell S.**Stilwell, Karen B.*

Department of Geology  
 Utah State University  
 Logan, Utah **84322-4505**

*Klipfel, Paul D.*

Placer Dome Exploration, Inc.  
**2085** Hamilton Avenue, Suite **150**  
 San Jose, California **95125**

*Krumhardt, Andrea P.*

Tectonics and Sedimentation Research Group  
 Geophysical Institute  
 University of Alaska Fairbanks  
 Fairbanks, Alaska **99775**

*McClelland, William C.*

Department of Geological Sciences  
 University of California  
 Santa Barbara, California **93106**

*Meyer, John F., Jr.*

Alaska State Division of Oil and Gas  
**3601** C Street, Suite **1380**  
 Anchorage, Alaska **99503**

*Miller, Lance D.*

Echo Bay Mines  
**3100** Channel Drive  
 Juneau, Alaska **99801**

*Mull, Charles G.*

Alaska State Division of Geological and  
 Geophysical Surveys  
**794** University Avenue, Suite **200**  
 Fairbanks, Alaska **99709**

*Murphy, John M.*

Department of Geology and Geophysics  
 University of Wyoming  
 Laramie, Wyoming **82071-3006**

*O'Sullivan, Paul B.*

School of Earth Sciences  
 LaTrobe University  
 Bundoora, Victoria, **3083**  
 Australia

*Sharp, Warren D.*

Berkeley Geochronology Center  
**2455** Ridge Road  
 Berkeley, California **94709**

*Stiles, Robert B.*

DRVEN Corporation  
**711** H Street  
 Anchorage, Alaska **99501**

# Geologic Studies in Alaska by the U.S. Geological Survey, 1995<sup>1</sup>

By Julie A. Dumoulin and John E. Gray

## INTRODUCTION

This collection of 20 papers continues the annual series of U.S. Geological Survey (USGS) reports on geologic investigations in Alaska<sup>1</sup>. Contributions cover a broad spectrum of earth science topics and report results from all parts of the State (fig. 1).

USGS activities in Alaska include studies of environment and climate, hazards, resources, and geologic framework. Five papers in this volume discuss aspects of environment and climate. Environmental geochemistry of parts of southwestern and south-central Alaska is the focus of four articles; a fifth study, of emergent postglacial lake shorelines in southwestern Alaska, contributes to ongoing investigations of paleoclimate. Two papers address geologic hazards. The first assesses ground deformation in Katmai National Park at Novarupta dome, site of the largest volcanic eruption in this century, and the second evaluates earthquake risks related to the "Twin Peak fault" near Anchorage. Resources, including metallic minerals in northern, southwestern, and southeastern Alaska and coal in south-central Alaska, are discussed in four articles. Nine geologic framework studies apply a variety of techniques to a wide range of subjects throughout Alaska, including tectonics, geophysics, geochronology, biostratigraphy, sedimentology, **paleogeography**, and paleomagnetism.

Two bibliographies at the end of the volume list reports about Alaska in USGS publications released in 1995 and reports about Alaska by USGS authors in non-USGS publications in 1995.

---

<sup>1</sup>This volume is the first to be published as a USGS Professional Paper. Prior volumes were published as USGS Bulletins (1988-1994) and USGS Circulars (1975-1987). The current title format was adopted for the 1985 volume; previous volumes were published under the title "The United States Geological **Survey** in Alaska: Accomplishments during 19\_\_."



Figure 1. Index map of Alaska showing 1:250,000-scale quadrangles and locations of study areas discussed in this bulletin.



# Hydrogeochemistry of Mine-Drainage Waters Associated with Low-Sulfide, Gold-Quartz Veins in Alaska

By Richard J. Goldfarb, Clifford D. Taylor, Allen L. Meier, William M. d'Angelo, and Richard M. O'Leary

## ABSTRACT

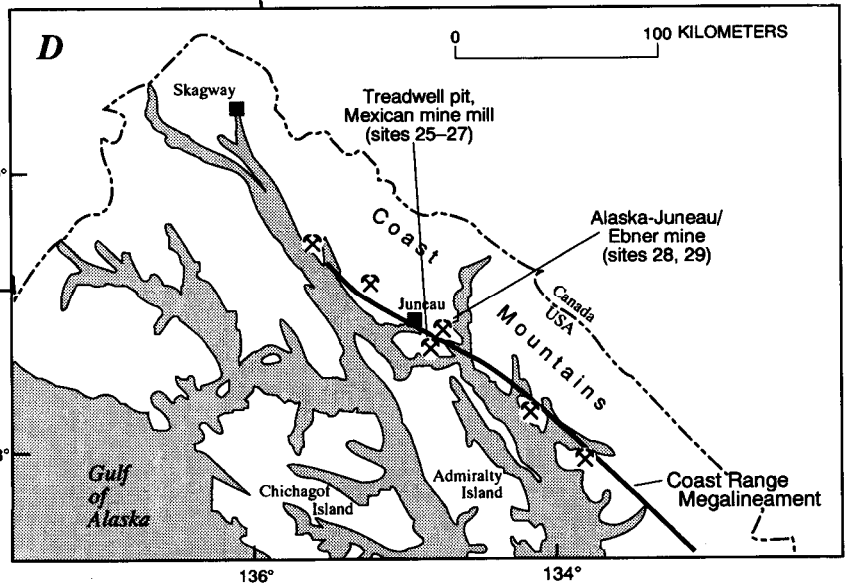
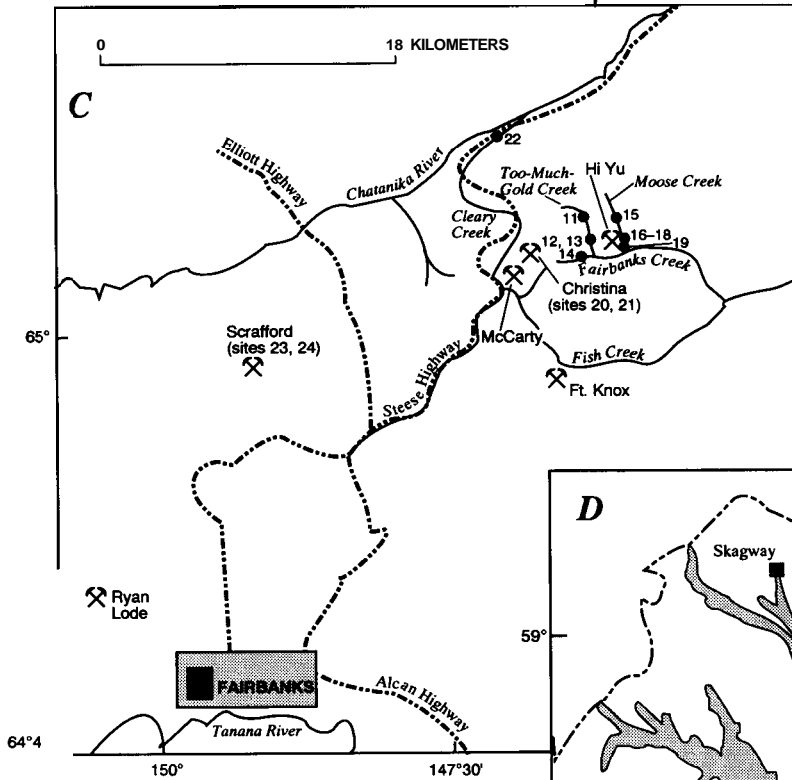
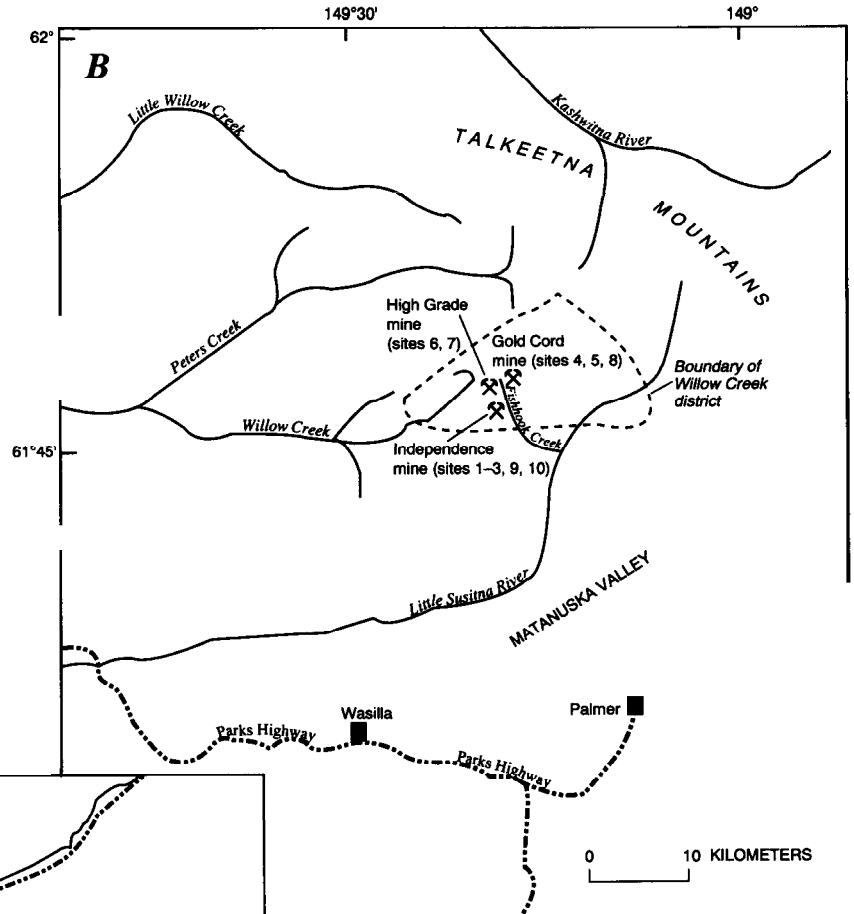
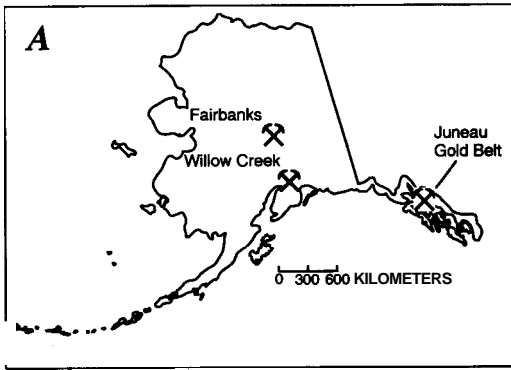
Surface waters were sampled above and below both abandoned and active mine workings associated with low-sulfide, gold-quartz veins in the Fairbanks, Willow Creek, and Juneau gold belt mining districts. All samples were analyzed for pH, dissolved and total cations, and dissolved anions. Waters were generally found to have near-neutral pH, with two exceptions. Waters flowing through mill tailings in the stream valley adjacent to the Hi-Yu mine in the Fairbanks district had a pH of 5.2. Near Juneau, processing of ore in the early 1900's at the Mexican mine on Douglas Island included concentrating sulfide minerals and dumping them in the adjacent forest. Effluent collected downstream from these mine wastes had a highly acidic pH of 2.9.

Iron, arsenic, and antimony in mine effluent are the constituents that are most consistently elevated above background concentrations. Because of the acidity of water draining the mill-waste pile near the Mexican mine, dissolved-iron concentrations exceeded 300,000 ppb. In more neutral waters, total-iron concentrations were elevated where an abundance of colloidal and suspended hydrous oxides were released into surface waters from lode and nearby placer-tailings piles. A concentration of 31,000 ppb total iron was measured for waters flowing from placer tailings along Too-Much-Gold Creek near Fairbanks, whereas dissolved iron at the same site was only 490 ppb. Within the Fairbanks district, maximum dissolved-arsenic levels of 260-270 ppb in stream waters were interpreted as background at one site and as elevated owing to mining activity at another site. Concentrations of as much as 8,900 ppb total arsenic were measured for waters associated with placer piles, the result of suspended or colloidal arsenic-bearing phases that were eroded from the piles or the absorption of dissolved arsenic onto ferric hydrous oxides. Where abundant stibnite occurs in the gold veins, waters associated with mine workings contained as much as 510 ppb Sb.

## INTRODUCTION

Low-sulfide, gold-quartz veins are common throughout the medium-grade metamorphic terranes of Alaska and historically have been the most widely developed deposit type in the state. Previous studies in Alaska focus on the environmental effects resulting from relatively small-scale mining of some of these vein systems on and near U.S. Forest Service and Park Service lands (Cieutat and others, 1994; Trainor and others, 1996). Data from these small deposits indicate minimal environmental impact as a result of acid mine drainage, although surface waters may be locally enriched in arsenic and iron. The purpose of this study is to evaluate how the development of much larger, low-sulfide, gold-quartz vein deposits may have impacted local surface-water quality. Resulting data are critical for identifying environmental problems associated with abandoned mine lands and for helping land planners better predict potential adverse effects of acid mine drainage and toxic metal contaminants that may result from future mining in Alaska. Additionally, identification of baseline levels of many elements are important in establishing reasonable standards for restoration of disturbed areas.

Hydrogeochemical studies were conducted in a number of Alaska's most economically significant past gold districts—the Willow Creek district, the Fairbanks district, and the Juneau gold belt (fig. 1A). Water samples were collected from adits and below waste piles at the Independence, Gold Cord, and High Grade mines in the Willow Creek district (fig. 1B). Near Fairbanks, surface waters were sampled that drained from adits and below mine and mill tailings of the Hi-Yu, Christina, and Scrafford mines (fig. 1C). Gold placer deposits are located downstream from many of the gold-quartz lodes in the Fairbanks district. We therefore also collected waters flowing through some of the placer-tailings piles. In the Juneau gold belt, we collected waters from the two largest lode gold deposits in Alaska (fig. 1D). We sampled surface waters at the



Treadwell deposit, including those of the abandoned glory hole at the Treadwell mine and below the mill tailings of the adjacent Mexican mine, and also those draining the underground workings of the Alaska-Juneau deposit. Samples for background metal levels were collected above mine **workings** in each of the three districts in order to establish baseline concentrations prior to mining. In addition to our collected data, we evaluated available hydrogeochemical information from private company reports for a few gold properties (Fort Knox and Alaska-Juneau) presently under development in Alaska.

The mineralogy of the deposits plays a major role in determining the chemical character of associated mine drainage (Smith and others, 1994). Low-sulfide, gold-quartz veins generally contain no more than a few percent sulfide minerals in the veins and in adjacent country rocks. The sulfide minerals that are present vary from one deposit to the next depending on what base metals are most enriched in local host rocks. In dioritic host rocks in the Willow Creek district and at the Treadwell deposit, pyrite is the dominant sulfide phase. At the Alaska-Juneau deposit, where veins lie along metagabbro-phyllite contacts, pyrrhotite, sphalerite, and galena are the dominant sulfide phases. In the schist-dominant part of the Fairbanks district where we conducted our field investigations, arsenopyrite and stibnite were the most common sulfide minerals in the gold lodes.

## FIELD AND LABORATORY METHODS

Water samples were collected in the period August 22-29, 1995, near abandoned and active gold mines in the Willow Creek district, Fairbanks district, and Juneau gold belt. At each of 29 sample sites, we measured water temperature, pH, and conductivity with standard meters and probes. Hach colorimetric kits were used in the field for determination of alkalinity. All resulting field measurements and descriptions of sampled sites are summarized in table 1.

Two water samples for cation analyses were collected in 60-mL polyethylene bottles at each site. One of these samples was unfiltered and was obtained for a combined measurement of total cations (both dissolved and suspended metal content). The second sample was collected, following filtration through 0.45- $\mu\text{m}$  filter, for determination of only dissolved-cation concentrations. Both samples were acidified in the field with concentrated nitric acid to a pH of less than 2. An additional unacidified, filtered sample was collected in a 125-mL polyethylene bottle at each site

for anion analysis. At about half of the sites, two additional samples were collected in 2-oz glass bottles, one unfiltered for total-mercury concentration and one filtered through a 45- $\mu\text{m}$  membrane for dissolved-mercury concentration. Both of these samples were acidified with nitric acid and potassium dichromate. Because mercury levels in natural waters are extremely low and would certainly be at concentrations below analytical determination limits, we restricted this sampling to localities downstream from mine **workings**.

Major, minor, and trace element contents of the acidified filtered and unfiltered, 60-mL samples were determined by inductively coupled plasma-mass spectrometry (ICP-MS) (Meier and others, 1994). Concentrations for more than sixty elements were determined directly from each sample, with lower determination limits for most elements at the parts per trillion level. Mercury concentrations for samples collected in the 2-oz glass bottles were determined by cold-vapor atomic absorption spectrophotometry using a technique modified from Kennedy and Crock (1987). Anion concentrations were determined on the filtered, unacidified 125-mL samples using ion chromatography (Fishman and Pyen, 1979).

## HYDROGEOCHEMISTRY OF MINE WATERS

Hydrogeochemical data were collected for samples of effluent emanating from some of Alaska's largest mine **adits**, mine-waste piles (fig. 2A), mill-tailings dumps (fig. 2B, C), and placer workings that are associated with low-sulfide, gold-quartz vein systems. These data were compared with natural background geochemical concentrations in surface waters from areas where mines and deposits are unknown. This comparison should identify whether potentially toxic concentrations of certain metals or **abnormal** pH conditions are being produced as a result of the oxidation of sulfide minerals and leaching of the weathered rock. Water geochemistry varies with season and discharge volume; the data in this study are for low flows in the late summer. However, the data presented here provide an indication of what, if any, geochemical constituents are significant environmental concerns associated with the mining of these gold-rich deposit types. Dissolved cations are summarized in table 2, total cations in table 3, and dissolved anions in table 4.

## BACKGROUND DATA

Waters collected at sites 3, 5, and 8 in the Willow Creek district, sites 11, 15, and 24 in the Fairbanks district, and site 25 in the Juneau gold belt (fig. 1) are representative of natural background conditions in areas undisturbed by mining. Values for pH at these sites are slightly alkaline, varying between about 7.2 and 7.8 (table 1). **Mea-**

◀ Figure 1. A, Location map of the major low-sulfide, gold-quartz vein districts in Alaska. B, Sampled mine locations from the Willow Creek district, south-central Alaska. C, Sampled mine locations from the Fairbanks district, central Alaska. D, Sampled water sites from the Juneau gold belt, southeastern Alaska.

Table 1. Field measurements and site descriptions for hydrogeochemical sampling near low-sulfide, gold-bearing vein deposits in Alaska

[Sites 3, 5, and 8 in the Willow Creek district, sites 11, 15, and 24 in the Fairbanks district, and site 25 from the Juneau gold belt were selected to reflect local background conditions]

Sample site	Temp. (°C)	Conductivity (µS/cm)	Alkalinity (mg/L as CaCO <sub>3</sub> )	Site Description	
Willow Creek district					
1	6.94	4	127	34	Below Independence mine-tailings pile
2	7.79	2	249	75	Flow from Independence mine portal
3	7.78	4	69	21	Background stream, north side of portal, Independence mine
4	7.28	4	166	48	Below Gold Cord mine-tailings pile
5	7.48	7	80	26	Upstream from Gold Cord mine
6	8.68	7	82	27	Flow from High Grade mine portal
7	7.45	4	66	21	Below High Grade mine-tailings pile
8	7.54	6	51	19.5	Stream in valley to the east
9	7.72	6	119	37	Main stream 40 m below Independence tailings
10	7.71	7	135	38	Main stream 1.5 km south of Independence mine
Fairbanks district					
11	7.66	6	173	75	Too-Much-Gold (TMG) Creek above trenches
12	6.73	8	172	43	Fe-stained seep in placer tailings, TMG Creek
13	7.50	9	149	50	TMG Creek flowing through placer tailings
14	7.85	11	210	85	Fairbanks Creek in tailings piles
15	7.49	6	133	60	Moose Creek 150 m upstream of Hi-Yu mill
16	5.18	9	339	<10	Moose Creek in Hi-Yu mill tailings
17	7.65	8	175	46	Branch of Moose Creek, west side of tailings
18	7.49	10	170	39	Branch of Moose Creek, immediately below tailings
19	7.14	9	182	42	Moose Creek above junction with Fairbanks Creek
20	6.27	13	38	<10	Holding pond at Christina mine
21	7.60	3	324	105	Drainage from Christina mine adit
22	7.28	5	383	155	Cleary Creek in placer tailings
23	8.09	6	532	250	Flow below Scrafford mine tailings
24	7.23	4	141	50	Creek above Scrafford mine workings
Juneau gold belt					
25	7.65	9	60	22	Waterfall before entering Treadwell pit
26	7.22	11	56	17	Treadwell pit
27	2.89	11	2350	<10	Below Mexican mine mill tailings
28	8.03	7	384	170	Ebner mine portal
29	8.04	6	897	160	Gold Creek tunnel draining Alaska-Juneau mine

sured alkalinities at the background sites ranged between about 20 to 26 mg/L as CaCO<sub>3</sub> for the Willow Creek district and the Juneau gold belt, and between about 50 to 75 mg/L as CaCO<sub>3</sub> for the Fairbanks district. Because calculated alkalinities approximate measured values at most sites (table 4), carbonate alkalinity from the dissolution of carbonate minerals is clearly dominant. Most sampled surface waters are dilute, calcium bicarbonate-type waters. In addition to carbonate, sulfate is the other dominant anion, with background concentrations ranging between 2.3 ppm in the Willow Creek district to 20 ppm in the Fairbanks district (table 4).

Background conductivities range from about 50 to 80 µS/cm for waters in the Juneau gold belt and Willow Creek district, and from about 133 to 173 µS/cm in the Fairbanks district (table 1). Calcium is consistently the dominant cation in solution, with background concentrations measured between 7 and 22 ppm (table 2). Background levels for the major cations (Ca, Mg, and K) are double to an order of

magnitude greater for stream waters in the Fairbanks area relative to those in the other gold districts. This difference likely reflects the much greater abundance of calc-silicate lithologies and the greater degree of water-rock interaction due to increased infiltration in the much more gentle terrain of the Fairbanks region. Background levels for dissolved minor and trace elements in all districts studied are generally below analytical determination limits and are estimated to be <40 ppb Fe, <0.1 ppb Co, ≤1 ppb Ni, <2 ppb Cu, <0.6 ppb Pb, <2 ppb Zn, 2 ppb Cd, ≤2 ppb As, <1 ppb Sb, and <0.1 ppb Hg. Total-cation concentrations in the unfiltered samples (table 3) are generally similar to those for dissolved concentrations. (In a few cases of mine drainage where total concentration of a species is significantly greater than dissolved concentration, the data for the unfiltered waters are discussed in detail below.)

All three of the background water samples from the Fairbanks district show high concentrations for dissolved arsenic and (or) antimony (table 2) relative to typical sur-

**A** face waters (Hem, 1992). For example, the acidified, filtered sample collected above any known workings on Too-Much-Gold Creek contained 260 ppb As and 23 ppb Sb (site 11). These elevated concentrations suggest the presence of sulfide-bearing rocks and undiscovered low-sulfide, gold-quartz vein occurrences within the upper part of the basin. Such high background arsenic concentrations may characterize natural waters throughout much of the highly mineralized Fairbanks district, especially near zones of ground-water discharge. A sample of well water that we collected from a private residence (adjacent to the University of Alaska) in Fairbanks contained 360 ppb As. Other workers have reported as much as 5,000 ppb As dissolved in ground water in the Fairbanks area (Hawkins and others, 1982; Krumhardt, 1982). Arsenic measurements of as low as 5 ppb for waters above the Scrafford mine (site 24), 10-30 ppb in many streams in the district (Wilson, 1975; Ray and others, 1992), and only a few parts per billion in surface and ground waters near the Fort Knox mine (Fairbanks Gold Mining, Inc., unpub. data) indicate large variability for dissolved-arsenic concentrations within natural waters across the district.



**B**



Whereas water at background site 24 contains only 5 ppb As, elevated concentrations of 500 ppb Fe, 120 ppb Al, 31 ppb Mn, 0.6 ppb Co, 2.9 ppb Ni, 4.8 ppb Sb, 0.10 ppb Hg, and 2.9 ppm  $\text{NO}_3^-$  at a pH of 7.2 were measured. The reason for these anomalies is uncertain. Because of the low arsenic concentration in these waters, it is unlikely that the waters interacted with sulfide-bearing mineral occurrences. One possibility is that the anomalies may result from a local, natural occurrence of colloidal ferric, aluminum, and manganese oxides that adsorbed many trace metals and ammonium cations.

### ACIDITY

Acid mine drainage is generally not a major concern in association with the prospecting or mining of low-sulfide, gold-quartz veins (Goldfarb and others, 1995). The low-sulfide mineral content of these ores, in combination with the presence of carbonate minerals that buffer water acidity, typically prevents the formation of acidic waters. Most

**C**



◀ **Figure 2.** **A**, Voluminous mine tailings at the Independence mine, Willow Creek district. The water sample at site 1 was collected a few meters below the point of discharge of a small stream at the base of the tailings pile. **B**, Finely ground mill tailings adjacent to the Hi-Yu mine, Fairbanks district. The water sample at site 16 was collected from Moose Creek in the middle of the tailings. **C**, Sulfide-rich mill tailings of the Mexican mine of the Treadwell orebody, Juneau gold belt on Douglas Island. The water sample at site 27 was collected in a bright-red discharge approximately 20 m downstream from the bulldozed pile.

**Table 2.** Concentrations of dissolved cations in filtered waters draining and (or) near major low-sulfide, gold-quartz vein deposits in Alaska  
 [All data in ppb except for Ca, Mg, and Na, which are in ppm; \* is background site]

Sample site	Ca (ppm)	Mg (ppm)	Na (ppm)	K	Fe	Al	Mn	Co	Ni	Cu	Pb	Zn	Cd	As	Sb	Hg
<b>Willow Creek district</b>																
1	14	6.2	3.6	460	<40	<10	0.6	<0.1	0.6	<2	<0.6	<2	2	3	2.3	<0.1
2	25	9.6	>8.0	600	<40	<10	0.4	0.1	1.0	<2	<0.6	3	2	37	3.9	<0.1
3*	9.7	0.98	0.95	280	<40	10	0.3	<0.1	<0.5	<2	<0.6	<2	2	2	0.4	—
4	20	5.0	1.6	460	<40	<10	<0.3	0.1	1.0	<2	<0.6	<2	2	3	3.2	<0.1
5*	10	0.99	0.93	290	<40	<10	<0.3	<0.1	0.5	<2	<0.6	<2	2	<2	0.6	—
6	12	0.63	1.3	330	<40	<10	<0.3	<0.1	0.6	<2	<0.6	<2	2	5	1.6	<0.1
7	9.3	0.49	0.94	270	<40	<10	<0.3	<0.1	0.6	<2	<0.6	<2	2	4	1.0	—
8*	6.7	0.80	0.78	240	<40	<10	0.9	<0.1	<0.5	<2	<0.6	<2	2	<2	0.3	—
9	13	2.9	2.7	330	<40	<10	1.9	<0.1	<0.5	<2	<0.6	<2	2	9	1.2	<0.1
10	14	3.4	2.3	380	<40	<10	0.4	<0.1	0.8	<2	<0.6	<2	2	12	0.9	<0.1
<b>Fairbanks district</b>																
11*	22	3.4	1.3	560	<40	<10	<0.3	<0.1	1.0	<2	<0.6	<2	2	260	23	—
12	19	5.3	1.5	540	490	<10	200	2.0	4.2	<2	<0.6	62	2	140	15	—
13	20	3.7	1.3	450	40	<10	8.5	0.2	2.0	<2	<0.6	2	2	100	21	<0.1
14	29	7.0	1.5	750	<40	<10	22	0.2	2.2	<2	<0.6	<2	2	44	20	<0.1
15*	21	3.3	1.2	470	<40	<10	0.5	<0.1	1.0	<2	<0.6	59	2	24	2.6	—
16	31	13	2.4	890	340	190	860	1.3	100	9.7	4.8	2000	20	80	14	<0.1
17	22	5.4	1.6	580	120	20	170	0.5	20	2	0.6	360	4.6	62	8.8	—
18	20	5.0	2.0	550	180	<10	240	0.6	2.2	<2	<0.6	16	2	49	18	<0.1
19	23	5.6	1.7	860	<40	<10	24	<0.1	6.7	<2	<0.6	110	2	38	8.3	0.11
20	3.1	0.70	0.33	1000	<40	10	23	0.3	2.7	<2	<0.6	29	2	270	510	—
21	49	9.4	1.5	600	130	<10	280	1.5	12	<2	<0.6	1500	3	84	200	—
22	57	14	2.9	2200	90	10	8.3	0.2	5.5	5	<0.6	2	2	14	22	—
23	74	30	2.8	1900	<40	<10	1.7	0.2	3.7	<2	<0.6	<2	2	92	200	—
24*	19	6.5	1.0	580	500	120	31	0.6	2.9	4	<0.6	<2	2	5	4.8	0.10
<b>Juneau gold belt</b>																
25*	11	0.59	1.2	260	70	20	0.5	<0.1	0.5	<2	<0.6	2	2	<2	0.3	—
26	9.6	0.72	1.3	280	140	40	7.6	<0.1	1.0	<2	<0.6	3	2	<2	0.3	<0.1
27	93	20	6.4	1700	330,000	7500	1800	160	120	380	21	2500	32	<2	<0.2	<0.1
28	34	11	>8.0	1400	200	<10	1.3	0.3	3.4	2	<0.6	6	1	7	2.0	—
29	120	37	6.2	3600	40	<10	0.8	0.4	10	<2	<0.6	44	2	2	1.0	<0.1

measured pH values for waters draining gold-mine workings in Alaska are alkaline and similar to waters away from the mines. Waters draining the underground workings of the Alaska-Juneau mine, Alaska's largest lode gold producer, had a pH of 8.0 (site 29), and those flowing out the portal of the large Independence mine had a pH of 7.8 (site 2).

Waters below a few of the studied mine tailings show minor pH decreases, having changed from slightly alkaline backgrounds to near-neutral levels where seeping from the base of tailings piles. For example, a small rill of water emanating from the base of the large tailings pile immediately east of the portal to the Independence mine had a pH of 6.9 (site 1). Oxidation of the 2-3 percent sulfide minerals, mainly pyrite, within the tailings produced a small amount of acid. Because water pH was 7.7, tens of meters downstream from the Independence mine (sites 9 and 10), influx from these tailings has little overall impact on waters of the Fishhook Creek basin. A pH measurement of 6.7 for water seeping through placer tailings along the lower reaches of Too-Much-Gold Creek (site 12) suggests that, like lode-tailings piles, oxidation of sulfides in placer piles may contribute small amounts of acid to local surface

flows. Alkaline pH values of 8.7 for water within the portal of the High Grade mine (site 6) indicate buffering by carbonate minerals.

We identified more strongly acid water in association with two broad, bulldozed zones of milling wastes. In the Fairbanks district, we measured a water pH of 5.2 from Moose Creek where water was flowing through the middle of the fine-grained mill tailings (fig. 2B) from the nearby Hi-Yu mine (site 16). The most acidic water that we measured (pH of 2.9) was for a bright-red, 1-m-wide stream flowing below mill tailings produced during the early 1900's (fig. 2C) at the abandoned Mexican mine on Douglas Island (site 27). The mined quartz-calcite veinlets contained only a few percent pyrite with lesser chalcopyrite, and the water data suggest that these tailings contain sulfide minerals concentrated from the processing of ore. Much of the gold at the Mexican mine is found in sulfide minerals. During processing, the ore was crushed and ground, and then sulfide minerals were concentrated for gold extraction by either amalgamation with mercury or by heap leaching (Kinzie, 1904; Redman and others, 1991). Because this processing was done at the turn of the century, little thought

**Table 3.** Concentrations of total cations in unfiltered waters draining and (or) near major low-sulfide, gold-quartz vein deposits in Alaska

[All data in ppb except for Ca, Mg, and Na which are in ppm; \* is background site]

Sample site	Ca (ppm)	Mg (ppm)	Na (ppm)	K	Fe	Al	Mn	Co	Ni	Cu	Pb	Zn	Cd	As	Sb	Hg
<b>Willow Creek district</b>																
1	12	5.8	29	410	<b>60</b>	<b>20</b>	12	0.1	0.6	<2	4.6	<2	1	3	23	0.27
2	23	9.1	7.1	610	280	<b>56</b>	43	0.2	20	2	0.9	5.1	2	39	39	4.1
<b>3*</b>	8.8	0.97	0.78	230	< <b>40</b>	< <b>10</b>	< <b>0.3</b>	4.1	4.5	<2	< <b>0.6</b>	<2	2	<2	0.5	—
4	18	5.2	15	470	3700	1100	57	20	20	10	5.8	11	1	80	4.8	0.24
<b>5*</b>	9.9	1.0	0.87	290	160	88	26	0.2	0.6	<2	< <b>0.6</b>	<2	2	2	0.7	—
6	11	0.62	1.2	310	320	130	5.0	0.1	0.6	<2	4.6	3.0	2	7.7	1.7	< <b>0.1</b>
7	8.8	0.51	0.88	260	< <b>40</b>	< <b>10</b>	< <b>0.3</b>	4.1	4.5	<2	4.6	<2	2	2	0.8	—
<b>8*</b>	7.2	0.93	0.80	260	< <b>40</b>	< <b>10</b>	4.3	4.1	0.7	<2	4.6	<2	2	<2	0.4	—
9	12	2.9	25	320	<b>90</b>	<b>30</b>	3.4	4.1	0.6	<2	< <b>0.6</b>	<2	1	9.5	1.1	4.1
10	14	3.3	21	370	< <b>40</b>	<b>10</b>	0.6	4.1	0.8	<2	< <b>0.6</b>	<2	2	10	0.9	< <b>0.1</b>
<b>Fairbanks district</b>																
<b>11*</b>	22	3.5	13	560	240	<b>120</b>	12	0.2	1.0	<2	4.6	5.0	2	290	20	—
12	20	5.8	1.6	580	31000	140	800	12	62	<2	21	170	3.2	8900	25	4.1
13	20	3.8	1.3	460	340	<b>96</b>	14	0.3	20	<2	1.0	4.0	2	140	21	< <b>0.1</b>
14	28	7.2	1.4	740	1900	640	70	12	37	2	53	6.9	2	110	23	—
<b>15*</b>	21	3.4	1.2	500	220	<b>94</b>	6.8	0.2	20	<2	0.8	6.4	2	30	26	—
16	31	13	2.4	920	470	190	860	13	99	10	63	1900	21	120	14	< <b>0.1</b>
17	22	5.5	1.5	560	580	61	180	0.6	18	3	3.8	380	5.2	150	11	—
18	20	5.2	2.0	550	<b>3200</b>	49	470	13	3.1	<2	13	28	2	410	28	0.58
19	24	5.8	1.7	860	160	10	30	0.2	68	<2	4.6	<b>110</b>	2	44	7.6	< <b>0.1</b>
20	3.0	0.78	0.33	1100	700	<b>260</b>	35	0.5	3.1	4	5.7	36	2	320	480	4.1
21	48	9.4	1.4	600	3800	220	1600	9.8	22	5	31	2200	5.3	810	250	4.1
22	57	14	3.0	<b>2200</b>	2200	630	22	1.0	7.0	10	10	5.6	2	24	22	< <b>0.1</b>
23	74	31	2.9	2000	40	< <b>10</b>	2.2	0.4	4.0	<2	4.6	<2	2	89	210	4.1
<b>24*</b>	20	7.0	1.1	840	770	140	38	0.7	2.6	4	< <b>0.6</b>	4.0	2	7.9	4.9	4.1
<b>Juneau gold belt</b>																
<b>25*</b>	12	0.66	1.2	290	170	43	27	0.2	0.8	<2	4.6	<2	2	<2	0.4	—
<b>26</b>	10	<b>0.75</b>	1.2	270	210	<b>49</b>	8.0	0.1	1.0	<2	< <b>0.6</b>	2.0	2	<2	0.2	< <b>0.1</b>
<b>27</b>	110	<b>23</b>	<b>7.5</b>	2000	360,000	> <b>8000</b>	2000	170	140	430	18	2600	27	4	0.4	< <b>0.1</b>
<b>28</b>	42	13	> <b>8.0</b>	1700	130	<b>20</b>	1.7	0.3	5.1	<2	< <b>0.6</b>	5.3	1	7.8	1.7	—
<b>29</b>	140	<b>43</b>	<b>7.0</b>	4200	40	< <b>10</b>	0.9	0.5	1.2	<2	< <b>0.6</b>	4.5	2	3	0.9	< <b>0.1</b>

was likely given at the time to the proper disposal of the tailings; they were generally piled up near the mill site. Their subsequent oxidation resulted in the acid generation.

### ARSENIC

Arsenopyrite is a common constituent of many gold-bearing quartz veins, and arsenic is a toxic metalloid that could potentially have a significant environmental impact during mining (Goldfarb and others, 1995). Arsenic concentrations are slightly elevated in mine drainage from studied workings in the Juneau gold belt and the Willow Creek district relative to local background levels. Arsenopyrite is a minor sulfide mineral in the Alaska-Juneau orebody, and therefore measured arsenic concentrations in waters draining the orebody did not exceed 7 ppb (site 28). Arsenopyrite is rare in the Treadwell orebody, and thus the arsenic content of waters emanating from the Mexican mill tailings is correspondingly low (<2 ppb As). In the Willow Creek district, waters draining from the Independence mine portal contained 37 ppb As (site 2), and the main creek 1.5 km

downstream from the mine contained 12 ppb As (site 10). Therefore, dissolved-arsenic concentrations of mine-drainage water in both of these major districts are below the State of Alaska MCL (maximum contaminant level) standard of 50 ppb (table 5).

Our unfiltered water sample collected below the tailings of the Gold Cord mine in the Willow Creek district (site 4) contained 80 ppb As (table 3), whereas the dissolved-arsenic concentration at this site was only 3 ppb (table 2). Relative to other waters from the district, the unfiltered water at site 4 also contained high levels of aluminum (1,100 ppb), iron (3,700 ppb), titanium (30 ppb), vanadium (2.9 ppb), chromium (1.0 ppb), manganese (57 ppb), cobalt (2.0 ppb), nickel (2.0 ppb), copper (10 ppb), zinc (11 ppb), lead (5.8 ppb), and many rare earth elements. This element suite is consistent with trace metals and especially arsenic being sorbed onto suspended hydrous ferric and aluminum oxide particles in waters emanating from the Gold Cord tailings pile. K.S. Smith and others (1992) noted that arsenic is strongly sorbed to iron-rich suspended matter in mine-drainage water at near-neutral pH conditions.

Table 4. Concentrations of dissolved anions in waters draining and (or) near major low-sulfide, gold-quartz vein deposits in Alaska

[All samples were also analyzed for Br<sup>-</sup> and HPO<sub>4</sub><sup>2-</sup>; all values for these anions were below lower determination limits of 0.2 ppm and 1 ppm, respectively. All data in ppm; alkalinities are as ppm CaCO<sub>3</sub>; \* is background site]

Sample site	F <sup>-</sup>	NO <sub>3</sub> <sup>-</sup>	Cl <sup>-</sup>	SO <sub>4</sub> <sup>2-</sup>	Measured alkalinity <sup>1</sup>	Calculated alkalinity <sup>2</sup>
1	4.05	0.92	0.12	32	34	35
2	0.11	0.56	0.27	38	75	63
3*	<0.05	<0.50	0.27	6.6	21	24
4	<0.05	0.55	0.12	18	48	50
5*	<0.05	0.62	0.13	7.7	26	25
6	<0.05	0.64	0.17	6.3	27	30
7	<0.05	0.65	0.17	6.2	21	23
8*	<0.05	<0.50	<0.10	2.3	19.5	17
9	<0.05	<0.50	0.18	14	37	33
10	<0.05	<0.50	0.16	14	38	35
11*	0.08	<0.50	0.24	10	75	55
12	0.15	<0.50	0.13	24	43	48
13	0.08	<0.50	0.20	20	50	50
14	0.10	<0.50	0.18	28	85	73
15*	0.07	2.1	0.19	11	60	53
16	0.17	0.60	0.18	150	<10	78
17	0.09	1.3	0.19	40	46	55
18	0.10	<0.50	0.22	39	39	50
19	0.10	<0.50	0.28	43	42	58
20	<0.05	<0.50	0.17	9.6	<10	8
21	0.16	<0.50	0.29	72	105	123
22	0.07	2.9	0.29	77	155	143
23	0.14	1.7	0.19	91	250	185
24*	0.07	2.9	0.18	20	50	48
25*	<0.05	<0.50	0.44	4.9	22	28
26	<0.05	<0.50	0.68	4.8	17	24
27	0.33	<0.50	2.2	1130	<10	233
28	0.33	2.7	2.1	48	170	85
29	<0.05	<0.50	0.53	349	160	300

<sup>1</sup> Data from table 1

<sup>2</sup> Calculated values assume all alkalinity as HCO<sub>3</sub> and are determined from measurements of Ca<sup>2+</sup> and pH using the assumption that dissolved-carbonate species contribute most of the alkalinity

Unlike waters associated with the workings in the Juneau and Willow Creek areas, waters in the Fairbanks region contain arsenic at concentrations that are of potential environmental concern. Even natural background levels in the Fairbanks district, as described above, commonly exceeded the 50 ppb State of Alaska MCL standard; hence, it is not possible to specifically attribute high-dissolved-arsenic concentrations to past mining activities. Drainage from the mouth of the Christina adit (site 21) contained 84 ppb As. It is uncertain whether this value would exceed premining concentrations of arsenic in waters infiltrating soils on the hillside. On the other side of the divide, however, and just about 2 km southeast of the Christina mine workings, Ray and others (1992) reported dissolved-arsenic concentrations on upper Fairbanks Creek that ranged from only 9 to 34 ppb over a 4-day-long period. These samples

were collected above known placer operations but directly downstream from the abandoned lode operations of the McCarty mine. A concentration of 270 ppb As, as well as a highly anomalous concentration of dissolved antimony, were measured in water ponded among a series of mineralized trenches a few hundred meters uphill from the Christina adit (site 20).

The presence of arsenopyrite, and its oxidized product scorodite, in lode mine tailings in the Fairbanks district is clearly the source for elevated arsenic concentrations in waters collected downstream from the studied lodes. At the Scrafford mine, waters flowing through waste rock exhibited an increase in arsenic concentration from 5 ppb above tailings (site 24) to 92 ppb below tailings (site 23). Similarly, the dissolved arsenic in waters of Moose Creek increased from 24 ppb As at 150 m above tailings (site 15) to



Table 5. Water standards for humans, aquatic life, and wildlife

[All data in ppb]

Constituent	U.S. Environmental Protection Agency's CMC <sup>1</sup>	State of Alaska's MCL <sup>2</sup>	Safe water quality criteria for wildlife <sup>3</sup>
Antimony	--	6	--
Arsenic	360	50	--
Cadmium	3.9	5	410-51,000
Chromium	--	100	--
Copper	18	1,000	410-589,000
Iron	--	300	--
Lead	82	--	1,015-2,640
Mercury	2.4	2	--
Nickel	--	100	--
Sulfate	--	250,000	--
Zinc	120	5,000	490-506,000

<sup>1</sup>Criteria maximum concentration (CMC), to protect against acute effects in aquatic life, is the highest 1-hour average *instream* concentration of the constituent not to be exceeded more than once every 3 years (Environmental Protection Agency, 1992). Values for cadmium, lead, and zinc assume a water hardness of 100 mg/L as CaCO<sub>3</sub>.

<sup>2</sup>Maximum contaminant level (MCL) is the State of Alaska's maximum allowable concentration for public drinking water (Alaska Department of Environmental Conservation, 1994).

<sup>3</sup>Data are presented as a range estimated from a variety of sources gathered in a 1992 study by Woodward-Clyde (Fairbanks Gold Mining, Inc., unpub. data, 1994).

80 ppb As in the Hi-Yu mill tailings that are bulldozed throughout the center of the stream valley (site 16). Although this concentration exceeds the State of Alaska MCL standard for arsenic, it is lower than the 260 ppb As concentration of the background water collected from Too-Much-Gold Creek, less than 2 km west of Moose Creek (site 11).

Although placer-tailings piles may contain concentrations of arsenopyrite and scorodite, dissolved-arsenic concentrations in waters collected downstream from placer mines in the Fairbanks district are similar to those at background sites. Near the center of a heavily placer-mined stretch of Cleary Creek (site 22), measured **dissolved-arsenic** concentrations were only 14 ppb. On Fairbanks Creek, immediately above its junction with Too-Much-Gold Creek (site 14), waters flowing through a heavily placer-mined area contained 44 ppm As. Ray and others (1992) reported dissolved-arsenic concentrations between 41 ppb and 84 ppb at essentially the same location over a 4-day-long period during 1991. Wilson (1975) reported somewhat higher levels of dissolved arsenic for water samples collected from streams with active placer mining in the district and filtered through 0.45-µm filters. He measured as much as

1,260 ppb dissolved arsenic within the waters of Cleary Creek, but this value came during a period of abundant sluicing that was associated with a high suspended load. Much of the "dissolved" material may thus have included fine colloidal particles (colloidal particles being material in the 0.003- to 10-µm range) that passed through the filter.

At many locations, total arsenic concentrations are not significantly greater than those for dissolved arsenic in corresponding samples. Total arsenic concentrations for waters collected below the Scrafford mine tailings (site 23), within the tailings on Cleary Creek (site 22), and within the tailings on Fairbanks Creek (site 14) were all no greater than 110 ppb. Similarly, Ray and others (1992) reported only a 30-50 percent increase from dissolved- to **total-arsenic** values for samples collected below placer operations on Fairbanks Creek.

Total-arsenic concentrations for some of the mine waters in the Fairbanks area are extremely high relative to dissolved concentrations. Measured values for total arsenic are nearly an order of magnitude greater than **dissolved-arsenic** values for waters immediately below the Hi-Yu mill tailings (site 18) and in waters flowing from the Christina **adit** (site 21). Total arsenic in waters from a small rill

in tailings piles near the mouth of Too-Much-Gold Creek (site 12) was 8,900 ppb, whereas dissolved arsenic from the same location was only 140 ppb. Wilson (1975) reported total-arsenic loads of about 12,000-17,000 ppb during one sampling period at a variety of sites on upper Cleary Creek. Total-iron concentrations of 3,200-3,800 ppb at our sampled sites 18 and 21, and of 31,000 ppb at site 12, suggest either that very fine grained suspended Fe- and As-bearing sulfide or oxide minerals were transported or that dissolved arsenic was sorbed onto the suspended material.

High-total-arsenic concentrations also are occasionally measured in ground water in the Fairbanks district. Water quality data from Fairbanks Gold Mining, Inc. (unpub. data) indicate that well water collected just north of the Fort Knox **orebody** on one occasion contained 1,060 ppb total As and 40 ppm total Fe, despite dissolved levels of 2 ppb As and 3.2 ppm Fe. These data suggest a correlation between total arsenic in waters and colloidal or suspended iron-rich particles. Arsenic- and iron-bearing sulfide minerals are virtually absent in the Fort Knox ore system, but these water data indicate that unexposed sulfide-rich mineral occurrences exist somewhere near Fort Knox.

### ANTIMONY

Antimony is often enriched in low-sulfide, gold-quartz veins. Though not as common as arsenopyrite, **antimony-bearing sulfide** phases such as stibnite and tetrahedrite are occasional minor minerals in ore veins. Minor tetrahedrite is found in the ores in the Willow Creek district and in the Alaska-Juneau deposit of the Juneau gold belt. **Antimony-bearing minerals** are common in the gold deposits of east-central Alaska within the Yukon-Tanana terrane. Many of the gold-vein deposits of the Fairbanks and Kantishna Hills districts (near Mt. Denali) contain abundant stibnite and Sb-rich sulfosalts.

Dissolved antimony increases by about an order of magnitude, from a background concentration of 0.3-0.6 ppb (sites 3, 5, and 8) to 2.3-3.9 ppb (sites 1, 2, and 4), for samples collected downstream from mine workings in the Willow Creek district. Similarly in the Juneau gold belt, waters draining the Alaska-Juneau **orebody** (sites 28-29) contain slight enrichments of 1-2 ppb Sb relative to background concentrations of <1 ppb. These concentrations are all below the State of Alaska's MCL standard of 6 ppb (table 5).

Antimony concentrations in surface waters from throughout the Fairbanks district, conversely, commonly exceed the State of Alaska MCL. Our data indicate that background levels for dissolved antimony may be in the 20-25 ppb range in parts of the Fairbanks region (i.e., site 11). One to two orders-of-magnitude increases above background in dissolved antimony characterize waters draining the boulangerite- and **jamesonite-bearing** veins at the Chris-

tina mine and the stibnite-bearing veins at the Scrafford mine. Anomalous concentrations include 510 ppb Sb in water collected from the holding pond at the Christina workings (site 20), 200 ppb Sb for waters draining the Christina **adit** (site 21), and 200 ppb Sb for waters collected below the Scrafford mine tailings (site 23). Ground-water samples in the Fish Creek basin near the Fort Knox **orebody** generally contain less than 3 ppb Sb, but values of 25-49 ppb Sb measured in a well in the area indicate episodic influxes of Sb-rich ground water (Fairbanks Gold Mining, Inc., unpub. data).

Total-antimony concentrations (table 3) are similar to those for dissolved antimony. Even for samples associated with mine workings, where arsenic levels increase by an order of magnitude between dissolved and total analyses (sites 12, 18, and 21), corresponding antimony concentrations only increase by 25 to 66 percent. Hence, adsorption of antimony onto suspended or colloidal particles is not as significant a phenomenon as is adsorption of arsenic.

### MERCURY

Mercury-bearing sulfide minerals are not common in low-sulfide, gold-quartz veins, and problems due to mercury toxicity would not be associated with the weathering of this type of mineral deposit. Historically, however, liquid mercury was used in the amalgamation method for gold extraction. As a result, high concentrations of mercury have been detected downstream from gold operations in many parts of the world decades after the cessation of mining (Fuge and others, 1992; Callahan and others, 1994). Because almost all of the abandoned gold-mine lands in Alaska were mined in the first half of the 20th century, the use of mercury for amalgamation of gold may have added additional amounts of the element into the environment in many parts of the state.

Our data indicate that dissolved-mercury dispersion from abandoned mining operations is not a significant environmental concern in the districts that we studied. Only one filtered water sample, downstream from the Hi-Yu mine (site 19), contained dissolved mercury above the 0.10 ppb lower determination limit (table 2). Mercury is likely contained in suspended sediment or adsorbed onto suspended organic matter, clay, and hydroxides. Evidence for such suspended transport of mercury is found in unfiltered water samples collected below some of the studied mine tailings (table 3). Measured total-mercury concentrations of 0.24 and 0.27 ppb characterized waters draining tailings piles in the Willow Creek district (sites 1 and 4), and a value of 0.58 ppb was determined for water immediately downstream from the Hi-Yu mill tailings (site 18). None of the dissolved- or total-mercury **determinations**, however, exceeded the State of Alaska MCL standard of 2 ppb (table 5).

## IRON

Iron is an important constituent in the study of the hydrogeochemistry of mine waters because Fe-bearing sulfide phases (i.e., pyrite and arsenopyrite) are the most common sulfide minerals in low-sulfide, gold-quartz veins. Dissolved-iron levels (table 2) are generally below the 300 ppb State of Alaska MCL standard (table 5), even in waters below mine workings. However, the abundant formation of hydrous ferric oxides in much of the mine-waste material often leads to significantly greater total iron concentrations (table 3).

All filtered waters collected from the Willow Creek district (sites 1-10) contained <40 ppb dissolved Fe; however, at many workings, total-iron concentrations were notably greater in unfiltered water samples. Waters collected a few meters below the inactive Independence and High Grade mine tailings (sites 1 and 7) contained  $\leq 60$  ppb total Fe, but those collected from the portals of the mines contained about 300 ppb total Fe (sites 2 and 6). Ferric oxyhydroxides may have precipitated on bacteria and other microorganisms within the mine adits, leading to the elevated total-iron levels. Water below the Gold Cord mine-tailings pile (site 4) contained a highly anomalous concentration of 3,700 ppb total Fe. Because the Gold Cord mining operation is active, associated tailings may be relatively permeable, allowing surface waters greater access to oxidizing sulfide minerals and the consequent release of iron hydroxides into the circulating waters.

Total- and dissolved-iron concentrations did not exceed 210 ppb for waters draining the Alaska-Juneau orebody (sites 28 and 29) and within the flooded Treadwell pit (site 26). The acidic water (pH 2.9) collected from below the Mexican mine mill tailings (site 27), however, contained 330,000 ppb dissolved Fe and 360,000 ppb total Fe. These are the highest iron concentrations that we have measured in any mine waters from Alaska; they are an order of magnitude greater than any acidic waters that drain workings of the iron-rich volcanogenic massive sulfide deposits in the Prince William Sound region (Goldfarb and others, 1996) and are similar in concentration to waters flowing from shale-hosted massive sulfide ores in the northwestern Brooks Range (Kelley and Taylor, in press).

Dissolved-iron concentrations are close to or exceed the MCL standard in a few water samples collected below the lode and placer mines in the Fairbanks district. Iron concentrations of 490 ppb were measured in a seep in placer tailings on Too-Much-Gold Creek (site 12), and of 340 ppb along Moose Creek within the Hi-Yu tailings (site 16). Similar concentrations are reported by Fairbanks Gold Mining, Inc. (unpub. data) in water collected from Fish Creek, where there are numerous placer mine tailings. However, a background water sample collected above the Scrafford mine workings (site 24) contained 500 ppb dissolved Fe, the highest concentration in the district (table 2). The high dis-

solved-iron and dissolved-aluminum concentrations at this site, located a few meters below where the water flows out from the mountainside, show that significant iron levels may locally occur near areas of chemically reduced groundwater discharge. Reduced ground water at near-neutral pH can commonly contain 1-10 mg/L (1 mg/L is about 1,000 ppb) of iron (Hem, 1992). Dissolved-iron concentrations exceeding 1,000 ppb characterize most of the ground water samples collected by Fairbanks Gold Mining, Inc. (unpub. data) from wells in the Fish Creek basin. We measured a concentration of 26,000 ppb dissolved Fe in well water from a private residence within the Fairbanks city limits.

Total-iron concentrations are much greater throughout most of the studied parts of the Fairbanks district. Iron concentrations of 2,220 ppb and 1,900 ppb characterize waters collected within the large placer piles along Cleary Creek (site 22) and Fairbanks Creek (site 14), respectively. The seep within the smaller placer piles on Too-Much-Gold Creek (site 12) contained 31,000 ppb total Fe; similar total-iron concentrations were found in waters from the Fish Creek basin (Fairbanks Gold Mining, Inc., unpub. data). The abundance of unconsolidated to poorly consolidated material resulting from placer mining is a major source of iron-rich suspended material released into the surface waters of the Fairbanks district.

## BASE METAL AND ADDITIONAL METALLOIDS

Most low-sulfide, gold-quartz veins contain much less than 1 percent base-metal sulfides, and hence waters draining workings at such vein deposits generally lack significant base-metal concentrations (fig. 3). For all samples collected in the Willow Creek district (sites 1-10), measured concentrations of dissolved trace metals are low (table 2) and similar to background levels; they do not exceed 0.1 ppb Co, 1.0 ppb Ni, <2 ppb Cu, <0.6 ppb Pb, 3 ppb Zn, 2 ppb Cd, 0.8 ppb Cr, and <0.6 Bi. Total concentrations for some of these elements in water collected below the Gold Cord mine tailings (site 4) are elevated (table 3), but they are still far below State of Alaska MCL standards (table 5). Even at the Alaska-Juneau deposit (sites 28 and 29), where the ore contains as much as a few percent base-metal-bearing sulfides, the filtered water samples contained a maximum concentration of <0.8 ppb Cr, 0.4 ppb Co, 10 ppb Ni, 44 ppb Zn, 2 ppb Cd, <0.6 ppb Pb, <0.6 ppb Bi, 2 ppb Cu, and 30 ppb W.

Despite rare base-metal sulfides in the ore removed from the Treadwell deposit, acid mine drainage (pH 2.9) at the Mexican mine mill (site 27) is highly metalliferous. At a pH below 3.0, most metals are mobile in solution. In addition to the high dissolved-iron concentrations discussed previously, the drainage from the mill tailings contained 11 ppb Cr, 160 ppb Co, 120 ppb Ni, 380 ppb Cu, 2,500 ppb Zn, 32 ppb Cd, and 21 ppb Pb. The dissolved-nickel and

dissolved-cadmium concentrations exceed State of Alaska MCL standards (table 5).

The most base-metal-rich mine waters identified in the Fairbanks district were associated with the mill tailings of the Hi-Yu mine; ore at the mine contained abundant sphalerite. As a result, the weakly acidic waters (pH 5.2) of Moose Creek flowing through the tailings (site 16) were found to contain 2,000 ppb Zn and 20 ppb Cd, in addition to anomalous levels of dissolved Ni, Cu, Pb, Mn, Fe, and Al. Cadmium exceeds the State of Alaska MCL standard but is below the cadmium standard estimated to be hazardous to wildlife in the area (column 3, table 5). Adsorption of some trace metals onto ferric hydroxides probably explains concentrations of 9.8 ppb total Co and 31 ppb total Pb in iron-rich waters draining the Christina mine adit (site 21) and of 12 ppb total Co in iron-rich waters along Too-Much-Gold Creek (site 12).

The Fort Knox deposit contains an extremely small volume of sulfide minerals, but bismuthinite and native bismuth are minor in the gold-bearing quartz veins. Almost all measurements by Fairbanks Gold Mining, Inc. (unpub. data) for waters on Fish Creek downstream from Fort Knox

contained less than their various reported lower analytical determination limits of 30 ppb, 44 ppb, or 56 ppb Bi. However, on a few occasions, these waters contained as much as 93 ppb dissolved Bi and 153 ppb total Bi. Elsewhere in the Fairbanks district, we found our collected samples to all contain <0.6 ppb Bi.

## SULFATE

None of our sulfate determinations in waters collected from the Willow Creek or Fairbanks districts (table 4) exceeded the 250 ppm State of Alaska MCL standard (table 5). In the Willow Creek district, sulfate concentrations ranged between background values of about 2-8 ppm (sites 3, 5, and 8) to a maximum concentration of 38 ppm at the Independence Mine portal (site 2). The lowest sulfate concentration from the Fairbanks district was 10 ppm for waters collected at higher elevations of Too-Much-Gold Creek (site 11). The corresponding anomalous dissolved-arsenic and dissolved-antimony values at site 11 are surprising given the relatively low sulfate measurement, but perhaps small

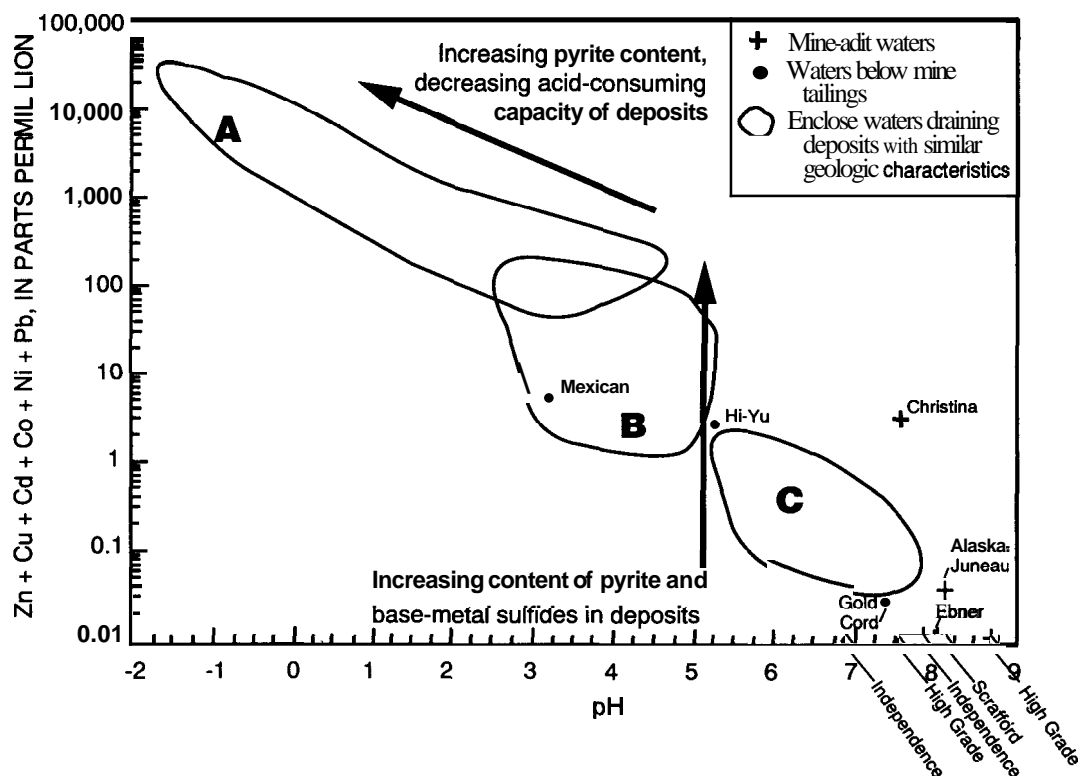


Figure 3. Ficklin diagram plotting pH vs. dissolved base-metal content of mine-drainage waters. Fields A, B, and C (from Plumlee and others, 1994) define fields for the West Shasta district volcanogenic massive sulfide deposits, sulfide-rich vein deposits in rocks with low-buffering capacity, and sulfide-rich vein deposits in carbonate host rocks, respectively. Data from this study indicate that mine waters draining workings at low-sulfide, gold-quartz vein deposits are typically high pH/low metal. Exceptions occur where ore-processing techniques increase sulfide-mineral/surface-water interactions.

and unexposed volumes of arsenic- and antimony-bearing sulfide minerals are present. The low iron concentration in waters at site 11 suggests that large amounts of pyrite are not present in these occurrences. The highest sulfate concentration from our study in the Fairbanks district was 150 ppm for waters of Moose Creek within the Hi-Yu mill tailings (site 16). Whereas sulfate concentrations in most ground-water samples were much lower, Fairbanks Gold Mining, Inc. (unpub. data) reported concentrations of as much as 65 ppm for dissolved sulfate and 325 ppm for total sulfate in well waters near the Fort Knox property.

Two anomalous sulfate concentrations were found in waters collected at **workings** in the Juneau gold belt. The metal-rich waters draining the mill tailings of the Mexican mine (site 27) contained 1,130 ppm sulfate due to oxidation and dissolution of sulfide concentrate. Despite relatively low dissolved-metal values, waters draining the Alaska-Juneau deposit from the Gold Creek tunnel (site 29) contained 349 ppm sulfate. This is the only dissolved constituent in waters from the workings of Alaska's largest gold mine that exceeds the State of Alaska MCL standard. However, sulfate levels in effluent from the Alaska-Juneau **orebody** are apparently quite variable. Measurements at the Gold Creek tunnel by Echo Bay Mines (unpub. data) vary between a maximum of also about 1,000 ppm sulfate and a minimum of 6.8 ppm sulfate. Such variation could reflect varying flow paths for the effluent within the extensive underground mine **workings**, changes in ground-water discharge volumes, or periodic influx of **surface-water** runoff.

## DISCUSSION

Mining and weathering of low-sulfide, gold-quartz vein deposits typically result in more limited environmental contamination than does the mining of more sulfide-rich deposit types (duBray, 1995). Arsenic from oxidized ores and mercury from processing procedures have characteristically been the trace elements of greatest concern. Thermodynamically favored As (V) is the most common inorganic arsenic species dissolved in natural waters, but the human metabolism tends to reduce the species to the more toxic As (III) following ingestion. If As (III) becomes bioavailable and migrates to the kidneys and other vital organs, it poses a major cancer threat in humans (Eisler, 1988; A.H. Smith and others, 1992). Little work has been published on arsenic speciation in Alaska's ground and surface waters. However, a limited amount of data collected by Hawkins and others (1982) indicates that As (III) makes up a high percentage of the total arsenic dissolved in ground waters in the Fairbanks district. In contrast to the relatively high toxicity of inorganic arsenic, organic forms of mercury (such as methylmercury) are the most toxic, are soluble in water, and are the most serious

mercury health concern to humans and other living organisms.

Effluent from the studied mine **adits** is generally metal poor and neutral to slightly alkaline in pH (fig. 3). Waters collected from the **adits** in the Willow Creek district (sites 2 and 6) contained only 5-37 ppb dissolved As, <40 ppb dissolved Fe, 1.6-3.9 ppb dissolved Sb, and 6-38 ppm sulfate; base metals at these sites are also at background levels. Similar low values characterized cations in waters draining the Alaska-Juneau **orebody** in the Juneau gold belt (sites 28 and 29), although sulfate levels were as great as 349 ppm. In contrast, much higher dissolved-metal levels of 130 ppb Fe, 84 ppb As, 200 ppb Sb, and 1,500 ppb Zn characterize drainage from the Christina mine in the Fairbanks district (site 21). Corresponding total-arsenic and total-iron concentrations are nearly an order of magnitude greater because of either the adsorption and colloidal transport with hydrous oxides or the transport of fine-grained suspended material.

The cause for the comparatively greater amounts of metal dissolution at the Christina mine is uncertain. An abundance of caved-in vein material within the **adit** may have enhanced water-rock interaction. Although uncommon, extremely acidic mine drainage has been reported from other **adits** in low-sulfide, gold-quartz vein deposits and also may be the result of waters interacting with pieces of sulfide-rich ore scattered along the **adit** floor. An abandoned **adit** at the Macres gold deposit in the Haast schist on the eastern side of the South Island of New Zealand was characterized by a neutral pH discharge carrying a dissolved load of 2,800-4,000 ppb As, 3,800-7,300 ppb Fe, and 180 ppm sulfate (BHP Gold New Zealand, unpub. environmental impact assessment, 1988). An abandoned **adit** in the Reefton district in older Paleozoic rocks on the western side of the same island had effluent with a pH measured at 2.9. Under such acidic conditions, increased metal solubilities led to dissolved concentrations of 77,000 ppb As, 80,000 ppb Fe, and 1,590 ppm sulfate (Macres Mining Company Ltd., unpub. environmental impact assessment, 1994).

The concentration of mined sulfide-bearing quartz vein and wall rock material stored in abandoned waste piles can be a significant source of hydrous ferric oxides with adsorbed metals and of mercury from ore processing. None of the measured mercury concentrations exceeded EPA-CMC or State of Alaska MCL standards (table 5), but the elevated mercury concentrations in waters below tailings at the Independence (site 1), Gold Cord (site 4), and Hi-Yu (site 18) mines (table 3) indicates the need for monitoring of mercury concentrations in waters draining historic mine operations. A roughly one order-of-magnitude increase in total iron relative to dissolved iron, with an associated increase in arsenic, occurred in waters below the tailings at the Hi-Yu and Gold Cord tailings piles. Waters flowing through placer piles showed a similar enrichment in **total-**

iron and total-arsenic concentrations on Too-Much-Gold (site 12), Fairbanks (site 14), and Cleary (site 22) Creeks.

Certain processing techniques used at historic mine workings may increase environmental problems if resulting tailings were abandoned in waste piles. At the Hi-Yu mine, ore was crushed to fine grain sizes before gold extraction. Hence, the mill tailings along Moose Creek offer a greater total surface area for water-rock interaction. As a result, acidic waters of a measured pH of 5.2 (site 16) can dissolve and transport greater-than-background metal concentrations. The concentration of sulfide grains prior to gold mining may lead to formation of increased acid mine drainage in association with a deposit type that normally lacks such problems. This must certainly be the case at the Mexican mine (site 27), where water below the milled tailings has a pH of 2.9 and is anomalously metal rich.

## SUMMARY

Our data from the Willow Creek district are typical of those from many low-sulfide, gold-quartz vein districts (Goldfarb and others, 1995). The lowest pH value measured in the district was near neutral (pH 6.9), and dissolved-ion concentrations draining all workings were below the Alaska and EPA water-quality standards. Total concentrations of 80 ppb As and 3,700 ppb Fe below the Gold Cord tailings piles indicate enhanced transport of ferric hydrous oxides from oxidized, poorly consolidated mine wastes.

All cation concentrations in waters draining workings of the Alaska-Juneau deposit, the State's largest past gold producer, are similar to background concentrations. Formation of sulfate during weathering of sulfide minerals leads to concentrations of as much as 349 ppm sulfate dissolved in mine effluent. At the nearby Treadwell mine glory hole, waters contain cation and anion concentrations similar to water samples collected from background sites. During mining and milling of ore at the Mexican mine, sulfide minerals were likely concentrated. During the ensuing weathering of the tailings, acidic waters of pH 2.9 were produced containing a dissolved load of 330,000 ppb Fe, 7,500 ppb Al, 1,800 ppb Mn, 160 ppb Co, 120 ppb Ni, 380 ppb Cu, 2,500 ppb Zn, 32 ppb Cd, and 1,130 ppm  $\text{SO}_4^{2-}$ .

The Fairbanks district is characterized by surface waters with variable, but often quite high, natural background levels of dissolved arsenic and dissolved antimony. We measured concentrations as high as 260 ppb As and 23 ppb Sb in surface waters upstream from mine workings. Dissolved-antimony concentrations were as much as 200 ppb in the Christina adit water samples and 200 ppb in water collected below the stibnite-rich tailings of the Scrafford mine. Total-iron and total-arsenic levels are elevated compared with background levels where abundant oxides form in lode and placer tailings piles. Concentrations of as much

as 31,000 ppb Fe and 8,900 ppb As were measured along Too-Much-Gold Creek.

## REFERENCES CITED

- Alaska Department of Environmental Conservation, 1994, Drinking water regulations: State of Alaska, Department of Environmental Conservation report 18-ACC-80, 195 p.
- Callahan, J.E., Miller, J.W., and Craig, J.R., 1994, Mercury pollution as a result of gold extraction in North Carolina, U.S.A.: *Applied Geochemistry*, v. 9, p. 235-241.
- Cieutat, B.H., Goldfarb, R.J., Borden, J.C., McHugh, J., and Taylor, C.D., 1994, Environmental geochemistry of mesothermal gold deposits, Kenai Fjords National Park, south-central Alaska, in Till, A.B., and Moore, T.E., eds., *Geological Studies in Alaska by the U.S. Geological Survey, 1993*: U.S. Geological Survey Bulletin 2107, p. 21-25.
- duBray, E.A., ed., 1995, Preliminary compilation of descriptive geoenvironmental mineral deposit models: U.S. Geological Survey Open-File Report 95-831, 272 p.
- Eisler, R., 1988, Arsenic hazards to fish, wildlife, and invertebrates—a synoptic review: U.S. Fish and Wildlife Service Biological Report 85(1.12), 92 p.
- Environmental Protection Agency, 1992, Water quality standards; establishment of numeric criteria for priority toxic pollutants; States' compliance; final rule: Federal Register, 40CFR Part 131, v. 57, no. 246, p. 60,847-60,916.
- Fishman, M.J., and Pyen, Grace, 1979, Determination of selected anions in water by ion chromatography: U.S. Geological Survey Water-Resources Investigations 79-101, 30 p.
- Fuge, R., Pearce, N.J.G., and Perkins, W.T., 1992, Mercury and gold pollution: *Nature*, v. 357, p. 369.
- Goldfarb, R.J., Berger, B.R., Klein, T.L., Pickthorn, W.J., and Klein, D.P., 1995, Low sulfide Au quartz veins, in duBray, E.A., ed., Preliminary compilation of descriptive geoenvironmental mineral deposit models: U.S. Geological Survey Open-File Report 95-831, p. 261-267.
- Goldfarb, R.J., Nelson, S.W., Taylor, C.D., d'Angelo, W.M., and Meier, A.L., 1996, Acid mine drainage associated with volcanogenic massive sulfide deposits, Prince William Sound, Alaska, in Moore, T.E., and Dumoulin, J.A., eds., *Geological studies in Alaska by the U.S. Geological Survey, 1994*: U.S. Geological Survey Bulletin 2152, p. 3-16.
- Hawkins, D.B., Forbes, R.B., Hok, C.I., and Dinkel, D., 1982, Arsenic in water, soil, bedrock, and plants of the Ester Dome area of Alaska: Institute of Water Resources, University of Alaska, Fairbanks, Report IWR-103, 82 p.
- Hem, J.D., 1992, Study and interpretation of the chemical characteristics of natural water: U.S. Geological Survey Water-Supply Paper 2254, 263 p.
- Kelley, K.D., and Taylor, C.D., in press, Natural environmental effects of silver-lead-zinc deposits in the Brooks Range, Alaska: *Applied Geochemistry*, v. 12, no. 3.
- Kennedy, K.R., and Crock, J.G., 1987, Determination of mercury in geological materials by continuous flow, cold-vapor, atomic-absorption spectrophotometry: *Analytical Letters*, v. 20, no. 6, p. 899-908.

- Kinzie, R.A., 1904, The Treadwell group of mines, Douglas Island, Alaska: Transactions of the American Institute of Mining Engineers, v. 34, p. 334-386.
- Krumhardt, A.P., 1982, Arsenic, nitrate, iron, and hardness in ground water, Chena Hot Springs road, Steele Creek road, and Gilmore trail, Fairbanks, Alaska: U.S. Geological Survey Open-File Report 82-356, 2 p.
- Meier, A.L., Grimes, D.J., and Ficklin, W.H., 1994, Inductively coupled plasma mass spectrometry—a powerful analytical tool for mineral resource and environmental studies [abs.], in Carter, L.M.H., Toth, M.I., and Day, W.C., eds., USGS research on mineral resources—1994, Part A—Program and Abstracts, V.E. McKelvey Forum on Mineral and Energy Resources, 9th, Tucson, Ariz., February 22-25, 1993: U.S. Geological Survey Circular 1103-A, p. 67-68.
- Plumlee, G.S., Smith, K.S., and Ficklin, W.H., 1994, Geo-environmental models of mineral deposits, and geology-based mineral-environmental assessments of public lands: U.S. Geological Survey Open-File Report 94-203, 7 p.
- Ray, S.R., Vohden, J., and Morgan, W., 1992, Investigation of trace metals related to placer mining on Fairbanks and Porcupine Creeks: Alaska Division of Geological and Geophysical Surveys, Public-Data File 92-13, 17 p.
- Redman, E.C., Maas, K.M., Kurtak, J.M., and Miller, L.D., 1991, Bureau of Mines minerals investigations in the Juneau mining district, Alaska, 1984-1988: U.S. Bureau of Mines Special Publication, Vol. 2—Detailed mine, prospect, and mineral occurrence descriptions, Section D—Juneau gold belt sub-area, 424 p.
- Smith, A.H., Hopenhayn-Rich, C., Bates, M.N., Goeden, H.M., Hertz-Picciotto, I., Duggan, H.M., Wood, R., Kosnett, M.J., and Smith, M.T., 1992, Cancer risks from arsenic in drinking water: Environmental Health Perspectives, v. 97, p. 259-267.
- Smith, K.S., Ficklin, W.H., Plumlee, G.S., and Meier, A.L., 1992, Metal and arsenic partitioning between water and suspended sediment at mine-drainage sites in diverse geologic settings, in Kharaka, Y.K., and Maest, A.S., eds., Water-rock interaction: Seventh International Symposium on Water-Rock Interaction, Park City, Utah, July 13-18, 1992, Proceedings: Rotterdam, A.A. Balkema, v. 1, p. 443-447.
- Smith, K.S., Plumlee, G.S., and Ficklin, W.H., 1994, Predicting water contamination from metal mines and mining wastes: U.S. Geological Survey Open-File Report 94-264, 112 p.
- Trainor, T.P., Fleisher, S., Wildeman, T.R., Goldfarb, R.J., and Huber, C.S., 1996, Environmental geochemistry of the McKinley Lake gold mining district, Chugach National Forest, Alaska, in Moore, T.E., and Dumoulin, J.A., eds., Geological studies in Alaska by the U.S. Geological Survey, 1994: U.S. Geological Survey Bulletin 2152, p. 47-57.
- Wilson, F.H., 1975, Arsenic and water, Pedro Dome-Cleary Summit area, Alaska: M.S. thesis, University of Alaska, Fairbanks, 80 p.

Reviewers: Lance Miller and Jim Rytuba

# Environmental Geochemical Study of the Nabesna Gold Skarn and Kennecott Strata-Bound Copper Deposits, Alaska

By Robert G. Eppinger, Stephen J. Sutley, and John B. McHugh

## ABSTRACT

An environmental geochemical study was undertaken at the Nabesna skarn and Kennecott strata-bound copper deposits to determine metal dispersion and metal-suite characteristics in various sample media, and to assess the present-day effects caused by historic mining and milling activities. Bedrock in the Nabesna mine area consists predominantly of Upper Triassic limestone, with subordinate exposures of underlying Triassic Nikolai Greenstone and overlying calcareous argillite and siltstone of the Jurassic to Cretaceous Nutzotin Mountain Sequence. The Triassic carbonate rocks were intruded by Early Cretaceous **granodiorite** stocks and dikes, resulting in the formation of **gold-bearing, pyrite-pyrrhotite-magnetite skarns**. Strata-bound copper deposits at Kennecott are within the lower part of the Upper Triassic Chitistone Limestone, near its **disconformable** contact with the underlying Nikolai Greenstone.

Water (stream, spring, pond) and solid (**stream-sediment**, heavy-mineral-concentrate, rock, mine waste, and mill tailings) samples were collected and analyzed for a broad suite of elements. All sampled natural waters had **near-neutral** pH values and contained low total dissolved metals. Surface waters are generally buffered by surrounding carbonate rocks in both areas, and such waters have a reduced capacity to transport metals. The highest dissolved-metal content in water from the Nabesna area was 360 ppb Zn in a sample collected below the Nabesna mill. At Kennecott, the highest dissolved-metal content in water was 67 ppb Cu in a sample collected below the Kennecott mill. Higher sulfate content in Nabesna area waters (mean  $\text{SO}_4^{2-}$  content, 190 ppm) compared with Kennecott area waters (mean  $\text{SO}_4^{2-}$  content, 8.9 ppm) is probably due to the widespread presence of pyrite, pyrrhotite, and associated sulfate salts in the Nabesna area, and to the relative lack of iron-bearing sulfides at Kennecott.

The overall metal suite Ag-As-Au-Bi-Cd-Cu-Fe-Mo-Pb-Zn is found in solid samples collected from mining and milling areas at Nabesna. A similar metal suite is found in sediments from adjacent unmined areas, suggesting the possibility of additional gold-skarn mineralization in these areas. Although highly variable, the naturally high metal

contents in sediments from unmined areas may be useful in deriving pre-mining background levels for some metals. Anomalous mercury concentrations, found throughout the Nabesna mill tailings samples and in sediment directly below the tailings, likely have an anthropogenic origin related to amalgamation processes.

The metal suite As-Cu-Hg characterizes sediments, concentrates, and rocks proximal to mining and milling areas at Kennecott. Distal sediments and concentrates have a similar, but less intense, metal suite.

Water leaches of eight Nabesna mill tailings and **mine-waste** samples had pH values below 3, high conductivities (mean conductivity, 5,200  $\mu\text{S}/\text{cm}$ ), and very high concentrations of Fe (mean concentration, 1,100 ppm), As (mean, 430 ppb), Co (mean, 260 ppb), Cu (mean, 8,400 ppb), Pb (mean, 1,200 ppb), Zn (mean, 1,300 ppb), and several other cations. Data from the water-leach test suggest a potential for acid generation and an influx of metals in waters during spring runoff or summer storm events. However, rapid downstream dilution by well-buffered waters would probably mitigate these effects.

## INTRODUCTION

In 1994, an environmental geochemical study was undertaken at the Nabesna mine, mill, and surrounding areas, and in the vicinity of the Kennecott mill and the nearby Bonanza and Erie mines. The purpose of the study was to determine the metal suites and extent of metal dispersion and to assess the present-day effects of past mining. Various sample media were collected and concentrations of a large suite of trace elements were determined to assess metal content in the different media.

The Nabesna gold mine is located in eastern Alaska, in the south-central part of the Nabesna  $1^\circ \times 3^\circ$  **quadrangle**, and is surrounded by Wrangell–St. Elias National Park and Preserve (fig. 1). Topography varies from relatively subdued near the valley bottom at the Nabesna mill (about 900 m in elevation), to the steep slopes and cliffs of White Mountain (about 1,860 m) immediately to the west. The Nabesna and nearby Rambler mines are located on the eastern flank of White Mountain (fig. 2A).



The Kennecott mill and its associated copper deposits are located south of Nabesna, in the central part of the McCarthy 1°×3° quadrangle, and also are surrounded by Wrangell–St. Elias National Park and Preserve (fig. 1). The Kennecott mill complex lies at the base of Bonanza Peak (2,128 m), along the edge of the Kennicott Glacier, at about 610 m in elevation. The mines which supplied the mill are located several thousand feet higher on the steep slopes of Bonanza Ridge (fig. 3).

## GENERAL GEOLOGY, DEPOSIT SETTING, AND MINING HISTORY

Deposits at both Nabesna and Kennecott are found within the Wrangellia terrane (Jones and others, 1977), one

of the accretionary terranes that constitute the geology of southern Alaska. Wrangellia originated at low paleolatitudes in the proto-Pacific region and probably was sutured to southern Alaska during the Late Cretaceous (Plafker and Berg, 1994).

## NABESNA

Rocks exposed at White Mountain, near the Nabesna mine, are predominantly Upper Triassic limestone; lesser underlying Nikolai Greenstone, an amygdaloidal subaerial basalt of Middle to Late Triassic age; and lesser overlying calcareous argillite and siltstone of the Upper Jurassic and Lower Cretaceous Nutzotin Mountain Sequence (fig. 2A) (Moffit, 1943; Wayland, 1943; Lowe and others, 1982; Newberry, 1986). The limestone, referred to as Chitistone

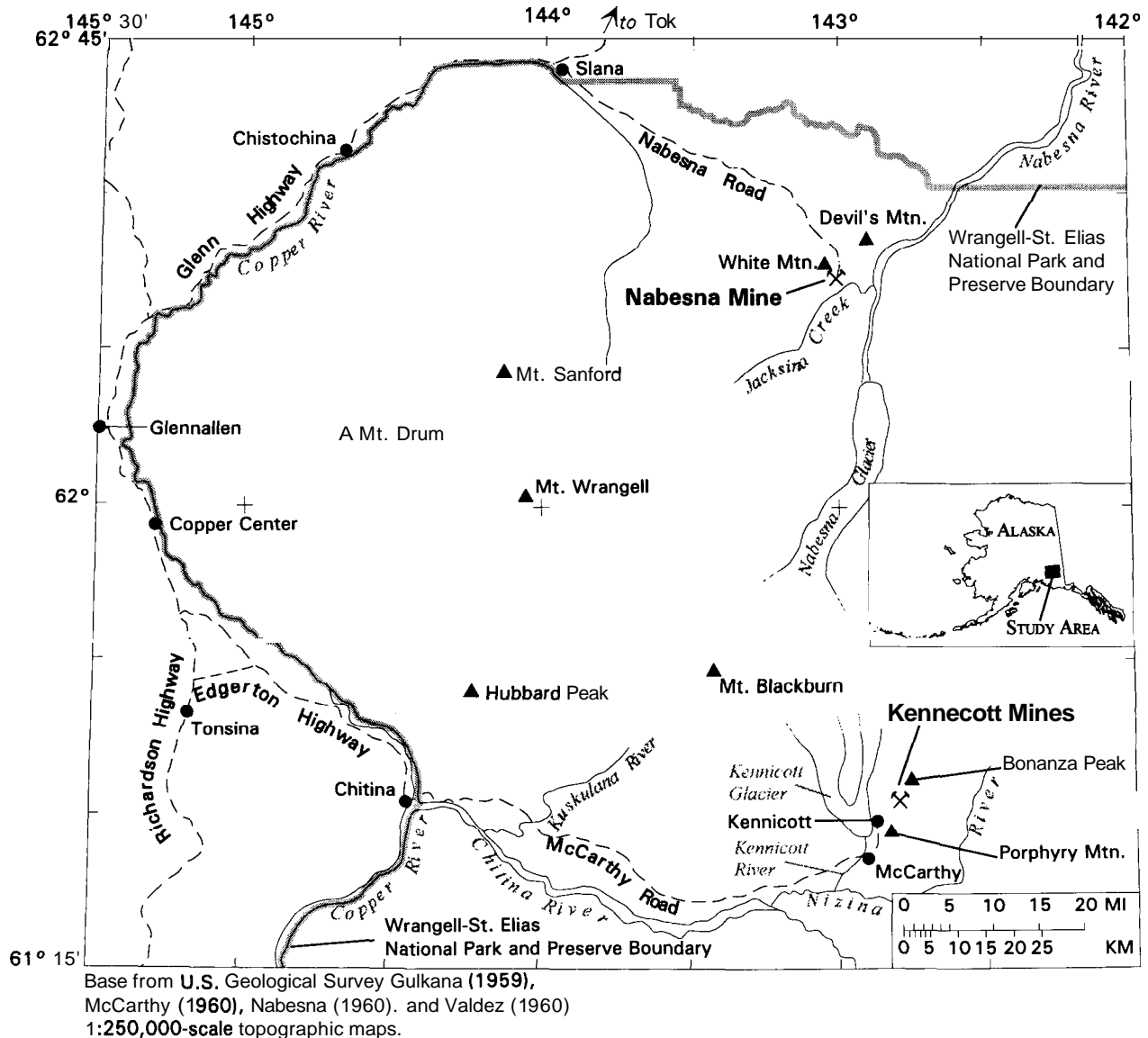


Figure 1. Location of the Nabesna and Kennecott mines within Wrangell–St. Elias National Park and Preserve, Alaska.

Limestone by **Wayland** (1943) but simply as Triassic massive limestone by **Lowe** and others (1982), consists of about 366 m of massive limestone, overlain by about 244 m of thin-bedded limestone (Wayland, 1943). It is intruded by Early Cretaceous stocks and dikes of granodiorite and quartz diorite (Wayland, 1943; **Lowe** and others, 1982; Newberry, 1986). The Triassic to Cretaceous rocks are overlain unconformably by andesitic and basaltic lavas of the Tertiary to Quaternary Wrangell Lava (**Lowe** and others, 1982). The intrusion of granodiorite into the carbonate sequence recrystallized some limestone and formed gold-bearing, iron-sulfide-rich skarn bodies. These skarns were exploited at the Nabesna and Rambler mines. Principal ore minerals were pyrite, pyrrhotite, magnetite, and chalcopyrite, with minor galena, sphalerite, arsenopyrite, and stibnite. Gangue minerals included garnet, wollastonite, vesuvianite, epidote, actinolite, hornblende, chlorite, scapolite, apatite, serpentine, and quartz (Wayland, 1943; Newberry, 1986). The main gold ores were pyrite veins along crosscutting fractures in limestone. Minor gold was produced from massive magnetite and pyrrhotite bodies (Wayland, 1943). Total gold production is listed in Theodore and others (1991) as 0.08 million metric tons at 25 g/t Au. **Wayland** (1943) also reports unquantified, but small, production of silver and copper. The Nabesna skarn deposit is classified as an iron skarn with byproduct gold (Theodore and others, 1991, table 3), although no iron was produced.

Gold was first panned at the foot of White Mountain in 1899 (Wayland, 1943). The earliest claims were located in the Nabesna mine area between 1903 and 1905, and sporadic work continued into the 1920's. In 1929, the Nabesna Mining Corporation was formed and mine development was accelerated (Hunt, 1996). By 1935, the operation was running year-round and a stamp mill was processing 60 tons of ore per day. By 1940, the deposits at the Nabesna mine were exhausted. However, the discovery in 1941 of a nearby gold-bearing pyrrhotite skarn body (probably the Rambler **orebody**) prompted small-scale exploration and mining (Moffit, 1944). Sporadic exploration and drilling continued at Nabesna into the 1980's. Presently, the mill and associated buildings are standing but in disrepair; a small amount of stockpiled ore remains near the old tram; mine-waste rock remains near the mill and on slopes below caved **adits** high on White Mountain; and a thin (locally about 1 m) veneer of fine, pyrite-rich and iron-oxide-rich mill tailings is present over a **several-thousand-square-meter** area below the mill.

## KENNECOTT

Strata-bound copper deposits in the Kennecott area are found in the lower part of the Chitistone Limestone, near the disconformable contact with the underlying Nikolai Greenstone (fig. 3). Basalt flows of the Nikolai Greenstone

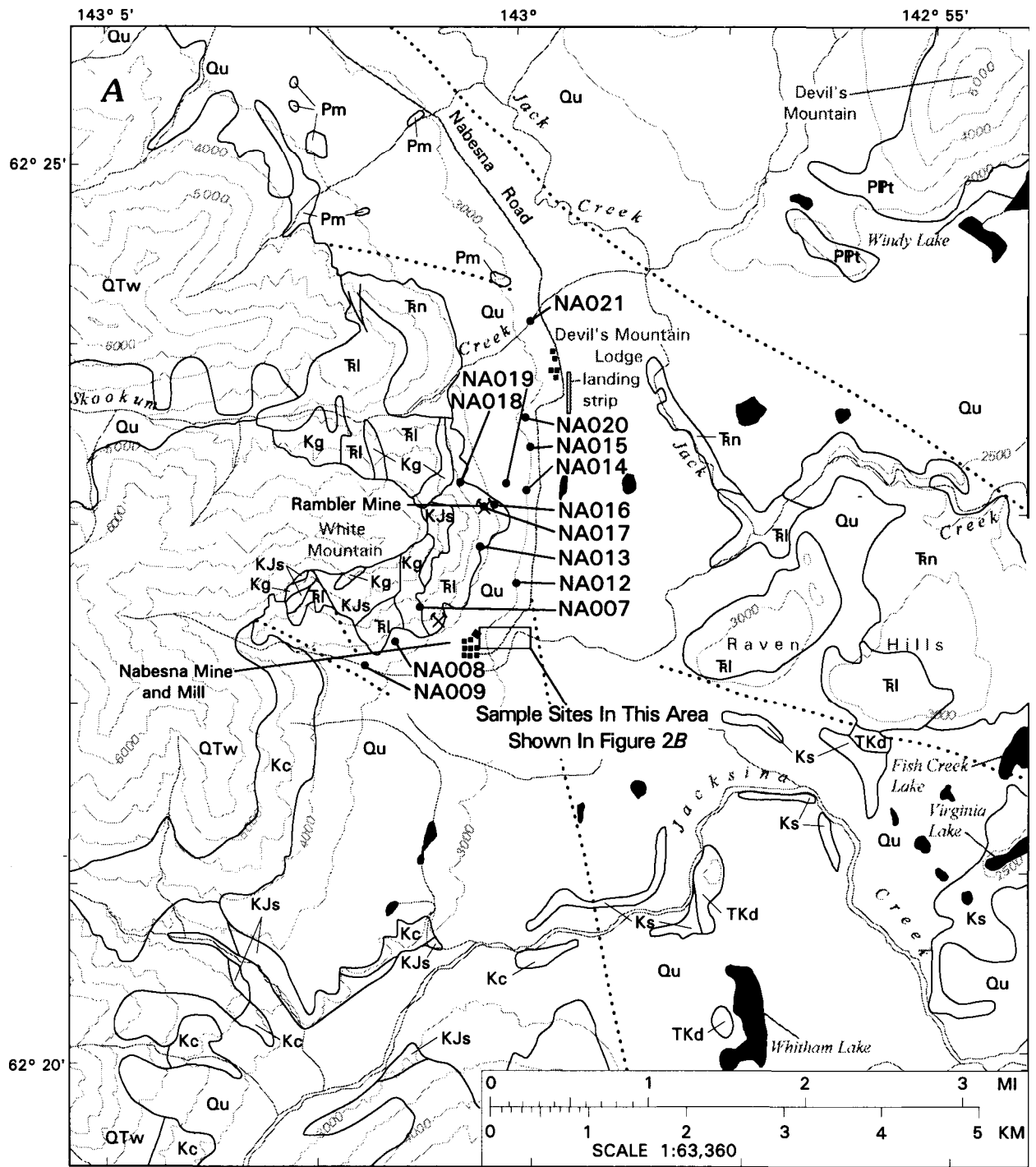
are mainly tholeiitic, have a high background copper content of around 150 ppm, and are more than 2,740 m thick in the Kennecott region (MacKevett and others, 1997). The Chitistone Limestone grades upward into the Nizina Limestone. The carbonate rocks represent a deepening-upward succession; the lower part of the Chitistone accumulated in an intertidal-supratidal, locally sabkha setting; whereas the Nizina was deposited in a moderately deep water marine environment (MacKevett and others, 1997). In the McCarthy quadrangle, the maximum thickness of the Chitistone Limestone is about 600 m and the maximum thickness of the Nizina Limestone is about 500 m (MacKevett, 1978).

The Kennecott deposits were mined for their spectacularly high-grade copper ore, which locally exceeded 70 percent. MacKevett and others (1997) suggest that the Kennecott deposits formed through the following sequence: (1) copper-enriched Nikolai Greenstone was extruded during the Middle or Late Triassic; (2) carbonate sediments (Chitistone Limestone) were deposited in a Late Triassic marine embayment on the Nikolai Greenstone; (3) sabkha-facies deposits, rich in sulfates and organic matter, formed locally in the embayment and restricted circulation, leading to evaporation that resulted in brine development; (4) karst features developed in exposed parts of the lower Chitistone Limestone following marine regression; (5) the Chitistone was buried by as much as 3,050 m of marine limestone, black shale, and other sedimentary rocks of the Nizina Limestone and the **McCarthy**, Nizina Mountain, and Root Glacier Formations; (6) the section was folded, faulted, and uplifted during the Late Jurassic to Early Cretaceous; (7) uplift and folding provided hydrologic head that caused brine circulation and leaching of copper from the Nikolai Greenstone; and (8) large orebodies formed in fissures and breccias in the lower Chitistone Limestone when migrating copper-rich brines mixed with reduced fluids derived from gypsum-organic matter mixtures in the sabkha horizons. The copper ore was mainly chalcocite and djurleite, with lesser chalcopyrite, bornite, covellite, digenite, anilite, luzonite, idaite, malachite, azurite, chalcanthite, and orpiment (**Bateman** and **McLaughlin**, 1920; MacKevett and others, 1997). More than 535,000 metric tons of copper and several million ounces of silver were produced from 1911 to 1938, the major period of mining activity (MacKevett and others, 1997).

Early Russian explorers reported implements of copper used by Copper River Indians at the mouth of the Copper River (Douglass, 1964). Prospecting in the region in the late 1890's probably was stimulated by the Klondike gold rush. The first Kennecott-type deposit was found by prospectors in 1900, who located extensive copper-stained outcrops crowning the Bonanza deposit, high above the Kennecott Glacier (Douglass, 1964; Hunt, 1996). The other principal deposits were located within the next few years. The first ore was shipped in 1911, but the peak of mining activity was from 1915 to 1929. Copper sulfide ore was

gravity-concentrated and shipped directly for processing in Washington. Copper was stripped from carbonate ore (malachite and azurite) at the mill using a Kennecott-developed ammonia leach process, and then it was shipped for further

refining. The mines ceased production in 1938 because of low reserves, low copper prices, and labor problems (MacKevett and others, 1997). Presently, much of the mill area remains intact, and carbonate-rich mine-waste rock



Base from U.S. Geological Survey Nabesna B-4 (1970) and Nabesna B-5 (1960) topographic maps.

Figure 2. A, Generalized geology and site locations for samples collected in the Nabesna mine area, Alaska. Geology generalized from Richter (1971) and Lowe and others (1982). B, Detailed site locations for samples collected at the Nabesna mill, Alaska.

remains below caved adits high above the mill on Bonanza Ridge.

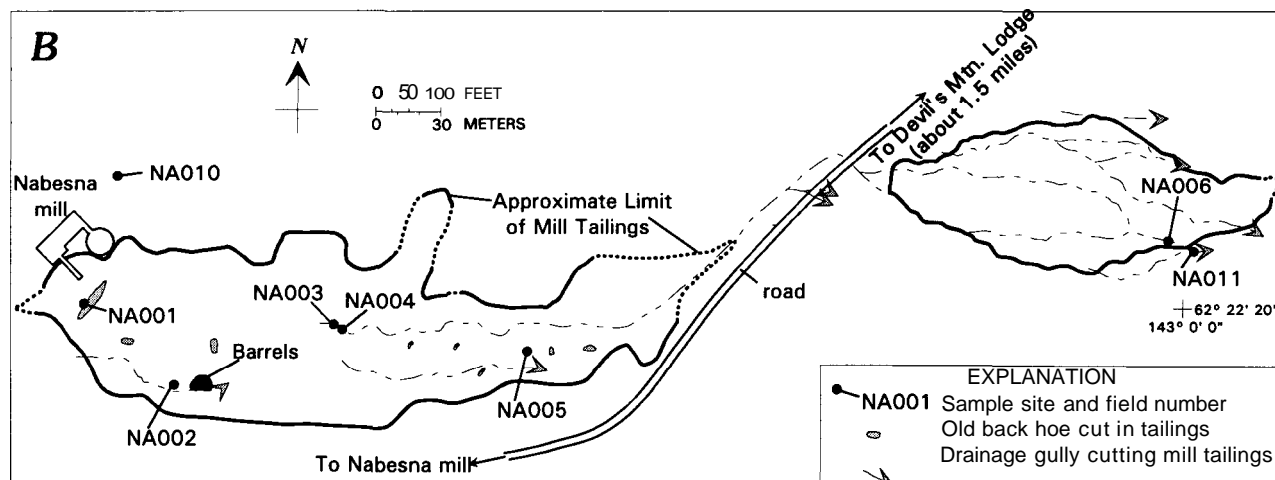
the various analytical methods, and a listing of analytical data are provided in Eppinger and others (1995).

**FIELD AND LABORATORY METHODS**

**SAMPLE COLLECTION AND PREPARATION**

Geochemical samples collected include water, stream-sediment, heavy-mineral-concentrate, rock, mine waste, and mill tailings. A brief description of sample collection, preparation, and analysis is provided here. A more detailed discussion, tables showing element determination limits for

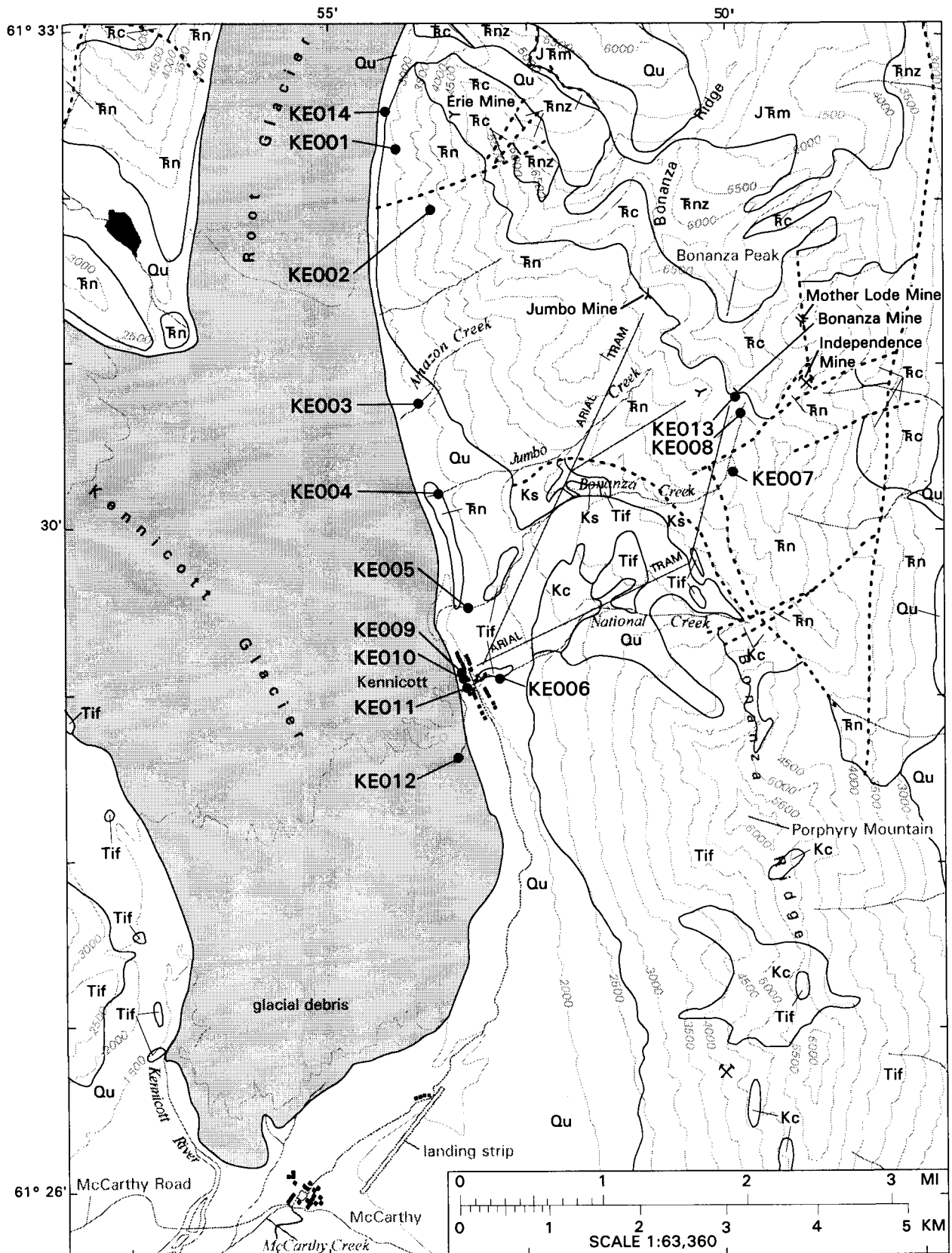
All samples were collected during a 9-day period in early August 1994. The principal sample medium was surface water, although water was scarce at many sites. The lack of surface waters in the region likely is due to three factors: (1) Near mineralization, carbonate rocks are preva-



**EXPLANATION**

- Qu Surficial deposits (Quaternary)--undivided alluvial, colluvial, and glacial deposits
  - QTw Wrangell Lava (Pleistocene, Pliocene, Miocene)--chiefly andesitic to basaltic flows and associated volcanic rocks
  - TKd Diorite (Tertiary to Cretaceous)--small diorite bodies
  - Kg Granodiorite to quartz diorite (Cretaceous)--stocks and dikes
  - Kc Chisana Formation (Cretaceous)--basaltic to andesitic flows, breccias, and interbedded volcanoclastic rocks
  - Ks Continental sedimentary rocks (Cretaceous)--arkosic sandstone, siltstone, and shale
  - KJs Nutzotin Mountain Sequence (Early Cretaceous and Late Jurassic)--calcareous argillite, siltstone, and graywacke
  - Til Limestone (Late Triassic)--includes thin-bedded (T<sub>tl</sub>) and massive (T<sub>ml</sub>) limestone units of Lowe and others (1982)
  - Tin Nikolai Greenstone (Middle to Late Triassic)--subaerial amygdaloidal basalt flows. Includes units Tin of Lowe and others (1982) and T<sub>Pb</sub> of Richter (1971)
  - Pm Mankomen Group (Early Permian)--argillite and subordinate interbedded calcareous siltstone and grit
  - PPt Tetelna Volcanics (Permian and Pennsylvanian)--interbedded andesitic flows, lahars, tuffs, and volcanoclastic rocks
- Contact, approximately located
  - - - Fault contact, approximately located, dotted where concealed
  - X Mine

Figure 2 Continued.



Base from U.S. Geological Survey McCarthy B-5 (1970).  
 B-6 (1959). C-5 (1959), and C-6 (1959) topographic maps.

Figure 3. Generalized geology and site locations for samples collected in the Kennecott mine area, Alaska. Geology generalized from MacKevett (1970, 1972, 1974) and MacKevett and Smith (1972).

lent in outcrop, alluvium, and colluvium. In such areas of carbonate terrane, surface waters tend to disappear underground over relatively short distances. This feature, particularly common at Nabesna, was less significant at Kennecott. (2) Samples were collected in late summer, well after ice breakup, spring runoff, and early summer precipitation. (3) There were unusually dry conditions throughout the region in the latter half of the summer of 1994. No precipitation occurred during the 9-day collection period. Sample sites are shown in figures 2A and 2B for the Nabesna area and in figure 3 for the Kennecott area.

Water samples were collected at 22 sites, 11 each from the Nabesna and Kennecott areas. Surface-water sources included flowing streams, springs, seeps, and, at Kennecott, ponded rainwater. Site duplicates were collected from two sites each at Nabesna and Kennecott. Water samples collected at each sample site include (1) a 125 mL, unacidified, unfiltered water sample, collected for anion analysis; and (2) a 60 mL sample, filtered to 0.45 μm and acidified to less than pH 2.0 with ultrapure, concentrated nitric acid, collected for trace and major cation analysis. The unacidified water samples were kept cool until they were analyzed. Other water data collected and recorded on-site include temperature, pH, conductivity, dissolved-oxygen content, alkalinity, and a visual estimate of the water flow rate (table 1).

Stream-sediment samples were collected at 21 sites, from below mines and mills and from nearby unmined ar-

reas. Sediment samples were collected at water-sample sites whenever possible; sediment site duplicates were collected at the same four sites that water site duplicates were collected. Stream-sediment samples consisted of composited 1-kg samples of active alluvium. In the laboratory, sediment samples were air dried, sieved to minus-200 mesh (0.074 mm), and pulverized for chemical analysis.

Since elements related to mineral deposits are commonly found in heavy minerals, pan concentrates were collected at 10 of the stream-sediment sample sites, as well as at 3 sites within mill tailings at the Nabesna mine. Samples weighing about 7 kg were collected from around boulders and in coarse-grained gravels where heavy minerals tend to accumulate, and these samples were panned at the site until 1 to 3 percent of the original sample remained. In the laboratory, panned concentrate samples were sieved to minus-20 mesh (0.84 mm), gravity separated using bromoform (specific gravity 2.89), and then separated with an electromagnet into magnetic, weakly magnetic, and nonmagnetic fractions. The nonmagnetic heavy-mineral fraction, which commonly contains ore-related minerals such as sulfide minerals, gold, and other native metals, was pulverized for chemical analysis.

Twenty-nine rock samples were collected in mined and unmined areas, generally as composite chip samples from outcrop, alluvium, mine-waste piles, and mill tailings. In the laboratory, rock samples were coarsely crushed to pea-sized pieces, split, and then pulverized for chemical analysis.

EXPLANATION

Qu	Surficial deposits (Quaternary)--undivided alluvial, colluvial, and glacial deposits
Tif	Dacite and dacite porphyry (Tertiary)--dikes and sills
Ks	Schulze Formation (Late Cretaceous)--siliceous shale with uncommon sandstone and siltstone
Kc	Chititu Formation (Cretaceous)--dominantly mudstone and shale with lesser siltstone and limestone. Includes metamorphosed Chititu Formation (Kch) of MacKevett (1974) and MacKevett and Smith (1972)
J <sup>RM</sup>	McCarthy Formation (Late Triassic and Early Jurassic?)--impure limestone, chert, shale, and minor siltstone. Includes both upper member (J <sup>RMu</sup> ) and lower member (J <sup>RMl</sup> ) of MacKevett (1970, 1972, 1974) and MacKevett and Smith (1972)
Rnz	Nizina Limestone (Late Triassic)--limestone with layered and nodular chert
Tic	Chitstone Limestone (Late Triassic)--limestone, dolomite, and minor nodular chert. Local solution pits and caverns
Tin	Nikolai Greenstone (Middle to Late Triassic)--subaerial amygdaloidal basalt flows
~	Contact, approximately located
-	Fault contact, approximatedly located
Y	Adit
X	Mine

Figure 3. Continued.

Table 1. On-site data and sample descriptions for water samples collected in the Nabesna and Kennecott areas, Alaska

[Shaded areas indicate samples collected from areas of historic mining or milling activities; unshaded areas indicate samples from unmined areas; " D in field number suffix indicates sample site duplicates; ppm, parts per million; cfs, cubic feet per second]

Index	Sample site no.	Site description	Temp. °C	pH	Conductivity $\mu\text{S/cm}$	Dissolved O <sub>2</sub> ppm	Alkalinity ppm	Estimated flow rate
<b>Nabesna</b>								
1	NA008	Spring on drill road above Nabesna mill site	25	7.8	1,310	8	190	<0.1 gal/min
2	NA011	Spring at base of lowermost Nabesna mill tailings; abundant iron oxides; unidentified white mineral coating pebbles	11	7.1	582	4	150	0.25 gal/min
3	NA016	Spring just below Rambler mine-waste pile; slight iron oxide staining	3	7.6	1,160	10	230	2 gal/min
4	NA009	Main stream south of Nabesna mine and mill site	24	8.0	144	8	60	<0.1 gal/min
5	NA012	Spring in muskeg	2	7.5	394	11	160	stagnant
6	NA013	Stream at base of limestone cliff; ion-oxide-rich sediments	17	7.9	740	9	80	5 gal/min
7	NA014	Spring in muskeg	3	7.5	780	7	350	2 gal/min
8	NA015	Spring in muskeg	8	7.5	870	7	200	0.5 gal/min
9	NA019	Spring along road heading to Rambler mine	4	7.5	770	7	260	0.5 gal/min
10	NA020	Spring in muskeg	8	7.4	535	7	260	<0.1 gal/min
11	NA021	Stream; Skookum Creek, upstream from the Nabesna road	14	8.0	132	8	55	10 cfs
12	NA013D	Site duplicate of NA013W1	17	7.9	740	9	75	5 gal/min
13	NA021D	Site duplicate of NA021W1	14	8.0	131	8	55	10 cfs
<b>Kennecott</b>								
1	KE008	Stream; head of Bonanza Creek, just below Bonanza mine; steel mining artifacts in drainage	2	8.2	147	10	60	20 gal/min
2	KE009	Ponded rainwater in Nikolai Basalt just below Kennecott mill; surrounded by mill tailings; white calcite crust around edge of pond	13	7.9	105	8	45	stagnant
3	KE010	Spring flowing from Kennecott mill tailings below ammonia leaching plant; white calcite crust along water's edge	6	7.9	436	11	230	5 gal/min
4	KE011	Stream; National Creek below Kennecott mill; slight light-colored orange-yellow staining on alluvium	8	8.0	145	11	60	15 cfs
5	KE012	Stream; National Creek at junction with Kennecott Glacier; slight light-colored orange-yellow staining on alluvium	18	8.1	149	11	65	15 cfs
6	KE002	Stream above small snowfield	4	8.0	145	11	60	50 gal/min
7	KE003	Stream; Amazon Creek about 15 m above Root Glacier trail	5	7.9	160	10	70	50 gal/min
8	KE004	Stream; Jumbo Creek about 15 m above Root Glacier trail	7	8.0	144	10	70	20 cfs
9	KE005	Stream; Bonanza Creek about 7 m above Root Glacier trail	9	8.1	188	11	80	8 cfs
10	KE006	Stream; National Creek above Kennecott mill; slight light-colored orange-yellow staining on alluvium	7	7.7	133	10	60	15 cfs
11	KE007	Spring in slightly brown-stained, amygdaloidal Nikolai Basalt	6	8.0	145	9	55	3 gal/min
12	KE004D	Site duplicate of KE004W1	7	8.0	144	10	70	20 cfs
13	KE010D	Site duplicate of KE010W1	6	7.9	437	11	220	5 gal/min
<b>Blank</b>								
	VA001W1	Blank sample, distilled water, unfiltered, unacidified	25	5.5	04	10	<10	--

Six tailings samples from the Nabesna mill, a mine-waste sample from the Rambler mine, and a mineralized bedrock sample from the Rambler mine were collected for a water-leach test. About 10 kg of material were collected for each sample from the upper 2 cm of the surface layer. Laboratory preparation for the samples followed a modification of the EPA Synthetic Precipitation Leaching Procedure 1312 (Environmental Protection Agency, 1994), a method designed to determine mobility of inorganic analytes in solid wastes. The sample was passed through a  $3/8$ -in. (9.5-mm) sieve. Deionized water, acidified to pH 5.0, was used for the leaching procedure, mixed in a ratio of 20:1 water to sample. Following mixing, measurements for pH, conductivity, temperature, oxygen content, and alkalinity were collected. Resultant leach-water aliquots for geochemical analysis were collected by filtering and acidifying as described above.

## ANALYTICAL TECHNIQUES

All acidified water samples were analyzed by inductively coupled plasma-mass spectrometry, following the semiquantitative method of Meier and others (1994), in which more than 60 cations are determined directly in the water sample without the need for preconcentration or dilution (table 2). Major element and selected trace element cations in waters were analyzed by inductively coupled plasma-atomic emission spectrometry (ICP-AES), following the procedure of Briggs and Fey (1996). Anions in waters were analyzed by ion chromatography (d'Angelo and Ficklin, 1996). Stream sediments and rocks were analyzed by a 40-element, total digestion, ICP-AES method (Briggs, 1990); and by a 10-element, partial extraction, ICP-AES method (Motooka, 1996). Several specific elements were determined using a variety of atomic absorption and

Table 2. Elements determined and analytical methods used for all sample media collected in the Nabesna and Kennecott areas, Alaska

[AA, atomic absorption spectrophotometry; AE, inductively coupled plasma-atomic emission spectrometry (total digestion); CV, cold-vapor atomic absorption spectrophotometry; ES, semiquantitative emission spectrography; GF, graphite-furnace atomic absorption spectrophotometry; HY, hydride generation atomic absorption spectrophotometry; IC, ion chromatography; IE, ion exchange inductively coupled plasma-atomic emission spectrometry; MS semiquantitative inductively coupled plasma-mass spectrometry; PA, inductively coupled plasma-atomic emission spectrometry (partial extraction)]

Sample media	Method: elements determined
Water, acidified/filtered	MS: Ag, Al, As, Au, Ba, Be, Bi, Ca, Cd, Ce, Co, Cr, Cs, Cu, Dy, Er, Eu, Fe, Ga, Gd, Ge, Hf, Ho, Ir, K, La, Li, Mg, Mn, Mo, Na, Nb, Nd, Ni, Os, Pb, Pd, Pr, Pt, Rb, Re, Rh, Ru, Sb, Sc, Sm, Sn, Sr, Ta, Tb, Te, Th, Ti, Tl, Tm, U, V, W, Y, Yb, Zn, Zr AE: Al, B, Ba, Be, Ca, Cd, Co, Cr, Cu, Fe, K, Li, Mg, Mn, Mo, Na, Ni, P, Pb, Si, Sr, Ti, V, Zn
Water, raw	IC: Cl, F, NO <sub>3</sub> <sup>-</sup> , SO <sub>4</sub> <sup>2-</sup>
Mill tailings leachates, acidified/filtered	MS: Ag, Al, As, Au, Ba, Be, Bi, Ca, Cd, Ce, Co, Cr, Cs, Cu, Dy, Er, Eu, Fe, Ga, Gd, Ge, Hf, Ho, K, La, Li, Mg, Mn, Mo, Na, Nb, Nd, Ni, Pb, Pr, Rb, Re, Sb, Sc, Sm, Sn, Sr, Ta, Tb, Te, Th, Ti, Tl, Tm, U, V, W, Y, Yb, Zn, Zr AE: Ag, Al, As, B, Ba, Be, Bi, Ca, Cd, Co, Cr, Cu, Fe, K, Li, Mg, Mn, Mo, Na, Ni, P, Pb, Sb, Si, Sn, Sr, Ti, V, Zn
Stream sediments and rocks	AE: Ag, Al, As, Au, Ba, Be, Bi, Ca, Cd, Ce, Co, Cr, Cu, Eu, Fe, Ga, Ho, K, La, Li, Mg, Mn, Mo, Na, Nb, Nd, Ni, P, Pb, Sc, Sn, Sr, Ta, Th, Ti, U, V, Y, Yb, Zn PA: Ag, As, Au, Bi, Cd, Cu, Mo, Pb, Sb, Zn HY: As, Sb, Se GF: Au CV: Hg AA: Tl IE: W
Heavy-mineral concentrates	ES: Ag, As, Au, B, Ba, Be, Bi, Ca, Cd, Co, Cr, Cu, Fe, Ga, Ge, La, Mg, Mn, Mo, Na, Nb, Ni, P, Pb, Pd, Pt, Sb, Sc, Sn, Sr, Th, Ti, V, W, Y, Zn, Zr

ICP-AES methods (O'Leary and Meier, 1990; O'Leary and others, 1990; Welsch and others, 1990; O'Leary, 1996; Doughten and Aruscavage, 1996). Nonmagnetic heavy-mineral-concentrate samples were analyzed by semiquantitative emission spectrography for 37 elements (Adrian and others, 1990).

## RESULTS

### NABESNA

#### WATER SAMPLES

Water close to the mines and mill was found at 3 of the 11 water-sample sites in the Nabesna area: a flowing spring at the base of the Nabesna mill tailings (site NA011, fig. 2B), a flowing spring below the Rambler mine-waste pile (NA016, fig. 2A), and a low-flowing spring in mineralized bedrock along the drill road above the Nabesna mill area (NA008, fig. 2A). Near-neutral pH values (7.1 to 8.0)

were found at all eleven surface-water sample sites in the Nabesna area (table 1); the lowest pH value was from the spring at the base of the Nabesna mill tailings (site NA011). Conductivities in water from the eleven sites ranged from 131  $\mu\text{S/cm}$  to 1,310  $\mu\text{S/cm}$  (table 1), with the highest conductivities from two sites near the mines and mill: site NA008 (1,310  $\mu\text{S/cm}$ ) and site NA016 (1,160  $\mu\text{S/cm}$ ). The spring at the base of the Nabesna mill tailings (site NA011) had a conductivity of 582  $\mu\text{S/cm}$ . Conductivities from the eight sites distal to the mines and mill ranged from 131  $\mu\text{S/cm}$  to 870  $\mu\text{S/cm}$ , with five of the sites having conductivities of 535  $\mu\text{S/cm}$  or greater.

None of the water samples collected from the Nabesna area contained extremely high anion or cation content when compared with worldwide surface-water and river-water averages (tables 3, 4). For anions, only sulfate was found in relatively high concentrations; many of the sulfate concentrations determined are an order of magnitude greater than worldwide averages for rivers (table 3). Two of the three samples collected proximal to mineralized rocks or



Table 3. Concentrations of dissolved anions determined on unacidified, unfiltered water samples collected in the Nabesna and Kennecott areas, Alaska

[Shaded areas indicate samples collected from areas of historic mining or milling activities; unshaded areas indicate samples from unmined areas; " D in field number suffix indicates sample site duplicates; ppm, parts per million; IC, ion chromatography; average values are world averages for rivers from Livingstone (1963)]

Index	Field no.	Cl <sup>-</sup> ppm-IC	F <sup>-</sup> ppm-IC	NO <sub>3</sub> <sup>-</sup> ppm-IC	SO <sub>4</sub> <sup>2-</sup> ppm-IC
Average	Value:	7.8	--	1	11
Nabesna					
1	NA008W1	3.2	0.23	<.5	615
2	NA011W1	.50	.08	<.5	178
3	NA016W1	1.3	.23	16	412
4	NA009W1	.42	.07	<.5	24
5	NA012W1	.34	.08	.56	36
6	NA013W1	1.3	.11	<.5	331
7	NA014W1	.86	.21	<.5	110
8	NA015W1	.99	.12	<.5	268
9	NA019W1	.67	.28	3.1	110
10	NA020W1	.85	.12	<.5	21
11	NA021W1	.21	.07	<.5	16
12	NA013W1D	1.3	.12	<.5	348
13	NA021W1D	.20	.07	<.5	16
Kennecott					
1	KE008W1	.17	<.05	.50	10
2	KE009W1	.37	.10	<.5	6.1
3	KE010W1	.33	.08	11	9.7
4	KE011W1	.14	.06	1.1	6.1
5	KE012W1	.16	.06	1.0	6.2
6	KE002W1	.13	<.05	<.5	12
7	KE003W1	.11	<.05	<.5	14
8	KE004W1	.20	<.05	<.5	6.3
9	KE005W1	.13	<.05	.98	7.8
10	KE006W1	.13	.06	.84	6.0
11	KE007W1	<.1	<.05	<.5	15
12	KE004W1D	.15	<.05	<.5	6.8
13	KE010W1D	.27	.07	11	9.8
Blank					
	VA001W1	<.1	<.05	<.5	<.5

tailings contained the highest sulfate content (NA008W1, 615 ppm SO<sub>4</sub><sup>2-</sup>; NA016W1, 412 ppm SO<sub>4</sub><sup>2-</sup>). However, several samples collected distal to mining areas also had high sulfate contents ranging from 110 to 348 ppm. Compared with the eight acidified, filtered water samples collected distal to the mines and mill, one or more of the three samples collected near the mines and mill contained elevated concentrations for the following cations: B (190 and 73 ppb), Mn (140 ppb), and Zn (360 ppb) (table 4). Elevated U concentrations (at or above 1 ppb U) were found in most water samples from the Nabesna area, with the highest

concentrations from sites near the mines and mill (U, 22 and 29 ppb). Similarly, anomalous Mo concentrations were found in several water samples (1.4 and 21 ppb near the mines and mill; 2.0 to 9.1 ppb in six samples distal to the mines and mill). All 11 water samples from the Nabesna area contained relatively high concentrations of Ca (mean, 111 ppm), Sr (mean, 220 ppb), and to a lesser degree, Mg (mean, 17 ppm).

For the cations and anions determined in this study, none of the surface-water samples analyzed from the Nabesna area had concentrations that exceed the State of

Table 4. Concentrations of selected dissolved cations determined on acidified, filtered water samples collected in the Nabesna and Kennecott areas, Alaska

[Shaded areas indicate samples collected from areas of historic mining or milling activities; unshaded areas indicate samples from unmined areas; "D" in field number suffix indicates sample site duplicates; ppm, parts per million; ppb, parts per billion; average values: a, worldwide values for surface waters from Hem (1985); b, values for rivers from Martin and Whitfield (1983); see table 2 for explanation of analytical methods codes AE and MS]

Index	Field no.	Al ppm-AE	Ca ppm-AE	Fe ppm-AE	K ppm-AE	Mg ppm-AE	Na ppm-AE	Si ppm-AE	As ppb-MS	B ppb-AE	Cd ppb-MS	Co ppb-MS
Average Value:		0.01-0.1's a	13.3 b	0.04 b	1.5 b	3.1 b	5.3 b	5 b	0.1-1's a	18 b	1's a	0.1's a
<b>Nabesna</b>												
1	NA008W3	0.2	200	< .02	2.9	48	22	14	4.3	190	< 2	0.3
2	NA011W3	.04	110	.6	2.0	11	4.2	16	< .8	73	4	1.6
3	NA016W3	.1	190	< .02	4.3	31	3.7	9.0	< .8	< 50	< 2	.2
4	NA009W3	< .02	19	< .02	1.2	2.9	3.2	10	< .8	< 50	< 2	.1
5	NA012W3	.03	77	.03	1.7	4.1	1.0	10	< .8	< 50	< 2	.2
6	NA013W3	.04	140	.03	1.9	10	5.5	14	1	< 50	< 2	1.4
7	NA014W3	.07	140	.03	2.2	17	2.1	15	< .8	< 50	< 2	.2
8	NA015W3	.06	150	< .02	3.0	16	6.1	15	< .8	< 50	< 2	.2
9	NA019W3	.07	110	.02	1.8	20	1.6	14	< .8	< 50	< 2	.1
10	NA020W3	.1	71	.1	.7	23	3.0	8.4	< .8	< 50	< 2	.2
11	NA021W3	.03	13	.03	1.0	5.1	4.7	9.3	< .8	< 50	< 2	< .1
12	NA013W3D	.04	140	.03	2.0	10	5.7	14	< .8	< 50	< 2	1.6
13	NA021W3D	.02	13	< .02	1.0	5.1	4.7	9.4	.9	< 50	< 2	< .1
<b>Kennecott</b>												
1	KE008W3	.02	19	< .02	.1	5.0	2.7	1.6	2.4	< 50	< 2	< .1
2	KE009W3	.02	18	< .02	.4	1.2	.4	< 1	< .8	< 50	< 2	.1
3	KE010W3	.04	72	< .02	.7	11	2.2	5.2	7.4	< 50	< 2	.1
4	KE011W3	< .02	16	< .02	.5	5.3	4.5	3.3	< .8	< 50	< 2	< .1
5	KE012W3	.03	17	< .02	.6	5.4	4.5	3.4	.8	< 50	< 2	< .1
6	KE002W3	< .02	19	< .02	.1	4.7	2.1	2.7	< .8	58	< 2	< .1
7	KE003W3	.02	22	< .02	.1	4.9	1.7	1.8	3.2	< 50	< 2	< .1
8	KE004W3	.02	19	< .02	.1	4.5	1.5	1.6	2.4	< 50	< 2	< .1
9	KE005W3	.03	24	< .02	.3	6.5	3.9	2.9	1	54	< 2	< .1
10	KE006W3	.03	15	< .02	.5	5.3	4.7	3.2	< .8	< 50	< 2	< .1
11	KE007W3	.02	16	< .02	.1	2.3	10	2.3	< .8	78	< 2	< .1
12	KE004W3D	.02	19	< .02	.1	4.5	1.5	1.6	2.2	< 50	< 2	< .1
13	KE010W3D	.04	72	< .02	.7	11	2.2	5.2	7.1	< 50	< 2	.1
Blank	VA001W3	< .02	.05	< .02	< .05	< .05	< .05	< 1	< .8	< 50	< 2	< .1

Index	Field no.	Cu ppb-MS	Mn ppb-MS	Mo ppb-MS	Ni ppb-MS	Pb ppb-MS	Sb ppb-MS	Sr ppb-MS	U ppb-MS	V ppb-MS	Zn ppb-MS
Average Value:		1-10's a	8.2 b	0.1's a	0.1-1's a	0.1-1's a	0.1-1's a	60 b	0.1-1's a	1's a	1-10's a
<b>Nabesna</b>											
1	NA008W3	2	6.4	21	2.2	< 0.1	0.2	970	29	0.9	6.6
2	NA011W3	7.5	140	48	4.2	< .1	< .2	220	.6	< .4	360
3	NA016W3	2.8	< 2	1.4	3.0	< .1	< .2	210	22	< .4	< 2
4	NA009W3	1	.4	.55	.4	.2	< .2	60	.2	2.2	< 2
5	NA012W3	6.2	.50	2.9	2.7	< .1	.2	96	.7	.4	< 2
6	NA013W3	6.4	1.0	9.1	2.5	< .1	.3	250	3.2	< .4	< 2
7	NA014W3	3.3	2.7	2.9	2.7	.1	< .2	150	5.9	< .4	< 2
8	NA015W3	2	1.3	2.0	2.9	< .1	< .2	210	2.3	< .4	< 2
9	NA019W3	2.9	.3	6.3	2.5	< .1	.69	110	8.9	< .4	4
10	NA020W3	1	18	.3	2.8	< .1	< .2	100	1	< .4	< 2
11	NA021W3	1	< 2	.61	.3	< .1	< .2	49	1.4	2.5	< 2
12	NA013W3D	6.7	.99	8.6	2.9	< .1	.3	240	2.9	< .4	< 2
13	NA021W3D	.6	< 2	.90	< 2	< .1	< .2	48	1.5	2.5	< 2
<b>Kennecott</b>											
1	KE008W3	2	< 2	< .1	.2	< .1	< .2	33	< .1	1.2	< 2
2	KE009W3	9.5	1.3	1.2	.5	.1	< .2	63	< .1	< .4	< 2
3	KE010W3	67	< 2	1.4	1.2	< .1	< .2	270	.4	< .4	< 2
4	KE011W3	2	< 2	.3	.3	< .1	< .2	63	.1	< .4	< 2
5	KE012W3	6.7	.3	.3	.3	.1	< .2	66	.2	< .4	< 2
6	KE002W3	< .6	.2	.2	< .2	< .1	< .2	93	.2	.9	< 2
7	KE003W3	< .6	.2	< .1	.2	< .1	< .2	50	< .1	.9	< 2
8	KE004W3	.9	< 2	.2	< 2	< .1	< .2	42	< .1	.8	< 2
9	KE005W3	2	.3	< .1	.2	< .1	< .2	69	< .1	.9	< 2
10	KE006W3	< .6	< 2	.2	< 2	< .1	< .2	58	< .1	< .4	< 2
11	KE007W3	< .6	.2	.1	< 2	< .1	< .2	40	< .1	2.0	< 2
12	KE004W3D	.8	< 2	.2	.3	< .1	< .2	42	.1	.7	< 2
13	KE010W3D	61	< 2	1.2	.75	.1	< .2	260	.2	< .4	< 2
Blank	VA001W3	< .6	< 2	< .1	< 2	< .1	< .2	< .1	< .1	< .4	< 2

Alaska's enforceable primary maximum contaminant levels (MCL) for public drinking water (Alaska Department of Environmental Conservation, 1994). However, secondary MCLs, which are merely goals for water quality set forth by the State of Alaska, were exceeded at Nabesna for Mn (secondary MCL, 50 ppb) and sulfate (secondary MCL, 250 ppn). The Mn secondary MCL was exceeded only at the spring at the base of the mill tailings (NA011W3, 140 ppb Mn, table 4). The sulfate secondary MCL was exceeded at two springs near the Nabesna and Rambler mines (NA008W1, 615 ppm  $\text{SO}_4^{2-}$ ; NA016W1, 412 ppm  $\text{SO}_4^{2-}$ ) and at two sites distal to the mines and mill: a stream containing iron oxide and pyrite in sediment (NA013W1, 331 ppn  $\text{SO}_4^{2-}$ ) and a spring in muskeg (NA015W1, 268 ppn  $\text{SO}_4^{2-}$ , table 3).

#### SOLID SAMPLES

Anomalous element concentrations found in minus-200 mesh stream-sediment samples collected from the Nabesna area include those of As, Au, Cu, Pb, and Zn and to a lesser degree Bi, Cd, Co, Hg, Mo, Sb, and Se (table 5). The sample collected below the Nabesna mill tailings (site NA011) contained anomalous concentrations of Ag, As, Au, Bi, Cu, Fe, Pb, and Zn, and weakly anomalous concentrations of Cd, Hg, Mo, and Sb. In contrast, the sample collected below the Rambler mine-waste pile (site NA016) contained anomalous concentrations of only Au and perhaps Sb. Sediments were also collected at eight sites from unmined areas. In these samples, Au was the most widespread anomalous element, found at five of the eight sites. Sediment sample NA013S1, collected from the unmined area mentioned previously with iron oxide and pyrite in the sediment, contained anomalous concentrations of As, Au, Co, Cu, Fe, and Zn, and weakly anomalous concentrations of Ag, Bi, Cd, Mo, Pb, and Sb. Other sediment samples collected from unmined areas contained sporadic, weakly anomalous concentrations of As, Bi, Cu, Pb, Sb, Se, and Zn. Weakly anomalous Hg in sediment was found only at one site, below the Nabesna mill (NA011S1; Hg, 0.43 ppm).

Twenty-one rock samples collected in the Nabesna area include mill tailings, stockpiled ore, mine waste, mineralized outcrop, and mineralized alluvial cobbles (table 6). Mill-tailings samples (sites NA001 through NA006) generally had highly anomalous concentrations of Ag, As, Au, Bi, Cd, Cu, Fe, Hg, Mo, Pb, and Zn and anomalous concentrations of Co, Sb, Se, and W (table 6). Mineralized outcrop, stockpiled ore, mine waste, and alluvial cobbles (sites NA007, NA008, NA010, and NA017) contained anomalous concentrations of essentially the same metal suite, except for a lack of anomalous Hg. Less consistent anomalies were found for Mn in several rock samples.

Nonmagnetic, heavy-mineral concentrates were collected from three sites within the Nabesna mill tailings (sites NA003, NA005, and NA006, fig. 2B) and from three

sites distal from the mines and mill (sites NA009, NA013, and NA021, fig. 2A). In mill tailings, highly anomalous metal concentrations were found for Ag (100 to 1,000 ppm), As (500 to 1,500 ppm), Au (100 to >1,000 ppm), Bi (20 to 150 ppm), Cu (5,000 to 15,000 ppm), Fe (7 to 50 percent), and Pb (500 to 700 ppm). Anomalous metals found in samples from sites distal to the mines and mill include Ag (20 ppm), Au (100 ppm), Cd (50 ppm), Cu (1,500 ppm), Pb (500 ppm) and Zn (1,500 ppm) at site NA009; Co (1,000 ppm), Cu (5,000 ppm), and Fe (15 percent) at site NA013; and As (1,000 ppm), Fe (10 percent), and Pb (300 ppm) at site NA021 (Eppinger and others, 1995).

#### LEACH SAMPLES

Leach waters derived from the Nabesna mill tailings, Rambler mine waste, and a mineralized outcrop sample above the Rambler mine had acidic pH values, high conductivities, and high concentrations of several cations (table 7). Six of the eight leach samples had pH values below pH 3. Particularly high cation concentrations were found for Fe (mean concentration, 1,100 ppm), As (mean, 430 ppb), Co (mean, 260 ppb), Cu (mean, 7,100 ppb), Pb (mean, 1,200 ppb), and Zn (mean, 1,300 ppb). Other cations found in anomalous concentrations include Ag, Al, B, Bi, Ca, Cd, Ce, Cr, Mg, Mn, Mo, Ni, Sb, Sr, Te, Th, Ti, Tl, U, and V.

Prior to leaching, splits of all the samples were analyzed for mineralogical content using X-ray diffractometry. A variety of minerals, particularly sulfate minerals, were found (table 8). Many of the sulfate minerals are highly soluble in water.

### KENNECOTT

#### WATER SAMPLES

Water near the mines and mill was collected from 5 of the 11 water-sample sites in the Kennecott area: a flowing stream below the Bonanza mine (site KE008), a small rain-water pool below the Kennecott mill (KE009), a small spring flowing from Kennecott mill tailings (KE010), National Creek flowing through the Kennecott mill-tailings area (KE011), and National Creek just above its junction with Kennecott Glacier (KE012; fig. 3). Near-neutral pH values (7.7 to 8.2) were found at all water-sample sites in the Kennecott area. Compared with Nabesna area waters, conductivities for all Kennecott water samples were relatively low, ranging from 105  $\mu\text{S}/\text{cm}$  to 188  $\mu\text{S}/\text{cm}$ , except at the mill-tailings spring sample site KE010 (conductivity, 436  $\mu\text{S}/\text{cm}$ , table 1).

Anion and cation concentrations were all relatively low for water samples collected from the Kennecott area (tables 3, 4). The spring sample in mill tailings at site KE010 had the highest Cu content, a surprisingly low value of 67 ppb (table 4). The sample at site KE012, about 0.8 km down-

Table 5. Concentrations of selected elements in minus-200 mesh stream-sediment samples collected in the Nabesna and Kennecott areas, Alaska

[Shaded areas indicate samples collected from areas of historic mining or milling activities; unshaded areas indicate samples from unmined areas; " D in field number suffix indicates sample site duplicates; ppm, parts per million; pct, percent; average crustal abundance values from Fortescue (1992, table 4); threshold values determined arbitrarily by inspection of data distributions and natural background data for various rock types (Rose and others, 1979); different thresholds for the Nabesna and Kennecott areas reflect differences in predominant lithologies in the two areas; see table 2 for explanation of analytical methods codes AE, CV, GF, HY, and PA; na, sample not analyzed for this element]

Index	Weld No.	Ag ppm-PA	As ppm-PA	Au ppm-GF	Bi ppm-PA	Cd ppm-PA	Co ppm-AE	Cu ppm-AE	Fe pct-AE	Hg ppm-CV	Mn ppm-AE	Mo ppm-PA	Pb ppm-PA	Sb ppm-HY	Se ppm-HY	Zn ppm-AE	Sample site description
Avg. crustal abundance		0.08	1.8	0.004	0.0082	0.16	29	68	6.22	0.086	1,060	1.2	13	0.2	0.05	76	
Threshold (Nabesna)		.5	10	.01	1	1	50	75	10	.3	1,500	5	25	1	1	100	
Threshold (Kennecott)		.5	20	.01	1	1	100	150	10	.3	1,500	5	25	1	1	120	
<b>Nabesna</b>																	
1	NA011S1	9.9	410	1.3	27	2	27	410	11	.43	700	5.2	480	<sup>1</sup> 3.4	na	330	Spring at base of Nabesna mill tailings
2	NA016S1	.1	5.5	.05	<1.0	.24	11	48	2.2		460	.45	2.8	1.1	.4	50	Spring below Rambler mine-waste pile
3	NA009S1		3.6	.006	<1.0	.11	23	45	5		1,000	.46	4.2	.7	<.1	82	Cabin Creek upstream of Nabesna mine
4	NA012S1	.18	10	.036	<1.0	.24	23	69	4.6		850	.91	28	1.3	.5	97	Unnamed spring
5	NA013S1	.52	510	.2	1.6	1.8	190	720	13	.05	980	6.9	28	<sup>1</sup> 3.4	1	380	Unnamed stream
6	NA014S1	.23	9.8	.026	1.1	.21	15	98	2.7	.03	560	.48	4.9	1.3	1	70	Unnamed spring
7	NA015S1	.092	5.9	.008	<1.0	.29	15	80	4.3	.03	730	1.3	9.5	1	1.3	130	Unnamed spring
8	NA018S1		2.9	.024	<1.0	.24	18	64	3.9		1,000	1	3.7	.7	.6	100	Unnamed dry streambed
9	NA020S1		2.2	<.002	<1.0	.082	17	31	3.6		670	.37	1.7	.7	<.1	53	Unnamed spring
10	NA021S1		4	.03	<1.0	.12	21	41	4.2	.11	900	.67	4.6	.5	.2	70	Skookum Creek upstream of Nabesna road
11	NA018S1D	.12	5.1	.004	<1.0	.27	17	62	3.9		1,000	1.1	5.9	.7	.1	100	Site duplicate of NA018S1
12	NA021S1D		3.6	.004	<1.0	.14	20	38	4.1		880	.66	12	.4	<.1	69	Site duplicate of NA021S1
<b>Kennecott</b>																	
1	KE008S1	3.8	170	.012	<1.0	1.4	12	6,100	2.3	.7	480	1.4	16	2.1	.3	59	Bonanza Creek just below the Bonanza
2	KE009S1	.17	17	.012	<1.0	.37	20	160	4.2	.1	690	1.5	27	<sup>1</sup> <1.0	na	72	Small rainwater pool just below Kennecott
3	KE010S1		110	.008	<1.0	5.2	5	4,900	1.1	.33	160	<1.0	11	2.7	.3	37	Unnamed spring draining Kennecott mill
4	KE011S1	.83	63	.3	<1.0	2.3	21	910	4.3	.75	980	1.1	60	<sup>1</sup> <1.0	.6	120	National Creek below Kennecott mill
5	KE012S1	.89	130	<.002	<1.0	6.3	6	5,000	1.2	.32	170	<1.0	16	2.6	.2	39	National Creek at junction with Kennecott
6	KE001S1		30	.004	<1.0	.15	33	140	5.2	.34	980	.65	1.5	.8	.2	58	Unnamed dry streambed
7	KE002S1		15	.004	<1.0	.061	54	170	8.3	.03	1,800	.5	1.2	.3	.9	89	Unnamed stream
8	KE003S1		45	.004	<1.0	.13	33	160	5.9	.47	1,000	.62	1.5	2.6	.7	77	Mouth of Amazon Creek
9	KE004S1		53	.006	<1.0	.15	35	230	6.4	.19	990	.67	2.1	1.4	.5	78	Mouth of Jumbo Creek
10	KE005S1	.56	58	.006	<1.0	.45	28	780	5.8	.32	920	.87	9.2	1.6	.2	99	Mouth of Bonanza Creek
11	KE006S1	.1	23	.002	<1.0	.14	22	100	4.6	.12	1,100	.83	14	1.4	1	110	National Creek just above the Kennecott
12	KE004S1D		51	.004	<1.0	.27	36	220	6.5	.16	1,000	.64	2.3	<sup>1</sup> <1.0	1	75	Site duplicate of KE004S1
23	KE010S1D	2.6	320	.016	<1.0	12	16	4,700	3.5	.12	730	1.6	41	<sup>1</sup> <1.0	na	90	Site duplicate of KE010S1

<sup>1</sup> Sample analyzed by PA.

Table 6. Concentrations of selected elements in rock samples collected in the Nabesna and Kennecott areas, Alaska

Index	Field no.	Ag ppm-PA	As ppm-PA	Au ppm-GF	Bi ppm-PA	Cd ppm-PA	Co ppm-AE	Cu ppm-PA	Fe pct-AE	Hg ppm-CV	Mn ppm-AE	Mo ppm-PA	Pb ppm-PA	Sb ppm-HY	Se ppm-HY	W ppm-IE	Zn ppm-PA	Sample description
1	NAD01R1	60	900	6.7	180	4.7	77	2,000	21	0.70	400	7.5	1,800	11	3.5	2.2	520	Fine py; Nabesna mine mill tailings
2	NAD01R2	< 1.2	860	1.5	< 15	49	110	4,500	19	< 1.5	53	< 1.5	1,800	11	3.5	2.2	520	Stuff and tail; Nabesna mine mill tailings
3	NAD01R3	15	1,800	3.6	47	50	69	2,800	23	38	1,100	4.4	550	5.9	1.9	6.7	2,700	Red to orange FeOx; Nabesna mine mill tailings
4	NAD01R4	35	470	3.0	69	2.0	130	1,100	29	1.2	150	1.8	1,500	10	4.1	1.4	190	White encrustation on py; Nabesna mine mill tailings
5	NAD02R1	27	930	3.6	82	8.9	33	1,700	13	2.7	1,100	9.7	910	9.5	1.3	3.6	810	Bright orange FeOx; Nabesna mine mill tailings
6	NAD03R1	100	950	7.4	280	1.2	36	1,400	14	1.5	240	29	4,900	< 15	3.4	4.8	300	Dark brown to tan FeOx; Nabesna mine mill tailings
7	NAD04R1	42	260	13	100	1.6	12	690	9.6	5.3	170	39	6,100	< 15	3.7	5.7	170	Mal. az. FeOx; Nabesna mine mill tailings
8	NAD04R2	39	220	11	86	1.2	12	750	10	4.8	130	40	3,800	< 15	2.0	6.6	100	Mal. az. FeOx; Nabesna mine mill tailings
9	NAD05R1	25	680	14	58	8.7	41	3,200	15	1.5	1,400	7.2	980	8.4	4.7	810	Bright orange-red FeOx; Nabesna mine mill tailings	
10	NAD06R1	16	1,500	60	49	7.9	20	330	13	1.1	400	3.0	970	13	3.3	3.9	1,100	White mix and bright orange-red FeOx; Nabesna mine mill tailings
11	NAD06R2	12	670	45	31	7.2	6	170	5.7	2.0	730	2.0	1,600	14	2.0	2.3	450	White mix crust; Nabesna mine mill tailings
12	NAD07R1	27	450	13	48	< 75	< 2	350	14	0.3	190	0.6	1,100	24	1.6	16	160	Spongy, py-gr FeOx; outcrop on Nabesna mine drill road
13	NAD07R2	4.4	< 15	20	< 15	3.2	59	6,200	26	< 0.2	5,200	4.2	< 15	3.8	1.1	15	880	Mal-gr-mag FeOx; outcrop on Nabesna mine drill road
14	NAD08R	9.2	< 15	35	< 15	2.4	39	13,000	26	< 0.2	6,100	4.8	< 15	6.8	16	930	Mal-py-mag-cp FeOx; outcrop on Nabesna mine drill road	
15	NAD08R	17	1,100	1.5	< 15	94	33	4,500	29	1.2	2,900	70	3,700	< 15	1.4	8,400	Py, mal. az. FeOx; mag; Nabesna mine ore stockpile	
16	NAD07R1	14	1,100	8.0	44	1.4	130	4,700	47	< 0.2	140	< 1.5	3.2	6.8	1.4	160	Py and possible py; outcrop above Rambler mine	
17	NAD07R2	12	6.5	3.6	19	< 75	24	2,100	43	< 0.2	100	7.6	3.2	6.8	7	53	61	White mix weathering rind on sulfide boulder; Rambler mine-waste pile
18	NAD07R3	42	32	210	22	< 75	24	2,700	21	< 0.2	37	3.2	460	14	1.8	2.2	61	FeOx; sulfur, and mix in steep zone; outcrop above Rambler mine
19	NAD01R1	< 1.2	3,200	1.0	38	< 75	20	660	45	< 0.2	230	6.9	< 15	2.1	2.1	22	21	Dark maroon-orange FeOx; alluvium
20	NAD01R2	< 1.2	50	< 15	< 15	< 75	31	240	49	< 0.2	41	< 15	< 15	2.3	2.4	< 1.0	22	Py-mag-FeOx stain; alluvium
21	NAD01R3	< 1.2	< 15	< 15	< 15	< 75	Z	150	1.1	< 1.5	38	< 1.5	< 15	7	1	< 1.0	41	White to gray vuggy silica; alluvium
1	KE01R	640	7,900	1.0	20	4.5	< 2	38,000	3.7	520	72	1.9	< 8	1.6	1.2	260	260	Mal. mal. az on Chitstone Limestone; Bonanza mine waste pile
2	KE007R	9.0	600	< 0.02	< 15	< 15	2	10,000	1.8	7.0	92	1.7	< 15	1.7	1.2	12	150	Mal. az on Chitstone Ls. lower grade diagenetic (?) FeOx mine-waste pile
3	KE007R	< 1.2	< 15	< 0.04	< 15	< 75	50	150	7.8	1.7	850	< 1.5	< 15	< 1.5	< 1.0	150	150	NiOx Basalt below Bonanza mine for background values; outcrop
4	KE009R1	< 1.2	< 15	1.42	< 15	< 75	28	69	5.6	1.1	1,200	< 1.5	< 15	< 1.5	< 1.0	46	46	NiOx Basalt outcrop with cc crusts; rainwater pool below Kennecott mill
5	KE009R2	< 0.80	1.34	0.04	< 1.0	< 0.50	51	69	9.3	1.3	1,400	0.31	< 1.0	< 1.0	< 1.0	64	64	NiOx Basalt for background values; outcrop
6	KE010R1	< 0.80	3.4	0.04	< 1.0	< 0.50	43	160	8.9	0.8	1,200	0.26	< 1.0	< 1.0	< 1.0	65	65	NiOx Basalt with maroon crust; outcrop at spring below Kennecott mill
7	KE011R1	< 0.80	Z.E	< 0.02	< 1.0	< 0.50	< 2	4.8	0.39	< 0.2	160	1.4	1.7	0.6	1.1	9.5	9.5	Tertiary (?) quartz porphyry for background values; alluvium
8	KE011R2	18	< 1.0	< 0.02	< 1.0	< 0.50	9	SE	ZI	15	700	0.37	4.5	2.4	0.5	74	74	Siltstone for background values; alluvium

Sample analyzed by AE.  
Sample analyzed by PA.  
Sample analyzed by HA.

[Shaded areas indicate samples collected from areas of historic mining or milling activities; unshaded areas indicate samples from unmined areas; ppm, parts per million; pct, percent; az-zaurite, cc-calcite, chal-chalcoite, ep-epidote, FeOx-iron oxide, gar-garnet, mal-malachite, mag-magnetite, py-pyrite, pyh-pyrrothite, qtz-quartz, Ls-limestone; see table 2 for explanation of analytical methods, codes AE, CV, GF, HY, and PA; na, sample not analyzed for this element; int, elemental interference]

**Table 7.** Concentrations of dissolved anions determined on water-leach samples from mill tailings, mine waste, and mineralized outcrop at the Nabesna and Rambler mines, Alaska

[ " D in field number suffix indicates sample site duplicates; ppm, parts per million; ppb, parts per billion; see table 2 for explanation of analytical methods codes AE and MS; na, sample not analyzed for this element; samples NA001L3 through NA006L3 are from the Nabesna mill tailings; sample NA017L3 is from the Rambler mine-waste pile; sample NA017L5 is from mineralized outcrop above the Rambler mine; sample NA001L3D is an analytical duplicate of NA001L3; sample VA002W3 is a blank sample]

Index	Field no.	pH	Conductivity µS/cm	O <sub>2</sub> ppm	Alkalinity ppm	Al ppm-AE	Ca ppm-AE	Fe ppm-AE	K ppm-AE	Mg ppm-AE	Na ppm-AE	Si ppm-AE	Ag ppb-MS
1	NA001L3	2.5	5,240	12	<1	16	570	1,500	1	10	1	<1	16
2	NA002L3	2.2	5,450	12	<1	23	630	580	1	19	<1	1	.1
3	NA003L3	2.4	5,120	12	<1	130	590	1,300	1	31	5	<1	.2
4	NA004L3	2.6	3,440	12	<1	5	670	170	1	3	<1	<1	1.3
5	NA005L3	6.4	2,410	6	220	<1	760	1	1	23	<1	6	<.1
6	NA006L3	3.4	2,600	5	<1	9	660	<1	2	66	5	<1	<.1
7	NA017L3	2.3	6,600	12	<1	4	540	2,800	1	51	<1	<1	2.8
8	NA017L5	2.2	5,570	12	<1	8	430	1,300	1	33	<1	<1	27
9	NA001L3D	2.5	5,240	12	<1	na	na	na	na	na	na	na	16
10	VA002W3	5.0	3.2	6	<1	<1	<1	1	1	<1	<1	<1	<.1

Index	Field No.	As ppb-MS	Au ppb-MS	B ppb-AE	Bi ppb-MS	Cd ppb-MS	Ce ppb-MS	Co ppb-MS	Cr ppb-MS	Cu ppb-MS	Mn ppb-MS	Mo ppb-MS	Ni ppb-MS
1	NA001L3	1,100	<.1	200	27	24	11	300	11	4,900	980	2.8	36
2	NA002L3	29	.1	<100	1.0	78	15	320	23	11,000	>4,000	<.2	55
3	NA003L3	2,200	<.1	200	2.2	16	29	440	28	12,000	1,200	35	56
4	NA004L3	38	<.1	<100	.8	11	8.5	36	4.1	1,400	450	2.8	15
5	NA005L3	2	.7	<100	<.6	6	<.1	12	<.8	18	1,800	<.2	13
6	NA006L3	26	<.1	<100	<.6	130	31	57	<.8	770	980	<.2	29
7	NA017L3	2	<.1	400	15	17	4.4	410	<.8	>20,000	830	<.2	12
8	NA017L5	20	<.1	200	21	7	2.2	470	4.4	7,800	560	<.2	12
9	NA001L3D	1,200	<.1	na	29	23	11	330	14	5,800	1,100	3.4	41
10	VA002W3	<.1	<.1	<100	<.6	<3	<.1	<.2	<.8	.8	<4	<.2	<.6

Index	Field No.	Pb ppb-MS	Sb ppb-MS	Sr ppb-MS	Te ppb-MS	Th ppb-MS	Ti ppb-MS	Tl ppb-MS	U ppb-MS	V ppb-MS	Zn ppb-MS
1	NA001L3	2,700	1	310	9.4	1.0	75	4.0	2.6	10	1,800
2	NA002L3	7.6	<.4	230	<.8	2.2	20	<.5	10	<.4	3,400
3	NA003L3	1.1	2.1	420	10	5.0	550	<.5	8.2	11	940
4	NA004L3	2,500	.6	280	.9	.4	30	1	1.4	1.2	410
5	NA005L3	.85	<.4	200	<.8	<.4	9	<.5	.6	<.4	33
6	NA006L3	54	<.4	680	<.8	<.4	20	.8	3.6	<.4	3,000
7	NA017L3	840	<.4	220	<.8	<.4	20	<.5	120	.4	340
8	NA017L5	3,500	.4	88	<.8	<.4	20	1	25	2.9	170
9	NA001L3D	2,700	.8	330	7.6	.9	85	4.4	3.6	12	2,000
10	VA002W3	<.2	<.4	<.1	<.8	<.4	<9	<.5	<.1	<.4	7.1

stream of site KE010, had a Cu concentration of 6.7 ppb. Other samples from sites near the mines and mill had Cu values ranging from 2 ppb to 9.5 ppb, while samples from sites distal to the mines and mill had Cu values from <0.6 ppb to 2 ppb. Other cations slightly enriched in waters collected from sites near the mines and mill include As (site KE010, 7.4 ppb), Mo (KE009, 1.2 ppb; KE010, 1.4 ppb), and Sr (KE010, 270 ppb). In water samples distal from the mines and mill, only two cations with weakly anomalous concentrations were found: As (three samples, 2.2 to 3.2 ppb) and B (three samples, 54 to 78 ppb). For the cations and anions determined in this study, none of the surface-water samples analyzed from the Kennecott area

had concentrations that exceed the State of Alaska's primary or secondary MCLs for public drinking water (Alaska Department of Environmental Conservation, 1994).

**SOLID SAMPLES**

Minus-200 mesh stream-sediment samples were collected from five sites below and proximal to the mines and mill and from six distal sites (table 5). Sediments near the mines and mill contained anomalous concentrations of As (63 to 170 ppm), Cu (160 to 6,100 ppm), and Hg (0.7 to 3.3 ppm), and weakly anomalous concentrations of Ag, Au, Cd, Pb, Sb, and Zn. Several sediment samples col-

Table 8. Minerals identified in mill tailings, mine-waste, and outcrop samples prior to water-leach test, Nabesna mill and Rambler mine, Alaska

[Minerals identified by X-ray diffraction; coding for likelihood: 1, definitely present; 2, probably present; 3, possibly present]

Sample site	Mineral	Chemical formula	Likelihood	Sample site	Mineral	Chemical formula	Likelihood
NA001	Pyrite	FeS <sub>2</sub>	1	NA005	Gypsum	CaSO <sub>4</sub> 2H <sub>2</sub> O	1
	Gypsum	CaSO <sub>4</sub> 2H <sub>2</sub> O	1		Calcite	CaCO <sub>3</sub>	1
	Rozenite	FeSO <sub>4</sub> 4H <sub>2</sub> O	1	NA006	Gypsum	CaSO <sub>4</sub> 2H <sub>2</sub> O	1
	Natrojarosite	NaFe <sub>3</sub> (SO <sub>4</sub> ) <sub>2</sub> (OH) <sub>6</sub>	1		Natrojarosite	NaFe <sub>3</sub> (SO <sub>4</sub> ) <sub>2</sub> (OH) <sub>6</sub>	1
	Kalinite	KAl(SO <sub>4</sub> ) <sub>2</sub> 11H <sub>2</sub> O	1		Jarosite, hydronian	(K,H <sub>3</sub> O)Fe <sub>3</sub> (SO <sub>4</sub> ) <sub>2</sub> (OH) <sub>6</sub>	3
	Copiapite	Fe <sub>14</sub> O <sub>3</sub> (SO <sub>4</sub> ) <sub>18</sub> 63H <sub>2</sub> O	1	NA017 (waste dump)	Sulfur	S	1
	Magnesiocopiapite	MgFe <sub>4</sub> (SO <sub>4</sub> ) <sub>6</sub> (OH) <sub>2</sub> 20H <sub>2</sub> O	1		Fibrofemte	Fe(OH)SO <sub>4</sub> 5H <sub>2</sub> O	1
	Butlerite	Fe(OH)SO <sub>4</sub> 2H <sub>2</sub> O	1		Goethite	FeO(OH)	1
	Rostite	Al(SO <sub>4</sub> )(OH)5H <sub>2</sub> O	1		Sepiolite, feman	(Mg,Fe) <sub>4</sub> Si <sub>8</sub> O <sub>15</sub> (OH) <sub>2</sub> 6H <sub>2</sub> O	1
	Cerussite	PbCO <sub>3</sub>	1		Copiapite	Fe <sub>14</sub> O <sub>3</sub> (SO <sub>4</sub> ) <sub>18</sub> 63H <sub>2</sub> O	1
	Magnetite	Fe <sub>3</sub> O <sub>4</sub>	1		Talc	Mg <sub>3</sub> Si <sub>4</sub> O <sub>10</sub> (OH) <sub>2</sub>	1
	Starkeyite	MgSO <sub>4</sub> 4H <sub>2</sub> O	2		Pyrite	FeS <sub>2</sub>	1
	Aplowite	CoSO <sub>4</sub> 4H <sub>2</sub> O	2		Chalcopyrite	CuFeS <sub>2</sub>	1
	Jarosite, hydronian	(K,H <sub>3</sub> O)Fe <sub>3</sub> (SO <sub>4</sub> ) <sub>2</sub> (OH) <sub>6</sub>	3		Pyrrhotite	Fe <sub>1-x</sub> S	1
Aluminocopiapite	(Mg,Al)(Fe,Al) <sub>4</sub> (SO <sub>4</sub> ) <sub>6</sub> (OH) <sub>2</sub> 20H <sub>2</sub> O	2	NA017 (outcrop)		Rozenite	FeSO <sub>4</sub> 4H <sub>2</sub> O	1
NA002	Gypsum	CaSO <sub>4</sub> 2H <sub>2</sub> O			1	Fibrofemte	Fe(OH)SO <sub>4</sub> 5H <sub>2</sub> O
NA003	Natrojarosite	NaFe <sub>3</sub> (SO <sub>4</sub> ) <sub>2</sub> (OH) <sub>6</sub>		1	Starkeyite	MgSO <sub>4</sub> 4H <sub>2</sub> O	2
	Gypsum	CaSO <sub>4</sub> 2H <sub>2</sub> O		1	Aplowite	CoSO <sub>4</sub> 4H <sub>2</sub> O	2
	Copiapite	Fe <sub>14</sub> O <sub>3</sub> (SO <sub>4</sub> ) <sub>18</sub> 63H <sub>2</sub> O		1	Sepiolite, feman	(Mg,Fe) <sub>4</sub> Si <sub>8</sub> O <sub>15</sub> (OH) <sub>2</sub> 6H <sub>2</sub> O	2
	Jarosite, hydronian	(K,H <sub>3</sub> O)Fe <sub>3</sub> (SO <sub>4</sub> ) <sub>2</sub> (OH) <sub>6</sub>	3	Cacoxenite	Fe <sub>4</sub> (PO <sub>4</sub> ) <sub>3</sub> (OH) <sub>3</sub> 12H <sub>2</sub> O	2	
Jarosite	KFe <sub>3</sub> (SO <sub>4</sub> ) <sub>2</sub> (OH) <sub>6</sub>	3	Carbonate hydroxylapatite	Ca <sub>10</sub> (PO <sub>4</sub> ) <sub>3</sub> CO <sub>3</sub> (OH)F	2		
NA004	Gypsum	CaSO <sub>4</sub> 2H <sub>2</sub> O	1				
	Magnetite	Fe <sub>3</sub> O <sub>4</sub>	1				

lected distal to the mines and mill contained anomalous As (23 to 58 ppm) and Cu (160 to 780 ppm), and weakly anomalous Ag, Hg, and Sb.

Nonmagnetic, heavy-mineral concentrates were collected from three sites below and close to the mines and mill (sites KE008, KE010, and KE012) and from four distal sites (sites KE003, KE004, KE005, and KE006). Highly anomalous metals found in samples from sites near the mines and mill include Ag (70 to 300 ppm), As (2,000 to 10,000 ppm), Cd (50 to 300 ppm), Cu (all >50,000 ppm), and Pb (300 to 1,500 ppm), whereas concentrates collected distal to the mines and mill contained anomalous Ag (70 ppm), As (500 ppm), Bi (70 ppm), Cu (1,500 to 50,000 ppm), Pb (500 to 10,000 ppm), and Sn (150 ppm) (Eppinger and others, 1995).

Two mineralized rock samples from the Bonanza and Erie mines contained anomalous concentrations of Ag, As, Au, Cd, Cu, Hg, and Zn, and weakly anomalous concentrations of Mo and Sb (table 6). **Unmineralized** rock samples

from six sites in the Kennecott area contained sporadic, weakly anomalous concentrations of Cu, Sb, and Zn.

## INTERPRETATIONS

### GENERAL

Overall, measured conductivities at water-sample sites were higher in the Nabesna area than in the Kennecott area (table 1). The higher conductivities are probably due to higher concentrations of dissolved Ca and, to a lesser degree, Sr and Mg. The high concentrations of these elements are likely derived from carbonate bedrock and alluvium, common throughout much of the Nabesna area. In contrast, water samples in the Kennecott area were collected generally at sites underlain by Nikolai Greenstone, below the overlying carbonate section, and consequently have lower dissolved Ca, Sr, and Mg contents.

Higher sulfate content in Nabesna waters (mean  $\text{SO}_4^{2-}$  content, 190 ppm) compared with Kennecott waters (mean  $\text{SO}_4^{2-}$  content, 8.9 ppm) is probably due to the widespread presence of pyrite and pyrrhotite and their alteration products in the Nabesna area. Color areal photographs of White Mountain near Nabesna reveal extensive unvegetated areas of outcrop stained orange, red, and tan, suggestive of altered iron sulfides beyond the limits of the mined areas. Wayland (1943) also noted the presence of pyrite, pyrrhotite, and magnetite near igneous intrusions in numerous places on White Mountain. In contrast, iron sulfide minerals are rare at Kennecott (MacKevett and others, 1997). Chalcocite and djurleite, the dominant copper sulfide minerals present at Kennecott (MacKevett and others, 1997), are relatively stable minerals at the deposits, are slower to oxidize, and subsequently do not generate high sulfate content in surficial waters.

Molybdenum content in water samples is enriched in Nabesna area samples (mean Mo content, 4.4 ppb) compared with Kennecott area waters (mean Mo content, 0.53 ppb; table 4). This finding agrees with overall Mo content in rocks and sediments from the two areas. Most Nabesna area waters have Mo contents an order of magnitude greater than worldwide averages for surface waters (table 4). Anomalous concentrations of Mo in several altered and mineralized rocks from Nabesna indicates that the Mo is likely derived from the mineralizing hydrothermal system rather than from high background Mo content in surrounding bedrock. If the Mo in water is similarly derived from mineralized or altered areas, then the elevated Mo content in waters distal to the mines and mill suggests that additional altered and mineralized areas are present. The widespread anomalous Mo content in the various sample media from the Nabesna area may be a surficial halo reflecting an underlying deposit similar to the Orange Hill and Bond porphyry Cu-Mo deposits about 20 km southeast of Nabesna (Nokleberg and others, 1995).

## NABESNA

Iron-bearing sulfides and sulfate salts formed by alteration of iron sulfides are extremely efficient in generating acid when combined with oxygenated water (Plumlee and Nash, 1995). The presence of abundant pyrite and pyrrhotite, and the diverse soluble sulfate salt assemblage in tailings (table 8) at the Nabesna mill and associated deposits, suggest high potential for acid generation and subsequent lowering of pH in waters draining the area. This potential acid generation is supported by the results of the mill-tailings and mine-waste water-leach test (discussed below), where highly acidic pH values were generated. However, all natural waters sampled in the area, including water collected below mine-waste piles and mill tailings, had near-

neutral pH values. The near-neutral pH values are no doubt due to the powerful acid-buffering capacity of the natural waters, a result of their passage through the abundant carbonate rocks in the area.

Near-neutral pH values in surface waters dramatically reduce the metal-carrying capacity of the waters, and as a result, waters both distal and proximal to the mines and mill do not contain high metal concentrations. For example, on a plot of pH versus the sum of  $\text{Zn}+\text{Cu}+\text{Cd}+\text{Ni}+\text{Co}+\text{Pb}$ , Nabesna surface waters collected near the mines and mill plot in the near-neutral, low-metal field when compared with waters generated around other mineral deposits (fig. 4). The water sample collected below the Nabesna mill (site NA011) plots highest in the field due to elevated concentrations of Zn, a metal that remains mobile in near-neutral pH waters.

Sorption is another important process in controlling element mobility (Smith and others, 1994). Hydrous iron oxides, present at several water-sample sites (table 1), were most abundant at site NA011. Their presence suggests that sorption is helping to suppress metal concentrations in water derived from the mill waste.

The synthetic precipitation leaching procedure used on samples from the Nabesna area is designed to determine mobility of organic and inorganic analytes in liquids, soils, and wastes. The pH of the leach water used is adjusted to mimic that of rainwater. The leach water pH used in this study, pH 5.0, is the recommended pH for samples collected west of the Mississippi River (Environmental Protection Agency, 1994), where acid rain is believed to pose minimal problems. This pH value is within the limits of several pH values for snow and rain from the west, which range from pH 4.9 to 6.4 (Hem, 1985). Data from the water-leach test suggest that during spring runoff or summer storm events, water that has precipitated on the Nabesna mill-tailings pile could become more acidic and then could carry more metals in solution. This feature is illustrated well in the Ficklin plot (fig. 4), where all but one of the tailings leach samples plot in the high-acid, high-metal and acid, high-metal fields (the single water-leach sample from site NA005, plotting in the near-neutral, low-metal field has a higher pH because of the presence of calcite in the tailings at that site; table 8). Natural mitigation processes likely would reduce the severity of the runoff or storm event in the following ways. Most importantly, rapid downstream dilution of the acidic waters by surrounding water released during the event would occur, a process that would raise pH and decrease the metal concentrations in the water through precipitation, sorption, or dilution mechanisms. Buffering capacity of the surrounding water would be increased as it flowed over and through the extensive carbonate rocks in the area. Finally, and perhaps of lesser importance, storm events are relatively short lived and do not provide a long residence time for water-tailings interaction.



Except for Hg, the anomalous metal suite that characterizes Nabesna mill-tailings rock samples, **Ag-As-Au-Bi-Cd-Cu-Fe-Hg-Mo-Pb-Zn-[Co-Sb-Se-W]**, also characterizes stockpiled ore, mine waste, mineralized outcrop, and mineralized alluvial cobbles. (Braces indicate weakly anomalous constituents.) Although more subdued, this same metal suite is found in minus-200 mesh stream-sediment samples from sites draining mined and unmined areas. In addition, most of these elements are found in anomalous concentrations in heavy-mineral concentrates from mill tailings and from unmined areas. There are three implications that can be drawn from these similarities.

First, the fact that anomalous concentrations of these metals are not confined to the mill and mine areas but are also found in unmined areas suggests that additional skarn deposits may exist in the area. As described above, the high-sulfate and high-Mo contents in waters collected throughout the area may also indicate additional mineralized areas. Anomalous Au in several sediment samples from unmined drainages implies that the additional skarn bodies may be gold bearing. Any additional deposits would probably be concealed, considering the large amount of pros-

pecting undertaken during the period of active exploration and mining in the Nabesna area.

Second, there are naturally occurring high-metal contents in some sediments from sites devoid of historic mining and milling activity. These natural high-metal concentrations in sediment may be useful in establishing locally derived, pre-mining background levels for certain metals. For example, natural sediment from site **NA013** contains 510 ppm As, 190 ppm Co, 720 ppm Cu, and 380 ppm Zn, indicating that, at least locally, natural As, Co, Cu, and Zn concentrations in sediment from the area can exceed average crustal abundance values by one to two orders of magnitude (table 5). However, other sediment samples from unmined areas at Nabesna contain much lower As, Co, Cu, and Zn content, illustrating a large variability in metal content in the sediments. This large natural variability needs to be taken into consideration when establishing pre-mining background levels in the area.

Third, the fact that anomalous Hg was found only in samples of the Nabesna mill tailings and in a single sediment sample directly below the Nabesna mill tailings, but not in mine waste, ore rocks, or other sediments, suggests

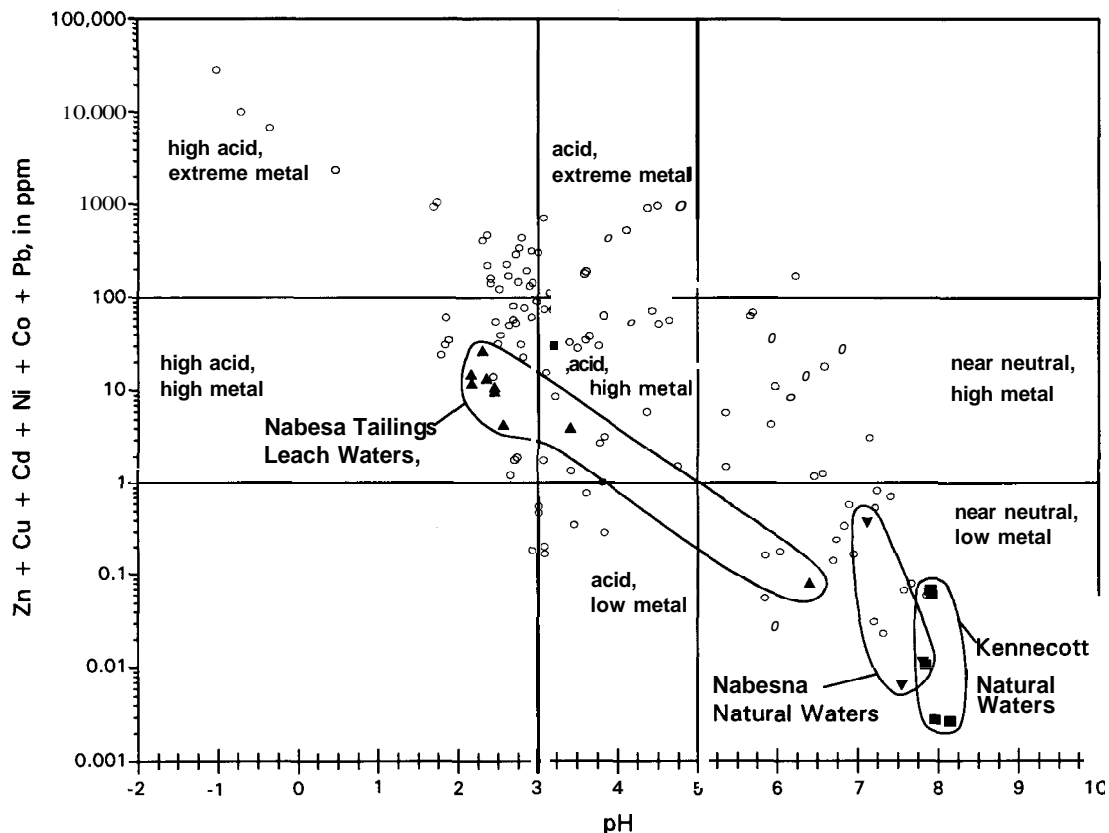


Figure 4. Ficklin diagram of pH versus dissolved metal content in water samples collected near mines and mills at Nabesna and Kennecott, Alaska. Open circles are values for mine-drainage waters from diverse mineral deposits for purposes of comparison (data from Plumlee and others, 1994).

that the Hg may have an anthropogenic origin. This conclusion is supported by **Wayland** (1943, p. 193), who mentions an unsuccessful attempt in the 1930's to use mercury amalgamation to recover gold. The anomalous Hg concentrations from mill-tailings samples are not extremely high (highest value 1.5 ppm Hg). Nevertheless, the fact that Hg was found at sites throughout the length of the mill-tailings pile (sites **NA001** through **NA006**, fig. 2B and table 6), and in sediment below the mill tailings (site **NA011**) suggests that Hg is present throughout the pile. The high density of native mercury and its natural liquid state together imply that higher Hg concentrations might be encountered at depth in the thickest parts of mill-tailings piles, a hypothesis that should be tested prior to disturbing the tailings in any future remediation efforts. Since water samples for Hg analysis were not collected in the present study, Hg concentrations in water below the mill are unknown. However, high-Hg concentrations in the water at site **NA011** would not be expected because of the high stability of native mercury in the surficial environment, which minimizes its dissolution in water (Eisler, 1987) and because of the high volatility of native mercury, a feature that tends to promote evaporation of native mercury when exposed to the atmosphere. Waters at the Nabesna mill should be analyzed for Hg content, and if present, the Hg species should be determined. Note: Mercury was not detected (Hg <0.10 ppb) in additional water samples collected in August 1996 at site **NA011** nor at additional sites downstream of this site (R.G. Eppinger, unpub. data).

## KENNECOTT

Surface-water samples collected in the Kennecott area have low metal concentrations that are generally comparable to worldwide average surface-water concentrations (table 4). Even water samples collected near the mines and mill do not contain high-metal content (fig. 4). This result is due primarily to two geologic controls: (1) the host carbonate rock greatly increases the buffering capacity of surface waters, resulting in near-neutral pH values; and (2) there is a general lack, in Kennecott-type deposits, of unstable sulfide minerals, such as pyrite, that commonly form acid waters during weathering. Further, minerals containing elements such as Zn or U, which could be mobilized in neutral or higher pH waters, are uncommon in Kennecott-type deposits. Even though rock and sediment data indicate that high concentrations of potentially toxic elements such as As, Cd, Cu, Hg, and Zn are found in mill and mine-waste piles, mobilization of these metals in water is unlikely because of the lack of acid-generating minerals in Kennecott-type deposits and the waste piles and mill tailings derived from them. If certain metals were mobilized from the waste or tailings piles, rapid dilution from adja-

cent streams and from the adjacent Kennicott River would minimize their downstream effects.

The overall metal suite that characterizes sediment samples below and close to the Kennecott mines and mill is As-Cu-Hg-[Ag-Au-Cd-Pb-Sb-Zn]. Corresponding heavy-mineral concentrates contain highly anomalous concentrations of several of the same metals: Ag-As-Cd-Cu-Pb. The anomalous metal suite in mineralized rocks from the **Bonanza** and **Erie** mine-waste piles is similar to that for the sediments: Ag-As-Cu-Hg-[Au-Cd-Mo-Sb-Zn]. Finally, **MacKevett** and others (1997) state that ore from the Kennecott deposits has anomalous Ag, As, and Cu, and sporadically anomalous Pb, Sb, and Zn. All metals found in anomalous concentrations in sediment and in heavy-mineral-concentrate samples were also found in mineralized rock samples from this study or are reported in rocks by **MacKevett** and others (1997). Thus, unlike the mercury at the Nabesna mill, none of the metals found in sediment samples from the Kennecott mines and mill appear to have an anthropogenic origin. The present high-metal concentrations in sediment from the mining and milling areas probably are a reflection of both high local background concentrations and ground disturbances created during the mining and milling.

In general, for sediments and heavy-mineral concentrates collected distal to the mines and mill, the anomalous metal suites are similar to those in mined areas: distal sediments, As-Cu-[Ag-Hg-Sb]; distal concentrates, Ag-As-Cu-Pb-[Bi-Sn]. For the distal sediments and concentrates, the magnitude of the anomalous metal concentrations is less and, for sediments, the metal suite is less extensive than for these same media collected proximal to the mines and mill. These data reveal that most of the drainage basins on the west side of **Bonanza Peak** and **Bonanza Ridge** (fig. 3) have metalliferous sediments. However, while naturally occurring high-metal concentrations were probable in many of these basins prior to mining in the area, one cannot readily ascribe the present metal concentrations in the sediments to natural processes alone because mining and prospecting probably has occurred in the upper parts of these basins as well. Thus, background metal concentrations in sediments in the Kennecott area probably should not be established using the present data alone. Samples need to be collected from similar unmined deposits nearby. Still, these data are useful in establishing the expected metal suite in sediments related to Kennecott-type deposits. Sediments derived from areas containing similar, but unmined, deposits will probably have elevated concentrations for most of these same metals.

**Acknowledgments.**—We would like to thank **Danny Rosenkrans** of **Wrangell–St. Elias National Park and Preserve** for logistical help and manuscript review, and **James Harrower** of the **Great Kennicott Land Co.** and **Kirk Stanley**, owner of the **Nabesna** and **Rambler** mines, for allowing access to their properties. We also thank the following U.S.

Geological Survey laboratory personnel for sample preparation and chemical analyses: Paul Briggs, Bill d'Angelo, Mike Doughten, David Fey, Phil Hageman, Tommy Hopkins, Roy Knight, Al Meier, Craig Motooka, Jerry Motooka, Rich O'Leary, Bruce Roushey, and Pete Theodorakos.

## REFERENCES CITED

- Adrian, B.M., Arbogast, B.F., Detra, D.E., and Mays, R.E., 1990, Direct-current arc emission spectrographic method for the semiquantitative analysis of rock, stream-sediment, soil, and heavy-mineral-concentrate samples, *in* Arbogast, B.F., ed., Quality assurance manual for the Branch of Geochemistry, U.S. Geological Survey: U.S. Geological Survey Open-File Report 90-668, p. 100-106.
- Alaska Department of Environmental Conservation, 1994, Drinking water regulations: State of Alaska, Department of Environmental Conservation report 18-AAC-80, 195 p.
- Bateman, A.M., and McLaughlin, D.H., 1920, Geology of the ore deposits of Kennecott, Alaska: *Economic Geology*, v. 15, p. 1-80.
- Briggs, P.H., 1990, Elemental analysis of geologic materials by inductively coupled plasma-atomic emission spectrometry, *in* Arbogast, B.F., ed., Quality assurance manual for the Branch of Geochemistry, U.S. Geological Survey: U.S. Geological Survey Open-File Report 90-668, p. 83-89.
- Briggs, P.H., and Fey, D.L., 1996, Twenty-four elements in natural and acid mine waters by inductively coupled plasma-atomic emission spectrometry, *in* Arbogast, B.F., ed., Analytical methods manual for the Mineral Resource Surveys Program, U.S. Geological Survey: U.S. Geological Survey Open-File Report 96-525, p. 95-101.
- d'Angelo, W.M., and Ficklin, W.H., 1996, Fluoride, chloride, nitrate, and sulfate in aqueous solution by chemically suppressed ion chromatography, *in* Arbogast, B.F., ed., Analytical methods manual for the Mineral Resource Surveys Program, U.S. Geological Survey: U.S. Geological Survey Open-File Report 96-525, p. 149-153.
- Doughten, M.W., and Aruscavage, P.J., 1996, Niobium, tungsten, and molybdenum by ion exchange/inductively coupled plasma-atomic emission spectrometry, *in* Arbogast, B.F., ed., Analytical methods manual for the Mineral Resource Surveys Program, U.S. Geological Survey: U.S. Geological Survey Open-File Report 96-525, p. 126-129.
- Douglass, W.C., 1964, A history of the Kennecott mines, Kennecott, Alaska: privately published, Seattle, Wash., 12 p.
- Eisler, Ronald, 1987, Mercury hazards to fish, wildlife, and invertebrates: a synoptic review: U.S. Fish and Wildlife Service Biological Report 85(1.10), 90 p.
- Environmental Protection Agency, 1994, Test methods for evaluating solid waste, physical/chemical methods (SW-846) (3d ed., update 2B): Environmental Protection Agency, National Center for Environmental Publications and Information, Cincinnati, Ohio 45268.
- Eppinger, R.G., McHugh, J.B., Briggs, P.H., d'Angelo, W.M., Doughten, M.W., Fey, D.L., Hageman, P.L., Hopkins, R.T., Knight, R.J., Meier, A.L., Motooka, J.M., O'Leary, R.M., and Roushey, B.H., 1995, Geochemical data for environmental studies at Nabesna and Kennecott, Alaska: water, leachates, stream-sediments, heavy-mineral-concentrates, and rocks: U.S. Geological Survey Open-File Report 95-645A, 91 p. and 95-645B (diskette version).
- Fortescue, J.A.C., 1992, Landscape geochemistry: retrospect and prospect—1990: *Applied Geochemistry*, v. 7, p. 1-53.
- Hem, J.D., 1985, Study and interpretation of the chemical characteristics of natural water (3d ed.): U.S. Geological Survey Water-Supply Paper 2254, 263 p.
- Hunt, W.R., 1996, Mountain wilderness, an illustrated history of Wrangell—St. Elias National Park and Preserve, Alaska: Anchorage, Alaska, Alaska Natural History Association, 224 p.
- Jones, D.L., Silberling, N.J., and Hillhouse, J.W., 1977, Wrangellia—a displaced terrane in northwestern North America: *Canadian Journal of Earth Sciences*, v. 14, p. 2565-2577.
- Livingstone, D.A., 1963, Chemical composition of rivers and lakes, data of geochemistry (6th ed.): U.S. Geological Survey Professional Paper 440-G, p. G1-G64.
- Lowe, P.C., Richter, D.H., Smith, R.L., and Schmoll, H.R., 1982, Geologic map of the Nabesna B-5 quadrangle, Alaska: U.S. Geological Survey Geologic Quadrangle Map GQ-1566, scale 1:63,360.
- MacKevett, E.M., Jr., 1970, Geologic map of the McCarthy C-5 quadrangle, Alaska: U.S. Geological Survey Geologic Quadrangle Map GQ-899, scale 1:63,360.
- 1972, Geologic map of the McCarthy C-6 quadrangle, Alaska: U.S. Geological Survey Geologic Quadrangle Map GQ-979, scale 1:63,360.
- 1974, Geologic map of the McCarthy B-5 quadrangle, Alaska: U.S. Geological Survey Geologic Quadrangle Map GQ-1146, scale 1:63,360.
- 1978, Geologic map of the McCarthy quadrangle, Alaska: U.S. Geological Survey Miscellaneous Investigations Map I-1032, scale 1:250,000.
- MacKevett, E.M., Jr., Cox, D.P., Potter, R.W., and Silberman, M.L., 1997, Kennecott-type deposits in the Wrangell Mountains, Alaska: High-grade copper ores near a basalt-limestone contact, *in* Goldfarb, R.J. and Miller, L.D., eds., Mineral deposits of Alaska: *Economic Geology Monograph* 9.
- MacKevett, E.M., Jr., and Smith, J.G., 1972, Geologic map of the McCarthy B-6 quadrangle, Alaska: U.S. Geological Survey Geologic Quadrangle Map GQ-1035, scale 1:63,360.
- Martin, J.M., and Whitfield, Michael, 1983, The significance of the river input of chemical elements to the ocean, *in* Wong, C.S., Boyle, E., Bruland, K.W., Burton, J.D., and Goldberg, E.D., eds., Trace metals in sea water: New York, Plenum Press, p. 265-296.
- Meier, A.L., Grimes, D.J., and Ficklin, W.H., 1994, Inductively coupled plasma mass spectrometry; a powerful analytical tool for mineral resource and environmental studies: U.S. Geological Survey Circular 1103-A, p. 67-68.
- Moffit, F.H., 1943, Geology of the Nutzotin Mountains, Alaska: U.S. Geological Survey Bulletin 933-B, p. 103-174.
- 1944, Mining in the northern Copper River region, Alaska, *in* Smith, P.S., Mineral industry of Alaska in 1941 and 1942: U.S. Geological Survey Bulletin 943-B, p. 25-47.
- Motooka, J.M., 1996, Organometallic halide extraction for 10 elements by inductively coupled plasma-atomic emission

- spectrometry, *in* Arbogast, B.F., ed., Analytical methods manual for the Mineral Resource Surveys Program, U.S. Geological Survey: U.S. Geological Survey Open-File Report 96-525, p. 102-108.
- Newberry, R.J., 1986, Compilation of data on Alaskan skarns: Alaska Division of Geological and Geophysical Surveys PDF 86-17, 835 p.
- Nokleberg, W.J., Bundtzen, T.K., Brew, D.A., and Plafker, George, 1995, Metallogeneses and tectonics of porphyry copper and molybdenum (gold, silver) and granitoid-hosted gold deposits of Alaska, *in* Schroeter, Tom, ed., Porphyry deposits of the Northwestern Cordillera: Canadian Institute of Mining, Metallurgy, and Petroleum Special Volume 46, p. 103-141.
- O'Leary, R.M., 1996, Tellurium and thallium by flame atomic absorption spectrometry, *in* Arbogast, B.F., ed., Analytical methods manual for the Mineral Resource Surveys Program, U.S. Geological Survey: U.S. Geological Survey Open-File Report 96-525, p. 37-41.
- O'Leary, R.M., Crock, J.G., and Kennedy, K.R., 1990, Determination of mercury in geologic materials by continuous flow-cold vapor-atomic absorption spectrophotometry, *in* Arbogast, B.F., ed., Quality assurance manual for the Branch of Geochemistry, U.S. Geological Survey: U.S. Geological Survey Open-File Report 90-668, p. 60-67.
- O'Leary, R.M., and Meier, A.L., 1990, Determination of gold in samples of rock, soil, stream-sediment, and heavy-mineral concentrate by flame and graphite furnace atomic absorption spectrophotometry following dissolution by  $\text{HBr-Br}_2$ , *in* Arbogast, B.F., ed., Quality assurance manual for the Branch of Geochemistry, U.S. Geological Survey: U.S. Geological Survey Open-File Report 90-668, p. 46-51.
- Plafker, George, and Berg, H.C., 1994, Overview of the geology and tectonic evolution of Alaska, *in* Plafker, George, and Berg, H.C., eds., The geology of Alaska: Boulder, Colo., Geological Society of America, The Geology of North America, v. G1, p. 989-1021.
- Plumlee, G.S., and Nash, J.T., 1995, Geoenvironmental models of mineral deposits—fundamentals and applications, *in* duBray, E.A., ed., Preliminary compilation of descriptive geoenvironmental mineral deposit models: U.S. Geological Survey Open-File Report 95-831, p. 1-9.
- Plumlee, G.S., Smith, K.S., and Ficklin, W.H., 1994, Geoenvironmental models of mineral deposits, and geology-based mineral-environmental assessments of public lands: U.S. Geological Survey Open-File Report 94-203, 7 p.
- Richter, D.H., 1971, Reconnaissance geologic map and section of the Nabesna B-4 quadrangle, Alaska: U.S. Geological Survey Miscellaneous Geologic Investigations Map I-656, scale 1:63,360.
- Rose, A.W., Hawkes, H.E., and Webb, J.S., 1979, Geochemistry in mineral exploration (2d ed.): Nepean, Ontario, Association of Exploration Geochemists, 657 p.
- Smith, K.S., Plumlee, G.S., and Ficklin, W.H., 1994, Predicting water contamination from metal mines and mining wastes, notes from a workshop presented at the International Land Reclamation and Mine Drainage Conference and the Third International Conference on the Abatement of Acidic Drainage, Pittsburgh, Pennsylvania, April 24, 1994: U.S. Geological Survey Open-File Report 94-264, 112 p.
- Theodore, T.G., Oms, G.J., Hammarstrom, J.M., and Bliss, J.D., 1991, Gold-bearing skarns: U.S. Geological Survey Bulletin 1930, 61 p.
- Wayland, R.G., 1943, Gold deposits near Nabesna: U.S. Geological Survey Bulletin 933-B, p. 175-199.
- Welsch, E.P., Crock, J.G., and Sanzolone, R.F., 1990, Trace-level determination of arsenic and selenium using continuous-flow hydride generation atomic absorption spectrophotometry (HG-AAS), *in* Arbogast, B.F., ed., Quality assurance manual for the Branch of Geochemistry, U.S. Geological Survey: U.S. Geological Survey Open-File Report 90-668, p. 38-45.

Reviewers: Danny Rosenkrans, Steven M. Smith, and Richard B. Wanty

# Mercury in the Terrestrial Environment, Kuskokwim Mountains Region, Southwestern Alaska

By Elizabeth A. Bailey and John E. Gray

## ABSTRACT

To evaluate environmental hazards of abandoned mercury mines in southwestern Alaska, mercury concentrations were measured in vegetation, soil, and stream-water samples collected from sites around the Cinnabar Creek and Red Devil mines, as well as from regional background sites. Mercury concentrations in all samples collected near the mines are elevated over those in background samples. Vegetation samples collected from the mines contain as much as 970 ppb Hg, whereas background vegetation samples contain no more than 190 ppb Hg. Soil samples collected from the mines contain as much as 1,500 ppm Hg, but background soil samples contain no more than 1.2 ppm Hg. In addition, concentrations of highly toxic methylmercury are low in samples of vegetation (no more than 37 ppb) and soil (no more than 133 ppb). Stream-water samples collected downstream from the mines contain no more than 0.28 ppb Hg and have nearly neutral pH values that range from 6.4 to 7.6. All stream-water mercury concentrations are well below the 2.0 ppb Hg drinking water standard recommended by the State of Alaska. Mercury concentrations in vegetation, soil, and stream-water samples collected from the Cinnabar Creek and Red Devil mines in this study are probably not hazardous to humans and wildlife in the region.

## INTRODUCTION

Mercury mines and deposits are found throughout southwestern Alaska (fig. 1); they represent significant sources of mercury that could potentially damage surrounding environments and may pose a potential health risk to residents and wildlife. As part of continuing mineral resource investigation in southwestern Alaska, the U.S. Geological Survey has been involved in assessing environmental mercury hazards in this region. Previous environmental studies have evaluated mercury contamination in fish collected downstream from mercury mines in the region to address effects to the aquatic food chain (Gray and others,

1994, 1996). Because mercury in aquatic systems can originate from terrestrial sources, such as mercury in mines, it is important to measure mercury concentrations in soil, water, and vegetation samples collected near such mines in order to better understand the behavior of mercury in both terrestrial and aquatic ecosystems. Certain vegetation species are important food sources for residents and wildlife in the region. Blueberries are consumed by humans and bears, alder twigs are eaten by ptarmigan, and willow leaves are an important food for moose. In this study, mercury concentrations were evaluated in vegetation, soil, and stream-water samples collected from the Cinnabar Creek and Red Devil mines. Variations in Hg concentration in different tissues of the same plant as well as between vegetation species were also investigated.

Mercury is a heavy metal with no known biological function in any organism. It comes in several forms, all of which are toxic to some degree (Agency for Toxic Substances and Disease Registry, 1994). When certain forms of Hg are ingested or inhaled by humans, the mercury adversely affects the central nervous system, the liver, and the kidneys; it can also cross the placental membrane in pregnant women, causing damage to the fetus (Clarkson, 1994). Mercury in the environment can be converted from inorganic forms such as HgS (cinnabar), Hg<sup>0</sup> (liquid mercury), or Hg<sup>2+</sup> (mercuric ion) to organic forms such as methylmercury (meHg) by aerobic and anaerobic bacteria. Organic mercury compounds, especially methylmercury, are the most toxic forms of mercury (Eisler, 1987). Methylmercury accumulates to a greater extent in biological tissues than do inorganic forms of mercury because of its affinity for the sulfhydryl (—SH) groups of some proteins (Agency for Toxic Substances and Disease Registry, 1994). Mercury concentrations increase in organisms that are higher in the food chain, a process called biomagnification. Concentrations of the organic forms of mercury in the terrestrial environment are generally at least one order of magnitude less than concentrations of inorganic forms of mercury, but in biological tissues methylmercury can constitute 70-100 percent of the total mercury concentration (Bloom, 1989; Baeyens, 1992; Gray and others, 1994).

## GEOLOGY

The Cinnabar Creek mine is located about 100 km southeast of Aniak in the southern Kuskokwim Mountains (fig. 1). Bedrocks in the area consist of interbedded graywacke, massive siltstone, volcanic rocks, and minor chert and limestone of the Triassic and Lower Cretaceous Gemuk Group (Cady and others, 1955; Sainsbury and MacKevett, 1965). Rocks of the Gemuk Group are locally cut by Late Cretaceous and early Tertiary mafic dikes (fig. 2) near the Cinnabar Creek mine.

Cinnabar was first discovered at Cinnabar Creek in 1941, and the mine operated intermittently from then until

1960 (Sainsbury and MacKevett, 1965). Mercury ore consists of massive replacements, disseminations, and vug fillings of cinnabar in quartz-carbonate veins (Sainsbury and MacKevett, 1965). Ore averaging about 3 to 4 percent mercury was retorted on site, and about 525 flasks (1 flask = 76 lb or 34.5 kg) of mercury were recovered (Nokleberg and others, 1987). The mine is located near the headwaters of Cinnabar Creek and consists of a small open-pit about 50 m long, 15 m wide, and 10 m deep. Veins containing cinnabar and native mercury in the open pit and small ore piles at the mine site are sources of mercury that have eroded into Cinnabar Creek. Abundant cinnabar and a few beads of native mercury have been observed in stream-

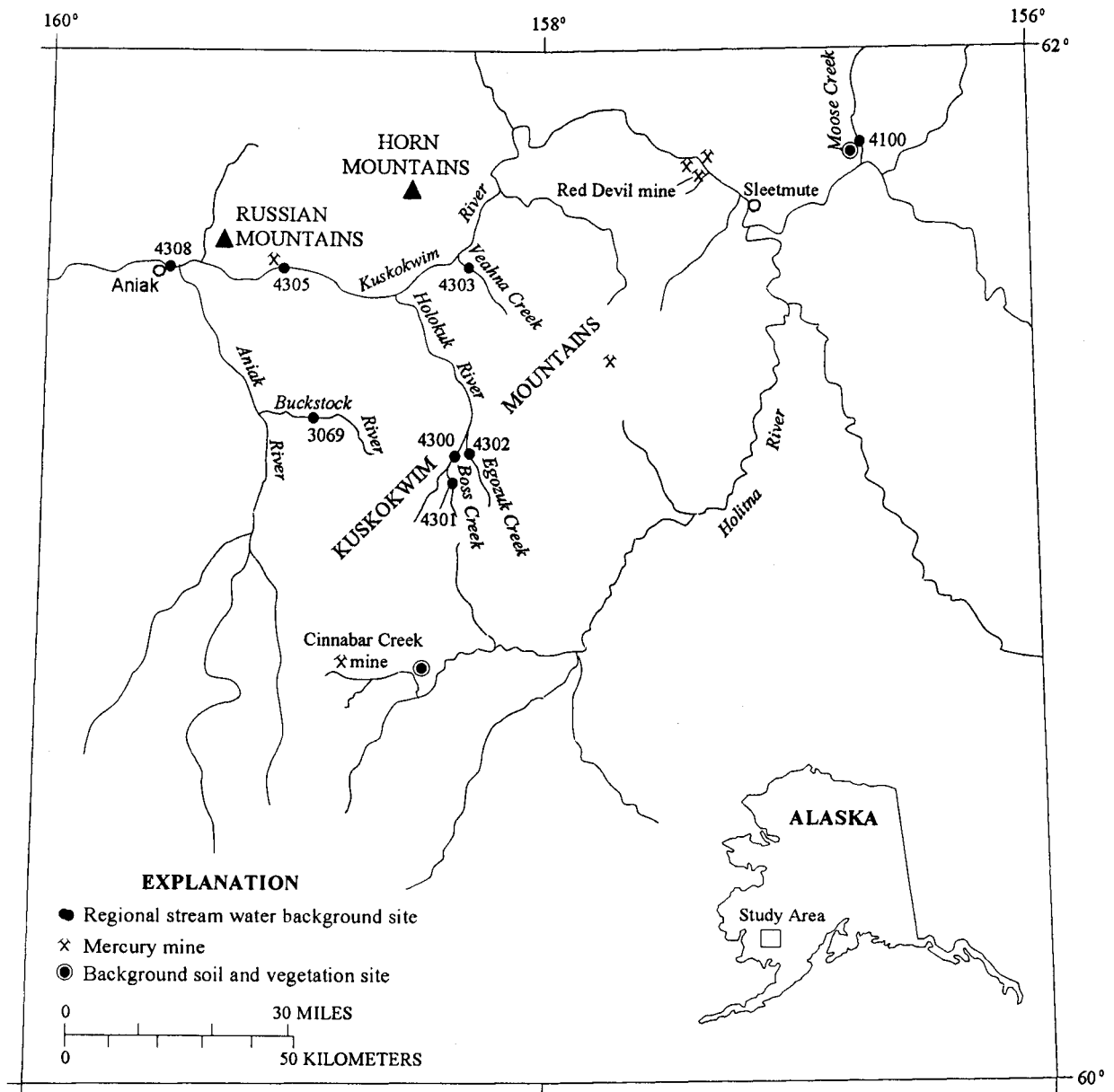


Figure 1. Map of study area, showing locations of the Cinnabar Creek and Red Devil mines and of background sample sites. Several smaller mercury mines are also shown. Background samples were collected distant or upstream from known mines.

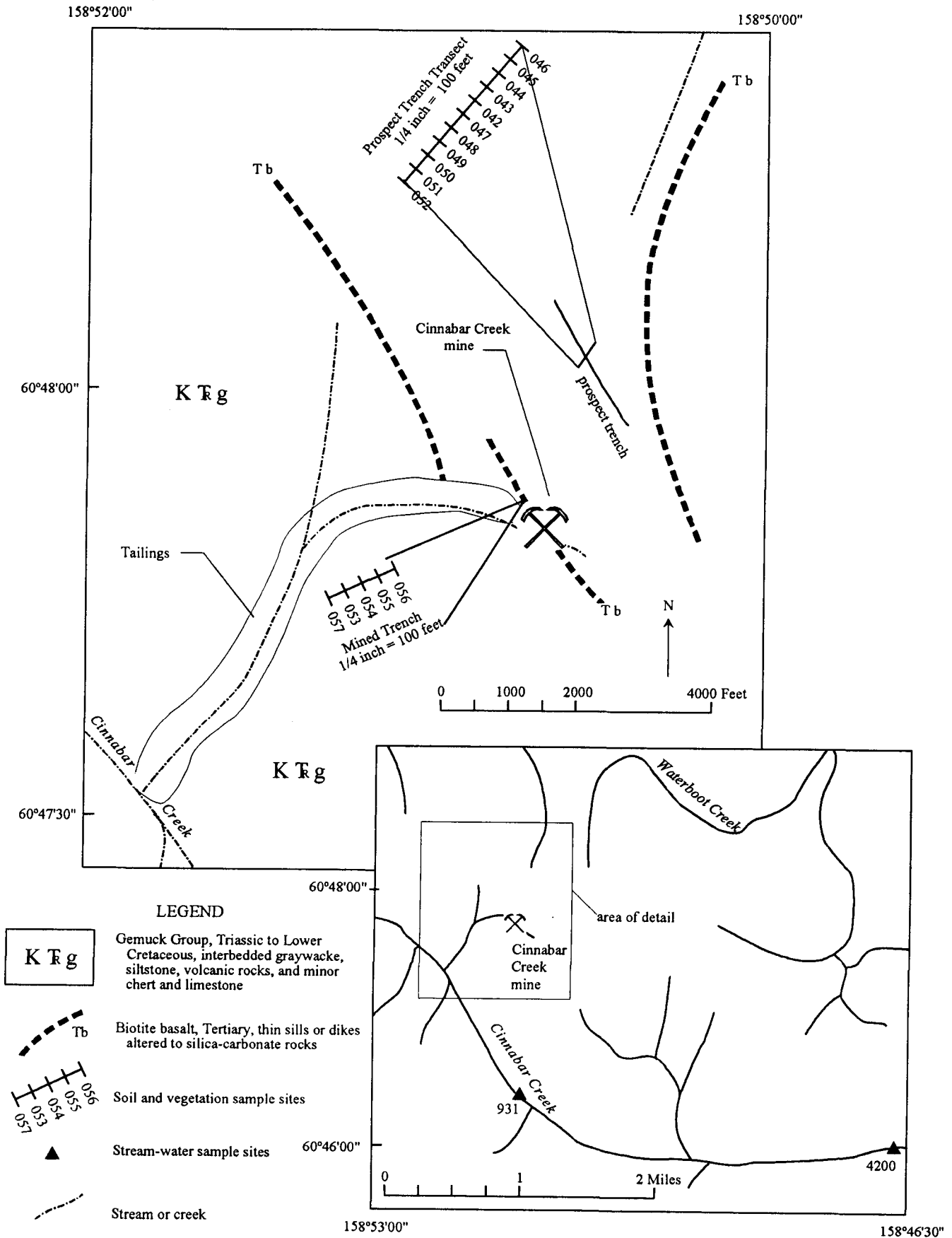


Figure 2. Sample locations and simplified geology, Cinnabar Creek mine. Geology generalized from Cady and others (1955).

sediment samples collected from Cinnabar Creek (Gray and others, 1991).

The Red Devil mine is located about 10 km northwest of the village of Sleetmute along the Kuskokwim River (fig. 1). Red Devil was Alaska's largest mercury mine; it operated intermittently from 1933 to 1971 and produced about 36,000 flasks of mercury (Miller and others, 1989). The deposit is found in rocks of the Cretaceous Kuskokwim Group (Cady and others, 1955), a thick sequence of interbedded graywacke and shale (fig. 3). These sedimentary rocks are cut locally by Late Cretaceous and early Tertiary dikes. Ore at Red Devil is in discontinuous open-space veins, vein breccias, and massive replacements localized along and near intersections between northeast-trending altered dikes and northwest-trending bedding plane faults (MacKevett and Berg, 1963). Principal metallic minerals are cinnabar and stibnite, with minor amounts of realgar, orpiment, and pyrite. Quartz, carbonate, dickite, and sericite are common gangue minerals (MacKevett and Berg, 1963).

The Red Devil mineralized zone covered an area about 150 m wide and 270 m long, which extended about 190 m vertically (MacKevett and Berg, 1963). Mineralized veins are mostly small, discontinuous, and less than 1 cm wide, but veins as much as 1 m wide and 10 m long were also observed (MacKevett and Berg, 1963). High-grade ore contained as much as 30 percent Hg, but most ore averaged about 2 to 5 percent Hg (Webber and others, 1947; MacKevett and Berg, 1963). **Workings** consisted of about 2,900 m of shafts, **adits**, drifts, crosscuts, and **stopes** (MacKevett and Berg, 1963), but the shafts and **adits** are presently caved. Numerous sloughed trenches total several hundred meters in length; most are heavily overgrown with alder and a few small spruce. Several ore and tailings piles on the site lie near the small Red Devil Creek that drains the mine area. The largest tailings pile is adjacent to the creek and is about 60 m wide and 75 m long. Abundant placer cinnabar and lesser stibnite are visible in Red Devil Creek.

## METHODS

### FIELD METHODS

At the Cinnabar Creek mine, vegetation and soil samples were collected at 15-m intervals along transects perpendicular to the mined trench and perpendicular to a prospect trench that had no recorded ore production (fig. 2). At the Red Devil mine, vegetation and soil samples were collected along a transect perpendicular to a large surface-mined area (fig. 3). Additional vegetation and soil samples were collected near the retort oven used during mining operations at Red Devil (fig. 3); no ore was actually mined from this area. The transects ranged from about 153 to 305 m long. Stream-water samples were also col-

lected from Cinnabar and Red Devil Creeks (figs. 2, 3) to evaluate mercury contamination in water downstream from the mines. To determine regional mercury background concentrations, vegetation, soil, and stream-water samples were collected from areas with geology similar to that of the mineralized areas, but where mercury deposits are not known (fig. 1).

Several vegetation samples were collected at each site. Species collected included alder (*Alnus crispa*), willow (*Salix* sp.), white spruce (*Picea glauca*), cottonwood (*Populus balsamifera*), black spruce (*Picea mariana*), blueberry (*Vaccinium uliginosum*), paper birch (*Betula papyrifera*), and dwarf birch (*Betula nana*). All of these plants are commonly found in the Kuskokwim Mountains region (Vioreck and Little, 1972), but all species were not present at each site. A minimum of two plant species were collected at each site. For each vegetation sample, first-year growth material was collected—generally, the outermost 15 to 20 cm on the larger woody species and 8 to 10 cm on the shrub species.

Soil samples typically included the upper 15-20 cm of material just below the surface organic layer. This is the zone of most active root development and is generally the primary zone of mercury accumulation in forest soils (Godbold, 1994). In the study area, soils are usually poorly developed below about 15 cm.

At each water-collection site two samples were collected—one for dissolved Hg, and one for total Hg. Samples for total Hg were collected unfiltered in a glass bottle and were acidified with nitric acid and potassium dichromate. Samples for dissolved Hg were obtained by filtering the stream water through a 0.45- $\mu\text{m}$  membrane into a glass bottle and were then preserved with nitric acid and potassium dichromate. Stream-water pH, conductivity, and turbidity were also measured at each sample site.

### ANALYTICAL METHODS

In the laboratory, vegetation samples were washed two times with distilled deionized water to remove surface contamination. They were then dried at 40°C and separated into leaves, stems, and flowers or fruit tissues for separate analyses. Soil samples were dried at 40°C, sieved to minus-10 mesh, and then pulverized to minus-100 mesh. No further preparation was required for the stream-water samples.

All vegetation (tables 1, 2 and 4), soil (tables 3 and 4), and stream-water samples (table 5) were analyzed for total mercury concentration by the cold-vapor **atomic-absorption** spectrophotometry (CVAAS) method of O'Leary and others (1990). Stream-water data from Cinnabar Creek and some of the background sites are from Gray and others (1996). A subset of the vegetation and soil samples were analyzed for methylmercury by the cryogenic gas chroma-



tography cold-vapor atomic-fluorescencespectrometry (GC-AFS) method of Bloom (1989) and are reported in tables 1 through 4.

Soil pH and total organic carbon (TOC) are reported in tables 3 and 4. Soil pH was determined by adding equal

volumes of soil and distilled deionized water to a 100-mL beaker and mixing to form a slurry. When most of the material had settled, the pH of the mixture was measured using a digital pH meter. Soil TOC was determined by the method of Curry (1990).

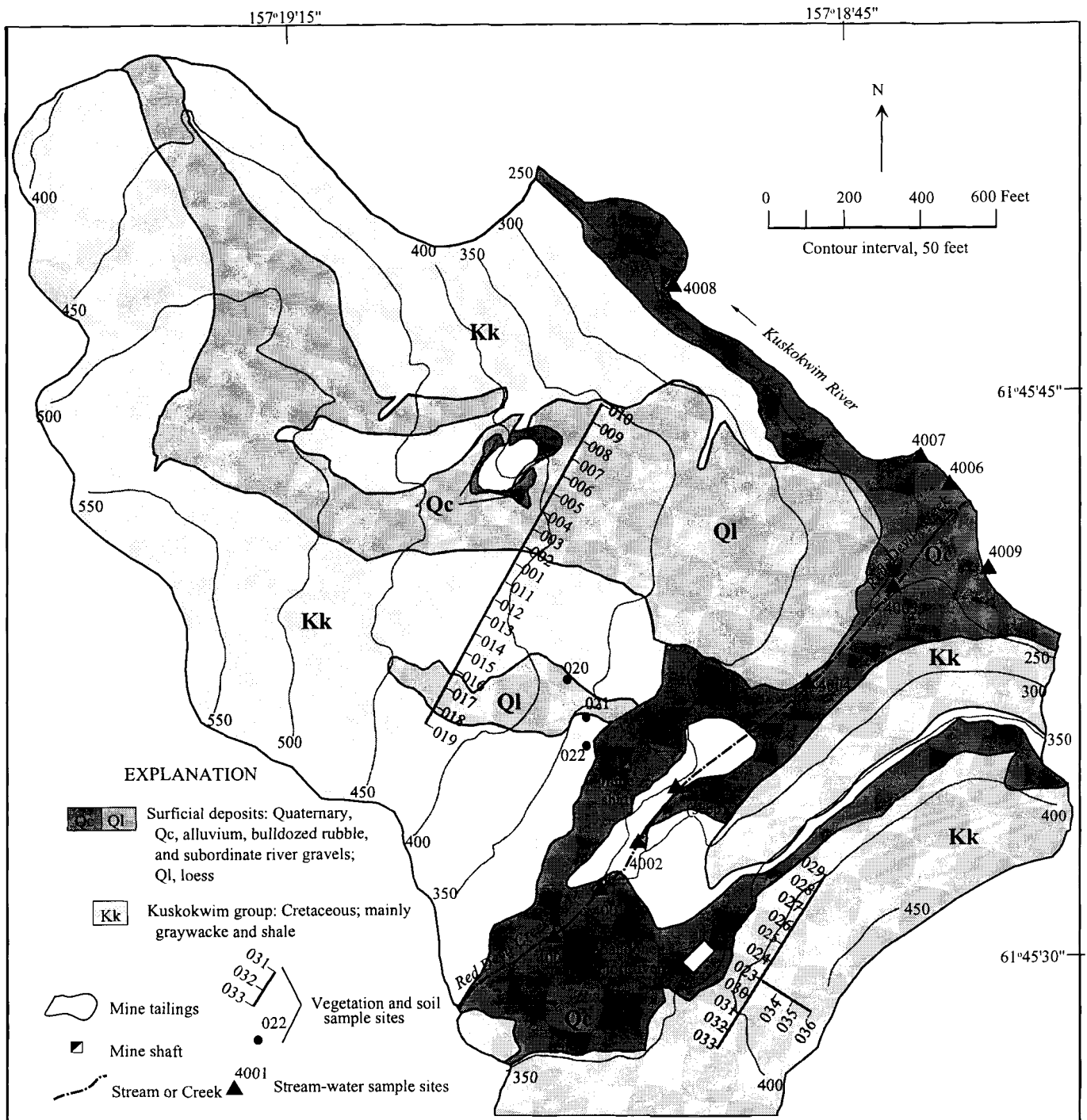


Figure 3. Sample locations and simplified geology, Red Devil mine. Geology generalized from MacKevett and Berg (1963).

Table 1. Geochemical data for vegetation samples collected at the Cinnabar Creek mine

[Analysis of total Hg by cold-vapor atomic-absorption spectrophotometry (CVAAS), lower limit of determination, 20 ppb; analysis of methylmercury (meHg) by cryogenic gas chromatography with atomic-fluorescence spectrometry; ppb, parts per billion; ---, not determined or sample not collected; <, less than]

Field no.	<sup>1</sup> A1 total Hg (ppb)	A1 meHg (ppb)	A2 total Hg (ppb)	A3 total Hg (ppb)	B1 total Hg (ppb)	B1 meHg (ppb)	B2 total Hg (ppb)	B2 meHg (ppb)	B3 total Hg (ppb)	C1 total Hg (ppb)	C2 total Hg (ppb)	E1 total Hg (ppb)	E2 total Hg (ppb)	F1 total Hg (ppb)	F1 meHg (ppb)	F2 total Hg (ppb)	F3 total Hg (ppb)	F3 meHg (ppb)	H1 total Hg (ppb)	H2 total Hg (ppb)	H3 total Hg (ppb)
Prospect area (unmined)																					
52	--	--	--	--	--	--	--	--	--	--	--	--	--	90	--	20	--	--	20	<20	50
51	--	--	--	--	--	--	--	--	--	--	--	--	--	40	--	<20	--	--	40	<20	70
50	40	--	<20	30	50	--	50	--	--	--	--	130	50	20	--	<20	--	--	--	--	--
49	--	--	--	--	--	--	--	--	--	--	--	--	--	60	0.74	20	60	0.73	90	30	90
48	130	--	<20	<20	40	--	40	--	--	20	<20	--	--	--	--	--	--	--	--	--	--
42	250	1.04	50	140	100	36.7	150	26.2	310	--	--	--	--	--	--	--	--	--	--	--	--
43	100	--	<20	20	30	--	30	--	--	--	--	--	--	--	--	--	--	--	--	--	--
44	--	--	--	--	--	--	--	--	--	--	--	--	--	30	--	20	--	--	30	<20	100
45	--	--	--	--	--	--	--	--	--	--	--	--	--	--	--	--	--	--	70	<20	40
46	--	--	--	--	--	--	--	--	--	--	--	--	--	--	--	--	--	--	20	<20	30
47	140	--	20	150	100	--	80	--	130	--	--	--	--	--	--	--	--	--	--	--	--
Mined area																					
53	970	0.98	200	170	760	1.27	180	--	--	--	--	--	--	--	--	--	--	--	--	--	--
54	250	--	30	80	670	--	50	--	270	--	--	--	--	--	--	--	--	--	--	--	--
54D	240	--	40	120	580	--	50	--	180	--	--	--	--	--	--	--	--	--	--	--	--
55	160	--	<20	--	--	--	--	--	--	--	--	--	--	--	--	--	--	--	--	--	--
56	90	--	<20	--	850	--	40	--	--	--	--	--	--	--	--	--	--	--	--	--	--
57	--	--	--	--	--	--	--	--	--	--	--	--	--	--	--	--	--	--	--	--	--

<sup>1</sup>Codes for vegetation species and tissue type for tables 1 and 2:

A1: alder (*Alnus crispa*) leaves

A2: alder (*Alnus crispa*) stems

A3: alder (*Alnus crispa*) flowers

B1: willow (*Salix* sp.) leaves

B2: willow (*Salix* sp.) stems

B3: willow (*Salix* sp.) flowers

C1: white spruce (*Picea glauca*) needles

C2: white spruce (*Picea glauca*) stems

C3: white spruce (*Picea glauca*) cones

D1: cottonwood (*Populus balsamifera*) leaves

D2: cottonwood (*Populus balsamifera*) stems

D3: cottonwood (*Populus balsamifera*) flowers

E1: black spruce (*Picea mariana*) needles

E2: black spruce (*Picea mariana*) stems

E3: black spruce (*Picea mariana*) cones

F1: blueberry (*Vaccinium uliginosum*) leaves

F2: blueberry (*Vaccinium uliginosum*) stems

F3: blueberry (*Vaccinium uliginosum*) fruits

G1: paper birch (*Betula papyrifera*) leaves

G2: paper birch (*Betula papyrifera*) stems

G3: paper birch (*Betula papyrifera*) flowers

H1: dwarf birch (*Betula nana*) leaves

H2: dwarf birch (*Betula nana*) stems

H3: dwarf birch (*Betula nana*) flowers

## RESULTS

### BACKGROUNDS

Vegetation, soil, and stream-water samples were collected near the Red Devil and Cinnabar Creek mines to determine regional background mercury concentrations for this study (fig. 1). Alder was the only vegetation species present at both mines and at the background sites studied.

At the background site for the Red Devil mine (fig. 1, samples 37-40), total-mercury concentrations range from <20 to 100 ppb in alder leaves, from <20 to 30 ppb in alder stems, and from <20 to 150 ppb in alder flowers (table 4). At the background site for the Cinnabar Creek mine (fig. 1, samples 58-61), total-mercury concentrations range from 40 to 190 ppb in alder leaves, <20 to 20 ppb in alder stems, and 20 to 110 ppb in alder flowers (table 4). These results are consistent with earlier studies that found total-Hg concentrations of 6 to 100 ppb in vegetation collected from

areas where there is no mercury contamination (Siegal and others, 1985, 1987; Kovalevsky, 1987; Rasmussen and others, 1991); however, most of the previously published data are for total-mercury concentrations in whole plants and not for specific tissues such as leaves, stems, and fruit. Methylmercury concentrations measured in two alder leaf samples are 0.49 ppb (Red Devil, sample 39) and 0.45 ppb (Cinnabar Creek, sample 60).

Total Hg in soils collected from the Red Devil background sites range from 0.10 to 0.39 ppm (table 4), whereas soils collected from the Cinnabar Creek background sites contain 0.16 to 1.2 ppm total Hg (table 4). Methylmercury concentrations in soil samples collected at two background sites for Red Devil (sample 39) and Cinnabar Creek (sample 61) were 0.88 and 0.90 ppb, respectively. Soil pH values for all background samples are slightly acidic and range from 4.0 to 5.5, similar to values reported by Gough and others (1988). TOC ranges from 1.1 percent up to 10.7 percent, consistent with values generally found in poorly

**Table 2.** Geochemical data for vegetation samples collected at the Red Devil mine

[Analysis of total Hg by cold-vapor atomic-absorption spectrophotometry (CVAAS), lower limit of determination, 20 ppb; analysis of methylmercury (meHg) by cryogenic gas chromatography with atomic-fluorescence spectrometry; ppb, parts per billion; —, not determined or sample not collected; <, less than]

Field no.	A1 total Hg (ppb)	A1 meHg (ppb)	A2 total Hg (ppb)	A2 meHg (ppb)	A3 total Hg (ppb)	A3 meHg (ppb)	B1 total Hg (ppb)	B1 meHg (ppb)	B2 total Hg (ppb)	B3 total Hg (ppb)	C1 total Hg (ppb)	C2 total Hg (ppb)	C3 total Hg (ppb)	D1 total Hg (ppb)	D2 total Hg (ppb)	E1 total Hg (ppb)	E2 total Hg (ppb)	E3 total Hg (ppb)	F1 total Hg (ppb)	F1 meHg (ppb)	F2 total Hg (ppb)	F3 total Hg (ppb)	F3 meHg (ppb)	G1 total Hg (ppb)	G2 total Hg (ppb)	G3 total Hg (ppb)	
Retort area (unmined)																											
33	310	0.45	30	--	90	--	310	--	40	--	--	--	--	--	--	--	--	--	210	2.76	60	100	2.60	--	--	--	
32	--	--	--	--	--	--	330	--	90	--	--	--	--	--	--	--	--	--	330	--	90	--	--	180	70	--	
31	--	--	--	--	--	--	280	--	60	--	--	--	--	--	--	210	210	--	260	--	70	70	--	--	--	--	
30	--	--	--	--	--	--	150	--	50	--	--	--	--	--	--	--	--	--	180	--	120	70	--	140	40	90	
23	--	--	--	--	--	--	180	--	70	--	--	--	--	--	--	--	--	--	190	--	50	40	--	160	40	--	
24	--	--	--	--	--	--	180	--	30	--	--	--	--	--	--	150	150	370	230	--	50	100	--	--	--	--	
25	--	--	--	--	--	--	160	--	40	--	--	--	--	--	--	90	40	100	230	--	70	80	--	100	30	120	
26	--	--	--	--	--	--	180	--	40	260	--	--	--	--	--	110	110	160	160	--	50	40	--	--	--	--	
27	--	--	--	--	--	--	130	--	90	--	--	--	--	--	--	90	100	60	110	--	40	30	--	--	--	--	
28	--	--	--	--	--	--	90	--	40	310	--	--	--	--	--	70	60	50	80	--	30	40	--	--	--	--	
29	--	--	--	--	--	--	160	--	30	--	--	--	--	--	--	70	80	210	80	--	40	60	--	--	--	--	
34	--	--	--	--	--	--	180	--	--	--	--	--	--	--	--	--	--	--	--	--	--	--	--	--	--	--	
35	--	--	--	--	--	--	140	--	--	--	--	--	--	--	--	--	--	--	--	--	--	--	--	--	--	--	
36	--	--	--	--	--	--	90	--	--	--	--	--	--	--	--	--	--	--	--	--	--	--	--	--	--	--	
Mined area																											
19	--	--	--	--	--	--	100	--	30	--	--	--	--	--	--	30	100	20	40	--	<20	50	--	40	<20	--	
18	--	--	--	--	--	--	380	--	70	--	60	20	30	--	--	--	--	--	60	--	30	40	--	130	30	40	
17	--	--	--	--	--	--	--	--	--	--	--	--	--	--	--	--	--	--	150	--	70	--	--	--	--	--	
16	--	--	--	--	--	--	40	--	<20	--	--	--	--	--	--	70	<20	200	30	--	<20	60	--	30	<20	--	
15	50	--	<20	--	30	--	--	--	--	--	--	--	--	--	--	20	40	60	--	--	--	--	--	--	--	--	
14	40	--	<20	--	30	--	--	--	--	--	--	--	180	30	--	--	--	--	--	--	--	--	--	--	--	--	
13	30	--	<20	--	<20	--	--	--	--	--	60	90	--	280	20	--	--	--	--	--	--	--	--	--	--	--	
12	80	--	20	--	30	--	150	--	30	--	50	60	--	60	30	--	--	--	--	--	--	--	--	--	--	--	
11	60	--	<20	--	30	--	--	--	--	--	--	--	--	100	40	--	--	--	--	--	--	--	--	--	--	--	
1	150	0.72	30	0.80	40	0.87	--	--	--	--	--	--	--	--	--	--	--	--	--	--	--	--	--	--	--	--	
2	900	0.54	40	--	40	--	560	2.73	70	--	140	130	--	--	--	--	--	--	--	--	--	--	--	--	--	--	
3	90	--	20	--	40	--	210	--	30	--	130	70	--	--	--	--	--	--	--	--	--	--	--	--	--	--	
4	100	--	30	--	50	--	--	--	--	--	--	--	--	--	--	--	--	--	--	--	--	--	--	--	--	--	
5	120	--	30	--	50	--	--	--	--	--	--	--	--	--	--	--	--	--	--	--	--	--	--	--	--	--	
6	320	--	20	--	60	--	--	--	--	--	--	--	--	--	--	--	--	--	--	--	--	--	--	--	--	--	
7	80	--	<20	--	<20	--	100	--	40	--	--	--	--	--	--	--	--	--	--	--	--	--	--	--	--	--	
8	40	--	<20	--	30	--	--	--	--	--	--	--	--	--	--	--	--	--	--	--	--	--	--	--	--	--	
9	110	--	<20	--	40	--	--	--	--	--	--	--	--	--	--	--	--	--	--	--	--	--	--	--	--	--	
10	40	--	<20	--	<20	--	100	--	20	--	--	--	--	--	--	--	--	--	--	--	--	--	--	--	--	--	
20	120	--	30	--	30	--	130	--	50	--	--	--	--	160	40	--	--	--	--	--	--	--	--	--	--	--	
21	300	--	30	--	60	--	--	--	--	--	--	--	--	--	--	--	--	--	--	--	--	--	--	--	--	--	
22	420	--	50	--	120	--	--	--	--	--	--	--	--	--	--	--	--	--	--	--	--	--	--	--	--	--	

<sup>1</sup>See table 1 for explanation of codes for vegetation species and tissue types.

drained boreal (northern) forest soils (Brady and Weil, 1996).

Background stream-water samples were collected from two sites upstream from the Red Devil mine and at several sites throughout the Kuskokwim River region (fig. 1). All stream-water samples collected from background sites contain less than 0.1 ppb Hg (table 5). These results are consistent with the low concentrations of mercury observed in natural surface waters, which are commonly less than 0.1 ppb (Wershaw, 1970). The pH of background stream waters are near neutral to slightly alkaline and range from 6.8 to 8.4. Conductivity values in samples collected from background sites range from 60 to 115  $\mu$ S/cm. Turbidity, a

measure of suspended matter such as clay, organics, and microorganisms, is generally low at most sites in streams measured for background in the region and ranges from 2 to 6 nephelometric turbidity units (NTU) at most sites; these values are similar to the 5-NTU State of Alaska drinking water standard (Alaska Department of Environmental Conservation, 1994). Turbidity measurements were somewhat higher on Red Devil Creek; for example, turbidity was 15 NTU in a small seep near the mine (table 5, sample RD4003). Turbidity as high as 30 NTU (table 5, sample KF4305) was measured on the Kuskokwim River and is probably related to suspended, glacially derived material in upstream tributaries that originate in the Alaska Range.



Table 5. Geochemical data for stream-water samples collected from the Red Devil mine, Cinnabar Creek mine, and background sites in the Kuskokwim River region

[Analysis of Hg by cold-vapor atomic-absorption spectrophotometry (CVAAS), lower limit of determination, 0.10 ppb; ppb, parts per billion; NTU, nephelometric turbidity units; RA, raw unfiltered water sample; FA, filtered water sample; —, not determined or sample not collected; <, less than]

Sample	Locality	Hg (ppb)	pH	Conductivity ( $\mu\text{S}/\text{cm}$ )	Turbidity (NTU)
RD4002RA	Red Devil	0.14	7.4	100	3.5
RD4002FA	Red Devil	<.10	--	--	--
RD4003RA	Red Devil	<.10	6.4	275	15
RD4003FA	Red Devil	<.10	--	--	--
RD4004RA	Red Devil	.28	7.1	115	3.5
RD4004FA	Red Devil	<.10	--	--	--
RD4005RA	Red Devil	.26	7.0	115	3.5
RD4005FA	Red Devil	<.10	--	--	--
RD4006RA	Red Devil	<.10	7.2	80	8.5
RD4006FA	Red Devil	<.10	--	--	--
RD4007RA	Red Devil	.16	7.4	80	8.5
RD4007FA	Red Devil	<.10	--	--	--
RD4008RA	Red Devil	<.10	7.5	80	8.5
RD4008FA	Red Devil	<.10	--	--	--
RD4009RA	Red Devil	.19	7.6	75	8.0
CC4200RA	Cinnabar Creek	.19	7.1	65	5.0
CC4200FA	Cinnabar Creek	<.10	--	--	--
CC931FA	Cinnabar Creek	<.10	6.4	190	--
Background sites					
RD4000RA	Red Devil	<0.10	7.6	105	3.5
RD4000FA	Red Devil	<.10	--	--	--
RD4001RA	Red Devil	<.10	7.6	105	2.0
RD4001FA	Red Devil	<.10	--	--	--
MC4100RA	Moose Creek	<.10	8.1	75	4.0
MC4100FA	Moose Creek	<.10	--	--	--
HK4300RA	Holokuk River	<.10	7.3	95	6.0
HK4300FA	Holokuk River	<.10	--	--	--
BS4301RA	Boss Creek	<.10	7.1	60	4.0
BS4301FA	Boss Creek	<.10	--	--	--
EZ4302RA	Egozuk Creek	<.10	8.4	80	4.5
EZ4302FA	Egozuk Creek	<.10	--	--	--
VH4303RA	Veahna Creek	<.10	7.6	75	5.0
VH4303FA	Veahna Creek	<.10	--	--	--
KF4305RA	Kuskokwim River	<.10	7.7	115	30
KF4305FA	Kuskokwim River	<.10	--	--	--
AN4308RA	Kuskokwim River	<.10	7.1	60	15
AN4308FA	Kuskokwim River	<.10	--	--	--
BR3069FA	Buckstock River	<.10	6.8	60	--

### CINNABAR CREEK

At the Cinnabar Creek mine, total-mercury concentrations in vegetation samples collected range from 20 to 970 ppb in leaves and needles, <20 to 200 ppb in stems, and <20 to 310 ppb in flowers (table 1). Leaf samples collected

from Cinnabar Creek contain methylmercury concentrations ranging from 0.73 to 36.7 ppb (table 1).

Soil samples collected from the Cinnabar Creek mine contain from 0.13 to 1,500 ppm total Hg, with a mean of 157 ppm (table 3). Mine-site soil samples contain from 5.03 to 133 ppb methylmercury (table 3). The soils are

slightly acidic to slightly alkaline; they range from pH 4.5 to 7.6 and have a mean pH of 5.0. Mean TOC content is 3.87 percent but ranges from 0.44 to 4.95 percent (table 3).

Mercury concentrations are slightly elevated in the raw unfiltered stream-water samples collected from Cinnabar Creek downstream from the main mine trench (0.19 ppb), but the filtered stream-water samples contained less than 0.10 ppb, similar to mercury concentrations in the stream-water samples collected from background sites (table 5). Stream-water samples collected from Cinnabar Creek had near neutral pH (6.4 and 7.1) and low conductivity (65 and 190  $\mu\text{S}/\text{cm}$ ) and turbidity values (5.0 NTU), similar to those measured at Red Devil Creek (table 5).

## RED DEVIL

At the Red Devil mine, total-mercury concentrations in all vegetation samples collected range from 20 to 900 ppb in leaves, <20 to 210 ppb in stems, and <20 to 370 ppb in flowers (table 2). Leaf samples analyzed for methylmercury have concentrations ranging from 0.45 to 2.76 ppb (table 2).

In the soil samples collected from the Red Devil mine, total-mercury concentrations range from 0.05 to 1,200 ppm, with a mean of 82 ppm (table 3). Soil methylmercury concentrations in samples from Red Devil range from 2.7 to 8.2 ppb (table 3). Soil pH ranges from 4.1 to 6.8, with a mean of 5.2. The average TOC content is 2.66 percent but ranges from 0.30 to 8.99 percent (table 3).

Stream-water samples collected in Red Devil Creek downstream from the mine contain as much as 0.28 ppb Hg in raw unfiltered stream-water samples. However, in all filtered water samples collected downstream from the mines, Hg concentrations are less than 0.10 ppb and similar to mercury concentrations in stream-water samples collected from background sites (table 5). The pH of the stream-water samples collected from the Red Devil mine varies between 6.4 and 7.6 (table 5). Conductivity values in samples collected downstream from the Red Devil mine range from 75 to 115  $\mu\text{S}/\text{cm}$ , with the exception of a water sample (RD4003) collected from a seep draining a caved **adit** at Red Devil that has a conductivity of 275  $\mu\text{S}/\text{cm}$  (table 5). In samples collected downstream from the mine, turbidity varies from 3.5 to 8.5 NTU, again with the exception of sample **RD4003**, which has a turbidity of 15 NTU (table 5).

## DISCUSSION

### VEGETATION SAMPLES

#### MERCURY VARIATIONS IN PLANT TISSUE TYPES

In all vegetation samples, total-mercury concentrations are generally highest in the leaves and lowest in the stems

(figs. 4, 5). Some plant tissues have a greater ability to absorb mercury than others (Kabata-Pendias and Pendias, 1992), but the data do not always clearly identify which plant tissues most readily absorb mercury (Warren and others, 1983; Kovalevsky, 1987; Rasmussen and others, 1991; Lodenius, 1994). Some studies suggest discarding stem tissue because stems generally contain low mercury concentrations (Rasmussen and others, 1991). Results of our study support this conclusion. However, Kovalevsky (1987) found that stems of some Siberian conifers contain higher mercury concentrations than do other parts of the plant. Lodenius (1994) reported that mercury concentrations are generally lower in the flowers and leaves than in other parts of plants. Warren and others (1983) found that in over 100 species collected from the **Pinchi** Lake mercury mine area in British Columbia, roots and flowers tended to have higher concentrations of mercury than did first-year leaves and first- or second-year stems. Our study suggests that leaves tend to concentrate mercury to a greater extent than do stems or flowers.

#### MERCURY VARIATIONS BETWEEN VEGETATION SPECIES

Plant species differ in their ability to take up mercury, as can be seen in the considerable variation between the species we sampled (figs. 4, 5). At the Red Devil and Cinnabar Creek mines, alders and willows concentrate mercury at levels as much as 20 times higher than those in the other species collected in this study. Data from Warren and others (1983) support this observation. The mechanism of mercury uptake and why certain species accumulate more mercury than others is unclear. Siegal and others (1985, 1987) suggested that some species are mercury accumulators, whereas other plant species reject mercury, or possibly that certain plants release their absorbed mercury as mercury vapor ( $\text{Hg}^0$ ) and thus lower their total concentration of mercury.

#### MERCURY IN VEGETATION—MINES VERSUS BACKGROUNDS

Total-mercury concentrations in alder samples are much higher in the mine-site samples than in the background samples (figs. 4, 5). Alder leaves collected near the mines contain mercury concentrations that range from 30 to 970 ppb. These values are similar to concentrations (28 to 1,150 ppb) measured by Warren and others (1966) and Siegal and others (1985) in various species collected near the **Pinchi** Lake mercury mine, but most of these values are for whole plants, not specific tissues. Alder leaves collected from background sites for our study contain from <20 to 100 ppb mercury at Red Devil and from 40 to 190 ppb mercury at Cinnabar Creek; these values are similar to worldwide background values in vegetation of 3 to 100 ppb reported by Lodenius (1994).

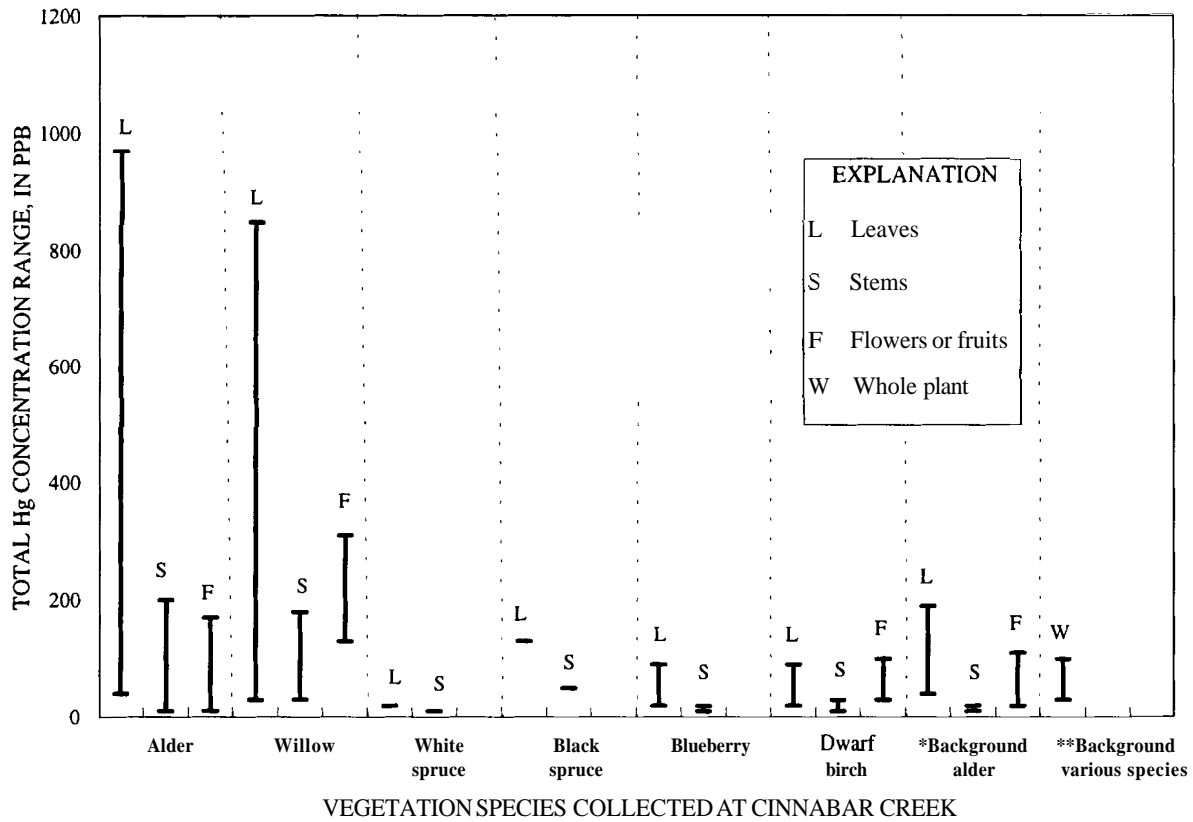


Figure 4. Variation in total-mercury concentrations (in parts per billion) between vegetation species sampled and between tissue type at the Cinnabar Creek mine. The single asterisk denotes background data from this study; the double asterisk represents background data from Rasmussen and others (1991), Siegal and others (1985), and Warren and others (1983).

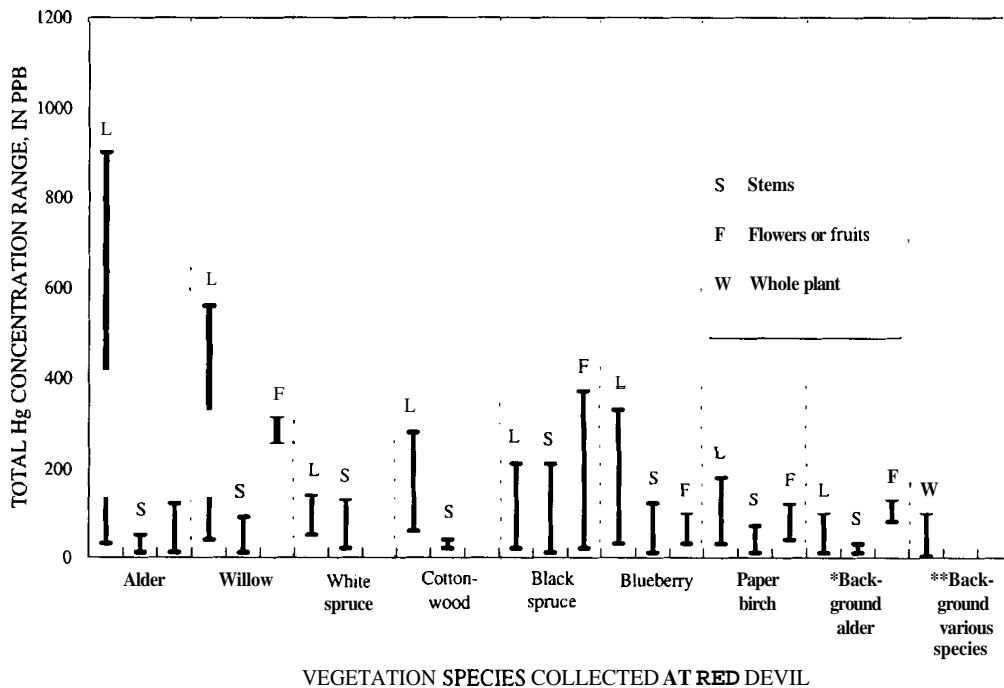


Figure 5. Variation in total-mercury concentrations (in parts per billion) between vegetation species sampled and between tissue type at the Red Devil mine. The single asterisk denotes background data from this study; the double asterisk represents data from Rasmussen and others (1991), Siegal and others (1985), and Warren and others (1983).

## SOIL SAMPLES

## SOIL MERCURY—MINES VERSUS BACKGROUNDS

Not surprisingly, total-mercury concentrations are significantly higher in soil samples collected from both the Red Devil and Cinnabar Creek mines (as much as 1,500 ppm) than in samples collected at the background sites (0.10 to 1.2 ppm, fig. 6). These elevated mercury concentrations in soils are somewhat higher than the values (14 to 500 ppm) found by other studies of abandoned mercury mines in British Columbia (Warren and others, 1966; Siegal and others, 1985) but are not substantially different. Most of the mercury present in soils at these abandoned mines probably occurs as cinnabar. It is the most stable *form* of mercury at the pH levels observed in these soils (Andersson, 1979).

We found somewhat higher background levels of mercury in soils (0.10 to 1.2 ppm) than those reported from organic-rich soils in other areas. For example, in Norway and Sweden, background mercury concentrations reported from organic-rich forest soils are less than 0.24 ppn

(Lindqvist, 1991). In the United States, mean concentrations reported from organic soils and loamy soils are 0.28 ppm Hg and 0.13 ppm Hg, respectively (Kabata-Pendias and Pendias, 1992). Background levels for organic soils in Canada as high as 0.40 ppm Hg are reported (Kabata-Pendias and Pendias, 1992). Shacklette and Boerngen (1984) report an average value of 0.058 ppm total Hg for background concentration in all soil types in the conterminous United States. The higher concentrations of mercury in soils sampled for background measurements in our study may indicate high regional background levels of mercury.

Methylmercury concentrations, like total-mercury concentrations, are higher in the mine-site soils in our study area (2.73 to 133 ppb; table 3) than in the background samples (0.88 to 0.90 ppb; table 4). In addition, methylmercury concentrations in soil samples collected from the Cinnabar Creek and Red Devil mines are as much as 50 times higher than the average background concentration of 2.5 ppb reported for sediments worldwide by Baeyens (1992), but the average methylmercury concentration for background soils collected in our study (0.89 ppb) is much lower than this worldwide average value.

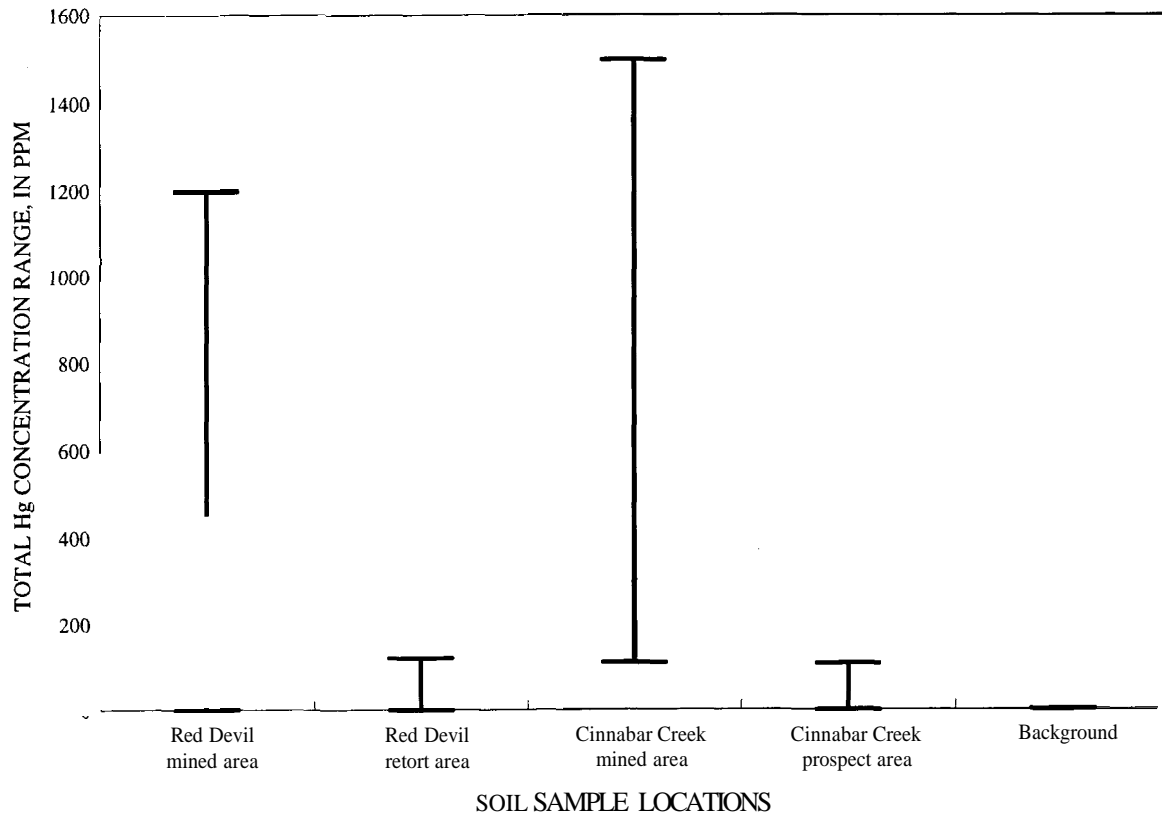


Figure 6. Comparison of total-mercury-concentration ranges (in parts per million) in soils collected from Red Devil and Cinnabar Creek mined areas and unmined areas and regional background sites.



## LIQUID MERCURY VERSUS CINNABAR

At the Red Devil mine, mercury concentrations are higher in the vegetation samples collected from the unmined area where the retort was located than in those samples collected from the mined trench (fig. 7). It is likely that during mining, retort operations released mercury vapor ( $\text{Hg}^0$ ) that later condensed as liquid mercury on the nearby soils. Liquid mercury, owing to its high solubility, is absorbed more readily by plants than is highly insoluble cinnabar (Lodenius, 1994), the most common form of mercury in soil in the mined trench. At the Cinnabar Creek mine, mercury concentrations are much higher in the vegetation samples collected from the mined trench, where liquid Hg has been noted (Gray and others, 1991), than in vegetation collected from a prospect trench where liquid mercury has not been noted and no ore was mined (fig. 7).

Methylmercury concentrations, like total-mercury concentrations, are higher in vegetation samples collected from both mines (0.45 to 36.7 ppb) than in vegetation samples collected from background sites (0.45 and 0.49 ppb). Methylmercury concentrations are generally higher in vegetation samples collected from Cinnabar Creek (0.73 to 36.7 ppb) than in those collected from Red Devil (0.45 to 2.76 ppb) (tables 1, 2). Liquid mercury ( $\text{Hg}^0$ ), a form of mer-

cury more commonly found at Cinnabar Creek mine than at Red Devil mine, is readily converted to the mercuric ( $\text{Hg}^{2+}$ ) ion, which in turn is easily converted to methylmercury. On the other hand, the conversions of mercury in cinnabar ( $\text{HgS}$ ) to methylmercury is slow (McLean and Bledsoe, 1992). Methylmercury levels in vegetation in our study area are generally low—less than 3 percent of total Hg levels—with the exception of sample 042 from the Cinnabar Creek mine, which contains 36.7 percent methylmercury. These data contrast with values from other types of biological tissue collected in southwestern Alaska; Gray and others (1994) reported fish samples in which methylmercury constituted greater than 90 percent of the total mercury content.

Methylmercury concentrations in soils collected from the mined trench at Cinnabar Creek and from the retort area at Red Devil are notably higher than those found at other locations at the mine sites (fig. 8). Liquid mercury is known to be present in the Cinnabar Creek mine trench. Likewise, near the Red Devil retort site, liquid mercury is probably present in the soils from past mining and retorting. In both cases, the presence of liquid mercury most likely explains the elevated methylmercury concentrations found in these soils compared with the levels found in soils collected from backgrounds.

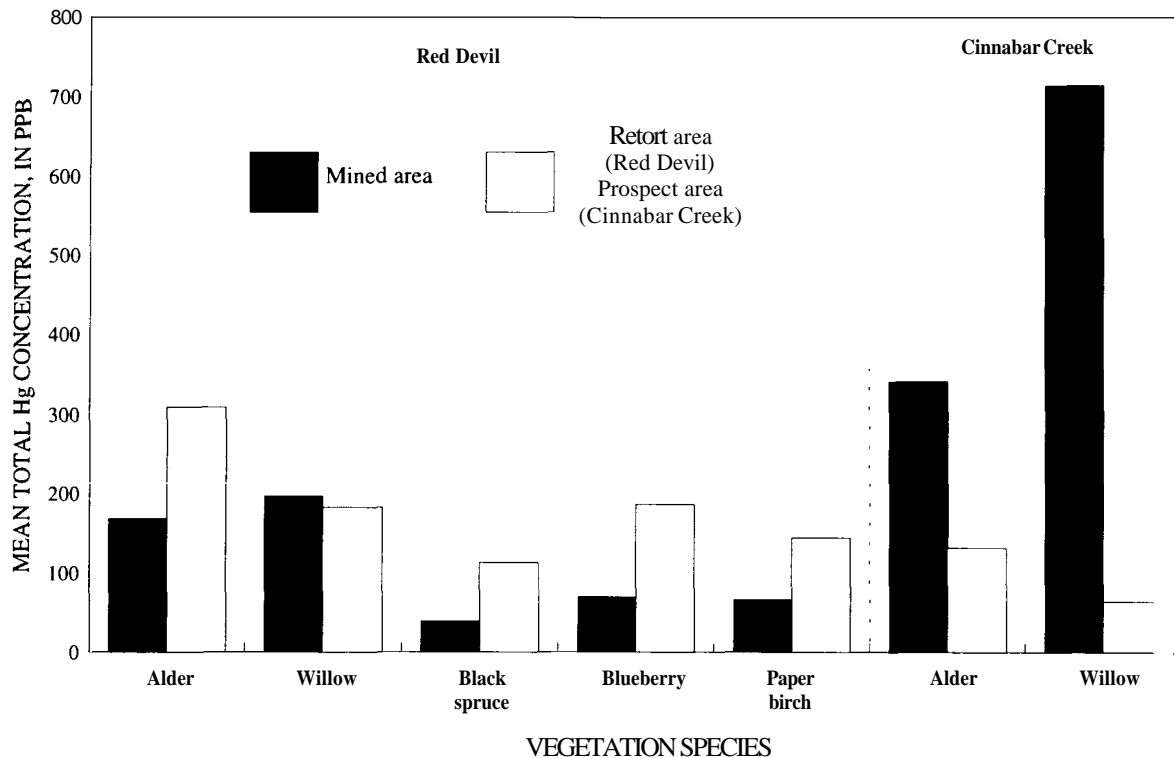


Figure 7. Comparison of average total-mercury concentrations (in parts per billion) in leaf-tissue samples from mined areas and unmined areas at Red Devil and Cinnabar Creek mines.

### STREAM-WATER SAMPLES

Some raw unfiltered stream-water samples collected downstream from the Red Devil and Cinnabar Creek mines contain mercury concentrations elevated above background values. Unfiltered stream-water samples collected downstream from the Red Devil mine contain as much as 0.28 ppb Hg, whereas background stream-water samples collected in the region contain less than 0.10 ppb Hg. However, the concentration of mercury in all stream-water samples is below both the 2 ppb drinking-water MCL recommended by the State of Alaska (Alaska Department of Environmental Conservation, 1994) and the 2.4 ppb maximum **instream** concentration recommended by the U.S. Environmental Protection Agency (Environmental Protection Agency, 1992). In addition, streams at these mines generally are not water supplies for human consumption. Mercury concentrations in the stream-water samples are low, even downstream from the mines, because the primary ore mineral is cinnabar, which is resistant to chemical and physical weathering. The stream-water mercury data indicate that only small amounts of mercury are transported in water, generally as suspended material, because the unfiltered water samples collected downstream from the mines were the only water samples with measurable concentrations of mer-

cury. Furthermore, even when mercury is converted to water-soluble forms and carried in water, it tends to be rapidly sorbed by sediment, including clays, microcrystalline oxides, and organic matter, in the stream environment (Jenne, 1970).

### CONCLUSIONS

Total-mercury and methylmercury concentrations in vegetation samples collected from the Cinnabar Creek and Red Devil mercury mines are elevated relative to regional background samples. We found considerable variation in mercury concentrations between different vegetation species; willow and alder generally contain the highest concentrations of mercury. Elevated mercury concentrations in vegetation are significant because alder twigs are eaten by ptarmigan and willow leaves are an important food for moose (Viereck, 1987). Blueberry, the species most likely to be consumed by residents of the Kuskokwim Mountains region, contains relatively low concentrations of total mercury (30 to 100 ppb in the edible fruit). Methylmercury, the highly toxic form of mercury, is probably not hazardous to humans or wildlife in the region. It generally represents less than 3 percent of the total mercury present in

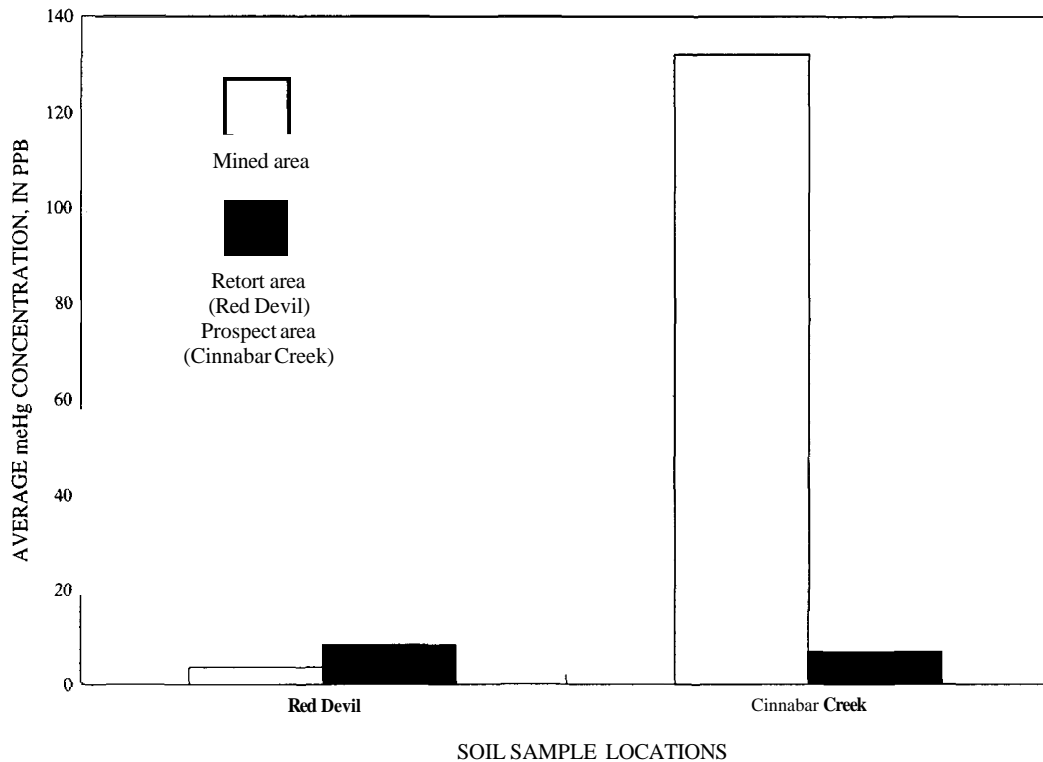


Figure 8. Comparison of average methylmercury concentrations (in parts per billion) in soils collected from Red Devil and Cinnabar Creek mined areas and unmined areas; regional background concentrations are less than 0.1 part per billion.

vegetation samples (although values as high as **36.7** percent occur locally); absolute values of methylmercury concentration are 0.45 to **36.7** ppb. Other studies (Agency for Toxic Substances and Disease Registry, 1994) indicate that chronic exposure (daily for **>365** days) to greater than 40 ppm methylmercury is necessary to produce detrimental effects in laboratory animals.

Total mercury-and methylmercury concentrations in soil samples collected from the Red Devil and Cinnabar Creek mines are as much as three to four orders of magnitude higher than those in background soil samples collected in this study. However, methylmercury constitutes only a small fraction (**<0.2** percent) of the total mercury present in the soil samples. Cinnabar is the most common form of mercury in soils collected from the mines, and the high total-mercury-to-methylmercury ratios in soils indicate low conversion rates of inorganic mercury (cinnabar) to organic mercury (methylmercury) at the mines studied. The low methylmercury concentrations in the soil samples collected in this study suggest that mercury contamination is not a problem at the Cinnabar Creek and Red Devil mines.

All concentrations of mercury in stream-water samples collected in this study are below the 2 ppb drinking-water MCL recommended by the State of Alaska. Stream-water pH in samples collected downstream from the mercury mines are neutral to slightly alkaline and are similar to background values. The dominant ore mineral in the mercury mines is cinnabar, which is highly insoluble in water and resistant to physical and chemical weathering. Therefore, these mines do not easily form acid drainage during weathering. Significant acid-drainage problems can result downstream from some sulfide-bearing mineral deposits and mines; however, acid formation in streams below the **mercury** mines in southwestern Alaska is insignificant.

Acknowledgments.—We thank Mike Balen (U.S. Bureau of Mines) and Bill Keith (USGS) for assistance with field work and **Marti** Miller (USGS) for helicopter use. Pete Theodorakos, Richard **O'Leary**, Kathleen Stewart, Tom Donley, David Dempsey, and Jim Hall (USGS) assisted with sample preparation, chemical analyses, and computer drafting. Jim Acher (Alaska Helicopters) provided helicopter support. June **McAtee** (Calista Corporation) also assisted in the field and provided access to Calista lands.

## REFERENCES CITED

Agency for Toxic Substances and Disease Registry, 1994, Toxicological profile for mercury: Agency for Toxic Substances and Disease Registry **ATSDR/TP-93/10**, 357 p.

Alaska Department of Environmental Conservation, 1994, Drinking water regulations: State of Alaska, Department of Environmental Conservation report 18-ACC-80, 195 p.

Andersson, A., 1979, Mercury in soils, *in* Nriagu, J.O., ed., The biogeochemistry of mercury in the environment: Amsterdam, **Elsevier/North-Holland** Biomedical Press, p. 82-103.

Baeyens, W., 1992, Speciation of mercury in different compartments of the environment: Trends in Analytical Chemistry, v. 11, p. 245-254.

Bloom, N.S., 1989, Determination of **picogram** levels of methylmercury by aqueous phase ethylation followed by cryogenic gas chromatography with cold vapor atomic fluorescence detection: Canadian Journal of Fisheries and Aquatic Sciences, v. 46, p. 1131-1139.

Brady, N.C. and **Weil**, R.R., 1996, The nature and properties of soils (11th ed.): Upper Saddle River, N.J., Prentice Hall, 740 p.

Cady, W.M., Wallace, R.E., Hoare, J.M., and Webber, E.J., 1955, The Central Kuskokwim region, Alaska: U.S. Geological Survey Professional Paper 268, 132 p., 5 pls.

**Clarkson**, T.W., 1994, The toxicology of mercury and its compounds, *in* Watras, C.J., and Huckabee, J.W., eds., Mercury pollution: integration and synthesis: Boca **Raton, Fla.**, Lewis Publishers, p. 631-641.

**Curry**, K.J., 1990, Determination of total carbon in geologic materials by combustion, *in* Arbogast, B.F., ed., Quality assurance manual for the Branch of Geochemistry, U.S. Geological Survey: U.S. Geological Survey Open-File Report 90-668, p. 114-118.

Eisler, Ronald, 1987, Mercury hazards to fish, wildlife, and invertebrates: a synoptic review: U.S. Fish and Wildlife Service Biological Report **85(1.10)**, 90 p.

Environmental Protection Agency, 1992, Water quality standards; establishment of numeric criteria for priority toxic pollutants; States' compliance; final **rule**: Federal Register, **40CFR** Part 131, v. 57, no. 246, p. 60,847-60,916.

**Godbold**, D.L., 1994, Mercury in forest ecosystems: risk and research needs, *in* Watras, C.J., and Huckabee, J.W., eds., Mercury pollution: integration and synthesis, Boca **Raton, Fla.**, Lewis Publishers, p. 295-303.

Gough, L.P., Severson, R.C., and Shacklette, H.T., 1988, Element concentrations in soils and other surficial materials of Alaska: U.S. Geological Survey Professional Paper 1458, 53 p.

Gray, J.E., Goldfarb, R.J., Detra, D.E., and Slaughter, K.E., 1991, Geochemistry and exploration criteria for epithermal cinnabar and stibnite vein deposits in the Kuskokwim River region, southwestern Alaska: Journal of Geochemical Exploration, v. 41, p. 363-386.

Gray, J.E., Meier, A.L., O'Leary, R.M., Outwater, Carol, and Theodorakos, P.M., 1996, Environmental geochemistry of mercury deposits in southwestern Alaska: mercury contents in fish, stream-sediment, and stream-water samples, *in* Moore, T.E., and Dumoulin, J.A., eds., Geologic studies in Alaska by the U.S. Geological Survey, 1994: U. S. Geological Survey Bulletin 2152, p. 17-29.

Gray, J.E., Theodorakos, P.M., Budahn, J., and O'Leary, R.M., 1994, Mercury in the environment and its implication, Kuskokwim River region, southwestern Alaska, *in* Till, A.B., and Moore, T.E., eds., Geologic studies in Alaska by the U.S. Geological Survey, 1993: U. S. Geological Survey Bulletin 2107, p. 3-12.

Jenne, E.A., 1970, Atmospheric and fluvial transport of mercury, *in* Mercury in the environment: U.S. Geological Survey Professional Paper 713, p. 40-49.

Kabata-Pendias, A., and Pendias, H., 1992, Trace elements in

- soils and plants (2d ed.): Boca **Raton**, Fla., CRC Press, Inc., p. 142-151.
- Kovalevsky, A.L., 1987, Biogeochemical exploration for mineral deposits (2d ed.): Utrecht, The Netherlands, VNU Science Press, 224 p.
- Lindqvist, O., ed., 1991, Mercury as an environmental pollutant—Proceedings from the International Conference, Gavle, Sweden: Water, Air, and Soil Pollution, v. 56, 847 p.
- Lodeniuss, M., 1994, Mercury in terrestrial ecosystems: a review, *in* Watras, C.J., and Huckabee, J.W., eds., Mercury pollution: integration and synthesis, Boca **Raton**, Fla., Lewis Publishers, p. 343-354.
- MacKevett, E.M., and Berg, H.C., 1963, Geology of the Red Devil quicksilver mine, Alaska: U.S. Geological Survey Bulletin 1142-G, 16 p.
- McLean**, J.E., and Bledsoe, B.E., 1992, Behavior of metals in soils: EPA Ground Water Issue, **EPA/540/S-92/018**, 25 p.
- Miller, M.L., **Belkin**, H.E., Blodgett, R.B., Bundtzen, T.K., Cady, J.W., Goldfarb, R.J., Gray, J.E., **McGimsey**, R.G., and **Simpson**, S.L., 1989, Pre-field study and mineral resource assessment of the Sleetmute quadrangle, southwestern Alaska: U.S. Geological Survey Open-File Report 89-363, 115 p.
- Nokleberg, W.J., Bundtzen, T.K., Berg, H.C., Brew, D.A., Grybeck, Donald, Robinson, M.S., Smith T.E., and **Yeend**, Warren, 1987, Significant metalliferous lode deposits and placer districts of Alaska: U.S. Geological Survey Bulletin 1786, 104 p.
- O'Leary**, R.M., Crock, J.G., and Kennedy, K.R., 1990, Determination of mercury in geologic materials by continuous flow-cold vapor-atomic absorption spectrophotometry, *in* Arbogast, B.F., ed., Quality assurance manual for the Branch of Geochemistry, U.S. Geological Survey: U.S. Geological Survey Open-File Report 90-668, p. 60-67.
- Rasmussen**, P.E., **Mierle**, G, and **Nriagu**, J.O., 1991, The analysis of vegetation for total mercury: Water, Air, and Soil Pollution, v. 56, p. 379-390.
- Sainsbury, C.L., and MacKevett, E.M., 1965, Quicksilver deposits of southwestern Alaska: U.S. Geological Survey Bulletin **1187**, **89** p.
- Shacklette, H.T., and Boerngen, J.G., 1984, Element concentrations in soils and other surficial materials of the conterminous United States: U.S. Geological Survey Professional Paper 1270, 105 p.
- Siegal, S.M., Siegal, B.Z., Barghigiani, C., Aratani, K., Penny, P., and Penny, D., 1987, A contribution to the environmental biology of mercury accumulation in plants: Water, Air, and Soil Pollution, v. 33, p. 65-72.
- Siegal, S.M., Siegal, B.Z., Lipp, C., Kruckeberg, A., Towers, G.H.N., and Warren, H., 1985, Indicator plant-soil mercury patterns in a mercury-rich mining area of British Columbia: Water, Air, and Soil Pollution, v. 25, p. 73-85.
- Viereck, E.G., 1987, Alaska's wilderness medicines: Anchorage, Alaska, Alaska Northwest Books, 107 p.
- Viereck, L.A., and Little, E.L., 1972, Alaska trees and shrubs: U.S. Department of Agriculture, Forest Service, Agricultural Handbook No. 410, 265 p.
- Warren, H.V., Delavault, R.E., and Barakso, John, 1966, Some observations on the geochemistry of mercury as applied to prospecting: Economic Geology, v. 61, p. 1010-1028.
- Warren, H.V., Horsky, S.J., Kruckeberg, A., Towers, G.H.N., and Armstrong, J.E., 1983, Biogeochemistry, a prospecting tool in the search for mercury mineralization: Journal of Geochemical Exploration, v. **18**, p. 169-173.
- Webber, B.S., Bjorklund, S.C., Rutledge, F.A., Thomas, B.I., and Wright, W.S., 1947, Mercury deposits of southwestern Alaska: U.S. Bureau of Mines Report of Investigations 4065, 57 p.
- Wershaw, R.L., 1970, Sources and behavior of mercury in surface waters, *in* Mercury in the environment: U.S. Geological Survey Professional Paper 713, p. 29-31.

Reviewers: ~~Mark~~ **Hines** and **Stephen Wilson**

# Distinguishing Between Natural Geologic and Anthropogenic Trace Element Sources, Denali National Park and Preserve

By Larry P. Gough and James G. Crock

## ABSTRACT

Geochemical and biogeochemical investigations in and near Denali National Park and Preserve (DNA), Alaska, were designed to (1) establish baseline elemental concentration information for selected native vegetation and the organic-rich Oa soil horizon, (2) define current spatial element trends as they may relate to emissions from a local coal-fired power plant, and (3) provide information useful in monitoring long-term landscape biogeochemical changes and in making biological resources management decisions. Critical to this assessment was the ability to distinguish between natural geologic and anthropogenic elemental sources. Two generally east-to-west traverses (Control and Stampede) and one north-to-south traverse (River Valley) were established. Sampling traverses extended outward from the existing Golden Valley Electric Association (GVEA) power plant located in Healy or near the Nenana River north of the GVEA facility. At each locality, samples of *Hylocomium splendens* (feather moss), *Peltigera aphthosa* (lichen), and the Oa soil horizon were collected. All materials were analyzed for their total major and trace element concentrations. Most elements show their highest concentrations close-in to the GVEA/Nenana River area and much lower concentrations beyond about 6 km from the GVEA facility. For example, Pb levels in moss averaged 6.2 ppm and 1.4 ppm (dry weight basis) when collected on the Stampede traverse at sites <6 km and >6 km, respectively, from the GVEA power plant. Elemental concentration baselines are presented based on the 6-km radius criterion.

## INTRODUCTION

The National Park Service (NPS) is concerned that emissions resulting from the operation of current and future coal-fired power plants near the northeastern border of the Denali National Park and Preserve (DNA) may negatively affect the biological resources of the region, especially the sulfur dioxide- and trace element-sensitive lichens (Nash and Wirth, 1988; Treshow and Anderson, 1989). This study, which is a cooperative one between the USGS

and NPS, was initiated in the fall of 1991 and was designed to (1) establish baseline elemental concentration information for selected nonvascular vegetation and the organic-rich Oa soil horizon, (2) define current elemental areal trends of the area, and (3) provide information useful in monitoring long-term landscape biogeochemical changes and in making biological resources management decisions. We hypothesized that observed baselines would include input from both natural geologic and anthropogenic elemental sources. The latter were thought to include emissions from the existing coal-fired power plant (the 25-MW Golden Valley Electric Association (GVEA) Healy Unit #1) and general emissions from local vehicle traffic and homes in the town of Healy. Critical to this assessment was the ability to distinguish between natural geologic and anthropogenic elemental sources.

Upon completion, this study provided background biogeochemical information that assisted in the evaluation of the potential impact of the new 50-MW Healy Clean Coal Project (HCCP) power plant. Construction began on the HCCP power plant in the spring of 1995, and it is scheduled for completion in early 1998 (Andrea Blakesley, DNA, oral commun., 1996). The GVEA facility has been operating since 1967, and the new HCCP facility is located adjacent to it. Both power plants are approximately 6.1 km from the boundary line of DNA, which is classified as a Class I airshed as defined by the Clean Air Act Amendments of 1977. Following a test period, the HCCP will burn local coal from the nearby Poker Flats mine. The mitigation documents that led to the permitting for the HCCP facility's construction have mandated maximum allowable emissions for both power plants; these limits will be monitored for compliance on a continuous basis (Alaska Industrial Development and Export Authority, 1992).

## MOSSES AND LICHENS AS BIOMONITORS

Vegetation, especially nonvascular species such as lichens and mosses, and organic-rich soils have been used successfully to assess the amounts and areal extent of industrial airborne emissions (Gough and Erdman, 1977;

Godbeer and others, 1981; Gough and others, 1988a, b; Onianwa, 1988; Puckett, 1988; Markert and Weckert, 1989; Berthelsen and others, 1995). Lichens and mosses are effective biomonitors of element deposition because they accumulate metals to a far greater level than is necessary for their physiological needs (Nash and Wirth, 1988; Berg and others, 1995). These and other studies have shown that the assessment of both floristic composition changes (due to morbidity and contaminant sensitivity) and trace element uptake make nonvascular vegetation particularly useful in point-source, metal contamination studies. Because of mainly adsorption processes, the organic-rich Oa soil horizon can also be an effective "trap" for metals. Its utility in delimiting point-source zones of influence was tested in this study.

### PHYSIOGRAPHY, CLIMATE, AND VEGETATION

A detailed discussion of the physiography and climate of Alaska is given by Péwé (1975). In general, the topography of the study area is dominated by the Alaska Range. The landscape consists of broad alluvial-fan complexes within river valleys covered with glacial outwash and eolian deposits. Lowlands containing many small lakes are scattered in the glacial till. Winds in the Healy region of the Nenana River valley vary with season but are predominantly out of the north and west. The vegetation is characterized by interior white spruce–birch forests with well-developed bogs and muskegs (Van Cleve and others, 1983; Gough and others, 1988c). Associated with these forests is an abundant shrub, lichen, and moss understory growth.

### GEOLOGY

The study area is underlain by a wide variety of sedimentary, volcanic, and igneous rocks ranging in age from Precambrian to Holocene (Csejtey and others, 1986, 1992; Wahrhaftig, 1987) (fig. 1). Most of the older formations have undergone some degree of metamorphism; for example, rocks of the Yukon-Tanana and McKinley terranes (Paleozoic and (or) Precambrian; see fig. 1) contain schist, gneiss, quartzite, and marble. The extensive Hines Creek and McKinley fault systems dominate the tectonics of the southern part of the study area.

In general, the river valleys (for example, Nenana River and Healy Creek) are predominantly undifferentiated Quaternary and Tertiary surficial deposits. These include glacial deposit, lake deposits, alluvium, and landslide debris. All of these deposits consist mainly of unconsolidated material ranging in size from huge boulders to very fine-grained clay. Clay, silt, and even sand (vegetated dunes are found both north and south of the DENA entrance) are the cause of massive dust clouds during high winds.

The coals of the study area are both Late Cretaceous (the Cantwell Formation which overlies the McKinley terrane) and Tertiary (coals that overlie the Cantwell Formation). The economic coals are associated with the Eocene and Miocene Usibelli Group, with the greatest number and thickest seams in the Healy Creek and Suntrana Formations. Coal seams are as thick as 20 m (Wahrhaftig and others, 1994) and range in apparent rank from lignite A to subbituminous B (Affolter and others, 1980; 1994). Seams 3 and 4 (and possibly 6) of the Suntrana Formation, Poker Flats mine, is the source of the very low sulfur (<0.5 percent) coal that was burned by the GVEA power plant during and immediately before the period of this study (Affolter and others, 1994). The concentration of many trace elements in these coals (whole-coal basis), such as Cr (15 ppm), La (7 ppm), Ni (10 ppm), and Yb (0.7 ppm), is elevated relative to coals from other U.S. sources (Swanson and others, 1976; Affolter and others, 1994). In this study, we pursue the possibility of using the presence of these and other trace elements in plant tissue as tracers of coal combustion.

### SOILS

Soils in the area are broadly classified as **Spodosols** (presence of an **Al** and Fe oxide accumulation zone (AO)) that vary from very shallow (a few centimeters) to deep (tens of meters). Soil parent material can be generally described as residual (developed over bedrock), glacial, or eolian. In this study, we focus on the organic-rich Oa horizon (usually 3–15 cm thick and about 3–4 cm below the surface); the Oa is the soil layer between the vegetation mat above and the **AO** spodic horizon below.

### METHODS

#### STUDY DESIGN

To discriminate between natural geologic and anthropogenic elemental sources we evaluated element-concentration trends in vegetation and soil with respect to distance from the GVEA emission source. An inverse log-linear relationship between element concentration in vegetation and (or) soil with distance from an emission source is frequently found near fossil-fuel power plants, refineries, or other types of point-source processing facilities (Gough and Erdman, 1977). Because emission-source-related trace element concentrations vary with vegetation types (owing to differences in longevity, absorptive surfaces, metabolism, growth form, habitat, and microenvironment), we sampled two potentially sensitive plant species.

In order to assess the potential influence of a proposed expansion of the existing GVEA facility at Healy on the air

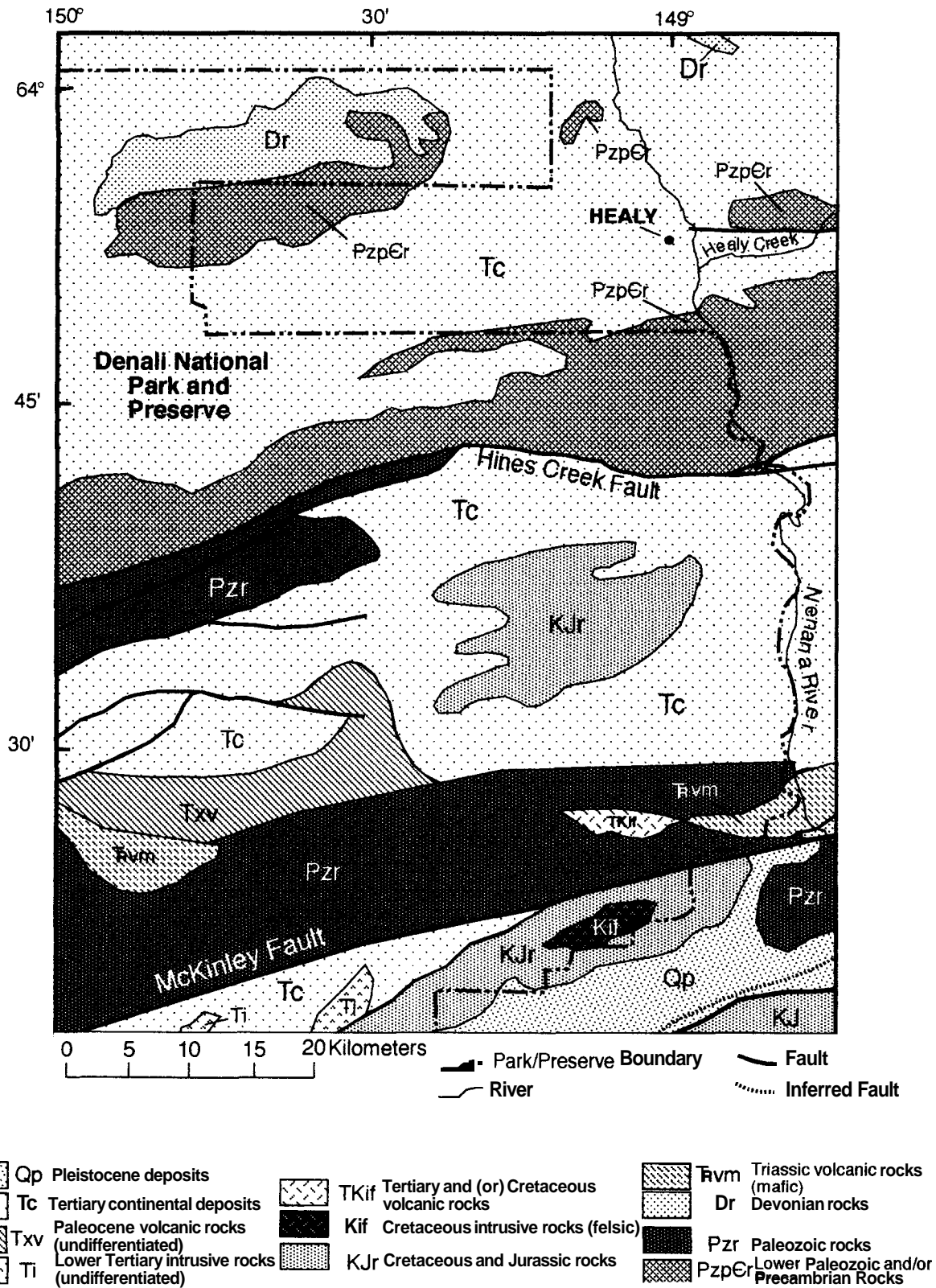


Figure 1. Generalized geologic map of the study area near Healy, Alaska (after Beikman, 1974; Csejty and others, 1992).

quality of DENA and surrounding environments, samples of *Hylocomium splendens* (feather moss), *Peltigera aphthosa* (dog-tooth lichen), and Oa-horizon soil were collected at sites along three traverses that ranged from 16 to 40 km in length. All of the samples were analyzed for their major and trace element concentrations (fig. 2). These element concentrations in moss, lichen, and soil, coupled with an examination of the chemistry of the coal to be utilized in the power plants, assisted in the process of evaluating the potential emission-related impact of the new HCCP facility on the local geochemical landscape.

Variations of element concentrations in sampled material, relative to distance from the GVEA site, were examined by linear regression. A least-squares equation was used for the regression, with the prediction model taking the form

$$X = a + b \log_{10} D,$$

where  $X$  is the concentration of the element in the material analyzed,  $D$  is the distance from the GVEA site, and  $a$  and  $b$  are, respectively, the regression constant and regression coefficient. The statistical significance of each regression was determined by analysis-of-variance (ANOVA) procedures. Coefficients of determination (between element concentration and log distance) estimate the proportions of the total variance in concentration that is associated with distance from an emission source. Large coefficients of determination are strong arguments for associating an emission source with element accumulation in vegetation or soil.

Geochemical and biogeochemical baselines were estimated by first assessing plots of distance from sources versus element concentrations in plant tissue or soil in order to choose which samples to incorporate into the determination of the baseline concentration ranges. If the coefficients of determination were large, these plots would usually demonstrate a marked decrease in element concentrations at about 6 km when plotted on an arithmetic scale. The zone beyond 6 km, therefore, shows a diminution of influence from the point source and points to a geographic region that contains material with baseline concentrations.

The study design consisted of three traverses (fig. 2): (1) the River Valley traverse (originating at the GVEA facility and progressed south roughly parallel to the Nenana River), (2) the Stampede traverse (originating at the GVEA facility and progressing west), and (3) the Control traverse (originating at the Nenana River 18 km north of the GVEA facility and progressing west). The Control traverse was incorporated into the overall study design in order to (1) factor out any observed GVEA power plant influence, and (2) assess the potential influence of airborne dust from the Nenana River basin as a natural geologic trace element source.

## FIELD SAMPLING

Sampling sites consisted of conifer stands, dominated by white spruce, with a canopy cover of between 30 and 60 percent (moderately dense). Sites were further classified according to the Viereck system (Viereck and others, 1986). The sampling sites were characterized by a moderate understory of mixed shrubs and a dense ground cover of mosses (*Hylocomium/Pleurozium/Polytrichum*) with scattered clumps of lichens (*Cladina/Cetraria/Peltigera*). The chosen sites were at least 200 m (if possible) from roads or railroads and at least 50 m from lakes or meadows and were selected to be as similar to one another as possible with regard to soil, vegetation, slope, and aspect (orientation relative to solar radiation). Uniformity in geology was maintained for the Control and Stampede traverses but was more variable along the River Valley traverse (figs. 1, 2). Minimization of site-related variability enhances the probability of defining variability associated with external sources.

Plant and soil samples were collected in close proximity to each other (less than 3 m apart). At each sampling site three separate plots were located within 200 m of each other, and about 200 g dry weight of moss and lichen were collected at each of these plots. The moss samples were usually thick, uniform mats and included the stratified old material (including rhizoids) as well as young material. Lichen samples consisted of small, scattered clumps. Attached organic detritus and extraneous vegetation were removed.

At all three sampling plots per site, living vegetation was removed from the soil surface and a 50-cm-diameter circle was cut into the top 10-15 cm of soil. The organic-rich Oa-horizon was then separated from the underlying AO mineral soil. Material from all three plots was subsequently composited and homogenized to make a single sample. About 1 kg of material was placed in paper soil-sample bags.

## LABORATORY ANALYSIS

Samples of moss and lichen were washed using distilled water, and attached foreign plant material was removed. The washed samples were then dried in a forced-air oven at ambient room temperature. Once dry, the plant samples were ground to minus-10 mesh using a Wiley mill. Each plant sample was divided with one part ashed at 450°C over a 24-hr period and the other part left unashed; ash yield (percent ash) was then calculated. Analytical procedures followed established quality-assurance and quality-control protocols of the USGS laboratories (Arbogast, 1990) and included the analysis of duplicate samples (randomly chosen for 10 percent replication), in-house lichen and moss



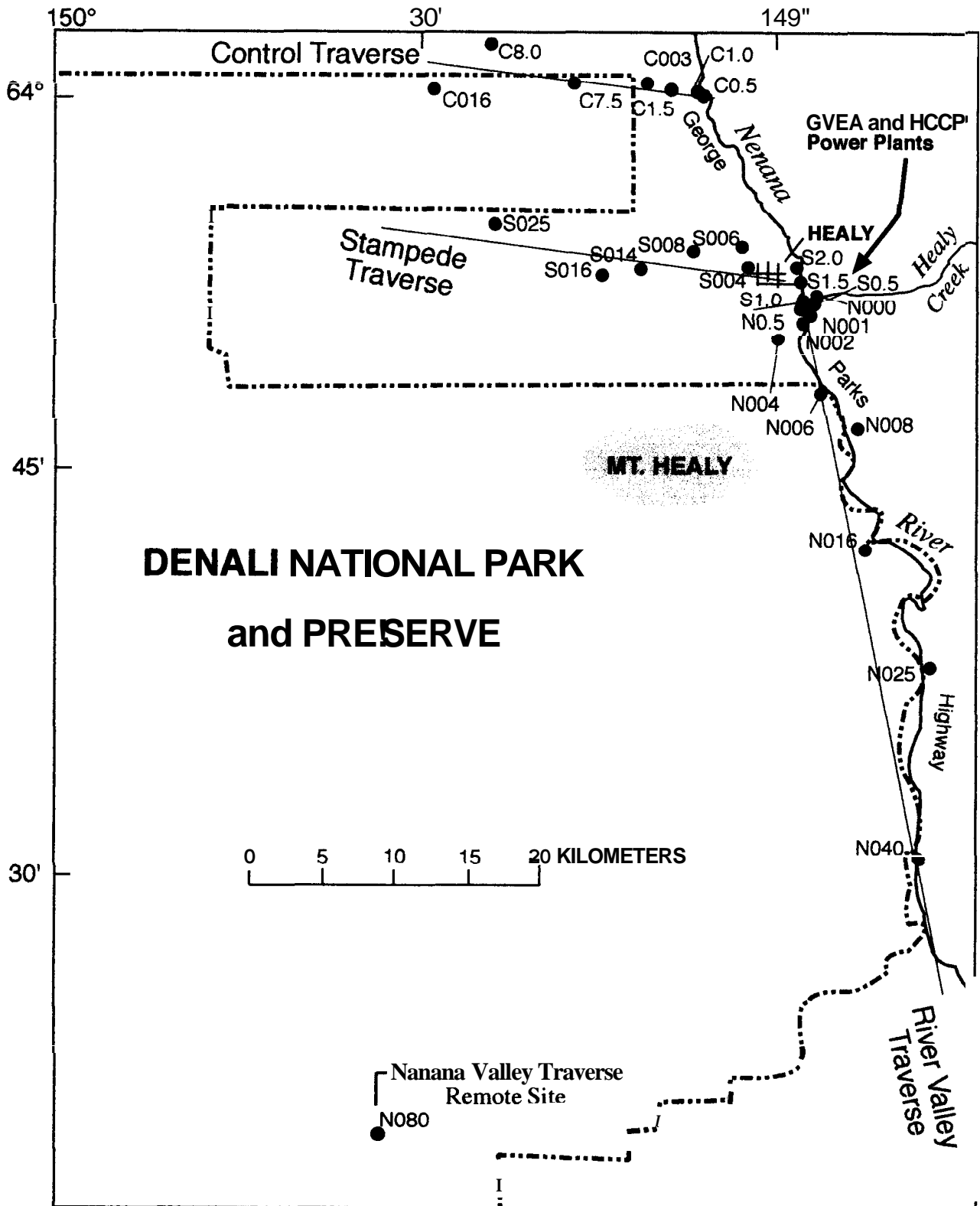


Figure 2. Location of sampling sites in and near Denali National Park and Preserve. Power plants GVEA and HCCP are near the confluence of Healy Creek and the Nenana River.

standards, and National Institute for Standards and Technology, Standard Reference Material (SRM) vegetation standards. All samples and analytical duplicates were submitted for analysis in random order.

Soil samples were dried under forced air at ambient temperature. All of the dry samples were disaggregated using a mechanical ceramic mortar and pestle and then sieved to minus-10 mesh. Sample splits were ground to minus-100 mesh in an agate shatter box, and a split of the material was ashed in a muffle furnace at 450°C; ash yield (percent ash) was then calculated.

One hundred milligrams of the ash were digested with mixed acids. After complete digestion of the ash, major, minor, and trace element concentrations were determined by inductively coupled plasma-atomic emission spectroscopy (ICP-AES) following the methods of Lichte and others (1987) and Arbogast (1990). Total sulfur and mercury were determined directly on a subset of the ground, unashed plant and soil material by combustion infrared detection and cold vapor atomic absorption, respectively (Jackson and others, 1985; Kennedy and Crock, 1987).

## RESULTS

### SPATIAL ELEMENTAL CONCENTRATION VARIABILITY

The total variance in the elemental concentration of sampled materials was partitioned among three sources (using a nested ANOVA design as presented by Miesch, 1976): (1) regional variation—that is, distance away from the GVEA power plant (Stampede and River Valley traverses) or the Nenana River (Control traverse); (2) site variation—that is, variation among plots within a site; and, (3) procedural or laboratory variation.

In general, when elemental concentrations were well above the limit of determination (limit of determination, expressed in parts per million or percent, plus about 10), procedural variance, or the analytical precision ANOVA component, for plant-tissue analyses was usually less than 3 percent (Crock and others, 1992a). In addition, close agreement of our analyses to the SRM's certified values indicate good laboratory analytical accuracy (usually less than 4 percent). The majority of the variation in our data, for most of the elements for both moss and lichen, was associated with distance from the emission source (the regional ANOVA component). The noticeable exceptions are the volatile elements Hg, total S, and Se, which show a greater amount of variation in the within-site ANOVA component. Replicate soil samples were not collected at each site; therefore, an ANOVA for the Oa-horizon soils was not performed.

### TRAVERSE TRENDS

Highly variable ash-yield data for plant tissue used in biomonitoring studies is always troublesome because of the implication that one may be measuring differences in the deposition and entrapment of airborne particles. We have found airborne particle entrapment to be of concern in semiarid environments (Gough and Erdman, 1977; Jackson and others, 1985; Gough and others, 1988a) but not as important in more humid environments (Gough and others, 1988b). Studies have shown fallout-derived particles deeply imbedded in intertwined lichen tissue that were difficult or impossible to remove by standard cleaning procedures (Gough and Erdman, 1977).

Feather moss grows in dense, tangled mats that add vertically to their mass with each growing season. It is possible that entrapped extraneous material in the moss mat was not completely removed through washing. Because ash yields ranged from <4 to 42 percent and <2 to 7.5 percent for moss and lichen, respectively, dust entrapment is possible (values of <10 percent and <5 percent, respectively, are common for noncontaminated samples). Several methods can be used to assess the relative degree of contamination originating from solid particles that might contribute to this variability. These include (1) assessing the absolute concentration of resistate, biologically inert elements, such as Ti and Sc; and (2) examining the relation between the concentration of these elements and ash yield.

Log-linear regression plots of ash yield versus the concentration of Ti, Sc, and Al in moss and lichen tissue from samples collected along the three major traverses were examined. The slopes of the regression lines were positive, and the  $r^2$  values indicate that these relations are strong for all 18 trends (table 1).

These data (table 1) indicate that the highly variable ash yields are probably the result of deeply entrapped soil particles. Because common ash-forming minerals, such as quartz and feldspar, are predominantly composed of the major elements (Ca, Fe, Mg, Na, Si, and Ti), entrapped soil particles would "dilute" the concentration of the trace elements that are of environmental concern. Therefore, entrapped soil particles usually cause an underestimation of the concentration of environmentally important trace elements.

Log-linear regression plots of element concentration versus distance from the GVEA site and the Nenana River (Stampede and River Valley traverses) or from the Nenana River only (Control traverse) were examined based on the data from moss, lichen, and soil samples. These plots are useful in assessing the overall strength of trends using the geometrically spaced sampling-site design. Plots for V and Y are shown in figures 3 and 4, respectively. Inverse trends with coefficients of determination >0.50 are arbitrarily considered important in this study (50 percent of the total vari-

**Table 1.** Coefficients of determination for relations between concentrations of Ti, Sc, and Al in moss and lichen and ash yield along the three major study traverses

Moss			Lichen		
Traverse	Element	$r^2$	Traverse	Element	$r^2$
Control	Ti	0.97	Control	Ti	0.81
	Sc	.80		Sc	.85
	Al	.96		Al	.90
Stampede	Ti	.99	Stampede	Ti	.94
	Sc	.98		Sc	.79
	Al	.99		Al	.94
River Valley	Ti	.83	River Valley	Ti	.83
	Sc	.97		Sc	.88
	Al	.98		Al	.96

ability in the data is being explained by the concentration versus distance trend) and may define emission point-source influences such as the GVEA power plant. Both V and Y have been used as coal-combustion tracers in studies involving coal-fired power plant emissions (Gough and Erdman, 1977; Markert and Weckert, 1989). The trends for V and Y in soil are weak, similar to those seen for most other trace elements examined. In contrast, the trends for V and Y in moss and lichen are strong. In addition, strong trends were found in moss and lichen for the environmentally important elements As, Cr, Cu, Ni, and Pb (Crock and others, 1992a).

#### ELEMENTAL CONCENTRATION BASELINES

Although log-linear plots help assess the relative strength of the concentration versus distance relationships, arithmetic plots of the same data are useful for evaluating the influence of emission point sources in a particular area. The data for Cr, Pb, Ni, and V in moss, lichen, and Oa soil for the Stampede traverse are plotted in figures 5 and 6. Most elements show their highest concentrations close-in to the GVEA power plant/Nenana River area and significantly lower concentrations beyond about 6 km. In addition, the >6-km zone was the area where most values were found at or near the detection limit for the analytical methods used. Because plots for many elements showed trends similar to those in these figures, we define the baseline as the observed range, for each of the three sampled media, for sites beyond 6 km from the GVEA power plant/Nenana River (table 2).

The Control traverse samples have many of the lowest element concentrations for moss, lichen, and soil (table 3; figs. 3, 4). Exceptions are concentrations of Mn, total S, and Zn, as well as the major elements such as Mg and P. For example, concentrations were low along the Control

traverse for Al, As, Cr, Ni, Se, and V (as well as ash yield) in all three sample media, and for Ca, Cu, Fe, La, Pb, and Y for moss and soil (but not lichen). The Control traverse appears to be outside the measurable potential influence of the present GVEA facility. For the Control traverse, observed inverse concentration versus distance trends are thought to result from the influence of airborne dust originating from the Nenana River alluvial plain.

The Stampede traverse crosses the eroded sideslope of the Nenana River and an upland Quaternary pediment (figs. 1, 2). This traverse has the highest overall element concentration levels of all three traverses in all three sample media (table 3); however, these higher concentration levels do not necessarily translate into stronger concentration versus distance trends. Some of these concentration levels appear elevated when compared with values cited in the general moss and lichen literature (Crock and others, 1992a, b), and the traverse trends indicate that the GVEA facility, or the town of Healy in general, or both, are probable sources for some elements.

The River Valley traverse follows the Nenana River. The base of the valley is filled with glacial material mixed with sideslope alluvium. The composition of these alluvial fans is determined by the upslope geological materials (fig. 1). Distance from the GVEA power plant, therefore, may not be the only variable contributing to the trends observed in the data; changes in the soil mineralogy and the geology would influence the local geochemistry. The River Valley traverse has intermediate concentration levels when compared with the data for the Control and Stampede traverses (table 3).

In general, elemental concentrations in samples collected from all three traverses follow the progression lichen < moss < soil. Concentrations of most elements were several times greater in moss than in lichen (table 3), with the notable exception of sulfur, for which moss and lichen

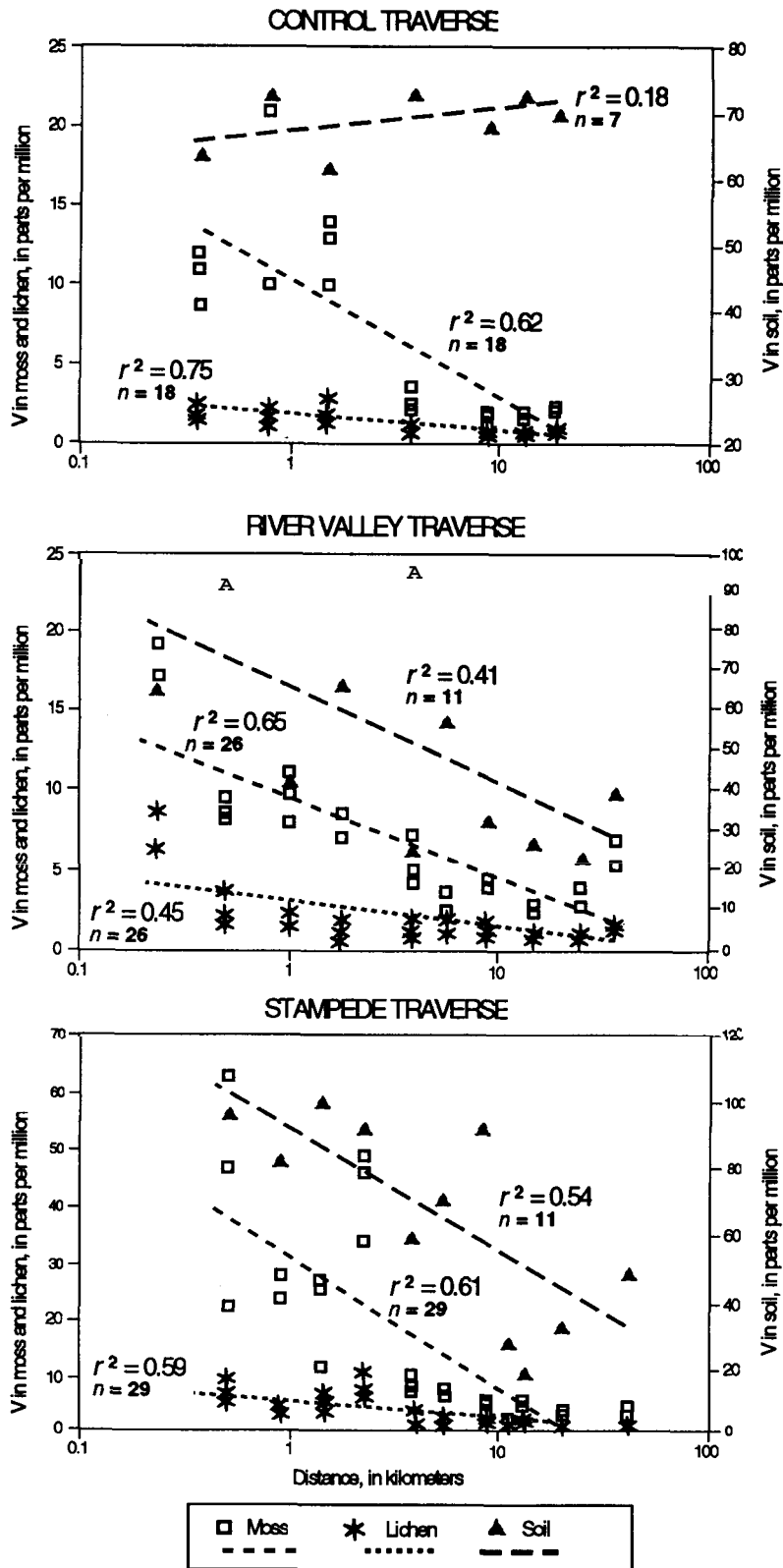


Figure 3. Regression trends for vanadium (V) versus distance (log scale) from the GVEA power plant for moss, lichen, and soil samples along the three major traverses.

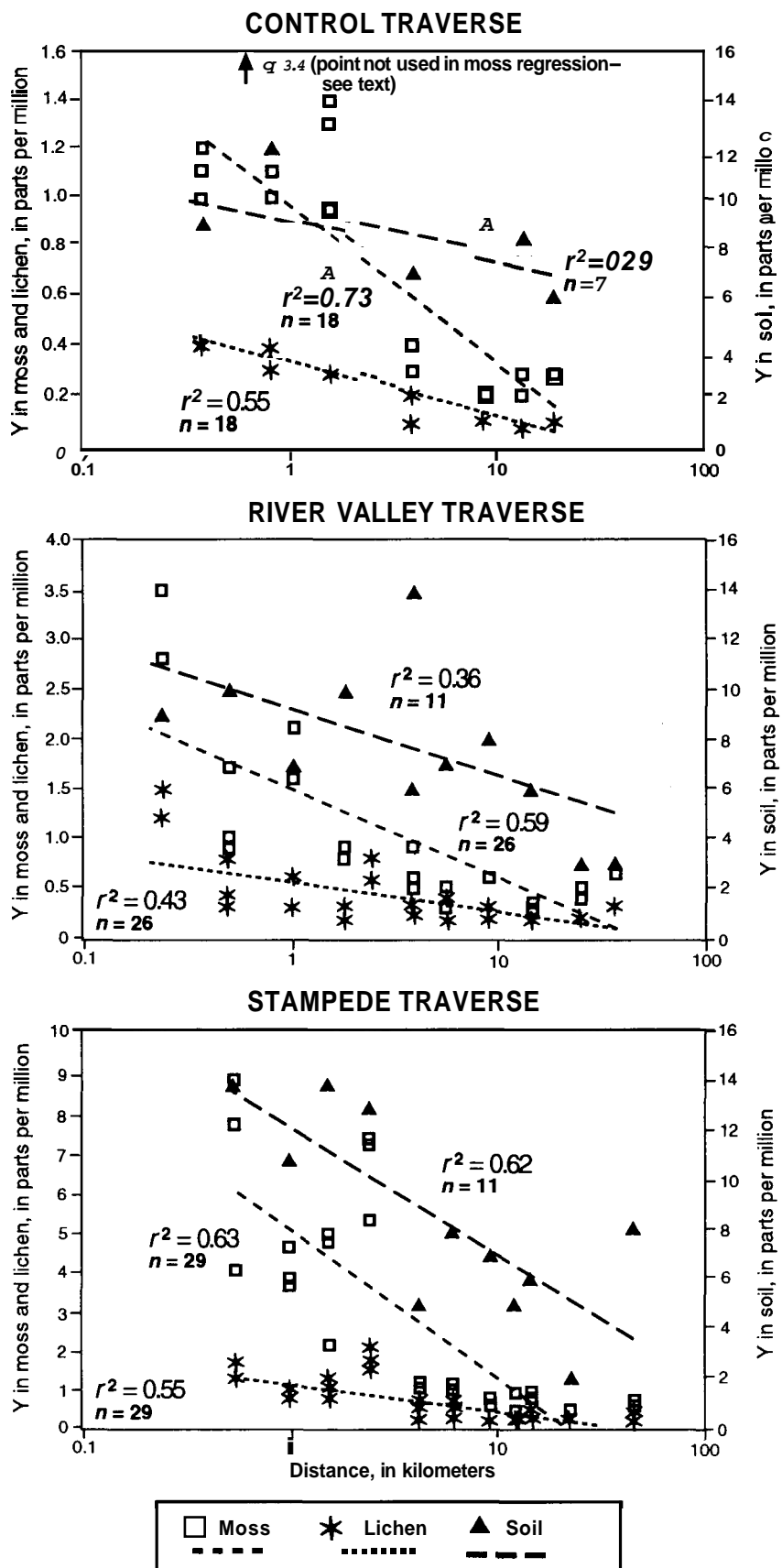


Figure 4. Regression trends for yttrium (Y) versus distance (log scale) from the GVEA power plant for moss, lichen, and soil samples along the three major traverses.

### STAMPEDE TRAVERSE

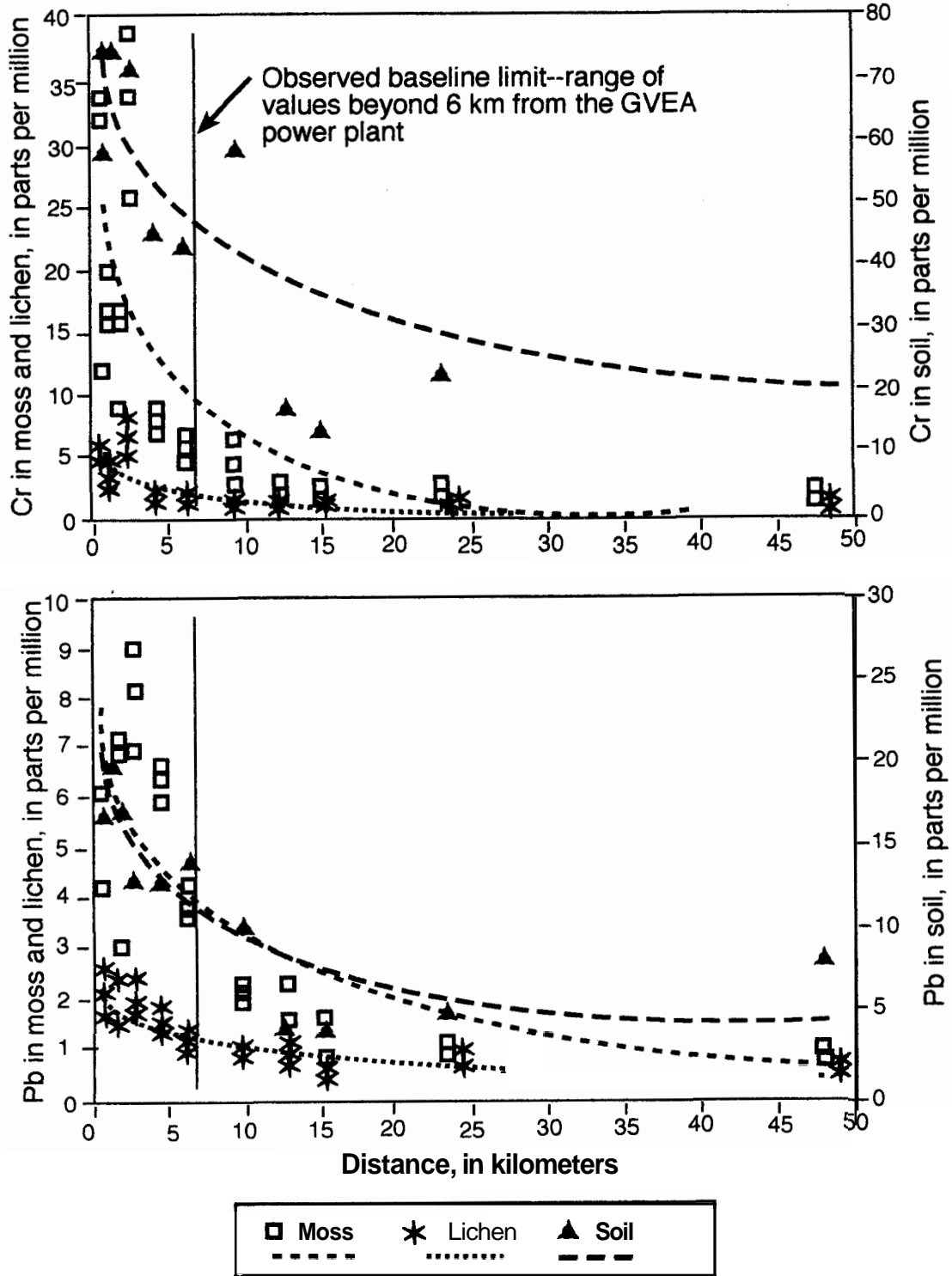


Figure 5. Observed baseline limit for chromium (Cr) and lead (Pb) in moss, lichen, and soil samples for the Stampede traverse.

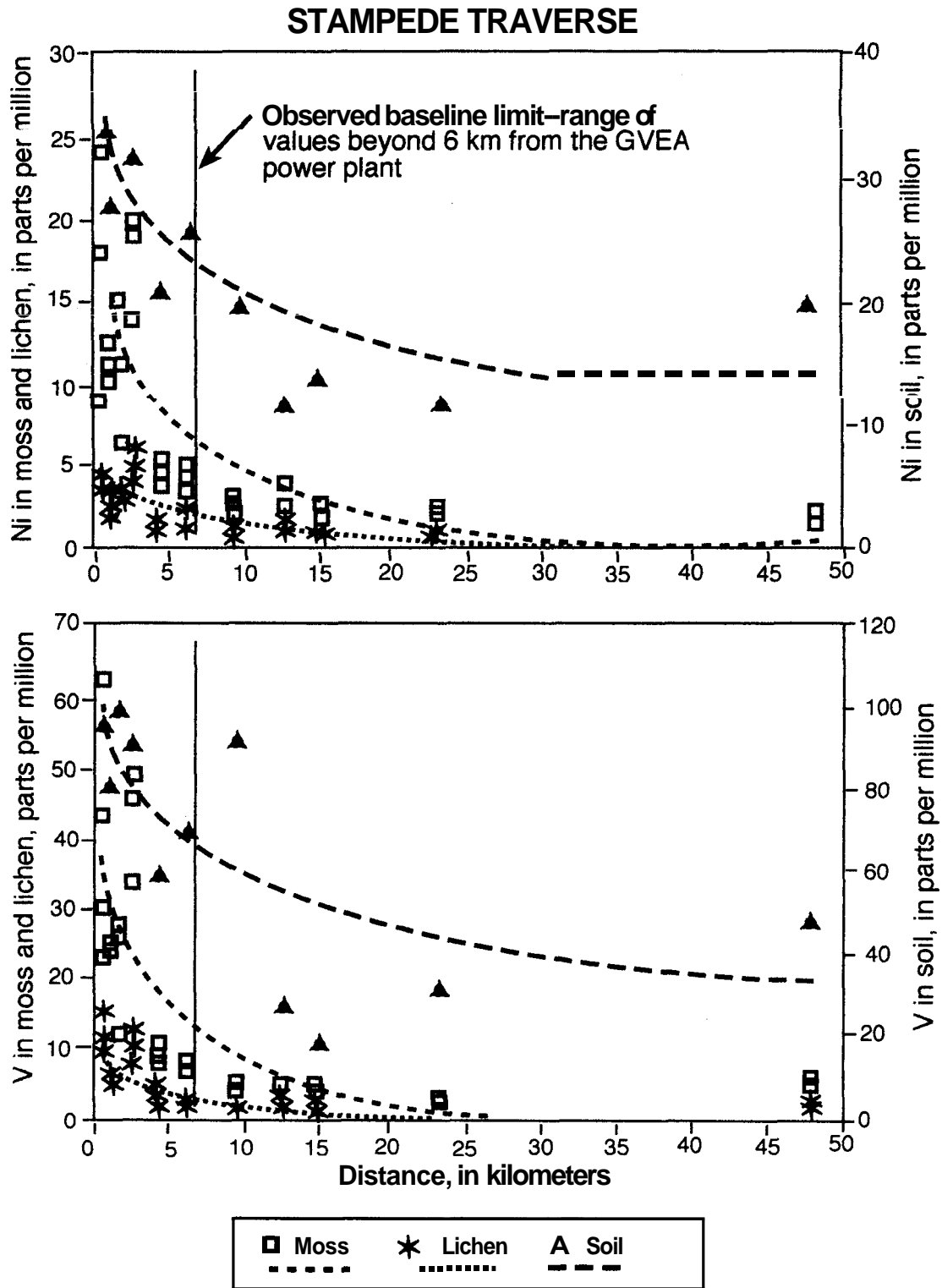


Figure 6. Observed baseline limit for nickel (Ni) and vanadium (V) in moss, lichen, and soil samples for the Stampede traverse.

**Table 2.** Observed baseline range for element concentrations (dry-weight basis) and ash yield for moss, lichen, and Oa-horizon soil, Denali National Park and Preserve, Alaska

Element	Moss (n = 45)		Lichen (n = 45)		Oa-soil (n = 21)	
Al <sup>1</sup>	0.064	- 0.78	0.022	- 0.24	1.2	- 6.0
Ca <sup>1</sup>	.60	- 1.1	.17	- .66	.28	- 3.2
Fe <sup>1</sup>	.048	- .53	.014	- .19	.73	- 4.0
K <sup>1</sup>	.15	- .54	.18	- .95	.27	- 2.2
Mg <sup>1</sup>	.15	- .28	.058	- .20	.15	- .65
Na <sup>1</sup>	.033	- .16	.012	- .045	.13	- .78
P <sup>1</sup>	.069	- .17	.099	- .37	.053	- .18
S <sup>1</sup>	.05	- .10	.08	- .14	.07	- .23
Ti <sup>1</sup>	.003	- .035	.0003	- .008	.034	- .33
As	.1	- 5.6	< .05	- .38	1.1	- 11
Ba	13	- 230	9.0	- 49	21	- 1700
Cd	< .1	- .7	< .1	- .4	< .4	- 1.7
Ce	.4	- 18	< .2	- 7.3	9.0	- 85
Co	.4	- 2.5	.2	- 2.0	5.0	- 19
Cr	.9	- 16	.4	- 3.6	14	- 75
Cu	9.0	- 25	5.0	- 18	10	- 42
Ga	.3	- 2.2	< .2	- .7	3.0	- 16
Hg	.05	- .13	< .02	- .14	.06	- .14
La	.3	- 10	< .1	- 4.1	5.0	- 47
Li	.3	- 5.0	< .1	- 1.0	4.0	- 23
Mn	56	- 1300	32	- 490	69	- 2400
Mo	.7	- 2.8	< .2	- 1.5	< .5	- 4.2
Nd	.4	- 8.2	< .2	- 3.5	6.0	- 37
Ni	1.1	- 9.5	.6	- 5.9	10	- 37
Pb	.7	- 4.7	.2	- 3.3	3.5	- 20
Sc	< .2	- 1.3	< .1	- .4	2.7	- 11
Se	< .03	- .62	< .03	- 0.07	.11	- .49
Sr	37	- 82	11	- 38	36	- 190
Th	< .3	- 2.8	< .2	- 1.5	1.5	- 16
V	1.1	- 20	.4	- 3.9	19	- 120
Y	.2	- 2.5	< .1	- .8	2.2	- 12
Zn	22	- 81	20	- 95	25	- 140
Ash yield <sup>1</sup>	3.36	- 12.6	2.02	- 7.29	14.3	- 85.2

<sup>1</sup> Range given in percent.

concentrations were similar. Concentrations of Mn and total S were elevated in lichen tissue.

Concentrations of the environmentally important elements (including total S) in Oa-horizon soils were found to be close to published values (Crock and others, 1992a, b;

Severson and others, 1992) for identical and similar species. We found no unusually high concentrations of any of the elements, including the rare-earth elements. Many of the element concentration versus distance trends observed for both moss and lichen were similar to those in soil. This



Table 3. Concentration of selected elements in moss, lichen, and Oa soil samples (dry-weight basis) from the three study traverses

Element		Concentration in moss			Concentration in lichen			Concentration in soil		
		Control	River Valley	Stampede	Control	River Valley	Stampede	Control	River Valley	Stampede
Al <sup>1</sup>	<6 km	0.55 (13) <sup>2</sup>	0.61 (18)	1.2 (21)	0.10 (12)	0.15 (17)	0.21 (21)	4.3 (4)	4.5 (8)	5.3 (6)
	>6 km	.12 (6) <sup>2</sup>	.28 (12)	0.20 (13)	.04 (8)	.08 (10)	.05 (13)	3.9 (4)	1.7 (4)	2.5 (6)
Ca <sup>1</sup>	<6 km	.83 (13)	.95 (18)	1.3 (21)	.25 (12)	.30 (17)	.36 (21)	1.0 (4)	1.3 (8)	1.2 (6)
	>6 km	.74 (6)	.81 (12)	.73 (13)	.20 (8)	.08 (10)	.22 (13)	.81 (4)	2.0 (4)	0.49 (6)
Fe <sup>1</sup>	<6 km	.32 (13)	0.36 (18)	.70 (21)	.06 (12)	.09 (17)	.13 (21)	2.1 (4)	2.8 (8)	3.0 (6)
	>6 km	.06 (6)	.15 (12)	.11 (13)	.20 (8)	.04 (10)	.03 (13)	1.8 (4)	1.1 (4)	1.9 (6)
As	<6 km	.72 (13)	.81 (18)	1.7 (21)	.17 (12)	.23 (17)	.39 (21)	7.5 (4)	9.2 (8)	9.2 (6)
	>6 km	.19 (6)	.30 (12)	.23 (13)	.07 (8)	.10 (10)	.11 (13)	5.1 (4)	3.5 (4)	3.8 (6)
Cu	<6 km	17 (13)	22 (18)	25 (21)	12 (12)	11 (17)	12 (21)	23 (4)	33 (8)	28 (6)
	>6 km	14 (6)	14 (12)	16 (13)	6.2 (8)	8.4 (10)	8.2 (13)	23 (4)	21 (4)	18 (6)
La	<6 km	2.8 (13)	3.6 (18)	6.8 (21)	.61 (12)	.97 (17)	1.3 (21)	23 (4)	25 (8)	33 (6)
	>6 km	.45 (6)	.89 (12)	1.0 (13)	.19 (8)	.34 (10)	.37 (13)	22 (4)	7.5 (4)	13 (6)
Mn	<6 km	530 (13)	470 (18)	460 (21)	150 (12)	160 (17)	136 (21)	329 (4)	1300 (8)	543 (6)
	>6 km	520 (6)	360 (12)	470 (13)	170 (8)	125 (10)	166 (13)	341 (4)	990 (4)	315 (6)
Nd	<6 km	2.7 (13)	3.2 (18)	21 (21)	.65 (12)	.87 (17)	1.2 (21)	20 (4)	21 (8)	28 (6)
	>6 km	.63 (6)	1.0 (12)	1.0 (13)	.27 (8)	.43 (10)	.37 (13)	19 (4)	8.2 (4)	12 (6)
S <sup>1</sup>	<6 km	.08 (13)	.10 (18)	.10 (21)	.12 (12)	.14 (17)	.13 (21)	.09 (4)	0.11 (8)	.07 (6)
	>6 km	.08 (6)	.07 (12)	.07 (13)	.10 (8)	.11 (10)	.10 (13)	.11 (4)	.18 (4)	.16 (6)
Zn	<6 km	46 (13)	61 (18)	56 (21)	37 (12)	48 (17)	36 (21)	60 (4)	80 (8)	97 (6)
	>6 km	56 (6)	40 (12)	36 (13)	42 (8)	36 (10)	34 (13)	72 (4)	68 (4)	52 (6)

<sup>1</sup> Concentrations given in percent.<sup>2</sup> Value in parentheses is the number of samples used to calculate the mean.

is to be expected if the soil organic matter is assumed to serve as a sink for the elements that are being transmitted through the atmosphere.

The coal being burned at the GVEA power plant is relatively homogeneous and is low in total S (<0.5 percent) and many of the potentially toxic metals (for example, As <50 ppm, Cr <200 ppm, Pb <40 ppm (dry-weight basis); Crock and others, 1992a). Although a mass-balance study was not performed, analysis of monthly composite coal and fly-ash samples did show that for most elements, including Hg, As, V, Co, Cr, and Cu, the amount being lost to the atmosphere during coal combustion was not great. Elements that probably are being lost in the flue gases include Cd, total S, Ni, Pb, and Zn.

## CONCLUSIONS

The HCCP coal-fired power plant is currently being built adjacent to the existing GVEA power plant at Healy, Alaska. Except for an experimental start-up period, coal to be utilized in the HCCP power plant is the locally mined Miocene subbituminous variety that is generally low in total S (<0.5 percent) and high in ash (~7 percent). This type of coal is also being burned in the GVEA power plant. Compared with coals from the lower 48 States, the Alaska coals are generally high in Cr, V, and Y and in the lanthanide elements (La, Nd, and Yb).

This study assessed the potential role that emissions from GVEA may have on the biological resources of nearby Denali National Park and Preserve (DNA). Objectives were to (1) establish baseline elemental concentration information for a common species of moss and lichen and the organic-rich Oa soil horizon, (2) define current spatial element trends as they may relate to the power-plant emissions, and (3) provide information useful in monitoring long-term landscape biogeochemical changes and in making biological resources management decisions. We hypothesized that observed baselines would include input from both natural geologic and anthropogenic elemental sources, and thus distinguishing between these two types of sources was essential.

Three traverses were established, with two (River Valley and Stampede) radiating from the GVEA facility. The third traverse (Control) progressed westward from the Nenana River and was judged to be generally outside the potential influence of the emission source. Plant and soil samples collected along these traverses were analyzed for >40 trace elements, and patterns of element concentration versus distance from the emission source were evaluated.

Concentrations of elements such as Cr, Pb, Ni, V, and Y in the material sampled close to the emissions source (<6 km) were found to have levels several times greater than material collected farther away. Baseline geochemical and biogeochemical levels were defined as the range of

elemental concentrations observed in material collected greater than 6 km from the GVEA power plant. Concentrations of elements in samples from the Control traverse were generally lower and had a fewer number of inverse concentration versus distance trends than were found in the other two traverses. Whereas each of the materials sampled (moss, lichen, soil) was effective in assessing the zone of influence of the elemental emissions, moss generally proved better than lichen, which in turn was more useful than soil. These data provide a snapshot of current biogeochemical trends and a basis against which future monitoring of geochemical landscape changes can be compared.

Acknowledgments.—This project was funded by the USGS Mineral Resources Program, the National Park Service, the Alaska Industrial Development and Export Authority, and the U.S. Department of Energy. All the chemical analyses were performed in the Denver Laboratories of the U.S. Geological Survey by P.H. Briggs, K.L. Curry, D.L. Fey, G. Gourdin, P.L. Hageman, C.S.E. Papp, and E.P. Welsch. Important field assistance was provided by Wyatt P. Gough, J. Benedict, P. Owen, P. Del Vecchio, H. Chakuchin, S. Carwile, M. Duffy, M.B. Cook, A. Blakesley, and M. Protti. Composite samples of feedstock coal and fly ash were graciously supplied by the GVEA.

## REFERENCES CITED

- Affolter, R.H., Simon, F.O., and Stricker, G.D., 1980, Analysis of coal samples from the Healy, Kenai, Seldovia and Utukok River Quadrangles, Alaska, in Rao, P.D., and Wolff, E.N., eds., Focus on Alaska's coal 1980: Fairbanks, Alaska, University of Alaska Press, p. 236-266.
- Affolter, R.H., Stricker, G.D., Flores, R.M., and Stanley, R.G., 1994, Geochemical evaluation of coal from the Tertiary Usibelli Group, Usibelli Coal Mine, Alaska—one of the lowest sulfur coals mined in the United States, in Rao, P.D., and Walsh, D.E., eds., Focus on Alaska's coal 1993: Fairbanks, Alaska, Mineral Industry Research Laboratory Report No. 94, University of Alaska, p. 167-182.
- Alaska Industrial Development and Export Authority, 1992, Permit application for Air Quality Program—prevention of significant deterioration (PSD) and air quality control—permit to operate, Healy Clean Coal Project, Healy, Alaska: Prepared by Stone and Webster Engineering Corporation, Denver, Colo.
- Arbogast, B.F., ed., 1990, Quality assurance manual for the Branch of Geochemistry, U.S. Geological Survey: U. S. Geological Survey Open-File Report 90-668.
- Beikman, H.M., 1974, Preliminary geologic map of the southeast quadrant of Alaska: U.S. Geological Survey Miscellaneous Field Studies Map MF-612, scale 1500,000.
- Berg, T., Royset, O., and Steinnes, E., 1995, Moss (*Hylocomium splendens*) used as biomonitor of atmospheric trace element deposition—estimation of uptake efficiencies: Atmospheric Environment, v. 29, p. 353-360.
- Berthelsen, B.O., Steinnes, E., Solberg, W., and Jingsen, L., 1995, Heavy metal concentrations in plants in relation to atmo-

- spheric heavy metal deposition: *Journal of Environmental Quality*, v. 24, p. 1018-1026.
- Crock, J.G., Gough, L.P., Mangis, D.R., Curry, K.L., Fey, D.L., Hageman, P.L., and Welsch, E.P., 1992a, Element concentrations and trends for moss, lichen, and surface soils in and near Denali National Park and Preserve, Alaska: U.S. Geological Survey Open-File Report 92-323, 149 p.
- Crock, J.G., Severson, R.C., and Gough, L.P., 1992b, Determining baselines and variability of elements in plants and soils near the Kenai National Wildlife Refuge, Alaska: *Water, Air, and Soil Pollution*, v. 63, p. 253-271.
- Csejtey, Béla, Jr., Mullen, M.W., Cox, D.P., Gilbert, W.G., Yeend, W.E., Smith, T.E., Wahrhaftig, Clyde, Craddock, Campbell, Brewer, W.M., Sherwood, K.W., Hickman, R.G., Stricker, G.D., St. Aubin, D.R., and Goertz, D.J. III, 1986, Geology and geochronology of the Healy Quadrangle, Alaska: U.S. Geological Survey Open-File Report 86-396, 90 p.
- Csejtey, Béla, Jr., Mullen, M.W., Cox, D.P., and Stricker, G.D., 1992, Geology and geochronology of the Healy Quadrangle, south-central Alaska: U.S. Geological Survey Miscellaneous Investigations Map I-1961, scale 1:250,000.
- Godbeer, W.C., Morgan, N.C., and Swaine, D.J., 1981, The use of moss to monitor trace elements: Proceedings of the Seventh International Clean Air Conference, Adelaide, Australia, p. 789-798.
- Gough, L.P., and J.A. Erdman, 1977, Influence of a coal-fired power plant on the element content of *Parmelia chlorochroa*: *The Bryologist*, v. 80, p. 492-501.
- Gough, L.P., Jackson, L.L., and Sacklin, J.A., 1988a, Determining baseline element composition of lichens: II. *Hypogymnia enteromorpha* and *Usnea* spp. at Redwood National Park and Preserve, California: *Water, Air, and Soil Pollution*, v. 38, p. 169-180.
- Gough, L.P., Severson, R.C., and Jackson, L.L., 1988b, Determining baseline element composition of lichens: I. *Parmelia sulcata* at Theodore Roosevelt National Park and Preserve, North Dakota: *Water, Air, and Soil Pollution*, v. 38, p. 157-167.
- Gough, L.P., Severson, R.C., and Shacklette, H.T., 1988c, Element concentrations in soils and other surficial materials of Alaska: U.S. Geological Survey Professional Paper 1458, 53 p.
- Jackson, L.L., Engleman, E.E., and Peard, J.L., 1985, Determination of total sulfur in lichens and plants by combustion-infrared analysis: *Environmental Science and Technology*, v. 19, p. 437-441.
- Kennedy, K.R. and Crock, J.G., 1987, Determination of mercury in geologic materials by continuous flow, cold vapor, atomic absorption spectrophotometry: *Analytical Letters*, v. 20, p. 899-908.
- Lichte, F.E., Golightly, D.W., and Lamothe, P.J., 1987, Inductively coupled plasma-atomic emission spectrometry, *in* Baedecker, P.A., ed., *Methods of geochemical analysis: U.S. Geological Survey Bulletin 1770*, p. B1-B10.
- Markert, B., and Weckert, V., 1989, Use of *Polytrichum formosum* (moss) as a passive biomonitor for heavy metal pollution (cadmium, copper, lead, and zinc): *The Science of the Total Environment*, v. 86, p. 289-294.
- Miesch, A.T., 1976, Geochemical survey of Missouri—methods of sampling, laboratory analysis, and statistical reduction of data: U.S. Geological Survey Professional Paper 954-A, 39 p.
- Nash III, T. J., and Wirth, V., eds., 1988, Lichens, bryophytes, and air quality: Berlin-Stuttgart, J. Cramer, 297 pp.
- Onianwa, P.C., 1988, Monitoring regional gradients in atmospheric heavy metal pollution—a comparative application of top-soil, epiphytic moss and plant litter as indicators: *Environmental Monitoring and Assessment*, v. 11, p. 25-31.
- Péwé, T.L., 1975, Quaternary geology of Alaska: U.S. Geological Survey Professional Paper 835, 145 p.
- Puckett, K. J., 1988, Bryophytes and lichens as monitors of metal deposition, *in* Nash, T. H. and Wirth, V., eds., Lichens, bryophytes, and air quality: Berlin-Stuttgart, J. Cramer, p. 231-268.
- Severson, R.C., Gough, L.P., and van den Boom, G., 1992, Baseline element concentrations in soils and plants, Wattenmeyer National Park and Preserve, North and East Frisian Islands, Federal Republic of Germany: *Water, Air, and Soil Pollution*, v. 61, p. 169-184.
- Swanson, V.E., Medlin, J.H., Hatch, J.R., Coleman, S. L., Wood, G.H., Woodruff, S.D., and Hildebrand, R.T., 1976, Collection, chemical analysis, and evaluation of coal samples in 1975: U.S. Geological Survey Open-File Report 76-468, 21 p.
- Treshow, M., and Anderson, F.K., 1989, Plant stress from air pollution: New York, John Wiley, 283 pp.
- Van Cleve, K., Dyrness, C.T., Viereck, L.A., Fox, J., Chapin, F.S., and Oechel, W., 1983, Taiga ecosystems in interior Alaska: *BioScience*, v. 33, p. 39-44.
- Viereck, L.A., Dyrness, C.T., and Batten, A.R., 1986, The 1986 revision of the Alaska vegetation classification: Institute of Northern Forestry, U.S. Department of Agriculture, Forestry Service and The University of Alaska Museum, Fairbanks, Alaska, Draft Technical Paper, final revision in print.
- Wahrhaftig, C., 1987, The Cenozoic section at Suntrana, Alaska, *in* Hill, M.L., ed., Cordilleran section of the Geological Society of America, Decade of North American Geology Project series, Geological Society of America, v. 1, p. 263-268.
- Wahrhaftig, C., Bartsch-Winkler, S., and Stricker, G.D., 1994, Coal in Alaska, *in* Plafker, G., and Berg, H.C., eds., The geology of Alaska: Boulder, Colo., Geological Society of America, The Geology of North America, v. G-1, p. 937-978.

Reviewers: Bill Miller and Ronald Severson

# Preliminary Evaluation of Emergent Postglacial Shorelines, Naknek and Iliamna Lakes, Southwestern Alaska

By Darrell S. Kaufman and Karen B. Stilwell

## ABSTRACT

Following late Wisconsin deglaciation of the Iliamna Lake and Naknek Lake basins, lowered lake levels created a flight of beach ridges and wave-cut terraces rimming the present-day lakes. Terraces at nearly identical altitudes above Iliamna Lake (at about 10, 25, 30, and 40 m above the present-day lake) and separated by over 70 km north-east to southwest indicate that there has been little if any tilting in this direction as a result of differential glacio-isostatic rebound or regional tectonism. Likewise, at Naknek Lake, the consistent altitudes of terraces at about 5, 15, and 30 m and separated by a maximum of 50 km southeast to northwest suggest that these shorelines are also horizontal, or nearly so. The most prominent terraces above both lakes lie about halfway between the highest terrace and the present-day lake level (24 m above Iliamna Lake and 15 m above Naknek Lake). If these terraces are correlative, then this correlation indicates some common control on lake-level fluctuations such as base level or climate. On the other hand, Iliamna Lake shows five terraces and Naknek Lake only three, suggesting that other factors, including different histories of outlet erosion, played a role in lake-level changes at the two lakes.

The 24-m terrace and higher terraces at Iliamna Lake and all three terraces at Naknek Lake were formed during latest Wisconsin and early Holocene time. The 40-m terrace at Iliamna Lake was probably cut during the Newhalen stade of the Brooks Lake glaciation. The 30-m terrace, and all higher terraces, are older than a prominent, pinkish-orange tephra, which is correlated by major element chemistry with the Lethe tephra, whose previously published  $^{14}\text{C}$  age is about 12.6 ka. Based on previously published  $^{14}\text{C}$  ages, the 24- and 17-m terraces at Iliamna Lake apparently formed at 8.5 and 5.5 ka, respectively. Lake level at Naknek Lake fell below about 9 m above present lake level before 7.4 ka and after the late-glacial Iliuk stade of the Brooks Lake glaciation.

## INTRODUCTION

Lakes along the northern Alaska Peninsula occupy troughs sculpted by glacier ice that flowed from east to

west and are dammed by end moraines of late Wisconsin age (fig. 1). Iliamna and Naknek are two of the largest lakes on the peninsula (125 km and 60 km in length, respectively); Iliamna Lake is larger than any lake in the United States with the exception of the Great Lakes. Following deglaciation of the lake basins, lake levels fluctuated, creating a flight of wave-cut terraces and beach ridges. The terraces are well preserved and in places are laterally traceable for tens of kilometers (fig. 2). They provide outstanding datums that can be used to assess the magnitude and direction of postglacial basin tilting. Such tilting may have occurred in response to tectonic forces or to postglacial isostatic rebound as a result of glacial unloading from the east, where ice was thickest.

Lake shorelines and terraces generally record lake-level stabilization for extended intervals followed by rapid lake-level change. Within open basins, such as present-day Iliamna and Naknek Lakes, shoreline features record intervals of lake-level stability during overall regression. Within closed or semiclosed basins, on the other hand, shoreline features form during both transgressive and regressive phases. Differentiating between these alternatives is often difficult and relies on accurate interpretations of sufficiently well-exposed stratigraphic relations. For example, at the east end of Iliamna Lake (fig. 1), Detterman and Reed (1973) described transgressive sand overlying a buried soil in a terrace at about 18 m above lake level. If their interpretation of the origin of this deposit is correct, then Iliamna Lake experienced a lake-level rise at a time either when its outlet was too small to accommodate the rising outflow or when the outlet altitude was higher than the lake level.

Lake-level transgressions, such as that interpreted by Detterman and Reed (1973), are typically controlled by climatic changes or by capture of inflows. Lake-level regressions, on the other hand, may or may not reflect climate forcing. Regressive shoreline features in an open basin typically record intervals of threshold stability followed by rapid outlet incision. The cause of episodic incision might be (1) climatic change leading to increased discharge and consequent accelerated incision, (2) base-level change resulting from tectonic or isostatic forces, (3) variability in the strength of the outlet constriction, or (4) some combination of these. If incisions are controlled by a common,

regionally synchronous mechanism, such as climatic or tectonic forces, then all lakes within the affected region should behave synchronously, possibly with similar amplitudes of change. Likewise, if the forcing is regional and episodic, then broader and more extensive terraces should form at all lakes during extended periods of stability compared with those that form during shorter intervals of lake-level stabilization. On the other hand, if the history of outlet incision is chaotic, with lake-level lowering in response to some variation in the stratigraphic or lateral strength of confining dams, then the lake-level fluctuations would not be expected to be in phase.

Our study expands upon previous work that established the altitudes of shorelines at a few sites around Iliamna (Detterman and Reed, 1973) and Naknek (Riehle and Detterman, 1993) Lakes. It is a preliminary effort to (1) determine whether the shorelines have been tilted, and if so, the amount and direction of deformation; and (2) limit the ages of the shorelines. More in-depth studies are needed

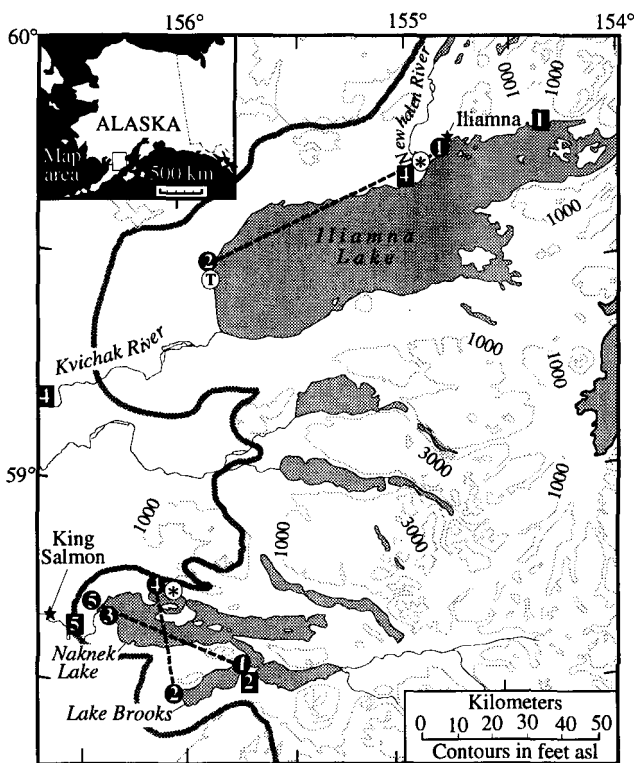
to fully understand the ages and physiography of the lake terraces. Although our study does not unequivocally resolve the mechanism of lake-level change at Iliamna and Naknek Lakes, it provides a reference for future studies aimed at evaluating such changes at other lakes along the Alaska Peninsula.

Iliamna Lake attained its maximum depth following retreat of the Iliamna lobe from its maximum late Wisconsin position (Kvichak stade of the Brooks Lake glaciation; table 1). At its highstand, the lake was about 20 percent larger than present and formed a shoreline about 45 m above the present-day lake level, which is about 14 m above sea level (asl) (Detterman and Reed, 1973). Below this level, Detterman and Reed (1973) identified four major terrace levels, at 12, 24, 30, and 39 m above the present-day lake level, which are well preserved on the west side of the Newhalen River near its mouth (fig. 2A). Less extensive terraces are developed at 17 and 36 m above the present-day lake level. The 12- and 24-m terraces are the broadest and most continuous, typically 0.3-0.9 km wide but locally as much as 1.5 km wide. Detterman and Reed (1973) suggested that the terraces may be tilted down to the southwest in response to isostatic adjustment following deglaciation. They presented no data, however, to assess this possibility, other than their inference, based on interpretation of aerial photographs, that the lake outlet has migrated southward.

At one site at Naknek Lake, Riehle and Detterman (1993) measured three approximately evenly spaced terraces, at 5, 15, and 30 m above present-day lake level (10 m asl). Naknek Lake apparently attained its highest stand sometime following late Wisconsin deglaciation of the basin. At this time, and during its subsequent lowering and stabilization to 15 m above present-lake level, Naknek Lake was connected with Lake Brooks. Once the lake level dropped below 9 m above the present-day level, the two lakes became separated (Dumond, 1981). Presently, Brooks Lake drains northeastward into Naknek Lake, whereas during glacial times it flowed southwestward (Stilwell, 1995).

## METHODS

Spot altitudes were measured at terrace shoreline angles (break in slope at back, wave-cut edge of terrace) using a digital barometric altimeter precise to 0.1 m. Lake level in 1994 was used as a datum. To account for the effects of barometric changes, base stations were reoccupied frequently and altitudes were corrected by linear interpolation between calibration points. The accuracy of measurements is a function of (1) the number of readings on a terrace, (2) the rate of change of barometric pressure, and (3) the length of time between measurements and calibrations. At 14 of the 17 terraces measured, repeat measurements varied by  $\pm 1$  m or less (table 2). At the remaining three terraces, the



**Figure 1.** Northern Alaska Peninsula showing locations of shoreline-altitude measurement sites (numbers in solid circles) and  $^{14}\text{C}$  collection sites (numbers in solid squares) at Iliamna and Naknek Lakes. Shoreline-altitude site numbers refer to those listed in table 2 and shown on transects in figure 3. Radiocarbon site numbers refer to those in table 3. T indicates location of tephra discussed in text. Asterisks indicate locations of terrace altitudes measured by Detterman and Reed (1973) at Iliamna Lake and by Riehle and Detterman (1993) at Naknek Lake. Gray line delimits termini of late Wisconsin glaciers.

range was 3 to 6 m. No attempt was made to estimate the error associated with each terrace altitude. Instead, we use a conservative estimate of  $\pm 2$  m as the error in altitude for all terraces. This value is nearly four times larger than the average range of repeated measurements made at 17 sites. Shoreline altitudes above Iliamna Lake were measured at two localities (fig. 1), and a topographic profile was measured at one (site 2). At Naknek Lake, shorelines were measured at five sites (fig. 1).

## TERRACE PHYSIOGRAPHY

We identified three prominent terraces at Iliamna Lake near the village of Iliamna (fig. 1, site 1), designated here as terraces IL-1, IL-2, and IL-3 (fig. 3; table 2). The lowest terrace is 12 m above the lake, an intermediate terrace is at 27 m, and the highest is at 39 m. (Hereafter, all altitudes are relative to present-day lake level and are considered accurate to within  $\pm 2$  m.) Near the northwest corner of Iliamna Lake (site 2), we identified five terraces, at 8, 24,

31, 35, and 41 m, designated as terraces IL-4 through IL-8, respectively. Of the eight terraces that we measured, six overlap with the altitudes of Detterman and Reed (1973), but the other two (IL-4 and IL-7, at 8 and 35 m, respectively) are at significantly different altitudes. The highest terraces measured were IL-3 (39 m) and IL-8 (41 m) at sites 1 and 2, respectively. At site 2, the 24-m terrace (IL-5) is approximately 120 m wide and is the broadest terrace; the 8-m terrace (IL-4) is 75 m wide (fig. 4). The widest terrace at site 1 is the 27-m terrace, although its width was not measured on the ground. All terrace widths vary laterally.

The mean altitudes of the highest terraces, IL-3 (39 m) at site 1 and IL-8 (41 m) at site 2, overlap within the measurement uncertainty, suggesting that these terraces form a single horizontal, or nearly horizontal, surface extending more than 70 km from northeast to southwest (fig. 3). This correlation is strengthened by the observation that both are the highest terraces cut onto drift of the Iliamna stage. Implicit in this correlation is the assumption that lower, presumably younger terraces are horizontal, or nearly hori-



**Figure 2.** Lake terraces and beach ridges. A, Vertical aerial photograph of the mouth of the Newhalen River, north side of Iliamna Lake. B, View to east of western end (outlet) of Naknek Lake; shoreline angles highlighted by dashed lines; spruce trees are 2-4 m tall.

zontal, as well. Therefore, the prominent IL-2 terrace (27 m) at site 1 should correspond to the broad IL-5 terrace (24 m) at site 2. Likewise, the IL-1 terrace (12 m), the lowest terrace at site 1, should correlate with the IL-4 terrace (8 m), the lowest at site 2. Although the mean altitudes for the lower terraces are 3-4 m lower at site 2 at the western end of the lake compared with site 1, we cannot differentiate them within our measurement uncertainty. The mean altitude of the highest terrace shows the opposite trend (higher to the west), although 2 m of down-to-the-southwest tilting is permissible within the  $\pm 2$  m uncertainty. Assuming that the highest, oldest terrace has been tilted at least as much and in the same direction as younger, lower terraces, and using a measurement uncertainty of  $\pm 2$  m, we may conclude that the terraces are either horizontal or, if they are tilted, then they are tilted downward to the southwest by no more than a few meters over the 70 km that separates the two sites.

At Naknek Lake, three distinct terrace levels are present, at 6, 15, and 31 m (fig. 3; table 2). These altitudes overlap within the measurement uncertainty with those reported by Riehle and Detterman (1993). The most prominent terrace, with the greatest width and most widespread distribution,

was found at 14 to 15 m at all sites. The lowest terrace at 6 m is present at the western end of *Iliuk Arm* (site 1; NL-1) and was also reported from the northwestern side of the lake, near site 4 (Riehle and Detterman, 1993).

The altitudes of the highest measured terraces at Naknek Lake (NL-3, 30 m; NL-6, 29 m; and NL-8, 31 m) average 30 m and overlap within  $\pm 2$  m, implying that these terraces form a single, roughly horizontal surface that extends more than 50 km northwest to southeast and, when including measurements made by Riehle and Detterman (1993), across 35 km from north to south (fig. 3). Similarly, the altitudes of the intermediate terraces (NL-2, 14 m; NL-4, 15 m; NL-5, 14 m; NL-7, 15 m; and NL-9, 15 m) average 15 m, overlap within  $\pm 2$  m, and suggest a consistent shoreline that has not been tilted by more than 4 m across 35 km from north to south or 50 km southeast to northwest (fig. 3).

The difference in the thickness of late Wisconsin glacier ice between the eastern, upglacier and western, terminal ends of both the Naknek Lake and Iliamna Lake basins should have led to a significant difference in isostatic loading and, therefore, in postglacial rebound and consequent shoreline tilting. Mann and Peteet (1994) recently calcu-

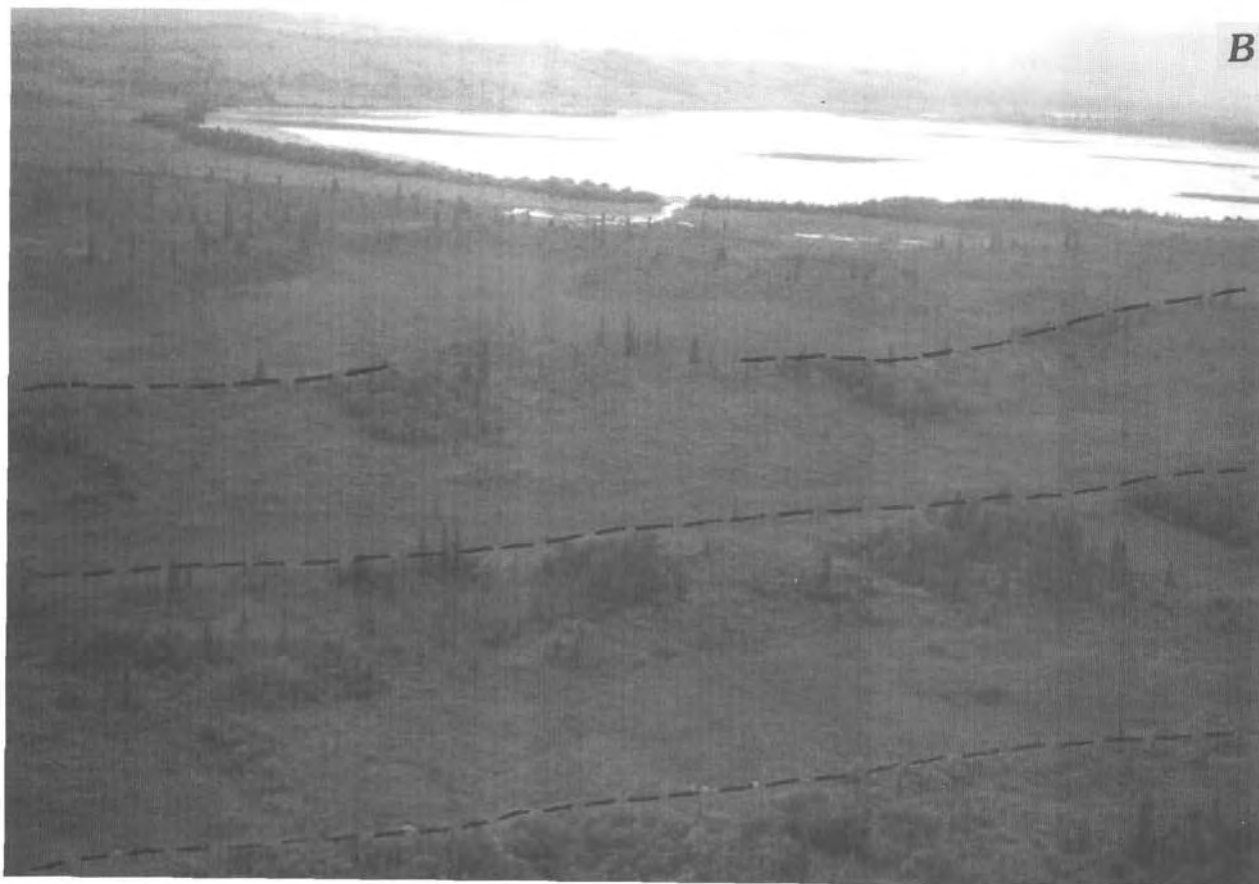


Figure 2. Continued.

Table 1. Geochronologic and climatologic units used in this report

[Climate units (glaciation and stade) are used informally for consistency with previous literature addressing the Brooks Lake glaciation]

Age (ka)	Epoch	Glaciation	Stade	Reference
0-10	Holocene			
26-10	late Pleistocene	Brooks Lake	Ukak Iliuk Newhalen Iliamna Kvichak	Pinney and Begét, 1991b Muller, 1952 Detterman and Reed, 1973 Detterman and Reed, 1973 Detterman and Reed, 1973

Table 2 Terrace altitudes measured at Iliamna and Naknek lakes

Site (fig. 1)	Terrace (fig. 3)	Altitude (m above lake level)		
		Range	Mean	N <sup>1</sup>
Iliamna Lake				
1	IL-1	12 - 12	12	2
1	IL-2	27 - 27	27	2
1	IL-3	38 - 41	39	3
2	IL-4	8 - 8	8	2
2	IL-5	24 - 25	24	3
2	IL-6	31 - 31	31	2
2	IL-7	35 - 35	35	2
2	IL-8	40 - 42	41	2
Naknek Lake				
1	NL-1	5 - 6	6	2
1	NL-2	11 - 16	14	8
1	NL-3	27 - 33	30	4
2	NL-4	14 - 16	15	2
3	NL-5	14 - 14	14	2
3	NL-6	29 - 29	29	2
4	NL-7	15 - 15	15	2
4	NL-8	31 - 31	31	2
5	NL-9	15 - 16	15	3

<sup>1</sup>Number of altitude measurements at terrace.

lated ice-surface profiles for these glaciers. Their reconstructions show glacier thicknesses of about 800 m at the eastern end of the lake basins, with ice surfaces that slope westward at about 4 m/km to the glacier termini. These reconstructions agree with our observations of the altitudes and gradients of lateral moraines and ice-marginal drainages on valley walls above Iliamna and Naknek Lakes

(Stilwell, 1995). Based on the simple assumption that the amount of isostatic depression caused by glacial loading was proportional to the ratio between the density of ice and underlying crust (about 0.3), elastic rebound should have resulted in differential uplift of about 1 m/km, which is typical for tilted postglacial shorelines (Andrews, 1975). Thus, we expected shorelines at the eastern ends of the Iliamna Lake and Naknek Lake basins to be tens of meters higher than correlative ones at the western ends. Instead, the shorelines are either horizontal in the direction of the transects or, if they are tilted, then their gradient is an order of magnitude lower than expected. This suggests that one or more of the following occurred: (1) Restrained rebound (elastic isostatic recovery that occurred while the area was still glaciated but under a diminishing ice load) allowed the basin to rebound before the shorelines were cut. (2) Ice advanced to the western ends of the basins too rapidly to establish full isostatic depression. (3) The ice load was more evenly distributed (lower surface slope and thinner) than expected, perhaps because the shear stress at the base of the glaciers was low. (4) The difference in the amount of depression was less than expected, perhaps reflecting atypical crustal rheology.

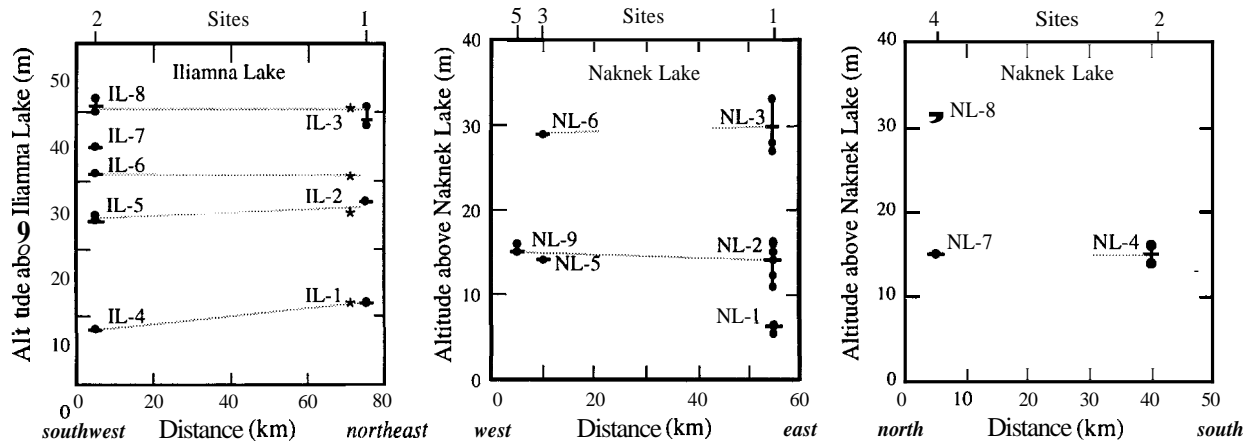
## GEOCHRONOLOGY

We constrained the ages of terraces surrounding Iliamna and Naknek lakes using <sup>14</sup>C dates (table 3), stratigraphic relationships, and tephrochronology. Together, the age evidence indicates that the terraces were formed during latest Wisconsin and early Holocene time (fig. 5). At its highest stand of 45 m above present-day lake level, Iliamna Lake was impounded by the prominent terminal moraine located 37 km downstream of the present outlet of Iliamna Lake. This moraine comprises the type drift of the Kvichak stade, the oldest phase of the Brooks Lake glaciation (Detterman and Reed, 1973). Peat that underlies **outwash gravel asso-**



ciated with the Kvichak moraine approximately 15 km downstream of the moraine along the Kvichak River (table 3, site 4) provides a maximum limiting age of  $26,155 \pm 285$  yr B.P. (all ages are in  $^{14}\text{C}$  years) on the highest terrace and, therefore, on all younger terraces (Stilwell and Kaufman, 1996). Following the retreat of the Kvichak stage glacier, the level of ancestral Iliamna Lake appears to have fallen below 31 m, enabling beach gravel, now exposed in bluffs at the west end of the lake, to **infill** the distal portion of the basin (Stilwell and Kaufman, 1996). The glacier

the northwestern shore (fig. 1, site T). Based on major element chemistry of glass shards (table 4), we correlate the tephra with the Lethe tephra of Pinney and **Begét (1991a)** (similarity coefficient = 0.96), which has been  $^{14}\text{C}$  dated at about 12.6 ka. The tephra at Iliamna Lake was found in massive sand at about  $28 \pm 3$  m above lake level. (Altitudes within the section were measured by locating vertical distances (eye-heights) against the bluff face using a hand-held level, and they are probably accurate to within  $\pm 10$  percent.) The tephra lies 10 cm above a planer contact cut

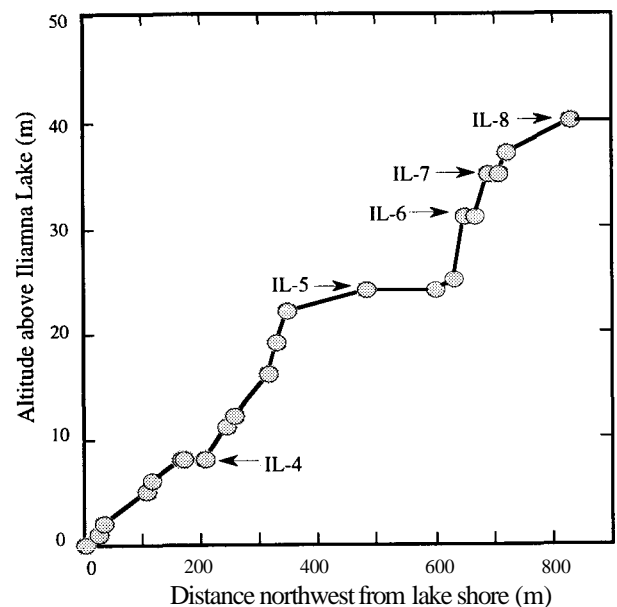


**Figure 3.** Lake-terrace altitudes measured at seven sites at Iliamna and Naknek Lakes plotted along three transects. Lines connect terraces at similar altitudes. Asterisks denote altitudes of terraces measured by Detterman and Reed (1973) west of Newhalen River (fig. 1) and by Riehle and Detterman (1993) near our site 4 on the north shore of Naknek Lake. Circles represent individual readings, some of which overlap; horizontal lines are averages of repeat readings on a terrace; and vertical lines span range of readings on a terrace.

then readvanced, depositing **outwash** and till of the Iliamna stage. The end moraine of the Iliamna stage presently encloses Iliamna Lake.

The next lower terrace (IL-3; 39 m) is notched into drift of the Iliamna stage at its type locality near the northeast corner of the lake. The length of time separating the formation of this terrace from the older, 45-m terrace is not known. Based on correlations with other moraine sequences in Alaska whose ages are more closely constrained, however, it appears that the **Iliamna** stage was complete prior to about 14 ka (Stilwell and Kaufman, 1996). The 39-m terrace would have been cut sometime after, perhaps during the Newhalen stage. This age assignment is based on an interpretation of 1:63,360-scale aerial photographs that show an **outwash** plain headed against the type Newhalen stage moraine and graded to a hanging delta 4.5 km northeast of the village of Iliamna. The delta, in **turn**, is graded to the 39-m terrace, thus tying it to the Newhalen stage, which is thought to be younger than about 14 ka (Stilwell and Kaufman, 1996).

The age of the next lower, relatively extensive terrace (IL-6; 31 m) at Iliamna Lake is constrained by a distinctive pinkish-orange tephra exposed in the high lake bluffs along



**Figure 4.** Topographic profile of terraces above Iliamna Lake at site 2 (fig. 1). Uncertainty in measurements is contained within plot symbol. Vertical exaggeration,  $\times 19$ .

Table 3. Radiocarbon ages that bear on the timing of lake-terrace formation at Iliamna and Naknek Lakes

Site (fig.1)	Age (yr B.P.)	Lab ID	Material	Stratigraphic position	Reference
1	5,520 ± 250	W-2147	Twigs, grass, and seed pods	From 17-m lake terrace	Detterman and Reed, 1973
2	7,360 ± 250	I-1160	Charcoal	From surface	Dumond, 1981
3	8,250 ± 350	W-1479	Organic matter	3.4 m below surface of 24-m terrace	Detterman and others, 1965
4	26,155 ± 285	AA-15092	Plant macrofossils	Underlies outwash associated with Kvichak moraine	Stilwell and Kaufman, 1996
5	26,570 ± 320	Beta-39578	Peat	Underlies outwash associated with Naknek moraine	Mann and Peteet, 1994

into till of the **Iliamna** stade, which we infer was eroded in a few meters of water depth when the lake level stabilized at **31** m. Although the depositional environment of the enclosing sand is equivocal, we suggest that the tephra was erupted after Iliamna Lake fell below **31** m, during an interval of eolian-sand aggradation.

Two previously published  $^{14}\text{C}$  ages from lower terraces at **Iliamna** Lake provide additional chronological con-

trol (Detterman and others, **1965**; Detterman and Reed, **1973**). An age of **8,250±350** yr **B.P.** (table 3, site 3) was determined on fine-grained organic matter contained in poorly stratified silt and sand thought to be of lacustrine origin (Detterman and others, **1965**). The sample was collected **3.4** m below the surface of a **24-m** terrace and apparently dates to the time that the lake occupied this level. Similarly, twigs, grass, and seed pods collected **30** cm be-

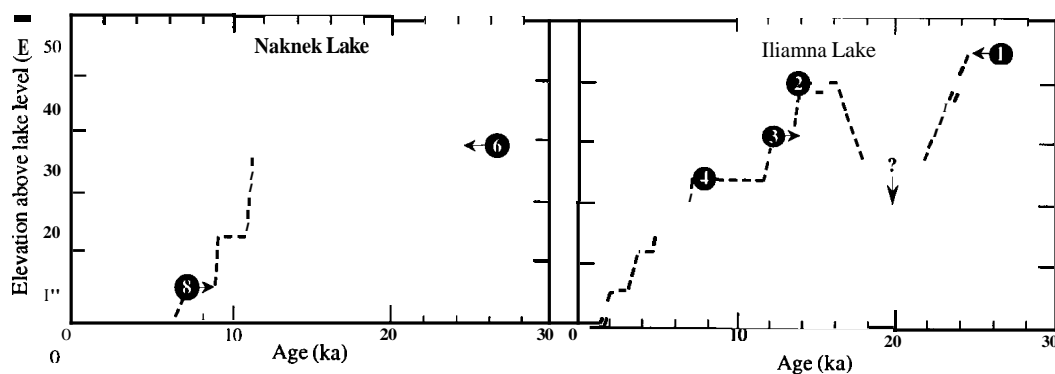


Figure 5. Hydrographs summarizing altitude and ages of terraces at Iliamna and Naknek Lakes. Left- and right-pointing arrows indicate maximum and minimum ages, respectively; down-pointing arrow indicates lake-level lowering between Kvichak and Iliamna stades. Circles lacking an arrow reflect ages that are thought to coincide closely with terrace formation. Geochronological control as follows: (1)  $^{14}\text{C}$  age (table 3, site 4; Stilwell and Kaufman, 1996) on peat underlying **outwash** associated with the Kvichak moraine; (2) age of hanging delta graded to 39-m shoreline and ascribed to the Newhalen stade, inferred (Stilwell and Kaufman, 1996) to have occurred after about 14 ka; (3)  $^{14}\text{C}$  age (Pinney and **Begét**, 1991a) of Lethe tephra, correlated by major element geochemistry (table 4) with the tephra deposited on the 30-m terrace (fig. 1,  $^{14}\text{C}$  site 1); (4)  $^{14}\text{C}$  age (table 3, site 3; Detterman and others, 1965) on organic matter from lacustrine deposits from a 24-m terrace; (5)  $^{14}\text{C}$  age (table 3, site 1; Detterman and Reed, 1973) on detrital organic matter from a 17-m terrace; (6)  $^{14}\text{C}$  age (table 3, site 5; Mann and Peteet, 1994) on peat underlying **outwash** associated with the Naknek moraine; (7)  $^{14}\text{C}$  ages (Pinney and **Begét**, 1991b) that limit the deposition of the Iliuk stade moraine, which is notched by the 30- and 15-m terraces; and (8)  $^{14}\text{C}$  age (table 3, site 2; Dumond, 1981) on charcoal from the 6-m terrace.

Table 4. Major element chemistry of glass separates of pinkish-orange tephra collected 28 m above lake level at northwest corner of Iliamna Lake (fig. 1,  $^{14}\text{C}$  site 1)

[Microprobe analyses performed by C. Meyer (U.S. Geological Survey)]

	Na <sub>2</sub> O	MgO	Al <sub>2</sub> O <sub>3</sub>	SiO <sub>2</sub>	K <sub>2</sub> O	CaO	TiO <sub>2</sub>	MnO	FeO	Total
Pinkish-orange tephra, Iliamna Lake										
Mean	4.44	0.65	13.80	71.37	2.43	2.35	0.62	0.07	2.84	98.57
1 $\sigma$	0.11	0.07	0.30	0.91	0.11	0.23	0.08	0.03	0.23	N = 18 <sup>1</sup>
Distal Lethe tephra analyzed by Pinney and <b>Begét (1991a)</b>										
Mean	4.31	0.70	13.88	72.37	2.34	2.56	0.62	nd	3.07	99.85
$\pm 1\sigma$	0.14	0.04	0.13	0.30	0.06	0.09	0.05	--	0.13	N = 16 <sup>1</sup>

<sup>1</sup>Number of glass shards analyzed.

low the surface of a 17-m terrace yielded a  $^{14}\text{C}$  age of  $5,520 \pm 250$  yr B.P. (table 3, site 1; Detterman and Reed, 1973). The organics are thought to have washed onto the beach during terrace formation, thereby providing an age for the 17-m shoreline.

Similar to the Kvichak moraine in the Iliamna Lake valley, the outer moraine at Naknek Lake is graded to an **outwash** plain comprising gravel that overlies organic matter with a  $^{14}\text{C}$  age of  $26,570 \pm 20$  yr B.P. (table 3, site 5; Mann and Peteet, 1994). This provides a maximum limiting age on the three Naknek Lake terraces. Both the 30- and 15-m terraces are notched into and are therefore younger than the deposition of the type moraine of the late-glacial Iliuk stade of the Brooks Lake glaciation, which is older than the eruption of Lethe **tephra** at 12.6 ka (Pinney and **Begét, 1991a**). Charcoal dated by  $^{14}\text{C}$  at  $7,360 \pm 250$  yr B.P. (table 3, site 2; Dumond, 1981) provides a minimum limiting age on the separation of Naknek and Brooks Lakes and is the oldest age that constrains the lowering of the lake below about 9 m above the present level of Naknek Lake.

## CONCLUSIONS

A 40-m terrace was found at two sites separated by 70 km southwest to northeast above Iliamna Lake, and terraces at 30 m were identified at two sites across 50 km southeast to northwest at **Naknek** Lake. These terraces, and lower ones at both lakes, appear to be horizontal or nearly horizontal; they are not tilted by more than about 4 m in the directions of and over the distances of our transects. The lack of significant tilting suggests either that **glacio-**

isostatic recovery was complete prior to the fall of the lakes from their highest stand, or that the ice had only a minor (differential) isostatic effect on the basins.

The 40-m terrace at Iliamna Lake probably dates to the Newhalen stade of the Brooks Lake glaciation; the 30-m terrace at Iliamna Lake is probably older than about 12.6 ka, and the 24-m terrace at the lake is older than 8.3 ka. At Naknek Lake, the 30- and 15-m terraces were formed after the late-glacial Iliuk stade of the Brooks Lake glaciation and prior to 7.4 ka. Therefore, the terraces were formed during the Pleistocene-Holocene transition, a period of major global climate change coincident with rapidly rising base level.

The most prominent terraces at both lakes—the 24-m terrace at Iliamna Lake and the 15-m terrace at Naknek Lake—lie about halfway between the highest terrace and present-day lake levels. This might be a coincidence, but their similarity in width and position in sequence might also suggest that they are correlative. If so, then this correlation indicates some regional climatic or tectonic control, or a common eustatic sea-level effect, on lake level. To construct the prominent terraces would seem to require an extended interval during which (1) effective moisture (precipitation minus evaporation) was sufficiently high to fill the basins to their thresholds, and (2) outlet altitudes remained stable. We infer that these conditions were met when lake water discharge was conveyed by a stable outflow channel unaffected by climatic, isostatic, or tectonic readjustments. We expect that downcutting occurred either during intervals of increased hydrologic budgets and consequent outflow or during adjustments to tectonic or eustatic perturbations. Apparently, conditions conducive to maintaining the outlet altitudes at Iliamna and Naknek Lakes

long enough to form the prominent intermediate terraces took place sometime between about 8 and 13 ka.

Whether some shorelines were formed following a lake-level rise in a closed basin, as suggested by Detterman and Reed (1973) for the 18-m terrace at Iliamna Lake, is presently unclear. The sites that we studied did not yield stratigraphic or geomorphic evidence to evaluate this alternative, nor did we recognize cut-in-fill river terraces downstream of the lake outlets that would support this possibility. We suggest that the altitudes of past lake levels at Iliamna and Naknek Lakes, like those of the present day, were dominantly controlled by the history of outlet incisions.

Precise correlation of terraces between Iliamna and Naknek Lakes is hampered by the differing numbers of terraces at each lake. The presence of five terraces at Iliamna Lake and three terraces at Naknek Lake suggests different histories of episodic outflow incisions at the two lakes. This interpretation is consistent with Riehle and Detterman's (1993) expectation that terrace levels at lakes along the Alaska Peninsula should not correspond exactly owing to regional differences in tectonism and local differences in outlet stability.

Acknowledgments. — We thank the King Salmon office of the National Park Service for logistical support in Katmai National Park, and the University of Washington Fisheries Institute for logistical support in Iliamna. C. Meyer (U.S. Geological Survey) provided the microprobe data on the tephra. This study was funded by the National Science Foundation Division of Polar Programs while Kaufman served as an intermittent employee of the U.S. Geological Survey.

## REFERENCES CITED

Andrews, J.T., 1975, *Glacial systems—an approach to glaciers and their environments*: Belmont, Calif., Duxbury Press, 191 p.

Detterman, R.L., and Reed, B.L., 1973, *Surficial deposits of the*

Iliamna Quadrangle, Alaska: U.S. Geological Survey Bulletin 1368-A, 64 p.

Detterman, R.L., Reed, B.L., and Rubin, M., 1965, Radiocarbon dates from Iliamna Lake, Alaska: U.S. Geological Survey Professional Paper 525-D, p. D34-D36.

Dumond, D.E., 1981, *Archaeology on the Alaska Peninsula—the Naknek Region, 1960-1975*: Eugene, Oreg., University of Oregon Anthropological Papers, no. 21, 276 p.

Mann, D.H., and Peteet, D.M., 1994, *Extent and timing of the Last Glacial Maximum in southwestern Alaska*: Quaternary Research, v. 42, p. 136-148.

Muller, E.H., 1952, *The glacial geology of the Naknek District, the Bristol Bay region, Alaska*: Urbana, Ill., University of Illinois, Ph.D. thesis, 98 p.

Pinney, D.S., and Begét, J.E., 1991a, Late Pleistocene volcanic deposits near the Valley of Ten Thousand Smokes, Katmai National Park, Alaska, in Reger, R.D., ed., *Short notes on Alaska Geology 1991*: Alaska Division of Geological and Geophysical Surveys Professional Report 111, p. 45-53

———, 1991b, *Deglaciation and latest Pleistocene and early Holocene glacier readvances on the Alaska Peninsula—records of rapid climate change due to transient changes in solar intensity and atmospheric CO<sub>2</sub> content?*, in Weller, G., Wilson, C.L., and Severing, B.A.B., eds., *International Conference on the Role of Polar Regions in Global Change*: Fairbanks, Alaska, University of Alaska, p. 634-640.

Riehle, J.R., and Detterman, R.L., 1993, *Quaternary geologic map of the Mount Katmai quadrangle and adjacent portions of the Naknek and Afognak quadrangles, Alaska*: U.S. Geological Survey Miscellaneous Geologic Investigations Map I-2032, scale 1:250,000.

Stilwell, K.B., 1995, *Late Quaternary glacial geology, shoreline morphology, and tephrochronology of the Iliamna/Naknek/Rooks Lake area, southwestern Alaska*: Logan, Utah, Utah State University, M.S. thesis, 162 p.

Stilwell, K.B., and Kaufman, D.S., 1996, *Late Wisconsin glacial history of the northern Alaska Peninsula*: Arctic and Alpine Research, v. 28, p. 475-487.

Reviewers: L. David Carter and James R. Riehle

# Geodetic Studies in the Novarupta Area, Katmai National Park, Alaska, 1990 to 1995

By Jack W. Kleinman, Eugene Y. Iwatsubo, John A. Power, and Elliot T. Endo



Note.—Jack W. Kleinman (1961-1994), a member of the geodesy group at the Cascades Volcano Observatory, Vancouver, Washington, died in a kayaking accident on the White Salmon River, Washington, on February 12, 1994. Jack started employment with the U.S. Geological Survey in the summer of 1985. In the spring of 1986, he began his career in volcano studies by participating in geodetic monitoring at Mount St. Helens. In the following years Jack worked on projects that took him to Yellowstone National Park, Long Valley, most of the Cascades volcanoes, the South Pole, Stromboli, Italy, and Alaska. Jack especially liked working in Alaska. He helped establish the first geodetic network near Novarupta, Katmai National Park, Alaska, in 1989, and served as crew chief for additional surveys there in 1990 and 1993. The job entailed long days of hard work in the face of unforgiving weather, logistical complexities, and a skin-tight budget. As in his kayaking, Jack relished the challenges of working in Alaska. For Jack, the colder and wetter, the more he liked field work. The physically demanding field work at Katmai National Park and on Augustine Island was perfect for Jack. He is missed by his colleagues and friends.

## ABSTRACT

A five-station electronic distance meter (EDM) network centered around the Novarupta dome in Katmai National Park, Alaska, was established in 1990 and resurveyed in 1993 and 1995. Both EDM and Global Positioning System (GPS) measurements were made in 1993. The 1995 survey was restricted to the more accurate GPS surveying method. Analysis of EDM data in 1993 suggested an aver-

age increase of 22.5 mm in slope distances between stations from 1990 to 1993. Those changes were about 2–3 times the expected error for lines of this length (1.5 to 4.7 km) and suggested that ground deformation was taking place in the Novarupta area. Loss of data from one of five GPS receivers in 1993 precluded complete comparison of GPS data with EDM results. In July 1995, the network was occupied with five P-code GPS receivers. Two 12-15 hour observations were made simultaneously at all five stations,

which were located relative to a reference GPS station in Fairbanks. For final L1-only solutions and EDM line lengths between stations, one station was held fixed using these new coordinates. The 1995 GPS results, when compared with recomputed EDM line lengths for 1990 and 1993 and available 1993 GPS line lengths, indicate that the Novarupta site moved about 15–20 mm to the west and the Mainstreet station moved a similar distance to the northwest during the interval from 1990 to 1993. There is a suggestion that the Mainstreet station also moved from 1993 to 1995. The movement at both stations is thought to be a result of a deformation source to the southeast outside the network or associated with the stability of the sites. The movement is not a result of volcano deformation centered at Novarupta. To further evaluate ground deformation in the Katmai area, extension of the network with GPS observations beyond the immediate vicinity of Novarupta is recommended.

## INTRODUCTION

Novarupta dome, located at the head of the Valley of Ten Thousand Smokes in Katmai National Park, Alaska (fig. 1), is the site of the largest volcanic eruption worldwide this century. During the 1912 eruption, approximately

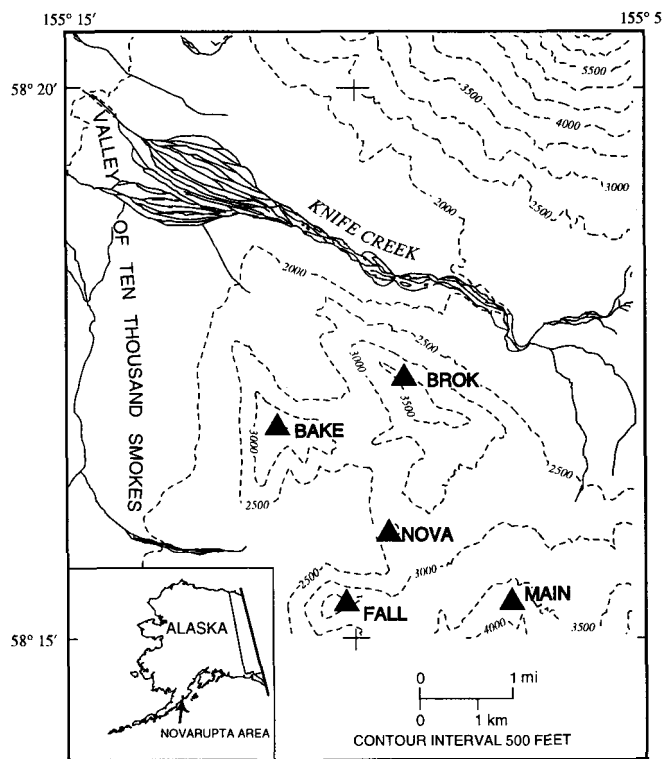


Figure 1. The braced quadrilateral geodetic network in the Novarupta area of the Valley of Ten Thousand Smokes. Benchmark locations are indicated by triangles and abbreviated names used in the text.

15 km<sup>3</sup> of compositionally mingled magma (Hildreth, 1983) erupted from the Novarupta vent area, which collapsed to form a 2-km-wide depression. The summit of nearby Mt. Katmai synchronously collapsed, presumably a result of a complex connection with the venting magma system (Hildreth, 1983, 1987). The eruptive sequence ended with the extrusion of the Novarupta rhyolite dome within the vent depression.

In conjunction with other geophysical studies initiated under the Continental Scientific Drilling Program (Eichelberger and Hildreth, 1986; Eichelberger and others, 1991), a geodetic network was established during 1989–90 to monitor ground deformation in the Novarupta area (Kleinman and Iwatsubo, 1991). The geodetic network consists of three stations from which measurements of slope distance and zenith angle can be made to each of the other stations. This technique was first used by the U.S. Geological Survey (USGS) in 1965 at the volcanoes Kilauea and Mauna Loa on the island of Hawaii. It was later used successfully to monitor ground deformation at Mount St. Helens both before and after the May 18, 1980, eruption (Lipman and others, 1981). Similar networks have been established at many of the other volcanoes in the Cascades Range to provide baseline geodetic information (Chadwick and others, 1985; Iwatsubo and others, 1988). A comparison of measurements of a three-station Novarupta electronic distance meter (EDM) network in 1989 and 1990 revealed no changes in slope distance larger than the expected measurement error (Kleinman and Iwatsubo, 1991). In 1990, part of the network was reestablished with more permanent marks and two stations were added to form the geodetic network resurveyed in 1993 and 1995.

The first opportunity to remeasure the network came in 1993. Following the Redoubt eruptions in 1990, the USGS Volcano Hazards Program began experimenting with Global Positioning System (GPS) receivers acquired for the purpose of monitoring geodetic networks on silicic volcanoes. With the availability of GPS equipment, a decision was made to occupy the Katmai network with both EDM and GPS receivers. GPS surveying does not require intervisibility between stations and thus could be accomplished in inclement weather. Dvorak and others (1994) describe the GPS surveying technique that was first applied in Hawaii and subsequently used at Novarupta.

## THE NOVARUPTA GEODETIC NETWORK

The geodetic network in the Novarupta area consists of one benchmark located on Novarupta (NOVA) and four additional benchmarks located on surrounding topographic highs (fig. 1). These four stations (Baked Mountain, BAKE; Broken Mountain, BROK; Falling Mountain, FALL; and Mainstreet, MAIN) formed a 2 km by 4 km braced quadri-

lateral approximately centered around Novarupta. The Falling Mountain, Broken Mountain, and Mainstreet benchmarks are fixed on 1.25-cm diameter copperweld rods driven 10.7 m into tephra at BROK and MAIN. The rod at FALL was driven to a depth of 2.4 m (Kleinman and Iwatsubo, 1991) into tephra. The benchmark on Novarupta, stamped 1989 K-2, is fixed in a hole drilled into a large rhyolite boulder and has a punch mark enclosed by a small rectangle for a centering target. The Baked Mountain benchmark is a brass disk approximately 7.6 cm in diameter cemented in shale. The brass disk is stamped BAKED and has a punch mark located about 2 cm from the center of the disk that was used as a target for centering. Benchmarks at other sites have small  $\dagger$  marks enclosed by a triangle for centering targets. Broken Mountain is stamped K-3, Mainstreet K-4, and Falling Mountain K-5. An older benchmark at Falling Mountain, K-1, has been abandoned. Owing to the topography and the weight of surveying equipment and batteries, all sites require helicopter support out of King Salmon. Baked Mountain, Novarupta, and Falling Mountain require short hikes from helicopter landing sites.

## GEODETIC FIELD WORK AND DATA ANALYSIS

### EDM MEASUREMENTS AND CORRECTIONS

The 10 lines of the braced quadrilateral network at Novarupta were measured in July 1990 and in June 1993. A Wild DI-5 EDM and a Wild T-2000 theodolite were used for the 1990 survey. In 1993, a Geodimeter 6000 EDM and a Wild T-2 theodolite were used. Prism sets mounted onto tripods and centered over permanent benchmarks were used for both surveys. Both the Wild DI-5 EDM and the Geodimeter 6000 EDM automatically measure distance. Hundreds of measurements at several different modulation frequencies are performed automatically by the EDM instruments with the push of a button. A mean distance and standard deviation is given for each set of measurements to a reflector. In 1990, as many as eight triangular clusters of three retro-reflectors were used because the DI-5 has a relatively weak laser source; vertical clusters of three retro-reflectors were used in 1993. Retro-reflectors used in 1993 could be tilted, but it is not known if the any clusters were tilted. Vertical angles were measured with a theodolite from each EDM setup to reflector sites. These vertical angles, along with instrument and reflector heights measured at each site, were used for conversion of slope distances to mark-to-mark distances. Mark-to-mark measured distances were corrected for atmospheric refraction (temperature, pressure, and humidity). The 1990 and 1993 EDM data were first reduced in 1993 with a hand calculator. The average change in line length was  $+22.5 \text{ mm}$  (where  $\dagger$  represents extension).

To gauge the validity of these changes, it was necessary to evaluate all likely sources of error in the measurements. One error source is the EDM instrument itself. Manufacturer specifications are  $3 \text{ mm} \pm 2$  parts per million (ppm) for the Wild DI-5 used in 1990 and  $5 \text{ mm} \pm 1$  ppm for the Geodimeter 6000 used in 1993. Because different EDM's and reflector sets were used for the two surveys, we checked the equipment sets against each other on a 1-km-long National Geodetic Survey calibration line. The two EDM's agreed with each other within manufacturer's specifications, but the two different types of reflector sets differed by a constant factor of 0.0056 m. This difference was accounted for in the 1993 analysis results that indicated an average line-length change of 22.5 mm.

Atmospheric factors can cause line-length changes, which introduces another potential source of error. Temperature, pressure, and relative humidity were measured at each endpoint so that the appropriate atmospheric corrections could be applied to the line-length measurements. Temperature corrections, the largest of the atmospheric corrections, are about 1 ppm for every  $1.0^\circ\text{C}$  change in temperature. Temperatures were measured 7.6 m above ground level at the top of a telescoping survey rod to minimize the effect of ground radiation.

Errors can also be introduced by instrument or reflector setup inaccuracies. Tribrach circular level bubbles and optical plummets can be out of true or height measurements can be made incorrectly. We attempted to minimize these potential sources of error by calibrating optical plummet tribrachs and by making redundant height measurements. High winds can also introduce error. The highest winds were encountered in 1990 while measuring the line from Baked Mountain to Novarupta, which shortened by 15 mm from 1990 to 1993. Benchmark instabilities as a result of slope creep or unstable rock are also possible sources of error.

To ensure consistently analyzed mark-to-mark slope distances, 1990 and 1993 EDM measurements were reduced in 1995 with a computer program written by Cascades Volcano Observatory staff for routine reduction of EDM data. The results of the analysis of EDM data are shown in table 1, including baseline lengths and differences between the 1993 and 1990 EDM surveys. There is no standard deviation record for EDM field measurements, and errors indicated in the table 1 explanation are based on manufacturers' specifications.

## GPS OBSERVATIONS AND ANALYSIS

### OBSERVATIONS DURING 1993

The 1993 Alaska field season was the first opportunity to utilize GPS receivers as a volcano deformation monitoring tool in the Novarupta area at Katmai. Five **Ashtech**

**Table 1.** Line lengths from repeated EDM measurements of the Novarupta geodetic network in 1990 and 1993

[Manufacturer's specification for the EDM used in the 1990 survey is 3 mm +2 ppm. Manufacturer's specification for the EDM used in 1993 is 5 mm +1ppm]

Line	Distance-meters		Changes 1993-1990
	1990	1993	
BAKE-NOVA	2566.0758	2566.0611	-0.015
BROK-NOVA	2795.7467	2795.7548	+0.008
MAIN-NOVA	2197.3964	2197.3972	+0.001
FALL-NOVA	1497.4217	1497.4070	-0.015
FALL-BAKE	3105.6921	3105.6878	-0.004
FALL-BROK	4070.6871	4070.6866	-0.001
FALL-MAIN	2663.3693	2663.3660	-0.003
MAIN-BAKE	4700.0450	4700.0297	-0.015
MAIN-BROK	4356.1728	4356.1608	-0.012
BROK-BAKE	2151.1032	2151.1045	+0.001

**Table 2.** Line lengths from GPS measurements of the Novarupta geodetic network in 1993

[Root-mean-square errors enclosed by parentheses. There were two 6-h observation sessions in 1993]

Station pair	Distance (meters)
BAKE-NOVA	2566.0555 (.009) 2566.0552 (.014)
BROK-NOVA	2795.7487 (.013) 2795.7534 (.015)
FALL-NOVA	1497.4040 (.006) 1497.4030 (.008)
FALL-BAKE	3105.6806 (.008) 3105.6809 (.013)
FALL-BROK	4070.6801 (.015) 4070.6783 (.012)
BROK-BAKE	2151.1062 (.008) 2151.1064 (.009)

dual-frequency receivers (no P-code capability) were deployed shortly after the completion of the EDM survey. Two 6-h observation sessions were made overnight. For unknown reasons, the receiver at MAIN failed and all data were lost. The loss of data from one receiver resulted in the loss of data for 4 baselines out of the 10 in the network around **Novarupta**. Using 1995 updated coordinates relative to Fairbanks, 1993 GPS data were processed using **Ashtech** GPS Post-Processing System (GPPS™) software

and broadcast orbits (predicted satellite orbits). Precise orbits (computed from actual satellite orbits) from the same source for orbits used in 1995 were not available for July 1993, and this lack of precise-orbit data was one reason for using GPPS software. We saw no advantage in processing 1993 GPS data with geodetic-grade software. BAKE, BROK and FALL were fixed to obtain all possible baselines distances. Root-mean-square (RMS) errors (Bevington, 1969) for baseline-length solutions varied from 6 mm to 15 mm. GPPS-determined baseline lengths are shown in table 2. Seeber (1993) and Hofmann-Wellenhof and others (1992)

**Figure 2.** The Mainstreet GPS station located on the northwest slope of Trident Mountain. The GPS receiver and battery are located under a plastic tarpaulin weighted down by tephra filled sample bags in the left foreground.



**Table 3. World Geodetic System (WGS)-84 latitude, longitude, height, and X, Y, and Z coordinates from repeated GPS observations**

[Root-mean-square errors for X, Y, and Z coordinates are enclosed by parentheses. There were three 12-h solutions for BAKE and MAIN, and two 12-h solutions for BROK, FALL, and NOVA]

Station	North latitude	West longitude	Height (meters)	X (meters)	Y (meters)	Z (meters)
BAKE	58° 16' 51.814832"	155° 11' 29.228658"	1141.8988	-3051806.0133 (.0037)	-1410684.8700 (.0018)	5403232.7216 (.0061)
	58° 16' 51.814127"	155° 11' 29.225605"	1141.9129	-3051806.0160 (.0027)	-1410684.9261 (.0014)	5403232.7221 (.0044)
	58° 16' 51.817122"	155° 11' 29.222761"	1141.8514	-3051805.8956 (.0100)	-1410684.9215 (.0069)	5403232.7185 (.0148)
BROK	58° 17' 24.871796"	155° 9' 33.149105"	1097.2164	-3050200.6339 (.0028)	-1412026.6719 (.0014)	5403732.4601 (.0045)
	58° 17' 24.877422"	155° 9' 33.143637"	1097.0376	-3050200.3768 (.0101)	-1412026.6511 (.0072)	5403732.3936 (.0152)
FALL	58° 15' 16.652979"	155° 10' 28.750913"	1171.2769	ω053679.4393 (.0029)	-1412637.6641 (.0014)	5401708.8943 (.0046)
	58° 15' 16.656674"	155° 10' 28.746263"	1171.0427	ω053679.2074 (.0106)	-1412637.6404 (.0071)	5401708.7554 (.0154)
MAIN	58° 15' 16.079094"	155° 7' 45.486891"	1197.9303	ω052586.7675 (.0037)	-1415066.5384 (.0018)	5401722.2124 (.0060)
	58° 15' 16.079319"	155° 7' 45.487474"	1197.9186	ω052586.7606 (.0028)	-1415066.5247 (.0014)	5401722.2102 (.0045)
	58° 15' 16.083213"	155° 7' 45.482769"	1198.2440	ω052586.7906 (.0100)	-1415066.6232 (.0068)	5401722.5502 (.0146)
NOVA	58° 15' 54.906988"	155° 9' 36.201614"	845.0910	-3052250.1535 (.0031)	-1412920.6042 (.0015)	5402054.2212 (.0051)
	58° 15' 54.911162"	155° 9' 36.193736"	844.9653	-3052249.9399 (.0111)	-1412920.6469 (.0076)	5402054.1823 (.0167)

present thorough discussions of the GPS surveying technique and data analysis.

**OBSERVATIONS DURING 1995**

In late July 1995, five Trimble SSE receivers (dual-frequency P-code receivers) were borrowed from the Hawaiian Volcano Observatory to occupy the Novarupta network. On July 22, receivers were set up at MAIN (fig. 2) and at BAKE. Receivers were programmed to record for 16-h (30-s epochs) during the best NAVSTAR (NAVigation Satellite Time And Ranging) satellite configuration for the day. On July 23, additional receivers were installed at BROK, FALL, and NOVA. The receiver at NOVA was programmed to record for two 12-h sessions because of a battery limitation. The goal of the survey was to obtain at least two simultaneous 12–16 h observations for all stations. These long observations, although not required for short-baseline GPS surveys, were used to establish precise locations for each station relative to known GPS sites in Kodiak and Fairbanks. On July 24, all five GPS receivers were retrieved without incident.

The 1995 Novarupta GPS data were processed with Bernese (version 3.5) geodetic-grade software (Rothacher and others, 1993). Precise orbits and pole data were obtained from CODE (Center for Orbit Determination Europe). All five Novarupta stations were first located relative to Fairbanks and Kodiak using L1 frequency and L2 frequency observations (table 3). ITRF93 (International Terrestrial Reference Frame) coordinates corrected for continental plate velocity were used for Fairbanks and Kodiak. These Bernese-determined locations for the Novarupta network were used as a priori station coordinates (initial locations required for data processing) for 1993 GPS data processing with GPPS. For final baseline calculations, BAKE was held fixed and data were processed for L1-only relative-coordinate solutions for BROK, FALL, MAIN, NOVA, and all baseline lengths. RMS errors for relative-coordinate solutions were 0.1–0.3 mm. Repeatabilities and scatter as defined by Dixon (1991) for observations are shown in figure 3. Computed baseline lengths and RMS errors are shown in table 4.

**RESULTS**

To determine if ground deformation had taken place in the Novarupta area from 1990 to 1995, we compared baseline lengths from the 1990 and 1993 EDM surveys with GPS-measured baselines in 1993 and 1995. As a check on consistency of the two surveying methods, we also compared 1993 GPS line lengths with 1993 EDM line lengths. All line-length data were placed in a spreadsheet to facilitate comparison of data and then plotted on geodetic-network diagrams.

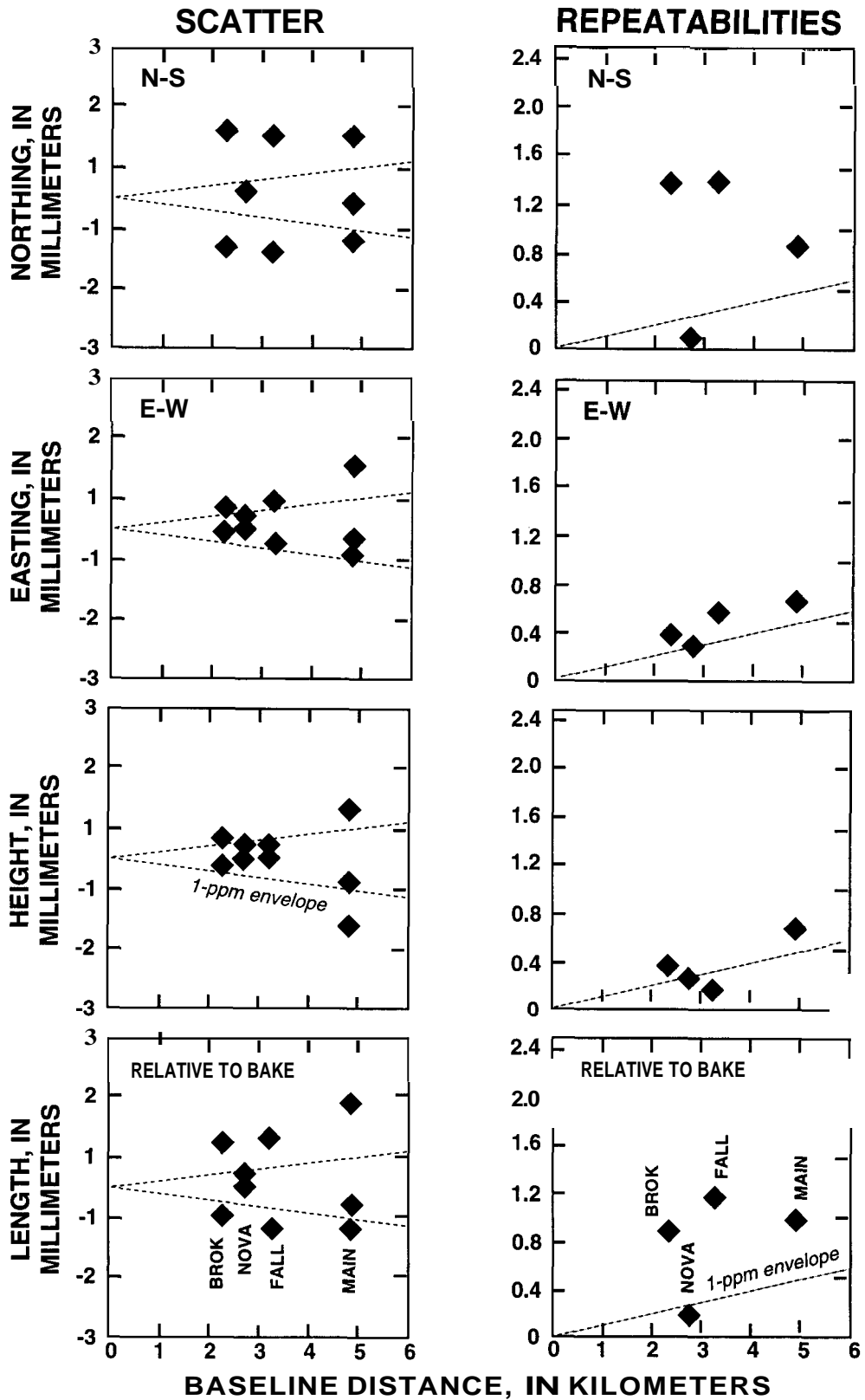


Figure 3. Plots of scatter and repeatability for L1-frequency-only Bemese-determined solutions for the 1995 GPS survey. The 1-ppm envelope is indicated by sloping dashed lines. Scatter plots show solutions plotted about a calculated mean. Repeatability is a statistical measure of the similarity of solutions.

Table 4. Line lengths from GPS measurements of the Novarupta geodetic network in 1995

[Root-mean-square errors enclosed by parentheses]

Station pair	Distance (meters)	Distance (meters)
BAKE-NOVA	2566.0545 (.0001)	2566.0544 (.0001)
BROK-NOVA	2795.7595 (.0002)	2795.7614 (.0002)
MAIN-NOVA	2197.3976 (.0001)	2197.3962 (.0001)
FALL-NOVA	1497.3951 (.0002)	1497.3966 (.0002)
FALL-BAKE	3105.6773 (.0001)	3105.6787 (.0001)
FALL-BROK	4070.6784 (.0002)	4070.6821 (.0002)
FALL-MAIN	2663.3618 (.0001)	2663.3609 (.0001)
MAIN-BAKE	4700.0227 (.0001)	4700.0210 (.0001)
MAIN-BROK	4356.1407 (.0001)	4356.1409 (.0001)
BROK-BAKE	2151.1101 (.0001)	2151.1113 (.0001)

Calculated line-length differences between the **1993 GPS** (six baselines) and the **1993 EDM** survey varied from 2 to 7 mm (fig. 4). The differences between the **1993 EDM** and **1993 GPS** surveys may be a result of unknown phase eccentricities of the **Ashtech GPS** antenna.

We have no way to evaluate **GPS** setup errors because there were no repeat surveys in **1993** and **1995**. As part of the preparation effort for the **1995** field season, **all** optical **tribrachs** used for the Novarupta **GPS** survey were calibrated by a Wild service center. Kern self-centering tripods were used in **1990**. We assume that antenna slant heights were measured correctly and baseline length errors that result from setup are comparable to the 5-mm-or-less errors encountered by other investigators (Larson, **1990**) for repeat **GPS** surveys.

The **1993 GPS** line-length differences relative to **1990 EDM** line lengths for the six baselines measured by both techniques are similar to **1993 EDM** and **1990 EDM** line-length differences. No similar comparison could be made for four baselines from MAIN because of the loss of data. Line-length differences from NOVA to FALL and from NOVA to BAKE for **1993** and **1990 EDM** measurements (fig. 5A) are nearly identical to line-length differences for **1993 GPS** data and **1990 EDM** data (fig. 5B). These data suggest that NOVA moved about **15–20 mm** to the west or northwest during the interval between **1990** and **1993**. Although length differences obtained by EDM surveys of lines from the MAIN station are close to the error limits for this surveying technique, the data suggest that MAIN may also have moved **15–20 mm** to the northwest. Data also indicate

that MAIN continued to move from **1993** through **1995** (fig. 6). The **1995 GPS** line lengths relative to **1990 EDM** line lengths show displacement similar to that suggested for NOVA during the **1990** to **1993** interval (fig. 7).

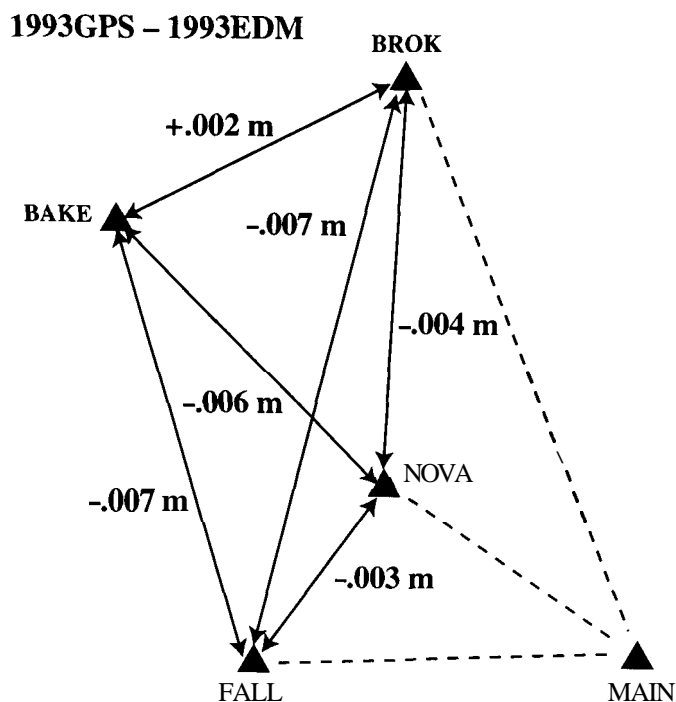


Figure 4. Novarupta line-length differences for 1993 GPS and 1993 EDM surveys.

1993EDM - 1990EDM

1993GPS - 1990EDM

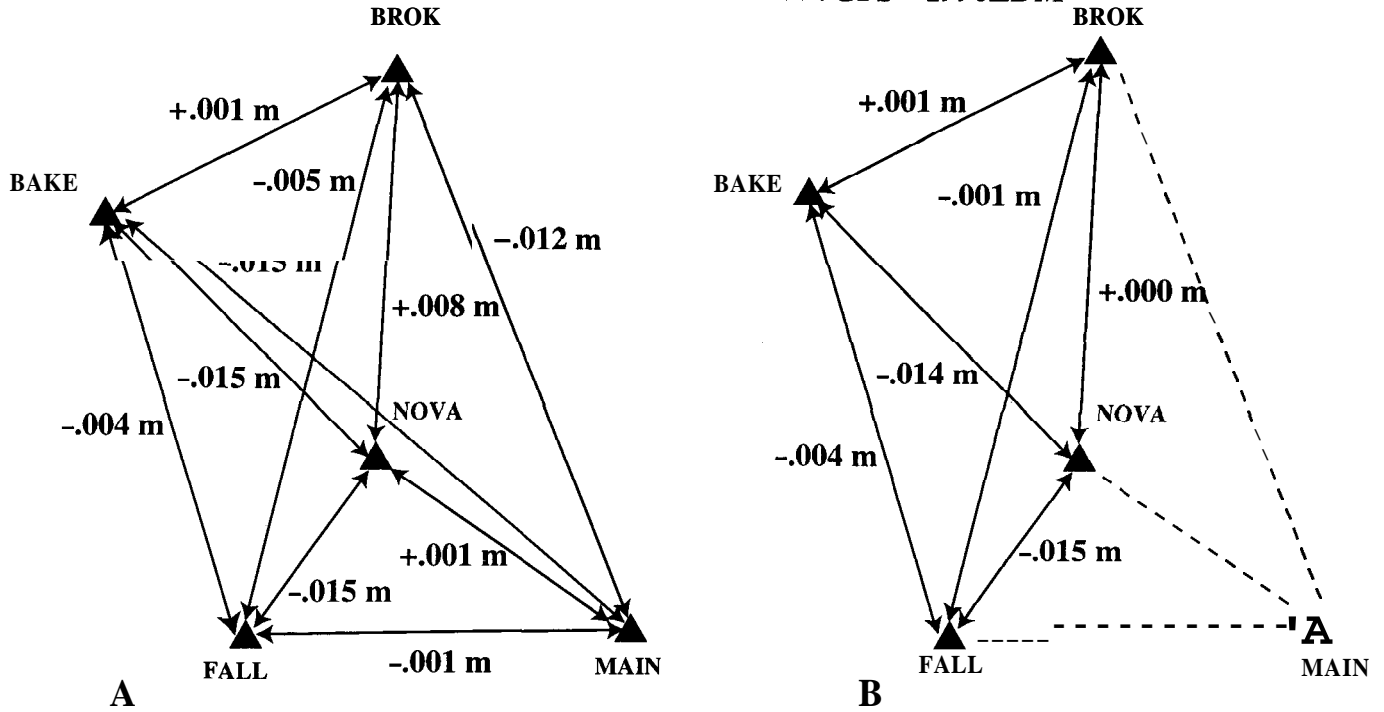


Figure 5. A, Novarupta line-length differences for 1993 EDM and 1990 EDM surveys. B, Novarupta line-length differences for 1993 GPS and 1990 EDM surveys

1995GPS - 1993EDM

1995GPS - 1990EDM

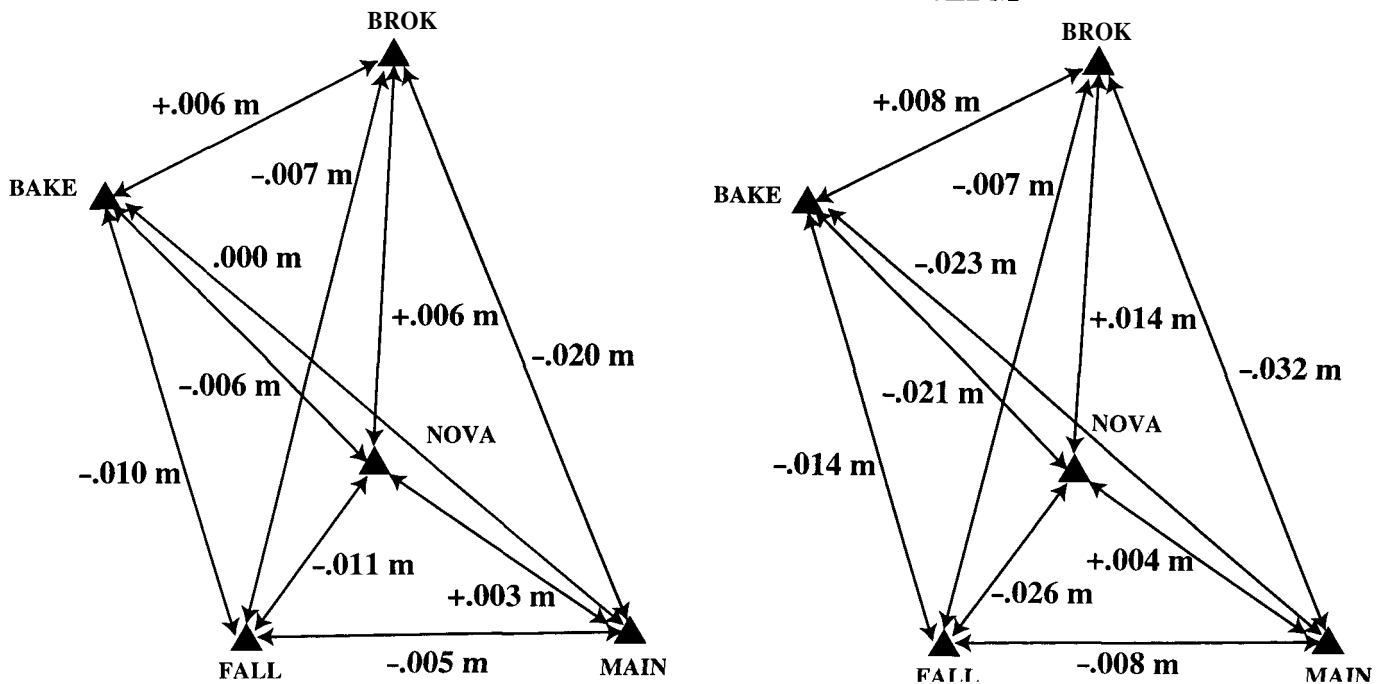


Figure 6. Novarupta line-length differences for 1995 GPS and 1993 EDM surveys.

Figure 7. Novarupta line-length differences for 1995 GPS and 1990 EDM surveys.

## DISCUSSION

It is not possible to definitively assess the magnitude of possible systematic errors in the Novarupta EDM surveys or the errors associated in comparing results from two surveying techniques and the use of different instruments. We tried to minimize such errors, and all appropriate corrections were applied to reduce any residual errors. Nevertheless, the lack of redundancy in the early measurements raises the possibility of larger-than-expected systematic errors.

Another approach to error assessment for the Novarupta EDM surveys is to compare them with similar repeated trilateration and distance-measurement networks elsewhere. An analysis of such surveys at 12 volcanoes in the Cascades Range indicated that repeatability was 2.46 mm  $\pm$ 2.26 ppm (Iwatsubo and Swanson, 1992). For the analysis, it was assumed that no real changes occurred at any of the volcanoes during the periods between surveys. For EDM surveys at Mount St. Helens during 1980, a period that included real ground displacements associated with eruptive activity, accuracies are believed to be  $\pm$ 10 mm over 2–4 km-long lines (Lipman and others, 1981). These line lengths are similar to those in the Novarupta network. By comparison with these earlier results, the 1- to 15-mm average line-length change in the Novarupta network from 1990 to 1993 is close to the probable total error in the measurements.

Unlike continuous GPS measurements of the type being made in California along the Hayward fault (King and others, 1995), errors associated with repeated GPS measurements like that at Novarupta in 1995 are difficult to assess because of few observations. For continuous measurements, a few parts per million RMS scatter in baseline length was observed for single-frequency measurements. The accuracy of results of the 1995 GPS survey near Novarupta cannot be any better than that achieved for continuous monitoring. We have to assume that satellite-signal multipath errors and random setup errors are possible sources of error for any GPS survey of the type done in 1993 and 1995. The 1995 GPS results are only slightly better than the EDM surveys of 1990 and 1993, and changes of less than 10 mm are probably due to some observation error.

The possibility that a nearby shallow magma body exists south of the Novarupta area has been suggested by Ward and others (1991) on the basis of P-wave travel-time residuals and a negative Bouguer gravity anomaly. In late 1992–early 1993 increased seismic activity was observed (Peter Ward, USGS, oral commun., 1993) in the area southwest of Baked Mountain (slightly west of the geodetic network). The relatively small geodetic network in this study does not well constrain the location of a hypothetical magma body. Expanding the size of the geodetic network to in-

clude the epicenters of seismic activity would be helpful in ascertaining the aerial extent of crustal deformation. The Novarupta network was tied to a regional GPS network in 1995, but the GPS network (Lisowski and others, 1993) is too regional in scope to help constrain a localized area of crustal deformation. To further evaluate ground deformation in the Katmai area, extension of the network with GPS observations beyond the immediate vicinity of Novarupta is recommended.

While the geodetic work in 1990, 1993, and 1995 did not result in evidence for volcano-related ground deformation centered at Novarupta, we now have a network that is tied into a worldwide coordinate system and locations for five stations that are accurate enough for future differential (real-time kinematic) GPS surveying for mapping or grid-type geophysical exploration in the Valley of Ten Thousand Smokes.

Acknowledgments.—The Katmai geodetic studies were supported by the Alaska Volcano Observatory and the USGS Volcano Hazards Program. Geodetic studies in the Valley of Ten Thousand Smokes were made possible with support and cooperation from Katmai National Park personnel and the National Park Service. We also thank the U.S. Fish and Wildlife Service for the generous use of their facilities in King Salmon. Our special thanks to the helicopter pilots for field support to and from King Salmon and Art Jolly for his help in 1995.

## REFERENCES CITED

- Bevington, P.R., 1969, Data reduction and error analysis for the physical sciences: New York, McGraw-Hill, 336 p.
- Chadwick, W.W., Jr., Iwatsubo, E.Y., Swanson, D.A., and Ewert, J.W., 1985, Measurements of slope distance and vertical angles at Mount Baker and Mount Rainier, Washington, Mount Hood and Crater Lake, Oregon, and Mount Shasta and Lassen Peak, California, 1980–1984: U.S. Geological Survey Open File Report 85-205, 96 p.
- Dixon, T.H., 1991, An introduction to the global positioning system and some geological applications: *Reviews of Geophysics*, v. 29, p. 249–276.
- Dvorak, J.J., Okamura, A.T., Lisowski, M., Prescott, W.H., and Svarc, J.L., 1994, Global positioning system measurements on the island of Hawaii from 1987 to 1990: *U.S. Geological Survey Bulletin* 2092, 33 p.
- Eichelberger, J.C., and Hildreth, W., 1986, Research drilling at Katmai, Alaska: *Eos (American Geophysical Union Transactions)*, v. 67, p. 733–735.
- Eichelberger, J.C., Hildreth, W., and Papike, J.J., 1991, The Katmai Scientific Drilling Project, surface phase: investigation of an exceptional igneous system: *Geophysical Research Letters*, v. 18, p. 1513–1516.
- Hildreth, Wes, 1983, The compositionally zoned eruption of 1912 in the Valley of Ten Thousand Smokes, Katmai National Park, Alaska: *Journal of Volcanology and Geophysical Research*, v. 18, p. 1–56.

- 1987**, New perspectives on the eruption of **1912** in the Valley of Ten Thousand Smokes, Katmai National Park, Alaska: *Bulletin of Volcanology*, v. **49**, p. **680–693**.
- Hofmann-Wellenhof, B., Lichtenegger, H., and Collins, J., **1992**, *Global Positioning System theory and practice*: New York, Springer-Verlag Wien, **326** p.
- Iwatsubo, E.Y., and Swanson, D.A., **1992**, Trilateration and distance-measuring techniques used at Cascades and other volcanoes, in Ewert, J.W., and Swanson, D.A., eds., *Monitoring volcanoes: techniques and strategies used by the staff of the Cascades Volcano Observatory, 1980-1990*: U.S. Geological Survey Bulletin **1966**, p. **103–114**.
- Iwatsubo, E.Y., Topinka, L., and Swanson, D.A., **1988**, Measurements of slope distance and zenith angles at **Newberry** and **South Sister** volcanoes, Oregon, **1985–1986**: U.S. Geological Survey Open File Report **88-377**, **51** p.
- King, N.E., Svarc, J.L., Fogleman, E.B., Gross, W.K., Clark, K.W., Hamilton, G.D., Stiffler, C.H., and Sutton, J.M., **1995**, Continuous GPS observations across the **Hayward** fault, California, **1991–1994**: *Journal of Geophysical Research*, v. **100**, no. **B10**, p. **20,271–20,283**.
- Kleinman, J.W., and Iwatsubo, E.Y., **1991**, A geodetic network in the **Novarupta** area, Katmai National Park, Alaska: *Geophysical Research Letters*, v. **18**, p. **1517–1519**.
- Larson, K.M., **1990**, Precision, accuracy, and tectonics from the Global Positioning System: **San Diego**, Calif., University of California, **Ph.D.** dissertation, **269** p.
- Lipman, P.W., Moore, J.G., and Swanson, D.A., **1981**, Bulging of the north flank before the May **18** eruption—geodetic data, in Lipman, P.W., and Mullineaux, D.R., eds., *The 1980 eruptions of Mount St. Helens*, Washington: U.S. Geological Survey Professional Paper **1250**, p. **143–155**.
- Lisowski, M., Savage, J.C., Svarc, J.L., and Prescott, W.H., **1993**, Deformation across the Alaska-Aleutian subduction zone near Kodiak, Alaska [abs.]: *Eos (American Geophysical Union Transactions)*, v. **74**, no. **43**, p. **191**.
- Rothacher, M., Buetler, G., Gurtner, W., Brockmann, E., and Mervart, L., **1993**, *Bernese software version 3.4 documentation*: Bern, Switzerland, University of Bern, **63** p.
- Seeber, Gunter, **1993**, *Satellite geodesy*: Berlin, Walter de Gruyter, **531** p.
- Ward, P.L., Pitt, A.M., and Endo, E., **1991**, Seismic evidence for magma in the vicinity of Mt. Katmai, Alaska: *Geophysical Research Letters*, v. **18**, p. **1537–1540**.

**Reviewers: Dan Dzurisin and Mike Lisowski**

# The "Twin Peaks Fault": Not a Tectonic or Seismogenic Structure

By Peter J. Haeussler and Robert S. Anderson

## ABSTRACT

The "Twin Peaks fault" in south-central Alaska is one of only two places along the Border Ranges fault system for which it has been argued that there is Holocene surface faulting. If true, then the "Twin Peaks fault" and the Border Ranges system in general could represent a significant earthquake hazard for the Anchorage area. We have reassessed evidence for surface faulting along the "Twin Peaks fault" and find that it is not a tectonic or seismogenic structure, but rather it is a coincidental alignment of bedrock structural fabric, swales related to sackungen and landsliding, and a headscarp related to landsliding within an inactive rock glacier.

## INTRODUCTION

The recognition and characterization of active faults is crucial to understanding the earthquake hazards in any region. If a fault is considered to be active, that is, having evidence of movement in Holocene time, it is likely that it moved suddenly and produced an earthquake. It is relatively simple to demonstrate that some faults are active; for example, the San **Andreas** fault in California has historical seismicity, including large earthquakes greater than magnitude 7, and a well-defined fault trace that includes a fault scarp, sag ponds, and a vegetation and topographic lineament (e.g., Wallace, 1990). Other active faults may not display all these features, but the presence of a scarp is typically regarded as evidence of surface faulting and of an active fault that can produce significant earthquakes.

The Border Ranges fault is one of the longest and most significant faults in southern and southeastern Alaska; it divides the accretionary complex to the south from its backstop, that is, the "continental" crust to the north (e.g., Plafker and others, 1994b). More than half the population of Alaska lives within a few tens of kilometers of the fault, and it is cited in local geotechnical reports and on seismic hazard maps (where it is often referred to as the "Knik fault" or "Knik fault zone"; Municipality of Anchorage,

1980–1982) as an active fault (fig. 1). There has been no seismicity that can be directly attributed to the Border Ranges fault (Page and others, 1991). Only two faults have been interpreted to be both active and associated with the Border Ranges fault. One of these is the Matanuska Glacier fault (located approximately 25 km east of the northeast corner of fig. 1; Burns and others, 1983; Plafker and others, 1994a). This 4-km-long east-west-striking fault apparently offsets tundra 30 cm vertically with a right-normal sense of offset (Gar Pessel, Alaska Division of Geological and Geophysical Surveys, written commun. to George Plafker, 1984). The other fault is the "Twin Peaks fault," mapped by **Urdike** and **Ulery** (1983), which lies 50 km northeast of Anchorage (figs. 1, 2).

The "Twin Peaks fault" as mapped by **Urdike** and **Ulery** (1983) is a 6-km-long, north-side-down normal fault with an average strike of 077°; it lies 1 to 1.5 km south of the Border Ranges fault *sensu strictu* (that is, the thrust fault that juxtaposes rocks of the accretionary prism with those of the backstop; Plafker and others, 1989) (fig. 2). The "Twin Peaks fault" does not offset any mapped con-

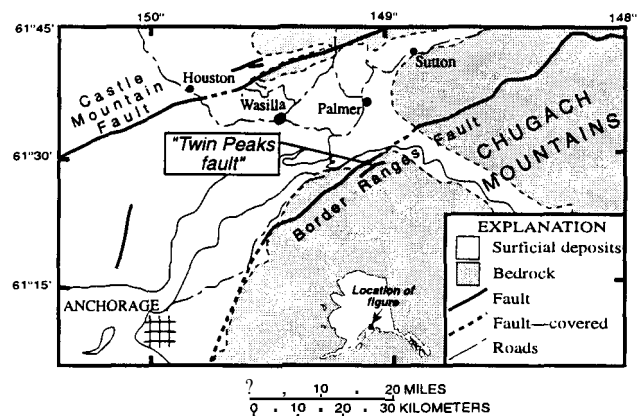


Figure 1. Map of the Anchorage area showing the trace of the Border Ranges fault (Winkler, 1992) and the "Twin Peaks fault" (Urdike and Ulery, 1983).

tact on the Updike and Ulery (1983) map but cuts across rocks of the McHugh Complex and, more significantly for earthquake hazards, "early-phase" rock glacier deposits in two locations. These early-phase rock glacier deposits are considered to be early to middle Holocene in age (Updike and Ulery, 1983), and thus the proposed faulting would have occurred in late Holocene time. Updike (1984, p. 20–21) said of the Twin Peaks fault, "Results obtained thus far strongly suggest that movement sufficient to generate major earthquakes has occurred within the past few thousand years." We examined aerial photographs of the "Twin Peaks fault" and inspected about 2.5 km of the proposed trace of the "fault" in order to further assess whether or not it is a seismogenic feature as interpreted by Updike (1984). A correct assessment of *this* structure is critical for evaluating earthquake hazards in south-central Alaska.

## AERIAL PHOTOGRAPHIC INTERPRETATIONS ALONG THE "TWIN PEAKS FAULT"

Aerial photographs were used to study structures and Quaternary deposits in the vicinity of the "Twin Peaks fault" (fig. 3). Our discussion of geomorphic features (denoted by letters on fig. 3) along the trace of the "Twin Peaks fault" (as defined by Updike and Ulery, 1983) follows from east to west (top to bottom on fig. 3).

(A)—This is an unusual linear trough with a crest on either side that appears to lie within talus and colluvium along the top of this horizontal mountain ridge. The feature appears to have the south side downthrown and has an uphill-facing scarp. It does not continue eastward beneath colluvium on the east side of the mountain. The swale is

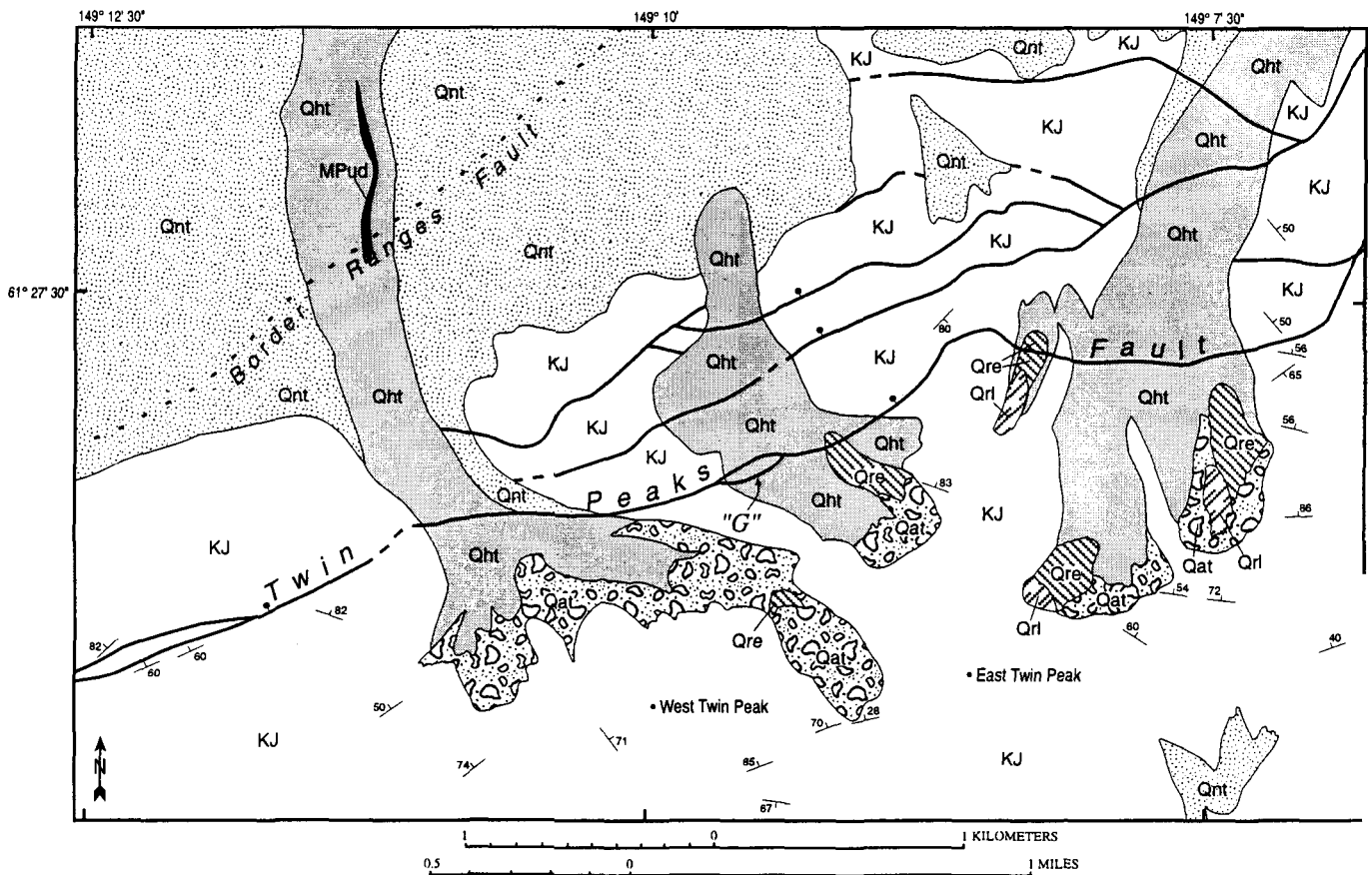


Figure 2. Simplified geologic map of the Twin Peaks area, modified from Updike and Ulery (1983). The map roughly corresponds in area to the aerial photographs in figure 3. Units are as follows: Qht, Holocene till, which includes all Holocene till units on the Updike and Ulery (1983) map; Qnt, Naptowne (late Quaternary) till, which includes all Naptowne till units on the Updike and Ulery (1983) map; Qat, large active talus deposits; Qre, rock-glacier deposits—early phase; Qrl, rock-glacier deposits—late phase; KJ, combined Jura-Cretaceous McHugh Complex metavolcanic and metasedimentary rocks and Valdez Group flysch deposits; Mpud, Eklutna ultramafic complex, dominantly dunite. Faults entirely within Mesozoic units are not shown. "G," locality G discussed in the text and shown on figures 3, 4, and 5.

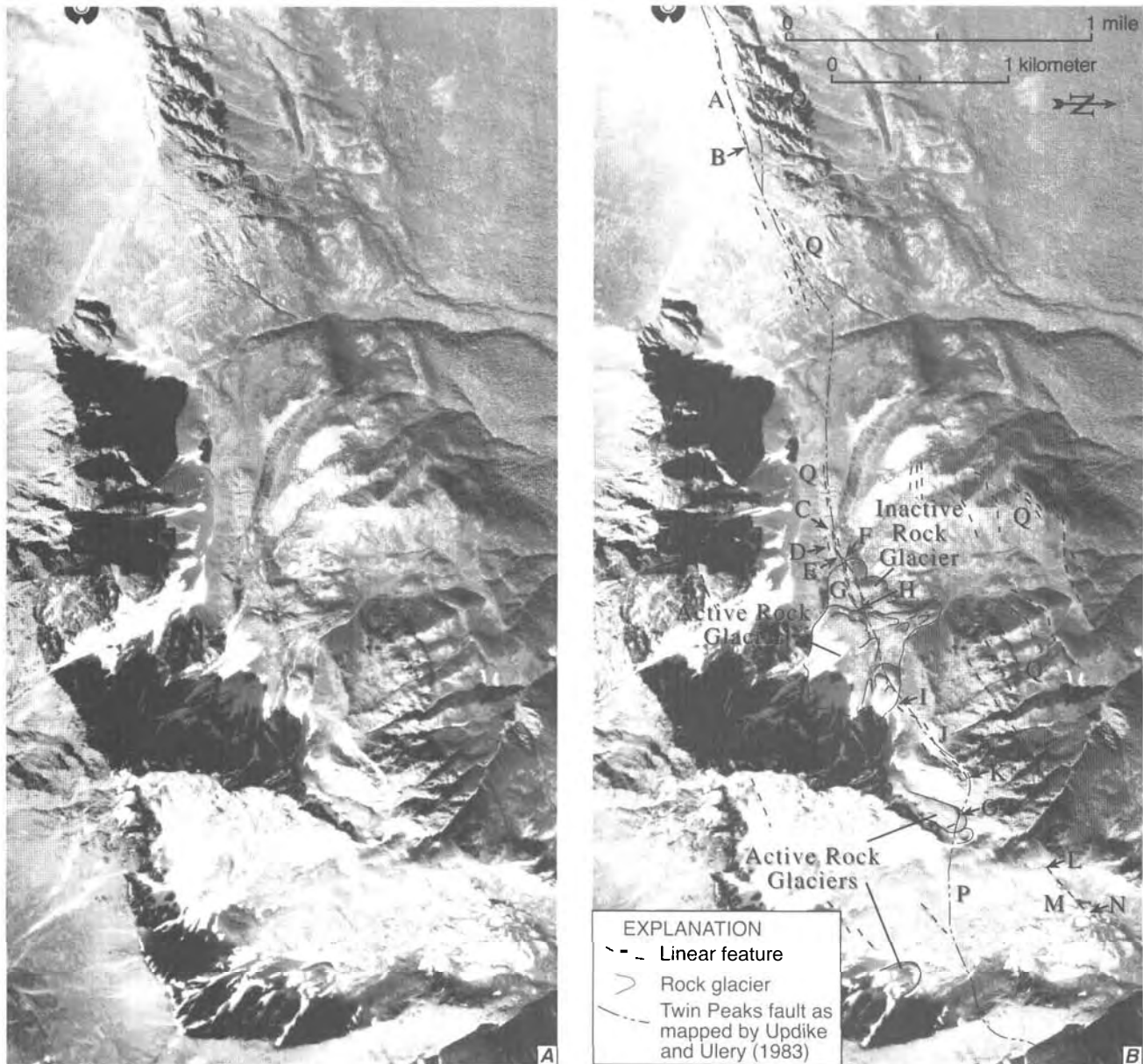


parallel to bedrock structural fabric on the north side of the mountain. The feature is probably a sackung, that is, a gravitational spreading ridge (e.g., Varnes and others, 1989). Yehle and Schmoll (1987) produced a surficial geologic map that includes this area, and they also considered this feature to be a sackung. Sackungen may be associated with seismic shaking in glaciated mountainous areas (Dohrenwend and others, 1978).

(Q)—At locations labeled Q, the structural fabric of the McHugh Complex is parallel to the mapped trace of the

"Twin Peaks fault" (Updike and Ulery, 1983) and has an east-northeast strike. Bedrock fabric in the McHugh Complex is dominated by numerous shear zones (e.g., Bradley and Kusky, 1992) and thus would be expected to have a geomorphic expression due to preferential weathering of the shear zones. In a number of places on the aerial photographs, such as north of location A, the bedrock fabric has a clear geomorphic expression.

(B) to (C)—There are no scarps or linear swales between these two locations. Bedrock exposures with east-



**Figure 3.** Aerial photographs of the Twin Peaks area, photograph 6-27-86 Eklutna 20 No. 8 from AeroMap U.S., Inc.; scale is 1 in. = 2,500 ft, or approximately 1:32,250. Note that north is to the right. A, Uninterpreted image. B, Interpreted image. Letters label parts of the photograph discussed in the text. Numerous north-northwest-striking late faults can be seen on the aerial photo, but none are illustrated in order to emphasize the east-northeast structural grain. The rock glaciers were determined to be active because of the lack of vegetation on their surfaces.

northeast-striking structures (labeled Q) are close to points B and C. It is unlikely that geomorphic processes would have buried or eliminated an escarpment because there is a lack of sediment to cover the scarp and because the bedrock is at least partly resistant to colluvial processes.

(D)—One large and two smaller flanking curving swales are located in a saddle along this ridge. These swales possibly cut bedrock, as indicated by small vegetated exposures of slate on the north side. The swales have a depth of 1–2 m and are *cusped* northward with a curve approximately  $30^\circ$  along a horizontal distance of 50 m (as determined from our field examination). The origin of the swales is uncertain. On aerial photos they appear to be related to landsliding because of their *cusped* shape. The swales do roughly parallel bedrock structure to the north, and thus the swales may be related to landsliding along the bedrock fabric.

(E) to (F)—There is no evidence on the aerial photos for a scarp or a linear swale between these two locations.

(G)—This is the scarp that has been cited as evidence for recent movement on the "Twin Peaks fault" (see photograph on p. 21 of *Updike, 1984*). Understanding the origin of this scarp is critical to establishing if the "Twin Peaks fault" is active. This scarp is approximately 200 m long and crosscuts colluvium and talus of an inactive rock glacier. In map view, the scarp is slightly concave toward the north, as shown by *Updike and Ulery (1983)*. There are more scarps located downhill and about 75 m to the north. One of these is weakly defined, is approximately 125 m long, and consists of two equal-length linear segments that, in map view, are slightly offset. Approximately 75 m to the east of this scarp there is another short (~30-m) linear swale. The relationship between this swale and the scarp with the two equal-length segments is unclear because colluvium between them is undisturbed.

(H) to (I)—An active rock glacier lies between these points, and there is no evidence for a scarp or linear swale along the inferred trace of the "Twin Peaks fault" in this area.

(J)—There is an uphill-facing bedrock escarpment in this knobby area. This uphill-facing scarp is parallel to other bedrock structural features to the north (labeled Q). All these linear features follow the "rule of V's" for a steeply southward-dipping structure. If there has been lateral spreading on the southward-dipping structure, then the uphill-facing scarp is consistent with a sacking.

(K) to (L)—There is no evidence for either a scarp or a linear swale between these two locations. One would expect to observe effects of faulting on the bedrock ridge, just to the northeast of point K, if a fault continued alongstrike from point J into this area.

(M)—There is a vague linear swale in the colluvium along the trend of the bedrock scarp at point J.

(N)—We observe no evidence for scarps or linear swales along the mapped trace of the "Twin Peaks fault" to the northeast of this point.

(O)—*Updike and Ulery (1983)* show the mapped trace of the "Twin Peaks fault" cutting across the toe of this rock glacier. We consider it unlikely that a steep, north-dipping fault (dip is close to vertical according to their mapping) would make such a sharp bend from point J or point K toward point O. The curvilinear feature through which they run the trace of the "Twin Peaks fault" appears to be a lobe of an active rock glacier.

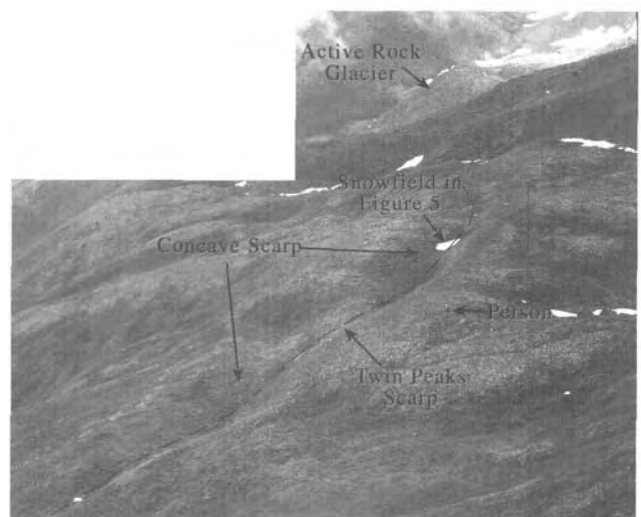
(P)—We observe no scarps or linear swales suggestive of a fault in this area, although *Updike and Ulery (1983)* map the "Twin Peaks fault" in this area.

Our interpretation of the aerial photographs is that the "Twin Peaks fault" as mapped by *Updike and Ulery (1983)* is not a continuous surficial feature, and that the trace of the mapped "fault" is parallel to the structural fabric in the *McHugh Complex* and includes a lobe near the front of an active rock glacier.

## FIELD INVESTIGATION OF THE "TWIN PEAKS FAULT"

We examined the "Twin Peaks fault" in the field at location A, and from halfway between points B and C to point H (fig. 3). In particular, we concentrated on examining the critical scarp at location G (fig. 3) because it was this scarp that *Updike (1984)* cited as evidence that the "Twin Peaks fault" is active.

The scarp at location G cuts a rock glacier that we consider to be inactive because it is covered with stable vegetation (figs. 4, 5). In contrast, the rock glacier to the east is presently active, as indicated by a complete lack of

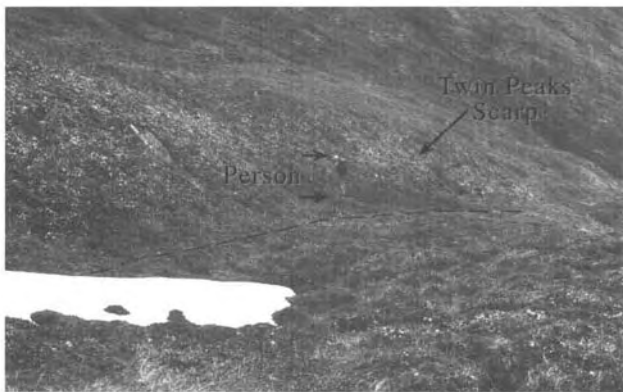


**Figure 4.** Oblique downward view of the Twin Peaks scarp at location G (figs. 2, 3). View is toward the northeast. Person in the photograph is about 2 m tall.

surface vegetation (fig. 4). The scarp is 3-4 m high on the inactive rock glacier, and it has a slope of about  $45^\circ$  (fig. 5). The curving linear swales at location D, in contrast, have a height of only about 1-2 m. The large scarp on the inactive rock glacier is located just above the steepest slope of the toe of the rock glacier. The scarp is slightly concave to the north (the downslope direction) and is generally oriented perpendicular to the downslope direction. The eastern end of the scarp strikes into—but is not visible within—the active rock glacier. The western end of the scarp dies out near, and slightly east of, the contact between the inactive rock glacier and the hillside to the west. We did not visit the lower scarps identified on aerial photographs due to time limitations, but we determined that the scarps were not sharply defined and they were covered with vegetation. Our field investigations confirmed the aerial photo interpretation that there was no evidence of a scarp on the hillside between locations E and F (fig. 3). We found no evidence for active faulting along the rest of the "Twin Peaks fault" from location F to the midpoint between locations B and C (fig. 3). There were no visible scarps, no springs, no sag ponds, no linear swales, no shutter ridges, no offset drainage channels, and no vegetation lineaments.

## INTERPRETATION

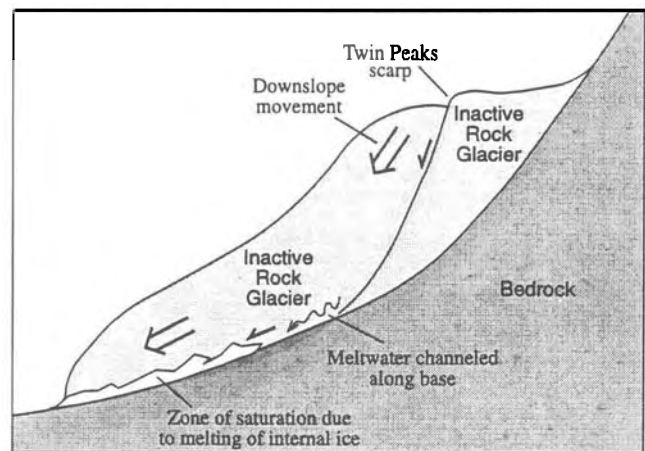
Active faults are generally planar features that display some sort of continuous surficial expression (e.g., Wallace, 1990), except where they are obscured by geomorphic processes after faulting. The orientation, shape, location, and discontinuous lateral extent of the "Twin Peaks fault" scarp and swales lead us to conclude that this feature is not an active fault. In addition, Yehle and Schmoll (1987), on a surficial geologic map that includes this area, did not map a fault scarp north of the Twin Peaks.



**Figure 5.** View westward along the Twin Peaks scarp at location G (figs. 2 and 3). Person in the photograph is about 2 m tall.

We interpret the scarp on the inactive rock glacier north of the Twin Peaks (location G, figs. 2 and 3) to be the result of degradation of the now-inactive rock glacier. Melting of internal ice may have promoted downslope motion of the toe of the inactive rock glacier as a discrete landslide, in which case the scarp would be the headscarp of a landslide. Landsliding may have been caused by water saturation of the rock-ice mixture beneath and near the toe of the inactive rock glacier (fig. 6). Although landslides within a rock glacier might be considered unusual owing to the abundance of boulders within the deposits, the cusped morphology of the scarp and its orientation perpendicular to the downslope direction support a landslide origin. The scarps downhill to the north, identified on aerial photos, are possibly minor scarps within the landslide and are not a splay of the "Twin Peaks fault" as shown by Updike and Ulery (1983).

Perhaps the most convincing argument against a fault-related origin for the Twin Peaks scarp is that the feature is not continuous through bedrock and the Quaternary deposits along its mapped length. In addition, the fact that the inferred trace is parallel to the dominant structural fabric in the underlying McHugh Complex suggests that other parts of the "Twin Peaks fault" we have not visited on the ground are actually related to bedrock fabric and not to recent faulting. We do not have a conclusive genetic explanation for the origin of every surficial swale or scarp along the mapped trace of the "Twin Peaks fault," but we consider the weight of the evidence to argue strongly against a throughgoing seismogenic fault in the Twin Peaks area. We consider the "Twin Peaks fault" of Updike and Ulery (1983) to be a coincidental alignment of bedrock structural fabric, swales related to sackungen, possible landslide headscarps, and a scarp related to landsliding within an inactive rock glacier.



**Figure 6.** Diagram showing how the Twin Peaks scarp might have developed from melting of internal ice within the rock glacier after its organized motion as a rock glacier ceased.

In addition, the fact that the scarp heights on the inactive rock glacier are significantly greater than the swale heights on the ridge to the west suggests that these scarps and swales were formed by different processes. The only plausible explanations for such height differences, if this were an active fault, would be drastic changes in either the dip of the fault or in the displacement along the fault, or the splaying of the fault into several strands. Over small distances (<1 km) extreme gradients in dip or in displacement are unlikely, and we saw no evidence for splaying of the feature. Moreover, both scarps and swales are **cusped**, and the lack of a scarp between the features at locations G and D argues against their being related to an active fault.

## DISCUSSION

If the "Twin Peaks fault" does not have any seismogenic potential, there is then no **surficial** evidence for Holocene activity on or near the Border Ranges fault close to Anchorage. Similarly, geologic evidence at numerous localities along the Border Ranges fault system indicates a lack of Quaternary activity on the fault, and that it has been inactive since Eocene time (Little and Naeser, 1989; Plafker and others, 1994a, b). This does not imply there has been no seismicity associated with late-stage faults near the Border Ranges fault (*sensu lato*), but rather that seismicity could not have been large enough to cause surface faulting. On 17 February 1995, there was a shallow magnitude 5.0  $m_b$  earthquake near Chickaloon, Alaska, that had a hypocenter about 5 km north of the mapped Border Ranges fault (Winkler, 1992), and a depth of 6 km. There are a number of steeply dipping brittle faults subparallel to the Border Ranges fault in the region where the earthquake occurred, and it is likely the earthquake occurred on one of these faults. These faults are not related to thrust faulting on the Border Ranges fault but rather to later stage faulting. Winkler (1992) considers these faults to be part of the "Border Ranges fault zone." While it appears that earthquakes large enough to cause extensive surface faulting (in the magnitude 7 range) along or near the Border Ranges fault have not occurred during Holocene time, the 17 February 1995 event implies that magnitude 5 earthquakes can be produced on nearby high-angle faults.

Finally, although we question the existence of the "Twin Peaks fault," we do not imply there has been no faulting at any time in the area. The Border Ranges fault lies 1 to 1.5 km to the north, and it is likely there are associated inactive faults nearby. In addition, geologic logs from a hydroelectric tunnel beneath Twin Peaks indicate abundant north-side-down normal faults occur to the north of the East Twin Peak (Bureau of Reclamation, 1958). However, we conclude the "Twin Peaks fault" is a coincidental alignment of bedrock structural fabric, swales related to

sackungen and landsliding, and a headscarp related to landsliding within an inactive rock glacier.

## REFERENCES CITED

- Bradley, D.C., and Kusky, T.M., 1992, Deformation history of the **McHugh** Complex, Seldovia quadrangle, south-central Alaska, in Bradley, D.C., and Ford, A.B., eds., *Geologic studies in Alaska by the U.S. Geological Survey, 1990: U.S. Geological Survey Bulletin 1999*, p. 17–32.
- Bureau of Reclamation, 1958, Eklutna dam, powerplant and tunnel: Technical Record of Design and Construction, U.S. Department of the Interior Bureau of Reclamation, 31 p.
- Bums, L.E., Little, T.A., Newbeny, R.J., Decker, J.E., and Pessel, G.H., 1983, Preliminary geologic map of parts of the Anchorage C-2, C-3, D-2, and D-3 quadrangles, Alaska: Alaska Division of Geological and Geophysical Surveys Report of Investigations 83-10, 3 pls., scale 1:25,000.
- Dohrenwend, J.C., **McCleary**, **Jefferson**, Hanson, Kathryn, and **Tillson**, D.D., 1978, Probable seismic triggering of sackung in the North Cascades, Washington [abs.]: *Geological Society of America Abstracts with Programs*, v. 10 (7), p. 390.
- Little, T.A., and Naeser, C.W., 1989, Tertiary tectonics of the Border Ranges fault system, Chugach Mountains, Alaska: deformation and uplift in a **forearc** setting: *Journal of Geophysical Research* v. 94, p. 4333–4359.
- Municipality of Anchorage, 1980-1982, Anchorage coastal resources atlas, v. 1–4.
- Page, R.A., Biswas, N.N., Lahr, J.C., and **Pulpan**, Hans, 1991, Seismicity of continental Alaska, in Slemmons, D.B., Engdahl, E.R., Zoback, M.D., and Blackwell, D.D., eds., *Neotectonics of North America: Boulder Colo., Geological Society of America, Decade of North American Geology Map Volume 1*, p. 47–67.
- Plafker, George, Gilpin, L.M., and Lahr, J.C., 1994a, Neotectonic map of Alaska, in Plafker, George, and Berg, H.C., eds., *The geology of Alaska: Boulder, Colo., Geological Society of America, The Geology of North America*, v. **G-1**, pl. 12, scale 1:2,500,000.
- Plafker, George, Moore, J.C., and Winkler, G.R., 1994b, Geology of the southern Alaska margin, in Plafker, George, and Berg, H.C., eds., *The geology of Alaska: Boulder, Colo., Geological Society of America, The Geology of North America*, v. **G-1**, p. 389–449.
- Plafker, George, Nokleberg, W.J., and Lull, J.S., 1989, Bedrock geology and tectonic evolution of the Wrangellia, Peninsular, and Chugach terranes along the trans-Alaska crustal transect in the Chugach Mountains and southern Copper River basin, Alaska: *Journal of Geophysical Research*, v. 94, p. 4255–4295.
- Updike**, R.G., 1984, Geological evaluations of earthquake hazards in the Anchorage area: *The Northern Engineer*, v. 16, no. 4, p. 18–25.
- Updike**, R.G., and Ulery, C.A., 1983, Preliminary geologic map of the Anchorage B-6 NW quadrangle (Eklutna Lake) Alaska: Alaska Division of Geological and Geophysical Surveys Report of Investigations 83-8, 2 sheets, scale 1:10,000.

Varnes, D.J., Radbruch-Hall, D.H., and Savage, W.Z., **1989**, Topographic and structural conditions in areas of gravitational spreading of ridges in the western United States: U.S. Geological Survey Professional Paper **1496**, **28** p.

Wallace, R.E., **1990**, Chapter **2**. Geomorphic expression, in Wallace, R.E., ed., The San **Andreas** fault system, California, U.S. Geological Survey Professional Paper **1515**, **283** p.

Winkler, G.R., **1992**, Geologic map and summary geochronology

of the Anchorage **1**°× **3**° quadrangle, southern Alaska: U.S. Geological Survey Miscellaneous Investigations Map **I-2283**, 1 sheet, scale **1:250,000**.

Yehle, L.A., and Schmoll, H.R., **1987**, Surficial geologic map of the Anchorage **B-7** NE quadrangle, Alaska: U.S. Geological Survey Open-File Report **87-416**, **20** p., scale **1:25,000**.

**Reviewers: Chris Waythomas and George Plafker**

# Silver-Lead-Zinc Mineral Occurrences in the Howard Pass Quadrangle, Brooks Range, Alaska

By Karen D. Kelley, Cliff D. Taylor, and Barrett A. Cieutat

## ABSTRACT

Nine occurrences of base-metal sulfide minerals in banded and brecciated veins (vein breccias) and one occurrence of sulfide-bearing concretions were discovered in the Howard Pass quadrangle during geochemical investigations. Most of these are small isolated mineral occurrences with little or no economic significance. However, the mineral occurrences are located in an east-west-trending belt in the southern part of the Howard Pass quadrangle that lies within a more broadly defined silver-lead-zinc province. The clustering of these occurrences in the southern part of the quadrangle, and the presence of numerous spatially associated barite mineral occurrences and other previously reported sediment-hosted Ag-Pb-Zn occurrences and deposits, indicate that this area was the focus for metal-rich fluids. The vein-breccia occurrences are hosted primarily by Upper Devonian and Mississippian clastic sedimentary rocks of the Endicott Group. They consist of sulfide-bearing banded quartz-calcite veins, quartz cemented breccias, and disseminated sulfide minerals. The dominant sulfide minerals are sphalerite and galena. Mineralized rock samples contain as much as 230 ppm Ag, 980 ppm As, 0.15 ppm Au, 730 ppm Cd, 3,300 ppm Cu, 2,400 ppm Ni, 100,000 ppm (10 percent) Pb, and 200,000 ppm (20 percent) Zn. Some samples contain anomalous concentrations of Sb (as much as 10,000 ppm) and Sn (100 ppm). Iron-rich, sulfide-bearing concretions hosted by black shale of Early Mississippian age are up to 0.3 m in diameter and probably formed during compaction and diagenesis of the shale. These concretions contain minor amounts of sphalerite and galena, as well as 3.7 percent Ca, 28 percent Fe, and 84 ppm Zn.

## INTRODUCTION

Stratiform sedimentary exhalative (SEDEX) massive sulfide deposits, sulfide-bearing concretions, and banded vein and breccia occurrences define a belt of silver-lead-zinc mineral occurrences and deposits that extends across the north-western and north-central Brooks Range (fig. 1). The apparent gap in the belt, suggested by only a single

occurrence in the Misheguk Mountain quadrangle, is probably due to the lack of geologic investigations in this area. The SEDEX deposits are hosted in chert, mudstone, and shale of Mississippian and Pennsylvanian age. Red Dog is the largest and highest grade deposit, but other important mineral occurrences include Su-Lik, Competition Creek, Suds, and Drenchwater (fig. 1). The banded and brecciated silver-lead-zinc veins are discordant but strata-bound in relatively older Upper Devonian and Lower Mississippian clastic rocks of the Endicott Group. Geologic and isotopic data suggest that most of the vein breccias are of similar age as the SEDEX deposits (Werdon and others, 1996). These data, together with other trace element geochemical data, indicate that the vein breccias may represent feeder zones to poorly developed, eroded, or structurally removed stratiform bodies (Kelley and Mull, 1995; Young, 1995; Schmidt, 1997). The best known examples of vein-breccia occurrences are in the Killik River and Howard Pass quadrangles. Several mineral occurrences in the Killik River quadrangle were discovered as part of mineral resource investigations of the area in the late 1980's and early 1990's (Duttweiler, 1987; Kelley and Kelley, 1992; Kelley and Mull, 1995; Kurtak and others, 1995), whereas many of those in the Howard Pass quadrangle were discovered during a mineral resource appraisal of the National Petroleum Reserve in Alaska (NPR) in the late 1970's (Jansons and Baggs, 1980; Jansons and Parke, 1981; Jansons, 1982). From 1990 to 1994, geochemical studies were conducted in the Howard Pass quadrangle as part of the Alaska Mineral Resource Assessment Program (AMRAP) (Kelley and others, 1996). Ten previously unknown mineral occurrences described in this study were discovered during follow-up investigations of geochemical anomalies in 1992 and 1994 (fig. 2). Although most of these new finds are small, isolated occurrences with little or no economic significance, they form an east-west-trending belt that extends across the southern part of the Howard Pass quadrangle, and they are of interest because of their spatial and perhaps genetic relationship to shale-hosted massive sulfide (SEDEX) deposits. The abundance of the vein breccias in the quadrangle and their spatial association with shale-hosted massive sulfide occurrences such as that at Drenchwater (Nokleberg and

**GEOLOGY**

Winkler, 1982; Werdon, 1996), with possible shale-hosted sulfide mineralization at **Twistem** Creek (Kelley and others, 1992), and with massive barite deposits directly north in the upper tributaries of Cutaway Creek (Kelley and others, 1993) indicate that metal-rich fluids were focused in this area (fig. 2). This paper briefly describes the local geologic and geochemical characteristics that led to discovery of the mineral occurrences. Additional information on individual silver-lead-zinc occurrences and (or) other types of mineral deposits in the quadrangle are provided by Jansons and Baggs (1980), Jansons and Parke (1981), Eilersieck and others (1982), Jansons (1982), Nokleberg and Winkler (1982), Kelley and others (1993), Kelley and Mull (1995), Kurtak and others (1995), and Werdon (1996).

Upper Proterozoic and lower Paleozoic sedimentary and igneous rocks in the central and southern Brooks Range record a passive pre-Devonian continental margin (Moore and others, 1994). Continental shelf to deep-marine-slope sedimentary strata, now exposed in the Brooks Range, were deposited along the passive margin. During Devonian time, a belt of volcanogenic massive sulfide (VMS) deposits, associated with **potassic** submarine rhyolites (Hitzman and others, 1986), formed a metallogenic province now exposed on the south side of the Brooks Range. A south-facing continental-margin shelf-platform sequence began to develop during a Late Devonian, rift-related extensional event

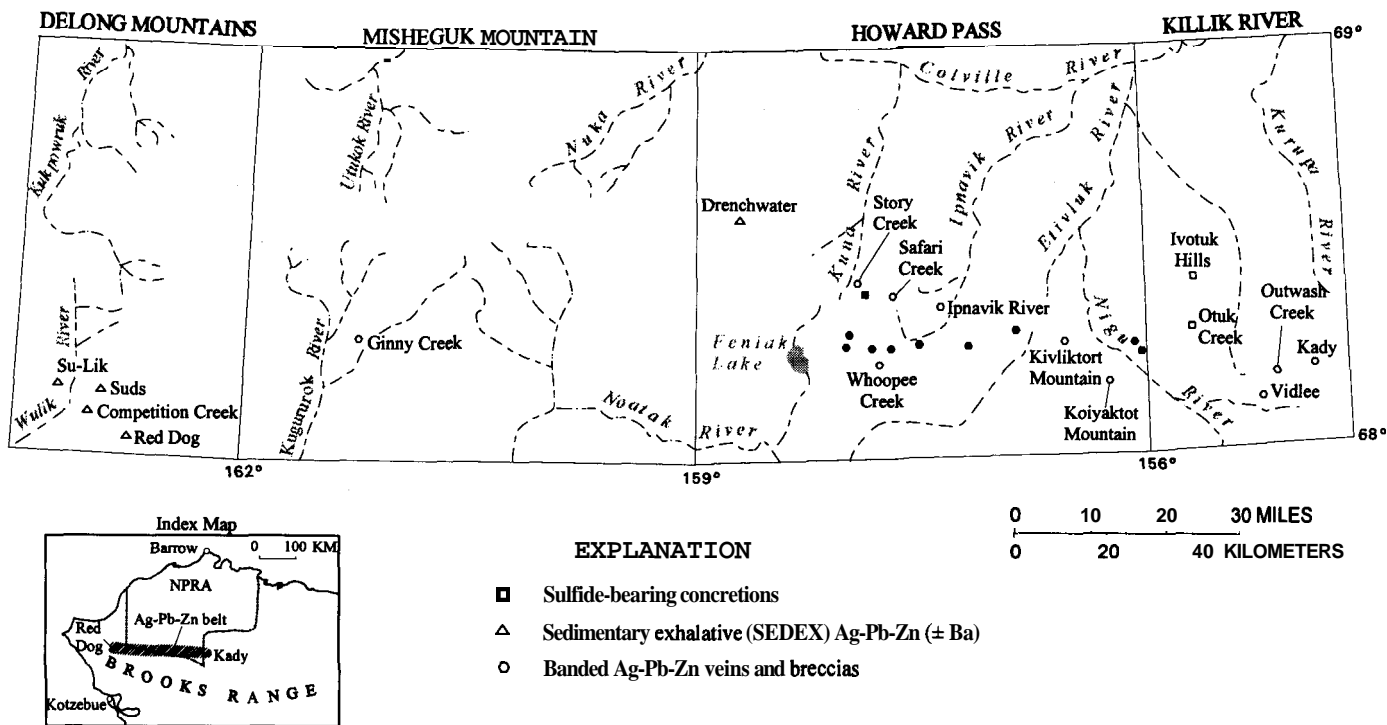
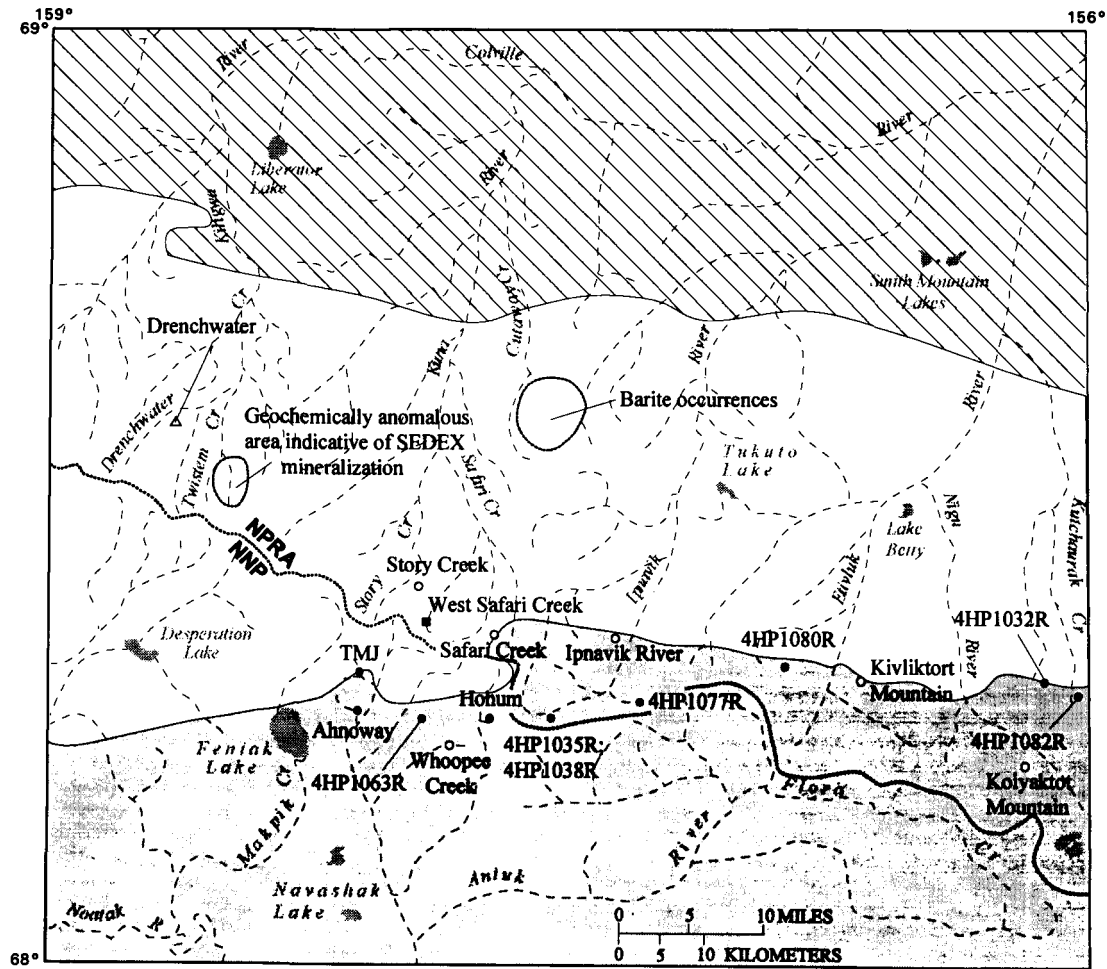


Figure 1. Locations of known Ag-Pb-Zn mineral occurrences and deposits within and adjacent to the Howard Pass quadrangle. Open symbols are previously reported mineral occurrences or deposits; closed symbols represent mineral occurrences described in this study and shown in more detail on figure 2. Inset shows the locations of the regional Ag-Pb-An province and of the National Petroleum Reserve in Alaska (NPR).

(Einaudi and Hitzman, 1986). Lower Mississippian marine shale and carbonate strata were deposited on older fluvial-deltaic sequences (Moore and others, 1994). Sedimentary-basin development during Mississippian and Pennsylvanian extension created an environment favorable for the formation of silver-lead-zinc massive sulfide (SEDEX) and barite deposits within carboniferous shale and, less commonly, within chert. These SEDEX and barite deposits now form a

metalogenic province on the north side of the Brooks Range. Latest Jurassic to earliest Cretaceous compressional deformation of the continental margin during the Brooks Range orogeny resulted in the formation of a north-directed fold-and-thrust belt with local blueschist metamorphism in its southern portion (Einaudi and Hitzman, 1986; Till, 1992). In the northern Brooks Range, the uplift and deformation resulted in a belt of intensively thrust-faulted middle



## EXPLANATION







-  Cretaceous continental and marine sedimentary rocks
-  Mississippian to Cretaceous marine sedimentary rocks
-  Devonian and Mississippian clastic sedimentary rocks of the Endicott Group
-  Banded Ag-Pb-Zn veins and breccias
-  Sulfide-bearing concretions
-  Sedimentary exhalative (SEDEX) Ag-Pb-Zn

Figure 2. Howard Pass quadrangle showing general distribution of sedimentary rocks (from Kurtak and others, 1995) and location of base-metal mineral occurrences. Open symbols are previously reported mineral occurrences; closed symbols are mineral occurrences described in this study. Abbreviations: NNP, Noatak National Preserve; NPR, National Petroleum Reserve in Alaska.



Paleozoic to Lower Cretaceous sedimentary rocks. Rocks of the foreland basin are exposed in the foothills north of the mountains and are predominantly siliciclastic rocks of Cretaceous age that were derived from the Brooks Range and prograded northward and eastward (Mull, 1982). Only Devonian through Cretaceous sedimentary rocks (fig. 2) and lesser mafic and ultramafic igneous rocks of Mississippian(?) through Jurassic age are exposed in the Howard Pass quadrangle. These rocks have been involved in large-scale thrust faulting that has obscured their original stratigraphic relations. They are overlain by upper Tertiary and Quaternary glacial and alluvial sedimentary deposits.

## MINERAL OCCURRENCES

The locations of nine occurrences of base-metal sulfide minerals in banded and brecciated veins and of one occurrence of sulfide-bearing concretions are shown on figure 2. Most of the mineralized vein breccias are small, isolated occurrences that were found in stream float and not traced to outcrop. These occurrences are listed by sample number on figure 2. Three vein-breccia occurrences, informally named the **Ahnoway**, Hohum, and **TMJ**, are exposed in outcrop. An additional occurrence of sphalerite-bearing concretions (informally named West Safari Creek) is exposed in outcrop along a western tributary of Safari Creek (fig. 2).

Although some of these mineral occurrences were discovered during regional reconnaissance geochemical sampling in 1992, most were discovered in 1994 by tracing geochemical anomalies upstream to their source. Nonmagnetic heavy-mineral-concentrate samples collected downstream from mineralized areas typically contain high concentrations of Ag (25 ppm), Pb (2500 ppm), and Zn (21,000 ppm), and stream-sediment samples contain anomalous Pb ( $\geq 70$  ppm) and Zn (2300 ppm). In addition, nonmagnetic heavy-mineral-concentrate samples collected downstream from some occurrences contain anomalous Cu (2100 ppm) and Au (50 ppm to  $>1,000$  ppm) (Kelley and others, 1994). Geochemical data for mineralized rocks from all of the mineral occurrences are included in table 1. A brief description of the four occurrences exposed in outcrop is given below.

### AHNOWAY

The **Ahnoway** occurrence is located in the Howard Pass B-4 (scale 1:63,360) quadrangle (N $1/2$  sec. 14, T. 33 N., R. 3 E.), about 7 km east of Feniak Lake (fig. 2) and within the Noatak National Preserve. Mineralized rocks are exposed on a low hill over an area of about 25 by 30 m in frost boils and "rubble-crop" (fig. 3A) north of a small, southeast-trending stream. Abundant mineralized float

(cobbles and boulders) was observed in the stream channel during reconnaissance stream-sediment sampling and was traced for about 0.4 km upstream to this outcrop.

Host rocks for this mineral occurrence are sandstone and siltstone of the Upper Devonian and Lower Mississippian Endicott Group. Mineralized rocks consist of sulfide-bearing banded veins and quartz- and sphalerite-cemented siltstone breccias (figs. 3B-D). The breccias consist of siltstone and sandstone clasts cemented by quartz; the quartz matrix commonly contains disseminated, fine-grained sphalerite (fig. 3B-C). The breccias have been cut by at least two generations of sulfide-bearing banded quartz-carbonate veins (fig. 3B, C). The most common sulfide minerals are sphalerite and galena. Pyrite and chalcopyrite are present but uncommon. The sulfide-rich breccias are extensively oxidized and weathered, and some exposures contain abundant secondary iron oxides and boxwork structures, indicating that sulfides have been leached and removed during weathering.

Mineralized rocks contain high concentrations of As (15-76 ppm), Au (0.05-0.15 ppm), Cd (58-680 ppm), Cu (85-530 ppm), Pb (3,400-92,000 ppm), and Zn (16,000-133,000 ppm) (table 1). Galena-rich samples contain high concentrations of Ag ( $>200$  ppm), and sphalerite-dominant samples contain high concentrations of Sn (32-45 ppm; table 1). The correlation between high Sn and sphalerite-rich samples suggests that the Sn is contained in the sphalerite. Trace element analyses of sphalerite from a variety of deposit types show that sphalerite can contain as much as 1 percent Sn (Levinson, 1974).

### HOHUM

The Hohum mineral occurrence lies within the Noatak National Preserve in the Howard Pass B-3 quadrangle (N $1/2$  sec. 16 and S $1/2$  sec. 9, T. 33 N., R. 5 E.), about 4 to 5 km northeast of the Whoopee Creek occurrence (Jansons, 1982) (fig. 2). Hohum is exposed on a large knoll about 200 m north of a small east-west-trending stream. The stream-sediment sample collected from this stream contained high concentrations of Pb (70 ppm) and Zn (300 ppm), and the nonmagnetic heavy-mineral-concentrate sample contained 200 ppm Ag,  $>1,000$  ppm Au, 5,000 ppm Pb, and 1,000 ppm Zn (Kelley and others, 1996). During follow-up investigations in 1994, mineralized cobbles and boulders were traced to outcrop.

The main zone of mineralized rocks extends in outcrop across a horizontal distance of about 30 m. Mineral textures are similar to those described for the **Ahnoway** mineral occurrence and consist primarily of banded quartz-calcite veins and quartz-cemented sulfide-bearing breccias hosted by thin-bedded sandstone and gray silty shale of the Endicott Group. Veins are typically about 2 cm wide but reach widths of at least 5 cm. Most veins strike northwest

Table 1. Selected geochemical data for Ag-Pb-Zn mineralized rock samples from the Howard Pass quadrangle

[**Occurrence** locations are shown on fig. 2. Names are given for occurrences exposed in outcrop; sample numbers are given for occurrences found only in float. Ag, As, Cd, Cu, Ni, Pb, and Zn analyzed by inductively coupled plasma-atomic emission spectrography (ICP-AES); Au analyzed by flame atomic absorption spectrophotometry. Sb and Sn analyzed by semiquantitative emission spectrography except for **Ahnoway** samples, which were analyzed for Sn by ICP-AES; NA, not analyzed; N, not detected at concentration shown; ccp, chalcopyrite; sp, sphalerite; gn, galena; py, pyrite; qtz, quartz; cal, calcite; ox, oxidized. More detail on analytical methods is included in Kelley and others (1996)]

Field No.	Occurrence	Latitude (° ' ")	Longitude (° ' ")	Ag (ppm)	As (ppm)	Au (ppm)	Cd (ppm)	Cu (ppm)	Ni (ppm)	Pb (ppm)	Sb (ppm)	Sn (ppm)	Zn (ppm)	Description
2HP615R1	Ahnoway	68 15 47	158 06 58	28	15	0.05	680	240	10	3,400	NA	45	133,000	sp-rich vein
2HP615R2	Ahnoway	68 15 47	158 06 58	110	76	.10	510	320	19	16,000	NA	32	124,000	sp-rich breccia
2HP615R3	Ahnoway	68 15 47	158 06 58	220	54	.10	260	530	47	83,000	NA	14	58,000	gn-rich qtz-cal vein
2HP615R4	Ahnoway	68 15 47	158 06 58	230	22	.15	58	85	8	92,000	NA	< 5	16,000	disseminated gn-qtz
4HP1051R	Hohum	68 15 57	157 45 35	20	29	NA	730	660	21	770	150	100	200,000	sp-rich breccia
4HP1052R	Hohum	68 15 54	157 45 02	N0.5	12	NA	< 2	26	9	430	N100	N10	220	oxidized qtz-cal vein
4HP1001R	Hohum	68 15 50	157 43 51	< .5	< 10	NA	2	7	10	610	N100	N10	900	gn-rich qtz-cal
4HP1002R	Hohum	68 15 51	157 44 14	100	< 20	0.1	280	140	15	19,000	N100	N10	67,000	gn-sp qtz-cal vein
4HP1003R	Hohum	68 16 02	157 43 43	50	980	< .05	200	3,300	2,400	16,000	10,000	N10	50,000	gn-ccppy-sp vein (ox)
2AKD832R	TMJ	68 18 30	158 05 11	1	31	NA	< 2	18	480	< 4	N100	N10	57	py vein
2TMJ001R	TMJ	68 18 29	158 04 56	< 2	42	< .002	< 2	71	63	6	N100	N10	29	py-rich qtz-cal vein
AKD833R	TMJ	68 18 29	158 05 09	N0.5	< 10	NA	< 2	34	170	< 4	N100	N10	170	py-rich qtz-cal vein
AKD834R	TMJ	68 18 29	158 05 09	N0.5	180	NA	< 2	21	140	14	N100	N10	29	pyritic black shale
AKD831R	TMJ	68 18 28	158 05 04	N0.5	91	NA	7	150	220	< 4	N100	N10	650	oxidized py-qtz-cal vein
2HP610R	W. Safari Cr.	68 22 26	157 54 36	< 2	< 10	NA	< 2	2	50	4	N100	N10	84	concretion; trace sp
4HP1080R		68 19 14	156 52 45	200	< 20	.05	160	100	19	100,000	1,000	N10	25,000	gn-sp qtz vein; float
4HP1032R		68 18 01	156 09 27	5	170	NA	220	53	9	2,700	N100	N10	87,000	gn-sp breccia; float
4HP1077R		68 17 02	157 19 49	50	< 20	.15	330	150	9	2,100	N100	N10	160,000	gn-sp breccia; float
4HP1035R		68 16 04	157 31 53	70	< 10	NA	< 2	38	21	36,000	150	N10	330	gn-rich breccia; float
4HP1038R		68 16 04	157 31 53	7	< 10	NA	< 2	< 1	8	3,700	N100	N10	120	gn-rich breccia; float
4HP1082R		68 16 52	156 03 08	3	< 20	< .05	< 4	27	5	6,300	N100	N10	260	gn-rich vein, float
4HP1063R		68 16 15	157 54 28	15	24	NA	380	140	12	11,000	N100	N10	100,000	gn-sp breccia, float

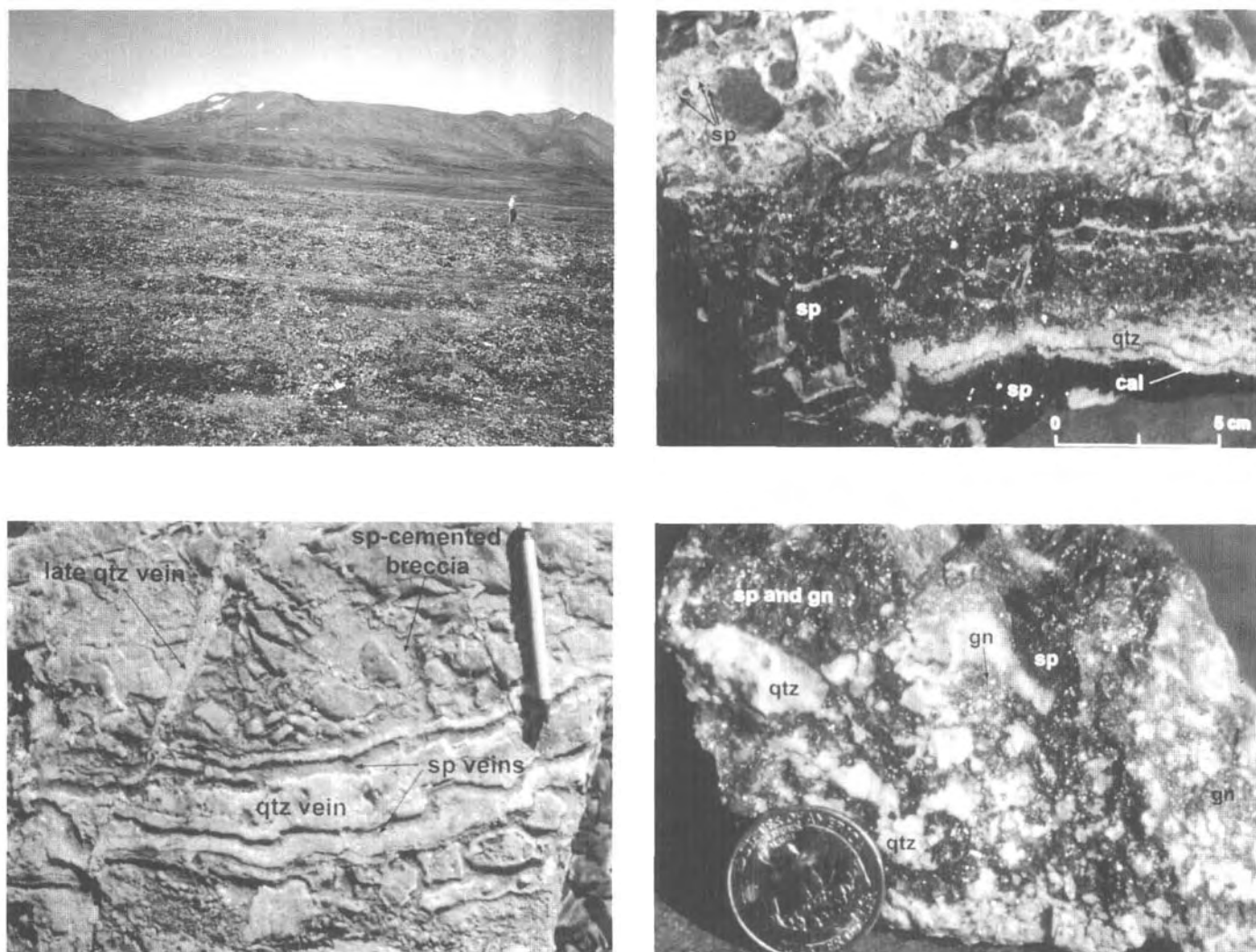
to east-west. Clots of galena up to several millimeters in size are common in some vein samples. Other samples contain massive, banded, red-brown sphalerite and galena in quartz-calcite veins. Some vein samples contain about 20 percent sulfide minerals, similar to banded veins at the **Ahnoway** occurrence (fig. 3B). Sphalerite and galena are the most abundant sulfide minerals, but pyrite and chalcocopyrite are also locally abundant. Minor iron oxides are found along some vein margins, and malachite staining is seen in some copper-rich veins and breccias.

The geochemical signature of mineralized rocks from the Hohum is similar to that at **Ahnoway** (table 1). Vein and breccia samples contain high concentrations of Ag (20-100 ppm), Cd (200-280 ppm), Pb (16,000-19,000 ppm), and Zn (up to 20 percent). Some lead-rich samples contain

high Sb concentrations (10,000 ppm), and sphalerite-bearing samples have as much as 100 ppm Sn (table 1). The arsenic, copper, and nickel contents of some samples reflect the abundance of pyrite (As and Ni substitute for Fe; Levinson, 1974) and of chalcocopyrite and associated oxidation products. For instance, a partly oxidized vein containing galena, chalcocopyrite, pyrite, and sphalerite from the Hohum contains 980 ppm As, 3,300 ppm Cu, and 2,400 ppm Ni (table 1).

### TMJ

The TMJ occurrence is located in the Howard Pass B-4 quadrangle (N<sup>1</sup>/<sub>2</sub> sec. 36, T. 34 N., R. 3 E.), about 5 km



**Figure 3.** The **Ahnoway** mineral occurrence. **A**, View to north; low rubble hill in foreground consists of mineralized veins and breccias in siltstone and sandstone of the Endicott Group. **B**, Weathered surface of vein breccia showing sphalerite-cemented breccia cut by at least two stages of quartz veining. **C**, Sphalerite-rich vein breccia shows different depositional textures. Quartz-cemented siltstone breccia with interstitial sphalerite appears to be cut by at least two generations of massive banded sphalerite in quartz-carbonate veins. **D**, Galena and quartz with minor sphalerite are in siltstone breccia with quartz matrix.

north of the **Ahnoway** occurrence (fig. 2). During reconnaissance stream-sediment sampling, sphalerite-bearing quartz was observed in stream float near the mouth of a southeast-trending stream. About 2.2 km upstream from this site, quartz-calcite veins, ranging from 10 to 25 cm wide, were found in outcrop along the northernmost of two branching tributaries of the stream (fig. 4). The veins are hosted in Endicott Group siltstone and sandstone, near a contact with black shale. Locally, the veins contain abundant pyrite; other sulfide minerals were not observed. About 25 m west of the siltstone–black shale contact is a 7-cm-wide, coarse-grained pyrite vein in shale that strikes north-west and dips steeply to the south. TMJ differs from the **Ahnoway** and **Hohum** mineral occurrences in its lack of mineralized breccias, its abundance of pyrite, and its lack of base-metal sulfide minerals.

Nearly all vein samples from this locality have high As (31-180 ppm) and Ni concentrations (140-480 ppm) that are probably contained in pyrite (table 1). Low concentrations of Pb in all samples reflect the absence of galena. However, elevated concentrations of Zn (as much as 650 ppm) in one pyrite-bearing quartz-calcite vein sample and the presence of sphalerite-bearing quartz in float down-

stream from the vein outcrop suggest that fine-grained sphalerite may be present in the veins.

### WEST SAFARI CREEK

Concretions in Lower Mississippian black shale (Kayak Shale; fig. 5) occur at stream level along a western tributary of Safari Creek about 10 km northeast of the TMJ mineral occurrence (fig. 2) in the Howard Pass B-4 quadrangle (SE<sup>1</sup>/<sub>4</sub> sec. 26, T. 12 s., R. 4 E.). The concretions are exposed over a horizontal distance of about 15 m along the east bank of the stream. During stream-sediment sampling, abundant concretions were found in float and traced 0.4 km upstream to outcrop.

The concretions range in diameter from 7 cm to 0.3 m. They are filled with abundant coarse-grained white calcite that apparently formed in open spaces and cracks in semi-consolidated mudstone, probably during compaction and diagenesis. Sparse clots of sulfide minerals in the core, or less commonly toward the rim, occur in some concretions. The most common sulfide mineral is coarse red-brown sphalerite, although a trace of galena was observed in one



**Figure 4.** The TMJ occurrence consists of pyrite-bearing quartz-calcite veins cutting siltstone and sandstone of the Endicott Group.

concretion. Secondary red-orange iron oxides have formed along the rims of some of the largest concretions.

The concretions contain 28 percent Fe, 3.7 percent Ca, and 84 ppn Zn (table 1; Kelley and others, 1996). Concretions similar to these were found at one locality in the Killik River quadrangle (Kelley and Mull, 1995) and at four localities in the Chandler Lake quadrangle (Kurtak and others, 1995) to the east, suggesting that metal-rich concretions are prevalent throughout the extent of the Kayak Shale.

#### OTHER OCCURRENCES

Several other occurrences of galena- and (or) sphalerite-rich veins and breccias were found during follow-up geochemical investigations. Most of these consisted of one or two large (10-50 cm) mineralized boulders that were probably the source of the stream-sediment and heavy-mineral-concentrate geochemical anomalies; the outcrop sources for these boulders were not identified. Geochemical analyses for these occurrences, listed by sample number, are given in table 1; sites are shown in figure 2.

#### DISCUSSION

The vein-breccia and sulfide-bearing concretion occurrences form an east-west-trending belt in the southern part of the Howard Pass quadrangle that lies within a more broadly defined silver-lead-zinc province (fig. 1). Strati-form sedimentary exhalative massive sulfide (SEDEX) deposits within the province were formed at least in part syngenetically with their enclosing Mississippian and Pennsylvanian host rocks (Moore and others, 1986; Werdon, 1996). Most vein breccias are discordant but strata-bound in clastic rocks of the Upper Devonian and Mississippian Endicott Group (fig. 2). The vein breccias are rich in silver (as much as 230 ppn), lead (as much as 100,000 ppn), and zinc (as much as 200,000 ppm), and they may also contain anomalous concentrations of gold (as much as 0.15 ppm) and copper (as much as 3,300 ppn). They characteristically lack significant concentrations of barium. In contrast, SEDEX deposits (for example, Drenchwater) are not associated with anomalous concentrations of gold and copper but contain highly anomalous concentrations of barium (Kelley and others, 1992). Goodfellow and others (1993)



**Figure 5.** The West Safari Creek mineral occurrence consists of iron-rich concretions in black shale of Early Mississippian age. Cores of some concretions contain sparse, red-brown sphalerite, and one concretion contains galena.

suggested that feeder zones that are discordant with their associated stratiform bodies typically contain lower **Zn/Pb**, **Pb/Ag**, **Fe/Zn**, and **Ba/Zn** ratios than the stratiform sulfide bodies themselves. The contrasting geochemical signatures of the vein breccias and shale-hosted massive sulfides at Drenchwater may reflect geochemical zoning, with the feeder zones (that is, the vein breccias) containing a different geochemical signature than overlying stratiform sulfides. These geochemical data suggest a genetic relationship between the two types of mineral occurrences and imply that both types formed primarily during Mississippian and Pennsylvanian time. Geologic mapping and isotopic data indicate that most vein-breccia occurrences are similar in age to SEDEX deposits in the central and western Brooks Range (Werdon and others, 1996), which further supports this interpretation. An alternative explanation by Kurtak and others (1995) and Werdon and others (1996) is that some of the vein breccias were formed by remobilization of metals from disseminated sources in the Endicott Group during the Jurassic to Cretaceous Brooks Range orogeny.

Acknowledgments.— We wish to thank Paul Briggs, Dave Fey, Jerry Motooka, and Elizabeth Bailey for chemical analyses. We also appreciate the efforts of Carter Borden and Elizabeth Bailey, who helped with field work during reconnaissance stream-sediment geochemical sampling.

## REFERENCES CITED

- Duttweiler, K.A., 1987, Use of factor analysis in locating base metal mineralization in the Killik River quadrangle, Alaska, *in* Hamilton, T.D., and Galloway, J.P., eds., *Geologic studies in Alaska by the U.S. Geological Survey during 1986*: U.S. Geological Survey Circular 998, p. 27-30.
- Einaudi, M.T., and Hitzman, M.W., 1986, Mineral deposits in northern Alaska: Introduction: *Economic Geology*, v. 81, p. 1583-1591.
- Ellersieck, Inyo, Jansons, Uldis, Mayfield, C.F., and Tailleur, I.L., 1982, The Story Creek and Whoopee Creek lead-zinc-silver occurrences, western Brooks Range, Alaska, in Conrad, W.L., ed., *The U.S. Geological Survey in Alaska—Accomplishments during 1980*: U.S. Geological Survey Circular 844, p. 35-38.
- Goodfellow, W.D., Lydon, J.W., and Turner, R.J.W., 1993, Geology and genesis of stratiform sediment-hosted (SEDEX) zinc-lead-silver sulphide deposits, *in* Kirkham, R.V., Sinclair, W.D., Thorpe, R.I., and Duke, J.M., eds., *Mineral deposit modeling*: Geological Association of Canada Special Paper 40, p. 201-253.
- Hitzman, M.W., Proffett, J.M., Jr., Schmidt, J.M., and Smith, T.E., 1986, Geology and mineralization of the Ambler district, northwestern Alaska: *Economic Geology*, v. 81, p. 1592-1618.
- Jansons, Uldis, 1982, Zinc-lead occurrences in and near the National Petroleum Reserve in Alaska: U.S. Bureau of Mines Mineral Lands Assessment Report MLA 121-82, 55 p.
- Jansons, Uldis, and Baggs, D.W., 1980, Mineral investigations of the Misheguk Mountain and Howard Pass quadrangles, Alaska: U.S. Bureau of Mines Open-File Report 38-80, 76 p.
- Jansons, Uldis, and Parke, M.A., 1981, 1978 mineral investigations in the Misheguk Mountain and Howard Pass quadrangles, Alaska: U.S. Bureau of Mines Open-File Report 26-81, 195 p.
- Kelley, J.S., Tailleur, I.L., Morin, R.L., Reed, K.M., Harris, A.G., Schmidt, J.M., and Brown, F.M., 1993, Barite deposits in the Howard Pass quadrangle and possible relations to barite elsewhere in the northwestern Brooks Range, Alaska: U.S. Geological Survey Open-File Report 93-215, 13 p.
- Kelley, K.D., Bailey, E.A., Briggs, P.H., Motooka, J.M., and Meier, A.L., 1996, Digital release of stream-sediment, heavy-mineral-concentrate, soil, water, and rock geochemical data collected in the Howard Pass quadrangle, Alaska: U.S. Geological Survey Open-File Report 96-711.
- Kelley, K.D., Bailey, E.A., Cicutat, B.A., and Borden, J.C., 1994, Gold in heavy-mineral-concentrate samples from the Howard Pass quadrangle, Brooks Range, Alaska, *in* Till, A.B., and Moore, T.E., eds., *Geologic studies in Alaska by the U.S. Geological Survey, 1993*: U.S. Geological Survey Bulletin 2107, p. 83-89.
- Kelley, K.D., Borden, J.C., Bailey, E.A., Fey, D.L., Motooka, J.M., and Roushey, B.H., 1992, Geochemically anomalous areas in the west-central part of the Howard Pass quadrangle, National Petroleum Reserve, Brooks Range, Alaska, *in* Bradley, D.C. and Dusel-Bacon, Cynthia, eds., *Geologic studies in Alaska by the U.S. Geological Survey, 1991*: U.S. Geological Survey Bulletin 2041, p. 60-69.
- Kelley, K.D., and Kelley, D.L., 1992, Reconnaissance exploration geochemistry in the central Brooks Range, northern Alaska: Implications for exploration of sediment-hosted zinc-lead-silver deposits: *Journal of Geochemical Exploration*, v. 42, p. 273-300.
- Kelley, K.D., and Mull, C.G., 1995, Maps showing areas of potential for mineral resources in the Killik River quadrangle, Brooks Range, Alaska: U.S. Geological Survey Miscellaneous Field Studies Map MF-2225-A, scale 1:250,000.
- Kurtak, J.M., Hicks, R.W., Werdon, M.B., Meyer, M.P., and Mull, C.G., 1995, Mineral investigations in the Colville mining district and southern National Petroleum Reserve in Alaska: U.S. Bureau of Mines Open-File Report 8-95, 217 p.
- Levinson, A.A., 1974, Introduction to exploration geochemistry: Calgary, Canada, Applied Publications Ltd., 612 p.
- Moore, D.W., Young, L.E., Modene, J.S., and Plahuta, J.T., 1986, Geologic setting and genesis of the Red Dog zinc-lead-silver deposit, western Brooks Range, Alaska: *Economic Geology*, v. 81, no. 7, p. 1696-1727.
- Moore, T.E., Wallace, W.K., Bird, K.J., Karl, S.M., Mull, C.G., and Dillon, J.T., 1994, Geology of northern Alaska, *in* Plafker, George, and Berg, H.C., eds., *The geology of Alaska*: Boulder, Colo., Geological Society of America, *The Geology of North America*, v. G-1, p. 49-140.
- Mull, C.G., 1982, The tectonic evolution and structural style of the Brooks Range, Alaska—an illustrated summary, *in* Powers, R.B., ed., *Geological studies of the Cordilleran thrust belt*: Denver, Colo., Rocky Mountain Association of Geologists, v. 1, p. 1-45.

- Nokleberg, W.J., and **Winkler**, G.R., 1982, Stratiform zinc-lead deposits in the Drenchwater Creek area, Howard Pass quadrangle, northwestern Brooks Range, Alaska: U.S. Geological Survey Professional Paper 1209, 22 p.
- Schmidt, J.M., 1997, Shale-hosted Zn-Pb-Ag and barite deposits of Alaska, in Goldfarb, R.J., and Miller, L.D., eds., Mineral deposits of Alaska: Economic Geology Monograph No. 9.
- Till, A.B., 1992, Detrital blueschist-facies metamorphic mineral assemblages in Early Cretaceous sediments of the foreland basin of the Brooks Range, Alaska, and implications for orogenic evolution: *Tectonics*, v. 11, no. 6, p. 1207-1223.
- Weldon, M.B., 1996, Drenchwater, Alaska: Zn-Pb-Ag mineralization in a mixed black shale- volcanic environment, in Coyner, A.R., and **Fahey**, P.L., eds., Geology and ore deposits of the American **Cordillera**—**Geological Society of Nevada Symposium Proceedings**, **Reno/Sparks**, Nev., April 1995, p. 1341-1354.
- Weldon, M.B., **Newberry**, R.J., Bums, L.E., and Mull, C.G., 1996, Probabilistic estimate of mineral resources in the Colville mining district, Alaska: Alaska Division of Geological and Geophysical Surveys Report of Investigations 96-5, 33p.
- Young, L.E., 1995, Empirical applications of common **lead-isotope** ratios to exploration: *Society of Economic Geologists Newsletter*, no. 22, p. 7-12.

Reviewers: **Tom** Nash and **Sherm** Marsh

# Areas Favorable for Metallic Mineral Resources and Newly Discovered Mineral Occurrences in the Buckstock Mountains Area, Southwestern Alaska

By John E. Gray and Peter M. Theodorakos

## ABSTRACT

The Buckstock Mountains area is located in the southwestern Sleetmute 1°×3° quadrangle and is remote and poorly studied. Few mineral occurrences are known in the Buckstock Mountains, but the geology is similar to that of other areas in southwestern Alaska where polymetallic Au-As-Sb-W vein and Hg-Sb vein deposits are found. We conducted a drainage-basin geochemical survey in the Buckstock Mountains area and collected stream-sediment and heavy-mineral-concentrate samples from 313 sites. These samples were chemically analyzed for several trace elements; in addition, the heavy-mineral-concentrate samples were microscopically examined for their mineralogical content. The resultant data were interpreted in order to identify areas favorable for metallic mineral resources in the Buckstock Mountains and surrounding areas. In a few of these areas, mineralized stream cobbles or outcrops of mineralized rocks were found.

Samples collected from seven areas in the Buckstock Mountains contain anomalous concentrations of Au, Ag, As, B, Bi, Cu, Hg, Sb, Sn, or W; these areas are considered favorable for polymetallic vein deposits. Five of these areas contain significant gold concentrations that indicate the possibility of upstream polymetallic gold vein lodes. Four areas delineated as favorable for the presence of Hg-Sb vein lodes are found on the periphery of the Buckstock Mountains. In these four areas, the most consistent anomalies are Hg in stream-sediment samples and cinnabar in heavy-mineral-concentrate samples. Generally, in the areas delineated as favorable for metallic mineral deposits, Late Cretaceous and Tertiary granite porphyry dikes cut Cretaceous sedimentary rocks of the Kuskokwim Group or Cretaceous and Triassic sedimentary and volcanic rocks of the Gemuk Group.

## INTRODUCTION

The Buckstock Mountains are located about 60 km southeast of **Aniak** in the southwestern Sleetmute 1°×3° quadrangle (fig. 1). The Buckstock Mountains are favor-

able for metallic mineral resources because these mountains contain rocks similar to those found at the nearby Fortyseven Creek polymetallic Au-As-Sb-W vein lode (Hawley, 1989) and at epithermal Hg-Sb vein lodes found throughout southwestern Alaska (Sainsbury and MacKevett, 1965). However, few metallic mineral occurrences have been previously reported in the Buckstock Mountains, probably because few geologic, geochemical, and geophysical studies have been conducted in this area. In 1993 and 1994, a geochemical survey was conducted in the southwestern part of the Sleetmute quadrangle as part of the Alaskan Mineral Resource Assessment Program (**AMRAP**). The survey covered about 2,200 km<sup>2</sup> and included the Buckstock Mountains and surrounding areas.

Reconnaissance drainage-basin geochemical surveys are a rapid and efficient means of locating areas with possible mineral deposits. The objective of this study was to use both geochemical data from stream-sediment samples and geochemical and mineralogical data from **heavy-mineral-concentrate** samples to identify areas favorable for the presence of mineral deposits. This report delineates drainage basins containing samples with anomalous concentrations of Au, Ag, As, B, Bi, Cu, Hg, Sb, Sn, or W. The presence of highly anomalous concentrations of these elements may indicate that mineral deposits such as polymetallic Au-As-Sb-W vein and epithermal Hg-Sb vein deposits are present upstream. At some localities, mineralized rocks were found in the streams or in outcrops near the headwaters of the streams; these sites are delineated as newly discovered mineral occurrences.

## GEOLOGY

The geology of the Buckstock Mountains consists largely of sedimentary and volcanic rocks of the Triassic and Cretaceous Gemuk Group, sedimentary rocks of the Cretaceous Kuskokwim Group, and Late Cretaceous and early Tertiary mafic to felsic volcanic rocks, small granitic intrusions, and granite porphyry dikes and sills (fig. 2; Cady and others, 1955; Miller and others, 1989). The Gemuk Group consists of massive siltstones interbedded with lesser



amounts of chert, andesitic flows and tuffs, and thin interbeds of limestone, graywacke, and breccia (Cady and others, 1955). Fossils from these rocks are of Late Triassic and Cretaceous age (Cady and others, 1955). These rocks represent deep-marine to shallow-water and subaerial **facies** (Cady and others, 1955; Miller and others, 1989) and are part of the Hagemeister subterrane of the Togiak **terrane** (Box, 1985). Rocks of the Togiak terrane have undergone prehnite-pumpellyite to low-grade greenschist-facies metamorphism, but they lack a penetrative metamorphic fabric (Decker and others, 1994). The Togiak terrane represents an accreted subduction-related, intraoceanic **arc-trench complex** (Box, 1985; Wallace, 1983; Decker and others, 1994).

The Kuskokwim Group is a sequence of flysch representing turbidite fan, foreslope, shallow-marine, and shelf facies formed primarily by turbidity currents depositing detritus into an elongate, northeast trending, fault-controlled Cretaceous basin (Decker and Hoare, 1982; Bundtzen and Gilbert, 1983; Miller and Bundtzen, 1994). The Kuskokwim Group was first described by Cady and others (1955), who suggested that graywacke and lesser siltstone compose almost all of the sequence, and that graywacke is about twice as abundant as siltstone. Conglomerates and interbeds of volcanic tuffs and flows of intermediate composition are found locally (Cady and others, 1955; Miller and Bundtzen, 1994). Paleontological evidence and radiometric K-Ar dating indicate that rocks of the Kuskokwim Group range in age from Albian to Campanian (Cady and others, 1955; Hoare and Coonrad, 1959; Box and Murphy, 1987; Box and Elder, 1992; Miller and Bundtzen, 1994). The Kuskokwim Group is postaccretionary, overlying rocks of adjacent tectonostratigraphic terranes (Miller and others, 1989).

Late Cretaceous and early Tertiary hypabyssal granite porphyry intrusions are common in the Buckstock Mountains. Granite porphyry dikes and sills cut all rock types in the study area but most commonly intrude sedimentary rocks of the Kuskokwim Group (fig. 2). In southwestern Alaska, granite porphyry intrusions are generally peraluminous in composition, with  $Al_2O_3$  exceeding  $Na_2O+K_2O+CaO$ , and locally they contain garnet (Bundtzen and Swanson, 1984; Moll-Stalcup, 1994). Granite porphyries in the Buckstock Mountains and throughout southwestern Alaska range in age from 72 to 62 Ma (Reifenstuhel and others, 1984; Robinson and Decker, 1986; Decker and others, 1986, 1995; Miller and Bundtzen, 1994). In the Buckstock Mountains, granite porphyry dikes generally trend southwest and are steeply dipping (Cady and others, 1955). Although typically small in outcrop, these intrusions are important in southwestern Alaska because they show a close spatial association with Au-As-Sb-W vein and Hg-Sb vein lodes (Cady and others, 1955; Gray and others, 1992).

Mafic to felsic volcanic rocks are found in the north-eastern part of the study area (fig. 2). These rocks are

generally volcanic flows interbedded with lesser tuff, agglomerate, and minor **lahar** units (Cady and others, 1955). Rocks of **mafic** composition are most common, but intermediate and felsic compositions are also present (Miller and others, 1989). These volcanic rocks have not been dated in the study area, but similar rocks located elsewhere in the Sleetmute quadrangle are Late Cretaceous and early Tertiary in age based on K-Ar determinations ranging from about 75 to 64 Ma (Reifenstuhel and others, 1984; Robinson and others, 1984; Robinson and Decker, 1986).

Small granitic intrusions are also found in the eastern part of the study area. The intrusions consist of monzonite, quartz monzonite, granodiorite, or granite, and they cut **sedimentary** rocks of the Kuskokwim Group. These small granitic intrusions have not been dated in the Buckstock Mountains, but similar rocks elsewhere in the Sleetmute quadrangle are Late Cretaceous and early Tertiary in age based on K-Ar determinations ranging from about 68 to 64 Ma (Decker and others, 1984; Reifenstuhel and others, 1984; Robinson and others, 1984; Robinson and Decker, 1986).

## MINERAL OCCURRENCES

Only three mineral occurrences have been reported in the Buckstock Mountains area. Cady and others (1955) reported that placer gold was prospected or known on Gold Run, Girl, and Timber Creeks (fig. 1), but the exact location of the gold occurrences on these creeks was not given. In the region surrounding the Buckstock Mountains are several polymetallic Au-As-Sb-W vein and Hg-Sb vein lodes. For example, the Fortyseven Creek polymetallic Au-As-Sb-W vein lode is located about 20 km east of the Buckstock Mountains, on the ridge crest at the headwaters of Fortyseven Creek, a tributary of the Holitna River (fig. 1). At Fortyseven Creek, rocks consist of interbedded graywacke and shale of the Kuskokwim Group (Cady and others, 1955). An altered granite porphyry dike cuts these rocks near the lode (Hawley, 1989). The Fortyseven Creek lode consists of massive, hydrothermal, quartz-rich veins in sheared and faulted sedimentary rocks. The veins contain arsenopyrite, scheelite, wolframite, jamesonite, argentite, stibnite, pyrite, and gold, as well as locally abundant coarse sericite and minor tourmaline (Hawley, 1989). Mineralized samples contain as much as 34 ppm Au (Hawley, 1989). The lode has not been mined, but 27.7 kg of gold (891 oz) have been recovered from a placer mine downstream from the lode on Fortyseven Creek (Hawley, 1989). Similar polymetallic vein lodes containing arsenopyrite, pyrite, chalcopyrite, bornite, sphalerite, galena, marcasite, tetrahedrite, gold, bismuthinite, stephanite, cassiterite, scheelite, barite, or wolframite are known in the Russian Mountains (fig. 1) (Bundtzen and Laird, 1991), the Horn Mountains (Bundtzen and others, 1993), and throughout southwestern Alaska (Bundtzen and Miller, in press). Many

of these polymetallic mineral occurrences contain significant concentrations of gold, although some contain little or no gold.

Numerous epithermal Hg-Sb vein lodes are scattered throughout southwestern Alaska. Cinnabar and stibnite are the dominant ore minerals, with lesser amounts of realgar, orpiment, native mercury, pyrite, gold, limonite, and hematite (Sainsbury and MacKevett, 1965; Gray and others, 1990). Gangue is typically quartz, carbonate, dickite, and sericite. The deposits are found in a variety of sedimentary and igneous rocks, but commonly they show a close spatial and temporal association with Late Cretaceous and Ter-

tiary igneous rocks (Gray and others, in press). Most of the Hg-Sb lodes are small, consisting of veins a few centimeters wide that extend for strike lengths of only a few meters. However, at Red Devil, the largest mercury mine in Alaska, veins exceeded a meter in width and 100 m in length (MacKevett and Berg, 1963). Red Devil produced about 36,000 flasks of mercury (1 flask = 76 lb or 34.5 kg) (Miller and others, 1989). Several other smaller mercury mines are found throughout southwestern Alaska (Sainsbury and MacKevett, 1965). Mercury mines with recorded production located near the Buckstock Mountains include Cinnabar Creek (525 flasks; Nokleberg and others, 1987),

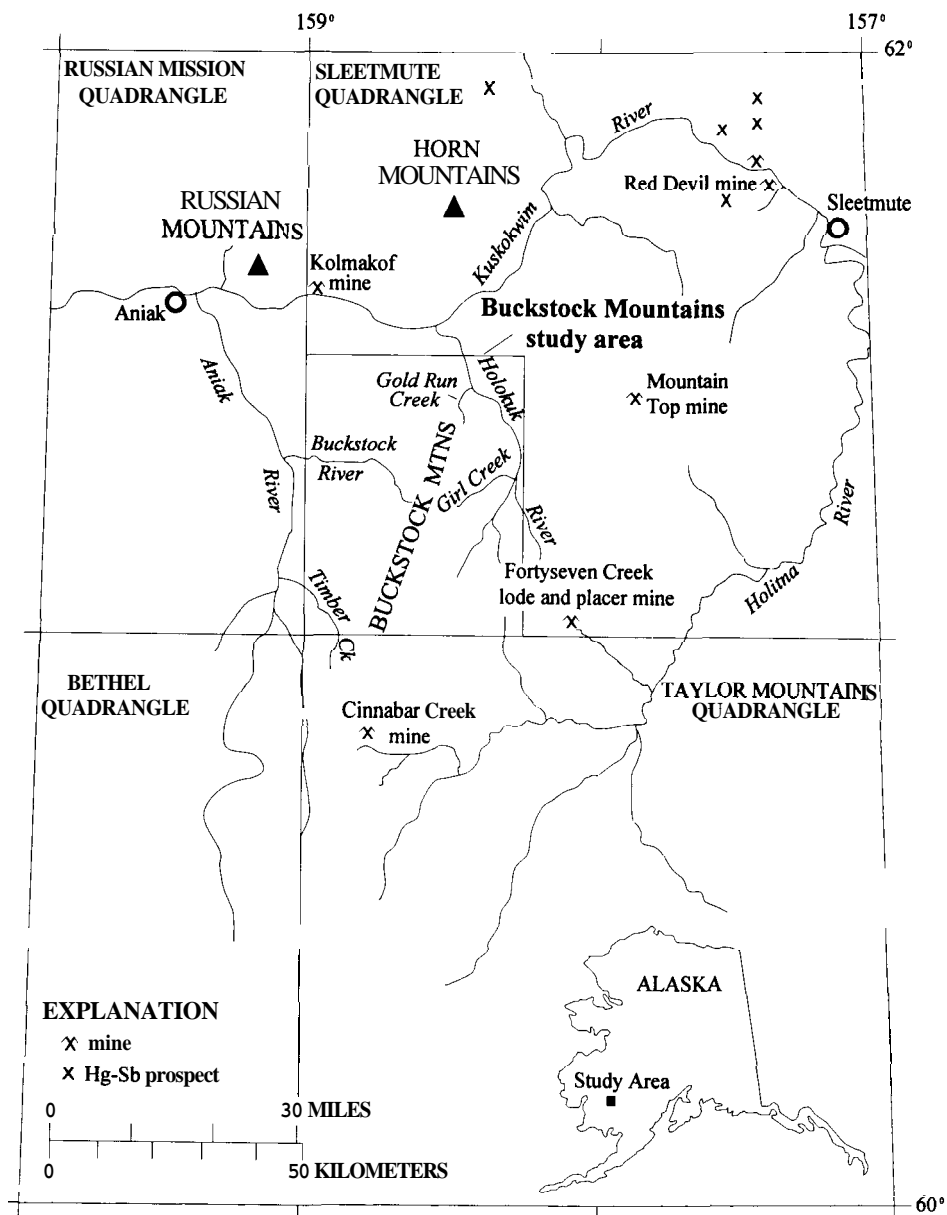
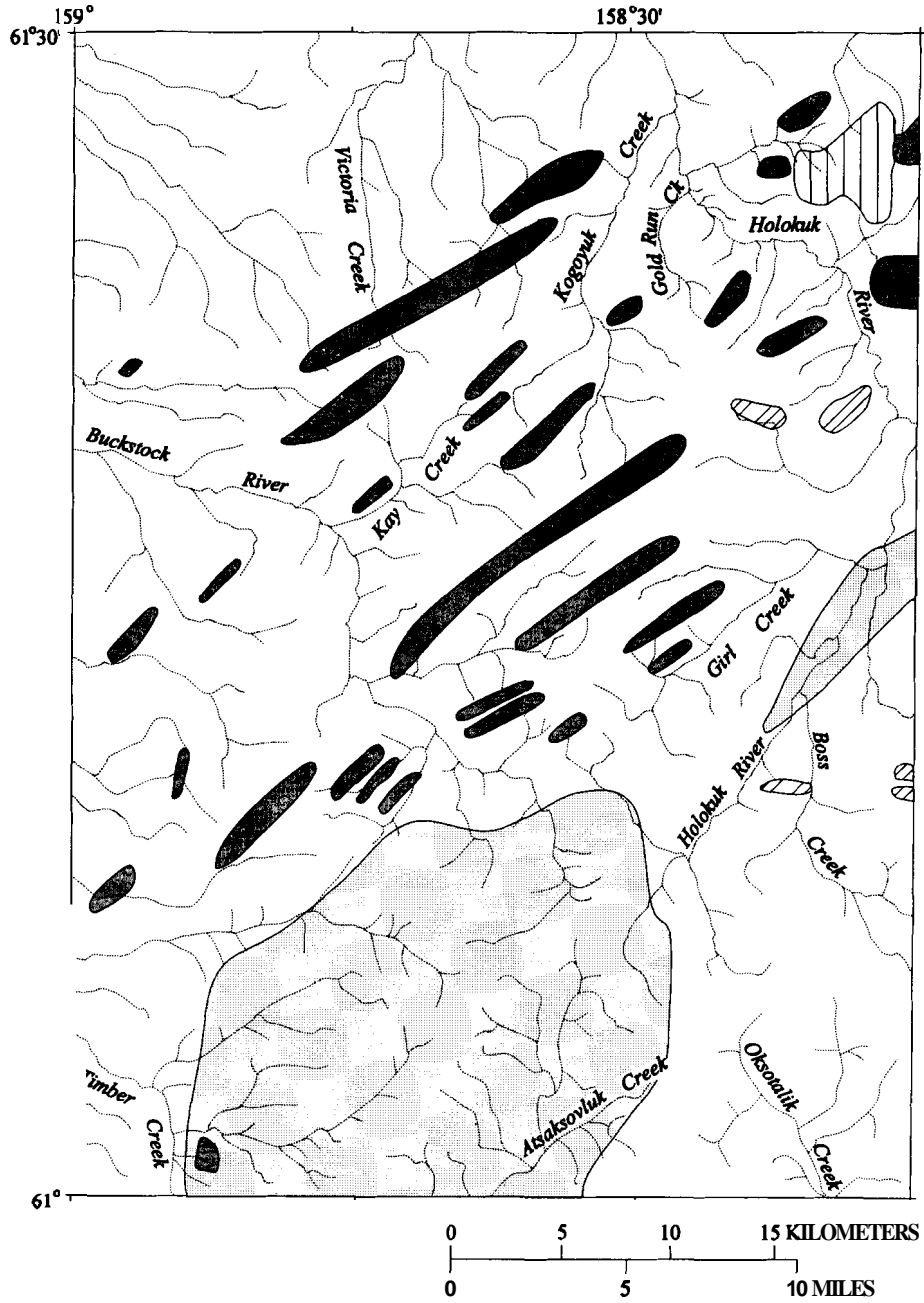


Figure 1. Location of the Buckstock Mountains study area and of mines and prospects in southwestern Alaska. Inset outline of the study area is shown for figures 2 and 3.



**EXPLANATION**



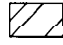

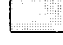
-  Granite porphyry (Tertiary and Late Cretaceous)
-  Mafic to felsic volcanicrocks (Tertiary and Late Cretaceous)
-  Intermediate to felsic intrusive rocks (Tertiary and Late Cretaceous)
-  Kuskokwim Group (Cretaceous) - Sedimentary rocks
-  Gemuk Group (Cretaceous and Triassic) - Sedimentary and volcanic rocks

Figure 2. Geology of Buckstock Mountains area (simplified from Cady and others, 1955).

Mountain Top (165 flasks; Miller and others, 1989), and Kolmakof (2 flasks; Cady and others, 1955) (fig. 1). Total mercury production from mines in southwest Alaska is about 41,000 flasks (Miller and others, 1989). The high concentrations of Hg, Sb, and As in minus-80-mesh **stream-sediment** samples and the presence of cinnabar in nonmagnetic heavy-mineral-concentrate samples collected downstream from Hg-Sb vein lodes are diagnostic indicators for this type of deposit (Gray and others, 1991). The presence of polymetallic Au-As-Sb-W and Hg-Sb mines, prospects, and mineral occurrences in areas with similar geology to that in the study area suggests that the Buckstock Mountains are favorable for similar mineral deposits.

## GEOCHEMICAL SAMPLING TECHNIQUES AND SAMPLE PREPARATION

Stream-sediment and panned concentrate samples were collected from the active stream channel at 313 sites (fig. 3). Stream sediment was screened to minus-10 mesh (2 mm) and collected in a 14-in. stainless-steel gold pan. Generally, about 2 kg of sediment was taken from the pan and saved as the stream-sediment sample. The pan was refilled with stream sediment and panned until most of the less dense minerals, organic materials, and clay were removed. In some places, stream cobbles or rocks from outcrops found upstream that appeared to be mineralized were also collected when samples large enough for geochemical analysis could be obtained.

In the laboratory, each stream-sediment sample was dried below 40°C, sieved to minus-80 mesh, pulverized, and chemically analyzed. Collected rock samples were crushed, pulverized, and chemically analyzed. The panned concentrate samples were further separated using bromoform to remove any remaining lighter minerals, primarily quartz and feldspar, then separated magnetically into magnetic, paramagnetic, and nonmagnetic heavy-mineral fractions. The nonmagnetic heavy-mineral fractions were ground and chemically analyzed, and splits were evaluated microscopically for their mineralogical content. Following bromoform and magnetic separations, 12 nonmagnetic **heavy-mineral-concentrate** samples had insufficient material for geochemical analysis, resulting in 307 concentrate samples for analysis.

## ANALYTICAL TECHNIQUES

### ATOMIC ABSORPTION SPECTROPHOTOMETRY

Concentrations of Au in the stream-sediment and rock samples were determined by an atomic absorption **spectrophotometry** (AAS) technique adapted from Hubert and Chao

(1985). The samples were digested using a series of hydrogen peroxide, hydrofluoric acid, aqua regia, and **hydrobromic acid-bromine** solutions. Gold was separated and concentrated by extraction into methyl isobutyl ketone and determined by flame AAS. Concentrations for Au in the range of 0.002 to 0.050 ppm were determined by graphite furnace atomic absorption spectrophotometry (GFAAS) on samples found to contain less than 0.050 ppm Au by the flame AAS technique. The GFAAS technique for Au was adapted from Meier (1980).

Mercury was measured in the stream-sediment and rock samples using a modified version of the cold vapor **AAS** technique (Kennedy and Crock, 1987). The samples were decomposed with nitric acid and sodium dichromate. Mercury was then reduced to elemental Hg with hydroxylamine **hydrochloride/sodium** chloride and stannous chloride in a continuous-flow system that releases the Hg vapor directly into an atomic absorption spectrophotometer.

### INDUCTIVELY COUPLED PLASMA SPECTROSCOPY

Concentrations of Ag, As, Sb, Bi, Cd, Cu, Mo, Pb, and Zn were determined in the stream-sediment and rock samples by inductively coupled plasma (**ICP**)-**atomic emission** spectrometry using the procedure developed by Motooka (1988). The sediments were decomposed with concentrated hydrochloric acid and hydrogen peroxide in a hot-water bath. The metals were extracted in diisobutyl ketone (DIBK) in the presence of ascorbic acid and potassium iodide. The DIBK phase was then aspirated directly into the plasma, and element concentrations were determined simultaneously with a multichannel ICP instrument. Tungsten in stream-sediment samples was determined by a laser ablation-ICP mass spectrometry technique described by Lichte (1995).

### SEMIQUANTITATIVE EMISSION SPECTROSCOPY

The nonmagnetic heavy-mineral-concentrate samples were analyzed by a semiquantitative, direct-current arc emission spectrographic (SQS) technique adapted from Grimes and Marranzino (1968). The 37 elements Ag, As, Au, B, Ba, Be, Bi, Ca, Cd, Co, Cr, Cu, Fe, Ga, Ge, La, Mg, Mn, Mo, Na, Nb, Ni, P, Pb, Pd, Pt, Sb, Sc, Sn, Sr, Ti, Th, V, W, Y, Zn, and Zr were determined in samples analyzed by SQS.

### MINERALOGICAL ANALYSIS

Gold, sulfide minerals (such as pyrite, cinnabar, **stibnite**, and arsenopyrite), and oxide minerals (such as

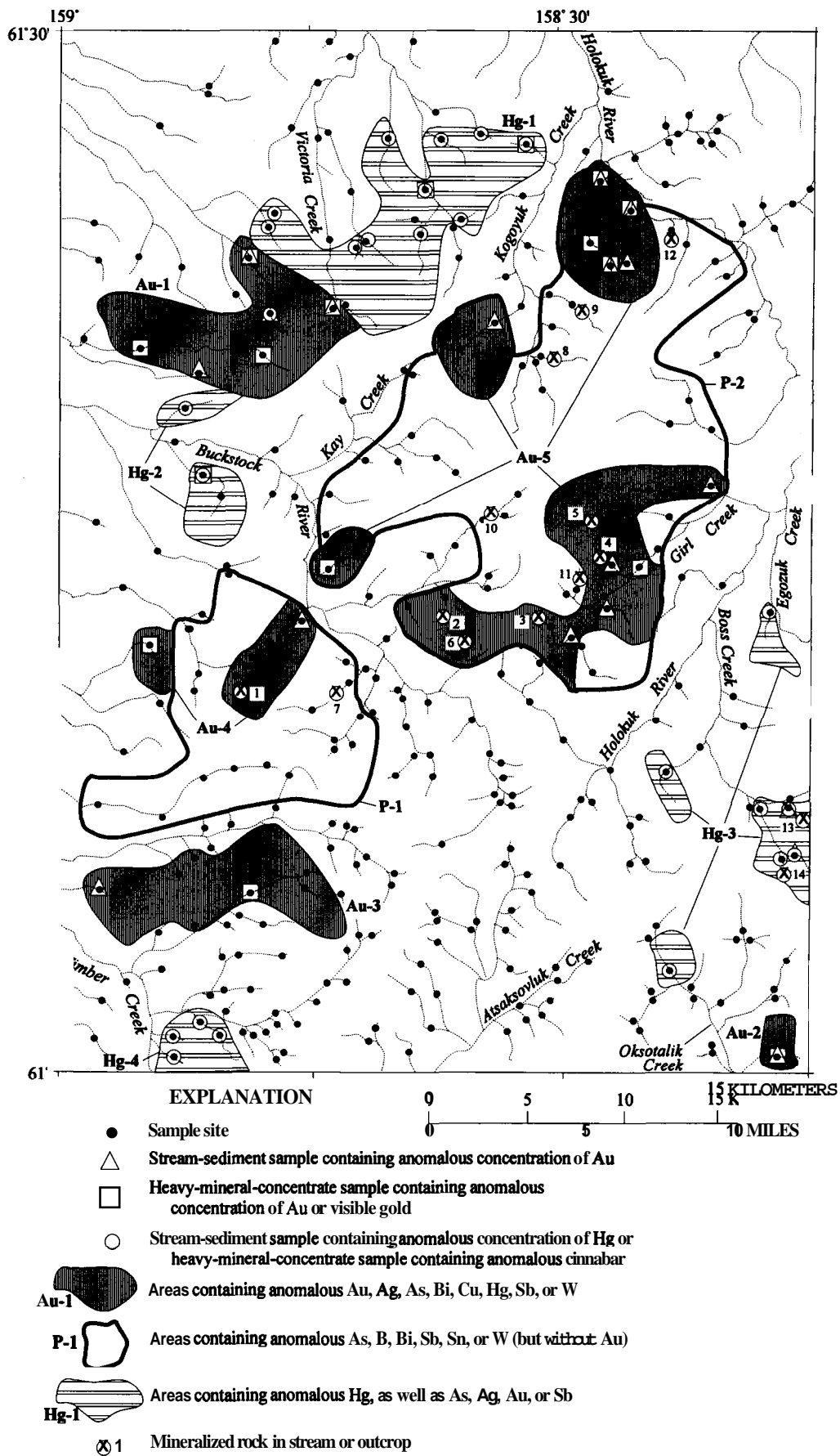


Figure 3. Location of sample sites and of areas favorable for metallic mineral resources in the Buckstock Mountains and surrounding areas.

scheelite) suggestive of possible upstream mineral occurrences are most commonly found in the nonmagnetic heavy-mineral-concentrate samples. Using a binocular microscope, mineral identifications were made in each nonmagnetic heavy-mineral-concentrate sample, and the amount of each mineral observed was estimated. These mineralogy data were used in conjunction with geochemical data from stream-sediment and heavy-mineral-concentrate samples to delineate areas with possible mineral deposits.

## INTERPRETATION

Anomalous concentrations of trace elements and minerals used in this study were determined by identifying breaks in the frequency distribution for each element or mineral; these breaks were usually found between the 90th and 99th percentiles. Selection of anomalous concentrations was also based on examination of background concentration data for various lithologies in southwestern Alaska. In particular, geochemical data were evaluated from rocks (McGimsey and others, 1988) and stream-sediment and heavy-mineral-concentrate samples (Gray and others, 1988) collected in the Iditarod quadrangle where rocks are similar to those exposed in the Buckstock Mountains area. A statistical summary of data used in this report is given in table 1, including anomalous concentrations for certain elements and minerals. Concentrations of Ag, As, Au, B, Bi, Cu, Hg, Sb, Sn, or W in the stream-sediment, heavy-mineral-concentrate, and rock samples were the most useful for delineating areas possibly containing mineral occurrences. Abundances of gold, pyrite, cinnabar, stibnite, arsenopyrite, and scheelite in the nonmagnetic heavy-mineral-concentrate samples were also important.

Geochemical data from the stream-sediment and heavy-mineral-concentrate samples collected in this study indicate that there are areas with (1) polymetallic As, Ag, Sb, Bi, Cu, Hg, or W anomalies that also contain significant Au concentrations; (2) polymetallic anomalies with dominant As, B, Bi, Sb, Sn, or W but without Au; and (3) Hg-dominant anomalies (fig. 3). Generally, the areas designated contain several samples (a cluster of sample sites) with anomalous concentrations of certain elements or minerals, but a few important single-site anomalies are also delineated.

## AREAS FAVORABLE FOR POLYMETALLIC VEIN DEPOSITS

Seven areas in the Buckstock Mountains are favorable for polymetallic vein deposits (fig. 3). Delineation of these areas is based primarily on geochemical or mineralogical anomalies in stream-sediment or heavy-mineral-concentrate

samples. The anomalies are grouped below as polymetallic metal suites with gold and those without gold. The drainage-basin geochemistry indicates that these areas are favorable for polymetallic Au-As-Sb-W vein lodes, similar to that at Fortyseven Creek (previously discussed).

### AREAS CONTAINING ANOMALOUS Au, Ag, As, Bi, Cu, Hg, Sb, OR W

#### AREA Au-1

Samples containing anomalous concentrations of Au, As, Sb, W, and Hg collected from seven sites are outlined as area Au-1 (fig. 3). Stream-sediment samples collected in Au-1 contained as much as 0.030 ppm Au, 250 ppm As, 4.0 ppm Sb, 3.7 ppm W, and 1.9 ppm Hg. Heavy-mineral-concentrate samples contained as much as 500 ppm W, 1 percent scheelite, and 1 percent cinnabar, and three concentrates each contained a grain of gold. At one site in this area, stream cobbles of oxidized siltstone hornfels contained small veins of quartz. Rocks in the area consist of sedimentary rocks of the Kuskokwim Group cut by several granite porphyry dikes (Cady and others, 1955).

#### AREA Au-2

Area Au-2 is defined by a single site where the collected stream-sediment sample contained 0.006 ppm Au and 4.4 ppm Sb; the heavy-mineral concentrate contained a grain of gold. Some stream gravel at this site consisted of sedimentary hornfels and small fragments of milky quartz vein, but this material was not collected for analysis. Rocks found in this area are sedimentary rocks of the Kuskokwim Group (Cady and others, 1955).

#### AREA Au-3

Area Au-3 consists of a cluster of eight sample sites on tributaries of Timber Creek (fig. 3). Stream-sediment samples collected in this area contained as much as 1.8 ppm Au, 16 ppm Sb, and 62 ppm As. Also in the area, one heavy-mineral-concentrate sample contained 150 ppm Au and 10 ppm Ag, and another concentrate contained 700 ppm Sb. The only rocks known in this area are sedimentary rocks of the Gemuk and Kuskokwim Groups. However, stream cobbles in this area consisted not only of graywacke and siltstone, but also monzonite and granite porphyry, indicating that igneous rocks may cut the sedimentary rocks upstream. In addition, some stream cobbles of siltstone hornfels containing minor quartz-vein stockworks were observed at sites in this area. These data indicate that the area is favorable for polymetallic vein deposits possibly with significant Au.

Table 1. Statistical summary of selected stream-sediment and heavy-mineral-concentrate data

[AAS, atomic absorption spectrophotometry; ICP, inductively coupled plasma-atomic emission spectroscopy; LA, laser ablation-inductively coupled plasma spectrometry; SQS, semiquantitative emission spectrography; MIN, mineralogical analysis; -, not applicable; <, less than. Element concentrations are in parts per million (ppm)]

Element	<sup>1</sup> Detection ratio	2N	3L	4G	Percentile concentrations					<sup>5</sup> Selected anomaly	
					Minimum	50th	90th	95th	99th		Maximum
Stream sediments											
Au-AAS	0.16	363	0	0	<0.002	<0.002	0.002	0.007	0.21	1.8	0.004
Hg-AAS	.93	22	0	0	<.02	.06	.17	.35	1.5	2.7	.20
Ag-ICP	.50	191	0	0	<.067	.10	.20	.27	.40	.76	.50
As-ICP	1.0	0	0	0	1.6	15	93	155	270	320	90
Bi-ICP	.19	253	0	0	<.67	<.67	2.5	4.4	16	26	2.0
Cu-ICP	1.0	0	0	0	4.2	25	44	50	66	84	80
Pb-ICP	1.0	0	0	0	3.2	9.5	16	18	21	29	30
Sb-ICP	.74	81	0	0	<.67	1.3	3.7	5.0	8.7	210	3.0
Zn-ICP	1.0	0	0	0	33	88	120	130	160	360	150
W-LA	.41	186	0	0	<1.0	<1.0	3.0	4.8	22	33	3.0
Nonmagnetic heavy-mineral concentrates											
Au-SQS	.02	296	3	0	<20	<20	<20	<20	150	300	20
Ag-SQS	.05	285	5	0	<1	<1	<1	<1	10	200	5
As-SQS	.01	396	4	0	<500	<500	<500	<500	<500	1,000	500
B-SQS	.91	1	13	13	<20	200	3000	5000	>5000	>5000	5000
Bi-SQS	.18	235	5	8	<20	<20	700	1,500	>2,000	>2,000	500
Cu-SQS	.31	198	9	0	<10	<10	150	200	700	1,000	500
Pb-SQS	.28	151	68	0	<20	<20	50	100	300	700	500
Sb-SQS	.05	283	7	0	<200	<200	<200	<200	1,000	5,000	200
Sn-SQS	.26	209	11	4	<20	<20	200	500	>2,000	>2,000	2,000
W-SQS	.25	203	24	0	<50	<50	200	500	1,000	3,000	200
Zn-SQS	.02	293	6	0	<500	<500	<500	<500	500	1,000	500
pyrite-MIN	.30	216	--	--	0	0	<1%	1-5%	5-20%	20-50%	1-5%
cinnabar-MIN	.16	259	--	--	0	0	<1%	<1%	1-5%	5-20%	1-5%
stibnite-MIN	.04	299	--	--	0	0	0	0	<1%	1-5%	<sup>6</sup> stibnite
gold-MIN	.03	302	--	--	0	0	0	0	<1%	<1%	<sup>6</sup> gold
arsenopyrite-MIN	.03	301	--	--	0	0	0	0	<1%	<1%	<sup>6</sup> arsenopyrite
scheelite-MIN	.40	185	--	--	0	0	<1%	1-5%	5-20%	5-20%	1-5%

<sup>1</sup>Number of uncensored values (those not qualified with N, L, or G) divided by total number of samples analyzed (313 stream-sediment samples, 304 heavy-mineral-concentrate samples, and 310 mineralogy samples).

2Number of samples in which concentrations were not detected at lower limit of determination.

3Number of samples in which concentrations were observed, but less than lower limit of determination.

4Number of samples in which concentrations were observed, but greater than upper limit of determination.

5Anomalous concentrations were selected by identifying breaks in frequency distribution of each data set.

6Any amount of visible gold, stibnite, or arsenopyrite in nonmagnetic heavy-mineral-concentrate samples is considered anomalous.

#### AREA Au-4

Samples collected from five sites define area Au-4. The stream-sediment sample collected from the easternmost site contained 0.010 ppm Au and 1.3 ppm Bi, and the heavy-mineral-concentrate sample from the same site contained 1,000 ppm Bi. One heavy-mineral-concentrate sample

collected from the westernmost site contained 30 ppm Au, 10 ppm Ag, 1,000 ppm W, and as much as 1 percent scheelite. Rocks in this area consist of sedimentary rocks of the Kuskokwim Group cut by granite porphyry dikes (Cady and others, 1955). Altered cobbles of granite porphyry containing minor quartz-vein stockworks were ob-

served at a sample site in the westernmost Au-4 area. At another site in the eastern part of Au-4, stream cobbles of siltstone hornfels with quartz veins contained as much as 130 ppm As, 0.014 ppm Au, and 73 ppm Bi (table 2).

#### AREA Au-5

In the central part of the study area, four subareas containing anomalous concentrations of gold define area Au-5. Stream-sediment samples collected in these subareas contained as much as 1.3 ppm Au, 150 ppm As, 14 ppm Bi, 8.3 ppm Sb, and 6.9 ppm W. Heavy-mineral concentrates contained as much as 200 ppm Au, 100 ppm Ag, 500 ppm Sb, 3,000 ppm W, and greater than 2,000 ppm Bi. Several concentrate samples collected from sites on Gold Run Creek (northernmost subarea) contained single grains of gold and (or) stibnite and as much as 20 percent scheelite and pyrite. Several sample sites in this area contained stream cobbles of mineralized sedimentary-rock hornfels and altered granite porphyry with quartz veins. Mineralized quartz veins and silicified graywacke hornfels in contact with an altered and silicified granite porphyry dike (southernmost Au-5 subarea) were found in an outcrop (table 2, #2) by tracing a geochemical anomaly upstream on a tributary of the Buckstock River in this area (fig. 3). Mineralized rock samples in this subarea contained vein and disseminated pyrite, arsenopyrite, and as much as 1,100 ppm As, 0.034 ppm Au, 13 ppm Bi, 590 ppm Cu, 1.6 ppm Hg, and 290 ppm Sb (table 2, #2-6). All of the Au-5 subareas are favorable for Au-As-Sb-W polymetallic lodes. In addition, Cady and others (1955) reported placer gold somewhere on Gold Run and Girl Creeks. The northernmost and southernmost Au-5 subareas delineated along these creeks are consistent with this placer gold, but the areas shown here extend the area favorable for the occurrence of gold to tributaries adjacent to Gold Run and Girl Creeks.

#### AREAS CONTAINING ANOMALOUS As, B, Bi, Sb, Sn, OR W (BUT WITHOUT Au)

##### AREA P-1

A large cluster of samples defines area P-1 (fig. 3). In this area, samples were collected from numerous sites from tributaries of the Buckstock River and Timber Creek. Stream-sediment samples collected in this area contained as much as 260 ppm As, 4 ppm Sb, 13 ppm Bi, and 33 ppm W; whereas heavy-mineral-concentrate samples contained as much as 2,000 ppm Sb, 700 ppm Bi, 1,000 ppm W, greater than 5,000 ppm B, greater than 2,000 ppm Sn, 1 percent scheelite, and 1 percent stibnite. Rocks in area P-1 are sedimentary rocks of the Kuskokwim and Gemuk Groups cut by granite porphyry dikes. At one site in this area, stream cobbles of graywacke hornfels with minor disseminated pyrite were found that contained as much as 150

ppm As, 8.4 ppm Bi, and 3.5 ppm Sb (table 2, #7). Although mineral occurrences have not been previously reported in this area, the drainage-basin geochemistry and mineralized rock samples indicate that the area is favorable for polymetallic vein lodes.

##### AREA P-2

Area P-2 is also defined by a large cluster of samples. In this area, samples were collected from numerous sites from tributaries of the Buckstock River, Holokuk River, Girl Creek, and Kogoyuk Creek (fig. 3). Samples collected in this area are highly anomalous in As, Sb, W, Bi, and B. Stream-sediment samples collected in this area contained as much as 320 ppm As, 210 ppm Sb, 26 ppm Bi, and 16 ppm W, whereas heavy-mineral-concentrate samples contained as much as 1,000 ppm As, 5,000 ppm Sb, 1,000 ppm W, greater than 2,000 ppm Bi, greater than 5,000 ppm B, and as much as 5 percent scheelite. Rocks in area P-2 are mostly shale and graywacke of the Kuskokwim Group cut by several granite porphyry dikes, but minor intermediate to felsic volcanic rocks are found in the eastern part of area P-2. Several sample sites in this area contained stream cobbles of mineralized sedimentary-rock hornfels with quartz-vein stockworks. These mineralized rock samples contained vein and disseminated pyrite and as much as 120 ppm As, 7.9 ppm Bi, and 8.0 ppm Sb (table 2, #8-12). The geology and geochemistry of mineralized rocks in this area is similar to that of polymetallic vein lodes in southwestern Alaska, such as the Fortyseven Creek lode. The data presented here indicate that additional polymetallic vein occurrences are likely in area P-2.

#### AREAS WITH ANOMALOUS Hg

The drainage-basin geochemistry in this study indicates that several areas are favorable for epithermal Hg-Sb vein deposits, similar to those deposits found throughout southwestern Alaska. Lode deposits of this type are not known in these study areas, but geochemical signatures in samples from these areas are similar to those in known epithermal Hg-rich vein deposits elsewhere in southwestern Alaska.

##### AREA Hg-1

Samples collected from 13 sites mostly along Victoria and Kogoyuk Creeks and their tributaries define area Hg-1 (fig. 3). Stream-sediment samples collected in this area contained as much as 2.7 ppm Hg, and heavy-mineral-concentrate samples contained as much as 5 percent cinnabar and 1 percent stibnite. Two concentrate samples each contained a grain of gold; one of these concentrates also contained



Table 2. Trace element concentrations in mineralized rock samples collected from newly discovered mineral occurrences in the Buckstock Mountains

[Newly discovered mineral occurrences are numbered and shown on figure 3; As, Bi, Cu, and Sb analyzed by inductively coupled plasma-atomic emission spectroscopy; Au and Hg analyzed by atomic absorption spectrophotometry; Sample sources as follows: o, outcrop; s, stream cobble]

Sample no.	Area	Latitude (° ' ")	Longitude (° ' ")	As (ppm)	Au (ppm)	Bi (ppm)	Cu (ppm)	Hg (ppm)	Sb (ppm)	Sample source	Description	
1.	3066R1	Au-4	61 11 23	158 49 31	110	<0.002	2.7	48	<0.02	1.0	s	Siltstone hornfels with quartz-vein stockworks
	3066R2	Au-4	61 11 23	158 49 31	130	.014	73	34	<.02	1.1	s	Siltstone hornfels with 5-cm-wide quartz vein
2.	3313RA	Au-5	61 13 01	158 37 27	220	.002	13	53	<.02	3.8	o	Graywacke hornfels with quartz <b>veinlets</b>
	3313RB	Au-5	61 13 01	158 37 27	290	<.002	3.4	20	<.02	7.5	o	Graywacke hornfels with quartz <b>veinlets</b>
	3313RC	Au-5	61 12 57	158 37 23	710	.006	<1.0	590	1.6	290	o	Silicified granite porphyry with iron oxide
	3313RD	Au-5	61 12 48	158 37 03	1,100	.034	<1.0	3.5	.06	16	o	<b>Pyrite-arsenopyrite</b> in vuggy quartz veins in granite porphyry
3.	4509R	Au-5	61 12 45	158 30 49	5.7	.004	<1.0	45	<.02	6.5	s	Silicified siltstone hornfels with disseminated pyrite
4.	4550R	Au-5	61 14 14	158 26 44	31	<.002	1.4	57	.13	5.8	s	Silicified graywacke hornfels with disseminated pyrite
5.	3266R	Au-5	61 16 00	158 27 15	70	<.002	<1.0	48	<.02	2.9	s	Siltstone hornfels with quartz-vein stockworks
6.	3032R	Au-5	61 11 50	158 35 43	240	<.002	2.6	58	<.02	6.5	s	Graywacke hornfels with quartz veins
7.	3031R	P-1	61 11 13	158 42 41	150	<.002	8.4	27	<.02	3.5	s	Graywacke hornfels with disseminated pyrite
8.	3097R1	P-2	61 20 28	158 31 08	50	.008	<1.0	12	.02	3.7	s	Oxidized siltstone hornfels with 2-cm-wide quartz veins
	3097R2	P-2	61 20 28	158 31 08	120	.004	<1.0	7.6	<.02	<.67	s	Altered monzonite with quartz-vein stockworks
9.	3099R	P-2	61 21 49	158 28 54	76	<.002	7.9	32	<.02	1.2	s	Siltstone hornfels <b>breccias</b> with <b>quartz-vein</b> stockworks
10.	3265R1	P-2	61 15 52	158 34 17	20	.004	<1.0	64	<.02	8.0	s	Oxidized siltstone hornfels with quartz veins
11.	4511R	P-2	61 13 37	158 29 12	69	<.002	1.9	55	.04	2.7	s	Siltstone hornfels with quartz veins and disseminated pyrite
12.	4546R	P-2	61 24 12	158 23 23	88	<.002	5.8	57	<.02	2.0	s	Graywacke hornfels with quartz-vein stockworks
13.	4527R	Hg-3	61 07 44	158 17 02	5.4	<.002	<1.0	12	.35	<1.0	s	Altered granite with disseminated pyrite
14.	4530R	Hg-3	61 06 22	158 17 24	1,000	.050	<1.0	0.8	<.02	6.1	s	Silicified graywacke with quartz veins and disseminated pyrite

300 ppm Au and 200 ppm Ag. Rocks in this area are sedimentary rocks of the Kuskokwim Group cut by granite porphyry dikes (Cady and others, 1955).

#### AREA Hg-2

Samples collected from tributaries of the Buckstock River define two small subareas that together define area Hg-2 (fig. 3). Stream-sediment samples collected in these subareas contained as much as 1.6 ppm Hg. Heavy-mineral-concentrate samples collected in area Hg-2 contained as much as 20 percent cinnabar, and one concentrate sample contained a grain of gold. Stream cobbles at sample sites in this area consist of siltstone containing small quartz veins, but these rocks were not collected. Rocks in this area are generally sedimentary rocks of the Kuskokwim Group cut by granite porphyry dikes (Cady and others, 1955).

#### AREA Hg-3

Four separate subareas are designated area Hg-3 (fig. 3). In these subareas, stream-sediment samples collected from Boss, Egozuk, and Oksotalik Creeks and their tributaries contained as much as 0.80 ppm Hg, 5.7 ppm Sb, and 0.35 ppm Au. Heavy-mineral concentrates collected in Hg-3 subareas contained as much as 1 percent each of cinnabar and pyrite. In the easternmost subarea, a stream cobble of altered and oxidized granite with disseminated pyrite (table 2, # 13) contained 0.35 ppm Hg, and a stream cobble of silicified graywacke with pyrite (table 2, #14) contained 1,000 ppm As and 0.050 ppm Au. In addition, at several sites in area Hg-3, fragments of quartz veins were observed in stream gravels. Rocks in these drainage basins are generally sedimentary rocks of the Kuskokwim Group (Cady and others, 1955).

#### AREA Hg-4

Anomalous area Hg-4 is a small region defined by four sample sites on tributaries of Timber Creek in the southwestern part of the study area (fig. 3). Stream-sediment samples collected in Hg-4 contained as much as 0.20 ppm Hg, and heavy-mineral-concentrate samples contained as much as 1 percent cinnabar and stibnite. Altered or mineralized rocks were not found in this area. Rocks in area Hg-4 are sedimentary rocks of the Gemuk Group and granite porphyry (Cady and others, 1955).

### SUMMARY

Several areas were identified as favorable for the occurrence of metallic mineral deposits in this drainage-basin geochemical and mineralogical study of the Buckstock Mountains area. Stream-sediment, heavy-mineral-concen-

trate, and mineralized rock samples were collected from these areas and contained anomalous concentrations of Au, Ag, As, B, Bi, Cu, Hg, Sb, Sn, or W; heavy-mineral concentrates in some areas contained microscopically visible gold, cinnabar, stibnite, arsenopyrite, pyrite, and scheelite. Few mineral occurrences were known in the study area prior to our study; only minor placer gold was previously reported on three streams. Our data suggest that the delineated areas are favorable for the presence of polymetallic **As-Sb-W±Au** vein lodes, Hg-Sb vein lodes, or minor placer gold occurrences. Throughout southwestern Alaska, **Au-As-Sb-W** vein deposits (such as Fortyseven Creek) and Hg-Sb deposits (such as Red Devil) are found in areas with geology and geochemistry similar to that of the Buckstock Mountains, indicating that undiscovered deposits of this type are possible in the areas delineated.

Acknowledgments.—The authors would like to thank John Bullock, Phil Hageman, Rich O'Leary, and Jerry Motooka for chemical analyses, and Greg Lee and Carter Borden for assistance with sample collection.

### REFERENCES CITED

- Box, S.E., 1985, Terrane analysis, northern Bristol Bay region, southwestern Alaska: development of a Mesozoic interoceanic arc and its collision with North America: Santa Cruz, University of California, Ph.D. dissertation, 163 p.
- Box, S.E., and Elder, W.P., 1992, Depositional and biostratigraphic framework of the Upper Cretaceous Kuskokwim Group, southwest Alaska, *in* Bradley, D.C., and Ford, A.B., eds., Geologic studies in Alaska by the U.S. Geological Survey, 1990: U.S. Geological Survey Bulletin 1999, p. 8-16.
- Box, S.E., and Murphy, J.M., 1987, Late Mesozoic structural and stratigraphic framework, eastern Bethel quadrangle, southwest Alaska, *in* Hamilton, T.D., and Galloway, J.P., eds., Geologic studies in Alaska by the U.S. Geological Survey during 1986: U.S. Geological Survey Circular 998, p. 78-82.
- Bundtzen, T.K., and Gilbert, W.G., 1983, Outline of geology and mineral resources of upper Kuskokwim region, Alaska: Journal of the Alaska Geological Society, v. 3, p. 101-119.
- Bundtzen, T.K., Hams, E.E., Laird, G.M., and Kline, J.T., 1993, Geologic map and data file tables of the Sleetmute C-7, C-8, D-7, and D-8 quadrangles, Alaska: Alaska Division of Geological and Geophysical Surveys Public-Data File 93-47, 1 pl., scale 1:63,360.
- Bundtzen, T.K., and Laird, G.M. 1991, Geology and mineral resources of the Russian Mission C-1 quadrangle, southwest Alaska: Alaska Division of Geological and Geophysical Surveys Professional Report 109, 24 p.
- Bundtzen, T.K., and Miller, M.L., in press, Precious metals associated with Late Cretaceous-early Tertiary igneous rocks of southwestern Alaska, *in* Goldfarb, R.J., and Miller, L.D., eds., Mineral deposits of Alaska: Economic Geology Monograph No. 9.
- Bundtzen, T.K., and Swanson, S.E., 1984, Geology and petrology of igneous rocks in the Innoko River area, western Alaska [abs.]: Geological Society of America Abstracts with Pro-

- grams, v. 16, no. 5, p. 273.
- Cady, W.M., Wallace, R.E., Hoare, J.M., and Webber, E.J., 1955, The central Kuskokwim region, Alaska: U.S. Geological Survey Professional Paper 268, 132 p.
- Decker, John, **Bergman**, S.C., Blodgett, R.B., Box, S.E., Bundtzen, T.K., Clough, J.G., **Coonrad**, W.L., Gilbert, W.G., Miller, M.L., Murphy, J.M., Robinson, M.S., and Wallace, W.K., 1994, Geology of southwestern Alaska, *in* Plafker, George, and Berg, H.C., eds., The geology of Alaska: Boulder, Colo., Geological Society of America, The Geology of North America, v. **G-1**, p. 285-310.
- Decker, John, and Hoare, J.M., 1982, Sedimentology of the Cretaceous Kuskokwim Group, southwest Alaska, *in* Coonrad, W.L., ed., The U.S. Geological Survey in Alaska: Accomplishments during 1980: U.S. Geological Survey Circular 844, p. 81-83.
- Decker, John, Reifentstuh, R.R., Robinson, M.S., and Waythomas, C.F., 1986, Geologic map of the Sleetmute A-5, A-6, B-5, and B-6 quadrangles, Alaska: Alaska Division of Geological and Geophysical Surveys Professional Report 93, 22 p., 1 sheet, scale 1:250,000.
- Decker, John, Reifentstuh, R.R., Robinson, M.S., Waythomas, C.F., and Clough, J.G., 1995, Geology of the Sleetmute A-5, A-6, B-5, and B-6 quadrangles, southwestern Alaska: Alaska Division of Geological and Geophysical Surveys Professional Report 99, 16 p.
- Decker, John, Robinson, M.S., Murphy, J.M., Reifentstuh, R.R., and Albanese, M.D., 1984, Geologic map of the Sleetmute A-6 quadrangle: Alaska Division of Geological and Geophysical Surveys Report of Investigations 84-8, scale 1:40,000.
- Gray, J.E., Arbogast, B.F., and Hudson, A.E., 1988, Analytical results and sample locality map of the stream sediment and nonmagnetic, heavy-mineral-concentrate samples from the Iditarod quadrangle, Alaska, U.S. Geological Survey **Open-File Report 88-221**, 69 p., 1 pl., scale 1:250,000.
- Gray, J.E., Frost, T.P., Goldfarb, R.J., and Detra, D.E., 1990, Gold associated with cinnabar- and stibnite-bearing deposits and mineral occurrences in the Kuskokwim River region, southwestern Alaska, *in* Goldfarb, R.J., Nash, T.J., and Stoesser, J.W., eds., Geochemical studies in Alaska by the U.S. Geological Survey, 1989: U.S. Geological Survey Bulletin 1950, p. **D1-D6**.
- Gray, J.E., Gent, C.A., Snee, L.W., and Wilson, F.H., in press, **Epithermal** mercury-antimony and gold-bearing vein deposits of southwestern Alaska, *in* Goldfarb, R.J., and Miller, L.D., eds., Mineral deposits of Alaska: Economic Geology Monograph No. 9.
- Gray, J.E., Goldfarb, R.J., Detra, D.E., and Slaughter, K.E., 1991, Geochemistry and exploration criteria for epithermal cinnabar and stibnite vein deposits in the Kuskokwim River region, southwestern Alaska: Journal of Geochemical Exploration, v. 41, p. 363-386.
- Gray, J.E., Goldfarb, R.J., Snee, L.W., and Gent, C.A., 1992, Geochemical and temporal conditions for the formation of mercury-antimony deposits, southwestern Alaska [abs.]: Geological Society of America Abstracts with Programs, v. 24, no. 5, p. 28.
- Grimes, D.J., and Marranzino, A.P., 1968, Direct-current arc and alternating-current spark emission spectrographic field methods for the semiquantitative analysis of geological materials: U.S. Geological Survey Circular 591, 6 p.
- Hawley, C.C., 1989, The Forty Seven Creek prospect, southwest Alaska, summary of data and recommendations: Unpublished report prepared for Holitna Basin Mining and Exploration, Inc., 7 p.
- Hoare, J.M., and **Coonrad**, W.L., 1959, Geology of the Bethel quadrangle, Alaska: U.S. Geological Survey Miscellaneous Geologic Investigations Map **I-285**, scale 1:250,000.
- Hubert, A.E., and Chao, T.T., 1985, Determination of gold, indium, tellurium and thallium in the same sample digestion of geological materials by atomic-absorption spectroscopy and two-step solvent extraction: Talanta, v. 32, p. 383-387.
- Kennedy, K.R., and Crock, J.G., 1987, Determination of mercury in geological materials by continuous flow, cold-vapor, atomic-absorption spectrophotometry: Analytical Letters, v. 20, p. 899-908.
- Lichte, F.E., 1995, Determination of elemental content of rocks by laser ablation inductively coupled plasma mass spectrometry: Analytical Chemistry, v. 67, no. 14, p. 2479-2485.
- MacKevett**, E.M., Jr., and Berg, H.C., 1963, Geology of the Red Devil quicksilver mine, Alaska: U.S. Geological Survey Bulletin 1142-G, p. **G1-G16**.
- McGimsey, R.G., Miller, M.L., and Arbogast, B.F., 1988, Paper version of analytical results, and sample locality map for rock samples from the Iditarod quadrangle, Alaska: U.S. Geological Survey Open-File Report 88-421-A, 110 p., 1 pl., scale 1:250,000.
- Meier, A.L., 1980, Flameless atomic-absorption determination of gold in geological materials: Journal of Geochemical Exploration, v. 13, p. 77-85.
- Miller, M.L., **Belkin**, H.E., Blodgett, R.B., Bundtzen, T.K., Cady, J.W., Goldfarb, R.J., Gray, J.E., McGimsey, R.G., and **Simpson**, S.L., 1989, Pre-field study and mineral resource assessment of the Sleetmute quadrangle, southwestern Alaska: U.S. Geological Survey Open-File Report 89-363, 115 p., 3 pls., scale 1:250,000.
- Miller, M.L., and Bundtzen, T.K., 1994, Generalized geologic map of the Iditarod quadrangle, Alaska, showing potassium-argon, major-oxide, trace-element, fossil, paleocurrent, and archaeological sample localities: U.S. Geological Survey Miscellaneous Field Studies Map MF-2219-A, 1 pl., scale 1:250,000.
- Moll-Stalcup, E.J., 1994, Latest Cretaceous and Cenozoic magmatism in mainland Alaska, *in* Plafker, George, and Berg, H.C., eds., The geology of Alaska: Boulder, Colo., Geological Society of America, The Geology of North America, v. **G-1**, p. 589-619.
- Motooka, J.M., 1988, An exploration geochemical technique for the determination of preconcentrated organometallic halides by ICP-AES: Applied Spectroscopy, v. 42, no. 7, p. 1293-1296.
- Nokleberg, W.J., Bundtzen, T.K., Berg, H.C., Brew, D.A., Grybeck, Donald, Robinson, M.S., Smith, T.E., and **Yeend**, Warren, 1987, Significant metalliferous lode deposits and placer districts of Alaska: U.S. Geological Survey Bulletin 1786, 104 p., 2 sheets.
- Reifentstuh, R.R., Robinson, M.S., Smith, T.E., Albanese, M.D., and Allegro, G.A., 1984, Geologic map of the Sleetmute B-6 quadrangle, Alaska: Alaska Division of Geological and

Geophysical Surveys Report of Investigations 84-12, scale 1:40,000.

Robinson, M.S., and Decker, John, 1986, Preliminary age dates and analytical data for selected igneous rocks from the Sleetmute, Russian Mission, Taylor Mountains, and Bethel quadrangles, southwestern Alaska: Alaska Division of Geological and Geophysical Surveys Public-Data File 86-99, 9 p.

Robinson, M.S., Decker, John, Reifstuhel, R.R., Murphy, J.M., and Box, S.E., 1984, Geologic map of the Sleetmute B-5 quadrangle, Alaska: Alaska Division of Geological and Geo-

physical Surveys Report of Investigations 84-10, scale 1:40,000.

Sainsbury, C.L., and MacKevett, E.M., Jr., 1965, Quicksilver deposits of southwestern Alaska: U.S. Geological Survey Bulletin 1187, 89 p.

Wallace, W.K., 1983, Major lithologic belts of southwestern Alaska and their tectonic implications [abs.]: Geological Society of America Abstracts with Programs, v. 15, no. 5, p. 406-407.

**Reviewers: Robert Eppinger and David Smith**

# Paleocene Molybdenum Mineralization in the Eastern Coast Batholith, Taku River Region, and New Age Constraints on Batholith Evolution

By Lance D. Miller, Richard J. Goldfarb, Lawrence W. Snee, William C. McClelland and Paul D. Klipfel

## ABSTRACT

Argon dating of hydrothermal muscovite at the Boundary Creek 2 molybdenite occurrence north of Taku Inlet indicates that molybdenite was formed at or later than  $59.7 \pm 0.1$  Ma. This new date, as well as those U-Pb ages of zircons separated from samples of nearby plutons of the Coast batholith, indicate that molybdenum mineralization was coeval with compressional tectonism and is similar in age to many of the molybdenum porphyry occurrences in nearby British Columbia. The Boundary Creek 2 mineral occurrence in the northern part of southeastern Alaska is not related to the Oligocene molybdenite-bearing extensional magmatism of the southern part of southeastern Alaska, as previously hypothesized.

## INTRODUCTION

Numerous molybdenite occurrences are distributed throughout intrusive rocks in southeastern Alaska in the Taku River region near the Canadian border (fig. 1). These mineral occurrences, spread along a 40-km-long stretch, are hosted by various stocks that make up the eastern side of the Coast batholith. They are mainly localized within granitic, granodioritic, and other leucocratic phases of the intrusive rocks. Molybdenite mineral occurrences recognized in the area (fig. 1) include Boundary Creek 1 (Brew and Ford, 1969), Boundary Creek 2 (Koch and others, 1987), Nan (Souther, 1971), and Yehring Creek (Clough, 1990).

Previous to our investigation, ages for the molybdenite occurrences in this area were unknown. Beley (1980) mentioned a K-Ar date of 69 Ma in association with the igneous rocks at the Nan prospect, but no information was given on what mineral was dated. More significantly, the sample site for the dated rock appears to be 25 km west of the Nan prospect. In addition, Brew and Ford (1969) correlated the intrusive host rocks at the Boundary Creek 1 mineral occurrence with the granodiorite at Turner Lake, located about 25 km to the south. The Turner Lake pluton has a

$50 \pm 2$  Ma age by U-Pb methods (Gehrels and others, 1984). Koch and others (1987) stated that the plutonic rocks at the Boundary Creek 2 mineral occurrence could be no older than 50 Ma because the rocks, in part, appeared similar in composition to the Turner Lake pluton. They further suggested that alkalic phases of the plutonic suite at the Boundary Creek 2 occurrence, the host for the molybdenite, are compositionally similar to the Oligocene plutonic rocks that host the world-class Quartz Hill molybdenum porphyry deposit 450 km to the south. Because of this compositional similarity, Koch and others (1987) hypothesized that these more northerly molybdenite occurrences might be similar to the Miocene-Oligocene Quartz Hill deposit with molybdenite ages of 30-15 Ma. If true, such a correlation would be highly significant in regard to the molybdenite mineral-resource potential of southeastern Alaska. Rather than a very localized extensional event in the southern part of southeastern Alaska being responsible for intrusion of the Quartz Hill porphyry, a major extensional episode could have impacted much of the length of the Coast batholith in the late Tertiary. Extension-related alkalic magmatism could produce an extensive mineral belt favorable for the occurrence of Quartz Hill-type porphyry deposits.

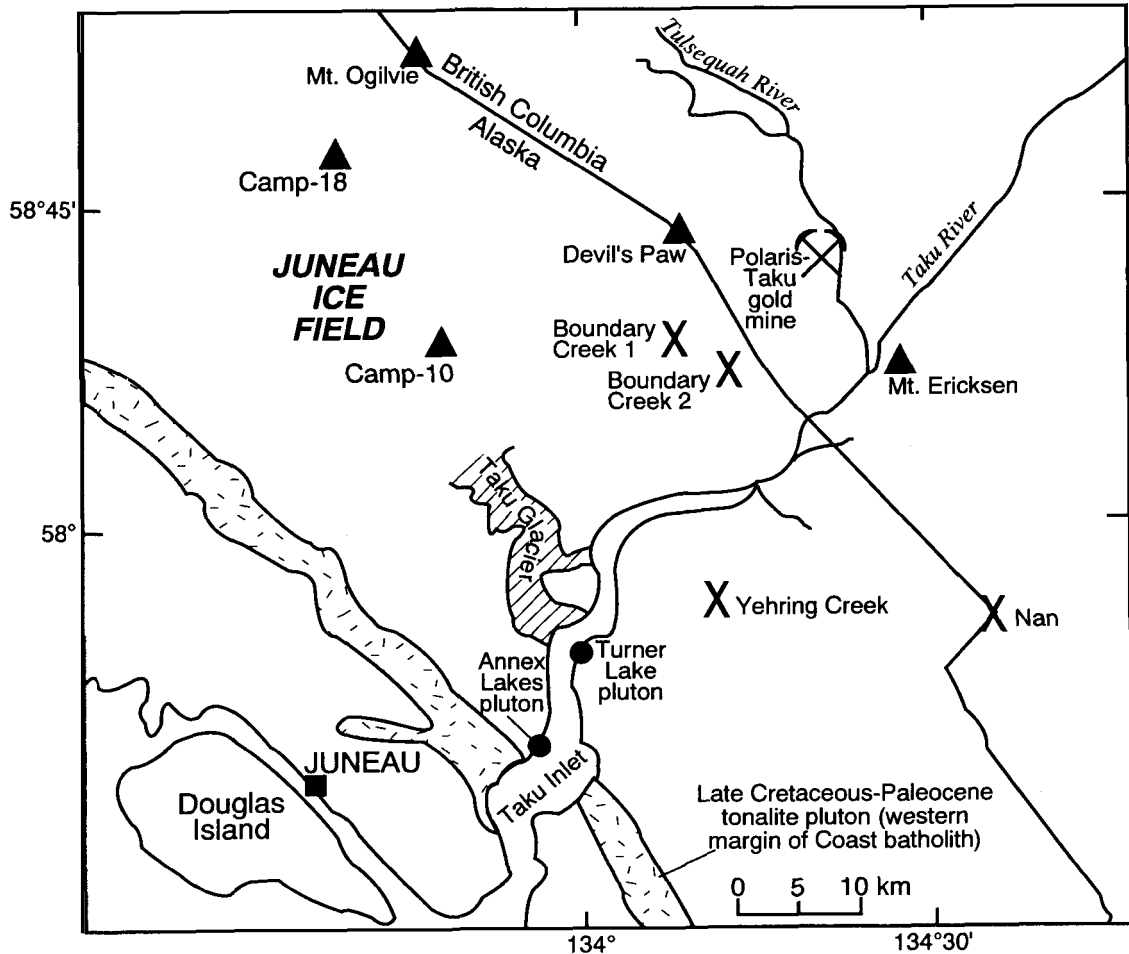
In addition to a lack of ages on the molybdenite occurrences, there has been only limited data available for the absolute ages of plutonic rocks of the Coast batholith to the northeast of Juneau. U-Pb geochronology in Gehrels and others (1991) confirmed the  $50 \pm 2$  Ma date for the Turner Lake pluton and determined a  $58.6 \pm 0.9$  Ma crystallization age for the Annex Lake tonalite-granodiorite complex located 10 km to the southwest of the Turner Lake pluton. These data collected from sites along Taku Inlet agree, as do additional age data from rocks collected to the west by Gehrels and others (1991), with the general younging-to-the-northeast pattern that characterizes much of the Coast batholith. Based on this trend for the batholith and on the general association of the molybdenite occurrences with relatively felsic igneous phases, the belt of molybdenite mineral occurrences might logically be assumed to be no older than middle Eocene (about 50 Ma). However, no

ages have been published prior to this work for the igneous rocks that compose the relatively inaccessible, high peaks of the Juneau ice field near the Canadian border.

### GEOLOGY AND MINERAL OCCURRENCES

The interior part of the northern Coast batholith that hosts the molybdenum occurrences includes a series of shal-

lowly **emplaced** tonalitic to granitic intrusions (Brew, 1994). Roof pendants (mainly high-grade metamorphosed sedimentary rocks of the Yukon-Tanana terrane; Miller and others, 1994) and dikes of **mafic** rocks, pegmatite, and aplite are common throughout this part of the batholith (Brew, 1994). Propylitic alteration of the **plutons** to the east of Juneau is widespread, particularly along 30°- to 60°-trending joints. Some of the late dikes, as well as disseminations and fracture fillings of pyrite, with lesser chalcopyrite and



#### EXPLANATION

- X Prospects and mineral occurrences
- ⚒ Mines
- Pluton
- ▲ Other sites referenced in this paper

**Figure 1.** Location of the Boundary Creek 2 and other molybdenum occurrences in the north part of the Coast batholith, southeastern Alaska. Also shown are the locations of the camp-10 and camp-18 granodiorite bodies.

traces of molybdenite, are associated with the joint sets (Klipfel, 1981).

The molybdenite occurrences in the study area are genetically associated with late, differentiated igneous phases. At the Nan prospect, Souther (1971) described molybdenite clots and fracture coatings restricted to aplite dikes and hydrothermally altered felsite. Molybdenite, along with iron- and copper-bearing sulfide minerals, is found in a quartz monzonite plug adjacent to its contact with a granodiorite stock at Yehring Creek (Clough, 1990). The mineral occurrence at Yehring Creek is fracture controlled along north-east-striking, subvertical joints. Granite float in the adjacent drainages also contains minor molybdenite. In the Boundary Creek area, the molybdenite occurrences are hosted by a highly altered and iron-stained, north- to northeast-trending aplite "dikelike unit" (Brew and Ford, 1969) and alkali granites (Koch and others, 1987).

Our field studies revealed that molybdenite at the Boundary Creek 2 mineral occurrence is localized along two sets of fractures that strike northeast and east-northeast and dip steeply. The most pervasive fracture set is oriented 80°-85° and dips 70° N.; the second set strikes 45°-50° and dips to the southeast at 56°-75°. Alteration associated with these joint sets includes epidote fracture coatings. Molybdenite occurs as coarse-grained rosettes associated with muscovite on fracture surfaces. A sample of molybdenite-bearing alaskite at the mineral occurrence contains 4,800 ppm Mo, 250 ppm Ag, 210 ppb Au, and 1,600 ppm Pb (Clough, 1990).

## METHODS

To determine the age of molybdenite mineralization, we sampled a biotite-rich, molybdenite-bearing granite dike at the Boundary Creek 2 mineral occurrence. Along the more altered parts of the dike, most of the coarse biotite had been replaced by hydrothermal muscovite. For argon thermochronology study, we separated both the fresh-looking, magmatic biotite and the muscovite from samples of the dike. To determine the age of nearby plutons, we sampled granodiorite bodies rising above the Juneau ice field at camp-10 (20 km west of the Boundary Creek occurrences) and at camp-18 (the Gilkey pluton, 35 km northwest of the Boundary Creek occurrences). Hornblende, biotite, and zircon were separated from the two sampled granodiorite bodies for isotopic dating.

Dates on the biotite, muscovite, and hornblende mineral separates (table 1) were determined using  $^{40}\text{Ar}/^{39}\text{Ar}$  techniques as described in Snee and others (1988). U-Pb analyses of zircons separated from the granodiorite samples were conducted at the University of California at Santa Barbara using methods outlined by Mattinson (1994). The U-Pb data are summarized in table 2.

## AGE RELATIONS

The  $^{40}\text{Ar}/^{39}\text{Ar}$  dates of micas associated with molybdenite at the Boundary Creek 2 mineral occurrence are interpreted to indicate that the molybdenum mineralization was probably Paleocene (about 60-63 Ma) and certainly no younger. Analysis of biotite from the Boundary Creek 2 sample yielded a highly disturbed profile (fig. 2), with the suggestion of an age from the middle part of the Paleocene (about 63 Ma). In contrast, an extremely well-defined plateau for the muscovite (fig. 2) from the mineral occurrence yielded a date of  $59.7 \pm 0.1$  Ma. This date indicates that alteration of the dike and associated molybdenite mineralization occurred in the late Paleocene.

New dates for the plutons (table 2) near the center of the batholith indicate that some of the voluminous magmatic activity was older than the one middle Eocene (50 Ma) pluton at Turner Lake dated by Gehrels and others (1984, 1991). A crystallization age of  $53.0^{+0.7}_{-0.2}$  Ma is interpreted for the granodiorite at camp-18 on the basis of linear regression of discordant conventional U-Pb analyses and partial-dissolution results (table 2, fig. 3). Relatively rapid cooling following early Eocene emplacement of the stock is suggested by a slightly younger hornblende  $^{40}\text{Ar}/^{39}\text{Ar}$  cooling age of  $51.48 \pm 0.15$  at camp-18 (table 1). The discordant, apparently older biotite date is interpreted to reflect the effect of  $^{39}\text{Ar}$  recoil from alteration chlorite. A U-Pb crystallization age of  $57.5 \pm 0.7$  Ma interpreted for the granodiorite at camp-10, also based on regression and partial-dissolution results (table 2, fig. 3), shows that major granodioritic pulses in the center of the batholith were at least as old as latest Paleocene. The  $^{40}\text{Ar}/^{39}\text{Ar}$  age spectra of both the hornblende and biotite from this sample are disturbed (table 1), but the dates are grossly equivalent to the U-Pb age for the camp-18 sample and reveal that much of the central part of the batholith that is now exposed within the Juneau ice field cooled below 300°C (the closing temperature of biotite) by the end of the early Eocene (53-52 Ma). These new ages of magmatism for the more evolved central and eastern part of the batholith are consistent with recent data from Mt. Ericksen in westernmost British Columbia, a few kilometers east of the junction between the Taku and Tulsequah Rivers (fig. 1). At that location, Mihalynuk and others (1996) describe a quartz monzonite porphyry with a U-Pb age of  $53.5 \pm 0.7$  Ma.

## DISCUSSION

Our new age data for a molybdenite occurrence from the Boundary Creek area reveal a temporal correlation with the bulk of the quartz monzonite-type molybdenum porphyry systems in western British Columbia. Emplacement ages for these subduction-related mineralized systems clus-

ter around 55 Ma (Dawson and others, 1992, fig. 19.15), overlapping the age of the final stages of compressional tectonics in this part of the Cordillera. The style of miner-

alization in the northern Coast batholith can be best classified within the differentiated monzogranite suite of low-grade molybdenum porphyry deposits of Carten and others

Table 1.  $^{40}\text{Ar}/^{39}\text{Ar}$  data for mineral separates from the Boundary Creek 2 molybdenum occurrence and the camp-10 and camp-18 granodiorites, northern part of the Coast batholith, southeastern Alaska

Temp. (°C)	$^2\text{Radiogenic}$ $^{40}\text{Ar}$	$^2\text{K-derived}$ $^{39}\text{Ar}$	$^{40}\text{Ar}/^{39}\text{Ar}_k^3$	$^{39}\text{Ar}/^{37}\text{Ar}^4$	Radiogenic yield (percent)	Percent $^{39}\text{Ar}$	Apparent age and error <sup>5</sup> (Ma)
<b>93RG52C; BIOTITE; BOUNDARY CREEK 2 DIKE</b>							
Total-gas date: <b>65.0±0.2 Ma</b> ; no plateau; isochron date (800-1,300°C): <b>65.2±0.6 Ma</b> ; ( $^{40}\text{Ar}/^{36}\text{Ar}$ ) <sub>i</sub> = <b>449±42</b> <b>J=0.007531±0.1</b> percent; wt., 51.1 mg							
650	0.0584	0.0347	1.69	40	24.1	0.9	22.8±1.9
750	.9143	.2468	3.70	67	82.5	6.6	49.65±0.08
800	1.3130	.2443	5.38	180	83.3	6.6	71.6±0.3
850	1.4084	.2817	5.00	267	97.6	7.6	66.7±0.2
900	1.6544	.3459	4.78	323	99.3	9.3	63.84±0.10
950	1.3812	.2898	4.77	449	98.8	7.8	63.6±0.2
1000	1.4697	.3090	4.76	145	97.9	8.3	63.49±0.10
1050	1.4209	.2933	4.84	101	96.5	7.9	64.65±0.10
1100	2.2652	.4147	5.46	86	96.7	11.2	72.72±0.11
1150	2.9032	.5612	5.17	62	97.8	15.1	68.95±0.11
1300	3.3067	.6970	4.78	11		10.6	63.78±0.10
<b>93RG52A; MUSCOVITE; BOUNDARY CREEK 2 DIKE</b>							
Total-gas date: <b>59.71±0.16 Ma</b> ; plateau date: <b>59.71±0.14 Ma</b> (850-1,300°C) <b>J=0.007547±0.1</b> percent; wt., 67.2 mg							
600	0.0136	0.0045	3.02	12	13.0	0.1	40.6±28.3
700	.1356	.0277	4.90	--	70.2	.7	65.4±0.8
750	.2041	.0469	4.36	37	44.0	1.1	58.3±1.0
800	.3879	.0877	4.42	200	77.8	2.1	59.2±0.4
850 <sup>P</sup>	.7422	.1664	4.46	495	88.9	4.0	59.7±0.3
900 <sup>P</sup>	3.1216	.7007	4.46	562	96.5	16.7	59.66±0.09
950 <sup>P</sup>	4.9095	1.1022	4.45	1332	98.8	26.3	59.65±0.09
1000 <sup>P</sup>	3.3397	.7485	4.46	406	98.5	17.9	59.75±0.09
1050 <sup>P</sup>	1.9059	.4266	4.47	652	97.8	10.2	59.83±0.09
1100 <sup>P</sup>	1.6872	.3773	4.47	--	98.0	9.0	59.88±0.09
1150 <sup>P</sup>	1.4891	.3342	4.46	--	98.7	8.0	59.67±0.12
1300 <sup>P</sup>	.7592	.1704	4.45	--	97.6	4.1	59.64±0.17
<b>93RG58; HORNBLLENDE; CAMP-18 GRANODIORITE</b>							
Total-gas date: <b>51.73±0.19 Ma</b> ; plateau date: <b>51.48±0.15 Ma</b> (1,125-1,450°C); isochron date: <b>51.5±0.6 Ma</b> (1,125-1,450°C) <b>J=0.007496±0.1</b> percent; 202.4 mg							
700	0.0516	0.0194	2.66	0.8	11.4	0.7	35.6±0.6
800	.3211	.0867	3.70	2.5	37.2	3.1	49.4±0.3
900	.7781	.1985	3.92	4.2	82.4	7.1	52.24±0.10
950	.7425	.1872	3.97	3.4	90.8	6.7	52.87±0.13
1000	.7238	.1847	3.92	1.8	89.9	6.6	52.23±0.26
1025	.5375	.1365	3.94	1.0	90.5	4.9	52.5±0.5
1050	.5053	.1279	3.95	.54	87.7	4.6	52.63±0.16
1075	.5810	.1469	3.95	.27	86.8	5.2	52.7±0.4
1100	.8315	.2118	3.92	.16	86.6	7.6	52.31±0.15
1125 <sup>P</sup>	1.4132	.3646	3.88	.13	90.2	13.0	51.66±0.10
1150 <sup>P</sup>	1.2655	.3285	3.85	.14	91.8	11.7	51.36±0.13
1200 <sup>P</sup>	1.0638	.2756	3.86	.20	90.0	9.8	51.46±0.12
1250 <sup>P</sup>	1.2083	.3135	3.85	.18	84.7	11.2	51.38±0.17
1450 <sup>P</sup>	.8440	.2183	3.87	.12	71.5	7.8	51.5±0.3



(1993). These arc-related mineral systems contrast with the Quartz Hill deposit, which has many characteristics transitional between these **calc-alkaline** systems and Climax-type molybdenum systems. Most importantly, the Quartz Hill deposit formed in an extensional setting during the Oligocene (Hudson and others, 1979).

Not only is the late Paleocene to early Eocene (58-52 Ma) magmatism obviously closely related to molybdenite mineralization, but we suggest it is possible to make a temporal link between the major part of the arc magmatism and widespread hydrothermal fluid flow on both sides of the batholith at the latitude of Juneau. Immediately west of

Table 1. Continued.

<b>93RG58; BIOTITE; CAMP-18 GRANODIORITE</b>							
Total-gas date: <b>51.8±0.3 Ma</b> ; no plateau							
<b>J=0.007465,±0.1 percent; 52.3 mg</b>							
600	0.0118	0.0078	1.52	--	10.7	0.2	20.4±16.5
700	.0347	.0160	2.16	--	30.8	.4	28.9±4.1
750	.0935	.0243	3.84	--	55.0	.7	51.1±0.9
800	.2517	.0680	3.70	--	48.6	1.8	49.2±0.6
850	.5355	.1376	3.89	--	86.2	3.7	51.65±0.16
900	.8455	.2166	3.90	--	91.8	5.8	51.82±0.29
950	1.0602	.2706	3.92	--	93.6	7.3	52.01±0.10
1000	1.0855	.2775	3.91	--	94.0	7.5	51.93±0.19
1050	1.0363	.2617	3.96	--	94.5	7.1	52.55±0.29
1100	1.2299	.3074	4.00	--	93.8	8.3	53.08±0.23
1150	1.3860	.3476	3.99	--	95.7	9.4	52.92±0.14
1200	1.9556	.4990	3.92	--	96.4	13.4	52.01±0.08
1350	4.9664	1.2776	3.89	--	97.4	34.4	51.60±0.08
<b>93RG59; BIOTITE; CAMP-10 GRANODIORITE</b>							
Total-gas date: <b>52.58±0.19 Ma</b> ; no plateau							
<b>J=0.007537,±0.1 percent; 75.1 mg</b>							
600	0.0025	0.0028	0.904	--	3.1	0.1	12.±29
700	.0480	.0244	1.96	--	13.1	.5	26.5±1.3
800	.9614	.2491	3.86	--	52.7	5.0	51.72±0.23
850	1.1659	.2994	3.89	--	84.4	6.0	52.18±0.23
900	1.8750	.4773	3.93	--	90.7	9.5	52.63±0.10
950	1.3204	.3308	3.99	--	91.6	6.6	53.47±0.09
1000	1.3648	.3455	3.95	--	89.1	6.9	52.92±0.16
<b>1050</b>	1.1895	.3012	3.95	--	82.0	6.0	52.90±0.19
1100	1.7103	.4246	4.03	--	80.5	8.4	53.95±0.08
1150	1.7259	.4340	3.98	--	86.8	8.6	53.28±0.15
1200	2.3335	.5942	3.93	--	91.6	11.8	52.62±0.08
1350	6.0279	1.5433	3.91	--	96.8	30.7	52.34±0.08
<b>93RG59; HORNBLLENDE; CAMP-10 GRANODIORITE</b>							
Total-gas date: <b>71.1±1.6 Ma</b> ; no plateau; isochron date: <b>63.1±0.7 Ma</b> (all); ( <sup>40</sup> Ar/ <sup>36</sup> Ar) <sub>i</sub> = <b>297±2</b>							
<b>J=0.007571±0.1 percent; 276.5 mg</b>							
750	0.1219	0.0081	15.02	94	0.4	0.9	194.4±12.3
900	.3933	.0683	5.76	.09	2.2	7.4	77.0±8.0
<b>1000</b>	.5476	.0926	5.91	.06	1.1	10.0	79.0±2.9
<b>1025</b>	.2196	.0926	5.49	.05	4.1	4.3	73.4±2.8
<b>1050</b>	.1255	.0206	6.08	.09	5.1	2.2	81.2±3.3
<b>1075</b>	.2604	.0477	5.46	.15	3.6	5.1	73.1±2.5
1100	.2931	.0598	4.91	.14	3.3	6.4	65.8±0.7
<b>1125</b>	.3747	.0771	4.86	.06	4.2	8.3	65.17±0.17
1150	.4580	.0937	4.89	.07	6.9	10.1	65.6±1.0
1175	.6306	.1320	4.78	.08	9.6	14.2	64.09±0.16
1200	.4095	.0788	5.20	.07	7.6	8.5	69.6±1.5
1250	.2838	.0500	5.68	.08	4.2	5.4	75.9±1.2
1300	.2417	.0428	5.64	.06	5.7	4.6	75.4±0.4
1450	.5692	.1167	4.88	.01	16.2	12.6	65.42±0.10

the batholith near Juneau, the similarity in ages of magmatism and widespread metamorphic fluid flow (about 56-52 Ma) leading to gold-vein formation has been well documented (Goldfarb and others, 1991; Miller and others, 1994). The data from the Boundary Creek area indicate that much of the magmatism on the eastern side of the batholith was also 5-10 m.y. older than Middle Eocene. A new  $^{40}\text{Ar}/^{39}\text{Ar}$  date of 63 Ma for hydrothermal fuchsite at the Polaris-Taku gold deposit (fig. 1), immediately east of the batholith (L.W. Snee, unpub. data) and 10-15 km north-east of the Boundary Creek area, indicates thermal pulses formed mesothermal vein deposits on both sides of the evolving batholith.

## CONCLUSIONS

Our age information elucidates two important elements related to molybdenite mineralization and the evolution of the Coast batholith. First, we have demonstrated that the significant, yet subeconomic, molybdenite mineralization

in the northern part of the Coast batholith is associated with Paleocene-Eocene (63-50 Ma) magmatism. Thus, assessment of mineral resources in the northern Coast batholith must consider the molybdenite potential relative to a calc-alkaline British Columbia-type model and not relative to Quartz Hill-type porphyry systems. Secondly, well-constrained ages of intrusive rocks distributed over many hundreds of square kilometers (as indicated by the samples from camp-18, camp-10 and those of the Taku River area) throughout the core of the Coast batholith indicate that great volumes of granite and granodiorite were **emplaced** over a 10- to 12-m.y.-long period beginning in the late Paleocene. Further, the differences in ages of a few million years at various locations attest to the composite nature of the batholith. These relations support a model whereby the batholith is composed of numerous stocks and plugs that are compositionally similar yet temporally separated by several millions of years.

Acknowledgments.—We would like to thank the Foundation for Glacier and Environmental Research for logistical support during part of this study.

Table 1. Continued.

<sup>1</sup> Samples of biotite-rich, molybdenite-bearing granite dike at the Boundary Creek 2 mineral **occurrence** and two granodiorite plutons at **camp-10** and **camp-18** were collected for hornblende, biotite, and zircon. Some of the biotite in the dike had been altered to hydrothermal muscovite. All three samples were crushed, ground, and sieved, and the 80-to-120-mesh-size sieve fractions were passed through heavy liquids and a magnetic separator to obtain muscovite, biotite, and hornblende concentrates. The concentrates were handpicked to 100 percent purity. The six mineral separates were cleaned in reagent-grade ethanol, acetone, and deionized water in an ultrasonic bath, air dried, **wrapped** in aluminum packages and sealed in silica vials along with monitor minerals prior to irradiation. Samples were irradiated in the **TRIGA** reactor at the U.S. Geological Survey in Denver, **Colo.** for 20 hrs at 1 MW.

<sup>2</sup> A Mass Analyser Products 215 **Rare Gas mass spectrometer** with a Faraday cup was used to measure argon-isotope **abundances**. Abundances of "Radiogenic  $^{40}\text{Ar}$ " and "K-derived  $^{39}\text{Ar}$ " are reported in volts. Conversion to moles can be made using  $1.838 \times 10^{-12}$  mol argon per volt of signal. Detection limit at the time of this experiment was  $2 \times 10^{-17}$  mol argon. Analytical data for "Radiogenic  $^{40}\text{Ar}$ " and "K-derived  $^{39}\text{Ar}$ " are calculated to five decimal places; " $^{40}\text{Ar}_k/^{39}\text{Ar}_k$ " is calculated to three decimal places. "Radiogenic  $^{40}\text{Ar}$ ", "K-derived  $^{39}\text{Ar}$ ", and " $^{40}\text{Ar}_k/^{39}\text{Ar}_k$ " are rounded to significant figures using analytical **precisions**. Apparent ages and associated errors were calculated from **unrounded** analytical data and then each rounded using associated errors. All analyses were done in the Argon Laboratory, U.S. Geological Survey, Denver, **Colo.** Decay constants are those of Steiger and **Jäger** (1977). The irradiation monitor, hornblende **Mmh-1** with percent **K**=1.555,  $^{40}\text{Ar}_k=1.624 \times 10^{-9}$  mol/g, and **K-Ar** age = 520.4 Ma (Samson and Alexander, 1987), was used to calculate J-values for this experiment.

<sup>3</sup> " $^{40}\text{Ar}_k/^{39}\text{Ar}_k$ " has been corrected for all interfering isotopes including atmospheric argon. Mass discrimination in low mass spectrometer was determined by measuring the  $^{40}\text{Ar}/^{36}\text{Ar}$  ratio of atmospheric argon; our measured value is 296.6 during the period of this experiment; the accepted atmospheric  $^{40}\text{Ar}/^{36}\text{Ar}$  ratio is 295.5. Abundances of interfering isotopes of argon from K and Ca were calculated from reactor production ratios determined by irradiating and analyzing pure  $\text{CaF}_2$  and  $\text{K}_2\text{SO}_4$  simultaneously with these samples. The measured production ratios for these samples are  $(^{40}\text{Ar}/^{39}\text{Ar})_k=9.76 \times 10^{-3}$ ,  $(^{38}\text{Ar}/^{39}\text{Ar})_k=1.307 \times 10^{-2}$ ,  $(^{37}\text{Ar}/^{39}\text{Ar})_k=1.10 \times 10^{-4}$ ,  $(^{36}\text{Ar}/^{37}\text{Ar})_{ca}=2.70 \times 10^{-4}$ ,  $(^{39}\text{Ar}/^{37}\text{Ar})_{ca}=6.81 \times 10^{-4}$ , and  $(^{38}\text{Ar}/^{37}\text{Ar})_{ca}=2.70 \times 10^{-3}$ . Corrections were also made for additional interfering isotopes of argon produced from irradiation of chlorine using the method of Roddick (1983). The reproducibility of split gas fractions from each monitor (0.05-0.2 percent, 1 sigma) was used to calculate imprecisions in J. J-values for each sample were interpolated from adjacent monitors and have similar uncertainties to the monitors. Uncertainties in calculations for the date of individual steps in a spectrum were calculated using modified equations of **Dalrymple** and others (1981).

<sup>4</sup> To calculate apparent **K/Ca** ratios, divide the  $^{39}\text{Ar}/^{37}\text{Ar}$  ratio value by 2.

<sup>5</sup> 1-sigma error.

<sup>6</sup> Fraction included in plateau date

**Table 2.** U-Pb isotopic data and apparent ages

Fraction-size <sup>a</sup> ( $\mu\text{m}$ )	Wt. concentration <sup>b</sup> (mg)	concentration <sup>b</sup> (ppm)		Isotopic composition <sup>c</sup>			Apparent ages <sup>d</sup> (Ma)			Th-corrected ages <sup>e</sup> (Ma)		
		U	Pb*	$\frac{206\text{Pb}}{204\text{Pb}}$	$\frac{206\text{Pb}}{207\text{Pb}}$	$\frac{206\text{Pb}}{208\text{Pb}}$	$\frac{206\text{Pb}^*}{238\text{U}}$	$\frac{207\text{Pb}^*}{235\text{U}}$	$\frac{207\text{Pb}^*}{206\text{Pb}^*}$	$\frac{206\text{Pb}^*}{238\text{U}}$	$\frac{207\text{Pb}^*}{206\text{Pb}^*}$	
<b>Sample C-10:</b>												
a	63-80	0.2	1445	13.4	4280	19.627	8.354	59.8	$60.2 \pm 0.1$	75	$59.9 \pm 0.1$	$72 \pm 2$
b	100-125A	.3	1165	10.7	5721	19.988	8.710	59.5	$59.8 \pm 0.1$	72	$59.5 \pm 0.1$	$69 \pm 2$
c	125-350A	.3	1135	10.8	3015	19.013	8.131	61.4	$62.0 \pm 0.1$	85	$61.5 \pm 0.1$	$82 \pm 2$
<b>Partial Dissolution Results:</b>												
<u>% U</u>												
L1	16.4	155	1.4	1805	17.979	8.514	58.5	$58.8 \pm 0.2$	73	$58.6 \pm 0.2$	$70 \pm 5$	
L2	31.4	298	2.6	2554	18.865	10.588	56.9	$57.0 \pm 0.2$	61	$56.9 \pm 0.2$	$59 \pm 3$	
L3	43.8	415	3.9	6797	20.140	9.513	60.7	$61.0 \pm 0.2$	74	$60.8 \pm 0.2$	$71 \pm 2$	
L4	7.7	73	.7	10,125	20.442	7.102	61.5	$61.8 \pm 0.2$	73	$61.6 \pm 0.2$	$71 \pm 4$	
R	.6	6	.1	275	9.468	3.348	60.8	$67.6 \pm 0.5$	314	$60.9 \pm 0.2$	$312 \pm 16$	
T(125-350)	1.5	327	2.9				59.2	$59.5 \pm 0.2$	71	$59.3 \pm 0.2$	$69 \pm 4$	
<b>Sample C-18:</b>												
a	63-80	0.2	652	5.7	3214	19.262	5.577	53.5	$53.8 \pm 0.1$	67	$53.6 \pm 0.1$	$63 \pm 3$
b	100-125A	.3	428	3.7	2898	19.006	6.015	54.2	$54.7 \pm 0.1$	77	$54.3 \pm 0.1$	$73 \pm 4$
c	125-350A	.3	369	3.2	1399	17.201	5.314	54.1	$54.7 \pm 0.1$	81	$54.2 \pm 0.1$	$77 \pm 4$
<b>Partial Dissolution Results:</b>												
<u>% U</u>												
L1	11.2	80	.8	463	12.596	4.261	58.6	$59.1 \pm 0.4$	78	$58.6 \pm 0.2$	$76 \pm 13$	
L2	20.8	148	1.2	1045	16.198	5.089	50.5	$51.1 \pm 0.2$	82	$50.5 \pm 0.2$	$79 \pm 6$	
L3	39.7	282	2.6	2165	17.788	5.329	56.3	$59.0 \pm 0.2$	168	$56.4 \pm 0.2$	$166 \pm 3$	
L4	25.5	181	1.7	6535	19.991	12.470	61.8	$62.5 \pm 0.2$	88	$61.9 \pm 0.2$	$86 \pm 3$	
R	2.7	19	.2	1852	18.152	6.462	53.5	$53.6 \pm 0.5$	59	$53.6 \pm 0.2$	$56 \pm 3$	
T(125-350)	2.4	296	2.7				56.7	$58.1 \pm 0.2$	117	$56.7 \pm 0.2$	$115 \pm 4$	

Table 2. Continued

- <sup>a</sup> a, b, and c designate conventional fractions; A designates conventional fractions abraded to 30 to 60 percent of original diameter; L1, L2, L3, and L4 designate *leachate* steps; R designates digestion of final residue; T designates mathematically recombined steps and residue. Partial dissolution procedure after Mattinson (1994). Partial dissolution schedule: 1 = 24 hours at 80°C; 2 = 24 hours at 150°C; 3 = 24 hours at 200°C; 4 = 6 hours at 245°C; R = 44 hours at 245°C. Conventional fractions were washed in warm 3N HNO<sub>3</sub> and 3N HCl for 15 minutes each, spiked with <sup>205</sup>Pb-<sup>235</sup>U tracer, and dissolved in a 50 percent HF>>14N HNO<sub>3</sub> solution within 3 mL Savillex™ capsules placed in 45 mL TFE Teflon™-lined Parr acid-digestion bomb. This procedure is similar to that outlined by Parrish (1987). Following evaporation and dissolution in HCl, Pb and U for all fractions were separated following techniques modified from Krogh (1973). Pb and U were combined and loaded with H<sub>3</sub>PO<sub>4</sub> and silica gel onto single degassed Re filaments. Isotopic compositions of Pb and U were determined through static collection on a Finnigan-MAT 261 multicollector mass spectrometer utilizing an ion counter for collection of the <sup>204</sup>Pb beam. All analyses were performed by W.C. McClelland at the University of California, Santa Barbara. Zircon fractions are nonmagnetic on Frantz magnetic separator at 1.8 A, a 15° forward slope, and a 1° side slope.
- <sup>b</sup> Pb\* is radiogenic Pb expressed as parts per million for conventional analyses and as nanograms for partial dissolution steps. U is expressed as parts per million for conventional analyses and as nanograms and percent of total U for partial-dissolution steps.
- <sup>c</sup> Reported ratios corrected for fractionation (0.125 ± 0.038 percent/AMU) and spike Pb. Ratios used in age calculation were adjusted for 6 to 10 pg of blank Pb with isotopic composition of <sup>206</sup>Pb/<sup>204</sup>Pb = 18.6, <sup>207</sup>Pb/<sup>204</sup>Pb = 15.5, and <sup>208</sup>Pb/<sup>204</sup>Pb = 38.4, 2 pg of blank U, 0.25 ± 0.049 percent/AMU fractionation for UO<sub>2</sub>, and initial common Pb with isotopic composition approximated from Stacey and Kramers (1975) with an assigned uncertainty of 0.1 to initial <sup>207</sup>Pb/<sup>204</sup>Pb ratio.
- <sup>d</sup> Uncertainties reported as 2 sigma. Error assignment for individual analyses follows Mattinson (1987) and is consistent with Ludwig (1991). An uncertainty of 0.2 percent is assigned to the <sup>206</sup>Pb/<sup>238</sup>U ratio based on our estimated reproducibility, unless this value is exceeded by analytical uncertainties. Calculated uncertainty in the <sup>207</sup>Pb/<sup>206</sup>Pb ratio incorporates uncertainties due to measured <sup>204</sup>Pb/<sup>206</sup>Pb and <sup>207</sup>Pb/<sup>206</sup>Pb ratios, initial <sup>207</sup>Pb/<sup>204</sup>Pb ratio, and composition and amount of blank. Linear regression of discordant data utilized the method of Ludwig (1991). Decay constants used: <sup>238</sup>U=1.5513 E-10, <sup>235</sup>U=9.8485 E-10. <sup>238</sup>U/<sup>235</sup>U = 137.88.
- <sup>e</sup> A 75 percent ± 25 percent efficiency in <sup>230</sup>Th exclusion during zircon crystallization is assumed, and <sup>207</sup>Pb/<sup>206</sup>Pb and <sup>206</sup>Pb/<sup>238</sup>U ratios have been adjusted accordingly. Age assignments presented are derived from the Th-corrected ratios.
-

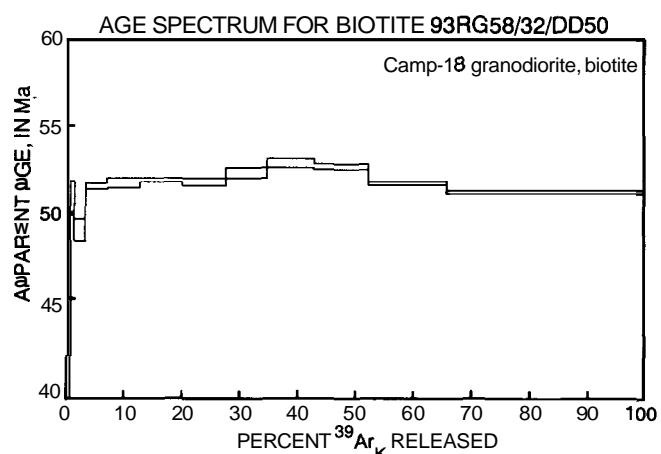
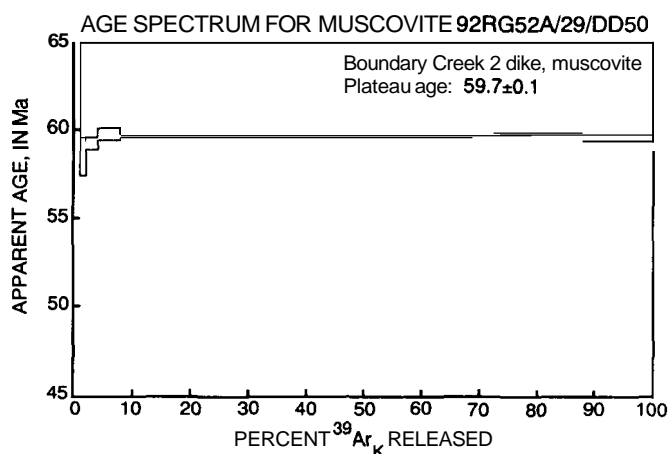
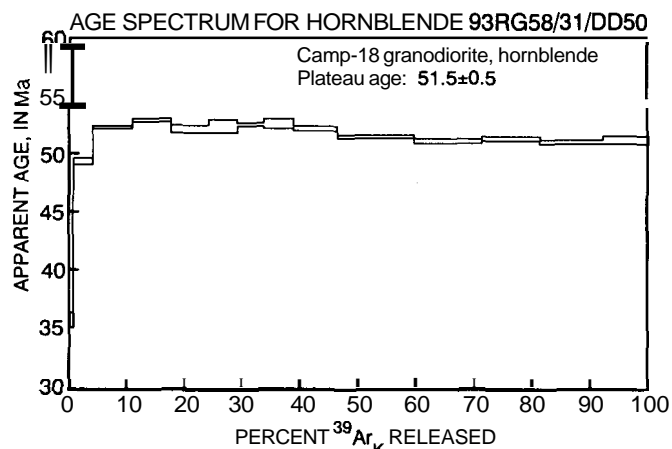
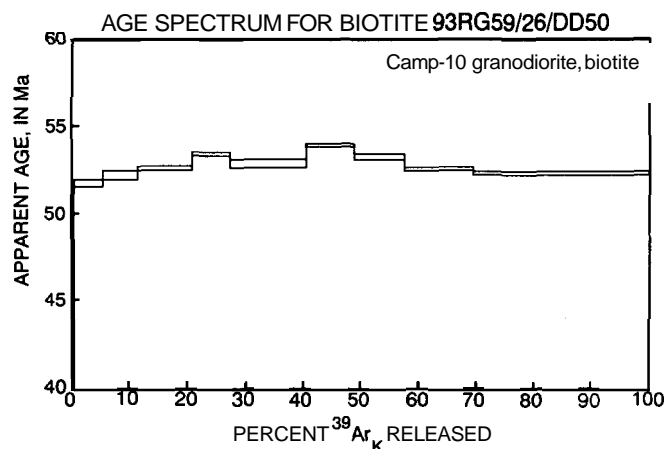
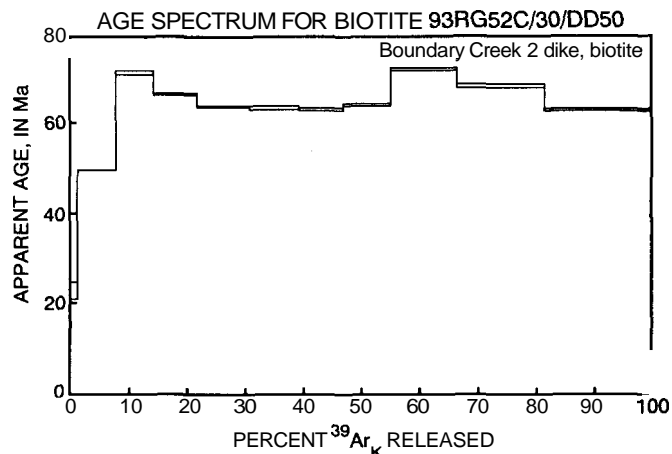
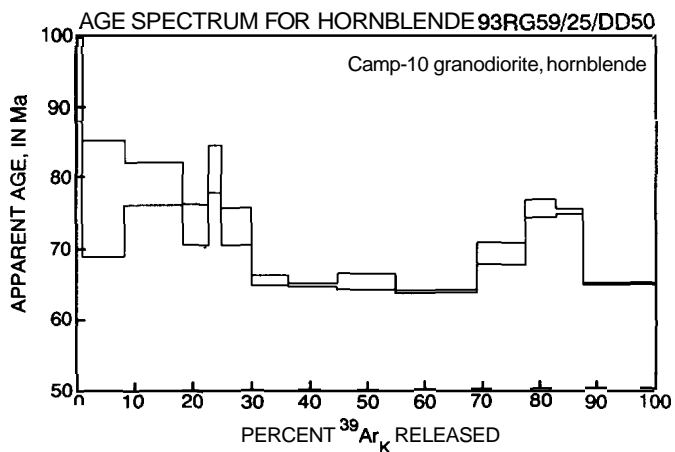
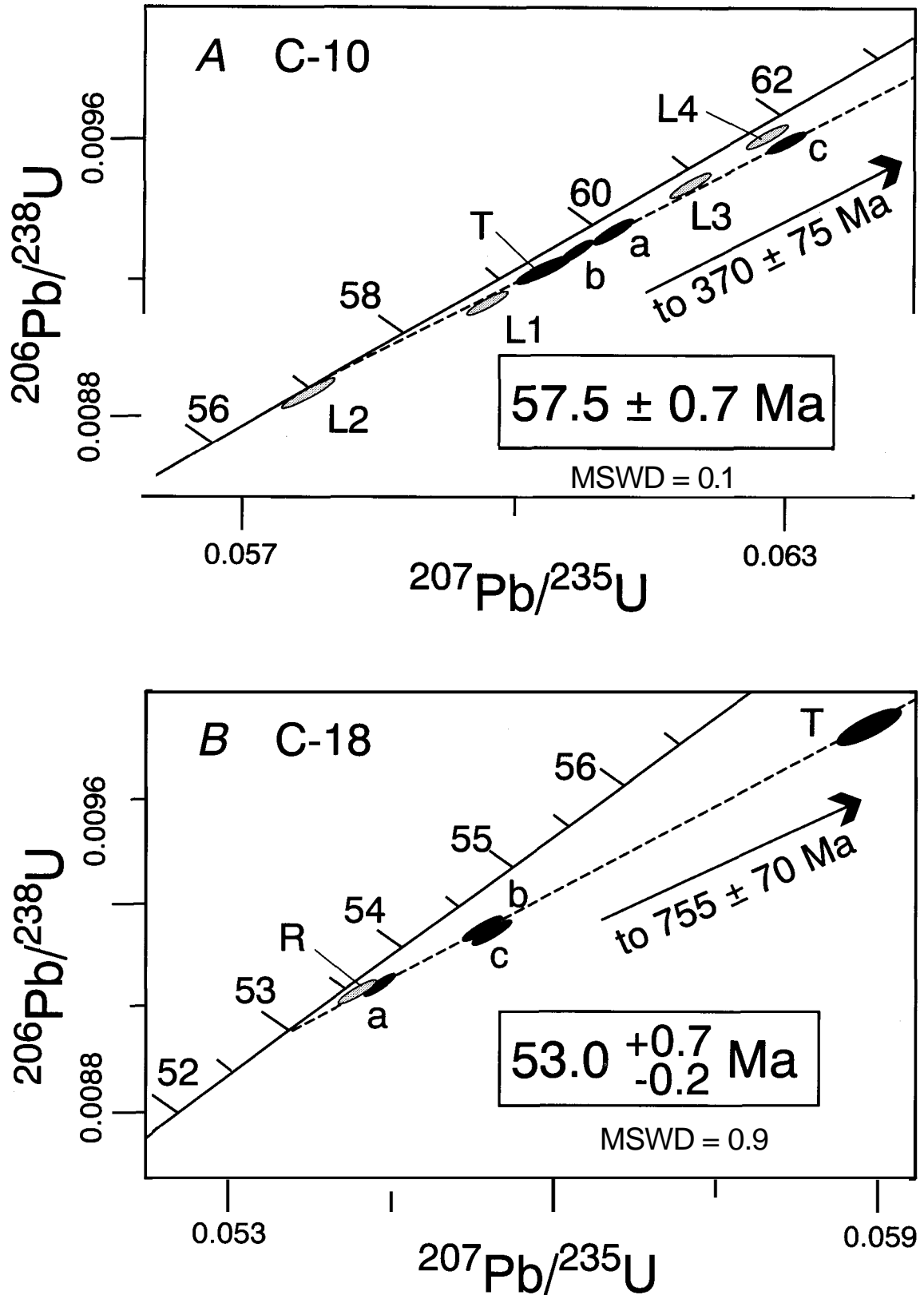


Figure 2. Argon-release spectra diagrams for minerals from the Boundary Creek 2 molybdenum occurrence and the camp-10 and camp-18 granodiorites. All errors are 1 sigma.



**Figure 3.** U-Pb concordia plots of conventional (solid) and partial-dissolution (shaded) data. Error ellipses are plotted at 95-percent confidence level. A, Samples from camp-10. B, Samples from camp-18. Abbreviations (see table 2): a, b, and c—conventional size fractions; L1, L2, L3, and L4—leachate steps; R—digestion of final residue; T—mathematically recombined steps and residue; MSWD—mean-student-weighted deviate.

## REFERENCES CITED

- Beley, M.J., 1980, Glaciers, mountains probed to find Mt Ogdén moly: Canadian Mining Journal, April, p. 55-62.
- Brew, D.A., 1994, Latest Mesozoic and Cenozoic magmatism in southeastern Alaska, *in* Plafker, George, and Berg, H.C., eds., The geology of Alaska: Boulder, Colo., Geological Society of America, The Geology of North America, v. G-1 p. 621-656.
- Brew, D.A., and Ford, A.B., 1969, Boundary Creek molybdenum-silver occurrence, southeastern Alaska: U.S. Geological Survey Circular 615, p. 12-15.
- Carten, R.B., White, W.H., and Stein, H.J., 1993, High-grade granite-related molybdenum systems: classification and origin, *in* Kirkham, R.V., Sinclair, W.D., Thorpe, R.I., and Duke, J.M., eds., Mineral deposit modeling: Geological Association of Canada, Special Paper 40, p. 521-554.
- Clough, A.H., 1990, Detailed mine, prospect, and mineral occurrence descriptions, Coast Range subarea, *in* Bureau of Mines mineral investigations in the Juneau Mining District, Alaska, 1984-1988: U.S. Bureau of Mines Special Publication, Section E, 44 p.
- Dalrymple, G.B., Alexander, E.C., Lanphere, M.A., and Kraker, G.P., 1981, Irradiation of samples for  $^{40}\text{Ar}/^{39}\text{Ar}$  dating using the Geological Survey TRIGA reactor: U.S. Geological Survey Professional Paper 1176, 56 p.
- Dawson, K.M., Panteleyev, A., Sutherland-Brown, A., and Woodsworth, G.J., 1992, Regional metallogeny, *in* Gabrielse, H., and Yorath, C.J., eds., Geology of the Cordilleran orogen in Canada: Geological Survey of Canada, Geology of Canada, no. 4., p. 707-768.
- Gehrels, G.E., Brew, D.A., and Saleeby, J.B., 1984, Progress report of U/Pb (zircon) geochronological studies in the Coast plutonic-metamorphic complex east of Juneau, southeastern Alaska, *in* Bartsch-Winkler, Susan, and Reed, K.M., eds., The U.S. Geological Survey in Alaska—Accomplishments during 1982: U.S. Geological Circular 939, p. 100-102.
- Gehrels, G.E., McClelland, W.C., Samson, S.D., Patchett, P.J., and Brew, D.A., 1991, U-Pb geochronology of Late Cretaceous and early Tertiary plutons on the northern Coast Mountains batholith: Canadian Journal of Earth Sciences, v. 28, p. 899-911.
- Goldfarb, Dick, Snee, L.W., Miller, L.D., and Newberry, R.J., 1991, Rapid dewatering of the crust deduced from ages of mesothermal gold deposits: Nature, v. 354, p. 296-298.
- Hudson, Travis, Smith, J.G., and Elliot, R.L., 1979, Petrology, composition, and age of intrusive rocks associated with the Quartz Hill molybdenite deposit, southeastern Alaska: Canadian Journal of Earth Sciences, v. 16, p. 1805-1822.
- Klipfel, P.D., 1981, Geology of an area near Mt. Ogilvie, northern Boundary Range, Juneau Icefield, Alaska: Moscow, University of Idaho, M.S. thesis, 112 p.
- Koch, R.D., Brew, D.A., and Ford, A.B., 1987, Newly discovered molybdenite occurrence near Boundary Creek, Coast Mountains, southeastern Alaska: U.S. Geological Survey Circular 988, p. 124-125.
- Krogh, T.E., 1973, A low contamination method for hydrothermal decomposition of zircon and extraction of U and Pb for isotopic age determinations: Geochimica et Cosmochimica Acta, v. 37, p. 488-494.
- Ludwig, K.R., 1991, Isoplot—a plotting and regression program for radiogenic-isotope data, version 2.53: U.S. Geological Survey Open-File Report 91-445.
- Mattinson, J.M., 1987, U-Pb ages of zircons—a basic examination of error propagation: Chemical Geology, v. 66, p. 151-162.
- 1994, A study of complex discordance in zircons using step-wise dissolution techniques: Contributions to Mineralogy and Petrology, v. 116, p. 117-129.
- Mihalynuk, M.G., McMillan, W.J., Mortensen, J.K., Childe, F.C., and Orchard, M.J., 1996, Age of host strata versus mineralization at the Ericksen-Ashby: a skarn deposit, *in* Grant, B., and Newell, J.M., eds., Geological fieldwork 1995: British Columbia Geological Survey, Paper 1996-1, p. 175-179.
- Miller, L.D., Goldfarb, R.J., Gehrels, G.E., and Snee, L.W., 1994, Genetic links among fluid cycling, vein formation, regional deformation, and plutonism in the Juneau gold belt, southeastern Alaska: Geology, v. 22, p. 203-206.
- Parrish, R.R., 1987, An improved microcapsule for zircon dissolution in U-Pb geochronology: Chemical Geology, v. 66, p. 99-102.
- Roddick, J.C., 1983, High precision intercalibration of Ar-Ar standards: Geochimica et Cosmochimica Acta, v. 47, p. 887-898.
- Samson, S.D., and Alexander, E.C.J., 1987, Calibration of interlaboratory  $^{40}\text{Ar}/^{39}\text{Ar}$  dating standard, MMhb-1: Chemical Geology, v. 66, p. 27-34.
- Snee, L.W., Sutter, J.S., and Kelly, W.C., 1988, Thermochronology of mineral deposits—dating the stages of mineralization at Panasqueira, Portugal, by high-precision  $^{40}\text{Ar}/^{39}\text{Ar}$  age spectrum techniques on muscovite: Economic Geology, v. 83, p. 335-354.
- Souther, J.G., 1971, Geology and ore deposits of Tulsequah map area, British Columbia: Geological Survey of Canada Memoir 362, 84 p.
- Stacey, J.S., and Kramers, J.D., 1975, Approximation of terrestrial lead isotope evolution by a two-stage model: Earth and Planetary Science Letters, v. 26, p. 207-221.
- Steiger, R.H., and Jager, E., 1977, Subcommittee on geochronology—Convention on the use of decay constants in geo- and cosmo-chronology: Earth and Planetary Science Letters, v. 36, p. 359-362.

Reviewers: Robert Eppinger and Fred Barker

# Tidal Influence on Deposition and Quality of Coals in the Miocene Tyonek Formation, Beluga Coal Field, Upper Cook Inlet, Alaska

By Romeo M. Flores, Gary D. Stricker, and Robert B. Stiles

## ABSTRACT

The Miocene Tyonek Formation in the Chuitna River basin in the southwestern part of the Beluga coal field contains several minable coalbeds that are as much as 10 m thick. These coalbeds, which include the Red 1, Red 2, Red 3, and Blue coals, are located in the Diamond Chuitna Project area, where data from 38 drillholes and 19 cores were studied. Analyses of the geophysical, driller, and lithofacies logs of these drillholes and cores suggest deposition of the Red 1 and Red 2 coalbeds in fluvially influenced raised mires, and of the Red 3 and Blue coalbeds in tidally influenced topogenous mires. Tidal deposits include intertidal, tidal channel, tidal sand flat, and supratidal sediments that exhibit burrowed flaser beds with double mudstone drapes, lenticular beds, tidal bundles, Ophiomorpha-like burrows, and rhythmic interlaminations.

Statistical analysis of coal-quality data indicates that the sulfur content of the Red 1 and Red 2 coalbeds is significantly lower than that of the Red 3 and Blue coalbeds. The relatively higher sulfur content at the latter two coalbeds is attributed to increased sulfate reduction in brackish-marine waters that inundated the peat mires after deposition. Ash and heat-value contents of these coals are not statistically different. Furthermore, differences in the depositional environments controlled the maceral composition of the coalbeds. The fluvially influenced raised peat mires were episodically oxidized above the ground-water table as organic matter accumulation from woody vegetation outpaced autocompaction. In contrast, the organic accumulation from woody vegetation in the tidally influenced topogenous peat mires evolved as a function of the ebb and flood tidal cycles.

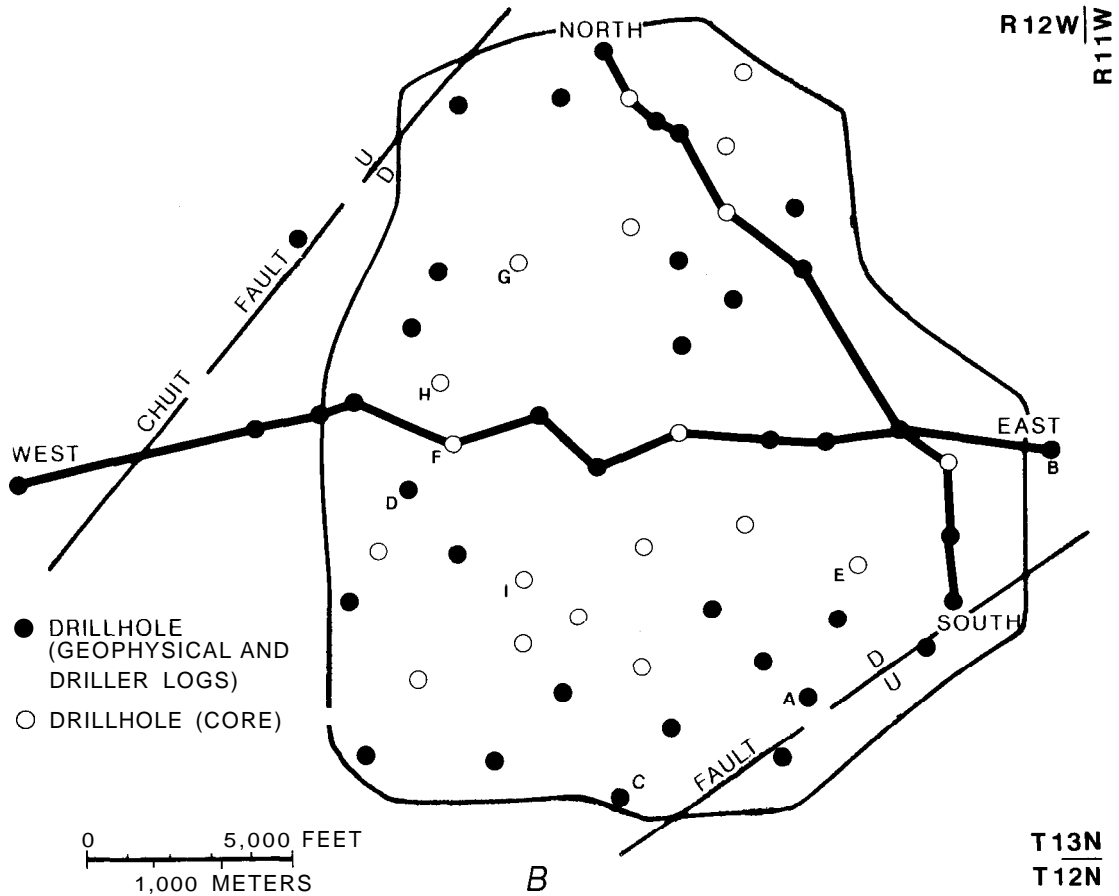
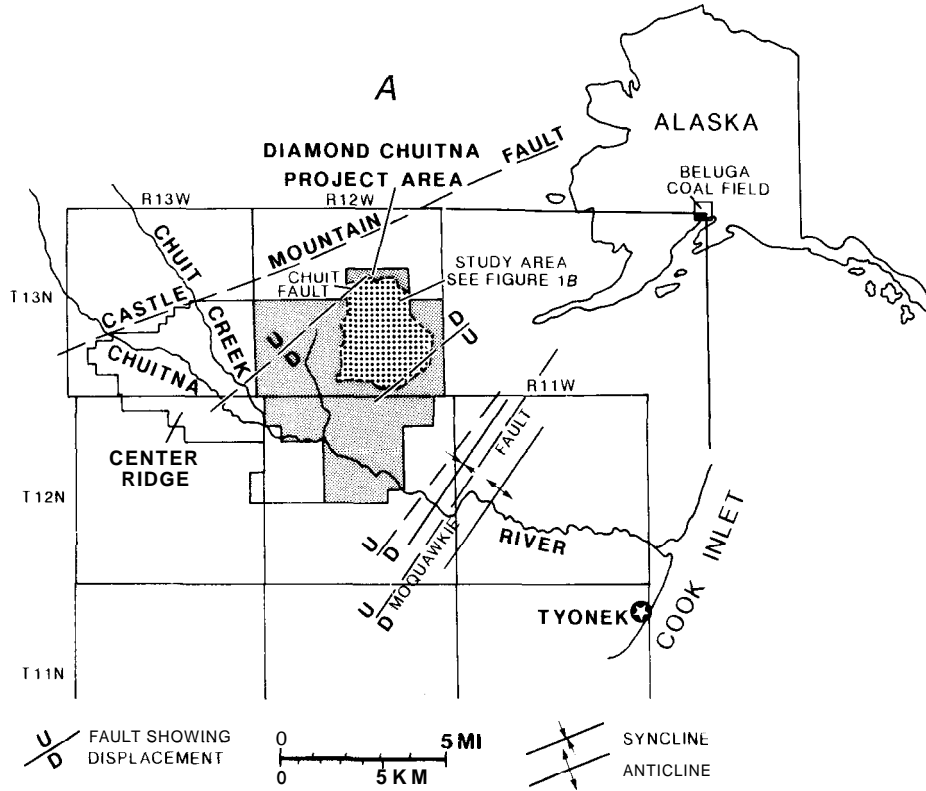
## INTRODUCTION

The southern part of the Beluga coal field, particularly in the Chuitna River basin (fig. 1A), has been the target of coal exploration and development during the past decade

(Ramsey, 1981; McFarland, 1987; Stiles and Franklin, 1987). The Center Ridge (CR), leased by Beluga Coal Company, and the Diamond Chuitna Project (DCP), leased by Diamond Alaska Coal Company, are areas (fig. 1A) that contain coal-bearing rocks of the Miocene Tyonek Formation of the Kenai Group; the formation is as much as 2,330 m thick (Calderwood and Fackler, 1972). In the CR and DCP areas, the surface minable coalbeds (Barnes, 1966) occur in the upper part of the Tyonek Formation and are as much as 10 m thick. The Tyonek coal-bearing interval (fig. 2) in the Chuitna River basin contains at least 18 coalbeds, of which 6 (Red 1, Red 2, Red 3, Blue, Green, and Brown coals) are considered minable in the DCP area (Stiles and Franklin, 1987). More importantly, the Red 1, Red 2, Red 3, and Blue coals are within a 30-100-m-thick interval and may be minable by a multiple-bed stripping method. The total maximum thickness of these four minable coalbeds is 28.9 m, but the average total thickness is about 21 m.

Rao and Smith (1987) indicated that minable coals from DCP drillhole cores range in rank from lignite to subbituminous (6,050-8,320 Btu/lb, as-received basis), which is typical for Beluga coals (Barnes, 1966). In addition, these coalbeds, as reported by Rao and Smith (1987), exhibit ash yields ranging from 3.64 to 32.5 percent (as-received basis) and sulfur contents ranging from 0.08 to 0.19 percent (as-received basis). The low sulfur contents of coals in the DCP area differ from those of other Tyonek coalbeds in the Beluga coal field reported by previous workers. Sulfur values were reported by Barnes (1966) as 0.1-0.4 percent (as-received basis), and by Affolter and Stricker (1993) as 0.08-0.32 percent (as-received basis). Thus, the Tyonek coalbeds in the Beluga coal field display varied sulfur contents. High and varied sulfur contents in coalbeds may be produced by marine or near-marine environmental settings (Gluskoter and Simon, 1968). Flores and others (1994) described tidal sedimentary structures (for example, burrows and associated flaser and lenticular bedding) in a mudstone-dominated facies below the Chuitna coalbed (Barnes, 1966; Brown coal of Ramsey, 1981) in outcrops along the Chuit Creek. Stratigraphically, the Chuitna coalbed is about





100 m above the minable Tyonek coalbeds in the DCP area (fig. 2).

The purpose of this investigation was to collect stratigraphic, sedimentologic, and geochemical data from the DCP area in order to determine the depositional environment of the minable coalbeds and associated interburden and overburden rocks. A thorough understanding of the stratigraphy of these rocks was aided by subsurface geophysical data provided by DRVEN Corporation of Anchorage, Alaska.

## METHODS

The stratigraphy and sedimentology (fig. 2) were studied using geophysical and driller logs of 38 drillholes as well as an additional 19 drillhole cores (fig. 1B). Lithology, thickness, color, grain size, petrology, sedimentary structures, and trace and body fossils were described from the drillhole cores. A total thickness of 785 m of 5-cm-diameter cores was described from the 19 drillholes. Vertical sedimentologic facies logs of the cores were constructed from these lithologic descriptions and utilized to interpret depositional processes and environments of the interburden and overburden rock types. The driller logs were used as guides for interpreting the lithotypes of the geophysical logs. The geophysical logs, which consist of gamma-ray and resistivity curves, were used to interpret the vertical and lateral variations of the coals and related interburden and overburden rocks. Cross sections were constructed from these geophysical logs and related field driller logs to establish two- and three-dimensional characteristics of the rocks. These cross sections were then used to determine the facies distribution and areal extent of the depositional settings. Coal quality (as-received basis), which includes heat value (Btu/lb), ash yield, and sulfur content, was compiled from analytical data of 20 coreholes. These data were used to compare and contrast characteristics of the coalbeds. Statistical analysis using the Student's T-test was performed to determine the significance of chemical differences between the coalbeds.

## GEOLOGIC SETTING

The Chuitna River basin (fig. 1A) extends across the Castle Mountain fault on the north and into the upper Cook Inlet on the south. Grantz (1966) interpreted the Castle

Mountain fault to be right-lateral and strike-slip from the Mesozoic through Tertiary and a steep reverse fault from the Oligocene to the present. This fault has been active for the past several million years, as indicated by several kilometers of net displacement (Barnes and Payne, 1956; Determan and others, 1976; Fuchs, 1980). The Castle Mountain fault generally separates conglomerates of the lower part of the Kenai Group to the northwest from the coal-bearing middle part of the Kenai Group (Tyonek Formation) to the southeast (Barnes, 1966). Flores and others (1994) suggested (1) that the Castle Mountain fault and related faults were active during deposition of the Tyonek Formation, and (2) that these southwest-trending faults controlled the trends of fluvial channels in the study area that deposited the Tyonek Formation.

The Chuitna River crosses an anticline about 13 km downstream from its confluence with the Chuit Creek (Barnes, 1966; fig. 1A). This anticline trends to the southwest and parallels the southwest-trending faults. An aeromagnetic survey (Grantz and others, 1963) indicates that the Moquawkie fault parallels an anticline-syncline axis (fig. 1A). The DCP area is located northwest of this synclinal axis. A north-south cross section (fig. 3A) shows southward-dipping coalbeds that are cut by a normal fault on the southern part of the property. An east-west cross section (fig. 3B) also shows a normal fault (Chuit fault) with westward-dipping coalbeds on the western part of the property. These cross sections together suggest that the study coalbeds (Red 1, Red 2, Red 3, and Blue) are near the surface in the central part of the study area but are deeper in the subsurface (as much as 135 m below the surface) westward near the confluence of the Chuitna River and Chuit Creek. In addition, these cross sections indicate that the part of the Tyonek Formation studied by Flores and others (1994), which includes the Chuitna and lower Chuitna coalbeds, is stratigraphically higher than the interval of the present study.

A composite section of part of the Tyonek Formation (as much as 300 m) in the DCP and the nearby Chuitna River-Chuit Creek areas consists of interbedded sandstone, conglomeratic sandstone, siltstone, mudstone, carbonaceous shale, and coal (fig. 2; Flores and others, 1994). The lower part of the above composite section of the Tyonek Formation in the DCP area is dominated by mudstone and siltstone with thick coalbeds and subordinate sandstone and conglomeratic sandstone (fig. 2).

## STRATIGRAPHY

The vertical succession and variation in related physical characteristics of rock types between coalbeds is interburden stratigraphy. Succession and variation in rocks above the coalbeds is overburden stratigraphy (figs. 3A, 3B). Important physical characteristics of the rocks that change through the section include lithology, color, grain

◀ **Figure 1.** A, Map showing location of Beluga coal field in the upper Cook Inlet and the study area in the Chuitna River basin. B, Map showing location of drillholes studied in the Diamond Chuitna Project (DCP) area. North-south and east-west cross sections are displayed in figure 3. Letters indicate location of drillholes shown in figures 4-8

size, sedimentary structures, and trace fossils. Many of these characteristics can be determined from the geophysical log curves, driller logs, or from drillhole core descriptions.

The gamma-ray curve measures the natural radioactivity of rock types, particularly shale, caused by absorption of thorium by clay minerals, potassium content of clay minerals (mainly illite), and uranium fixed by associated organic matter (Doveton, 1994). In general, low levels of radioactivity are observed in sandstones, limestones, and

dolomites. However, elevated gamma radiation in sandstones may be produced by their clay mineral, potassium feldspar, mica, and heavy-mineral contents. Coal displays the least gamma radiation compared with these rock types, and thus it is readily identifiable by the gamma-ray log curve.

Continuous drillhole cores of the interburden and overburden rocks were described for the intervals between the Red 1, Red 2, Red 3, and Blue coalbeds. Although the

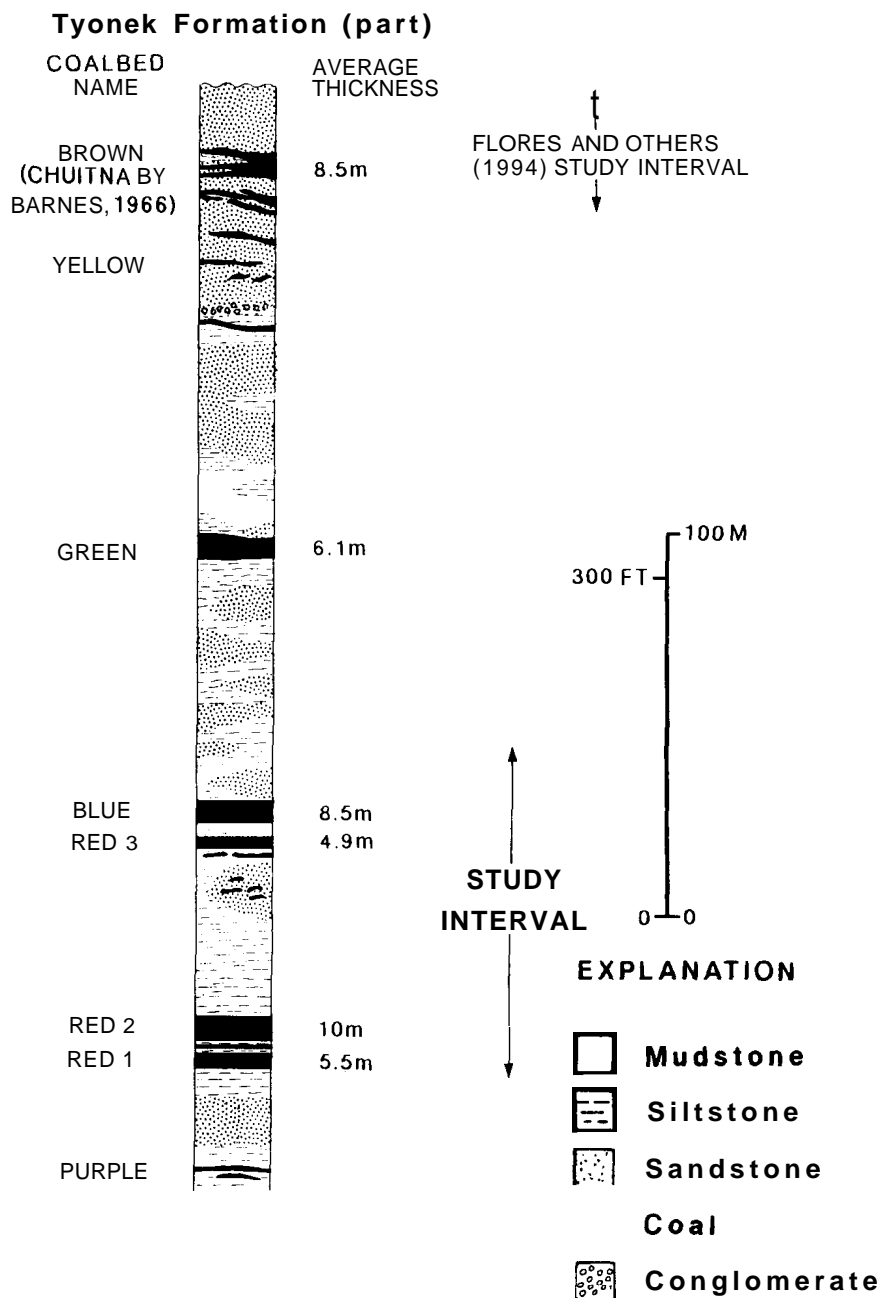


Figure 2. Generalized composite stratigraphic column of part of the Tyonek Formation in the Chuitna River basin (DCP) area, showing the study interval.

cores of 19 drillholes were described for this study, only 5 cores (figs. 4A, 4B, 5A, 5B, and 6) are presented in this paper; these cores represent the greatest variety in the stratigraphy and sedimentology encountered in the study interval and reflect interburden and overburden intervals comparable to those described from the geophysical and driller logs.

**RED 1 COALBED TO BASE OF RED 2 COALBED**

The Red 1 coalbed is as much as 3.5 m thick and is split into a thicker lower bench and a thinner upper bench (fig. 4A). Rao and Smith (1987) characterized this bed as containing 68-88 percent vitrinite, 8-25 percent liptinite, and 2-5 percent inertinite (mainly fusinite and semifusinite).

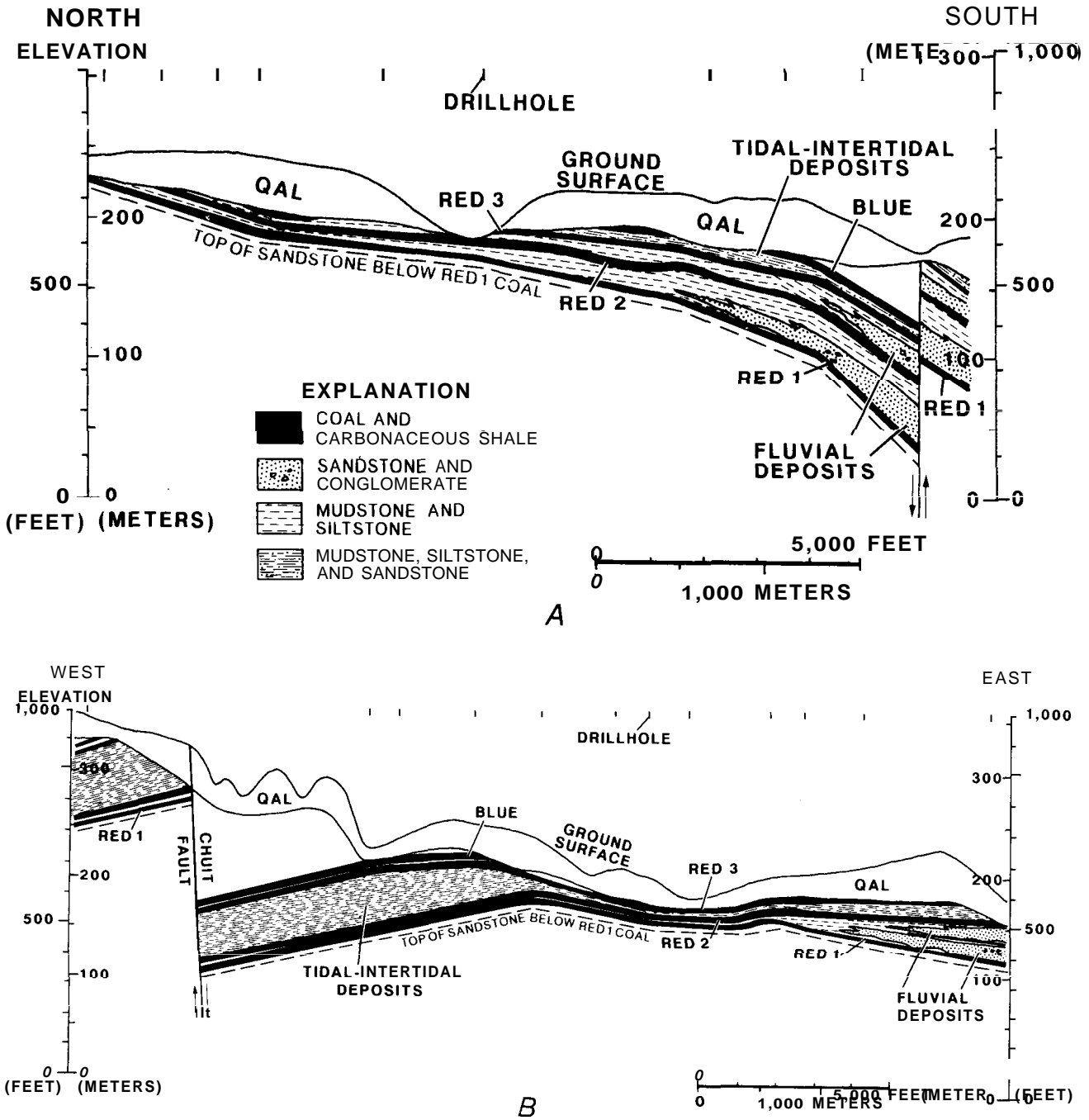


Figure 3. Cross sections of part of the Tyonek Formation in the DCP area. See figure 1A for location of lines of cross sections. QAL is Quaternary gravel, sand, silt, mud, and organic deposits. All drillholes were drilled to the top of the sandstone below the Red 1 coalbed. A, North-south cross section. B, East-west cross section.

**Figure 4 Drillholes** showing geophysical and lithologic logs, sedimentary structures, and facies interpretation of cores. See figure 1B for location of drillholes. A, Drillhole E, from below Red 1 coalbed to above the Blue coalbed. B, Drillhole F, from below Red 1-Red 2 coalbeds to below Red 3 coalbed; shows type 1 facies profile.

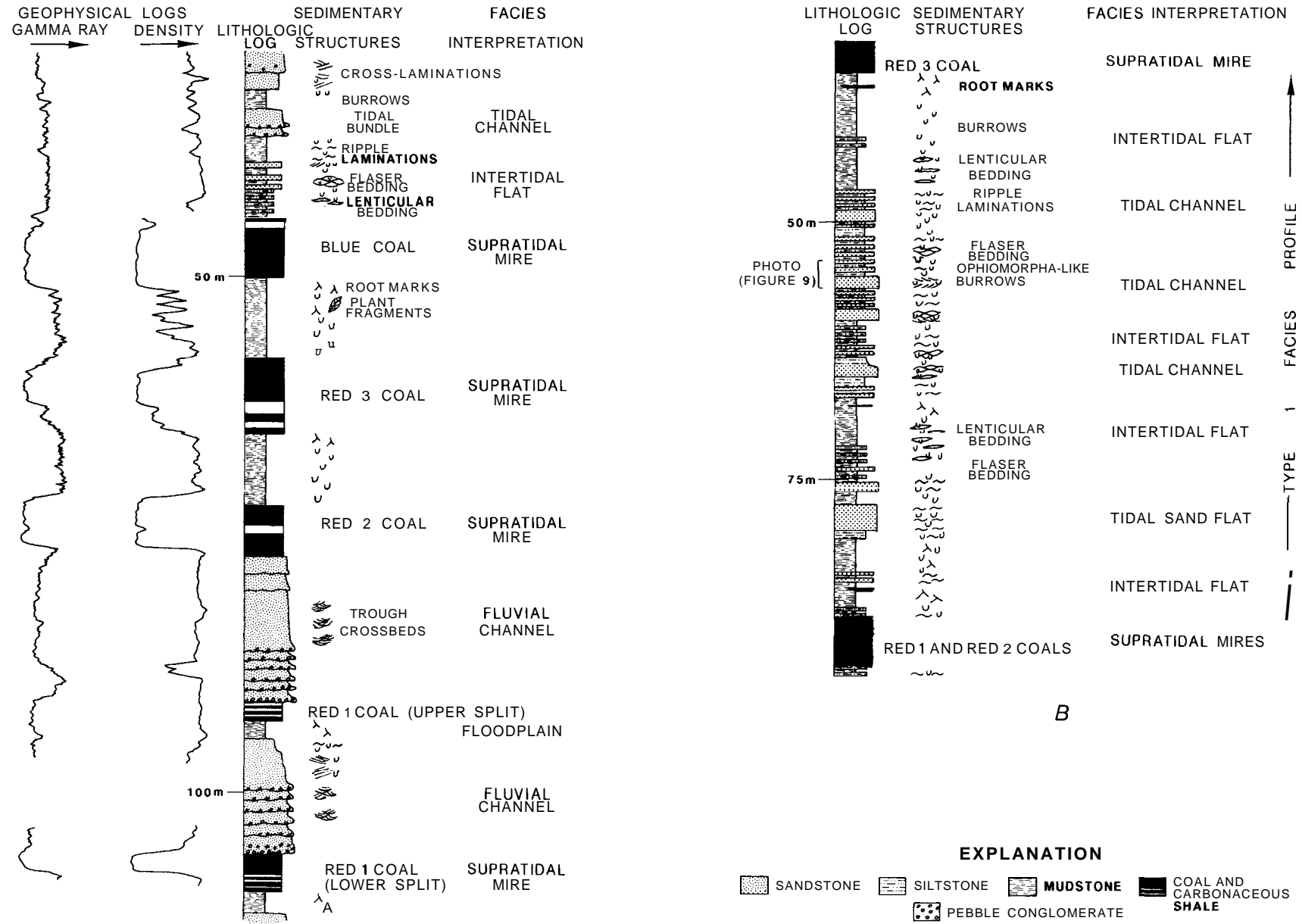
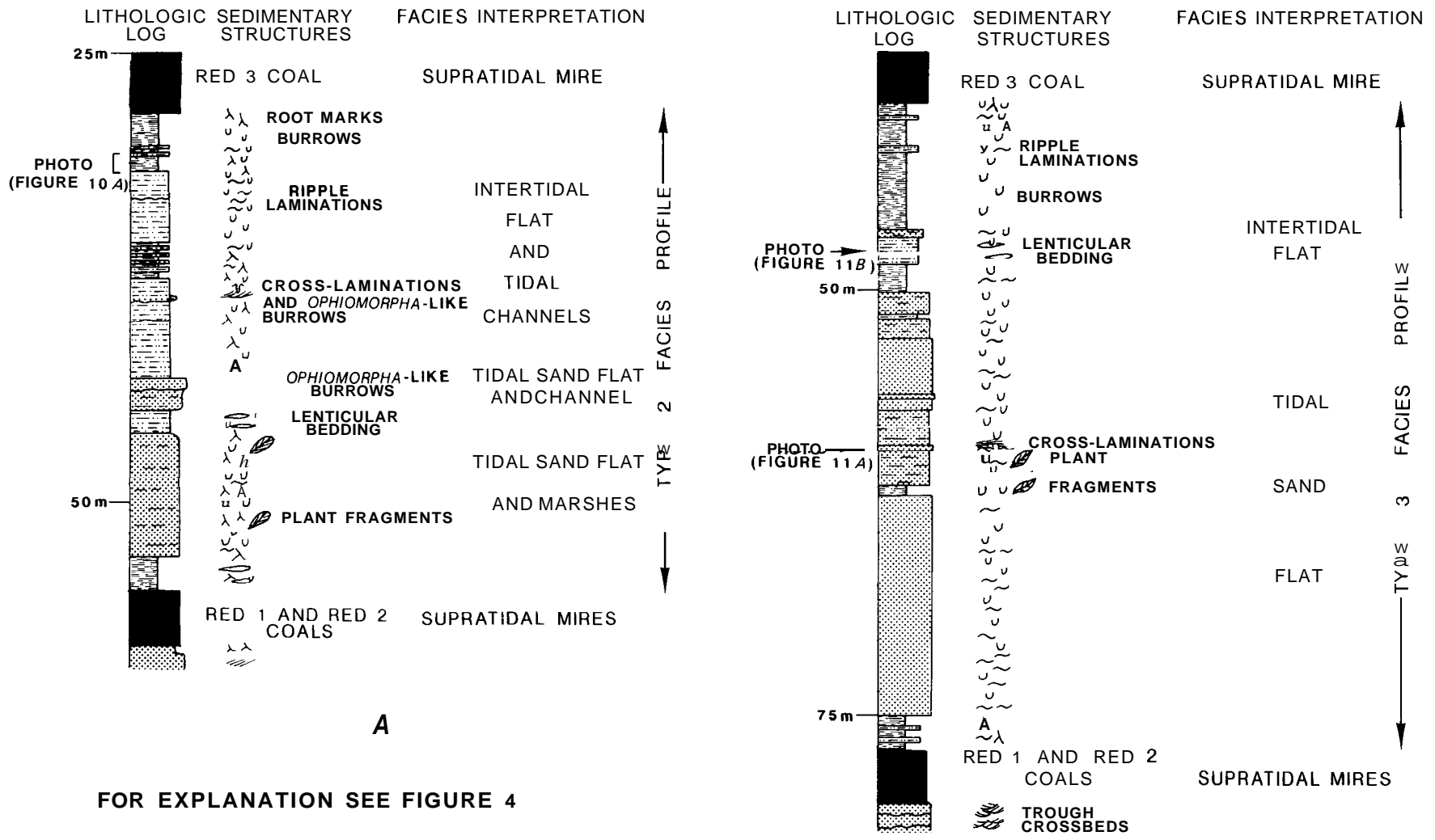


Figure 5. Lithologic log, sedimentary structures, and facies interpretation of drillhole cores from below Red 1 and Red 2 coalbeds to below Red 3 coalbed. See figure 1B for drillhole locations. A, Drillhole G; shows type 2 facies profile. B, Drillhole H; shows type 3 profile.



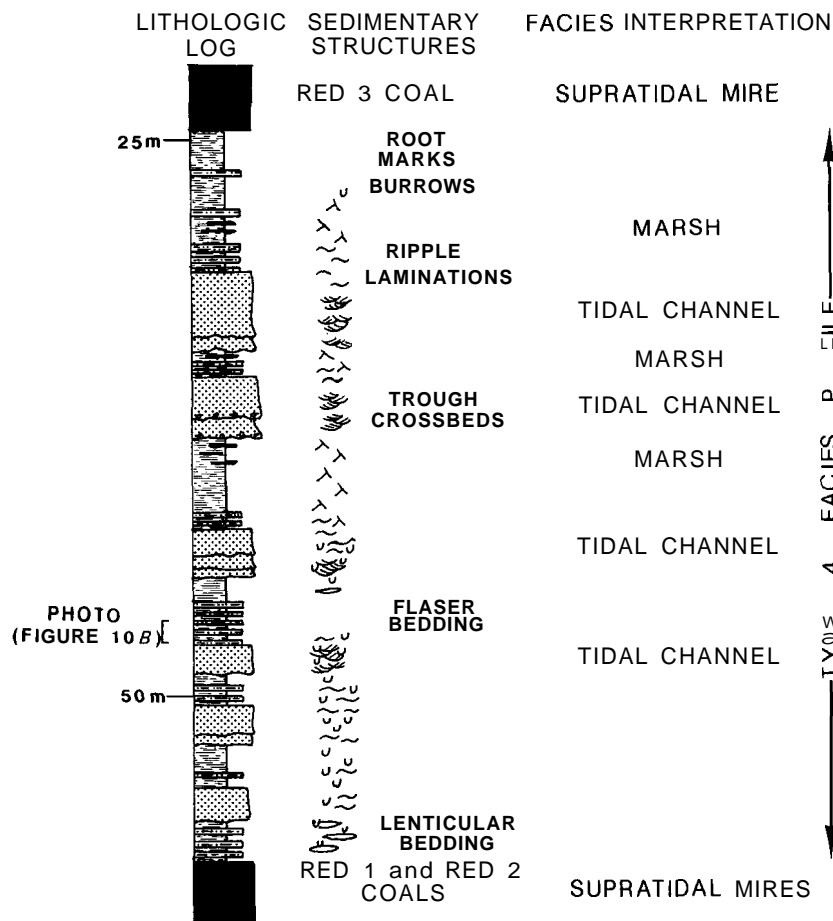
FOR EXPLANATION SEE FIGURE 4

The interburden between the Red 1 and Red 2 coalbeds ranges from 0.3 to 38 m in thickness. A comparison of the gamma-ray and resistivity logs of interburden rocks between these coalbeds shows that these logs have significantly different patterns (fig. 7A). The gamma-ray log curve shows a "blocky, shallow serrated pattern, whereas the resistivity log curve shows a "peaks and valleys" pattern (depths of 60 to 95 m in fig. 7A). The better definition of the resistivity log curve into a "peaks and valleys" pattern is probably due to vertical changes in the lithotypes. The driller log between the top of the Red 1 coalbed and the base of the Red 2 coalbed (depths of 60 to 95 m in fig. 7A) indicates that the interburden consists mainly of medium- to fine-grained sandstone, 45 percent gravel, and some clay. The "peaks" (rightward excursions) probably reflect the gravelly units, and the "valleys" (leftward excursions) represent the sandy units. Similar conglomeratic sandstones in the Tyonek Formation contain gravelly units underlain by

erosional surfaces and overlain by sandy units (Flores and others, 1994); hence, the gravels mark the lower parts of generally fining-upward units.

The interburden between the Red 1 and Red 2 coalbeds includes interbedded mudstone and 20 percent fine-grained sandstone, as shown in depths 103-122 m (fig. 7B). Interbedded mudstones and sandstones were described by Flores and others (1994), in a Tyonek interval in the nearby Chuitna River and Chuit Creek drainage area, as occurring either overlying or interfingering with conglomeratic sandstones.

Vertical and lateral lithologic variations of the interburden between the Red 1 and Red 2 coalbeds can be seen in figures 4B, 5, and 6. In contrast to the interburden between the Red 1 and Red 2 coalbeds shown in figure 4A, which includes vertically stacked conglomeratic sandstones, the interburden between the Red 1 and Red 2 coalbeds in figures 4B and 5A consists mainly of mudstones in the driller logs. This is interpreted as a condensed section of



FOR EXPLANATION SEE FIGURE 4

Figure 6. Lithologic log, sedimentary structures, and facies (type 4 facies profile) interpretation of a drillhole core (drillhole I) from above the Red 1 and Red 2 coalbeds to below Red 3 coalbed. See Figure 1B for location of drillhole.

**mudstone** parting as a result of merging of the Red 1 and Red 2 coalbeds. This **mudstone** parting, which ranges from 0.3 to 0.8 m thick, is laminated, rooted, and contains **interbedded carbonaceous shale** and **coaly lenses**. In figure 6, the interburden between the Red 1 and Red 2 coalbeds is missing in the core but consists of a parting of interbedded **mudstone** and an 0.8-m-thick **coalbed** in the driller log; this parting may be a split from Red 1 and (or) Red 2 coalbeds.

In cores, the interburden between the Red 1 and Red 2 coalbeds consists mainly of conglomeratic, coarse- to fine-grained sandstone. The conglomerate, which occurs along

erosional bases of beds, is clast supported and comprises rounded to subrounded pebble quartz, black chert, and ironstone fragments. The sandstone is trough crossbedded (troughs are 7.6-15.2 cm in height), and the uppermost crossbeds contain muddy cross-laminations (2.5-5.1 cm thick) and are vertically burrowed (depths of 97-98 m in fig. 4A). The sandstone is thin- to thick-bedded (0.6-6.4 m) and overlies the pebbly conglomerate. This basally erosional conglomerate-sandstone occurs as fining-upward and vertically stacked couplets. Two vertically stacked bodies consist of these conglomerate-sandstone couplets; the lower

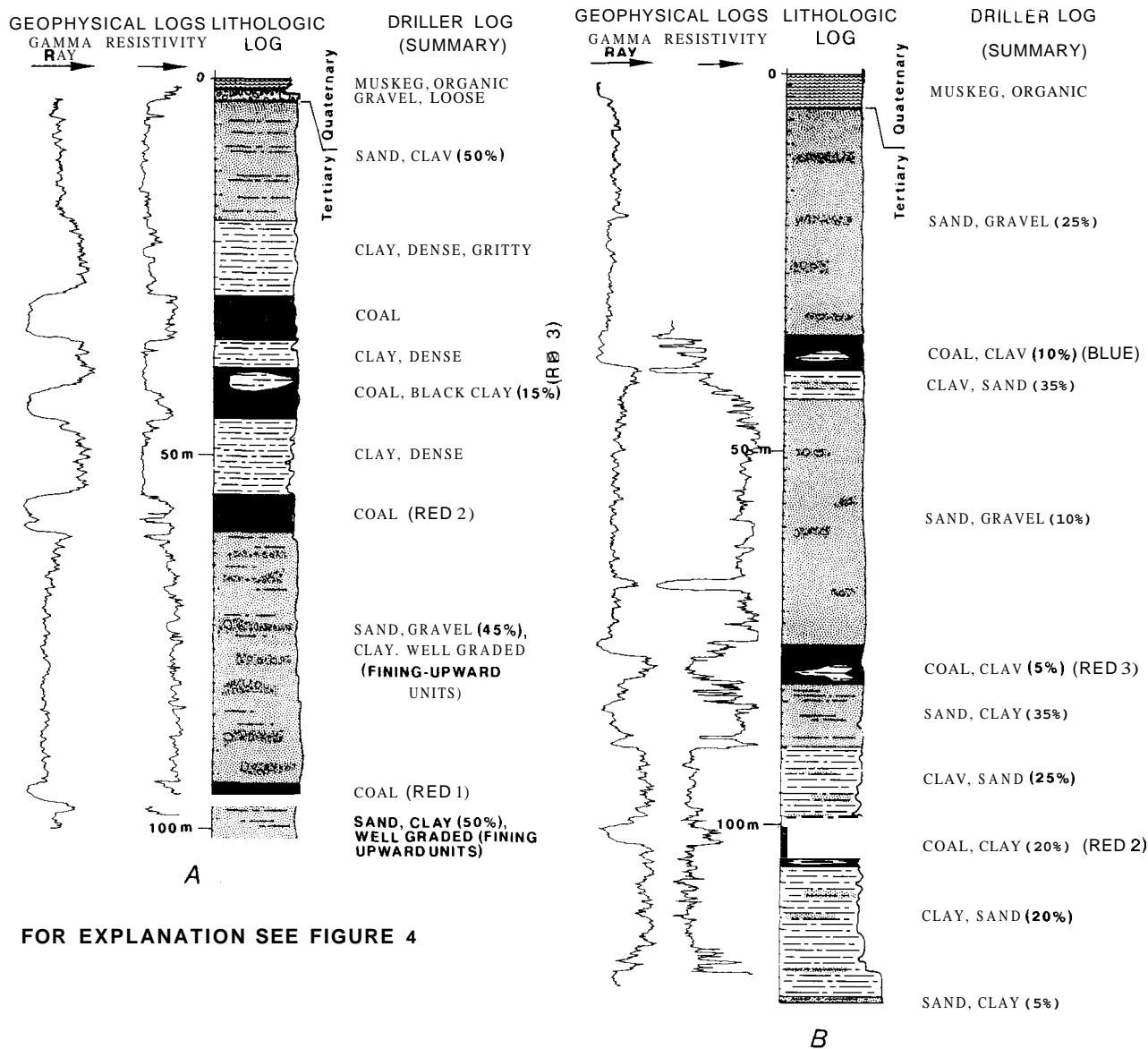


Figure 7. Drillhole showing geophysical, lithologic, and driller logs of rocks. See figure 1B for location of drillholes. Arrows represent increasing natural gamma radiation and resistivity to applied electrical currents. Metric units represent depths below the ground surface. A, Drillhole A, from below Red 1 coalbed to ground surface. B, Drillhole B, from below Red 2 coalbed to ground surface.



body is overlain by rooted, burrowed, and rippled mudstone, siltstone, and silty sandstone. Thinner conglomerate-sandstone couplets generally developed in the lower part of each body and thicker couplets formed in the upper part. The two bodies are separated by 1.5 m of coal and carbonaceous shale.

### RED 2 COALBED TO BASE OF RED 3 COALBED

The Red 2 coalbed is as much as 8.3 m thick. This coal is composed of 68-93 percent vitrinite, 3-19 percent liptinite, and 1-10 percent inertinite (mainly semifusinite; Rao and Smith, 1987). The interburden interval between the Red 2 and Red 3 coalbeds ranges from 3.6 to 46 m in thickness. The gamma-ray and resistivity log curves of the interburden rocks between the Red 2 and Red 3 coalbeds in three drillholes show different patterns for the same muddy interval (figs. 7A, 7B, 8A). This difference in patterns is caused by slight variations in the amounts of siltstone and sandstone interbeds with the mudstone. Drillhole cuttings of the interburden rocks indicate the presence of mudstone interbedded with siltstone and sandstone in this interval, and the geophysical logs (figs. 7A, 7B) confirm the presence of coarser grained interbeds. The interburden between Red 2 and Red 3 coalbeds in figure 8A (depths 95-108 m) shows a similar resistivity log pattern, confirming the presence of siltstone (10 percent) interbeds.

The mudstone interburden between the Red 2 and Red 3 coalbeds is locally overlain by a sandstone that contains as much as 35 percent mudstone (depths 80-89 m in fig. 7B). The gamma-ray and resistivity log curves of this interburden reflect the interbedded nature of sandstone and mudstone. The intercalation of subordinate mudstone, which subdivides the sandstone into three thick units, is similar to that of the sandstone above the Red 3 coalbed shown in figure 7A (depth 19 m). The sandstone above the Red 3 coalbed, which contains 50 percent mudstone (driller log in fig. 7A), has less pronounced gamma-ray and resistivity log curves than the sandstone in figure 7B. The contacts between these sandstone types and the underlying mudstones in both intervals (figs. 7A, 7B) are best defined by the gamma-ray log curve (depth 19 m in fig. 7A; depth 89 m in fig. 7B).

In cores, the interburden between the Red 2 and Red 3 coalbeds is mainly moderately to heavily bioturbated mudstone. The burrows are mainly short (1-3 mm long), narrow (1-2 mm wide) tubules filled with siltstone. Similar but larger horizontal burrows (as much as 1 cm in length) are also present. Thin (average 1 mm), flat lenses of siltstone, which are dissected by vertical burrows, are common in the mudstone. The uppermost part of the mudstone interburden is silty, sparsely burrowed, and exhibits abundant root marks.

### RED 3 COALBED TO BASE OF BLUE COALBED

The Red 3 coalbed is as much as 6.6 m thick and locally contains mudstone and carbonaceous shale partings. This coal consists of 65-89 percent vitrinite, 8-16 percent liptinite, and 1-15 percent inertinite (mainly semifusinite; Rao and Smith, 1987). The Red 3 coalbed is split into two benches by a mudstone parting that ranges from 0.9 to 4 m in thickness (figs. 7A, 7B, 8B). The lower coal bench, in turn, is split by mudstone and carbonaceous shale partings (fig. 7A). The interburden interval between the Red 3 and Blue coalbeds ranges from 0.9 to 58 m thick and contains gravelly sandstone, carbonaceous shale, and mudstone (depth 38-75 m, fig. 7B; depth 38-80 m, fig. 8B).

The gamma-ray log curve shows a "serrated" pattern representing a sandstone with gravel (fig. 7B). Cementation of gravel lenses may be indicated by pronounced "spiking" of the resistivity log curve (for example, depth 67 m in fig. 7B). The stratigraphy of the interburden between the Red 3 and Blue coalbeds is best displayed by the gamma-ray log curve (fig. 8A). The upper part of the gamma-ray log curve (depths 30-59 m) consists of "blocky with serrated" patterns representing sandstones. A break in this "blocky" pattern, both in the gamma-ray and the resistivity log curves, represents mudstone with siltstone interbeds (depths 47-51 m, fig. 8A). The basal contacts of these sandstones, as shown by the gamma-ray log curve (depths 47-59 m), indicate sharp boundaries with the underlying units. The lower part of the gamma-ray log curve (depths 59-90 m), like the resistivity log curve, exhibits thin to thick "peaks and valleys" representing a mudstone with sandstone interbeds (fig. 8A). The gamma-ray and resistivity log curves display a combination of "peaks and valleys" separated by pronounced "spikes" and "fine- to coarse-tooth comb" patterns typical of a mudstone (fig. 8B). Sandstone interbeds, some of which may be well cemented, produce the "spikes" (fig. 8B).

In core, the interburden between the Red 3 and Blue coalbeds is dominated by a mudstone. It contains burrows similar to those in the interburden between the Red 2 and Red 3 coalbeds. However, the upper part of this mudstone contains more rooted horizons than does the interburden between the Red 2 and 3 coalbeds. In addition, this mudstone contains sparse thin, flat siltstone lenses.

### BLUE COALBED TO THE SURFACE

The Blue coalbed is as much as 7.5 m thick and is split into two benches by a 4-m-thick parting consisting of mudstone and carbonaceous shale. This coalbed is composed of 71-87 percent vitrinite, 8-20 percent liptinite, and 0.5-3 percent inertinite (mainly semifusinite; Rao and Smith, 1987). The overburden interval between the Blue coalbed and the surface is best displayed in figures 7B and 8A. In

these figures, this interval, which is as much as 34 m thick, contains Quaternary organic, sand, gravel, silt, and clay surficial deposits (Barnes, 1966). However, figure 8B shows a different type of Quaternary deposit, consisting of gravel, sand, and clay, which directly overlies the Blue coalbed (depth 24 m). In this locality (fig. 8B), the uppermost part of the Blue coalbed may have been eroded by glaciation.

The gamma-ray log curves shown in figures 7B and 8A reflect a mainly sandstone overburden. However, the gamma-ray log curves vary with the gravel (25 percent in fig. 7B), siltstone (25 percent in fig. 8A), and mudstone contents of the sandstones (see driller logs). The gamma-ray log patterns of the sandstone overburden indicate both

the presence of gravel lenses and the cementation of these coarse materials (fig. 7B). Gamma-ray patterns shown in figure 8A are probably caused by the siltstone and mudstone interbeds of the generally sandstone overburden. The sharp basal contact of these sandstones reflected by the gamma-ray log curve is best displayed in figure 8A (depth of 25 m) where the silty and muddy sandstone directly overlies the Blue coalbed.

In core, the Blue coalbed is locally interbedded with 1.5-m-thick, rooted mudstone parting, and the overburden above the coalbed is 45 m thick and includes interbedded mudstone, siltstone, and sandstone (fig. 4A). The mudstone is moderately to heavily bioturbated (silt-filled vertical and

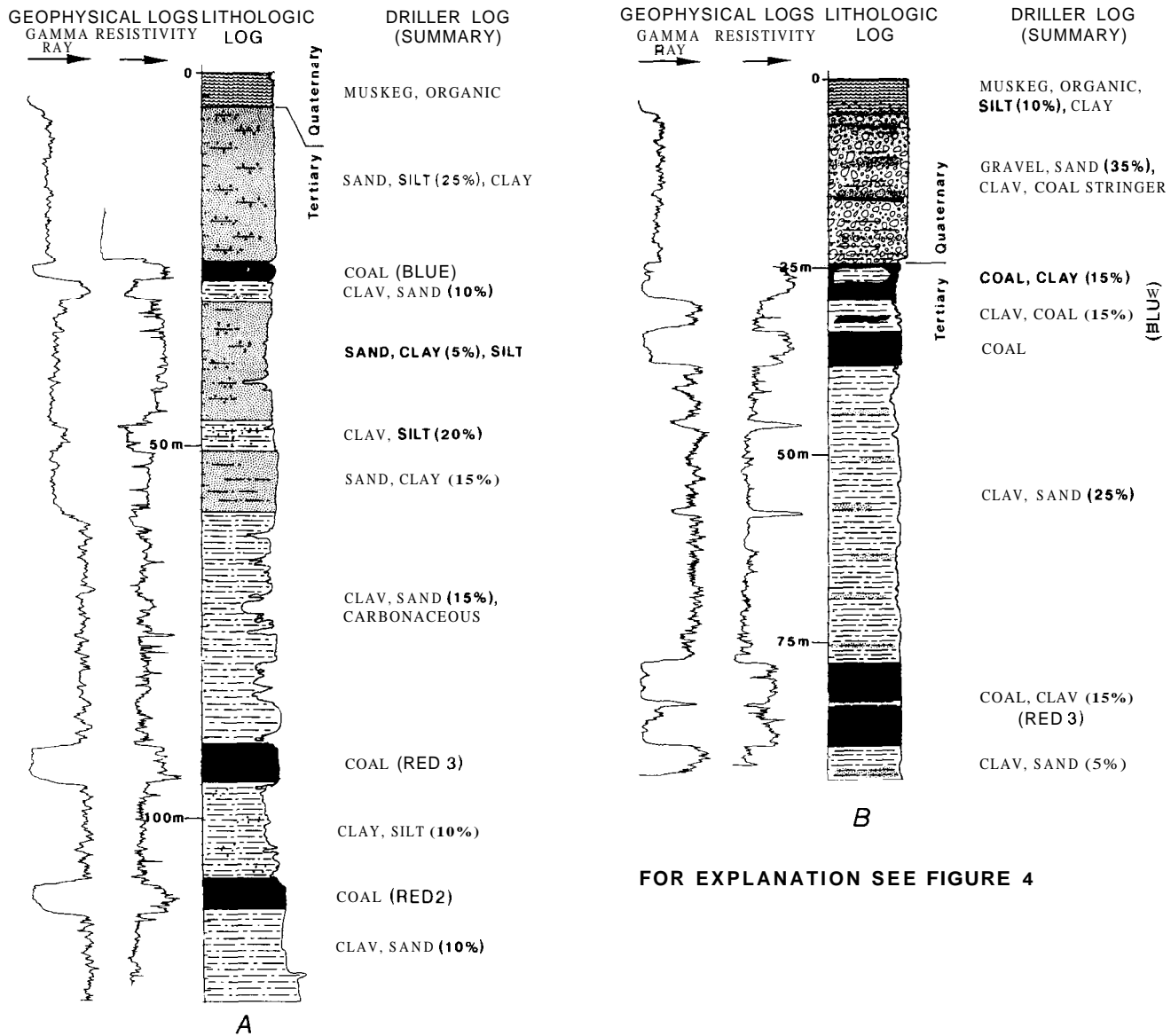


Figure 8. Drillholes showing geophysical, lithologic, and driller logs of rocks. See figure 1B for location of drillholes. Arrows represent increasing natural gamma radiation and resistivity to applied electrical currents. Metric units represent depths below the ground surface. A, Drillhole C, from below Red 2 coalbed to ground surface. B, Drillhole D, from below Red 3 coalbed to ground surface.

horizontal tubular burrows) and contains thin, burrowed, flat lenses of siltstone. In addition, burrows occur in 2.5-7.6-cm-thick layers, particularly in the lowermost part of the overburden (fig. 4A, at depths of 40-41 m). Here the siltstone is moderately burrowed and contains ripple laminations; elsewhere, laminae have been destroyed by vertical and horizontal tubular burrows. The sandstone varies from very fine to medium grained and contains some pebble (quartz and chert fragments) conglomerate. It displays sharp to erosional basal contacts; the latter type of contact is lined with pebble conglomerate. The medium-grained, pebbly sandstone is trough crossbedded (troughs are 7.6-10.1 cm in height) and contains vertical tubular burrows (2 cm long and 0.2 cm wide). This pebbly sandstone is overlain by fine-grained sandstone that occurs in alternating **foresets** (<15 cm in height) draped by thin (a few millimeters to 3 cm) layers or beds of rippled siltstone and mudstone. The fine-grained sandstone exhibits a sharp base, ripple laminations, and cross-laminations (5.1-7.6 cm in height). It contains sparse to abundant vertical burrows. Also, it contains abundant burrowed **mudstone** and siltstone lenses forming flaser and lenticular bedding. The fine-grained sandstone (fig. 4A) formed either as the upper part of a generally coarsening-upward burrowed **mudstone** and **burrowed-rippled** siltstone succession or as a single, fining-upward body.

## FACIES PROFILES

The interburden between the Red 2 and Red 3 coalbeds has four types of facies profile (figs. 4B-6). The type 1 facies profile consists of a succession of **coarsening-upward** siltstone and silty to very fine grained sandstone interbedded with **mudstone** in the lower part (depth 64-88 m, fig. 4B). This succession is capped by a 30-cm-thick unit of coal and carbonaceous shale interbeds (depth 36 m, fig. 4B) and contains a 3.0-cm-thick coal in the lowermost part (depth 67 m, fig. 4B). The **mudstone** is moderately to heavily bioturbated, mainly by vertical tubular burrows (1-2 mm long and 1 mm wide) but also by subordinate horizontal tubular burrows (2-4 mm long and 1 mm wide), and it is also rooted (roots represented by vertical coaly stringers), particularly where **mudstone** underlies coalbeds. The **mudstone** locally contains thin (1-2 mm), burrowed siltstone lenses. The siltstone is moderately burrowed and sparsely rippled; ripple laminations are masked locally by heavy bioturbation. The siltstone commonly underlies the **coarsening-upward** units. The sandstone is mainly **ripple-laminated**, intercalated with 2.5-5.1-cm-thick units containing tubular vertical and horizontal burrows (1-3 mm long and 1 mm wide). In addition, the sandstone exhibits alternating sandy rippled laminations and silty burrowed laminations.

The upper part of the type 1 facies profile (depth 35-63 m, fig. 4B) is a succession of fining-upward, silty to

very fine grained sandstone and siltstone interbedded with mudstone. The **mudstone** and siltstone are similar to those in the lower part of the facies; however, here in the upper part of the facies, the **mudstone** and siltstone are alternating laminae associated with sandstones and form a 5-m-thick succession of large-scale rhythmic interlaminations or rhythmites. The sandstone consists of cross-laminations (5.1-7.6 cm in height), ripple laminations, and flaser laminations (as much as 15 cm thick; fig. 9A). The upper part of this sandstone contains small-scale **rhythmites** (2-3 cm thick), which consist of cross-laminated silty sandstone separated by very thin rippled and burrowed siltstone and subordinate burrowed **mudstone** drapes (fig. 9B). Some burrows (fig. 9C) in the silty sandstone are >5.1 cm long and 0.1 cm wide, bifurcate in the lowermost part, and exhibit walls that are partly lined with mud and have a crenulated (corn-cob) texture that resembles the Ophiomorpha-like burrows described by Kamola (1984).

The type 2 facies profile, exemplified in figure 5A, is dominated by siltstone and includes subordinate **mudstone** and sandstone. The siltstone is commonly interbedded with **mudstone** (fig. 10A) that is both vertically and horizontally burrowed (2-mm-long and 1-mm-wide tubules) and rooted (tubules as much as 10 cm long). This siltstone also contains a few zones with Ophiomorpha-like vertical burrows marked by corn-cob walls (5.1 cm long). Sedimentary structures of the siltstone, where not destroyed by burrows, are mainly ripple lamination and subordinate lenticular bedding. The sandstone is sharp based and cross-laminated (laminae as much as 12.7 cm in height) and is separated by zones containing Ophiomorpha-like burrows. Sandstone is common in the lower part of the interburden.

The type 3 facies profile shown in figure 5B is generally fining upward and is dominated by silty to fine-grained sandstone in the lower two-thirds of the interburden and subordinate **mudstone** and siltstone in the upper one-third of the interburden. The sandstone is moderately to heavily bioturbated by tubular vertical burrows (>3 mm long and 1-2 mm wide; see fig. 11) and horizontal burrows (>5 mm long and 1 mm wide). Ripple laminations range from 2.5 to 5.1 cm in height and occur as discrete zones and (or) interspersed with the burrows. Cross-laminations (fig. 11) are as much as 5.1 cm in height. The lowermost part of the sandstone (depth 75-78 m, fig. 5B) is interbedded with carbonaceous **mudstone** that is rooted. The **mudstone** is moderately burrowed (2-mm-long and 1-mm-wide tubules; fig. 11) and rooted; roots are concentrated in the uppermost part of the mudstone. The siltstone is ripple laminated, lenticular bedded, and burrowed (3-mm-long and 1-mm-wide tubules; fig. 11).

The type 4 facies profile exhibited in figure 6 is a succession of fining-upward, very fine to silty sandstone interbedded with **mudstone** and siltstone. The sandstone beds have sharp to erosional bases that are marked by coal spars. Sandstone occurs either as a single fining-upward

body or as multiple-stacked bodies. Two single fining-upward sandstone bodies (depths 47-49 m and 54-56 m, fig. 6) are trough crossbedded (troughs 5.1-7.6 cm in height) in the lower part and ripple laminated in the upper part; a few nondescript burrows are found in these sandstone bodies. Single fining-upward sandstone bodies are directly overlain by bioturbated and rippled couplets of mudstone and siltstone (rhythmites) and are interbedded with bioturbated mudstone drapes (fig. 10B). Four multiple-stacked sandstone bodies (depths 31-34 m, 36-39 m, 42-44 m, and 50.5-52 m; fig. 6) are trough crossbedded (troughs 5.1-10.1 cm in height) and capped by rooted, carbonaceous mudstone, coal, and rippled siltstone.

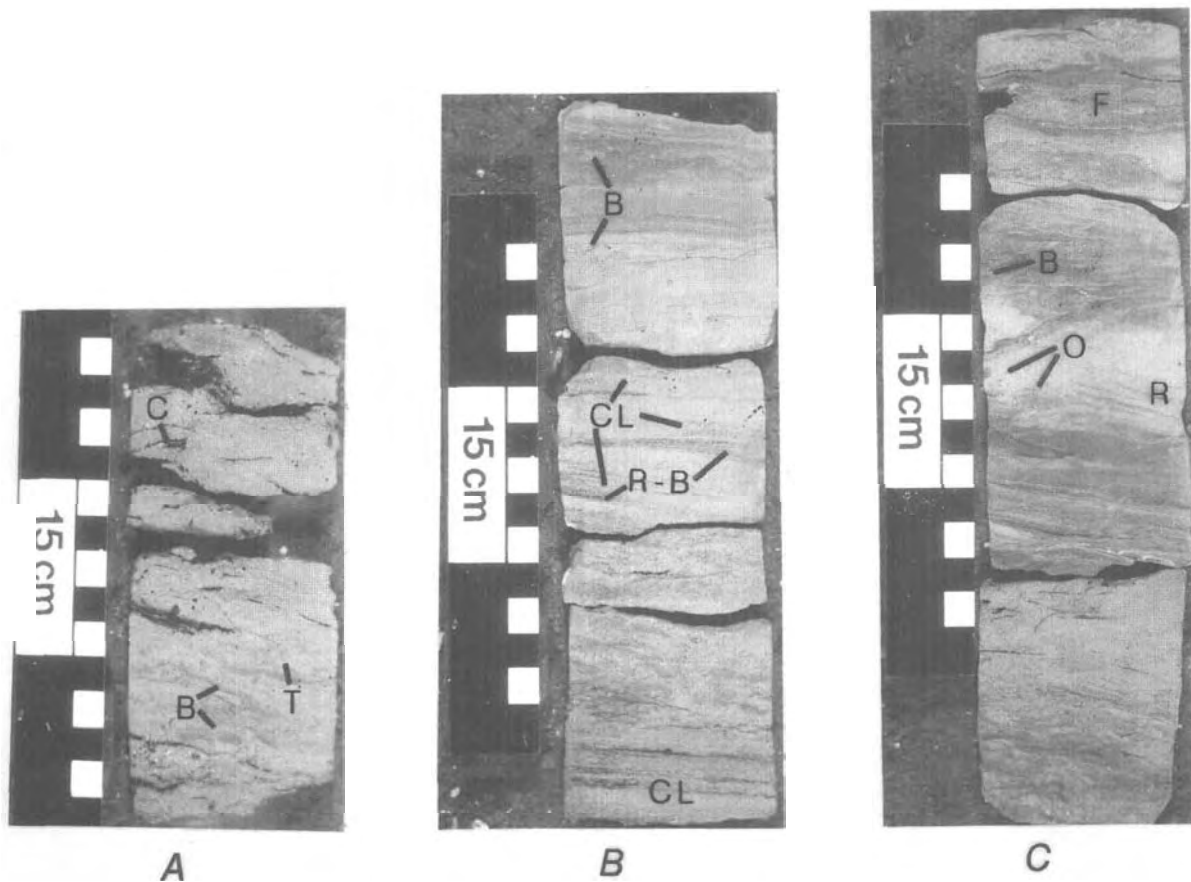
### SEDIMENTOLOGICAL FACIES INTERPRETATION OF THE CORES

The core descriptions were used to interpret sedimentary processes and environments of deposition of the interburden and overburden rocks. Thus, the sedimentol-

ogy of the interburden and overburden rocks between the Red 1 and Blue coalbeds provides a general interpretation of the depositional setting within the study interval. Descriptions of the interburden rocks between the Red 1 and Red 3 coalbeds yield specific interpretations of the processes and environments of deposition.

### RED 1 TO BLUE COALBEDS INTERBURDEN AND OVERBURDEN

The succession of fining-upward sandstone, which is underlain by conglomerate-lined erosional surfaces, between the Red 1 and Red 2 coalbeds (fig. 4A) was probably deposited by repeated scouring and filling of low-sinuosity channels similar to those studied by Lawrence and Williams (1987). The trough crossbeds in this channel sandstone probably represent rapid cut and fill by dune bedforms (Smith, 1970; Ethridge, 1980; Tunbridge, 1981, 1984). The erosionally based pebble conglomerate underlying the sandstone represents a channel-bottom lag deposit. Multiple



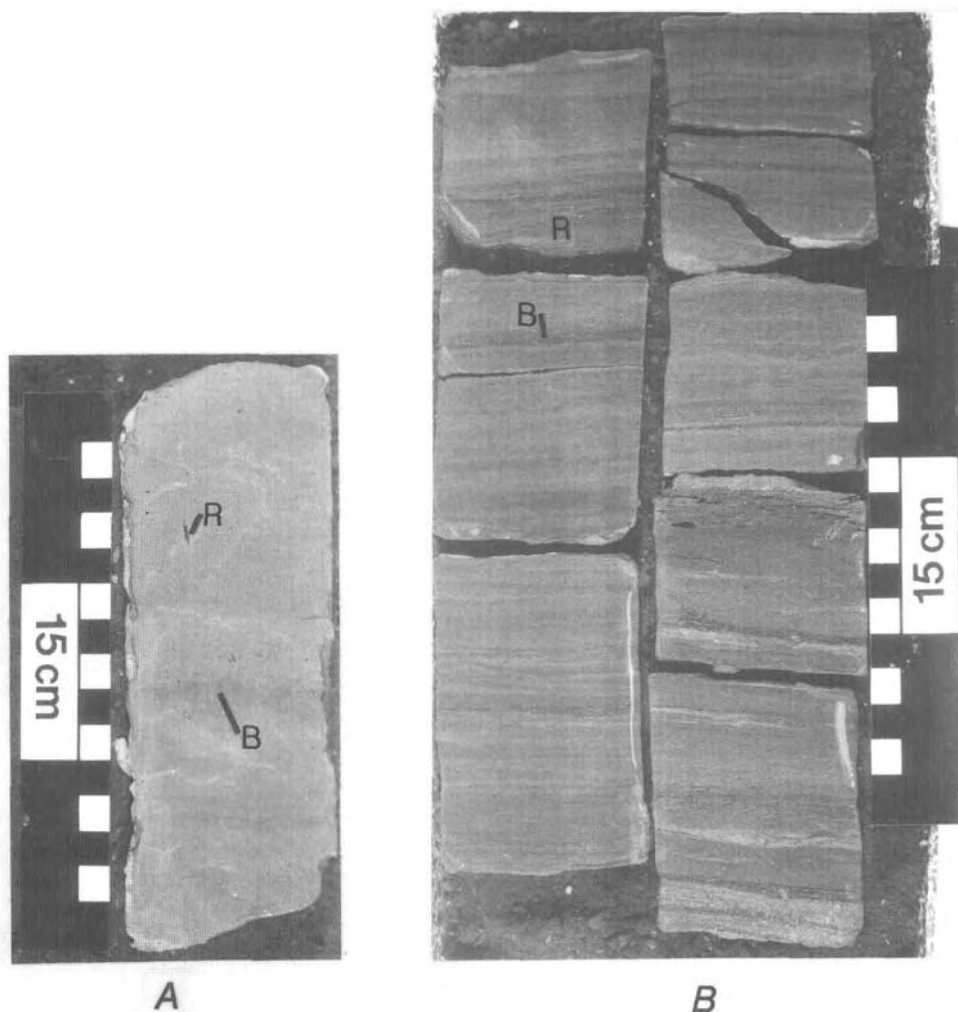
**Figure 9.** Photos of core (A, bottom; B, middle; C, top) of the tidal-channel interval shown in figure 4B. A, Trough crossbedded (T), burrowed (B) sandstone with coal spar lag deposits (C) at depth 54.6 m. B, Alternating cross-laminated (CL) silty sandstone and rippled and burrowed (R-B) siltstone and mudstone (rhythmites) at depth 54 m. C, Rippled (R), burrowed (B), flaser (F) bedded silty sandstone, siltstone, and mudstone (double drapes) at depth 53 m. Upside-down Y-shaped Ophiomorpha-like burrow (O) penetrates rippled silty sandstone.

stacking of conglomeratic lag-sandstone couplets (fig. 4A) within a vertical sequence suggests deposition in small- and large-scale low-sinuosity channels of braided streams. The thin conglomerate-sandstone couplets (fig. 4A) in the lower parts of the two sequences indicate deposition in small-scale narrow, shallow channels. The thick conglomerate-sandstone couplets (fig. 4A) in the upper parts of the sequences suggest deposition in large-scale wide, deep channels. This sequential order probably reflects braidbelt evolution from inactive (small-scale channels) to active (large-scale channels) (Smith, 1970; Rust, 1979). These braided stream deposits probably formed in a fluvial environment, even though one of the sandstone sequences is capped by bioturbated fine-grained sediments; bioturbation suggests a subaqueous setting in an abandoned channel.

The moderately to heavily bioturbated mudstone, siltstone, and sandstone (fig. 4B) were probably deposited in tidal and intertidal flat environments (Ginsburg, 1975; Reineck and Singh, 1980; de Boer and others, 1988; Smith and others, 1991). The presence of burrowed lenticular and flaser beds in the fining-upward siltstone and sandstone

and of burrowed, flat silty lenses in the mudstone indicate an intertidal-subtidal environment (Reineck and Wunderlich, 1968; Evans, 1975; Larsonneur, 1975). In addition, alternating cross-laminations draped by rippled siltstone and burrowed mudstone or mud drapes (fig. 9B) resemble "bundles" in tidal environments (Visser, 1980; Nio and Yang, 1991). Facies association of these "tidal bundles" in the upper part of a erosionally based, trough crossbedded, fining-upward conglomeratic sandstone suggests deposition in a tidal channel (Berg, 1982; Reinson, 1989; Nio and Yang, 1991). The tidal channel was probably rapidly infilled by tidal flood-ebb flow cycles. Small and large rhythmic interlamination or rhythmites of sandstones, siltstones, and mudstones represent deposition during tidal cycles (Nio and Yang, 1991)

The Red 1, Red 2, Red 3, and Blue coalbeds were probably deposited in mires in a fluvio-tidal coastal environment. Facies association of the Red 1 and Red 2 coalbeds with braided-stream conglomeratic sandstone suggests accumulation in raised mires developed on abandoned braidbelt ridges (Flores and others, 1994). The low ash



**Figure 10.** A, Photo of a core of the intertidal flat interval in figure 5A. Burrowed (B) and rooted (R) mudstone at depth 31 m. B, Photo of core of tidal-channel interval in figure 8. Alternating or rhythmic silty sandstone and mudstone containing burrowed mud drapes (B) of flaser bedding, ripple laminations (R), and lenticular bedding. The core on the right is at depth 47-46.6 m, and the core on the left is at depth 46.4-46.3 m.

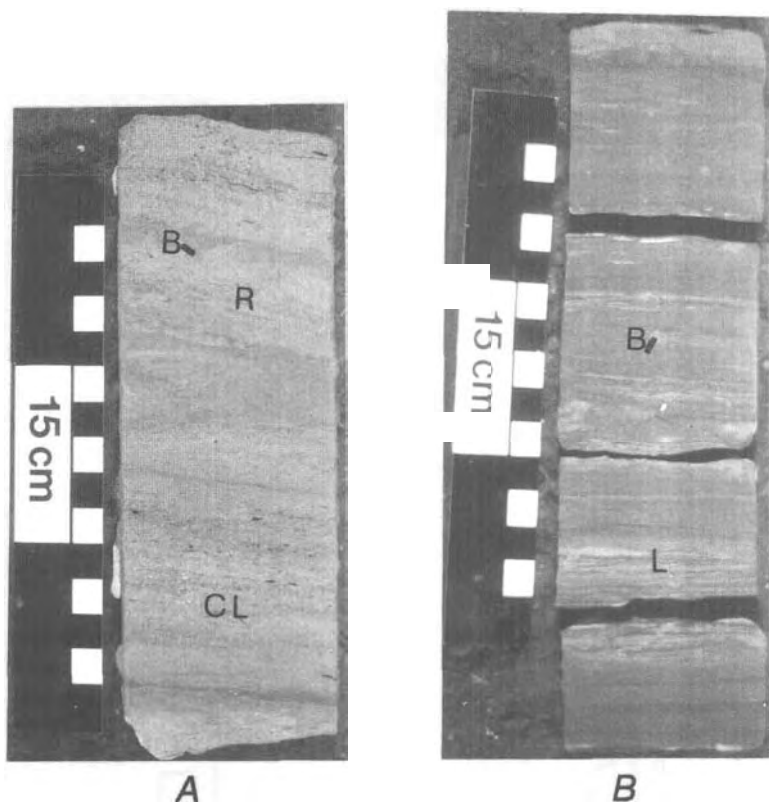
content (3.6-6 percent; Rao and Smith, 1987) of the Red 2 coalbed above the fluvial channel sandstone indicates that the peat-forming mires were relatively protected from detrital influx. In contrast, the Red 3 and Blue coalbeds, which are interbedded with tidal deposits and probably formed in a topographically low (topogenous) mire, contain higher ash contents (4.2-21.7 percent; Rao and Smith, 1987), indicating effects of sediment floods. Although the sulfur content of the combined Red 1, Red 2, Red 3, and Blue coalbeds is generally low (0.08-0.19 percent; Rao and Smith, 1987), the Red 2 coalbed contains less sulfur (0.08-0.13 percent) than do the Red 3 and Blue coalbeds (0.12-0.19 percent). These higher sulfur contents in the Red 3 and Blue coalbeds may be explained by accumulation in tidally influenced mires. That is, high sulfur content was produced by sulfate reduction of brackish-marine waters that were introduced over the peat mires (Gluskoter and Simon, 1968).

The vertical variations of the maceral composition of the Red 1, Red 2, Red 3, and Blue coalbeds probably reflect differences in depositional environments of the mires (Rao and Smith, 1987). Rao and Smith (1987) reported cyclic variations of the maceral composition (for example, vitrinite) from bottom to top of the Red 1 and Red 2 coalbeds. This cyclic variation of vitrinite in the Red 1 and Red 2 coalbeds suggests episodic woody vegetal growth in the mire. Rao and Smith (1987) also reported high liptinite for the Red 1 and 2 coalbeds, which suggests decomposition of vegetal matter yielding concentration of resistant exinite. Decomposition probably involved episodic oxida-

tion of the woody vegetal matter in the raised mires on the abandoned fluvial braidbelts and yielded liptinites as accumulation reached above the ground-water table. The organic matter accumulated episodically as the peat mire underwent autocompaction. In contrast, Rao and Smith (1987) reported a general upward increase in vitrinite and liptinite composition in the Red 3 coalbed and a general upward decrease of vitrinite and liptinite composition of the Blue coalbed. These findings suggest a gradual occupation by, and then demise of, woody vegetation in the topogenous mires. That is, upward increase of vitrinite in the Red 3 coalbed indicates subaqueous to subaerial evolution of the tidally influenced peat mire permitting woody vegetation to take root through time. The upward decrease of vitrinite in the Blue coalbed, in contrast to patterns seen in the underlying Red 1, Red 2, and Red 3 coalbeds, indicates short-lived occupation of woody vegetation in the peat mire prior to tidal inundation.

### RED 1 TO RED 3 COALBED INTERBURDEN

The facies of the interburden between the Red 1 and Red 2 coalbeds (depths of 77-106 m, fig. 4A), which consists of sandstone and an intervening condensed section of rooted mudstone, is interpreted as a channel and floodplain deposit that is laterally equivalent to the fluvial channel (braidbelt) sandstones between 60 and 93 m on figure 7A. Splitting of the Red 1 and (or) Red 2 coalbeds reflects



**Figure 11.** Photo of cores of the tidal sand flat and intertidal flat intervals in figure 5B. **A**, Cross-laminated (CL), rippled (R), and burrowed (B) sandstone at depth 60 m. **B**, Lenticular bedded (L) and burrowed (B) siltstone at depth 47 m.

interruptions of the mires by **overbank** detrital sedimentation. Variations in the tidal depositional environment are best displayed by the facies between the Red 2 and Red 3 **coalbeds** (facies types 1-4 described previously).

The type 1 facies profile (fig. 4B) represents local variations within the intertidal deposits. The succession of **coarsening-upward**, burrowed and rippled siltstone and sandstone interbedded with burrowed **mudstone** containing silty lenticular beds is interpreted as intertidal-tidal sand flat deposition (Knight and Dalrymple, 1975; Thompson, 1975). The sandstone containing alternating sandy rippled laminations and burrowed silty laminations represents a tidal sand flat deposit. This tidal sand flat probably formed above the high-water level reworked by tidal currents (Thompson, 1975). The burrowed, lenticular-bedded **mudstone** and burrowed, rippled siltstone represent intertidal deposits. The presence of rooted horizons and thin **coalbeds** indicates that these deposits were transformed into supratidal mires. The fining-upward, erosionally based sandstone capped by alternating rippled and burrowed silty sandstone, siltstone, and **mudstone** in the upper part of the type 1 facies profile suggests that the intertidal environment was drained by tidal channels. Ophiomorpha-like burrows in these sediments strengthen the argument for a marine influence. The flaser and rhythmic beds associated with the tidal-channel sandstone indicate small- to large-scale tidal-flood and ebb flows (Nio and Yang, 1991).

The type 2 facies profile, which is dominated by burrowed, lenticular beds of sandy siltstone and subordinate burrowed mudstone, represents a tidal sand-silt flat (fig. 5A). The presence of a few bioturbated zones with Ophiomorpha-like burrows suggests that this tidal sand-silt flat was partly formed in high-current areas (Harrison, 1975). The presence of sharp-based, cross-laminated sandstone with Ophiomorpha-like burrows indicates that the tidal flat was aggraded by sand ridges that developed above high-water level. The occurrence of rooted horizons in the tidal sand-silt flat supports the idea of high-water level sedimentation and suggests sparse vegetal growth in local marshes that developed in this high-water area.

The type 3 facies profile, which is dominated by a thick, burrowed and rippled, silty to fine-grained sandstone, is interpreted as a tidal sand flat (fig. 5B). However, unlike the tidal sand flats described for the types 1 and 2 facies profiles, this tidal-sand-flat deposit contains moderately to heavily bioturbated zones interbedded with a discrete zone containing ripple laminations. The presence of alternating bioturbated, cross-laminated, and rippled zones indicates deposition in low- and high-water areas in a broad tidal sand flat. The overlying burrowed **mudstone** interbedded with burrowed-rippled siltstone indicates that this tidal sand flat was aggraded by a tidal mud flat. This mud flat was later transformed into a marsh, as suggested by the occurrence of rooted horizons in the upper part of the type 3 facies profile.

The type 4 facies profile, which consists of a succession of sharp- to erosional-based, fining-upward, very fine to silty sandstone interbedded with burrowed and rippled **mudstone** and siltstone, rooted carbonaceous mudstone, and coal, is interpreted as a tidal channel-intertidal-supratidal complex (fig. 6). The tidal channel consists of single- to multiple-stacked, trough-crossbedded, locally burrowed sandstone. The presence of overlying rhythmite of burrowed **mudstone** and rippled siltstone and silty sandstone suggests that this sandstone was deposited in a tidal setting (Smith, 1987). The succession of burrowed **mudstone** and rippled siltstone that overlies the sandstone indicates that these tidal-channel deposits culminated in intertidal flats. The channel deposits are best depicted in the lower part of the type 4 facies profile between 45 and 49 m in figure 6. The upper part of the type 4 facies profile contains similar tidal-channel sandstone that is successively overlain by rooted **mudstone** and coal. This pattern indicates development of ephemeral to long-lived supratidal marshes over abandoned tidal-channel deposits.

The interburden between the Red 2 and Red 3 **coalbeds** contains prevalent tidal-channel, tidal-flat, intertidal, and supratidal facies types. Facies association of these tidal deposits, particularly with the overlying Red 3 **coalbed**, suggests accumulation in tidally influenced mires (Flores and Johnson, 1995). Rao and Smith (1987) reported that the Red 3 **coalbed** comprises, from bottom to top, 21.73 to 7.11 percent ash and 0.15 to 0.19 percent sulfur (as-received basis). The decreasing ash content toward the top of the **coalbed** is consistent with progressive sheltering of the mires from detrital influx, and with peat accumulation initially in topogenous mires but above water drainage or in raised mires through maturity. Raised mires were recognized to form in coastal-plain settings by Cameron and others (1989). The upward-increasing sulfur content of the **coalbed** may suggest a tidal influence (Flores and Sykes, 1996).

## COAL-QUALITY ANALYSIS

Our coal-quality data (table 1) from the Red 1, Red 2, Red 3, and Blue **coalbeds** yielded a total of 165 samples from 20 drillholes. Sample density ranged from 21 samples for the Red 3 **coalbed** to 53 samples for the Blue **coalbed**; this number of samples allows a meaningful statistical analysis. The coal-quality data consist of heat values in British thermal units per pound (**Btu/lb**), and ash yield and sulfur content are in percent (all values are on an as-received basis). The coal-quality study by Rao and Smith (1987) in the **DCP** area represents a detailed characterization of the Red 1, Red 2, Red 3, and Blue **coalbeds** in a single drillhole. Although their study provides an adequate knowledge of vertical qualitative differences between these coalbeds, statistically significant differences cannot be determined from

Table 1. Arithmetic means and standard deviations of ash, sulfur, and heat-value contents of the Red 1, Red 2, Red 3, and Blue coalbeds

variable <sup>1</sup>	Number of samples	Range		Arithmetic mean	Standard deviation
		Minimum	Maximum		
<b>BLUE COALBED</b>					
Ash yield	53	4.18	34.36	11.88	7.65
Total sulfur	53	.07	.26	.14	.04
Heat value	53	4,190	8,130	7,000	930
<b>RED 3 COALBED</b>					
Ash yield	21	5.34	47.70	11.15	9.17
Total sulfur	21	.09	.25	.14	.05
Heat value	21	2,950	7,970	7,040	1,080
<b>RED 2 COALBED</b>					
Ash yield	49	4.11	49.97	11.49	10.88
Total sulfur	49	.04	.24	.12	.04
Heat value	49	2,960	8,500	7,070	1,230
<b>RED 1 COALBED</b>					
Ash yield	42	5.30	41.11	12.26	9.04
Total sulfur	42	.07	.30	.12	.05
Heat value	42	3,950	8,070	7,050	980

<sup>1</sup> Ash and total sulfur are in percent; heat value is in British thermal units per pound. All values are on an as-received basis.

their data because of the limited number of samples available for each coalbed. To aid comparison with our results, we summarize below the data of Rao and Smith (1987); all values are on an as-received basis.

According to Rao and Smith (1987), the Red 1 coalbed has heat values that range from 6,050 to 7,470 Btu/lb and contains 9.0-23.5 percent ash (highest values toward the top and bottom of the bed) and 0.13-0.16 percent sulfur. The Red 2 coalbed ranges in heat value from 7,790 to 8,320 Btu/lb and contains 3.6-6.0 percent ash and 0.08-0.13 percent sulfur. The Red 3 coalbed ranges in heat value from 6,260 to 7,810 Btu/lb and contains 6.8-21.7 percent ash and 0.13-0.19 percent sulfur. The Blue coalbed ranges in heat value from 7,740 to 8,020 Btu/lb and contains 4.2-5.6 percent ash and 0.12-0.14 percent sulfur.

The arithmetic means of the heat values of the Red 1, Red 2, Red 3, and Blue coalbeds calculated from our data range from 7,000 to 7,070 Btu/lb. The arithmetic means of the ash yields and sulfur contents of these coalbeds range from 11.15 to 12.26 percent, and from 0.12 to 0.14 percent, respectively. Visual observations of these values indicate that there appears to be no difference between the heat values of the coalbeds.

Statistical analyses using Student's T-test (at the 95-percent confidence limit) were performed on the heat values, ash yields, and sulfur contents of the Red 1, Red 2, Red 3, and Blue coalbeds. Tests between all coalbeds show similarity in heat value and ash yields, suggesting similar heat values regardless of the depths of occurrence of the coalbeds and similar ash yields regardless of the depositional setting of the peat-accumulating mires. In addition, the tests between the Red 1 and Red 2 coalbeds, as well as between the Red 3 and Blue coalbeds, show similarities in sulfur content. Tests between the Red 1 and Blue, Red 1 and Red 3, Red 2 and Red 3, and Red 2 and Blue coalbeds, however, show differences in sulfur contents. The Student's T-test suggests that the sulfur content of the Red 3 and Blue coalbeds is statistically higher than that of the Red 1 and Red 2 coalbeds. This difference is attributed to the tidal influence on the mires forming the Red 3 and Blue coalbeds. A direct relationship between coal roof rocks deposited in a marine environment and high-sulfur content of underlying coalbeds has been reported by Gluskoter and Simon (1968); high-sulfur coals were attributed to sulfate reduction of brackish-marine waters that inundated the peat mires after deposition. Thus, the statistical analysis sup-



ports the sedimentological interpretation of tidal deposits from below the Red 3 to above the Blue **coalbeds** in contrast to **fluvial** deposits between the Red 1 and Red 2 **coalbeds** (fig. 4A).

## SUMMARY AND CONCLUSIONS

The Tyonek coal-bearing interval in the DCP area contains at least four **coalbeds** (Red 1, Red 2, Red 3, and Blue) between 30 and 135 m below the surface. These **coalbeds**, which have a total cumulative thickness in excess of 21 m, are amenable to strip mining and are generally **subbituminous** in rank with moderately low ash yields (range from 4.11 to 49.97 percent, mean of 11.74) and low-sulfur contents (range from 0.04 to 0.30 percent, mean of 0.12 percent). Affolter and Stricker (1993) report that Alaskan coals of similar age and apparent rank have ash yields ranging from 1.16 to 40.30 percent (mean of 10.71 percent) and sulfur contents ranging from 0.01 to 1.65 percent (mean of 0.29 percent). Our stratigraphic and sedimentologic investigations of these minable **coalbeds** indicate that their sulfur contents may be influenced by the depositional environments of the mires and related interburden and overburden rocks and by the coalification process. The higher sulfur contents of the Red 3 and Blue **coalbeds** relative to the Red 1 and Red 2 **coalbeds** may reflect accumulation in mires influenced by tidal processes. The statistical similarity (Student's T-test at the 95-percent confidence level) in the ash yields of these **coalbeds** suggests that the mires were equally exposed to sediment floods regardless of their tidal and (or) **fluvial** origin. We interpret that the Red 3 and Blue **coalbeds** accumulated in topogenous mires probably formed in a tidally influenced coastal plain. The Red 1 and Red 2 **coalbeds** accumulated on raised mires formed on abandoned channel deposits along alluvial-ridge belts in a fluvially influenced coastal plain. The difference in the environments of deposition of these peat mires controlled maceral composition of the **coalbeds**. That is, the raised peat mires were episodically oxidized above the groundwater table as organic matter accumulation from woody vegetation overcame autocompaction. In comparison, the organic accumulation from woody vegetation in the topogenous peat mires evolved through the ebb and flood of the tidal cycle.

Finally, the presence of tidal deposits in the drillhole cores of our study interval in the DCP area indicates that tidal influence in the Tyonek Formation is more pervasive than was originally suggested by Flores and others (1994) in their study of the Tyonek of the nearby Chuitna **River-Chuit** Creek area. The Tyonek Formation in the upper Cook Inlet basin has generally been interpreted as **nonmarine** braided **fluvial** deposits (McGee, 1972; Adkison and others, 1975; Hite, 1976; Dickinson and Campbell, 1978; Dickinson and others, 1995). The Tyonek tidal deposits in

the DCP area include (1) intertidal-flat sediments with burrowed flaser (containing double-draped mudstones) and lenticular bedding, tidal bundles, and Ophiomorpha-like burrows; (2) tidal-channel sediments that are burrowed, basally erosional, and fining upward, overlain by alternating burrowed **mudstone** and siltstone beds, and by **cross-laminated** and rippled sandstone beds (large-scale rhythmites); (3) tidal-sand-flat sediments that are moderately to heavily bioturbated and sparsely cross-laminated and rippled; and (4) supratidal sediments consisting of rooted, burrowed, and carbonaceous fine-grained detritus.

## REFERENCES CITED

- Adkison, W.L., Kelley, J.S., and Newman, K.R., 1975, Lithology and palynology of Tertiary rocks exposed near Capps Glacier and along Chuitna River, Tyonek quadrangle, southern Alaska: U.S. Geological Survey Open-File Report 75-21, 58 p.
- Affolter, R.H., and Stricker, G.D., 1994, Chemical characterization of Alaska's coal—a state wide summary, in Rao, P.D., and Walsh, D.E., eds., Focus on Alaska's coal '93: Fairbanks, Alaska, Mineral Industry Research Laboratory Report, v. 94, p. 190-227.
- Barnes, F.F., 1966, Coal resources of the Beluga-Yentna region, Alaska: U.S. Geological Survey Bulletin 1202-C, 54 p.
- Barnes, F.F., and Payne, T.G., 1956, The Wishbone Hill district, Matanuska coal field, Alaska: U.S. Geological Survey Bulletin 1016, 88 p.
- Berg, J.H. van den, 1982, Migration of large-scale **bedforms** and preservation of cross-bedded sets in highly accretional parts of tidal channels in the Ooterschelde, SW Netherlands: *Geologie en Mijnbouw*, v. 61, p. 253-263.
- Calderwood, K.W., and Fackler, W.C., 1972, Proposed stratigraphic nomenclature for Kenai Group, Cook Inlet basin, Alaska: American Association of Petroleum Geologists Bulletin, v. 56, p. 739-754.
- Cameron, C.C., Esterle, J.S., and Palmer, C.A., 1989, The geology, botany and chemistry of selected peat-forming environments from temperate and tropical latitudes, in Lyons, P.C., and Alpern, B., eds., Peat and coal: origin, facies, and depositional models: *International Journal of Coal Geology*, v. 12, p. 105-156.
- de Boer, P.L., Gelder, A., van, and Nio, S.D., 1988, Tide-influenced sedimentary environments and facies: Dordrecht, The Netherlands, Reidel Publishing Company, 530 p.
- Detterman, R. L., Plafker, George, Tysdal, R.G., and Hudson, Travis, 1976, Geology and surface features along part of the Talkeetna segment of the Castle Mountain-Caribou fault system: U.S. Geological Survey Miscellaneous Field Studies Map MF-738, scale 1:63,360.
- Dickinson, K.A., and Campbell, J.A., 1978, Sedimentary facies in Tertiary rocks in the Tyonek quadrangle, in Geological Survey research 1978: U.S. Geological Survey Professional Paper 1100, p. 84.
- Dickinson, K.A., Campbell, J.A., and Dula, W.F., Jr., 1995, Geology, geochemistry, and uranium favorability of Tertiary

- continental sedimentary rocks in the northwestern part of the Cook Inlet area, Alaska: *U.S. Geological Survey Bulletin* 2098, p. **B1-B37**.
- Doveton, J.H., 1994, Geologic log interpretation: Society of Economic Paleontologists and Mineralogists Short Course Notes No. 29, 169 p.
- Ethridge, F.G., 1980, **Fluvial** and related depositional systems—depositional models in the search for minerals and fuels: Fort Collins, Colo., Colorado State University, Short Course Notes, 285 p.
- Evans, G., 1975, Intertidal flat deposits of the Wash, western margin of the North Sea, *in* Ginsburg, R.N., ed., Tidal deposits—a **casebook** of recent examples and fossil counterparts: New York, Springer-Verlag, p. 13-20.
- Flores, R.M., and Johnson, S.Y., 1995, Sedimentology and lithofacies of the Eocene Skookumchuck Formation in the Centralia coal mine, southwest Washington, *in* Fritsche, A.E., ed., Cenozoic paleogeography of the western United States—II: Pacific Section, SEPM (Society for Sedimentary Geology), Book 75, p. 274-290.
- Flores, R.M., Stricker, G.D., and Roberts, S.B., 1994, Miocene coal-bearing strata of the Tyonek Formation: braided-stream deposits in the Chuit Creek-Chuitna River drainage basin, southern Alaska, *in* Till, A.B., and Moore, T.E., eds., Geologic studies in Alaska by the U.S. Geological Survey, 1993: U.S. Geological Survey Bulletin 2107, p. 95-114.
- Flores, R.M., and Sykes, R., 1996, Depositional controls on coal distribution and quality in the Eocene Bmner Coal Measures, Buller Coal field, South Island, New Zealand: *International Journal of Coal Geology*, v. 29, p. 291-336.
- Fuchs, W. A., 1980, Tertiary tectonic history of the Castle Mountain-Caribou fault system in the Talkeetna Mountains, Alaska: Salt Lake City, Utah, University of Utah, Ph.D. dissertation, 152 p.
- Ginsburg, R.N., ed., 1975, Tidal deposits—a **casebook** of recent examples and fossil counterparts: New York, Springer-Verlag, 428 p.
- Gluskoter, H.J., and Simon, J.A., 1968, Sulfur in Illinois coals: Illinois State Geological Survey Circular 432, 28 p.
- Grantz, Arthur, 1966, Strike-slip faults in Alaska: *U.S. Geological Survey Open-File Report* 267, 82 p.
- Grantz, Arthur, Zietz, Isidore, and Andreasen, G.E., 1963, An aeromagnetic reconnaissance of the Cook Inlet area, Alaska: *U.S. Geological Survey Professional Paper* 316-G, p. 117-134.
- Harrison, S.C., 1975, Tidal-flat complex, **Delmarva** Peninsula, Virginia, *in* Ginsburg, R.N., ed., Tidal deposits—a **casebook** of recent examples and fossil counterparts: New York, Springer-Verlag, p. 31-38.
- Hite, D.M., 1976, Some sedimentary aspects of the Kenai Group, Cook Inlet, Alaska, *in* Miller, T.P., ed., Recent and ancient sedimentary environments in Alaska, Proceedings of the Alaska Geological Society Symposium: Alaska Geological Society, p. **I1-I22**.
- Kamola, D.L., 1984, Trace fossils from marginal-marine facies of the Spring Canyon Member, Blackhawk Formation (Upper Cretaceous), east-central Utah: *Journal of Paleontology*, v. 58, p. 529-541.
- Knight, R.J., and Dalrymple, R.W., 1975, Intertidal sediments from the south shore of Cobequid Bay, Bay of Fundy, Nova Scotia, Canada, *in* Ginsburg, R.N., ed., Tidal deposits—a **casebook** of recent examples and fossil counterparts: New York, Springer-Verlag, p. 47-56.
- Larsonneur, C., 1975, Tidal deposits, Mont Saint-Michel Bay, France, *in* Ginsburg, R.N., ed., Tidal deposits—a **casebook** of recent examples and fossil counterparts: New York, Springer-Verlag, p. 21-30.
- Lawrence, D.A., and Williams, B.P.J., 1987, Evolution of drainage systems in response to Acadian deformation: the Devonian Battery Point Formation, eastern Canada, *in* Ethridge, F.G., Flores, R.M., and Harvey, M.D., eds., Recent developments in **fluvial** sedimentology: Society of Economic Paleontologists and Mineralogists Special Publication No. 39, p. 287-300.
- McFarland, C.E., 1987, Placer's Beluga coal project—mining and marketing plans, *in* Rao, P.D., ed., Focus on Alaska's coal '86: Fairbanks, Alaska, Mineral Industry Research Laboratory Report No. 72, University of Alaska, p. 127-131.
- McGee, D.C., 1972, Coal reserves, Beluga and Chuitna Rivers and Capps Glacier areas Alaska: Alaska Geological and Geophysical Surveys Open-File Report 35, 5 p., 3 pls., scale 1:15,840.
- Nio, S.D., and Yang, C., 1991, Diagnostic attributes of clastic tidal deposits—a review, *in* Smith, D.G., Reinson, G.E., Zaitlin, B.A., and Rahmani, R.A., eds., Clastic tidal sedimentology: Canadian Society of Petroleum Geology Memoir 16, p. 3-28.
- Ramsey, J.P., 1981, Geology-coal resources and mining plan for the Chuitna River field, Alaska, *in* Rao, P.D., ed., Focus on Alaska's coal '80: Fairbanks, Alaska, Mineral Industry Research Laboratory Report No. 50, University of Alaska, p. 92-110.
- Rao, P.D., and Smith, J., 1987, Characterization of Chuitna coal from deep drill core with possible applications to seam correlation, *in* Rao, P.D., ed., Focus on Alaska's Coal '86: Fairbanks, Alaska, Mineral Industry Research Laboratory No. 72, University of Alaska, p. 157-182.
- Reineck, H.E., and Singh, I.B., 1980, Depositional sedimentary environments: New York, Springer-Verlag, 549 p.
- Reineck, H.E., and Wunderlich, F., 1968, Classification and origin of flaser and lenticular bedding: *Sedimentology*, v. 11, p. 99-104.
- Reinson, G.E., 1989, Tide-influenced channel deposits in the Lower Cretaceous Glauconitic Member, southern Alberta, *in* Reinson, G.E., ed., Modern and ancient examples of clastic tidal deposits—a core and peel workshop: Canadian Society of Petroleum Geologists, Second International Research Symposium on Clastic Tidal Deposits, Calgary, p. 98-104.
- Rust, B.R., 1979, Facies models 2: coarse alluvial deposits, *in* Walker, R.G., ed., Facies models: Geoscience Canada Reprint Series, p. 9-23.
- Smith, D.G., 1987, Meandering river point bar lithofacies models: modern and ancient examples compared, *in* Ethridge, F.G., Flores, R.M., and Harvey, M.D., eds., Recent developments in **fluvial** sedimentology: Society of Economic Paleontologists and Mineralogists Special Publication No. 39, p. 83-91.

- Smith, D.G., **Reinson**, G.E., Zaitlin, B.A., and Rahmani, R.A., 1991, Clastic tidal sedimentology: Canadian Society of Petroleum Geology Memoir 16, 387 p.
- Smith, N.D., 1970, The braided stream depositional environment: comparison of the Platte River with some Silurian **clastic** rocks, north-central Appalachians: Geological Society of America Bulletin, v. 81, p. 2993-3014.
- Stiles, R.B., and Franklin, L.C., 1987, DCP summary, in Rao, P.D., ed., Focus on Alaska's coal '86: Fairbanks, Alaska, Mineral Industry Research Laboratory Report No. 72, University of Alaska, p. 132-141.
- Thompson, R. W., 1975, Tidal-flat sediments of the Colorado River delta, northwestern Gulf of California, in Ginsburg, R.N., ed., Tidal deposits—a **casebook** of recent examples and fossil counterparts: New York, Springer-Verlag, p. 57-66.
- Tunbridge, **I.P.**, 1981, Sandy high-energy flood **sedimentation**—some criteria for recognition with an example from the Devonian of S.W. England: Sedimentary Geology, v. 28, p. 79-85.
- 1984, Facies model for a sandy ephemeral stream and playa lake complex: the Middle Devonian Trentishoe Formation of North Devon, U.K.: Sedimentology, v. 31, p. 697-715.
- Visser, M.J., 1980, Neap-spring cycles reflected in Holocene **subtidal** large-scale **bedform** deposits: a preliminary note: Geology, v. 8, p. 543-546.
- Reviewers: Michael Brownfield and Richard Stanley

# Tectono-Geophysical Domains of Interior Alaska as Interpreted From New Gravity and Aeromagnetic Data Compilations

By Richard W. Saltus, John F. Meyer, Jr., David F. Barnes, and Robert L. Morin

## ABSTRACT

We identify and discuss 20 "tectono-geophysical domains" that span interior Alaska (61°-66°N., 144°-159°W.). The boundaries of these domains are based on analysis of gradients and patterns in new compilations of aeromagnetic and gravity data along with previously mapped lithotectonic boundaries. The aeromagnetic compilation is a mosaic of 23 different surveys flown between 1954 and 1982. The gravity compilation comprises about 9,800 gravity measurements collected between 1958 and 1992. Half of the 20 tectono-geophysical domains are identified here for the first time, and half are consistent with previous geophysical interpretations by other workers based on previous geophysical data compilation. The tectono-geophysical domains (1) trace parts of the Peninsular, Wrangellia, Kahiltna, Yukon-Tanana, Ruby, and Koyukuk lithotectonic terrane boundaries beneath postaccretionary cover rocks; (2) suggest subdivision of the Chugach, Peninsular, Kahiltna, Yukon-Tanana, and Tozitna lithotectonic terranes; (3) delineate the newly recognized Nowitna-Sischu tectono-geophysical domain based on magnetic anomaly patterns; and (4) extend to the south the Lower Yukon Basin, Koyukuk, Kanuti, and Ruby geophysical domains previously defined by Cady north of 65°N.

## INTRODUCTION

Interior Alaska (fig. 1) is a collage of amalgamated lithotectonic terranes. These terranes are, by definition, fault-bounded geologic packages with individual geologic histories. In many cases, these individual geologic histories have created structural and stratigraphic contrasts that are reflected in the gravity and magnetic patterns observed in these terranes. In particular, the faulted boundaries between terranes often mark sharp contrasts in density or magnetic properties that cause gradients in the gravity and magnetic fields. We use new regional gravity and aeromagnetic data compilations to interpret the locations of geophysical boundaries. We then use the geophysical boundaries in combination with previously mapped lithotectonic boundaries to

define "tectono-geophysical domains." In many cases our tectono-geophysical domains correspond well with previously mapped lithotectonic terranes, often allowing them to be tracked beneath postaccretionary cover rocks. In some cases, the tectono-geophysical domains suggest subdivision or modification of existing lithotectonic terranes. The geophysical boundaries may also reflect postaccretionary geologic structures.

Previous studies have examined regional geophysical data for portions of interior Alaska using earlier data compilations. Cady (1989, 1991) examined magnetic and gravity data north of 65°N. He identified "geophysical domains," defined as "three-dimensional regions having characteristic physical properties that express themselves as distinctive patterns of geophysical anomalies." Our "tectono-geophysical domains" are analogous to Cady's "geophysical domains," but we also include previously mapped lithotectonic terrane boundaries when defining domains. Our domains are consistent with Cady's domains north of 65°N. and extend those domains south of 65°N. Griscom and Case

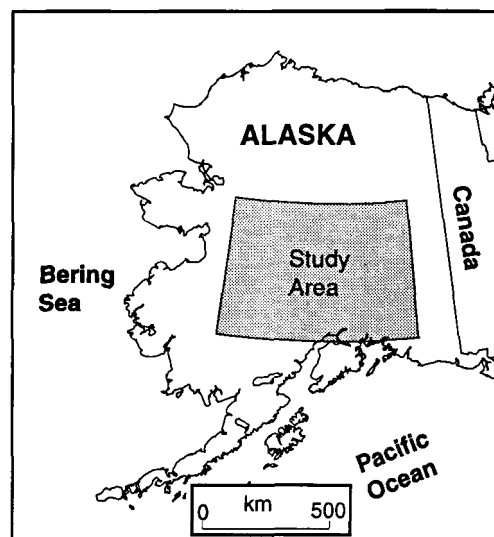


Figure 1. Index map showing the study area relative to the state of Alaska.

(1982, 1983) discussed magnetic anomalies in southern Alaska (south of the Denali-Farewell fault; fig. 2). They described the general magnetic character of the major southern Alaska lithotectonic terranes and discussed several discrete anomalies, including those related to (1) the northern boundary of the Chugach terrane, (2) remanent magnetization in the Wrangell volcanic field (fig. 2), and (3) possible deep magmatism associated with Mesozoic and Cenozoic extension of the Copper River basin and the Cook Inlet. Our tectono-geophysical domains south of the Denali-Farewell fault are consistent with the interpretations of Griscom and Case (1982, 1983).

### GRAVITY COMPILATION

The data sets used in this study were produced by cooperative effort of the State of Alaska, Division of Oil and Gas, and the U.S. Geological Survey (USGS). The gravity data grid is constructed from about 9,800 measurements made by the USGS, the State of Alaska, and other groups between 1958 and 1992 (fig. 3). The data are tied to the International Gravity Standardization Net-71 (Morelli, 1974) and were reduced using the 1967 ellipsoid (International Association of Geodesy, 1971). Because topographic maps of Alaska contain elevation errors of up to 25 m

## Interior Alaska Geography

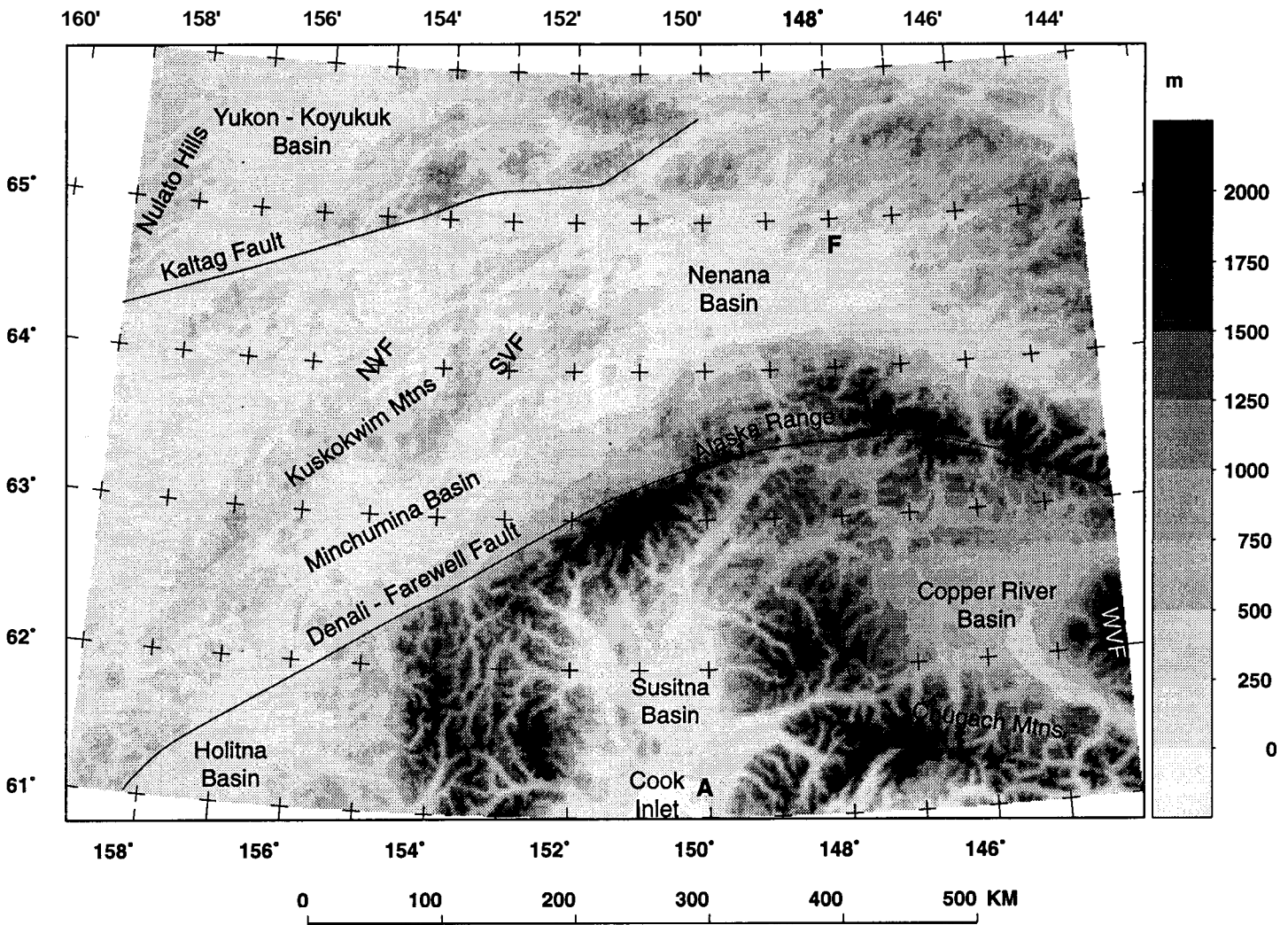


Figure 2 Interior Alaska geography with selected cities, basins, mountain ranges, volcanic fields, and faults identified. Topography gray-scale interval is 250 m. Cities: F, Fairbanks; A, Anchorage. Volcanic fields: WVF, Wrangell volcanic field; NVF, Nowitna volcanic field; SVF, Sischu volcanic field.

(Barnes, 1984), **altimetry** was used to reduce most of the Alaskan gravity measurements included in this compilation (Barnes, 1972). Complete Bouguer anomalies were calculated with terrain corrections from 0.39 to 166.7 km from each measurement point using a digital elevation model (Barnes, 1984). Most of the gravity data are accurate to better than 5 mGal ( $1 \text{ mGal} = 10^{-5} \text{ m/s}^2$ ).

The gravity data were interpolated onto a 1-km grid. In order to contain maximum information at this scale, each 1-km grid cell should be controlled by at least one gravity measurement. However, only about 2 percent of

the grid cells meet this criteria. Instead, grid values were defined for cells within 10 km of a gravity measurement. The large area of "white space" (regions more than 10 km from a gravity measurement) in figure 3 shows the need for additional gravity-data coverage in interior Alaska, particularly in the western half of the study area.

To emphasize density distributions in the uppermost crust, we display (fig. 3) the isostatic residual gravity anomalies, which are constructed from the Bouguer anomalies by subtraction of an isostatic regional field. This subtraction removes the broad wavelength features of the Bouguer **grav-**

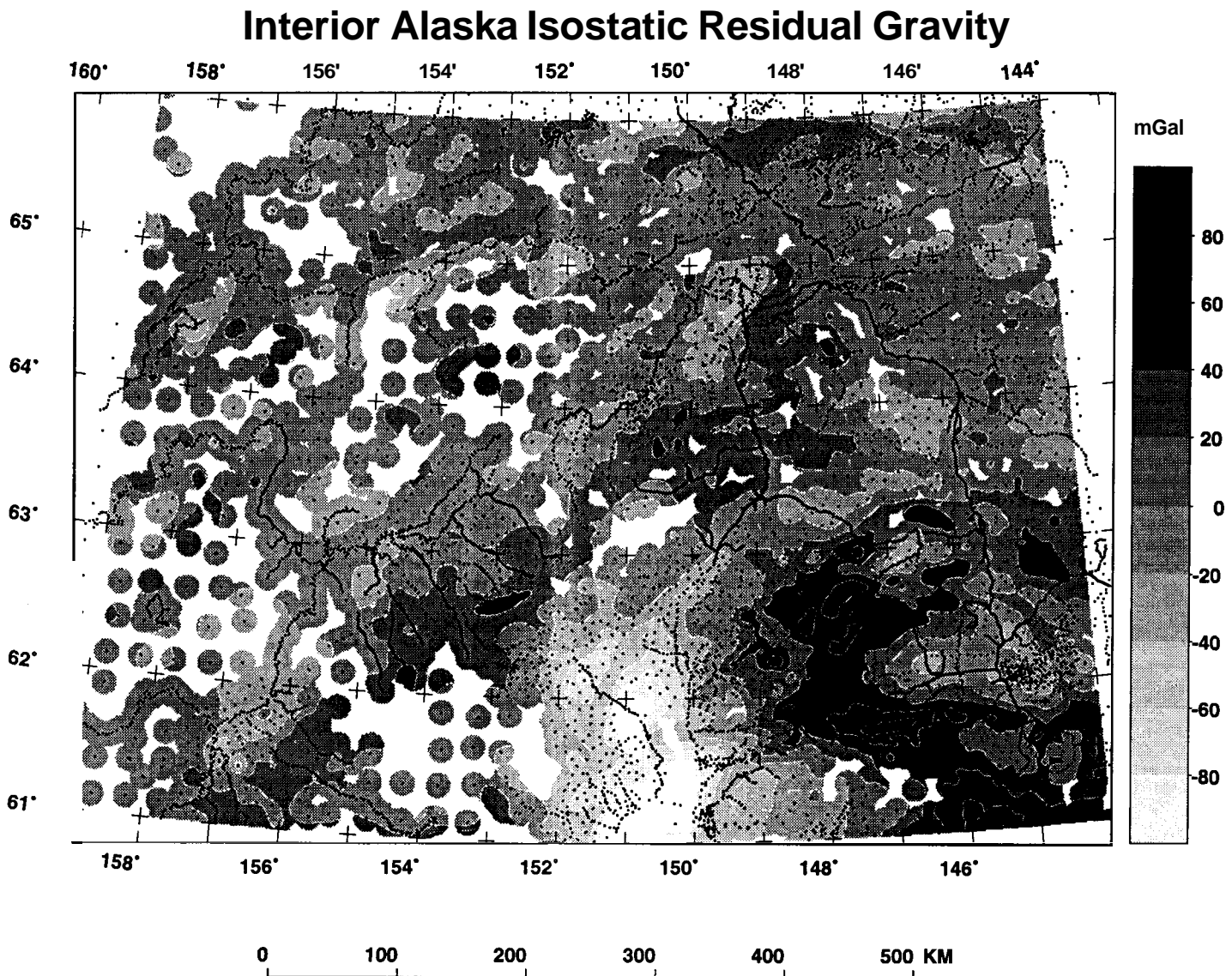


Figure 3. Gravity grid and data. Isostatic residual gravity anomalies are based on about 9,800 measurements made between 1958 and 1992. Individual observation locations are plotted as small dots. These locations mostly follow rivers and roads. The contour interval is 20 mGal ( $1 \text{ mGal} = 10^{-5} \text{ m/s}^2$ ). The isostatic regional gravity anomaly is primarily sensitive to density variations in the upper crust and was constructed from the complete Bouguer gravity values by subtraction of an isostatic regional field. The isostatic regional field is from Barnes and others (1994).

ity field that are caused by isostatic support of topography (Simpson and others, 1986). A local support (Airy) model was assumed, but the isostatic regional field is not strongly model dependent. The isostatic regional field is from Barnes and others (1994). The Bouguer gravity data grid is available from the National Geophysical Data Center in Boulder, Colorado (send inquiries to [info@ngdc.noaa.gov](mailto:info@ngdc.noaa.gov)). Color contour maps of the complete Bouguer anomaly values are available from the USGS (Meyer and others, 1996).

## TERRACED RESIDUAL GRAVITY AND BOUNDARIES

The terraced residual gravity map (fig. 4) accentuates upper-crustal rock density boundaries, some of which coincide with previously mapped lithotectonic terrane boundaries in interior Alaska. Other important gravity boundaries outline postaccretionary basins. The gravity-defined boundaries are of particular interest where they allow **extrapola-**

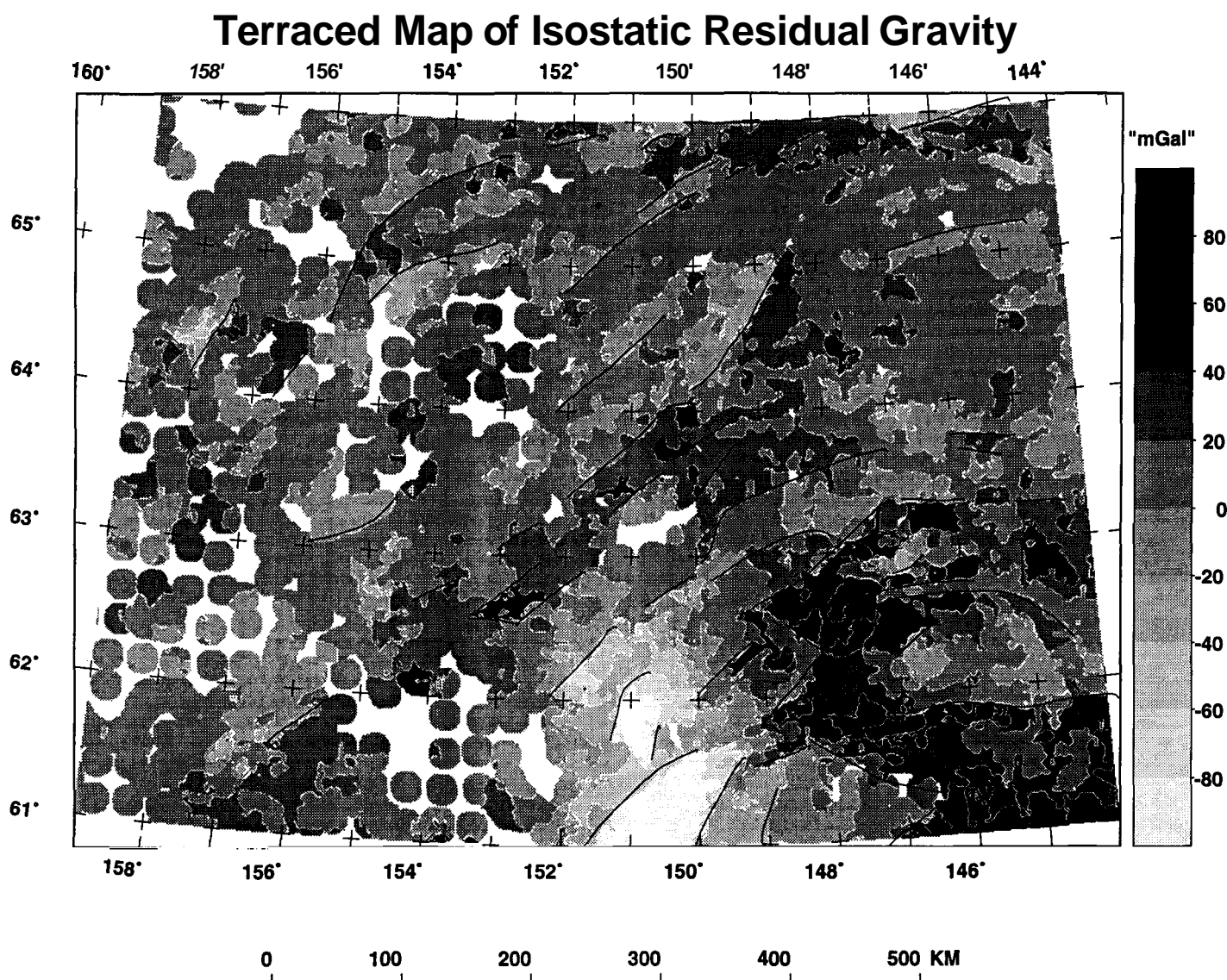


Figure 4. Terraced residual gravity and boundaries. This map is constructed from the complete isostatic residual gravity map of figure 3 by application of the terracing operator of Cordell and McCafferty (1989) and highlights domains with contrasting upper-crustal rock density. Lines mark major density boundaries identified from these data. These boundaries are used, along with magnetic and lithotectonic boundaries, to define tectono-geophysical domains (fig. 8).

tion of terranes beneath postaccretionary cover rocks. The terraced residual gravity map (fig. 4) was constructed from the isostatic residual anomaly map (fig. 3) by applying the terracing transform of Cordell and McCafferty (1989). This transform highlights upper-crustal rock-density boundaries by steepening gradients. We have traced the major density boundaries (black lines, fig. 4) and use these to help define the tectono-geophysical domains discussed below.

## AEROMAGNETIC DATA COMPILATION

Aeromagnetic data processing (editing and merging) was performed by Paterson, Grant & Watson, Ltd., Toronto, Canada under contract with the State of Alaska. Two grids were produced at 1-km spacing: a composite grid and a merged grid. These grids comprise data from 23 surveys with flight-line spacings that vary from 800 m (1/2 mi) to

10 km (6 mi) and flight elevations that vary from 120 m (400 ft) above ground to 1.2 km (4,000 ft) barometric (fig. 5, table 1). For the composite grid (fig. 6), all surveys were included at their original flight elevations. For the merged grid, all surveys were mathematically continued to a common flight height of 300 m (1,000 ft) above ground (Meyer and Saltus, 1995; Meyer and others, in press). This required upward continuation of the National Uranium Resource Exploration (NURE, flown at 122 m above ground) surveys and level-to-drape continuation (to convert the constant-flight-elevation survey to one "draped" over topography) of the USGS Copper River survey (table 1). In addition to the mathematical continuation, some adjustments of datum levels and of values along survey boundaries were done (Meyer and others, in press; Paterson, Grant & Watson, Ltd., written commun., 1994). Both gridded aeromagnetic data sets are publicly available from the National Geophysical Data Center in Boulder, Colorado. Color contour

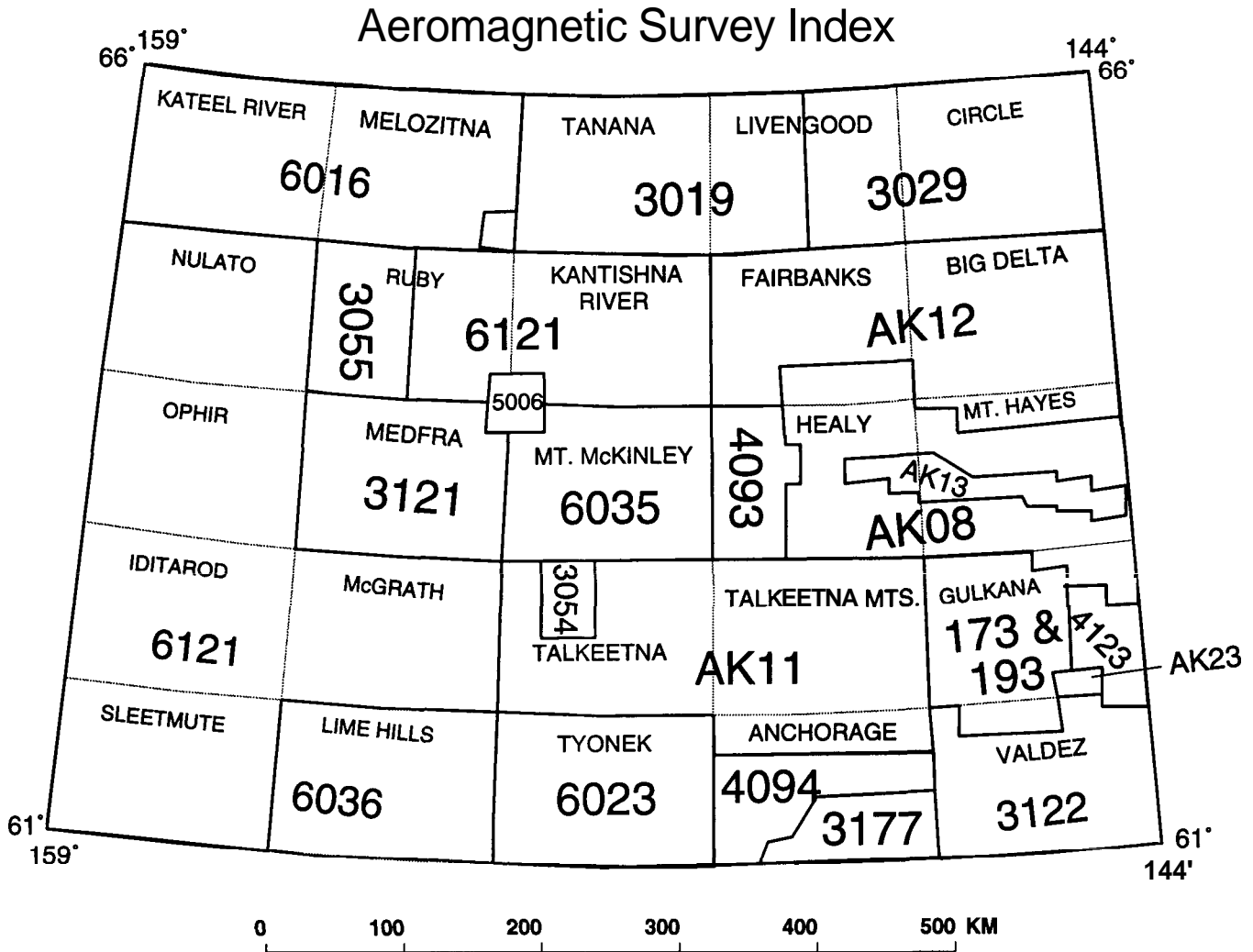


Figure 5. Index map of individual aeromagnetic surveys. Specifications are listed in table 1.



Table 1. Aeromagnetic survey specifications keyed to figure 4

[AG, above ground; B, barometric elevation]

Survey number	Date flown	Contractor	Area	Flight-line spacing		Direction	Flight elevation		Flight surface
				(km)	(miles)		(meters)	(feet)	
173	1954	USGS	Copper River	3	2	N-S.	1,219	4,000	B
193	1955	USGS	Copper River	2	1	N.S.	1,219	4,000	B
3019	1972	Aero Service	Northeast Alaska	2	1.2	N.S.	305	1,000	AG
3029	1973	GeoMetrics	Northeast Alaska	2	1	N-S.	305	1,000	AG
3054	1975	LKB	Talkeetna	2	1	N-S.	305	1,000	AG
3055	1975	Applied Geophysics, Inc.	Ruby	2	1	N.S.	305	1,000	AG
3121	1978	LKB	Medfra	2	1	N. 35° W.	305	1,000	AG
3122	1978	LKB	Valdez	2	1	N-S.	305	1,000	AG
3177	1979	LKB	Chugach	2	1	N. 50° W.	305	1,000	AG
4093	1982	Diversified Technical Service	Healy	2	1	N.S.	305	1,000	AG
4094	1982	Diversified Technical Service	Anchorage	2	1	N. 30° W.	305	1,000	AG
4123	1984	Airborne Systems	Wrangell Mountains	2	1	E-W.	305	1,000	AG
5006	1979	Aero Service	Four Corners	2	1	N-S.	122	400	AG
6016	1976	Texas Instruments	Yukon	10	6	E-W.	122	400	AG
6023	1976/77	LKB	NURE - Cook Inlet	10	6	E-W.	122	400	AG
6035	1977	Texas Instruments	NURE - Eagle/Talkeetna	10	6	E-W.	122	400	AG
6036	1977	Texas Instruments	NURE - Lime Hills/Lake Clark	10	6	E-W.	122	400	AG
6121	1979	Aero Service	NURE - West-central Alaska	10	6	E-W.	122	400	AG
AK08	1971	LKB	East Alaska Range	1	.75	N.S.	305	1,000	AG
AK11	1972	LKB	Talkeetna/Anchorage	1	.75	N-S.	305	1,000	AG
AK12	1973	LKB	Big Delta/Fairbanks	1	.75	N.S.	305	1,000	AG
AK13	1973	LKB	Healy/Mt. Hayes	1	.75	N-S.	305	1,000	AG
AK23	1982	Ertec	Eastern Copper River	1	.5	N-S.	152	500	AG

aeromagnetic maps have been produced using the merged data set (Meyer and Saltus, 1995).

The patterns and amplitudes of the magnetic anomalies on the composite aeromagnetic map (fig. 6) reflect the depth to and the magnetic character of crystalline basement, the distribution and volume of intrusive and extrusive volcanic rocks, and the nature of boundaries between domains with contrasting magnetic rock properties. In interior Alaska, magnetic domain boundaries correlate strongly with previously mapped lithotectonic terrane boundaries. The magnetic domain boundaries are also important to both mineral and petroleum exploration as potential zones of concentrated deformation, fluid flow, magmatism, and heat flow.

## TERRACED MAGNETICS AND BOUNDARIES

The terraced magnetic map (fig. 7) accentuates boundaries between upper-crustal regions with contrasting magnetic character. These magnetic boundaries generally follow previously mapped boundaries between lithotectonic terranes (fig. 8) and often allow these terrane boundaries to be traced beneath postaccretionary cover rocks. The magnetic boundaries are the primary information used to define the tectono-geophysical domains outlined below.

The terraced magnetic map (fig. 7) was produced from the merged aeromagnetic grid by the following process: (1) reduction-to-pole of the total field magnetic anomaly, and (2) application of the terracing operator of Cordell and McCafferty (1989). Reduction-to-pole is a mathematical

operation that eases interpretation by shifting aeromagnetic anomalies to lie directly over their magnetic rock sources. The terracing operator further aids in identification of magnetic rock source boundaries by steepening horizontal magnetic gradients. As with any derivative product, care should be taken when interpreting features that have been affected by processing. The magnetic boundaries used for tectono-geophysical domain delineation in this report were examined on a larger scale version of the composite map to verify the nature of interpreted boundaries and also to check that boundaries between surveys were not inadvertently interpreted as tectonic features.

## LITHOTECTONIC TERRANES

Interior Alaska encompasses parts of about 20 different lithotectonic terranes (Silberling and others, 1994; Nokleberg and others, 1994). These terranes have been grouped (Plafker and Berg, 1994) into seven composite terranes and two undifferentiated categories (fig. 8). As defined by Plafker and Berg (1994, p. 991), a composite terrane is "an aggregate of subordinate terranes which are grouped based on an interpretation of similar lithotectonic kindred or affinity." Further, "there is no implication regarding whether the terranes came together before or after accretion to the continent" (Plafker and Berg, 1994, p. 991). In the composite-terrane descriptions that follow, terrane names are from Silberling and others (1994) unless otherwise specified. The seven composite terranes are listed below, proceeding roughly from south to north, with all descriptions condensed from Plafker and Berg (1994):

1. SCT, Southern Margin composite terrane (includes parts of the Chugach and Prince William terranes within the study area), is a complexly deformed accretionary prism containing Upper Triassic to Paleogene oceanic rocks, **mélange**, and flysch. The rocks of this terrane record Early Jurassic to middle Eocene crustal convergence of arc-related volcanoclastic and volcanic rocks against the Pacific margin of the Wrangellia composite terrane; Early Jurassic and mid-Cretaceous blueschist metamorphism; Eocene high-**temperature/low-pressure** metamorphism and intrusion of anatectic tonalitic plutons; and **16°-30°** northward displacement relative to the craton since the Late Cretaceous.

2. WCT, Wrangellia composite terrane (includes parts of the Wrangellia and Peninsular terranes within the study

area), is composed of Late Proterozoic and younger magmatic arc, oceanic plateau, and rift fill. The rocks record several periods of arc magnetism from Late Proterozoic to post-Eocene; Middle to Late Triassic emplacement of basalt and gabbro; younger Jurassic volcanism with comagmatic granitic intrusion; up to **25°** northward displacement relative to the North American craton during the Late Triassic to mid-Cretaceous; and emplacement by mid-Cretaceous and subsequent contractional deformation and collapse of flysch basins.

3. CCT, Central composite terrane (includes the Dillinger, Livengood, **Nixon** Fork, Minchumina, Mystic, Wickersham, and White Mountains terranes of Silberling and others, 1994—note that several of these (Mystic, White

## Interior Alaska Composite Aeromagnetics

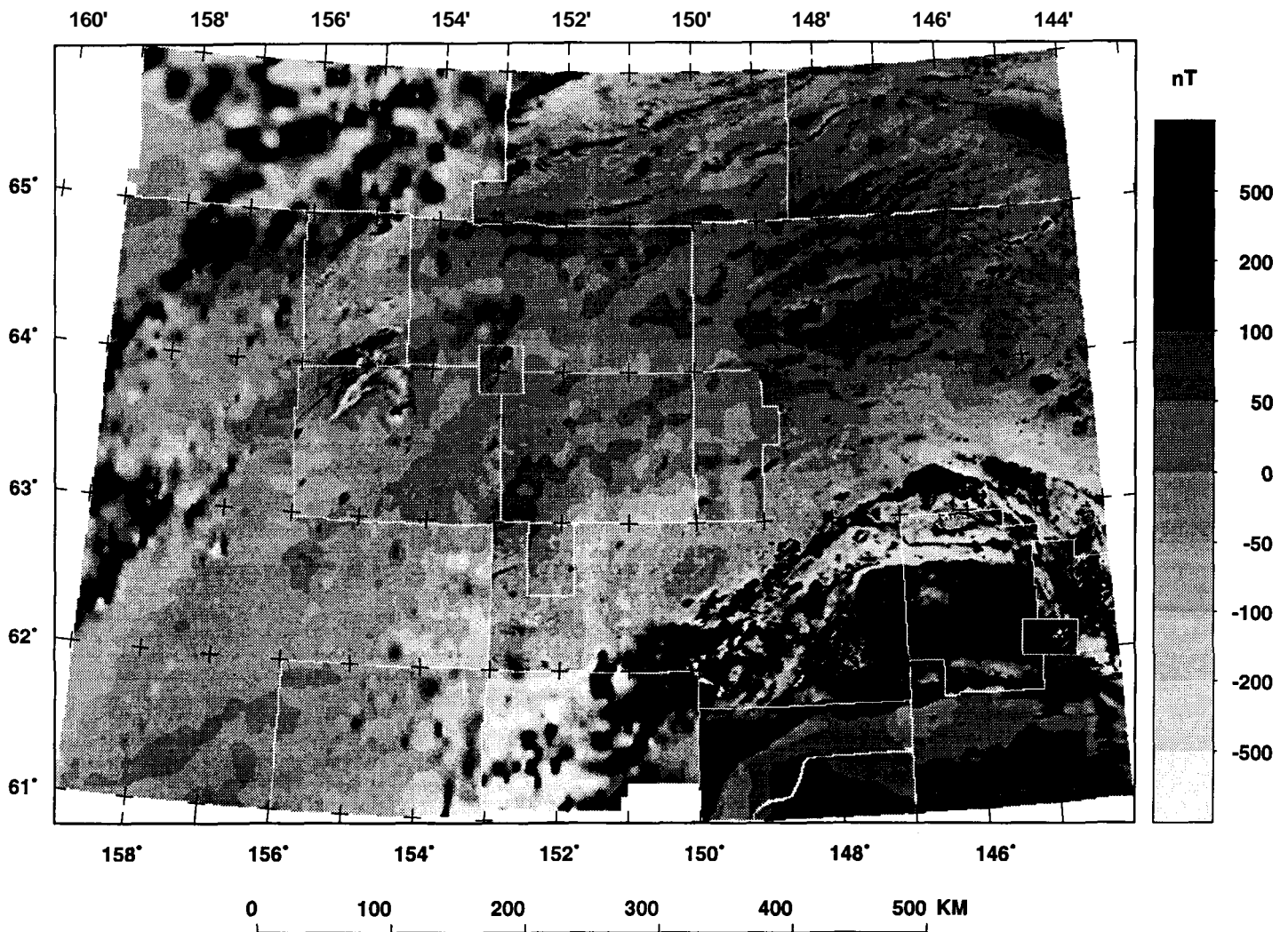


Figure 6. Composite aeromagnetic map, showing aeromagnetic anomalies from 23 different surveys flown between 1954 and 1982. White lines show boundaries between individual aeromagnetic surveys (fig. 5, table 1). The aeromagnetic data have a large amplitude range, and it is difficult to show all the features with a limited number of contour levels.

Mountains, Dillinger, and **Nixon Fork**) are grouped as sequences within the Farewell Terrane by Decker and others, 1994), is made up primarily of rifted, rotated, translated, and imbricated miogeoclinal fragments. Rock exposure is generally poor and relations between and among terranes are not well known. This composite terrane consists of Late Proterozoic and Cambrian clastic deposits (Wickersham terrane), Late Proterozoic metamorphic basement overlain by Middle Cambrian to Upper Devonian carbonate rocks and terrigenous Permian, Triassic, and Lower Cretaceous marine sedimentary rocks (**Nixon Fork terrane**); Ordo-

vician bimodal volcanic rock, volcanoclastic rocks, and conglomerate overlain by Silurian and Devonian carbonate rocks and capped by undated clastic sedimentary rocks (White Mountains terrane); a Paleozoic sequence of shales, cherts, turbidites, pillow basalt, limestone, and conglomerate (Minchumina, Mystic, and Dillinger terranes); and small areas of Early Cambrian or older ultramafic and gabbro units that underlie Ordovician chert, mafic volcanic, and carbonate rocks (Livengood terrane). The rocks record late Precambrian to Ordovician emplacement of ultramafic and deep-marine rocks; deposition of a shelf sequence that

## Terraced map of Interior Alaska Merged Reduced-to-Pole Magnetics

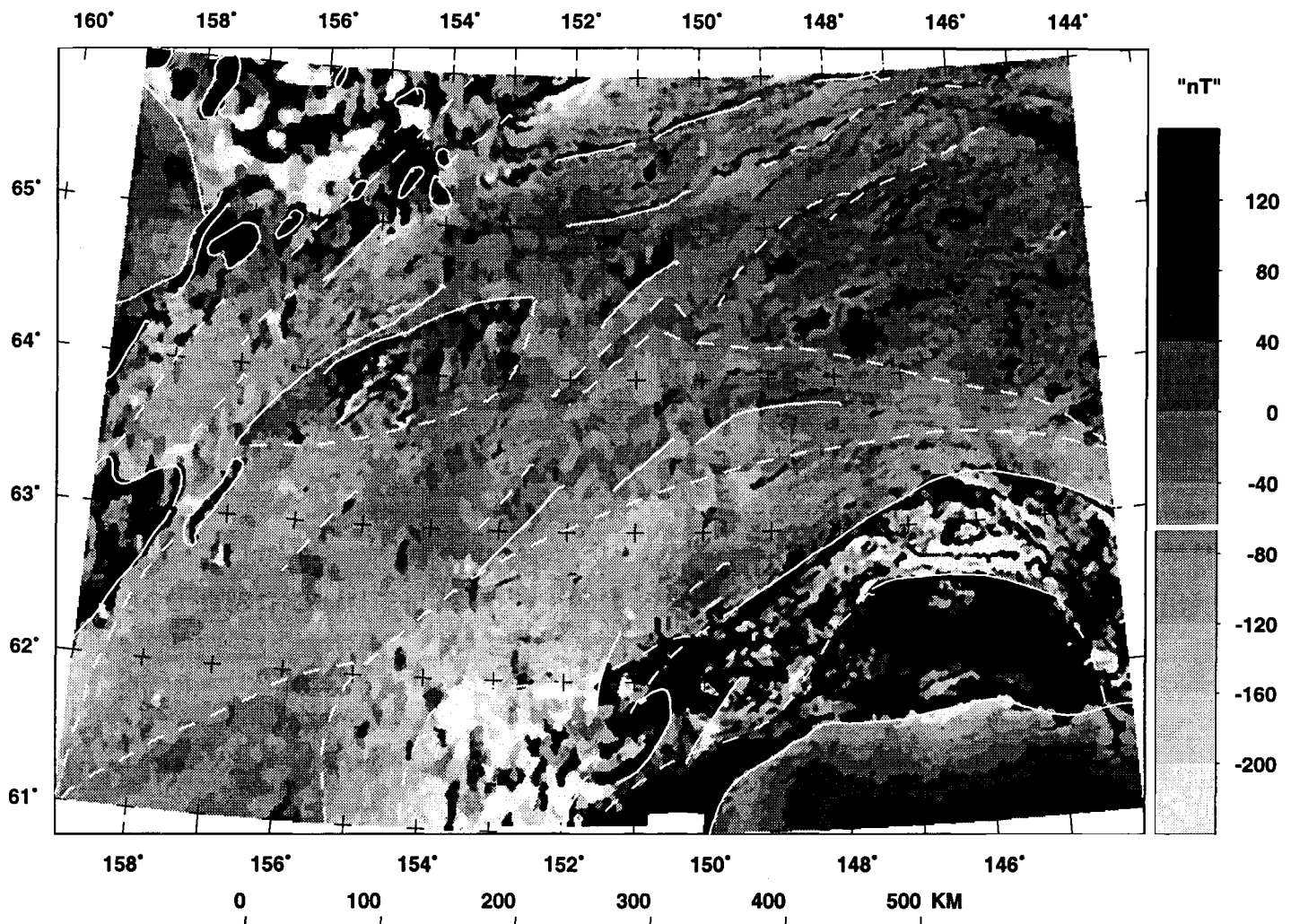


Figure 7. Terraced reduced-to-pole magnetics and boundaries. This map is constructed from the composite aeromagnetic anomaly map (fig. 6) by a three-step process: (1) mathematical merging of individual surveys to a common flight altitude of 300 m (1,000 ft) above ground, (2) reduction-to-pole to center the anomalies over their causative magnetization sources, and (3) application of the terracing operator of Cordell and McCafferty (1989) to accentuate the boundaries between domains with contrasting magnetization. The map is displayed with a 40-nT contour interval to accentuate features in domains with low magnetic amplitudes. The solid white lines mark primary boundaries marked by steep magnetic gradients. The dashed white lines mark secondary boundaries identified by contrasts in magnetic-anomaly patterns.

interfingering with slope and basin facies including mafic volcanic and ultramafic rocks; and Devonian folding and northeast-verging thrusting toward the craton in the White Mountains terrane.

4. YCT, Yukon composite terrane (includes just the Yukon-Tanana terrane within the study area), is a mainly crystalline terrane with overlying arc-related rocks. The crystalline rocks of the Yukon composite terrane are Late Proterozoic to Mississippian schists and gneisses with strong affinities to rocks of the North American craton margin. The rocks record several periods of arc magmatism from

the Late Devonian to the mid-Cretaceous; Middle Jurassic accretion of the Yukon composite terrane against the continental margin; Early Jurassic episodes of regional plutonism and metamorphism; and mid-Cretaceous plutonism and crustal extension in east-central Alaska.

5. RB, Ruby composite terrane, is a poorly known and structurally complex metamorphic terrane. The rocks of the Ruby terrane include schists, gneisses, marbles, and metabasalts that probably originated as a continental margin assemblage. The rocks contain fossils as old as Proterozoic and as young as Devonian. The terrane is locally

## Lithotectonic Terranes

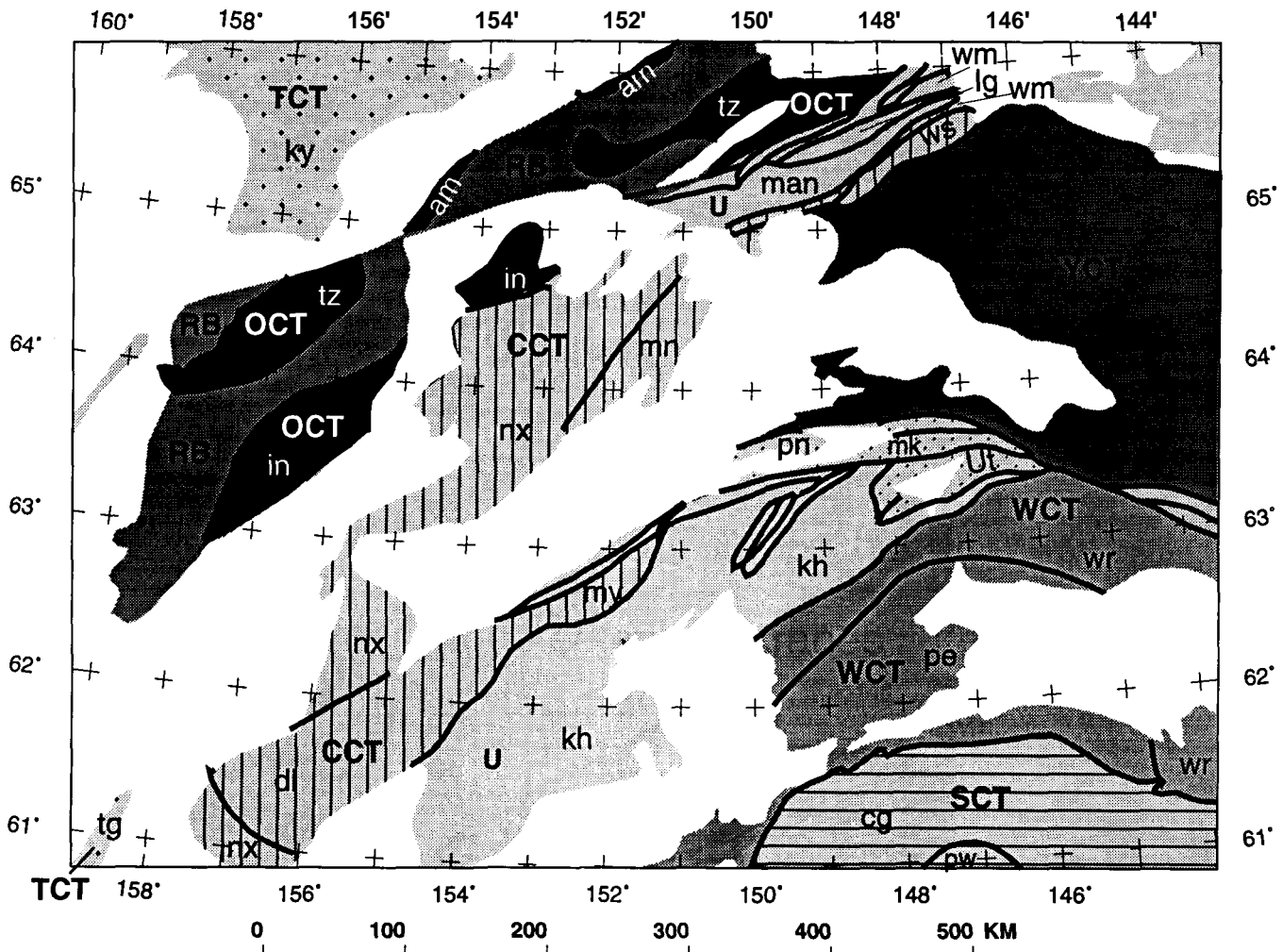


Figure 8. Composite lithotectonic terranes and postaccretionary cover rocks, modified from Silberling and others (1994) and Plafker and Berg (1994). The composite terranes and undifferentiated categories are as follows: OCT, Oceanic composite terrane; SCT, Southern Margin composite terrane; WCT, Wrangellia composite terrane; YCT, Yukon-Tanana composite terrane; CCT, Central composite terrane; RB, Ruby composite terrane; TCT, Togiak-Koyukuk composite terrane; U, undifferentiated Mesozoic and Cenozoic basal deposits and deformed flysch basins; Ut, undifferentiated terranes. White regions are areas of postaccretionary cover rocks. Heavy black lines are mapped boundaries between individual lithotectonic terranes (Silberling and others, 1994). Selected individual terranes are labeled as follows: am, Angayucham; cg, Chugach; dl, Dillinger; in, Innoko; kh, Kahiltna; ky, Koyukuk; lv, Livengood; man, Manley; mk, McKinley; mn, Minchumina; my, Mystic; nx, Nixon Fork; pe, Peninsular; pn, Pingston; pw, Prince William; tz, Tozitna; wm, White Mountains; wr, Wrangellia; ws, Wickersham.

intruded by mid-Cretaceous granitic plutons, especially to the north of the Kaltag fault (fig. 2). The rocks record early Paleozoic continental-margin sedimentation followed by emplacement of granitic plutons; Late Jurassic to Early Cretaceous high-pressure-high-temperature metamorphism related to ophiolite **obduction** and arc accretion; and mid-Cretaceous plutonism.

6. OCT, Oceanic composite terrane (includes the Innoko, Tozitna, and Angayucham terranes—note that all of these terranes are identified as part of the Angayucham terrane in the compilation by Nokleberg and others, 1994), is composed mainly of oceanic basalt, sedimentary rocks, and minor **ultramafic** rocks. Plafker and Berg (1994) interpret this composite terrane as composed of **obducted** fragments of the paleo-Pacific crust that were thrust onto the continental margin before and during the accretion of the Togiak-Koyukuk composite terrane in Late Jurassic and Early Cretaceous time.

7. TCT, Togiak-Koyukuk composite terrane (includes the Koyukuk and Togiak terranes), is a poorly exposed terrane consisting of Late Triassic through Early Cretaceous arc-related volcanic and volcanoclastic rocks and their intrusive equivalents. The arc rocks of the composite terrane are overlain by mid-Cretaceous marine and nonmarine sedimentary rocks and by Upper Cretaceous and Paleogene volcanic and marine sedimentary rocks. The rocks record Middle Jurassic metamorphism; Middle Jurassic through Early Cretaceous arc volcanism; latest Jurassic or earliest Cretaceous emplacement against the continental margin; arc accretion and regional metamorphism of lower plate rocks; and mid-Cretaceous plutonism and early Tertiary arc volcanism and related plutonism.

The two undifferentiated categories are (1) U, undifferentiated Mesozoic and Cenozoic basinal deposits and deformed flysch basins (includes parts of the Kahiltna, Manley, Livengood, and Windy-McKinley terranes); and (2) Ut, other undifferentiated terranes (includes about eight small terranes that fall in the tectonic wedge between the YCT and WCT composite terranes).

The full extent and boundaries of many of these terranes are obscured by postaccretionary cover (fig. 8). Previously mapped exposed boundaries between the terranes (Silberling and others, 1994) show significant correspondence with the gravity and magnetic gradients observed in our data compilations (figs. 3, 6).

## DEFINITION OF TECTONO-GEOPHYSICAL DOMAINS

By comparing lithotectonic boundaries (Silberling and others, 1994) to geophysical boundaries defined in this study we have provisionally identified 20 "tectono-geophysical" domains (fig. 9). The domains are defined chiefly by magnetic boundaries (fig. 7). Gravity boundaries play a sec-

ondary role, partly because data coverage is much poorer and partly because gravity is generally more sensitive to structure within the postaccretionary section than to tectonically significant basement structure (because of the greater contrast in density between the postaccretionary section and the basement than between intrabasement units). North of 65°N, our domains are consistent with geophysical domains previously identified by Cady (1989, 1991). South of the Denali-Farewell fault (fig. 2; the southern boundary of the YCT, fig. 8), our tectono-geophysical domains agree broadly in character and boundaries with the interpretations of Griscom and Case (1982, 1983).

Proceeding roughly from south to north, our domains are as follows (fig. 9):

1. CG, Chugach tectono-geophysical domain. This domain corresponds to the Chugach lithotectonic terrane (cg, fig. 8), part of the Southern Margin composite terrane (SCT, fig. 8). The northern boundary is sharply defined by the magnetic data. The magnetic expression of the domain is a broad gradient with decreasing magnetic values to the north; these values possibly trace the top of magnetic basement (an oceanic slab?) as it dips to the north beneath a (mostly) magnetically transparent upper crust. Gravity data suggest three subdivisions of this domain based on average density of the upper crust ( $g_1$ ,  $g_2$ ,  $g_3$ , fig. 9). These subdivisions increase in average density from west to east. This terrane is mostly nonmagnetic, with a few major positive and negative anomalies that are caused locally by mafic and **ultramafic** bodies as well as by thick sequences of mafic submarine volcanic rocks (Griscom and Case, 1983). A narrow series of major magnetic anomalies marks the northern boundary of this domain. These discrete anomalies are probably caused by Jurassic gabbros, diorites, and tonalites (Griscom and Case, 1983). Griscom and Case (1983) suggested that this narrow unit should be regarded as a separate terrane. This narrow band of anomalies falls in our PE1 domain, which is discussed next.

2. PE1, Peninsular tectono-geophysical domain #1. This domain encompasses a portion of the Peninsular lithotectonic terrane (pe, fig. 8) which is part of the Wrangellia composite terrane (WCT, fig. 8). The magnetic data suggest that this terrane extends to the southwest beneath the postaccretionary cover rocks (fig. 8). The PE1 domain is sharply delineated by the magnetic data, and the northern boundary is also traced by the gravity data. PE1 is a domain of broad magnetic highs that suggest a high crustal concentration of magnetite with induced and **normal-polarity** remanent magnetization. It is also a domain of high average crustal density based on the gravity data. The **high-amplitude** magnetic anomalies are caused by plutons of Jurassic, Cretaceous, and Tertiary age, and by the Cenozoic volcanic rocks at the surface (Griscom and Case 1983). This domain also contains, at its southern margin, the narrow, high-amplitude anomaly identified by Griscom and Case (1983) as the Chugach Mountains anomaly. They **sug-**

gested that this anomaly should be classified as a separate terrane, but we feel it encompasses too small a region to warrant subdivision at this scale of study.

3. PE2, Peninsular tectono-geophysical domain #2. This domain encompasses a portion of the Peninsular lithotectonic terrane, part of the Wrangellia composite terrane. The southern boundary is sharply delineated by the magnetic data. The northern boundary is defined by the mapped lithotectonic boundary (Silberling and others, 1994) but is not expressed geophysically. On the basis of geophysics alone, PE2 would be part of the Wrangellia tectono-geophysical domain (David Campbell, oral commun., 1996). PE2 is a domain of high-amplitude, short-wavelength, magnetic highs and lows, and generally characterized by high gravity. The magnetic lows may be topographic or geomet-

ric effects or they may indicate reverse-polarity remanent magnetization. Like WR (discussed below), the magnetic anomaly patterns in PE2 are caused by "numerous magnetic anomalies with complex sources: Triassic basalt flows, a folded mafic-ultramafic sheet, Mesozoic and Cenozoic plutons, and Cenozoic volcanic rocks" (Griscom and Case, 1983).

4. WR, Wrangellia tectono-geophysical domain. WR corresponds to the Wrangellia lithotectonic terrane (wr, fig. 8), part of the Wrangellia composite terrane (WCT, fig. 8). The geophysical data suggest that this terrane extends to the southwest beneath the postaccretionary cover rocks. The northern boundary of WR is sharply defined by the magnetic data and is partially traced by the gravity data. As mentioned above, WR is geophysically similar to the PE2

## Tectono-Geophysical Domains

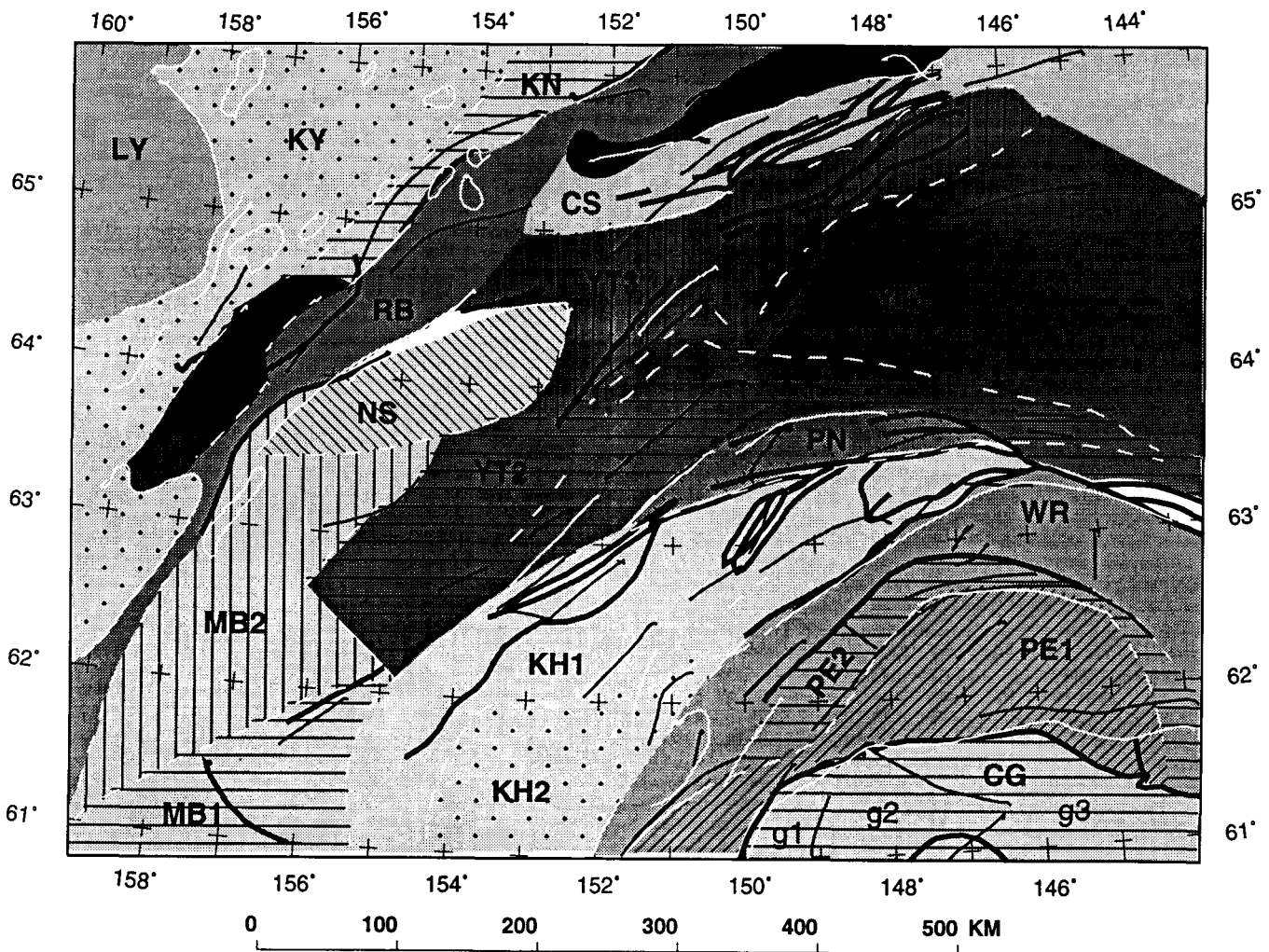


Figure 9. Tectono-geophysical domains. Twenty tectono-geophysical domains are interpreted from the gravity boundaries (thin black lines) and anomalies of figure 4, the magnetic boundaries (solid white lines are primary boundaries marked by steep magnetic gradients, and dashed white lines are secondary boundaries identified by contrasts in magnetic-anomaly patterns) and anomalies of figure 7, and the lithotectonic boundaries (thick black lines) of Silberling and others (1994). The domain abbreviations are defined in the text.

domain to the south and has similar complex volcanic and ultramafic sources for the magnetic anomalies.

5. **KH1**, Kahiltna tectono-geophysical domain #1. This domain encompasses portions of the Kahiltna (kh, fig. 8) and Dillinger (dl, fig. 8) lithotectonic terranes, which are part of the Central composite terrane (CCT, fig. 8) and of the undifferentiated Mesozoic and Cenozoic basinal deposits and deformed flysch basins (U, fig. 8). **KH1** is a domain of generally low magnetic relief punctuated by scattered discrete magnetic highs. The northern boundary is subtly expressed in the magnetic data and is also expressed in a few isolated places by the gravity data. **KH1** (and **KH2**; see below) is relatively nonmagnetic but contains some plutons that have discrete anomalies (Griscom and Case, 1983). Contact metamorphic aureoles associated with some plutons that intruded flysch have reversed-polarity remanent magnetization associated with pyrrhotite (Griscom and Case, 1983).

6. **KH2**, Kahiltna tectono-geophysical domain #2. This domain encompasses a portion of the Kahiltna lithotectonic terrane (kh, fig. 8), part of the undifferentiated Mesozoic and Cenozoic basinal deposits and deformed flysch basins (U, fig. 8). It is a domain of neutral magnetic values punctuated with isolated magnetic highs. This domain is similar in magnetic character to **KH1** but has a more negative average residual magnetic value (caused by a contrast in basement rock lithology?); it also has generally broader magnetic highs (caused by deeper magnetic sources?). **KH2** is a domain with poor gravity-data coverage. **KH2** may owe its magnetic character to the interaction of plutonic intrusions with flysch basins (Griscom and Case, 1983).

7. **PN**, **Pingston** tectono-geophysical domain. This domain corresponds to the **Pingston** (pn, fig. 8) and **McKinley** (mk, fig. 8) lithotectonic terranes (Silberling and others, 1994), part of the undifferentiated terranes of Plafker and Berg (1994; Ut, fig. 8). Geophysically, **PN** is a domain of generally low magnetic relief and high average density. Its boundaries are traced by a combination of subtle magnetic and gravity gradients. The coincidence of these subtle geophysical gradients with the mapped lithotectonic boundaries strengthens the case for defining **PN** as a distinct tectono-geophysical domain; this case would be more difficult to make on the basis of the overall geophysical character of the domain, which is similar to that of the **YT2** domain to the north. The generally high average density of **PN** may be caused by higher average metamorphic grade in this domain compared with surrounding terranes.

8. **MB1**, Mesozoic Basin tectono-geophysical domain #1. This domain encompasses portions of the **Nixon Fork** (nx, fig. 8) and **Dillinger** (dl, fig. 8) lithotectonic terranes, which are part of the Central composite terrane (CCT, fig. 8), as well as areas of postaccretionary cover (white areas of fig. 8). Both the **Nixon Fork** and **Dillinger** lithotectonic terranes consist primarily of sedimentary-rock units including abundant carbonates. This geology is reflected geo-

physically in **MB1** as low magnetic relief and generally positive gravity values. This domain has strong geophysical affinity to the **YT2** domain described below.

9. **MB2**, Mesozoic Basin tectono-geophysical domain #2. This domain encompasses a portion of the **Nixon Fork** (nx, fig. 8) lithotectonic terrane, which is part of the Central composite terrane (CCT, fig. 8), but mostly it corresponds to exposures of postaccretionary cover rocks (white areas of fig. 8). **MB2** is a domain of low magnetic relief and near-zero average residual magnetic values and of near-zero to slightly negative residual gravity values. Both of these geophysical signatures suggest the presence of a thick sedimentary section above the crystalline basement. A greater thickness of the postaccretionary rock section in **MB2** may be the primary difference between **MB2** and the adjacent **MB1** and **YT2** domains.

10. **YT1**, Yukon-Tanana tectono-geophysical domain #1. This domain encompasses a portion of the Yukon-Tanana lithotectonic terrane, which is the same as the Yukon composite terrane (YCT, fig. 8) within the study area. **YT1** is a domain of distinctive magnetic-anomaly patterns that consist of generally high average values with short-wavelength highs superimposed. These generally high average magnetic values reflect the crystalline makeup of this metamorphic terrane, and the short-wavelength highs may reflect gneissic plutons and scattered ophiolites. The geophysical distinctions between **YT1**, **YT2**, and **YT3** are relatively subtle and may relate, at least partly, to differences in aeromagnetic data quality over the three domains. **YT1** is a domain of zero to low positive values of residual gravity.

11. **YT2**, Yukon-Tanana tectono-geophysical domain #2. This domain encompasses a portion of the Yukon-Tanana lithotectonic terrane, which is the same as the Yukon composite terrane (YCT, fig. 8) within the study area, although much of the domain is obscured by postaccretionary cover rocks. It is a domain of low-amplitude magnetic highs and lows and distinctive "riftlike" en-echelon features in both the magnetic and gravity data. The geology of the domain is dominated by postaccretionary exposures, with some areas of crystalline Yukon-Tanana rocks mapped. Based on the "riftlike" patterns in the geophysical data for **YT2**, we speculate that the lower average magnetic values of **YT2** compared with **YT1** may reflect thinning of the **YT2** domain by postaccretionary extension.

12. **YT3**, Yukon-Tanana tectono-geophysical domain #3. This domain encompasses portions of the Yukon-Tanana terrane, which is the same as the Yukon composite terrane (YCT, fig. 8) within the study area, and several small, primarily clastic terranes of the Central composite terrane (Manley, White Mountains, and Wickersham). It is a domain of positive, low-relief magnetics and generally positive gravity. The northern boundary is defined by a string of sinuous high-amplitude magnetic anomalies, possibly suture zones containing ophiolitic rocks. The geophysical con-

tinuity of YT3 with Y1 suggests that the Yukon-Tanana crystalline basement extends beneath the (thin-skinned?) Central composite terrane in the northern part of YT3.

13. NS, Nowitna-Sischu tectono-geophysical domain. This domain encompasses portions of the Innoko terrane (in, fig. 8), which is part of the Oceanic composite terrane (OCT, fig. 8), and the Nixon Fork terrane (nx, fig. 8), which is part of the Central composite terrane (CCT, fig. 8). It is also partly covered by postaccretionary rocks (white areas, fig. 8). NS is a domain of high-amplitude, short-wavelength magnetic anomalies that are unlike those in surrounding domains. NS encompasses parts of the mapped Nowitna and Sischu Late Cretaceous to early Tertiary volcanic fields (fig. 2; Moll-Stalcup and Arth, 1989) and spans the region between them. The distinctive magnetic-anomaly pattern is probably caused by the andesites and rhyolites of these volcanic fields and their associated intrusions. Gravity anomalies in NS are not distinctive, although data coverage is very sparse.

14. CS, Complex Sutured tectono-geophysical domain. This domain encompasses all or parts of a number of miscellaneous small terranes (Livengood, Wickersham, White Mountains, and Tozitna) of the Central composite terrane (CCT, fig. 8) north of the Yukon-Tanana terrane. The geology exposed in these small terranes is quite variable and includes Paleozoic sedimentary, carbonate, and volcanic rocks. CS is a domain of variable magnetic character bounded by sinuous, high-amplitude magnetic anomalies (oceanic crust trapped in suture zones?). The domain also contains discontinuous domains of linear gravity gradients that probably mark boundaries of the smaller terranes. This domain was labeled as "Miscellaneous domains outside the study area" by Cady (1989). At the scale of this study, we have chosen to lump this domain together; at larger scale, the geophysical data would probably suggest further subdivision of this domain.

15. TZ1, Tozitna tectono-geophysical domain #1. This domain encompasses part of the Tozitna lithotectonic terrane (tz, fig. 8), which is part of the Oceanic composite terrane (OCT, fig. 8). TZ1 is a domain of discrete magnetic highs and lows, many with east-west trend, and is bounded on the south by a sinuous magnetic high (suture zone?). TZ1 is consistent with the Tozitna domain as defined by Cady (1989, 1991). The east-west-trending gravity and magnetic highs are caused by sills of layered gabbro and cumulus wehrlite (Cady, 1991). The high-amplitude magnetic character of this domain contrasts sharply with the quiet magnetic field of the TZ2 domain (discussed below), suggesting a lack of these magnetic source rocks in TZ2.

16. TZ2, Tozitna tectono-geophysical domain #2. This domain corresponds to (although not exactly) part of the Tozitna lithotectonic terrane (tz, fig. 8), which is part of the Oceanic composite terrane (OCT, fig. 8). TZ2 is a domain of very quiet magnetics with a near-zero mean re-

sidual value. A pair of gravity gradients define the eastern and western boundaries of the northern part of the domain. TZ2 differs geophysically from the high-amplitude magnetic patterns in TZ1. The difference in geophysical character suggests that if TZ2 is part of the Tozitna lithotectonic terrane, it does not contain the same highly magnetic sills present in TZ1.

17. RB, Ruby tectono-geophysical domain. This domain corresponds to the Ruby lithotectonic terrane (RB, fig. 8). RB is a domain of low-amplitude, short-wavelength magnetic highs and lows with a near-zero mean residual value. Although gravity-data coverage is poor in this area, sections of the boundary are marked by discontinuous gravity gradients. RB is consistent with the Ruby domain as defined by Cady (1989). Short-wavelength magnetic highs and lows in RB are caused by mid-Cretaceous plutons that tend to cause magnetic lows in the south and magnetic highs in the north (Cady, 1989). This pattern of magnetic pluton signature may be related to the composition of lower-crustal rocks (felsic in the south to more mafic in the north) that were melted in forming the plutons (Arth and others, 1989).

18. KN, Kanuti tectono-geophysical domain. This domain encompasses part of the Angayucham lithotectonic terrane (am, fig. 8), which is part of the Oceanic composite terrane (OCT, fig. 8). KN is a domain of large-amplitude magnetic highs and generally higher gravity than adjacent domains. The northern and southern boundaries are defined by contrasts in magnetic-anomaly patterns. The northern boundary of KN agrees in part with a gravity-gradient boundary. KN is consistent with the Kanuti domain as defined by Cady (1989). The geophysical patterns of this domain are caused by three suites of ultramafic rocks that include a cumulus plutonic suite, an underlying ultramafic tectonite, and sills of wehrlite and associated layered gabbro (Cady, 1989). KN is distinguished from a separate Angayucham domain north of 67°N. by its complexity and higher amplitude magnetic anomalies (Cady, 1989).

19. KY, Koyukuk tectono-geophysical domain. This domain encompasses the Koyukuk lithotectonic terrane (ky, fig. 8), which is part of the Togiak-Koyukuk composite terrane (TCT, fig. 8), and areas of postaccretionary cover rocks. KY is consistent with the Koyukuk domain as identified by Cady (1989) north of 65°N. and extends that domain to the south. KY is a prominent domain of large-amplitude, long-wavelength residual magnetic highs and lows and generally neutral to slightly positive residual gravity. The geophysical signature reflects the dense, magnetic rocks of a magmatic arc (Cady, 1989). Magnetic and gravity lows are caused by granitic plutons that intrude the arc, although aeromagnetic data resolution is insufficient to resolve much about the igneous variability within the domain (Cady, 1989).

20. LY, Lower Yukon Basin tectono-geophysical domain. This domain encompasses an area of postaccretionary



cover rocks. LY is consistent with the "Lower Yukon (sub) Basin" as identified by Cady (1989) north of 65°N, and extends that domain to the south. LY is a domain of low magnetic relief, in sharp contrast to the adjacent KY domain. LY has poor gravity coverage. Analysis of the low-amplitude aeromagnetic anomalies in LY suggests that the mid- and Late Cretaceous sedimentary rocks of the Nulato Hills (fig. 2) are underlain by magnetic basement at a depth of about 8 km (Zietz and others, 1959).

## SUMMARY

We analyzed new compilations of aeromagnetic and gravity data for interior Alaska in order to delineate geophysical boundaries. Comparison of these geophysical boundaries and previously mapped boundaries of lithotectonic terranes allowed us to identify 20 "tectono-geophysical domains." Most of these domains can be directly associated with lithotectonic terranes. In many cases, the domains trace the lithotectonic terrane boundaries as they extend beneath postaccretionary cover rocks. In other cases, the domains suggest modification or subdivision of previously mapped lithotectonic terranes. North of 65°N, our domains agree with the previously defined Koyukuk, Kanuti, Ruby, Tozitna, and Lower Yukon Basin geophysical domains of Cady (1989, 1991); We extend all but the Tozitna domain to the south in this study. South of the Denali-Farewell fault, our tectono-geophysical domains agree broadly with the geophysical characterization of lithotectonic terranes previously done by Griscom and Case (1982, 1983).

Our most important conclusions are the following:

1. Magnetic data trace the northward-dipping basement of the Chugach terrane.
2. Based on magnetic-anomaly patterns, the Peninsular lithotectonic terrane should be subdivided into two geophysical subunits (PE1 and PE2, fig. 9). PE2 has similar magnetic-anomaly patterns to the Wrangellia tectono-geophysical domain.
3. Magnetic anomaly patterns suggest subdivision of the Kahiltna lithotectonic terrane based on inferred basement-rock variation (KH1, KH2, fig. 9).
4. The Pingston and McKinley terranes (our PN tectono-geophysical domain) are distinct geophysically from the neighboring terranes, possibly as a result of higher metamorphic grade.
5. The Mesozoic basins of southwestern interior Alaska can be divided into two tectono-geophysical domains based on the inferred total thickness of the sedimentary section.
6. The Yukon-Tanana lithotectonic terrane is subdivided based on magnetic anomaly patterns into three separate domains that may represent differing postaccretionary tectonic histories (that is, possible extension in YT2 com-

pared with no extension in YT1) and continuation beneath thin-skinned terranes (YT3).

7. The Nowitna-Sischu tectono-geophysical domain outlines a connection between the Nowitna and Sischu volcanic fields.

8. The Complex Sutured tectono-geophysical domain is a lumped domain where sutures between smaller terranes are distinctive geophysically.

9. Two different parts of the previously mapped Tozitna lithotectonic terrane are very different geophysically (TZ1, TZ2).

10. Our tectono-geophysical domains show the southern continuation of Cady's Ruby, Koyukuk, Kanuti, and Lower Yukon domains to the south of 65°N.

*Acknowledgments.*— Esther Castellanos accurately and rapidly digitized numerous analog aeromagnetic maps for the data compilation. Pat Hill provided essential assistance in locating original data for aeromagnetic surveys.

## REFERENCES CITED

- Arth, J.G., Zmuda, C.C., Foley, N.K., Criss, R.E., Patton, W.W., Jr., and Miller, T.P., 1989, Isotopic and trace element variations in the Ruby batholith, Alaska, and the nature of the deep crust beneath the Ruby and Angayucham terranes: *Journal of Geophysical Research*, v. 94, p. 15,941-15,955.
- Barnes, D.F., 1972, Notes on processing and presentation of U.S. Geological Survey Alaskan gravity data: U.S. Geological Survey Open-File Report 72-16, 25 p.
- 1984, Digital elevation models improve processing of Alaskan gravity data, in Coonrad, W.L., and Elliot, R.L., eds., *The U.S. Geological Survey in Alaska: Accomplishments during 1981*: U.S. Geological Survey Circular 868, p. 5-7.
- Barnes, D.F., Mariano, J., Morin, R.L., Roberts, C.W., and Jachens, R.C., 1994, Incomplete isostatic gravity map of Alaska, in Plafker, George, and Berg, H.C., eds., *The geology of Alaska: Boulder, Colo., Geological Society of America, The Geology of North America*, v. G-1, pl. 9.
- Cady, J.W., 1989, Geologic implications of topographic, gravity, and aeromagnetic data in the northern Yukon-Koyukuk province and its borderlands, Alaska: *Journal of Geophysical Research*, v. 94, p. 15,821-15,841.
- 1991, Angayucham and Tozitna geophysical domains—geophysical and geochemical ties between parts of the Angayucham and Tozitna terranes, northern Alaska [abs.]: *Eos (American Geophysical Union Transactions)*, v. 72, p. 296.
- Cordell, Lindrieth, and McCafferty, A.E., 1989, A terracing operator for physical property mapping with potential field data: *Geophysics*, v. 54, p. 621-634.
- Decker, J., Bergman, S.C., Blodgett, R.B., Bundtzen, T.K., Clough, J.G., Coonrad, W.L., Gilbert, W.G., Miller, M.L., Murphy, J.M., Robinson, M.S., and Wallace, W.K., 1994, Geology of southwestern Alaska, in Plafker, George, and Berg, H.C.,

- eds., *The geology of Alaska: Boulder, Colo., Geological Society of America, The Geology of North America, v. G-1*, p. 285-310.
- Griscom, Andrew, and Case, J.E., 1982, Magnetic expression of geologic terranes in southern Alaska: Technical Program Abstracts and Biographies, 52d Annual Meeting and Exposition, October 17-21, 1982, Society of Exploration Geophysicists, p. 230-232.
- 1983, Magnetic expression of geologic terranes in southern Alaska: *Geophysics*, v. 48, p. 444-445.
- International Association of Geodesy, 1971, *Geodetic Reference System 1967: International Association of Geodesy Special Publication*, v. 3, 116 p.
- Meyer, J.F., Jr., Racic, L.J., and Saltus, R.W., in press, The compilation and application of aeromagnetic data for hydrocarbon exploration in interior Alaska, *in* Gibson, R., ed., *Gravity and magnetic case histories: American Association of Petroleum Geologists special volume*.
- Meyer, J. F., Jr., and Saltus, R.W., 1995, Merged aeromagnetic map of interior Alaska: U.S. Geological Survey GP Map, GP-1014, scale 1:500,000, 2 sheets.
- Meyer, John F., Jr., Saltus, R.W., Barnes, D.F., and Morin, R.L., 1996, Bouguer gravity maps of interior Alaska: U.S. Geological Survey GP Map GP-1016, scale 1:500,000, 2 sheets.
- Moll-Stalcup, E., and Arth, J.G., 1989, The nature of the crust in the Yukon-Koyukuk province as inferred from the chemical and isotopic composition of five Late Cretaceous to early Tertiary volcanic fields in western Alaska: *Journal of Geophysical Research*, v. 94, p. 15,989-16,020.
- Morelli, C., 1974, The international gravity standardization net 1971: *International Association of Geodesy Special Publication*, v. 4, 194 p.
- Nokleberg, W.J., Moll-Stalcup, E.J., Miller, T.P., Brew, D.A., Grantz, A., Reed, J.C., Jr., Plafker, G., Moore, T.E., Silva, S.R., and Patton, W.W., Jr., 1994, Tectonostratigraphic terrane and overlap assemblage map of Alaska: U. S. Geological Survey Open-File Report 94-194, scale 1:2,500,000, 1 map sheet with 53 p. pamphlet.
- Plafker, G., and Berg, H.C., 1994, Overview of the geology and tectonic evolution of Alaska, in Plafker, George, and Berg, H.C., eds., *The geology of Alaska: Boulder, Colo., Geological Society of America, The Geology of North America, v. G-1*, p. 989-1021.
- Silberling, N.J., Jones, D.L., Monger, J.W.H., Coney, P.J., Berg, H.C., and Plafker, George, 1994, Lithotectonic terrane map of Alaska and adjacent parts of Canada, in Plafker, George, and Berg, H.C., eds., *The geology of Alaska: Boulder, Colo., Geological Society of America, The Geology of North America, v. G-1*, pl. 3, scale 1:2,500,000.
- Simpson, R.W., Jachens, R.C., Blakely, R.J., and Saltus, R.W., 1986, A new isostatic residual gravity map of the conterminous United States with a discussion on the significance of isostatic residual anomalies: *Journal of Geophysical Research*, v. 91, p. 8348-8372.
- Zietz, I., Patton, W.W., Jr., and Dempsey, W.J., 1959, Preliminary interpretation of total intensity aeromagnetic profiles of the Koyukuk area, Alaska: U.S. Geological Survey Open-File Report 59-501.

Reviewers: Dave Campbell, Carol Finn, and John Cady

# Provenance of the Carboniferous Nuka Formation, Brooks Range, Alaska: A Multicomponent Isotope Provenance Study with Implications for Age of Cryptic Crystalline Basement

By Thomas E. Moore, Sidney Hemming, and Warren D. Sharp

## ABSTRACT

Arkose, arkosic limestone, and limestone of the Carboniferous Nuka Formation are present as thin thrust imbricates, fault slivers, and olistoliths along the length of the central and western Brooks Range at the highest structural levels of the Arctic Alaska terrane. Although the composition, depositional facies, and texture of the Nuka Formation are consistent with derivation from a local granitic source, the allochthonous position of the Nuka precludes identification of its source area. Possible granitic source areas for the Nuka in the Arctic Alaska terrane are sparse Late Proterozoic and Early Devonian granitic rocks in the southern Brooks Range, but derivation of the Nuka from these rocks would require structural restoration of the Nuka along presently unrecognized out-of-sequence faults.

To help identify the nature of the source area of the Nuka Formation, a combination of U-Pb zircon and rutile geochronology, K-Ar geochronology of potassium feldspar, Pb isotopic composition of detrital quartz and feldspar grains, and Nd and Pb isotopic compositions and rare earth element patterns of whole-rock samples of the Nuka were investigated from samples collected at its type locality in the northern Brooks Range. These data indicate that the arkosic detritus in the Nuka Formation was derived from about 2.0–2.1 Ga granitic sources with mantlelike initial Pb and Nd isotopic compositions. Discordant U-Pb ages of sparse, dark-brown zircon grains suggest that country rocks of the granitic rocks are at least as old as 2.2 Ga. A near-concordant U-Pb age for detrital rutile and K-Ar ages from detrital feldspar suggest that the subsequent thermal history of the Nuka and its source did not exceed about 400°C since 1.9 Ga and 200°C since 1.2–1.8 Ga. Detrital quartz grains, combined with detrital feldspar grains and whole-rock samples, provide a Pb-Pb age of  $1,954 \pm 56$  Ma, supporting the interpretation that the Nuka was derived from an Early Proterozoic region with a limited age range.

The isotopic data indicate that the Nuka Formation was not derived from a source area in the presently exposed rocks of the southern Brooks Range. Although a

source in the Arctic Alaska terrane cannot be ruled out, the data support the hypothesis that the Nuka Formation was derived from a continental land mass located to the south of the Arctic Alaska margin (present coordinates) during the middle Carboniferous. Crust of 2.0–2.1 Ga age is rare or absent in both autochthonous and allochthonous parts of western North America; only allochthonous granitic rocks in the Kilbuck and Idoon terranes of southwestern Alaska share similar age and isotopic characteristics. Recent paleogeographic models suggest that possible source areas for the Nuka may have been in the Australian or Siberian cratons that were rifted away from North America, leaving stranded crustal fragments that provided granitic detritus to the Nuka.

## INTRODUCTION

The Brooks Range of northern Alaska (fig. 1) is a west-trending north-vergent fold-and-thrust belt that comprises the northernmost mountain range of the North American Cordillera. The fold belt resulted from south-dipping (present coordinates) A-type subduction (Bally, 1975) of the continental Arctic Alaska terrane beneath the oceanic Angayucham terrane during the Jurassic and Early Cretaceous (Box, 1985; Mayfield and others, 1988; Moore and others, 1994a). Oceanic crustal rocks (Angayucham terrane) preserved at the highest structural levels may represent the underpinnings and (or) forearc region of a Jurassic to Early Cretaceous island arc (Harris, 1988; Moore and others, 1994a) (fig. 2). These oceanic rocks are structurally underlain by imbricated Devonian to Lower Cretaceous sedimentary rocks of the continental Arctic Alaska terrane. Structurally higher imbricates of the Arctic Alaska terrane are principally siliceous basinal sequences that were distal to sources of continental detritus, whereas structurally lower imbricates consist of siliciclastic and carbonate strata that were relatively proximal to sources of continental detritus. Simple restorations of these rocks indicate that they formed a south-facing passive continental margin succession that

is inferred to have developed following rifting along the southern margin of the Arctic Alaska terrane in the Devonian (Moore and others, 1994a).

A major enigma in reconstruction of the Mississippian to Early Cretaceous paleogeography of the Arctic Alaska terrane is the source region for the arkosic strata of the

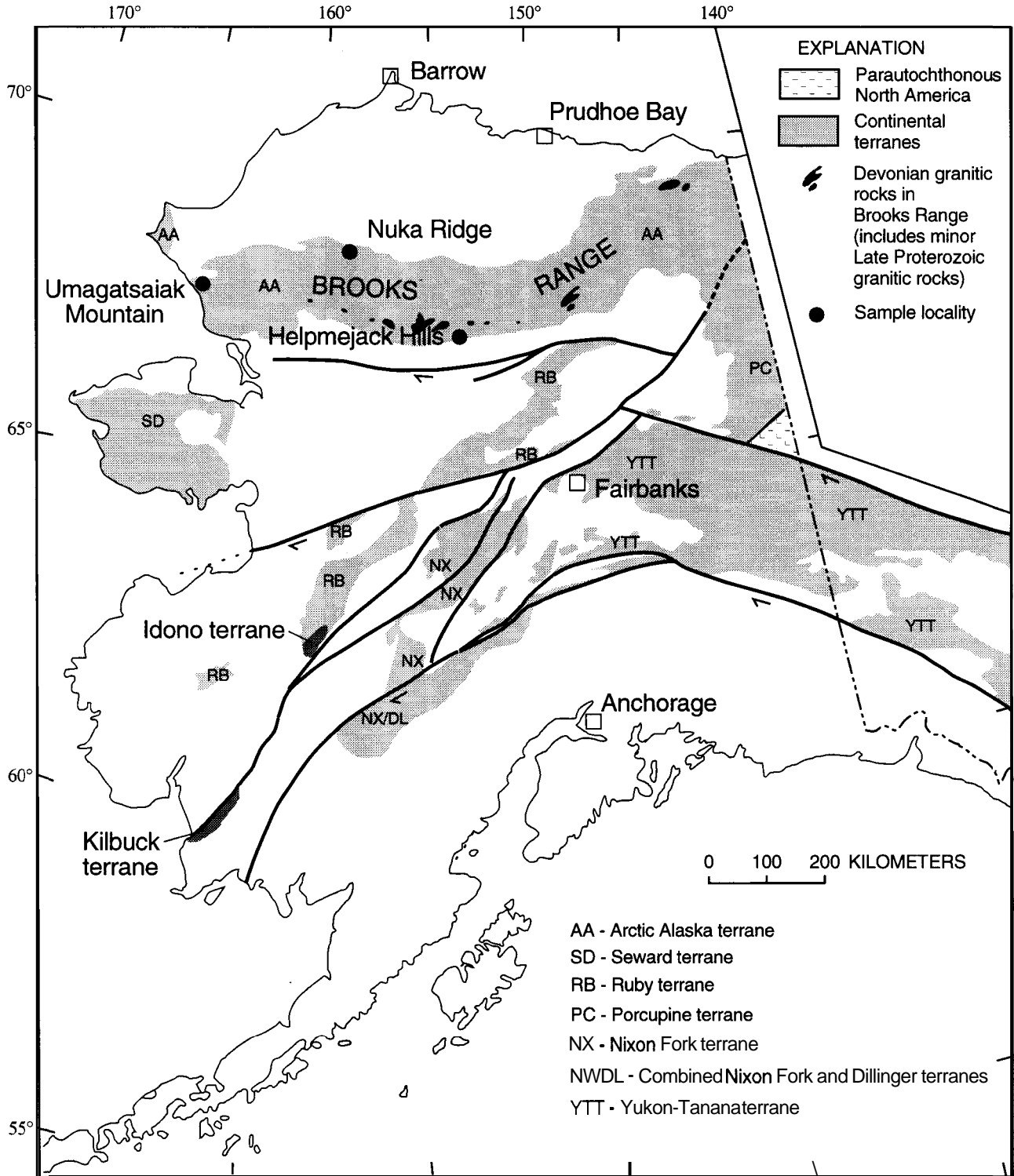
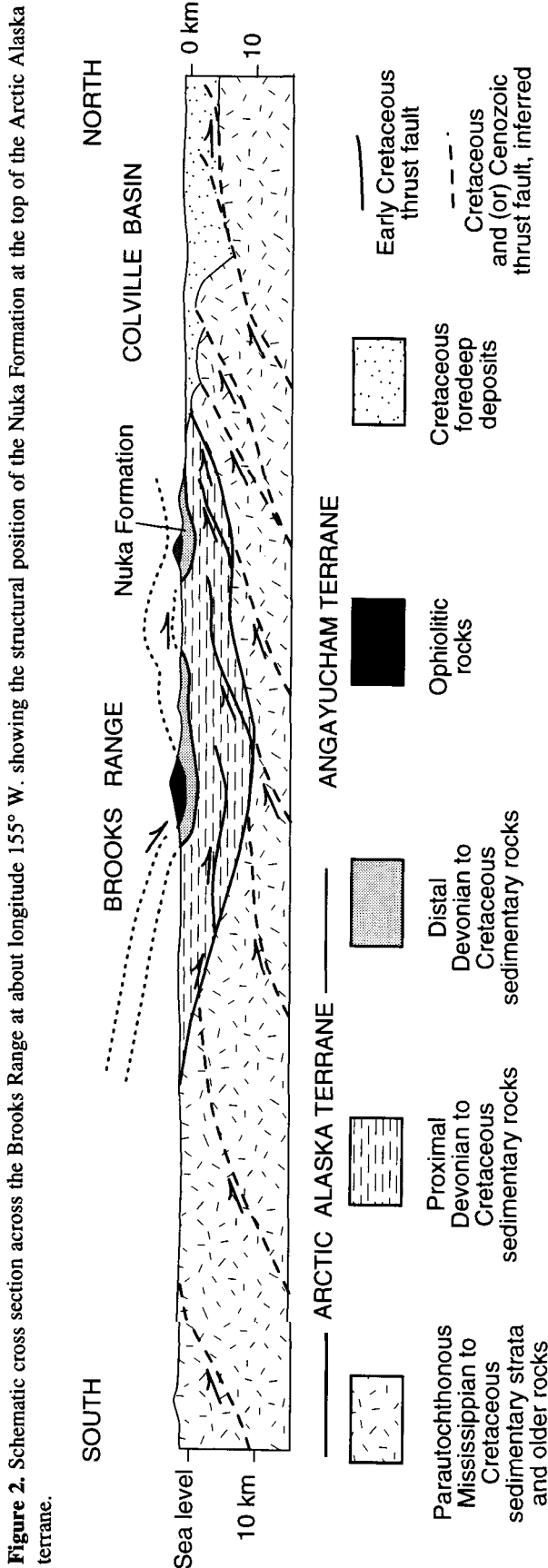


Figure 1. Map of Alaska showing the location of sample localities at Nuka Ridge and other locations mentioned in the text. The shaded areas show terranes with known evidence for Proterozoic crust; the Kilbuck and Idono terranes have yielded 2.0–2.1 Ga zircon crystallization ages (Box and others, 1990; Moll-Stalcup and others, 1996). Terranes discussed in text are shown for reference.

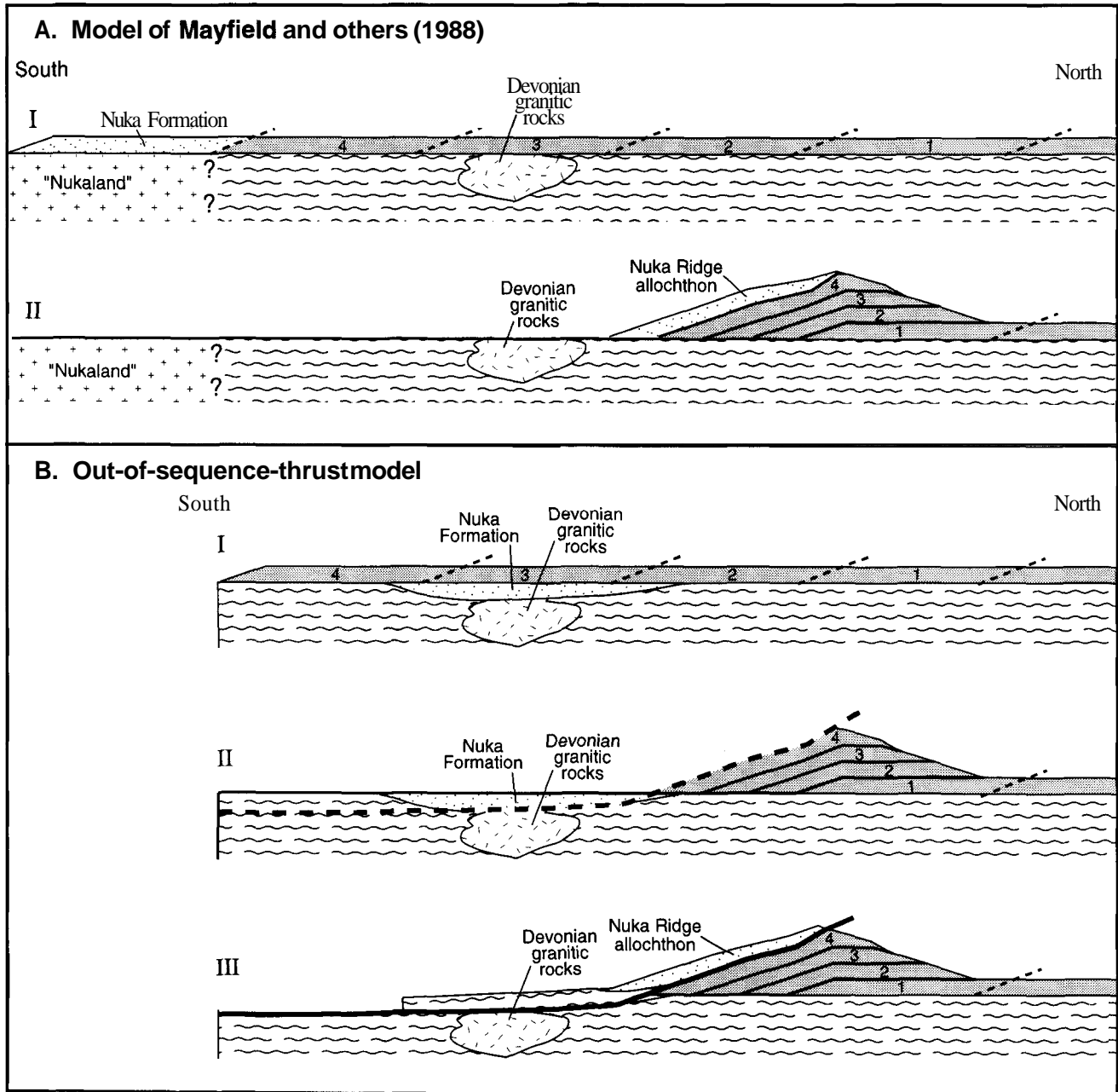


Mississippian and Pennsylvanian(?) Nuka Formation. This unit, less than 300 m thick, forms a distinctive part of thin, allochthonous, siliceous sequences and fault slivers preserved at the highest structural levels of the Arctic Alaska terrane (fig. 2). It is the only arkosic unit known in northern Alaska and consists of fine- to coarse-grained sandstone, minor granule conglomerate, and limestone deposited primarily in shallow- to deep-marine and possibly nonmarine environments (Moore and others, 1994a). The locally coarse grain size and sedimentary facies, coupled with the arkosic composition of the Nuka, indicate that the Nuka was derived from a nearby granitic source area, but its present allochthonous position prevents identification of that source. The only possible source areas exposed in northern Alaska are the Late Proterozoic and Devonian granitic rocks in the southern and northeastern Brooks Range (Dillon and others, 1980, 1987; Karl and Aleinikoff, 1990).

Identification of the source region of the arkosic sandstones of the Nuka Formation would help constrain Carboniferous paleogeographic reconstructions and the kinematic history of the allochthonous sedimentary rocks of the Arctic Alaska terrane. Mayfield and others (1988) have reconstructed the paleogeography of Mississippian to Jurassic strata of the Arctic Alaska terrane in the western Brooks Range by a simple southward **unstacking** of its allochthonous sequences (fig. 3A). Based on its high structural level and regional extent, they suggested that the Nuka Formation provides evidence of a hypothetical southern area of granitic **highlands** ("Nukaland"). The facies associations in the Nuka Formation are consistent with its deposition in fan-delta settings within grabens or pull-apart basins on a block-faulted continental borderland (Moore and others, 1994a). If the restoration of Mayfield and others (1988) is correct, the age of the granitic source region for the Nuka Formation probably would be different from the age of the granitic rocks of the southern Brooks Range because the Nuka is restored to a paleogeographic location widely separated from that of the granitic rocks. If, on the other hand, the Nuka Formation was derived from Late Proterozoic or Devonian granitic rocks of the southern Brooks Range, it would require that the Nuka was transported from structurally lower levels of the Arctic Alaska terrane to its present high structural position, probably along presently unidentified out-of-sequence thrust faults. In figure 3B, we provide a hypothetical model that shows this restoration, which implies a more complicated structural history than that proposed by Mayfield and others (1988). Oldow and others (1987) and Till and others (1988) have recognized **out-of-sequence** faults in the southern Brooks Range, providing support for this alternative hypothesis. An **out-of-sequence**-thrust model would require less total shortening than the model of Mayfield and others (1988), but this model, at least as presently understood, does not provide an explanation for the presence of Permian to Jurassic rocks in the Nuka Ridge allochthon (fig. 4).

This paper reports the results of U-Pb analysis of **detrital** zircon grains from sandstone of the Nuka Formation and thereby tests the paleogeographic reconstructions for northern Alaska. We also provide detrital **rutile** U-Pb data, Nd and Pb isotopic data, and feldspar **K-Ar** data that help

constrain the petrogenesis and cooling history of the granitic source region of the Nuka Formation. These data show that the granitic rocks of the southern Brooks Range could not have provided the granitic detritus that composes the Nuka Formation. The isotopic data instead point to source



**Figure 3.** Models for emplacement of the Nuka Formation during the Brookian orogeny. A, Model of Mayfield and others (1988) showing the Nuka Formation as deposited adjacent to southern granitic highlands ("Nukaland") (I) and later **emplaced** at high structural levels along a northward-propagating thrust system (II). B, An alternative model, proposed here, showing the Nuka Formation as deposited adjacent to Devonian granitic rocks now exposed in the southern Brooks Range (I) and later **emplaced** at high structural levels along out-of-sequence faults (II and III) following large-scale thrusting as proposed by Mayfield and others (1988). Numbers indicate relative positions of allochthons before and after thrusting.

terraces that once were exposed along the margin of North America and may now be found in cratonal areas of Australia, Antarctica, or Siberia.

## U-Pb, Nd, AND REE ANALYSIS

### LOCATION AND LITHOLOGY OF SAMPLES

Two samples of coarse-grained sandstones from the Nuka Formation were collected at its type section at Nuka Ridge (Misheguk Mountain quadrangle) in the western Brooks Range for U-Pb, Pb, and Nd isotopic analysis (fig. 1). The Nuka Formation (Tailleur and Sable, 1963; Tailleur and others, 1973, 1977) at the type area at Nuka Ridge is underlain by the Mississippian Kayak Shale (fig. 4) and is overlain by Pennsylvanian to Permian chert and siliceous shale of the Etivluk Group (Mayfield and others, 1984), which locally contains arkosic silt and radiolarians (figs. 4, 5). The entire succession is about 700 m thick and is repeated by imbrication along detachments in the Kayak Shale and overlying Jurassic to Lower Cretaceous foredeep strata (Okpikruak Formation; fig. 5). The basement of this succession is not exposed. Conodont color alteration indices (CAI) from the Nuka Formation at Nuka Ridge are 1.5–2 (Mayfield and others, 1984), which indicate that postdepositional diagenesis of the Nuka occurred at temperatures less than about 90°C (Epstein and others, 1977).

The Nuka Formation at Nuka Ridge consists of about 250 m of interbedded arkose, arkosic limestone, and limestone. The sandstone is massive to medium bedded, fine to very coarse grained, and locally contains minor interbed-

ded granule conglomerate. The coarse and angular grains and granitic composition lend a gruslike appearance to these sandstones (fig. 6A). In most sections of the Nuka Formation in its type area, shallow-marine sedimentary features are common; these include herringbone cross-stratification; low-angle, inclined planar lamination; glauconitic zones; and beds rich in megafossils (for example, echinoderms, brachiopods, and bryozoans; Moore and others, 1994a). Some sections lack fossils and have a distinct red color, which suggests a nonmarine origin (Moore and others, 1994a).

Two samples, each approximately 10 kg, were collected for U-Pb zircon geochronology. Sample DT-84-14 (N. 68°37'46", W. 159°12'34") was collected from parallel-stratified sandstone in the lower of two well-exposed, 20-m-thick, fining- and thinning-upward, shallow-marine sandstone bodies in the fifth highest of six asymmetrically folded thrust imbricates within the Nuka Ridge allochthon mapped by Mayfield and others (1984) (fig. 5). Sample DT-84-15 (N. 68°38'00", W. 159°12'29") is from a boulder of massive granule conglomerate, collected from float derived from the same sandstone interval as DT-84-14, about 250 m to the north. Point counts of thin sections indicate that both samples consist almost entirely of granitic detritus and consist of approximately 25–50 percent quartz, 30–50 percent potassium feldspar, 1–5 percent plagioclase, and as much as 42 percent carbonate lithic grains (fig. 6B; table 1). Sparse lithic grains are mostly granitic rock fragments, but rare quartzite and quartz-mica schist fragments are also present. The point counts indicate that sample DT-84-14 is an arkosic limestone, whereas no carbonate detritus or cement was observed in sample DT-84-15.

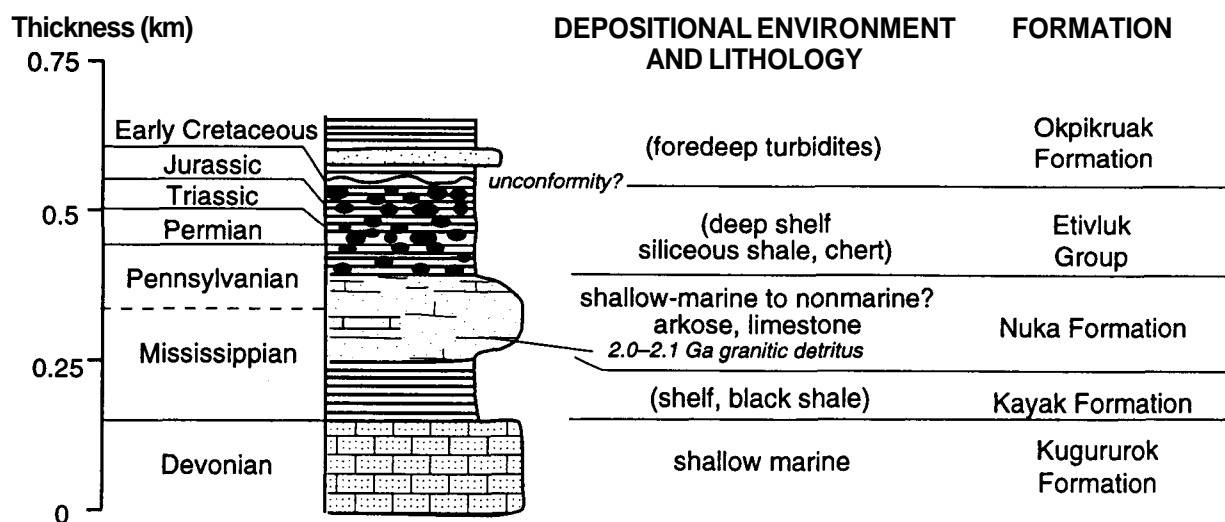


Figure 4. Generalized stratigraphic section of the Nuka Ridge allochthon.

**ANALYTICAL PROCEDURE**

**MINERAL SEPARATION AND SORTING**

Both samples were crushed and separated using a wiffly table and heavy liquids at the laboratory of Donald L. Turner at the University of Alaska and magnetically separated at the State University of New York, Stony Brook. Zircons were hand-picked from the nonmagnetic heavy-mineral separates and are by far the most abundant heavy mineral

in both samples. Rutile is also present but is less abundant. No monazite or xenotime was observed (consistent with rare earth element abundances reported below). In general, the zircons are euhedral with both prism and pyramid faces and aspect (length-to-width) ratios of about 2:1 to 4:1. Most of the grains (greater than 90 percent) are colorless; others are very light pink or yellow. In an effort to identify age diversity within the zircon population, samples were hand-picked and grouped on the basis of color and shape (table

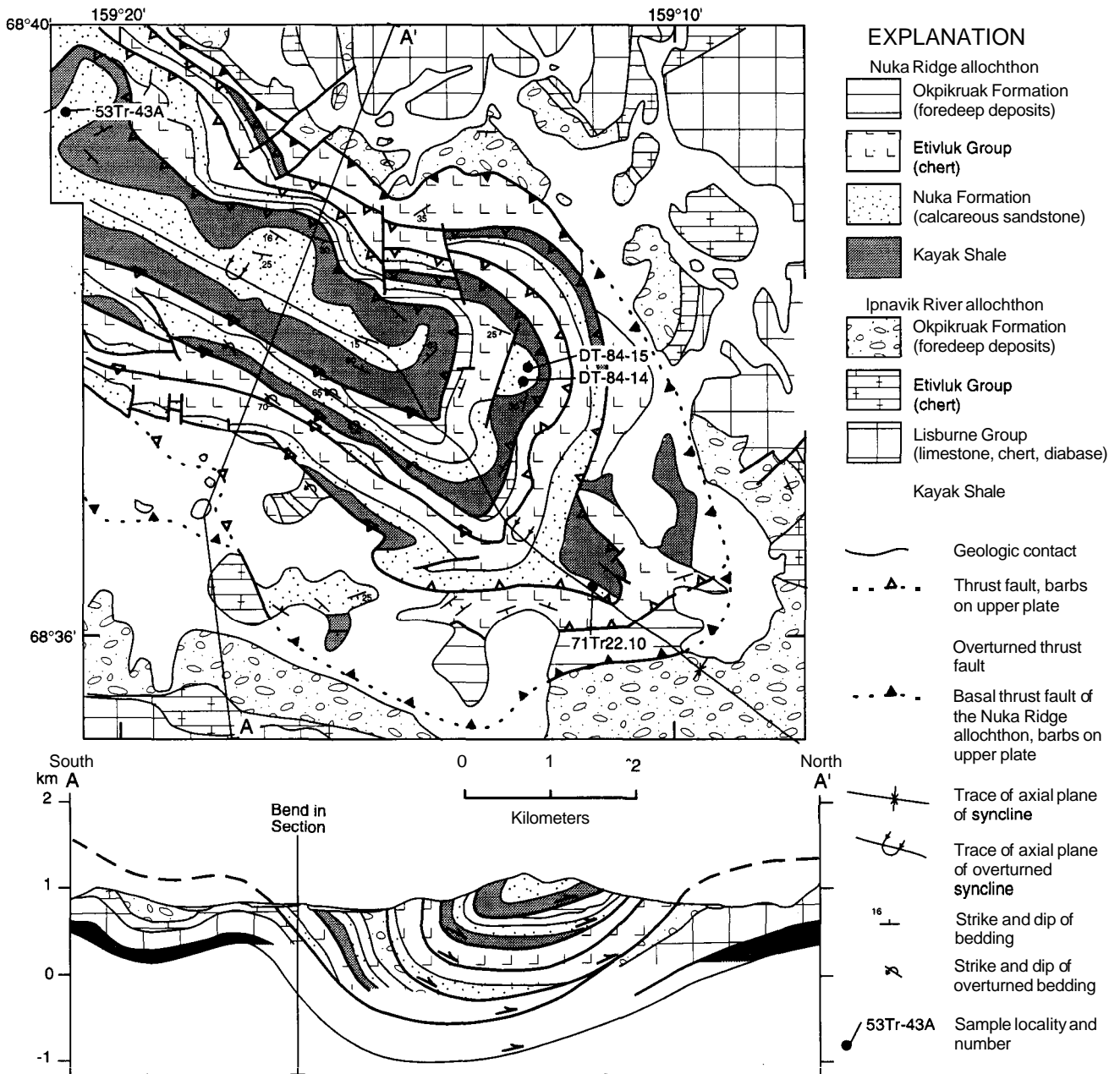


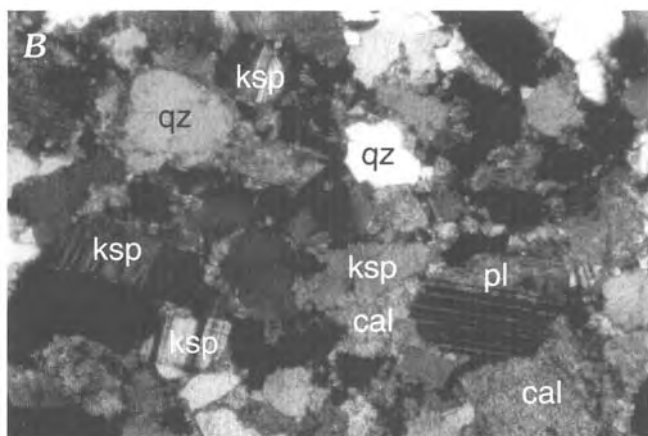
Figure 5. Geologic map of the Nuka Ridge area showing sample locations. Geology from Mayfield and others (1984).



2). Although fraction 5 (table 2) is an especially large, single subhedral crystal with a pitted surface, the remainder of the zircons are much smaller and were consequently analyzed as **multigrain** fractions. Portions of the bulk zircon populations of both samples (fractions 3, 10; table 2) were abraded (method of Krogh, 1982). Rutile was hand-picked from the magnetic heavy-mineral separate. Most rutile grains are well rounded; they have appearances that range from bright, translucent orange to opaque black. Quartz and feldspar were picked from a small sample of DT-84-14, which was crushed in such a way that many grains were separated but not broken.

#### COMMON Pb AND U-Pb ISOTOPIC ANALYSIS

After the initial hand-picking and weighing, all handling was conducted in a laminar flow hood. Zircon and rutile samples were dissolved in teflon bombs using HF-HNO<sub>3</sub> and prepared according to the zircon method of Krogh (1973), using 0.5 mL of 100- to 200-mesh AG1-X8



**Figure 6.** A, Photo of Nuka Formation sandstone at sample locality DT-84-15. B, Photomicrograph of sample DT-84-14 showing K-feldspar-rich, arkosic composition of Nuka Formation. Long dimension of photomicrograph is 2.7 mm. Abbreviations: qz, quartz; ksp, K-feldspar; pl, plagioclase; cal, calcite.

**Table 1.** Point count, rare earth element, and Nd isotopic data from the Nuka Formation at Nuka Ridge

[Counted constituents are reported in percent, with 300 counts per thin section. Carbonate is mostly calcite with subequal amounts of grains and cement. Rare earth element concentrations are in parts per million.  $f_{Sm/Nd}$  is the deviation in  $^{147}Sm/^{144}Nd$  from CHUR (chondritic uniform reservoir).]

Sample	DT-84-14	DT-84-15
K-feldspar	27	50
Plagioclase	5	1
Quartz	26	49
Carbonate	42	--
La	7.75	6.80
Ce	9.35	8.16
Nd	6.07	4.08
Sm	1.11	.691
Eu	.374	.389
Gd	1.03	.601
Dy	.914	.513
Er	.528	.373
Yb	.480	.375
Eu/Eu*	1.07	1.84
Ce/Ce*	.625	.680
$^{147}Sm/^{143}Nd$	.117	.102
$f_{Sm/Nd}$	-.404	-.479
$^{143}Nd/^{144}Nd$	.511850	.511676
$\epsilon_{Nd(0)}$	-15.2	-18.7
$\epsilon_{Nd(350)}$	-11.8	-14.6
$\epsilon_{Nd(2050)}$	+5.59	+6.05
$T_{CHUR}$ (Ga)	1.50	1.55

resin. Pb blank corrections were 300 pg $\pm$ 30 percent for analyses 1–8, 11 and 12. In cases where the total common Pb was less than 300 pg, all common Pb was subtracted as blank. When the rutile sample and fraction 10 were analyzed, the procedural blank was approximately 50 pg. The isotopic composition of the blank in the lab is estimated to be  $^{206}Pb/^{204}Pb=18.055$ ,  $^{207}Pb/^{204}Pb=15.6591$ , and  $^{208}Pb/^{204}Pb=37.865$ . The Stacey and Kramers (1975) model Pb curve for the appropriate Pb-Pb age was used for the initial Pb corrections, and a generous uncertainty of  $\pm 0.5$  for  $^{206}Pb/^{204}Pb$  and  $\pm 0.45$  for  $^{207}Pb/^{204}Pb$  was used, which is half the difference between the model curves for upper and lower crust (Doe and Zartman, 1979). Zircon data were corrected using the Stacey and Kramers (1975) model rather than the detrital feldspar data in an attempt to keep the provenance information from these two data sets as independent as possible.

Table 2. Detrital zircon and rutile data from the Nuka Formation

[Analytical uncertainties shown in parentheses]

Fraction <sup>1</sup>	Fraction type	Sample	Total Pb (ng)	Sample size	Measured <sup>206</sup> Pb/ <sup>204</sup> Pb	Blank-corrected <sup>206</sup> Pb/ <sup>204</sup> Pb	<sup>208</sup> Pb*/ <sup>206</sup> Pb*	<sup>207</sup> Pb*/ <sup>206</sup> Pb* age (Ma)	<sup>206</sup> Pb*/ <sup>238</sup> U age (Ma)	<sup>207</sup> Pb*/ <sup>235</sup> U age (Ma)
1	Bulk	DT-84-15	382	8.95 mg	2,432(28)	2,549	0.1440	0.12493(19) 2,028(3)	0.14172(38) 854	2.441(78) 1,255
2	Bulk	DT-84-14	416	7.7 mg	5,989(196)	6,809	.1424	.12465(15) 2,024(2)	.17585(53) 1,044	3.022(99) 1,413
3	Abraded	DT-84-15	120	2.04 mg	4,377(188)	5,425	.1474	.12462(18) 2,023(2)	.19518(246) 1,149	3.354(43) 1,494
4	Slightly rounded	DT-84-14	17.2	60 xls	1,985(40)	5,059	.1528	.12653(18) 2,050(2)	.18927(62) 1,117	3.302(121) 1,482
5	Large, pitted	DT-84-15	1.3	1 xl	174.3(6)	786	.2148	.12854(75) 2,078(10)	.24359(145) 1,405	4.317(41) 1,697
6	Pale pink	DT-84-14	7.6	30 xls	1,748(38)	5,821	.1462	.12653(20) 2,050(2)	.25974(84) 1,488	4.531(17) 1,737
7	Pale pink	DT-84-14	5.3	20 xls	1,143(37)	3,625	.1415	.12570(40) 2,039(6)	.19437(51) 1,145	3.369(15) 1,497
8	Dark-brown fragments	DT-84-14	2.8	2 xls	1,250(18)	5,009	.1246	.14086(20) 2,238(3)	.19347(52) 1,140	3.757(12) 1,584
9	Rutile, orange fragments	DT-84-15	.285	3 xls	108.0(5)	3,077	.0044	.11648(105) 1,903(16)	.33562(357) 1,866	5.390(91) 1,883
10	Abraded	DT-84-14	9	67 xls	782(2)	848	.1460	.12527(44) 2,033(9)	.25979(71) 1,488	4.487(25) 1,729
11	With inclusions	DT-84-14	17.5	50 xls	454.7(5)	579	.1542	.12433(80) 2,019(17)	.17877(55) 1,060	3.064(24) 1,424
12	<200 mesh, abraded	DT-84-15	.45	20 xls	119(1.6)	61,604	.1363	.12390(199) 2,013(34)	.34560(385) 1,913	5.904(134) 1,962

<sup>1</sup> All fractions are zircon except fraction 9. Zircon fractions are clear and colorless, euhedral, greater than 200 mesh, and nonmagnetic at 1.8 A with a 15° side tilt and 2° front tilt, except where otherwise noted. Rutile was hand-picked from magnetic fraction. Abbreviation: xls, crystals.

Large single feldspar grains (about 10 mg each) were cleaned vigorously with hot 6N HCl and 6N HNO<sub>3</sub>, and then leached with concentrated HF for approximately 10 min. These procedures are estimated to remove less than 50 percent of the grain. Following leaching, the remaining feldspar sample was dissolved in HF, and the Pb was separated using 0.5 mL of 200- to 400-mesh AG1-X8 resin, with three 2N HCl wash steps of 5 column volumes and two complete column passes. The Pb from the procedural blank was approximately 100 pg, and the Pb from the feldspar was greater than 50 ng. The resulting sample-to-blank ratio of <sup>206</sup>Pb/<sup>204</sup>Pb yields a measured ratio less than 0.1 percent different for <sup>206</sup>Pb/<sup>204</sup>Pb and less than 0.02 percent different for <sup>207</sup>Pb/<sup>204</sup>Pb, and no blank corrections were made.

Quartz grains were cleaned in 2N HCl, and dissolved in HF-HNO<sub>3</sub> in 3 mL Savillex vials on a hot plate at about 100°C. U and Pb separation procedures were the same for quartz as for zircon and rutile but were scaled down to 0.1-mL resin volumes and used 200- to 400-mesh resin. The Pb blank for quartz analyses was 35±15 pg.

Whole-rock powders (about 0.1 g) were dissolved in bombs in HF-HNO<sub>3</sub>, dried down with HCl, and redissolved in a bomb with 12N HCl. Column procedures were the same as for feldspars but with three column passes.

Pb isotopic compositions and Pb and U concentrations were determined with a NBS design, 12-inch single-sector Nier-type mass spectrometer. Pb was run using the H<sub>3</sub>PO<sub>4</sub>/silica gel method (Cameron and others, 1969) at filament temperatures between 1,200°C and 1,500°C. The average ratios obtained from 10 runs of the NBS Pb standard 982 throughout this study were (2-sigma deviations) as follows: <sup>208</sup>Pb/<sup>206</sup>Pb=0.99853±0.1 percent; <sup>207</sup>Pb/<sup>206</sup>Pb=0.46669±0.043 percent; and <sup>206</sup>Pb/<sup>204</sup>Pb=36.653±0.1 percent. Samples were corrected for mass fractionation of 0.1±0.02 percent per amu (atomic mass unit). U samples were run with H<sub>3</sub>PO<sub>4</sub> on a single outgassed Re filament precoated with a graphite slurry, followed by a second coat of graphite. U was analyzed at filament temperatures of about 1,750°C to 1,850°C. The average <sup>235</sup>U/<sup>238</sup>U ratio for 10 runs of NBS standard U-930 during the course of this study were 17.381±0.2 percent (2-sigma deviations). Uncertainties in the age (2-sigma deviations) were calculated using the program of Ludwig (1980).

#### Nd ISOTOPIC AND RARE EARTH ELEMENT ANALYSIS

Whole-rock powders (0.2 g) were fused with LiBO<sub>2</sub> flux at 1,100°C in high-purity graphite crucibles for 15 min. Fused samples were dissolved in 30 mL of 1N HNO<sub>3</sub>, precipitated using ammonium hydroxide, and centrifuged. The precipitates were rinsed with distilled water and centrifuged again. Separate fusions were made for Nd isotopic composition (IC) and rare earth element (REE) isotope dilution (ID) analyses. ID samples were combined with a

mixed REE spike. REE were separated from other elements using AG-50-1X8 resin with 2N HCl and 4N HNO<sub>3</sub> wash steps and with 4N HNO<sub>3</sub> elution. The REE were separated into groups using methylactic acid as described in Stern and Hanson (1991).

Nd was loaded on a Re side filament in 2N HNO<sub>3</sub> and run with a double Re filament assembly on a Finnigan MAT 262. Data were collected in multicollector static mode. Ratios were normalized with a linear fractionation correction, using <sup>146</sup>Nd/<sup>144</sup>Nd=0.7219, and corrected to a value consistent with the <sup>143</sup>Nd/<sup>144</sup>Nd standard of La Jolla equal to 0.511865. During the interval in which these data were collected, the 2-sigma uncertainty on the La Jolla standard runs was 0.005 percent.

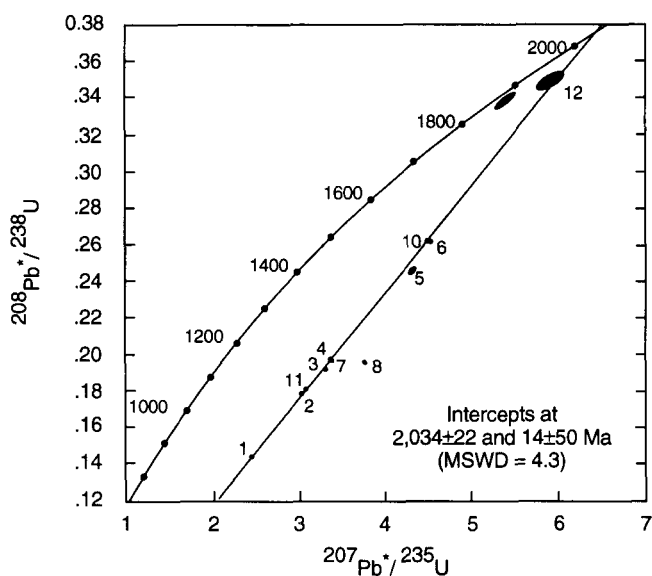
The REE were analyzed by isotope dilution on an NBS design, 6-inch single-sector Nier-type mass spectrometer. All REE cuts were taken up in 2N HNO<sub>3</sub>. Gd was loaded with TaO<sub>2</sub> slurry and phosphoric acid on a Re center filament and run as an oxide. Nd, Sm, and Eu were loaded on a Re side filament on the same assembly as Gd and run as metals. La and Ce were loaded with silica gel and phosphoric acid on a Re center filament and run as oxides at source vacuums at or lower than 2×10<sup>-7</sup> torr to reduce baseline effects on the La analysis (McDaniel and others, 1994). Yb, Er, and Dy were loaded on a Re side filament on the same assembly as La and Ce and run as metals.

## RESULTS

### ZIRCON

Multigrain fractions of nonmagnetic, clear zircons from both samples are strongly discordant (fig. 7) but yield identical Pb-Pb ages of 2,028±3 and 2,024±2 Ma (fractions 1, 2; table 2). The abraded fraction from sample DT-84-15 (fraction 3; table 2) is less discordant than the unabraded fraction (fraction 1; table 2), although it yielded an identical Pb-Pb age of 2,023±2 Ma. All three of these bulk samples, which were the only ones large enough to weigh, have U concentrations of 270–280 ppm. The small abraded separate from DT-84-14 (fraction 10; table 2) yielded a Pb-Pb age of 2,033±9 Ma. These four analyses span an approximately linear array from 27 to 58 percent discordant and yield a model 2 fit (Ludwig, 1988) with an upper-intercept age of 2,034±22 Ma, a lower intercept of 14±50 Ma, and a MSWD (mean standard weighted deviation) of 4.2. This line is plotted on figure 7 for reference. If these data were from a single granite, the upper intercept would be interpreted as the crystallization age and the lower intercept would be interpreted as a result of recent Pb loss. However, given the large discordance and the potential for mixed sources in a sedimentary rock, it is possible that the similarity of these ages resulted from a fortuitous mixing of different age sources.

In an attempt to test the homogeneity of the source age of the detrital zircons in the Nuka Formation, small fractions of zircon were selected by hand-picking on the basis of color and shape to represent possible diverse components of the zircon population (fractions 4–8, 10–12; table 2). These smaller fractions are all more concordant than the unabraded bulk fractions. A clear, colorless euhedral fraction (fraction 12; table 2), the predominant type of zircon, yielded a Pb-Pb age of  $2,013 \pm 34$  Ma. A rounded fraction (fraction 4; table 2) of pale-yellow and pale-pink zircons yielded a Pb-Pb age of  $2,050 \pm 2$  Ma. A single large, pitted but euhedral zircon (fraction 5; table 2) yielded a Pb-Pb age of  $2,078 \pm 10$  Ma. The light-pink fractions seem to be gradational in appearance with the more abundant colorless population. In some cases, the zircons appear colorless in one orientation and light pink in another. Two light-pink euhedral fractions yielded Pb-Pb ages of  $2,050 \pm 2$  Ma (fraction 6; table 2) and  $2,039 \pm 6$  Ma (fraction 7; table 2). A clear, colorless, euhedral fraction with acicular inclusions (fraction 11; table 2) yielded a Pb-Pb age of  $2,019 \pm 17$  Ma. Two dark-brown fragments of zircon yielded a discordant Pb-Pb age of  $2,238 \pm 3$  Ma (fraction 8; table 2). More data



**Figure 7.** Concordia diagram of zircon (1 to 8, 10 to 12) and rutile (9) data. Numbers show fractions listed in table 2. Data from fractions 5, 9, and 12 are shown as error ellipses. The other fractions have error ellipses smaller than the dots that mark them. Fraction 8 is dark-brown opaque fragments. The reference line is a Ludwig (1988; ISOPLOT program) model 2 fit through the two pairs of unabraded and abraded bulk samples (1 and 3, 2 and 10). The age implied by this line is only appropriate assuming the zircons were derived from a granitic source with a single age and a single Pb-loss event. As described in the text, there is good evidence that the zircons were derived almost exclusively from Early Proterozoic granite, but a small range of Early Proterozoic ages is likely.

on this dark-brown component would be useful, but no more zircons of that description were found.

## RUTILE

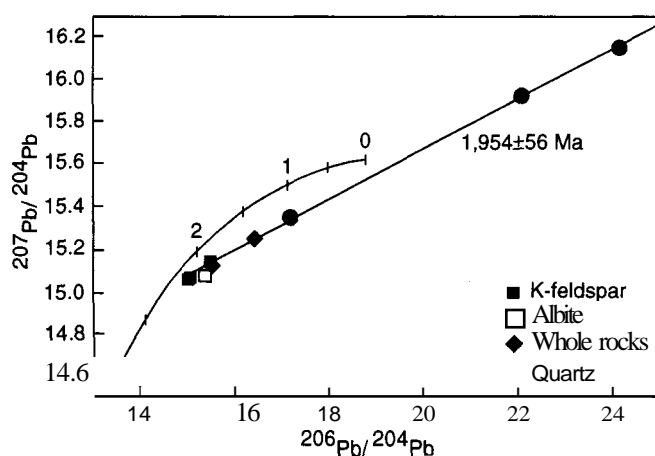
A small fraction of the grains in the zircon separate were identified as rutile using Energy-Dispersive X-Ray Spectroscopy (EDS). These grains were broken and angular, and they ranged in color from orange and translucent to black and opaque. A sample of three of the orange grains yielded a near-concordant age of  $1,903 \pm 16$  Ma (fraction 9; table 2; fig. 7).

## FELDSPAR Pb ISOTOPIC COMPOSITIONS

The Pb isotope compositions of the feldspars (fig. 8, table 3) are consistent with derivation from an Early Proterozoic source. For example, the least radiogenic analysis has a Stacey and Kramers (1975) model age of 1,967 Ma, and an  $m_1$  ( $^{238}\text{U}/^{204}\text{Pb}$ ; Ludwig, 1988) of 9.101. The single-stage model age of the same sample is 1,765 Ma with an  $m$  from primordial values (Tatsumoto and others, 1973) of 7.886, and a  $k$  ( $^{232}\text{Th}/^{238}\text{U}$ ) of 4.033. The results are consistent with an isotopically juvenile, Early Proterozoic granitic source of the Nuka Formation.

## QUARTZ Pb ISOTOPIC COMPOSITIONS AND FELDSPAR-WHOLE ROCK-QUARTZ Pb-Pb ISOCHRON

Pb isotope data from a single quartz grain and two fractions of five grains are presented in figure 8 and table 3. The quartz is significantly more radiogenic than the whole-rock samples. Quartz, feldspar, and whole-rock analyses from the Nuka Formation lie on a  $1,968 \pm 66$  Ma slope,



**Figure 8.** Pb isotope data from feldspar, quartz, and whole-rock samples. Growth curve is from Stacey and Kramers (1975) with tick marks at 500-Ma intervals. Regression was calculated using K-feldspar, quartz, and whole-rock data. The mean standard weighted deviation (MSWD) is 3.27 (Ludwig, 1988).

Table 3. Pb isotope data from feldspar, quartz, and whole-rock samples from the Nuka Formation

[Analytical uncertainties are less than 0.1 percent except as otherwise noted in parentheses]

	$^{206}\text{Pb}/^{204}\text{Pb}$	$^{207}\text{Pb}/^{204}\text{Pb}$	$^{208}\text{Pb}/^{204}\text{Pb}$
<b>DT-84-14</b>			
Albite	15.342	15.080	34.888
K-feldspar	15.452	15.145	35.154
	15.021	15.072	35.687
	14.960	15.064	34.643
Single quartz grain	17.140(0.15)	15.356(0.17)	35.449(0.18)
Five quartz grains	21.986(0.16)	15.923(0.14)	35.533(0.16)
Five quartz grains	24.032(0.19)	16.153(0.14)	36.493(0.15)
Whole rock	15.497	15.128	34.981
<b>DT-84-15</b>			
Whole rock	16.376	15.260	35.780

with an MSWD of 6.23 (Ludwig, 1988), an age within analytical uncertainty of the corresponding zircon data. Removing the albite analysis (it appears to be slightly off the line and may have been recrystallized during diagenesis) results in a  $1,954 \pm 56$  Ma slope (fig. 8).

#### REE AND Nd ISOTOPIC COMPOSITION

Both samples have low REE abundances (fig. 9, table 1), consistent with the apparent absence of monazite and xenotime. The samples have slightly to significantly positive Eu anomalies and significant negative Ce anomalies. Positive Eu anomalies are generally attributed to the concentration of feldspar during sedimentary processes (for example, Nance and Taylor, 1977; McLennan, 1989). The high Er and Yb abundances relative to Dy in DT-84-15 may be caused by concentration of zircon during sedimentary sorting. The strong negative Ce anomalies may have been formed during weathering of the granitic source (Nesbitt, 1979; Rosenblum and Mosier, 1983; Banfield and Eggleton, 1989) or perhaps during recent weathering (Zhao and others, 1992). Both samples have Nd isotopic compositions consistent with derivation from a depleted mantle source at 2.050 Ga (table 1, fig. 10).

#### K-Ar ANALYSIS

The results of conventional K-Ar analysis of K-feldspar of two rock samples from Nuka Ridge plus two

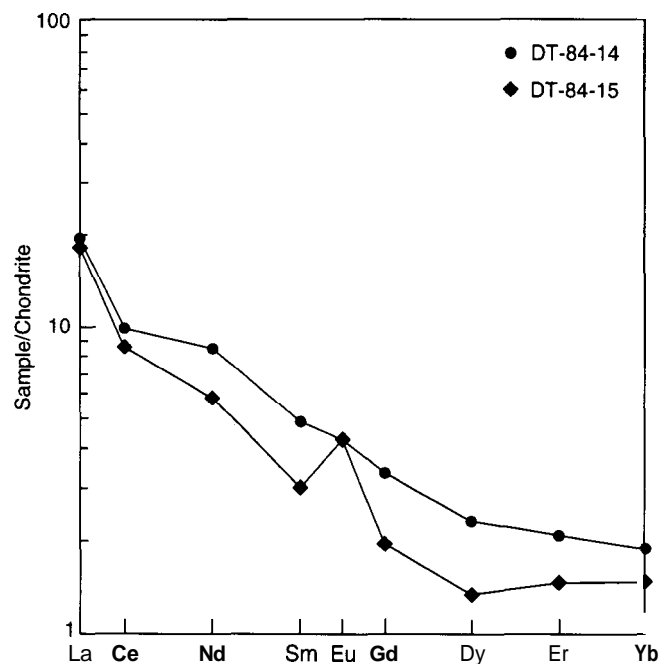


Figure 9. Rare earth element patterns from Nuka Formation whole-rock samples. Note the low abundances, positive Eu anomalies, and negative Ce anomalies. The upward trend in the HREE of DT-84-15 may be caused by concentration of zircon owing to sedimentary processes. The positive Eu anomaly could be from sorting of feldspar (for example, Nance and Taylor, 1977; McLennan, 1989). The Ce anomalies may result from weathering (for example, Banfield and Eggleton, 1989; Zhao and others, 1992).

analyses from elsewhere in the Brooks Range were reported by I.L. Tailleir (Tailleur, 1985). These ages, with previously unpublished accompanying analytical data, were graciously provided to us by Tailleir and are shown in table 4.

The locations of the samples (samples 71Tr22.10 and 53Tr-43A) from Nuka Ridge are shown in figure 5. These samples were taken from Nuka Formation strata in thrust imbricates below and above the site of samples DT-84-14 and DT-84-15 collected for this study. The K-Ar samples consist of pebble conglomerate and very coarse-grained sandstone, respectively, and have proportions of K-feldspar, quartz, and plagioclase that are similar to those of the U-Pb samples. K-Ar age determinations from K-feldspar in these samples yielded similar ages of 1,150±58 Ma and 1,187±59 Ma, respectively (table 4).

K-Ar samples from outside the Nuka Ridge area were collected from the south flank of Umagatsaiak Mountain, 25 km north of the village of Kivalina in the westernmost Brooks Range, and from the Helpmejack Hills in the southern Brooks Range (fig. 1). The sample from the western Brooks Range (68Tr-147B) (fig. 11) is a granule conglomerate of composition similar to that of the Nuka Formation in the Nuka Ridge area. Conodonts from the Nuka Formation near this location are Late Mississippian to Early Pennsylvanian, whereas foraminifera from the same location are Late Mississippian (Viséan) (Mayfield and others, 1987). The conodonts have a CAI of 1, indicating that the Nuka

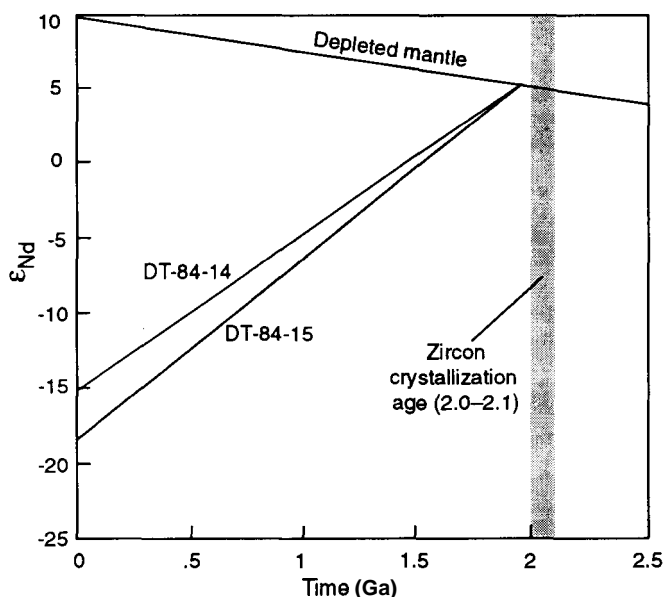


Figure 10.  $\epsilon_{Nd}$  versus time plot for whole rock samples from the Nuka Formation. Depleted-mantle model is from Taylor and McLennan (1985). The depleted-mantle model age is approximately equal to the detrital zircon crystallization ages, suggesting that the granitic source from which the Nuka detritus was shed was derived from a source with a short crustal residence time.

**Table 4. Conventional K-Ar feldspar age data from the Nuka Formation at Nuk Ridge, Umagatsaiak Mountain, and Helpmejack Hills**

[Abbreviation: scc, cubic centimeters at standard temperature and pressure]

Sample <sup>1</sup>	Lab no.	Location	Latitude	Longitude	Mineral <sup>2</sup>	K (percent)	40Ar (percent)	40Ar (scc/g x 10 <sup>-5</sup> )	Radiometric age
71Tr22.10	KA84-195	Nuka Ridge	68°39'13"	159°21'05"	Microcline	1.02, 1.03	95.8, 97.4	6.30, 6.52	1,150 ± 58
53Tr-43A	KA84-196	Nuka Ridge	68°36'10"	159°11'22"	Microcline	8.33, 8.34	99.4, 99.4, 99.1	52.9, 54.2, 56.2	1,187 ± 59
68Tr-147B	KA84-197	Umagatsaiak Mountain	67°57'09"	164°33'35"	Microcline	.61, .61	94.7, 96.8	7.07, 7.26	1,775 ± 8
84Tr-02b4	KA85-0815	Helpmejack Hills	66°59'10"	153°51'27"	Feldspar	.03, .04	70.0, 72.4	.245, .260	1,276 ± 64

<sup>1</sup> Analyzed by Teledyne.

<sup>2</sup> Separates of feldspar and feldspar partially hand-picked separates.

has undergone little postdepositional heating (<80°C) (Epstein and others, 1977) in this area. This sample yielded a K-feldspar K-Ar age of 1,775±8 Ma (table 4).

The sample from the southern Brooks Range (84Tr-02b4) was collected from a fault sliver (fig. 12) in a regional zone of down-to-the-south normal faulting of Cretaceous age along the margin of the southern Brooks Range described elsewhere by Christiansen and Snee (1994) and Little and others (1994). In contrast to other samples of the Nuka Formation, this sample consists of arkose rich in plagioclase and displays a cataclastic texture that was likely

imposed during the episode of normal faulting. The CAI for a probably redeposited Late Devonian conodont collected from this site is 5 to 5.5 (A.G. Harris, USGS, written commun. to I.L. Tailleir, 1984), corresponding to a temperature of 330–350°C (Epstein and others, 1977). Feldspar in this sample is partly replaced by carbonate and (or) albite. Despite the mesoscale to microscopic scale evidence of young deformation and alteration, the sample yielded a feldspar K-Ar age of 1,276±64 Ma (table 4).

The K-Ar systematics of K-feldspar are very complex and depend on the nature of the constituent diffusional domains and the thermal history of the rocks (McDougall and Harrison, 1988; Lovera and others, 1989; Harrison, 1990). As a result, the closure temperature of K-feldspars may range from a low of 120°C to a high of 300°C. Assuming that the K-feldspar in the Nuka Formation is largely microcline, the closure temperatures for K-feldspars in the Nuka likely range from 120°C to 200°C (McDougall and Harrison, 1988). In addition, K-feldspar may incorporate excess argon and yield anomalously old ages. Without more detailed study, the significance of these data are not certain. Nonetheless, these data do provide some information. The K-Ar feldspar ages from the Nuka Ridge area are significantly younger than the 2-Ga U-Pb ages from the same

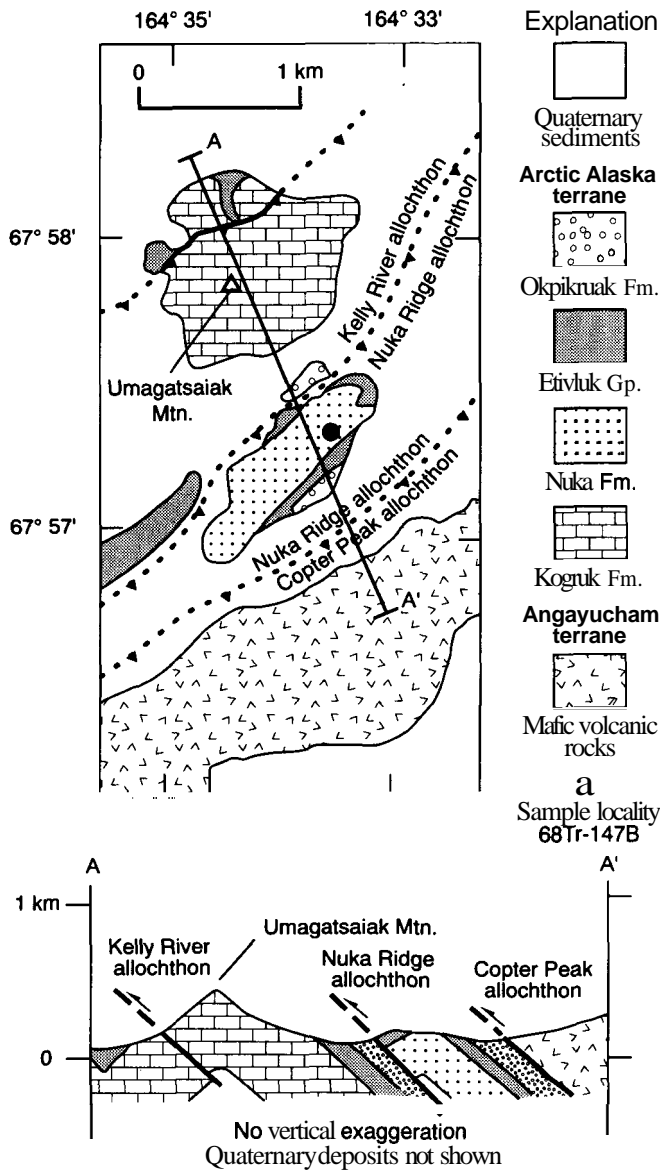


Figure 11. Simplified geologic map and section showing Nuka Formation on the south flank of Umagatsaiak Mountain, where K-Ar sample 68Tr-147B was collected (Noatak 1:250,000 quadrangle). Map relations from Mayfield and others (1987).

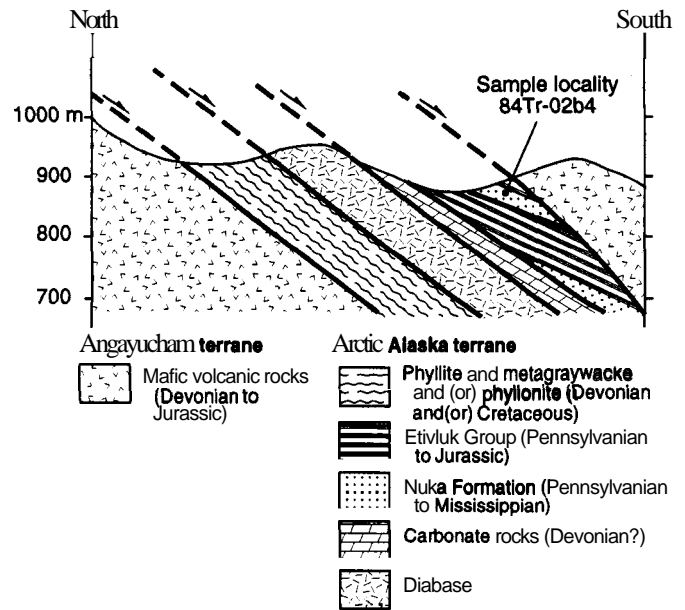


Figure 12. Schematic structural section of Nuka Formation outcrop from which K-Ar sample 84Tr-02b4 was collected in the Helpmejack Hills (Hughes 1:250,000 quadrangle) (I.L. Tailleir, USGS, written commun., 1996). Fault slivers of Nuka Formation, chert of the Eivluk Group, and mafic volcanic and hypabyssal rocks of the Angayucham terrane are interleaved along a regional zone of down-to-the-south normal faulting described elsewhere by Christiansen and Snee (1994) and Little and others (1994).

rocks, which indicates that the K-Ar ages are not magmatic cooling ages and that the feldspars are unlikely to contain excess argon. Simple interpretations of the K-Ar data include (1) cooling from several regional or local metamorphic events ranging from 1.2–1.77 Ga, (2) partial resetting of the 2.0–2.1 age of crystallization by a 1.2 Ga or younger metamorphic event, or (3) protracted cooling for more than 800 m.y. due to uplift in the source area. The data indicate that the Nuka detritus in the Nuka Ridge area has not been heated above 200°C since 1.2 Ga. The generally comparable K-Ar results from the Nuka from three locations in the Brooks Range suggest that the source region of the Nuka was extensive and uniformly older than 1.2 Ga over a wide region.

### PROVENANCE OF THE NUKA FORMATION

Discordance is difficult to interpret in detrital zircon populations where mixing of zircons of different ages is likely. Relevant observations from our data that bear on the age of the zircon population in the Nuka Formation are that (1) the petrography is consistent with a simple granitic source (quartz, microcline, sodic plagioclase, and granitic rock fragments); (2) the zircons are generally euhedral and, where seen in thin section, are always included within quartz and feldspar clasts; (3) a large single zircon yielded a Pb-Pb age of  $2,078 \pm 1$  Ma; (4) although picked to represent as much color and morphological variation as possible, small fractions yielded only Early Proterozoic Pb-Pb ages (table 1, fig. 7); (5) bulk abraded and unabraded fractions, with significant differences in degree of discordance, give similar Pb-Pb ages within analytical error; and (6) all other isotopic data are consistent with an Early Proterozoic granitic provenance. These observations indicate that the dominant, light-colored euhedral zircon population in the Nuka Formation was derived mainly from a 2.0–2.1 Ga (Early Proterozoic) granitic source. The petrographic and isotopic data indicate that granitic detritus from source areas with a large range of ages (for example, **Archean** and Devonian) is not likely. However, a mix of Early Proterozoic source rocks is possible given the range in Pb-Pb ages and the age of the distinct, but minor, dark-brown, opaque zircon fragments that yielded a Pb-Pb age of  $2,238 \pm 3$  Ma (fraction 8; table 2). Although the latter result is a single discordant analysis and can only be interpreted as a minimum age, it indicates that a minor amount of detritus was contributed from rocks older than 2.2 Ga in the source area.

There is no evidence in the Nd isotopic data for contamination from significantly older crustal rocks. The older zircons, with a minimum age of 2.24 Ga, could have come from inclusions of older rocks within this complex, but we suggest, on the basis of the Nd data, that they must represent a minor component. Whatever the details of the zircon

systematics, substantial Pb loss occurred recently, perhaps during the Mesozoic and Tertiary Brookian orogeny. With aggressive abrasion of the zircons, it might be possible to eliminate part of the complexity, and analysis of single zircons would provide better constraints on the age range of the source. We believe that neither the Nuka Formation nor its source of rutile was heated above ~400°C, the probable closure temperature for rutile of this size (Mezger and others, 1989) after 1.9 Ga. Likewise, the K-feldspar K-Ar ages from Nuka Ridge indicate that neither the Nuka Formation nor its source of K-feldspar have been subjected to heating above 200°C since 1.2 Ga. The CAI data suggest that postdepositional thermal heating of the Nuka was variable, ranging from a maximum of 80°C in the western Brooks Range to a high of 330–350°C in the southern Brooks Range. The post-Devonian temperatures required by the CAI data from the southern Brooks Range are higher than the maximum temperatures allowed by the K-Ar feldspar age data (300°C) since 1.3 Ga from the same location. We are uncertain how to reconcile these conflicting data but suggest that (1) the CAI of the single conodont found in the southern Brooks Range location may be anomalous for the location, (2) the temperatures determined by Epstein and others (1977) for conodont alteration may not be accurate under conditions of high strain, (3) the feldspar K-Ar age may have been partially reset from an older (greater than 1.3 Ga) age during post-Devonian, probably Cretaceous time, and (or) (4) the K-Ar age from the southern Brooks Range dates white mica (closure temperature ~350°C) enclosed in the feldspar. Other interpretations are possible for these data.

### IS THE SOURCE FOR THE NUKA IN THE SOUTHERN BROOKS RANGE?

The present position of the Nuka Formation in allochthonous sequences at high structural levels in the Brooks Range orogen may be explained by (1) systematic south-over-north (present coordinates) stacking of imbricates of the sedimentary cover of the Arctic Alaska terrane during the Late Jurassic and Early Cretaceous, or (2) emplacement of structurally lower parts of the orogen into higher levels along presently unrecognized out-of-sequence thrust faults (fig. 3). If derived from structurally lower parts of the Brooks Range orogen, the granitic detritus in the Nuka Formation may have come from the belt of granitic rocks in the southern Brooks Range. If not **emplaced** by out-of-sequence faults, the Nuka Formation was probably derived from a granitic source area that would lie in the present position of the Late Jurassic to Late Cretaceous rocks exposed in the Koyukuk basin. This source area is now not exposed in northern Alaska and is thus of uncertain character.



The belt of plutonic and metaplutonic rocks now exposed in the southern Brooks Range consists of orthogneiss that ranges in composition from tonalite to alkali-feldspar granite. These rocks intrude Upper Proterozoic and lower Paleozoic metasedimentary rocks and are locally overlain by quartz-rich metasiliciclastic rocks and metalimestone of Mississippian age (Mull and Tailleux, 1977; Nelson and Grybeck, 1980). Metamorphism of the granitic rocks and the associated sedimentary rocks occurred during the Brookian orogeny in the Late Jurassic and Cretaceous. Most of the largest plutons of the plutonic belt yield discordant U-Pb ages of about 390 Ma (Dillon and others, 1987; Aleinikoff and others, 1993). Some smaller plutonic bodies in the belt are older, yielding U-Pb ages of 700-750 Ma (Karl and others, 1989; Karl and Aleinikoff, 1990). Nelson and others (1993) reported that the Late Proterozoic and Devonian plutons have Nd- and Sr-isotope compositions consistent with derivation, in part, from Middle to Early Proterozoic crust. Proterozoic metasedimentary rocks associated with these plutons have calculated Nd crustal residence ages of 2.0 Ga.

Comparison of the Devonian and Late Proterozoic ages of the granitic rocks of the southern Brooks Range with the Early Proterozoic age of the granitic detritus in the Nuka Formation show unequivocally that the Nuka Formation could not have been derived from granitic rocks related to those exposed in the southern Brooks Range. Because Devonian and Mississippian clastic sedimentary rocks (now metamorphosed) are exposed with the plutons in the southern Brooks Range, it seems unlikely that deeper levels of the southern Brooks Range were exposed during the Mississippian. Thus, the Nuka Formation cannot be directly correlated to possible granitic source areas in the southern Brooks Range. On this basis, it is doubtful that the Nuka Ridge allochthon could have been derived from structurally lower levels of the orogen in the southern Brooks Range and **emplaced** at structurally higher levels along hypothetical out-of-sequence thrust faults (for example, our restoration in fig. 3B). Our data instead support the **structural** model of Mayfield and others (1988) (fig. 3A), which proposes that the source area of the Nuka was a highland that once lay south of the Brooks Range orogen. That highland has since disappeared or has been tectonically removed or buried, so the source area of the Nuka can only be characterized through the petrographic and isotopic character of the detritus in the Nuka Formation.

#### OTHER POSSIBLE SOURCE AREAS FOR NUKA DETRITUS

The petrographic and isotopic data indicate that the detritus in the Nuka Formation was derived from a source area that consisted of evolved 2.0–2.1 Ga granitic rocks and older Lower Proterozoic country rocks. The granitic

rocks were derived from partial melts of depleted mantle at about 2 Ga and were not significantly contaminated by older wall rocks. The granitic rocks cooled to below 400°C by about 1.9 Ga and were not significantly reheated above the bulk closure temperature of K-feldspar (120–200°C) after 1.2 Ga. The generally similar feldspar-rich composition and Proterozoic K-Ar feldspar ages from widely separate localities of the Nuka Formation in the Brooks Range suggest that similar conditions were present regionally in the source region of the Nuka and that the source area had a considerable regional extent. A diagram summarizing the cooling history of Nuka Formation detritus is shown in figure 13.

The source area for the Nuka Formation should have characteristics that are comparable to those summarized above for the Nuka Formation. Although we can eliminate the granitic rocks of the southern Brooks Range as the source area for the Nuka, the Arctic Alaska terrane in the southern Brooks Range contains metasedimentary rocks that were derived from continental crust with an average crustal residence of 2.0 Ga (Nelson and others, 1993) and thus may contain other possible source areas. Other continental terranes with isotopic characteristics similar to those of the southern Brooks Range are exposed over wide areas of

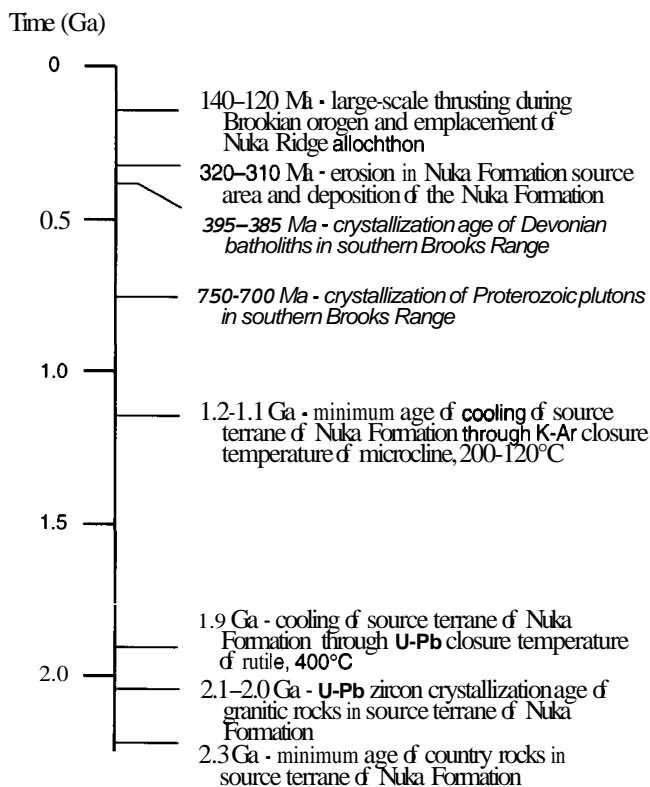


Figure 13. Diagram summarizing known or inferred geologic history for the Nuka Formation and its source area. Shown in italics are ages of plutonic rocks known from the Arctic Alaska terrane. Time scale is that of Harland and others (1990).

Alaska (fig. 1) and may contain alternative source regions for the Nuka, although only the Kilbuck and Idono terranes contain known exposures of Early Proterozoic granitic rocks. We compare below the data from the Nuka to these possible source areas and to other possible source areas elsewhere in the Cordillera.

#### ARCTIC ALASKA TERRANE

The Nd isotopic compositions of the Late Proterozoic metasedimentary rocks in the southern Brooks Range suggest that the Devonian magmatic belt was an arc that was built on Early Proterozoic continental crust (Nelson and others, 1993). While the source area for the Nuka Formation arkose could not have been the Devonian magmatic belt itself, it is possible that granitic rocks may form part of the Early Proterozoic crust at depth beneath the arc. The hypothesized granitic rocks may have been a source for the Nuka if they were uplifted above sea level in the Mississippian.

The presence of younger sedimentary cover and the absence of exposures of Early Proterozoic rocks seemingly would preclude such an uplift in the southern Brooks Range. However, the southward continuation of Early Proterozoic basement rocks from their restored position to the edge of the Mississippian continental margin of Arctic Alaska provides a hypothetical site for their exposure. Such a distal location is supported by (1) the deep-shelf depositional environment of the siliceous shale and chert that overlie the Nuka Formation (fig. 4); (2) the basinal aspect of coeval sedimentary rocks of the allochthonous successions that lie structurally below, and that restore paleogeographically continentward (northward in present coordinates) of the Nuka Ridge allochthon (Moore and others, 1994a); and (3) the structural model of Mayfield and others (1988) that interpreted the Nuka Ridge allochthon as the most distal or outboard part of the Arctic Alaska terrane. Rifting along this continental margin is thought to have occurred in the Middle and Late Devonian and culminated in opening of the Angayucham ocean and development of a passive margin on the adjacent Arctic Alaska terrane by the latest Devonian (Moore and others, 1994a). Extension, aided by thermal heating along this margin, may have uplifted thinned Early Proterozoic crust and exposed the hypothetical Early Proterozoic granitic rocks as a horst or rifted fragment. However, such thermal heating in the Devonian of the Early Proterozoic crust might be expected to reset the K-Ar ages of the K-feldspar grains to younger ages, which cannot be demonstrated with the present data set.

#### KILBUCK AND IDONO TERRANES

In southwestern Alaska, orthogneisses in the Kilbuck and Idono terranes (fig. 1) have yielded zircon U-Pb crys-

tallization ages similar to those from detrital zircons of the Nuka Formation (Turner and others, 1983; Box and others, 1990; Miller and others, 1991; Moll-Stalcup and others, 1996). The Kilbuck terrane consists of tonalitic gneiss, granite gneiss, and amphibolite and rare pelitic schist and marble that were metamorphosed to eclogite and upper amphibolite facies (12–13 kbar, 550–600°C) (Moll-Stalcup and others, 1996). Discordant zircons from a tonalitic gneiss have an intercept of 2.07 Ga, whereas two samples from granite gneiss, which intrudes the tonalitic gneiss, have intercepts of 2.04 Ga and 2.05 Ga, respectively (Box and others, 1990; Moll-Stalcup and others, 1996). Other granite gneisses are undated but yield Nd model ages of approximately 1.8 Ga. Two samples from the diorite-tonalite-trondhjemite suite within the Kilbuck terrane have  $\epsilon_{Nd}(2.05 \text{ Ga})$  of +2.1 and +2.7, consistent with a dominantly depleted mantle derivation (Box and others, 1990). A granite within the same area has  $\epsilon_{Nd}(2.05 \text{ Ga})$  of -5.7, requiring a significant Archean input (Box and others, 1990). Box and others (1990) and Moll-Stalcup and others (1996) interpreted the Kilbuck terrane as a 2.05-Ga volcano-plutonic arc proximal to an Archean craton. A U-Pb sphene age indicates that the terrane was metamorphosed at 1.77 Ga (Moll-Stalcup and others, 1996) and was further thermally disturbed during the Mesozoic, creating complicated K-Ar systematics (Turner and others, 1983).

A similar scenario has been presented for the Idono terrane (Idono complex of Miller and others, 1991), located about 275 km northeast of the Kilbuck terrane. Miller and others (1991) reported U-Pb discordia intercept ages of 2.05 Ga and 148 Ma for fractions from one of three samples. Zircons from the three samples appear collinear and give intercepts of 2.06 Ga and 183 Ma, which Miller and others (1991) interpreted as the ages of crystallization of the suite and of major episodic Pb loss, respectively. Although the zircon systematics are complicated, it appears that there is at least a component of the Idono terrane that crystallized at about 2.05 Ga.

There are some striking similarities between the Idono and Kilbuck terranes and the source terrane of the Nuka Formation. These include (1) the zircon crystallization ages, (2) the highly discordant nature of the zircons, (3) the juvenile nature of the Nd, and (4) the REE patterns, especially the low overall abundances and positive Eu anomalies. There are also some differences, as follows: (1) The detrital rutile age from the Nuka Formation requires that its source was not subjected to temperatures higher than 400°C between 1.9 Ga and the time of deposition of the Nuka. This is in contrast to the amphibolite- to eclogite-grade metamorphism at about 1.77 Ga recorded in the Kilbuck terrane. (2) The intermediate granitic rocks in both the Kilbuck and Idono terranes record substantial crustal contamination in their Nd system, but the granitic source of the Nuka Formation has significantly higher  $\epsilon_{Nd}$ . (3) The Kilbuck and Idono terranes are themselves allochthonous, and most tectonic

reconstructions restore them southeastward to positions along the Canadian Cordillera (Moore and others, 1994b; Plafker and Berg, 1994). In short, although the Kilbuck and Idono terranes were probably not sources for the Nuka Formation, it is possible that a larger Early Proterozoic terrane contained both of those fragments as well as the source for the Nuka Formation (fig. 14).

#### OTHER CONTINENTAL TERRANES IN ALASKA

Other continental terranes in Alaska, including the Seward, Ruby, Yukon-Tanana, and Nixon Fork terranes (fig. 1), contain Upper Proterozoic but no known Lower Proterozoic rocks (Plafker and Berg, 1994, and references therein). The Seward, Ruby, Yukon-Tanana, and Nixon Fork terranes have yielded isotopic evidence from Late Proterozoic and younger plutonic rocks that suggests the presence of an Early Proterozoic or older crustal component at depth (Arth, 1994). However, the isotopic evidence from these terranes does not require a crustal contaminant of Early Proterozoic igneous crust but could result from contamination by mixtures of Archean and younger crust or by younger

sedimentary rocks with Early Proterozoic or similar mixed sources (Nelson and others, 1993).

#### THE SIGNIFICANCE OF 2.0–2.1 Ga CRUST IN THE CORDILLERA

Possible source regions of Early Proterozoic zircons (2.0–2.1 Ga) in the Nuka Formation may lie in the Precambrian basement of western Canada (Hoffman, 1989). Nd model ages from about 1.9-Ga granitoids from the Wopmay orogen in the Northwest Territories of Canada indicate that the orogen was generated on 2.0–2.4 Ga crust (Bowring and Podosek, 1989). Isotopic data from drillcore from stable Precambrian basement in Alberta indicate that parts of the cratonal interior consist of 2.0–2.4 Ga crust (Thériault and Ross, 1991). Exposures of Early Proterozoic rocks are reported from the Omineca belt in the southern part of the Canadian Cordillera (Armstrong and others, 1991; Murphy and others, 1991). On the basis of the U-Pb and Nd isotopic data, Bowring and Podosek (1989) suggested that a large part of western Canada is underlain by 2.0–2.4 Ga crust. However, Nd isotopic data from the Omineca belt are generally evolved ( $\epsilon_{Nd}(0)$  is negative with model ages of 2.3–2.6 Ga; G.M. Ross, Geological Survey of Canada, written commun., 1995), and 2.0–2.4 Ga basement rocks in Alberta were formed by mixing of a depleted-mantle component with Archean crust (Thériault and Ross, 1991). In addition, both the Wopmay orogen and Omineca belt are invaded by gneisses that yield 1.8–1.9 Ga U-Pb ages and crystalline rocks of 2.0–2.4 Ga age are rare or absent at the present level of exposure. Detrital zircons with Early Proterozoic crystallization ages have been reported from quartz-rich rocks of the Omineca belt but are apparently absent in less mature arkosic strata of the Windemere Supergroup (Ross and Parrish, 1991). This suggests that 2.0–2.4 Ga crust is a relatively minor component of the Precambrian basement of western Canada, and this basement is thus not a likely location of the Nuka Formation provenance terrane.

Hints of the existence of 2.0–2.1 Ga crust in the Cordillera have been reported as far south as California and Nevada. For example, Carboniferous sedimentary rocks of the Klamath Mountains contain a 2.1 Ga detrital component (Miller and Saleeby, 1989). Detrital zircons with similar ages have been reported from Paleozoic sandstones from the allochthonous Shoo Fly Complex in the northern Sierra Nevada and from Ordovician sedimentary rocks of the Roberts Mountain allochthon (Girty and Wardlaw, 1985), and inheritance in zircon of about this age has been observed in plutons in the central Sierra Nevada (Sharp, 1988). The detrital zircon studies of Gehrels and others (1995) show that U-Pb ages of 2.0–2.1 Ga compose a minor component of miogeoclinal sandstones in the northern Cordillera and are nearly absent from miogeoclinal strata in the southern Cordillera (Gehrels and others, 1995).

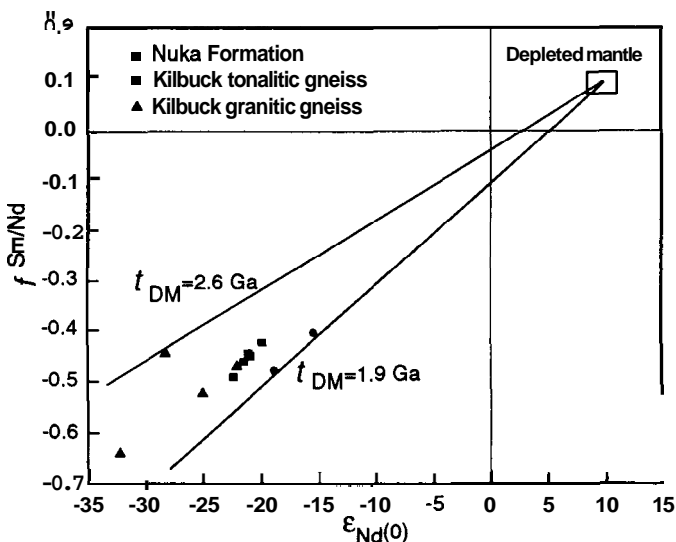


Figure 14.  $f_{Sm/Nd}$  vs  $\epsilon_{Nd}(0)$  plot showing data from the Nuka Formation as well as from gneisses of the Kilbuck terrane (Moll-Stalcup and others, 1996). For reference, the approximate composition of modern depleted mantle (DM) and reference model age slopes that span the range of data are included. Although the zircon crystallization ages are the same, it is evident that Nuka Formation samples have substantially younger Nd model ages than do samples from the Kilbuck terrane. However, the source region for the Nuka and the Kilbuck terrane could reasonably have been components of the same larger terrane with a geographic gradient in the amount of contamination by ancient continental crust. Nuka Formation samples do not appear to have had their Sm-Nd system disturbed by sedimentary processes because the two samples show a relatively large range in Sm/Nd, yet lie along an Early Proterozoic slope.

The above data suggest that the distribution and volumetric significance of 2.0–2.1 Ga crust in the Cordillera is uncertain. Even though 2.0–2.1 Ga gneisses are locally present, they are subordinate to 1.8–1.9 Ga orthogneisses that intrude them (G.M. Ross, written commun., 1995). Furthermore, most rocks in the North American Cordillera that have zircon ages of about 2 Ga generally have older Nd model ages, and those with Nd model ages of 2 Ga have younger U-Pb zircon ages (Moll-Stalcup and others, 1996). We therefore conclude that the Early Proterozoic rocks of western North America, as presently known, are not a good match for the source area of the Nuka Formation as determined by our multicomponent isotopic provenance study of its detrital components.

### PROTEROZOIC SUPERCONTINENT

Hoffman (1989) interpreted the Early Proterozoic rocks of the Wopmay orogen as terranes that were accreted to an **Archean** protocraton. The evolved Nd isotopic data suggest that this continental growth occurred through interaction with older **Archean** rocks and juvenile crust. As summarized above, these rocks are present along the margin of northwestern North America and commonly underlie allochthonous Paleozoic and Mesozoic rocks of oceanic affinity at their westernmost extent in North America. The nature of the Early Proterozoic crust that once was to the west of these exposures is unknown, but it may have consisted of 2.0–2.1 Ga crust that was less evolved than the coeval rocks exposed in the Omineca belt and Wopmay orogen and hence more like the crust interpreted as the source area for the Nuka Formation. The existence of a western continuation of Early Proterozoic crust is substantiated by sedimentological evidence of a western source for the Proterozoic Belt-Purcell strata (Ross and others, 1992).

If there once was an Early Proterozoic terrane with the isotopic character of the source area of the Nuka Formation outboard of the present exposures of Early Proterozoic basement in the northwestern Cordillera, where are those rocks now and how did they provide detritus for the Nuka in the Mississippian? The Cordilleran margin of North America was formed by rifting sometime after 750 Ma, probably along the  $^{87}\text{Sr}/^{86}\text{Sr}$  initial isopleth of 0.706, which approximates the edge of thick continental basement (Kistler and Peterman, 1978). The rifting led to **seafloor** spreading and the opening of Panthalassa, the ancestral Pacific Ocean (Dickinson, 1977). The present position of the conjugate margin of the rift is unknown, but recent speculation centers on the composite Australia-Antarctic shield (Moores, 1991; Dalziel, 1991; Hoffman, 1991) (fig. 15). The hypothetical source area for the Nuka might be a small crustal block derived from the Australia-Antarctic shield that was stranded along the northwestern margin of North America during this rifting event (fig. 16). However, Early Proterozoic rocks in Australia and Antarctica suggested to be cor-

relative to the northwestern part of the North American margin apparently lack magmatic rocks with juvenile characteristics similar to those of the source area for the Nuka (see summary map in Ross and others, 1992). Similarly, if fragments of the rifted source area were stranded along the margin of North America, then evidence of these rocks might be expected to be more abundant in the Phanerozoic sedimentary record of North America.

Alternatively, the source area for the Nuka Formation may be in the Russian Far East. If the allochthonous rocks in the Brooks Range are unstacked southward and the **Arc-**

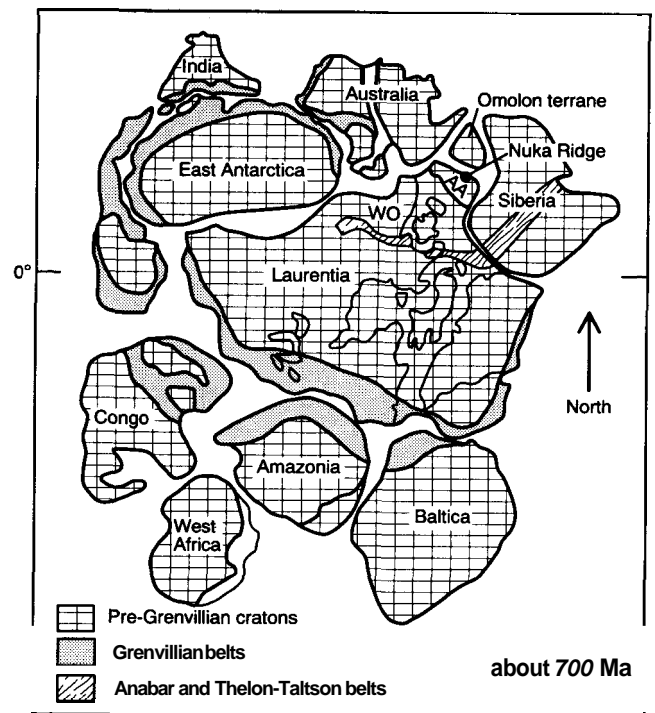


Figure 15. Schematic paleogeographic reconstruction of Late Proterozoic supercontinent proposed by Hoffman (1991). Reconstruction is based on correlation of Grenvillian belts and correlation of Anabar and Thelon-Taltson belts in Siberia and northern Canada, respectively. Figure modified to show possible position of Omolon terrane, which is the cratonic core of the Kolyma-Omolon superterrane of Nokleberg and others (1994). Position of the Arctic Alaska terrane (AA) depicted prior to  $67^\circ$  of counterclockwise rotation in the Jurassic and (or) Cretaceous as proposed by many workers (for example, Halgedahl and Jarrard, 1987). If restored by this rotation and unstacking of Brookian thrust faults, the Nuka Formation would be located in a position along the northern margin of Laurentia and adjacent to the Siberian and Omolon cratons as shown. If Arctic Alaska is held fixed in its present position, the Nuka Formation would lie along the northwestern margin of Laurentia adjacent to Australia. Wopmay orogen (WO) shown for reference. The loose fit in parts of the reconstruction reflects changes in the size and shapes of cratonic areas as a result of tectonic shortening during subsequent deformation episodes.

tic Alaska terrane in northern Alaska is restored by rotation about a pole in the Mackenzie River delta to its inferred position in pre-Cretaceous time (for example, Halgedahl and Jarrard, 1987), the Nuka Formation would lie along the outboard part of the northern margin of North America. The reconstructions of Moores (1991) and Hoffman (1991) discussed above place the Siberian craton adjacent to the northern margin of North America in Proterozoic time (fig. 15) but do not specify the time of rifting along this margin. Stratigraphic evidence and faunal evidence from the Arctic Alaska terrane indicate that rifting occurred in the Devonian and is approximately coeval with rifting of the cratonal rocks of the Omolon terrane away from the Siberian craton in the Russian Far East (Nokleberg and others, 1994). Furthermore, paleontological data from some lower Paleozoic rocks of northern Alaska show affinities with Siberian faunas (Palmer and others, 1984; Grantz and others, 1991; R.B. Blodgett, consultant, oral commun., 1996). These relations suggest that rifting between the Siberian craton, the Omolon terrane, and the northern margin of North America occurred in the Devonian. The source region for the Nuka may have been crustal fragments of the Siberian craton or Omolon terrane that were stranded by this rifting along the outboard edge of the Arctic Alaska terrane (as depicted in fig. 16). Unfortunately, present isotopic data from the Omolon terrane and the Siberian craton are insufficient to test this hypothesis. This scenario implies that the granitic rocks of the Kilbuck and Idono terranes of southwestern Alaska, which share many isotopic characteristics with the arkosic detritus in the Nuka Formation, may also have origi-

nated from positions adjacent to the Omolon terrane (W.J. Nokleberg, U.S. Geological Survey, oral commun., 1996).

### CONCLUSIONS

Sandstone from the Nuka Formation at its type section in the western Brooks Range consists chiefly of K-feldspar-rich arkosic debris that was derived from a 2.0–2.1 Ga granitic source area that had little contamination from older crustal material. Because the Nuka Formation occurs only in allochthonous thrust sheets, fault slivers, and olistoliths at high structural positions in the Brooks Range, the location of its source area is unknown. The widespread distribution of the Nuka in the western Brooks Range suggests that the source area was extensive. On the basis of U-Pb, Nd, and Pb isotopic data from the arkosic detritus, we eliminate the exposed granitic rocks in the southern Brooks Range as a possible source area for the detritus in the Nuka Formation. Only the Kilbuck and Idono terranes of southwestern Alaska are known to contain granitic rocks of approximately the same age and isotopic character as the detritus in the Nuka Formation, but they are allochthonous relative to the North American craton and also differ somewhat from the Nuka detritus in their isotopic characteristics.

Zircons with 2.0–2.1 Ga crystallization ages seem to represent an important crustal component along the Cordillera. However, many of these rocks have Archean Nd model ages, which distinguishes them from the Proterozoic Nd

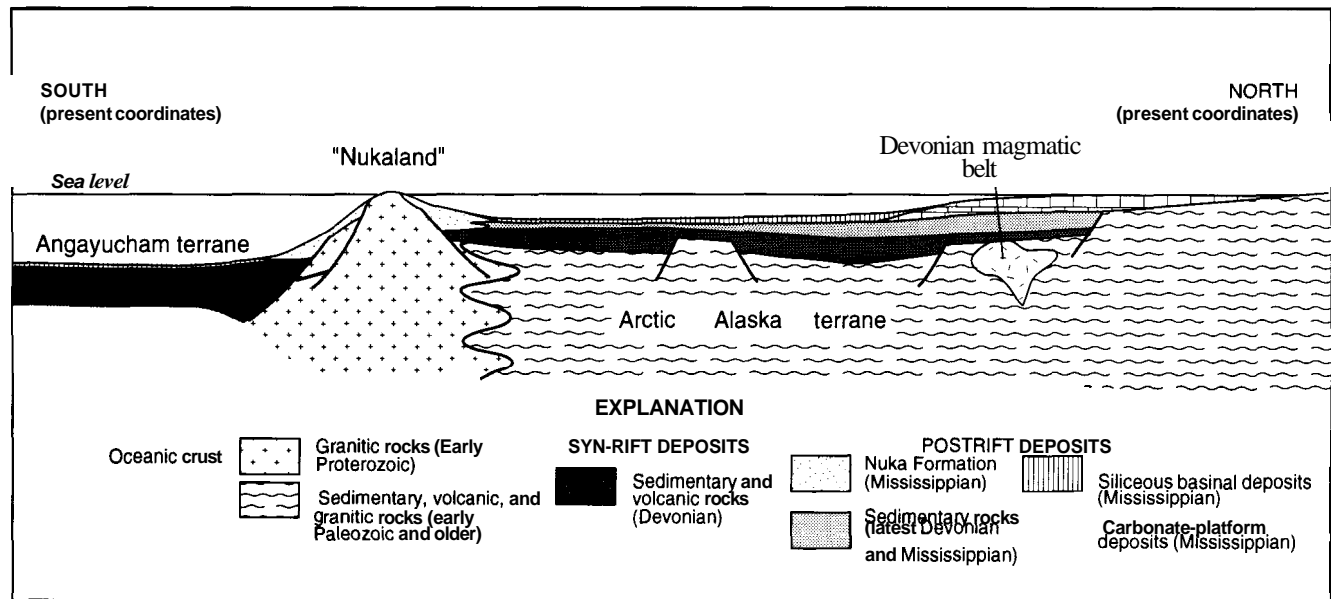


Figure 16. Paleogeographic restoration of the Nuka Formation as inferred by isotopic data and known geologic relations. The data suggest that the Nuka Formation was deposited adjacent to an offshore highland composed of Early Proterozoic granitic rocks near the outer edge of a Devonian to Jurassic passive continental margin. The Early Proterozoic granitic rocks may have been stranded by older (Proterozoic or Devonian) rifting along the margin of North America (see text for explanation).

model ages of the Nuka Formation detritus. The generally allochthonous nature of the terranes in which much of this evidence is preserved precludes any direct correlation among these terranes and the source for the Nuka Formation. Geologic relations and plate reconstructions for Proterozoic time suggest that the source area for the Nuka could have been crustal blocks stranded by rifting along the western margin of North America in the neo-Proterozoic or by rifting along the northern margin of North America in the Devonian.

Acknowledgments.—Sidney Hemming was partially supported by National Science Foundation Presidential Young Investigator award EAR8957784 to Scott McLennan. Thanks to Wesley K. Wallace, Michael Churkin, Jr., and Donald L. Turner, who helped collect the samples, and to ARCO Alaska, Inc., who provided funding for zircon analysis. Crushing and initial separation of the samples were done in the lab of D.L. Turner at the University of Alaska, and Carl Leighton did some additional separations at Stony Brook. Analyses were done in G.N. Hanson's lab at Stony Brook. Klaus Mezger helped with zircon analyses and data reduction. Dave Moecher identified the rutile by EDS. J.S. Oldow, Elizabeth Moll-Stalcup, and S.E. Box provided us with preprints. Thanks to Scott McLennan, Gerry Ross, Irv Tailleir, Gary Hemming, Klaus Mezger, Owen Evans, Eirik Krogstad, G.N. Hanson, Diane McDaniel, and Barbara Bock for reading various drafts of this manuscript. We are grateful to Elizabeth Moll-Stalcup, J.L. Wooden, W.W. Patton, S.C. Bergman, and Arthur Grantz, who provided thorough and helpful reviews of early drafts of the manuscript, and J.L. Wooden and David Brew, who reviewed the present version.

## REFERENCES CITED

- Aleinikoff, J.N., Moore, T.E., Walter, Marianne, and Nokleberg, W.J., 1993, U-Pb ages of zircon, monazite, and sphene from Devonian metagranites and metafelsites, central Brooks Range, Alaska, *in* Dusel-Bacon, Cynthia, and Till, A.B., eds., *Geologic studies in Alaska by the U.S. Geological Survey, 1992: U.S. Geological Survey Bulletin 2068*, p. 59–70.
- Armstrong, R.L., Parrish, R.R., Van der Heyden, P., Scott, K., Runkle, D., and Brown, R.L., 1991, Early Proterozoic basement exposures in the southern Canadian Cordillera: core gneiss of Frenchman Cap, unit I of the Grand Forks Gneiss, and the Vaseaux Formation: *Canadian Journal of Earth Sciences*, v. 28, no. 8, p. 1169–1201.
- Arth, J.G., 1994, Isotopic composition of the igneous rocks of Alaska, *in* Plafker, George, and Berg, H.C., eds., *The geology of Alaska: Boulder, Colo., Geological Society of America, The Geology of North America*, v. G-1, p. 781–795.
- Bally, A.W., 1975, A geodynamic scenario for hydrocarbon occurrences: Tokyo, 9th World Petroleum Congress, v. 2, p. 23–44.
- Banfield, J.F., and Eggleton, R.A., 1989, Apatite replacement and rare earth mobilization, fractionation, and fixation during weathering: *Clays and Clay Minerals*, v. 37, p. 113–127.
- Bowring, S.A., and Podosek, F.A., 1989, Nd isotopic evidence from Wopmay orogen for 2.0–2.4 Ga crust in western North America: *Earth and Planetary Science Letters*, v. 94, p. 2170–2230.
- Box, S.E., 1985, Early Cretaceous orogenic belt in northeastern Alaska: internal organization, lateral extent, and tectonic interpretation, *in* Howell, D.G., ed., *Tectonostratigraphic terranes of the circum-Pacific region: Houston, Tex., Circum-Pacific Council for Energy and Mineral Resources (American Association of Petroleum Geologists), Earth Science series*, no. 1, p. 137–145.
- Box, S.E., Moll-Stalcup, E.J., Wooden, J.L., and Bradshaw, J.Y., 1990, Kilbuck terrane: oldest known rocks in Alaska: *Geology*, v. 18, p. 1219–1222.
- Cameron, A.E., Smith, D.H., and Walker, R.L., 1969, Mass spectrometry of nanogram-size samples of lead: *Analytical Chemistry*, v. 41, p. 525–526.
- Christiansen, P.P., and Snee, L.W., 1994, Structure, metamorphism, and geochronology of the Cosmos Hills and Ruby Ridge, Brooks Range schist belt, Alaska: *Tectonics*, v. 13, no. 1, p. 193–213.
- Dalziel, I.W.D., 1991, Pacific margins of Laurentia and East Antarctica–Australia as a conjugate rift pair: evidence and implications for an Eocambrian supercontinent: *Geology*, v. 19, p. 598–601.
- Dickinson, W.R., 1977, Paleozoic plate tectonics and the evolution of the Cordilleran continental margin, *in* Stewart, J.H., Stevens, C.H., and Fritsche, A.E., eds., *Paleozoic paleogeography of the western United States: Society of Economic Paleontologists and Mineralogists, Pacific Section, Pacific Coast Paleogeography Symposium 1*, p. 137–155.
- Dillon, J.T., Pessel, G.H., Chen, J.H., and Veach, N.C., 1980, Middle Paleozoic magmatism and orogenesis in the Brooks Range, Alaska: *Geology*, v. 8, p. 338–343.
- Dillon, J.T., Tilton, G.R., Decker, John, and Kelly, M.J., 1987, Resource implications of magmatic and metamorphic ages for Devonian igneous rocks in the Brooks Range, *in* Tailleir, I.L., and Weimer, Paul, eds., *Alaskan North Slope geology, Society of Economic Paleontologists and Mineralogists, Pacific Section, Bakersfield, Calif., Book 50*, v. 2, p. 713723.
- Doe, B.R., and Zartman, R.E., 1979, Plumbotectonics, the Phanerozoic, *in* Barnes, Hubert L., ed., *Geochemistry of hydrothermal ore deposits (2d ed.)*: New York, John Wiley, p. 22–66.
- Epstein, A.G., Epstein, J.B., and Harris, L.D., 1977, Conodont color alteration—an index to organic metamorphism: *U.S. Geological Survey Professional Paper 995*, 27 p.
- Gehrels, G.E., Dickinson, W.R., Ross, G.M., Stewart, J.H., and Howell, D.G., 1995, Detrital zircon reference for Cambrian to Triassic miogeoclinal strata of western North America: *Geology*, v. 23, no. 9, p. 831–834.
- Girty, G.H., and Wardlaw, M.S., 1985, Petrology and provenance of pre-Late Devonian sandstones, Shoo Fly complex, northern Sierra Nevada, California: *Geological Society of America Bulletin*, v. 96, p. 516–521.
- Grantz, Arthur, Moore, T.E., and Roeske, S.M., 1991, Continent-ocean transect A-3: Gulf of Alaska to Arctic Ocean: *Boul-*

- der, Colo., Geological Society of America, scale 1:500,000, 3 sheets.
- Halgedahl, S.L., and Jarrard, R.D., 1987, Paleomagnetism of the Kuparuk River Formation from oriented drill core: evidence for rotation of the Arctic Alaska plate, *in* Tailleir, I.L., and Weimer, Paul, eds., *Alaskan North Slope geology: Pacific Section, Society of Economic Paleontologists and Mineralogists*, Bakersfield, Calif., Book 50, p. 581–617.
- Harland, W.B., and others, 1990, *A geologic time scale 1989*: Cambridge, England, Cambridge University Press, 263 p.
- Harris, R.A., 1988, Origin, emplacement and attenuation of the Misheguk Mountain allochthon, western Brooks Range, Alaska [abs.]: *Geological Society of America Abstracts with Programs*, v. 20, p. A112.
- Harrison, T.M., 1990, Some observations on the interpretation of feldspar  $^{40}\text{Ar}/^{39}\text{Ar}$  results: *Chemical Geology*, v. 80, p. 219–229.
- Hoffman, P.F., 1989, Precambrian geology and tectonic history of North America, *in* Bally, A.W., and Palmer, A.R., eds., *The geology of North America; an overview*: Boulder, Colo., Geological Society of America, *The Geology of North America*, v. A, p. 447–512.
- 1991, Did the breakout of Laurentia turn Gondwanaland inside-out?: *Science*, v. 252, p. 1409–1412.
- Karl, S.M., and Aleinikoff, J.N., 1990, Proterozoic U-Pb zircon age of granite in the Kallarichuk Hills, western Brooks Range, Alaska: evidence for Precambrian basement in the schist belt, *in* Dover, J.H., and Galloway, J.P., eds., *Geologic studies in Alaska by the U.S. Geological Survey, 1989*: U.S. Geological Survey Bulletin 1956, p. 95–100.
- Karl, S.M., Aleinikoff, J.N., and Dickey, C.F., 1989, Age and chemical composition of the Proterozoic intrusive complex at Mount Angayukaqraq, western Brooks Range, Alaska, *in* Dover, J.H., and Galloway, J.P., eds., *Geologic studies in Alaska by the U.S. Geological Survey, 1988*: U.S. Geological Survey Bulletin 1903, p. 10–19.
- Kistler, R.W., and Peterrnan, Z.E., 1978, Reconstruction of crustal blocks of California on the basis of initial strontium isotopic compositions of Mesozoic granitic rocks: U.S. Geological Survey Professional Paper 1071, 17 p.
- Krogh, T.E., 1973, A low contamination method for the hydrothermal decomposition of zircon and extraction of U-Pb for isotopic age determinations: *Geochimica et Cosmochimica Acta*, v. 37, p. 485–494.
- 1982, Improved accuracy of U-Pb zircon ages by the creation of more concordant systems using an air abrasion technique: *Geochimica et Cosmochimica Acta*, v. 46, p. 637–649.
- Little, T.A., Miller, E.L., Lee, J., and Law, R.D., 1994, Extensional origin of ductile fabrics in the schist belt, central Brooks Range, Alaska—I. Geologic and structural studies: *Journal of Structural Geology*, v. 16, no. 7, p. 899–918.
- Lovera, O.M., Richter, F.M., and Harrison, T.M., 1989, The  $^{40}\text{Ar}/^{39}\text{Ar}$  thermochronometry for slowly cooled samples having a distribution of diffusion domain sizes: *Journal of Geophysical Research*, v. 94, p. 17,917–17,935.
- Ludwig, K.R., 1980, Calculations of uncertainties of U-Pb isotope data: *Earth and Planetary Science Letters*, v. 46, p. 212–220.
- 1988, ISOPLOT for MS DOS. A plotting and regression program for radiogenic-isotope data, for IBM-PC compatible computers, version 1.00: U.S. Geological Survey Open-File Report 88-577, 39 p.
- Mayfield, C.F., Curtis, S.M., Ellersieck, Inyo, and Tailleir, I.L., 1984, Reconnaissance geologic map of southeastern Misheguk Mountain quadrangle, Alaska: U.S. Geological Survey Miscellaneous Investigations Map 1-1503, scale 1:63,360.
- Mayfield, C.F., Ellersieck, Inyo, and Tailleir, I.L., 1987, Reconnaissance geologic map of the Noatak C5, D5, D6, and D7 quadrangles, Alaska: U.S. Geological Survey Miscellaneous Investigations Map I-1814, scale 1:63,360.
- Mayfield, C.F., Tailleir, I.L., and Ellersieck, Inyo, 1988, Stratigraphy, structure, and palinspastic synthesis of the western Brooks Range, northwestern Alaska, *in* Gryc, George, ed., *Geology and exploration of the National Petroleum Reserve in Alaska, 1974 to 1982*: U.S. Geological Survey Professional Paper 1399, p. 143–186.
- McDaniel, D.K., Hemming, S.R., McLennan, S.M., and Hanson, G.N., 1994, Resetting of neodymium isotopes and redistribution of REE during sedimentary processes: the Early Proterozoic Chelmsford Formation, Sudbury Basin, Ontario, Canada: *Geochimica et Cosmochimica Acta*, v. 58, p. 931–941.
- McDougall, I., and Harrison, T.M., 1988, Geochronology and thermochronology by the  $^{40}\text{Ar}/^{39}\text{Ar}$  method: Oxford Monograph on Geology and Geophysics no. 9: New York, Oxford University Press, 212 p.
- McLennan, S.M., 1989, Rare earth elements in sedimentary rocks: influence of provenance and sedimentary processes, *in* Lipin, B.R., and McKay, G.A., eds., *Geochemistry and mineralogy of the rare earth elements: Reviews in Mineralogy*, v. 21, p. 169–196.
- Mezger, K., Hanson, G.N., and Bohlen, S.R., 1989, High-precision U-Pb ages of metamorphic rutile: application to the cooling history of high-grade terranes: *Earth and Planetary Science Letters*, v. 96, p. 106–118.
- Miller, M.L., Bradshaw, J.Y., Kimbrough, D.L., Stem, T.W., and Bundtzen, T.K., 1991, Isotopic evidence for Early Proterozoic age of the Idono Complex, west-central Alaska: *Journal of Geology*, v. 99, p. 209–223.
- Miller, M.M., and Saleeby, J.B., 1989, Proterozoic detrital zircon from the Carboniferous Bragdon Formation, E. Klamath terrane, California: continent-influenced arc sedimentation [abs.]: *Geological Society of America Abstracts with Programs*, v. 21, p. 347.
- Moll-Stalcup, E.J., Wooden, J.L., Bradshaw, J.Y., and Aleinikoff, J.N., 1996, Elemental and isotopic evidence for 2.1-Ga arc magmatism in the Kilbuck terrane, southwestern Alaska, *in* Moore, T.E., and Dumoulin, J.A., eds., *Geologic studies in Alaska by the U.S. Geological Survey, 1994*: U.S. Geological Survey Bulletin 2152, p. 111–130.
- Moore, T.E., Grantz, Arthur, and Roeske, S.M., 1994b, Continent-ocean transition in Alaska: the tectonic assembly of eastern Denalia, *in* Speed, R.C., ed., *Phanerozoic evolution of North American continent-ocean transitions*: Boulder, Colo., Geological Society of America, *The Geology of North America*, v. CTV-1, p. 399–441.
- Moore, T.E., Wallace, W.K., Bird, K.J., Karl, S.M., Mull, C.G. and Dillon, J.T., 1994a, Geology of northern Alaska, *in* Plafker, George, and Berg, H.C., eds., *The geology of Alaska*:

- Boulder, Colo., Geological Society of America, *The Geology of North America*, v. G-1, p. 49–140.
- Moore, E.M., 1991, Southwest U.S.-Antarctic (SWEAT) connection: a hypothesis: *Geology*, v. 19, p. 425–428.
- Mull, C.G., and TAILLEUR, I.L., 1977, Sadlerochit(?) Group in the Schwatka Mountains, south-central Brooks Range, in Blean, K.M., ed., *The United States Geological Survey in Alaska: Accomplishments during 1976*: U.S. Geological Survey Circular 751-B, p. B27–B29.
- Murphy, D.C., Walker, R.T., and Parrish, R.R., 1991, Age and geological setting of Gold Creek gneiss, crystalline basement of the Windermere Supergroup, Cariboo Mountains, British Columbia: *Canadian Journal of Earth Sciences*, v. 28, no. 8, p. 1217–1231.
- Nance, W.B., and Taylor, S.B., 1977, Rare earth element patterns and crustal evolution—II. Archean sedimentary rocks from Kalgoorlie, Australia: *Geochimica et Cosmochimica Acta*, v. 41, p. 225–231.
- Nelson, S.W., and Grybeck, Donald, 1980, Geologic map of the Survey Pass quadrangle, Brooks Range, Alaska: U.S. Geological Survey Miscellaneous Field Studies Map MF-1176A, scale 1:250,000.
- Nelson, B.K., Nelson, S.W., and Till, A.B., 1993, Nd- and Sr-isotope evidence for Proterozoic and Paleozoic crustal evolution in the Brooks Range, northern Alaska: *Journal of Geology*, v. 101, p. 435–450.
- Nesbitt, H.W., 1979, Mobility and fractionation of rare earth elements during weathering of a granodiorite: *Nature*, v. 279, p. 206–210.
- Nokleberg, W.J., and 23 others, 1994, Circum-North Pacific tectonostratigraphic terrane map: U.S. Geological Survey Open-File Report 94-714, 221 p., 5 sheets.
- Oldow, J.S., Seidensticker, C.M., Phelps, J.C., Julian, F.E., Gottschalk, R.R., Boler, K.W., Handschy, J.W., and Avé Lallemant, H.G., 1987, Balanced cross sections through the central Brooks Range and North Slope, Arctic Alaska: American Association of Petroleum Geologists publication, 19 p., 8 pls., scale 1:200,000.
- Palmer, A.R., Dillon, J.T., and Dutro, J.T., Jr., 1984, Middle Cambrian trilobites with Siberian affinities from the central Brooks Range, northern Alaska: *Geological Society of America Abstracts with Programs*, v. 16, p. 327.
- Plafker, George, and Berg, H.C., 1994, Overview of the geology and tectonic evolution of Alaska in Plafker, George, and Berg, H.C., eds., *The geology of Alaska*: Boulder, Colo., Geological Society of America, *The Geology of North America*, v. G-1, p. 989–1021.
- Rosenblum, S., and Mosier, E.L., 1983, Mineralogy and occurrence of europium-rich dark monazite: U.S. Geological Survey Professional Paper 1181, 67 p.
- Ross, G.M., and Parrish, R.R., 1991, Detrital zircon geochronology of metasedimentary rocks in the southern Omineca belt, Canadian Cordillera: *Canadian Journal of Earth Sciences*, v. 28, no. 8, p. 1254–1270.
- Ross, G.M., Parrish, R.R., and Winston, D., 1992, Provenance and U-Pb geochronology of the Mesoproterozoic Belt Supergroup (northwestern United States): implications for age of deposition and pre-Panthalassa plate reconstructions: *Earth and Planetary Science Letters*, v. 113, p. 57–76.
- Sharp, W.D., 1988, Pre-Cretaceous crustal evolution in the Sierra Nevada region, California, in Ernst, W.G., ed., *Metamorphism and crustal evolution of the western United States*, Rubey Volume VII: Englewood Cliffs, N.J., Prentice-Hall, p. 823–864.
- Stacey, L.S., and Kramers, J.D., 1975, Approximation of terrestrial lead isotope evolution by a two-stage model: *Earth and Planetary Science Letters*, v. 26, p. 207–221.
- Stern, R.A., and Hanson, G.N., 1991, Archean high-Mg granodiorite: a derivative of light rare earth element-enriched monzodiorite of mantle origin: *Journal of Petrology*, v. 32, p. 201–238.
- Tailleur, I.L., 1985, Letter to the editor: *Newsletter of the Alaska Geological Society*, v. 15, no. 2.
- Tailleur, I.L., Mamet, B.L., and Dutro, J.T., Jr., 1973, Revised age and structural interpretation of Nuka formation at Nuka Ridge, northwestern Alaska: *American Association of Petroleum Geologists Bulletin*, v. 57, p. 1348–1352.
- Tailleur, I.L., Mayfield, C.F., and Eilersieck, I.F., 1977, Late Paleozoic sedimentary sequence, southwestern Brooks Range, in Blean, K.M., ed., *The United States Geological Survey in Alaska: Accomplishments during 1976*: U.S. Geological Survey Circular 751-B, p. B25–B27.
- Tailleur, I.L., and Sable, E.G., 1963, Nuka Formation of Late Mississippian to Late Permian age, new formation in northern Alaska: *American Association of Petroleum Geologists Bulletin*, v. 47, p. 632–642.
- Tatsumoto, M., Knight, R.J., and Allegre, C.J., 1973, Time differences in the formation of meteorites as determined from the ratio of lead-207 to lead-206: *Science*, v. 180, p. 1279–1283.
- Taylor, S.R., and McLennan, S.M., 1985, *The continental crust: its composition and evolution*: Oxford, Blackwell, 312 p.
- Thériault, R.J., and Ross, G.M., 1991, Nd isotopic evidence for crustal recycling in the ca. 2.0 Ga subsurface of western Canada: *Canadian Journal of Earth Sciences*, v. 28, no. 8, p. 1140–1147.
- Till, A.B., Schmidt, J.M., and Nelson, S.W., 1988, Thrust involvement of metamorphic rocks, southwestern Brooks Range, Alaska: *Geology*, v. 10, p. 930–933.
- Turner, D.L., Forbes, R.B., Aleinikoff, J.N., Hedge, C.E., and McDougal, Ian, 1983, Geochronology of the Kilbuck terrane of southwestern Alaska [abs.]: *Geological Society of America Abstracts with Programs*, v. 15, p. 407.
- Zhao, J.X., McCulloch, M.T., and Bennett, V.C., 1992, Sm-Nd and U-Pb zircon isotopic constraints on the provenance of sediments from the Amadeus Basin, central Australia: evidence for REE fractionation: *Geochimica et Cosmochimica Acta*, v. 56, p. 921–940.

Reviewers: Joseph L. Wooden and David A. Brew



# Comparison of Conodont and Calcareous Microfossil Biostratigraphy and Lithostratigraphy of the Lisburne Group (Carboniferous), Sadlerochit Mountains, Northeast Brooks Range, Alaska

By Anita G. Harris, Paul L. Brenckle, John F. Baesemann, Andrea P. Krumhardt, and Paul D. Gruzlovic

## ABSTRACT

Comparison of the lithostratigraphy and microfossil assemblages in two sections in the eastern and western Sadlerochit Mountains shows that deposition of the Alapah Limestone (Lisburne Group) began earlier and the entire formation formed under more restricted conditions in the western section. In both sections, appearances of the calcareous microfossils *Skippella?* sp. and *Koninckopora minuta?* help position the Meramecian-Chesterian boundary in the lower Alapah. Microfossils in the upper half of the formation are middle to late Chesterian, and the uppermost beds are probably very late Chesterian. Fossil assemblages in the overlying Wahoo Limestone are more diverse and slightly more biostratigraphically diagnostic than in the Alapah. The conodonts *Cavusgnathus unicornis* and *Adetognathus tythus* with the foraminifer *Brenckleina rugosa* likely indicate a very late Chesterian age for the lowest Wahoo strata. In both eastern and western sections, the Mississippian-Pennsylvanian boundary is at approximately the same stratigraphic level, 50-56 m above the base of the lower member of the Wahoo, and is marked by a chert-rich interval. The conodont *Declinognathodus noduliferus* and foraminifers *Pseudostaffella* spp. or *Eoschubertella* spp. appear to be the most reliable fossils for local and regional correlation of the base of the **Morrowan** and Atokan Series, respectively.

The Pennsylvanian part of the lower member and all of the upper member of the Wahoo Limestone are much thinner in the western section because of greater erosion along the pre-Echooka Formation unconformity, slower deposition, and (or) intraformational unconformities. The presence of glauconite and some cosmopolitan conodont species in the western section suggests that at least part of the Wahoo was deposited more slowly in somewhat deeper water open-marine conditions than to the east.

The microfossil succession in the Lisburne Group is generally consistent along depositional strike in northeast-

ern Alaska and is reliable for local Mississippian-Pennsylvanian correlation. However, correlation of the Lisburne with coeval rocks in sub-Arctic North America remains difficult because some biostratigraphic indices are absent and many that do occur seem to appear earlier in northern Alaska than southward.

## INTRODUCTION

The Lisburne Group (chiefly Carboniferous) is a thick sequence of predominantly carbonate rocks that extends across the Brooks Range and into the subsurface of the North Slope, where the upper part of the Lisburne (Wahoo Limestone) is a hydrocarbon reservoir (Jameson, 1994). In the northeast Brooks Range, the Lisburne is at least 400 m thick and is subdivided into the Alapah Limestone and overlying Wahoo Limestone. Calcareous microfossils (Armstrong and others, 1970; Mamet and Armstrong, 1972) and, more recently, conodonts (Krumhardt and others, 1996) have been used as the primary biostratigraphic controls for the Lisburne in the northeast Brooks Range.

Two sections of the Lisburne Group, about 40 km apart in the Sadlerochit Mountains (fig. 1), were measured and systematically sampled for conodonts, calcareous microfossils (foraminifers, algae, and *incertae sedis* (taxonomic position uncertain)), and microlithofacies. The eastern Sadlerochit Mountains (ESM) section was measured, sampled, and analyzed by Krumhardt and others (1996). Their study focused on the conodont biostratigraphy and microlithofacies of the Wahoo Limestone; a few samples were analyzed from the lower and upper parts of the underlying Alapah Limestone at lithostratigraphic boundaries. The western Sadlerochit Mountains (WSM) section, near the Katakaturuk River, is a composite section (figs. 1, 2) and was measured and sampled in 1985 by P.L. Brenckle, J.F. Baesemann, and C.E. Bartberger, Amoco Corporation. The calcareous microfossils, conodonts, and microlithofacies

were analyzed by Brenckle, Baesemann, and P.D. Gruzlovic, respectively.

The relationship of the Lisburne Group to coeval strata in **sub-Arctic** North America is not straightforward because of the absence of key taxa and (or) migration of taxa between the two regions. Krumhardt and others (1996) showed that most of the established Chesterian to early Atokan conodont zones of North America could not be recognized in the eastern Sadlerochit Mountains as well as elsewhere in the northeast Brooks Range because of the absence of many key species. For correlation, these authors developed a conodont biostratigraphic framework for the Wahoo Limestone using some established North American conodont zones together with local faunal intervals. P.L. Brenckle and J.F. Baesemann encountered the same biostratigraphic problems in their Lisburne section in the western Sadlerochit Mountains and elsewhere in the northeast Brooks Range. In addition, both groups of investigators recognized that previous workers in the Sadlerochit Mountains had incon-

sistently positioned series boundaries for a variety of biostratigraphic and lithostratigraphic reasons, including redefinition of series boundaries, inconsistent recognition of stratigraphic units, diachroneity in ranges of taxa between the Arctic and other areas, and changing taxonomic concepts and incomplete identification of assemblages of calcareous microfossils (see Krumhardt and others, 1996, fig. 8).

The above biostratigraphic dilemmas involving a widespread stratigraphic unit that is also an important hydrocarbon reservoir in the subsurface of the North Slope provided the impetus for this collaborative report. The two Lisburne Group sections that were independently sampled and analyzed not only allowed a comparison of conodont and calcareous microfossil biostratigraphy, but they also **confirmed** the influence of local variations in differential erosion and depositional regime on correlation.

In this report, we present a lithologic column for the WSM section (fig. 2), a range chart for calcareous micro-

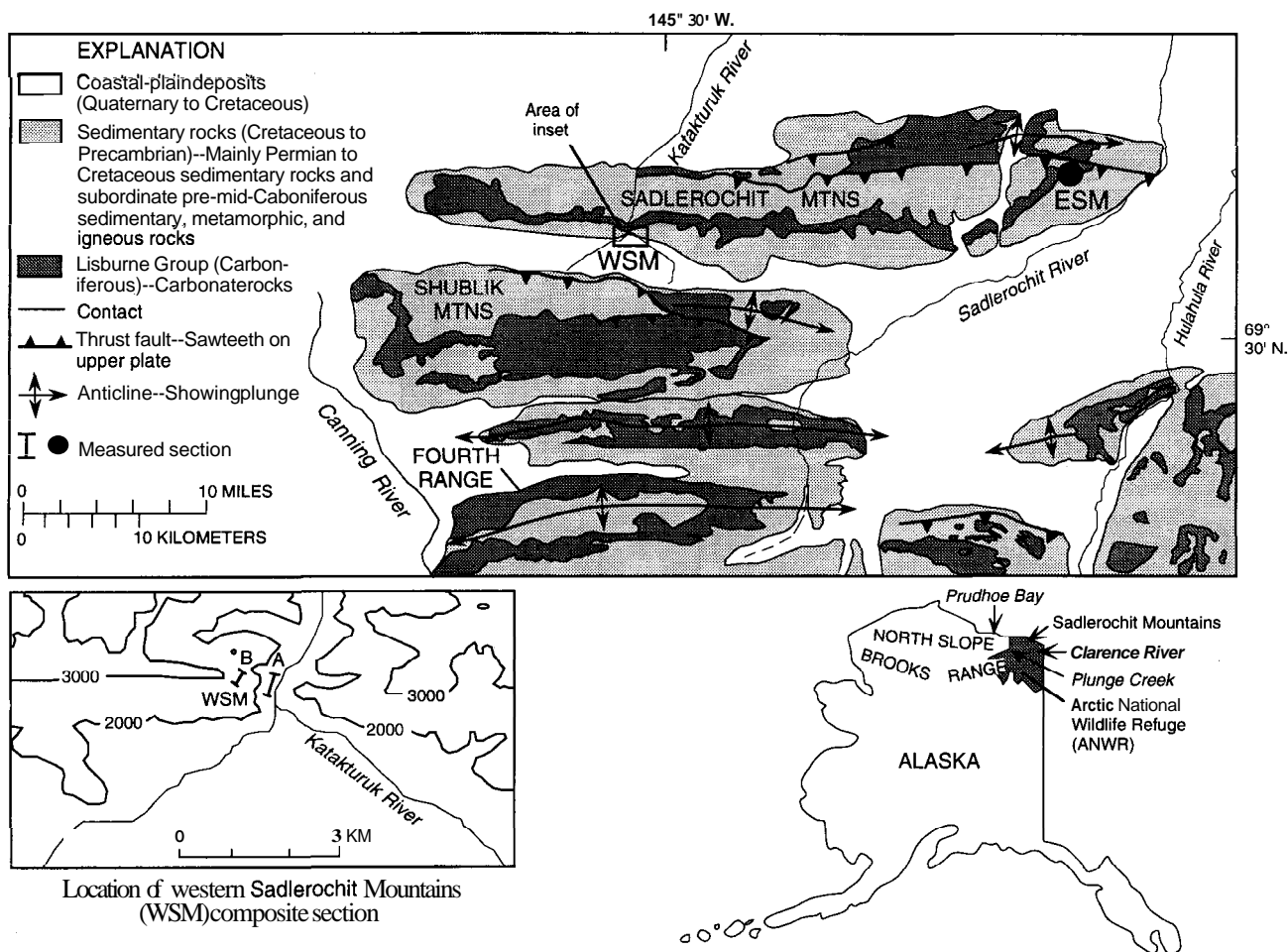


Figure 1. Generalized geologic map of the Sadlerochit Mountains showing location of the eastern (ESM) and western (WSM) Sadlerochit Mountains sections, northeast Brooks Range (modified from Krumhardt and others, 1996). Base for inset generalized from Mt. Michelson 1:250,000 quadrangle (1956 edition, revised 1983); contour interval is 1,000 ft. Lithologic columns for sections A and B are shown in figures 2A and 2B, respectively.

fossils found in the section (fig. 3), a comparison of the ranges of significant calcareous microfossils and conodonts in the eastern and western sections (figs. 4, 5), and photographs of significant calcareous microfossils in the western section and of conodonts thus far restricted to that section (figs. 6-10). A detailed lithologic column and micro-lithofacies analysis of the ESM section and photographs of all conodont species found there are provided in Krumhardt and others (1996). The conodont **biostratigraphic** scheme given by Krumhardt and others (1996, fig. 7) is much the same as that used here (see fig. 5).

### MICROPALAEONTOLOGICAL SAMPLING AND ANALYSIS

Conodont samples averaging 7 kg were collected at 5-m intervals in the ESM section; closer intervals were sampled near lithostratigraphic and chronostratigraphic boundaries. Three samples were collected from the Alapah Limestone and 72 from the Wahoo Limestone; all produced conodonts. P.L. Brenckle analyzed the calcareous microfossils from key lithostratigraphic and **chronostratigraphic** levels in this section: from 42 to 70 m above the base of the lower member of the Wahoo and from the basal 11 m and between 82 and 118.5 m above the base of the upper member.

Conodont samples averaging 5 kg were collected at 2- to 5-m intervals and calcareous microfossil samples were collected at closer intervals in the WSM section (fig. 2). Of 95 conodont samples collected, 46 are from the Alapah Limestone and 49 are from the Wahoo Limestone. Ten samples, all from the Alapah, lacked conodonts. Harris and Krumhardt independently analyzed the western section conodont collections previously analyzed by Baesemann. Our biostratigraphic interpretations are in agreement, as are virtually all of our taxonomic assignments.

## COMPARISON OF THE WESTERN AND EASTERN SADLEROCHIT MOUNTAINS SECTIONS

### LITHOSTRATIGRAPHY

#### ALAPAH LIMESTONE (MISSISSIPPIAN)

An angular unconformity separates the Alapah Limestone from the underlying Nanook Limestone of Cambrian and Ordovician age in the WSM section and from the **Katakturuk** Dolomite of Proterozoic age in the ESM section. In the WSM section, the Alapah is approximately 224 m thick (fig. 2A). The lower 83 m is about two-thirds exposed and is mainly composed of peloidal to skeletal packstone and cross-bedded grainstone in cycles 12-15 m thick. The middle part of the Alapah is about 70 m thick;

only one-third of this part is exposed in the WSM and consists of bryozoan-pelmatozoan packstone and grainstone. The unexposed intervals are mostly covered by platy to blocky dolomitic rubble. The upper part of the Alapah is 69 m thick, about 90 percent exposed, and is chiefly dolomitic mudstone, wackestone, and packstone containing bryozoans and pelmatozoans and lesser amounts of grainstone. Sponge spicules increase in abundance in the upper 10 m. The lower part of the Alapah formed in intertidal, **restricted**-to open-platform and shoal environments. The middle part of the Alapah was deposited in an open-platform and (or) open-marine environment, and the upper part formed in restricted-platform to intertidal settings. Locally, **recrystallization** at the top of the Alapah in the WSM section (fig. 2A) obliterated many of the original grains. The origin of the recrystallized zone is unclear. It may have formed during a tectonic event or local exposure, but its presence seems to have no significant effect on the faunal succession, which is neither repeated nor noticeably truncated.

The Alapah Limestone is about 175 m thick in the eastern Sadlerochit Mountains (Watts and others, 1994). Major rock types include (1) spiculitic dolomite and dolomitic lime mudstone-wackestone containing cryptalgal **laminite**; (2) bryozoan-pelmatozoan limestone; and (3) skeletal grainstone and packstone. Lithostratigraphy, **micro-lithofacies**, and conodont biofacies indicate the Alapah formed in a variety of shallow-water depositional settings on a carbonate **platform** (Watts and others, 1994).

Lithologically, the Alapah Limestone is similar in the eastern and western sections. The formation is about 50 m thicker and appears more dolomitic in the western section. Deposition of the Alapah began earlier in the west. Here, the lower 40 m are most likely late Meramecian, whereas the entire Alapah is of Chesterian age in the eastern Sadlerochit Mountains (**Mamet** and Armstrong, 1984). The contact between the Alapah and the overlying Wahoo Limestone is sharp and conformable in the eastern section and is placed at the base of the first light-weathering, **cliff**-forming, fossiliferous limestone above the slope-forming, darker limestone and dolostone characteristic of the Alapah. The boundary is probably the same in the western section, where it is placed at the top of a recrystallized zone. In both sections the formation is interpreted to have formed in a restricted- to open-platform depositional setting, although restricted settings are more prevalent in the western section.

#### WAHOO LIMESTONE (MISSISSIPPIAN AND PENNSYLVANIAN)

The Wahoo Limestone, which is approximately 262 m thick in the ESM section and 142 m thick in the WSM section, has been informally subdivided into lower and upper members by Watts and others (1994). The general lithologic succession is similar in both sections. The western

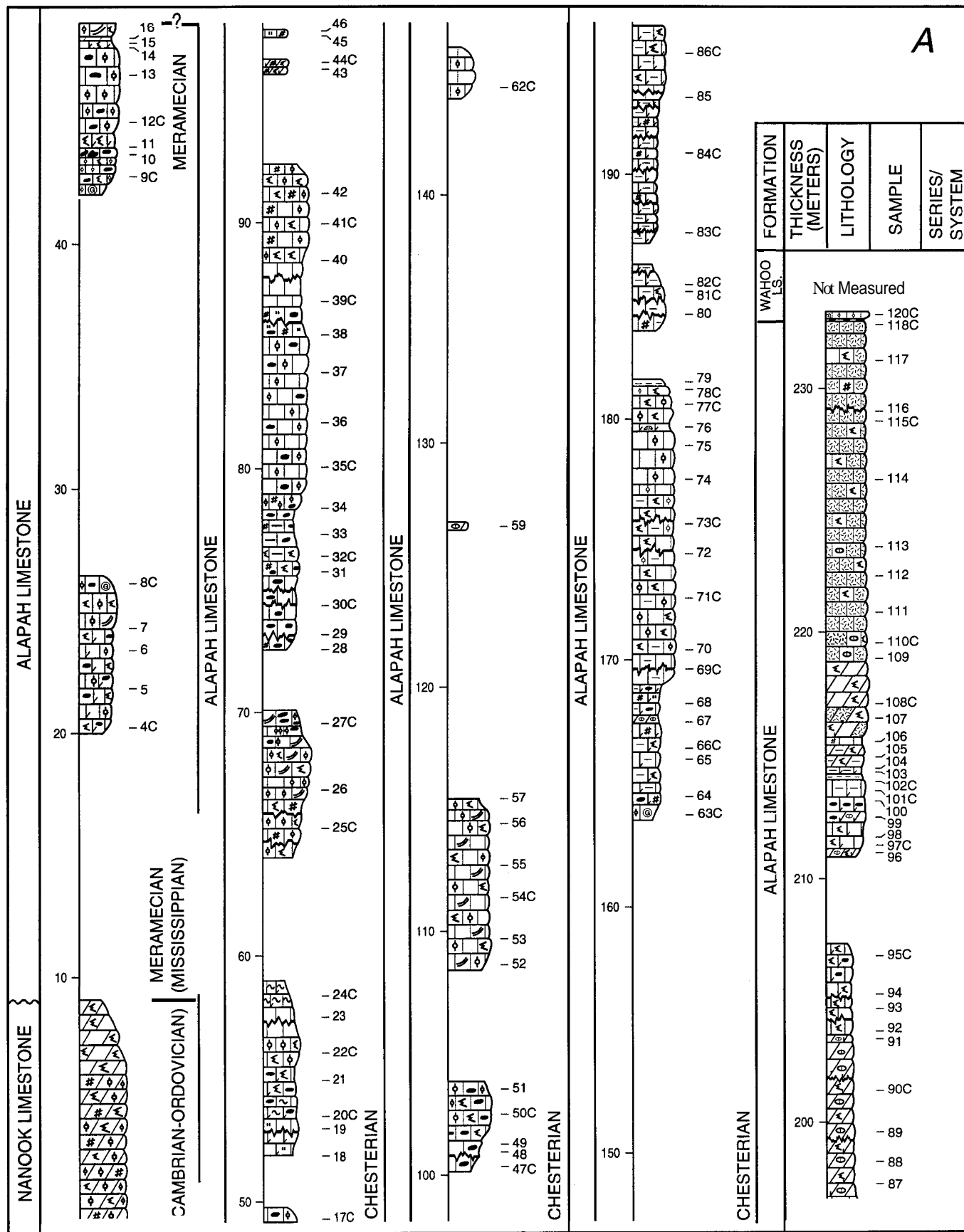


Figure 2. Stratigraphic succession at the western Sadlerochit Mountains (WSM) composite section at **Katakturuk** River showing lithology and sample locations. Gaps in lithologic column are covered intervals. Samples for grain-type and calcareous microfossil analysis were taken at every location; C indicates conodont sample also collected. Sections A (lower part) and B (upper part) have a composite thickness of 377 m. The sections overlap slightly and are correlated at the Alapah Limestone–Wahoo Limestone contact.

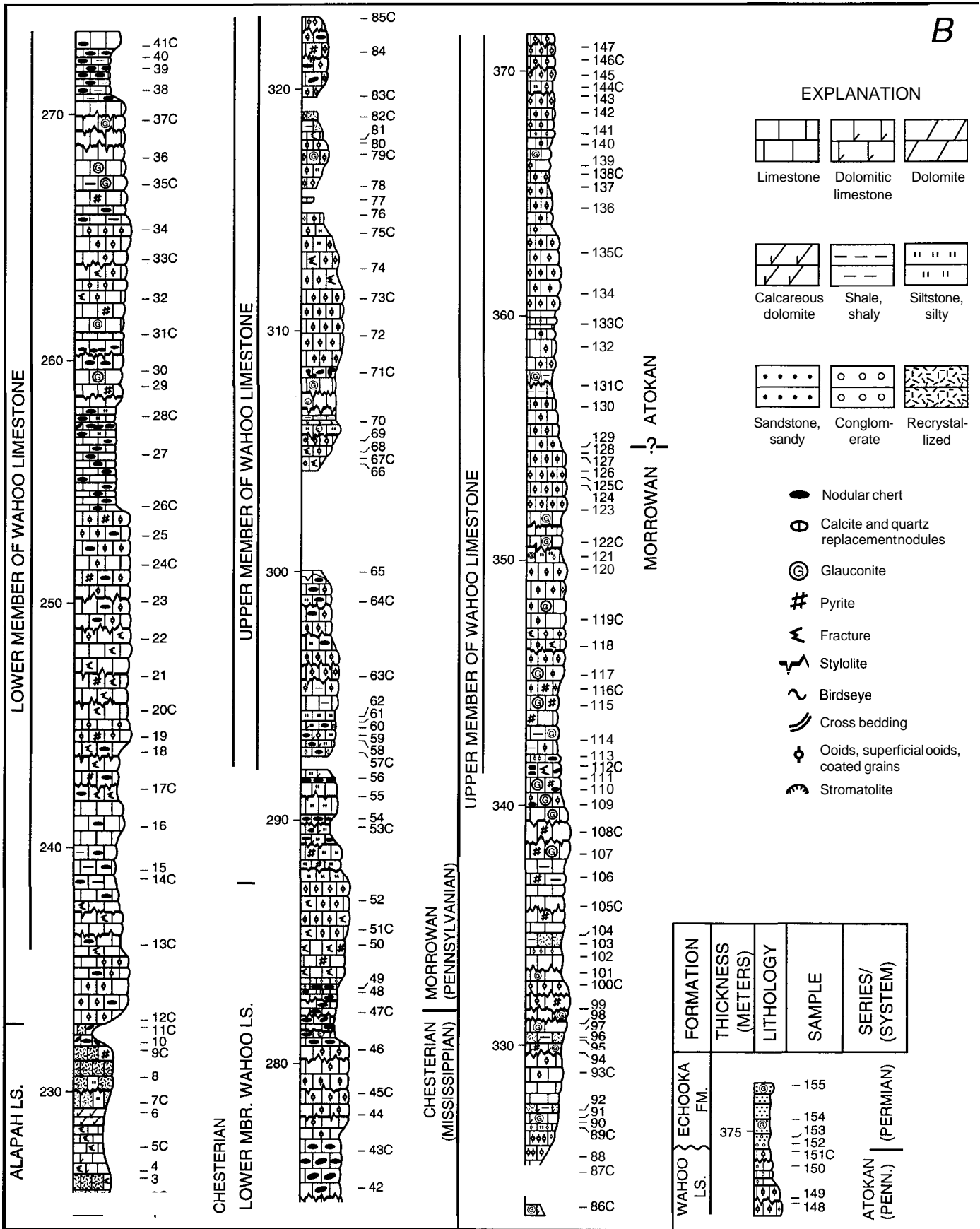


Figure 2. Continued

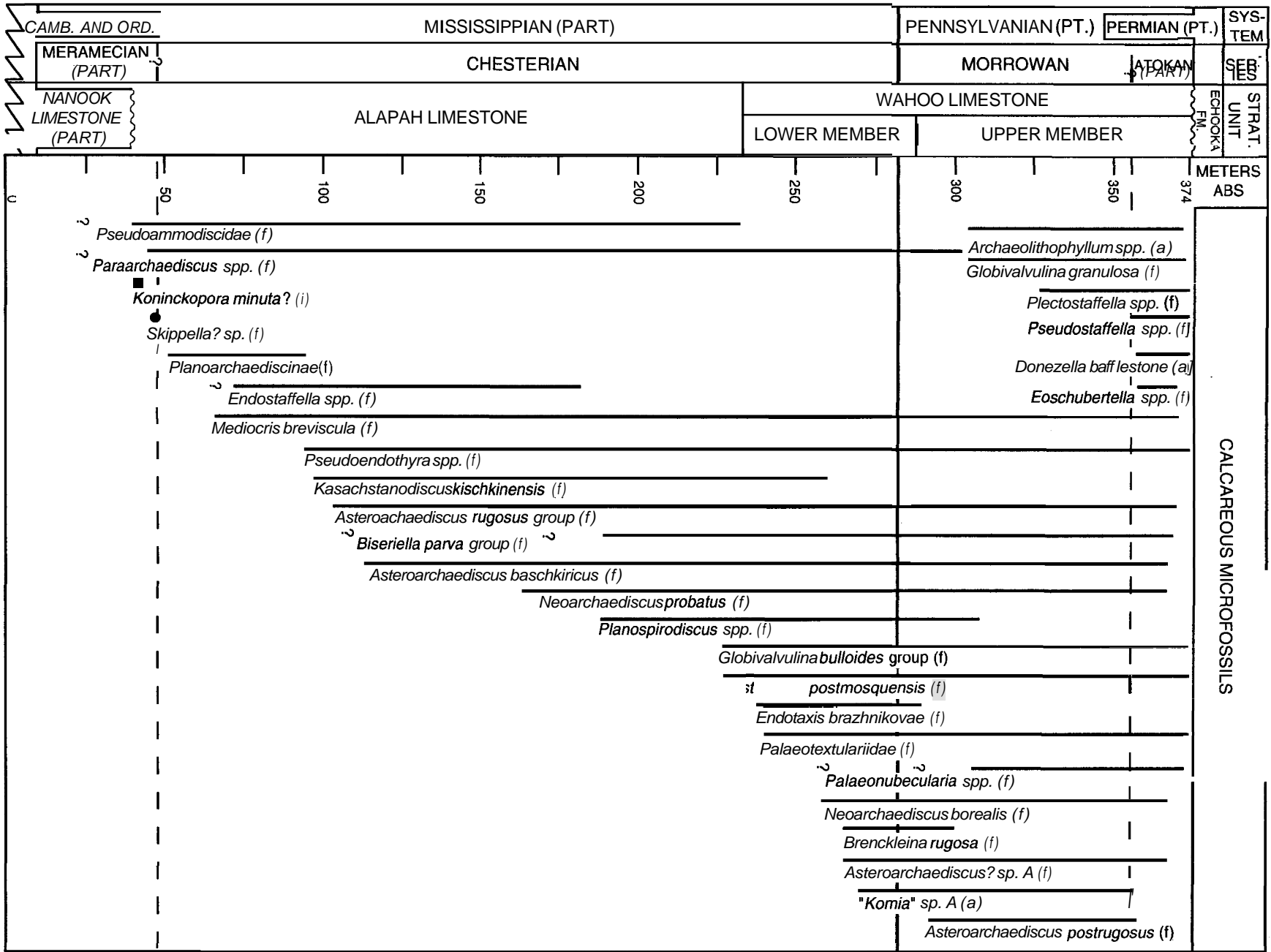
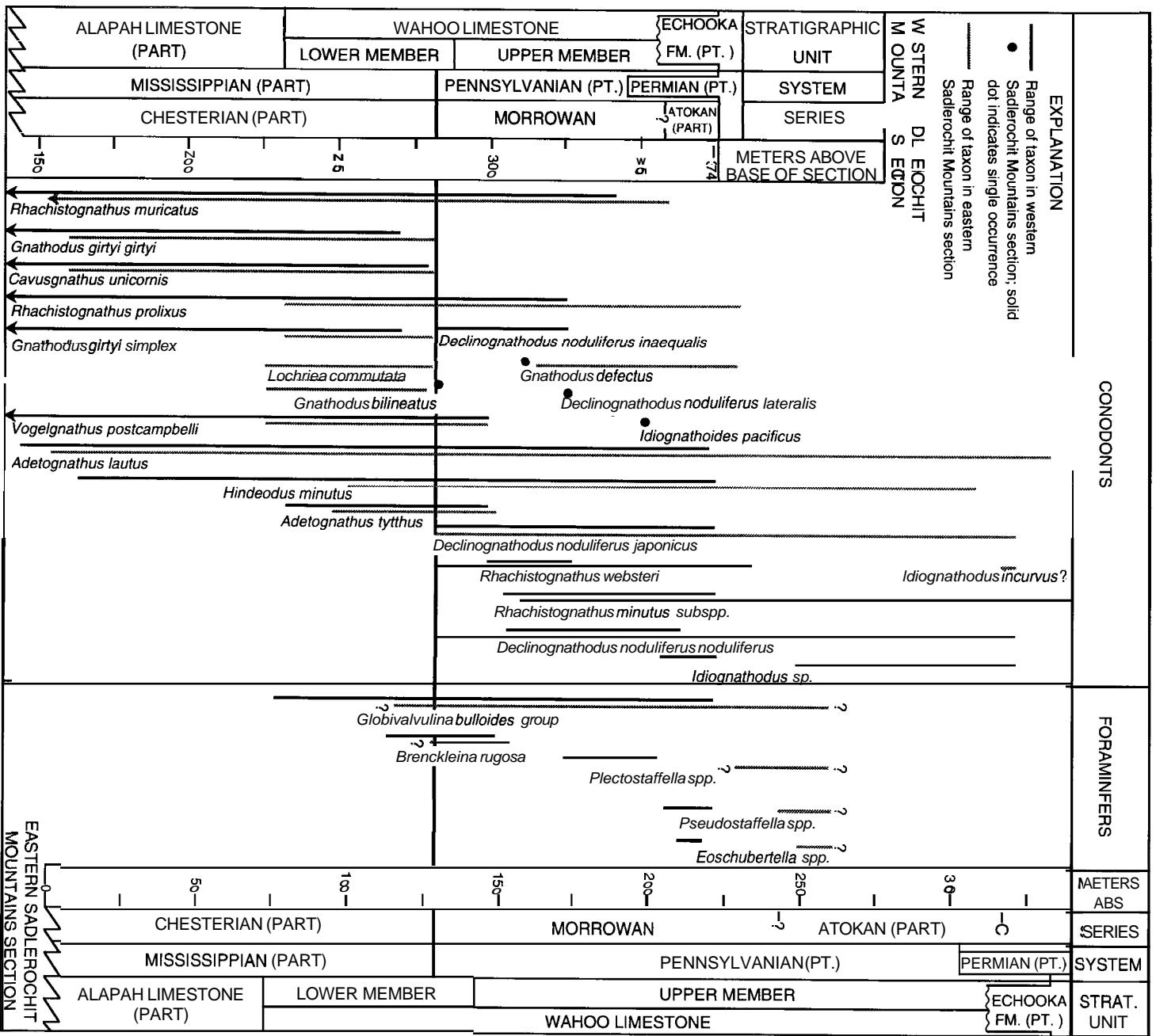


Figure 3. Range of selected calcareous microfossils in the western Sadlerochit Mountains composite section. Range line extend between first and last positive occurrence; query above or below range line indicates uncertain taxonomic assignment. Abbreviations: ABS, above base of section; a, alga; f, foraminifer; i, incertae sedis.



**Figure 4.** Comparison of the ranges of selected conodonts and biostratigraphically important foraminifers in the eastern (ESM) and western (WSM) Sadlerochit Mountains sections. Sections are correlated at the Mississippian-Pennsylvanian boundary. Ranges are shown just for the upper part of the Alapah Limestone because only a few microfossil samples were collected from the Alapah in the ESM section. Arrow at end of range line indicates taxon continues in the section; query indicates no data above or below range line. Abbreviation: ABS, above base of section.

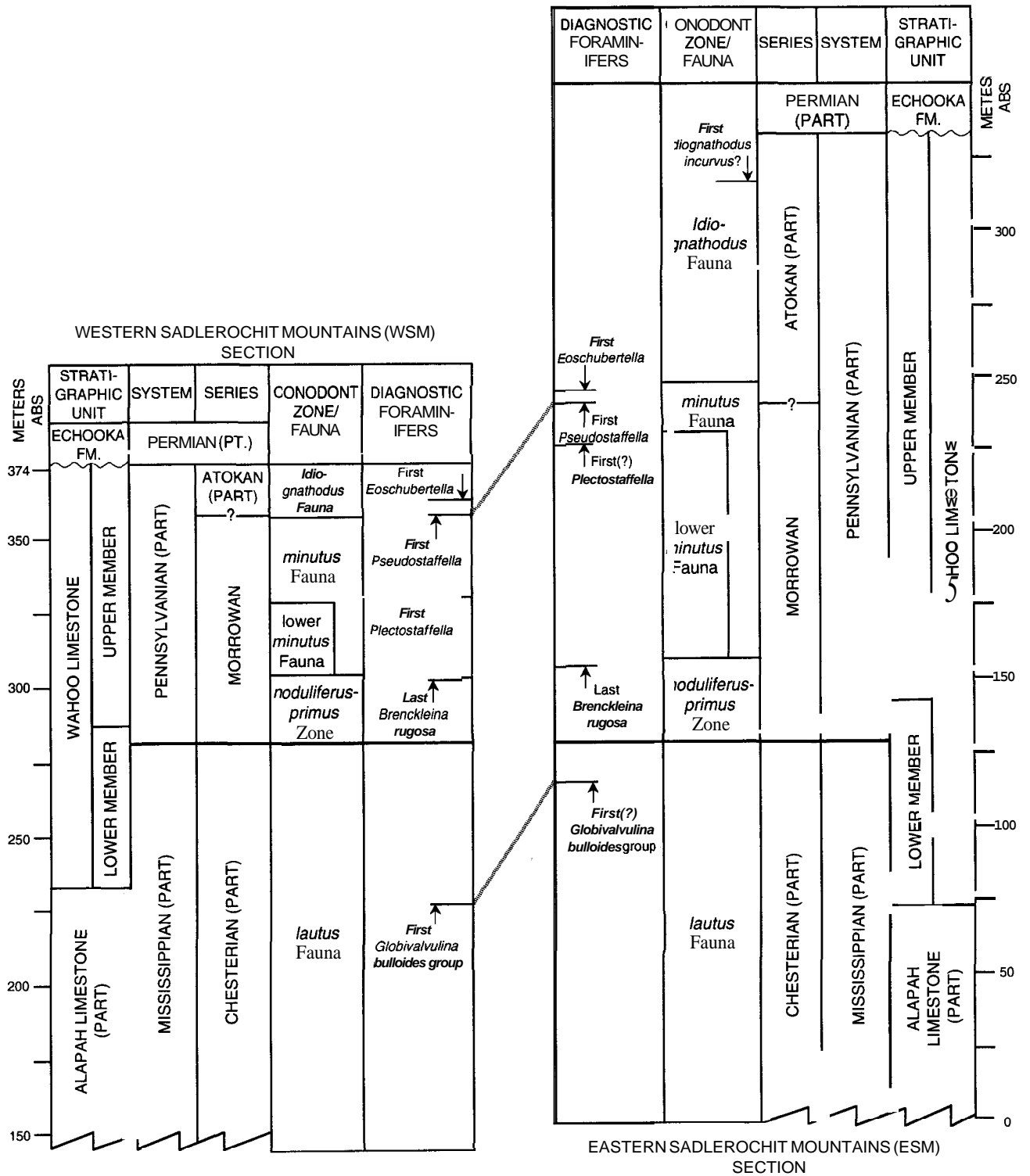


Figure 5. Comparison of biostratigraphic intervals and first or last occurrences of key taxa in the eastern and western Sadlerochit Mountains sections. Sections are correlated at the Mississippian-Pennsylvanian boundary. The late appearance of *Globivalvulina bulloides* and *Plectostaffella* in the eastern section in comparison to the western section is probably an artifact of insufficient sampling in the upper part of the Alapah Limestone and in the lower part of the upper member of the Wahoo Limestone in the eastern section. Abbreviation: ABS, above base of section.



section was deposited on the relatively positive Sadlerochit high (Armstrong and Mamet, 1974; Mamet and Armstrong, 1984) and represents one of the thinnest Wahoo Limestone sequences in the northeast Brooks Range (Watts and others, 1994).

#### LOWER MEMBER (MISSISSIPPIAN AND PENNSYLVANIAN)

The lower member of the Wahoo Limestone is 54 m thick in the western section and 70 m thick in the eastern section. In both sections, it is typically massive, light-gray, cliff-forming, fossiliferous limestone.

Bryozoan-pelmatozoan grainstone and packstone containing common dark-gray replacement chert nodules characterize the lower member in both the western and eastern sections. In the western section, peloids, ooids, and superficial ooids are rare (fig. 2B); oolitic grainstone first appears in the upper 3 m. In the eastern section, rare beds of mixed skeletal wackestone and packstone occur particularly near the base and near the Mississippian-Pennsylvanian boundary. Peloids, including completely micritized bioclasts, are a common constituent, becoming abundant near the Mississippian-Pennsylvanian boundary. Oolitic grainstone, a lithology that typifies the upper member, first appears as a 2-m-thick interval 8 m below the top of the lower member. Lithology, grain types, and fossils in both sections indicate the member formed in a range of partly restricted to open-marine environments.

The Mississippian-Pennsylvanian boundary is 50 m above the base of the lower member in the western section and 6 m higher in the eastern section (figs. 4, 5). In both sections it is marked by a chert-rich interval. In the WSM section, this interval is 3 m thick, straddles the systemic boundary, and consists of bryozoan-pelmatozoan packstone and grainstone containing abundant dark-gray chert. In the ESM section, the interval is below the systemic boundary, consists of a 0.5- to 1-m-thick peloidal-spiculitic wackestone that is partly replaced by reddish-brown and gray nodular chert, and appears to have been deposited above an irregular surface with as much as 1 m of relief. The surface has been interpreted to have formed during subaerial exposure (Carlson, 1990; Watts and others, 1994). Elsewhere in the eastern Sadlerochit Mountains, the chert interval is immediately above the systemic boundary at some sections and immediately below it at others (Krumhardt and others, 1996, fig. 6). Some of the variation in thickness of the lower member may be related to variations in erosion at the exposure surface that marks the Mississippian-Pennsylvanian boundary.

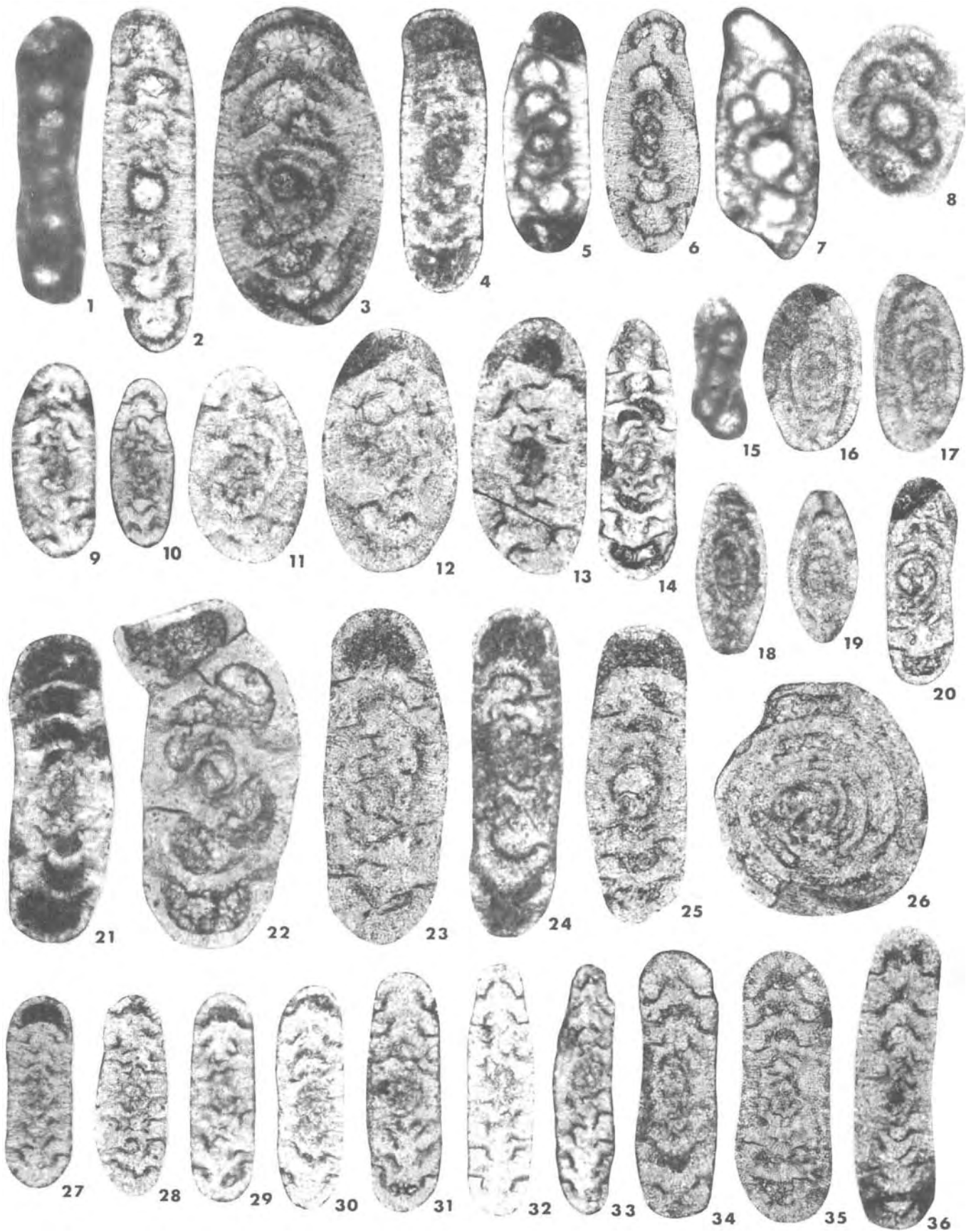
The Pennsylvanian part of the lower member is thicker in the eastern section than in the western section (14 m versus 4 m). The boundary between the two members in the eastern section is marked by an increase in detrital quartz (Krumhardt and others, 1996). In the western section, detrital quartz makes up as much as 2 percent of the

chert-rich interval that straddles the Mississippian-Pennsylvanian boundary and, as in the eastern section, detrital quartz increases in the lower part of the upper member. In addition, possibly redeposited, latest Mississippian conodonts are found sporadically in the Pennsylvanian part of the lower member in the eastern section and increase in abundance a meter below the contact with the upper member. Only one possible redeposited form, *Gnathodus bilineatus*, was found in the base of the Pennsylvanian part of the lower member in the western section. The contact between the lower and upper members is planar in both the eastern and western sections. The uppermost beds of the lower member at the eastern section represent a significant regressive sequence of peloidal-skeletal packstone, spiculitic limestone, and cryptalgal laminites; erosion channels were observed near the eastern section (Krumhardt and others, 1996). These features along with the notable increase in detrital quartz and possibly redeposited conodonts suggest exposure and erosion at the lower-upper member contact that could have contributed to variations in thickness of the lower member in the Sadlerochit Mountains. The contact between the lower and upper members is well exposed in the eastern section and is marked by a change from cliff-forming, light-gray packstone below to orange-weathering, silty, cryptalgal(?) dolostone above.

#### UPPER MEMBER (PENNSYLVANIAN)

The upper member of the Wahoo Limestone is 88 m thick in the western section and 192 m thick in the eastern section. Both sections contain many progradational, shallowing-upward parasequences, 3 to 13 m in thickness, that form a characteristic ledge-and-slope topography. Fifteen parasequences are recognizable in the upper member in the western section, whereas 24 can be recognized in the eastern section. The parasequences of the western section chiefly contain various proportions of bryozoan-pelmatozoan to mixed skeletal grainstone, packstone, and wackestone, and oolitic grainstone. Those in the eastern section mainly contain, in ascending order, various proportions of bryozoan-pelmatozoan grainstone and packstone, oolitic grainstone and mixed skeletal packstone, and oncolitic and peloidal packstone and grainstone. In both sections, the member formed in a range of restricted- or partly restricted- to open-platform, shoal, tidal-channel, and open-marine depositional settings on a southward-dipping carbonate ramp.

Relatively few conodonts and foraminifers are found in the lower beds of the upper member, possibly owing to inhospitable environmental conditions. According to Watts and others (1994), the lower beds of the upper member in the northeast Brooks Range formed on a predominantly restricted platform during a major regression and contain some of the shallowest water deposits in the Wahoo Limestone. The interval contains cryptalgal laminites, common



**detrital** quartz sand (averaging 12 percent in the lower 20 m of the upper member), and, locally, exposure surfaces (Krumhardt and others, 1996).

Ooid grainstone, indicative of a shoal environment, first occurs 25 m above the base of the upper member in the ESM section, is common to 144 m above the base, becomes rare in the succeeding 24 m, and is absent in the upper 24 m. The upper 24 m are mostly beds of peloidal, oncolitic, and bryozoan-pelmatozoan packstone and grainstone that indicate deposition in more restricted conditions than those that prevailed during deposition of much of the underlying part of the upper member. In comparison, oolitic grainstone first appears 10 m above the base of the member in the WSM section, does not become common until 45 m higher, and remains common to the top of the section. Oncoids were not identified in the western section. That section has a 10-m aggregate thickness of oolitic grainstone compared to 38 m in the eastern section. Glauconite is a minor constituent in the western section from the middle part of the lower member through the upper

member but is absent in the eastern section. The presence of glauconite in the western section may indicate a slower rate of deposition and may account for some of the disparity in thickness between the two sections.

The greatest difference in thickness between the eastern and western sections is within the upper member, in the interval of the *Rhachistognathus minutus* and *Idiognathodus* faunas (71 m in the western section versus 178 m in the eastern section). The interval of the *R. minutus* Fauna is 40 m thicker in the eastern section than in the west. We infer that more sediment accumulated in the eastern section during this time interval. Much of the remaining variation in thickness of the upper member may be related to differential erosion along the top of the Lisburne Group. The interval of the *Idiognathodus* Fauna is 67 m thicker in the eastern section but may have been at least as thick in the western section prior to pre-Echooka Formation erosion. Similarly, the thin Lisburne interval above the appearance of *Pseudostaffella* in the western section compared to the eastern section (fig. 5) supports differential erosion along the

◀ **Figure 6.** Foraminifers from the western Sadlerochit Mountains composite section (thin sections). Explanation of sample designations: A, lower part of section (fig. 2A), from Alapah Limestone except as noted; B, upper part of section (fig. 2B), from Wahoo Limestone except as noted; stratigraphic position of sample shown in figure 2. All illustrated specimens are repositied in the U.S. National Museum (USNM), Washington, D.C.

1, 15, *Planoarchaediscinae*, ×200.

1, *Viseidiscus* sp., axial section, sample A-19, USNM 489224.

15, *Planoarchaediscus* sp., axial section, sample A-44C, USNM 489238.

2, *Kasachstanodiscus kischkinensis* Marfenkova, 1978, axial section, sample A-46, ×200, USNM 489225.

3, *Paraarchaediscus kokjubensis* (Rauzer-Chernousova, 1948), slightly oblique axial section, sample B-46, ×200, USNM 489226.

4-6, *Paraarchaediscus stilus* (Grozdilova and Lebedeva in Grozdilova, 1953), axial sections.

4, Sample B-49, ×200, USNM 489227.

5, Sample A-102C, ×200, USNM 489228.

6, Sample B-5C, Alapah Limestone, ×100, USNM 489229.

7, *Paraarchaediscus pachythea* (Petryk, 1971), axial section, sample A-78C, ×200, USNM 489230.

8, *Paraarchaediscus pauxillus* (Shlykova, 1951), axial section, sample B-40, ×200, USNM 489231.

9, 10, 13, *Asteroarchaediscus rugosus* (Rauzer-Chernousova, 1948), axial sections, ×200.

9, Sample B-34, USNM 489232.

10, Sample B-113, USNM 489233.

13, Sample B-80, USNM 489236.

11, 12, *Asteroarchaediscus baschkiricus* (Krestovnikov and Theodorovich, 1936), axial sections, ×200.

11, Sample B-102, USNM 489234.

12, Sample B-125C, USNM 489235.

14, *Neoarchaediscus probatus* (Reitlinger, 1950) (= *Archaediscus incertus* Grozdilova and Lebedeva, 1954), axial section, sample B-122C, ×100, USNM 489237.

16, 17, 19, *Brenckleina rugosa* (Brazhnikova, 1964), ×200.

16, Sagittal section, sample B-34, USNM 489239.

17, Oblique-sagittal section, sample B-56, USNM 489240.

19, Axial section, sample B-56, USNM 489242.

18, *Eosigmoilina robertsoni* (Brady, 1876), axial section, sample B-56, ×200, USNM 489241.

20, 25, 26, *Planospirodiscus absimilis* (Sosipatrova, 1962), sample B-70, ×200.

20, 25, Axial sections, USNM 489243, 48.

26, Sagittal section, USNM 489249.

21, *Neoarchaediscus borealis* (Reitlinger, 1949), axial section, sample B-31C, ×200, USNM 489244.

22, *Archaediscus* sp., axial section, sample B-122C, ×200, USNM 489245.

23, 24, *Asteroarchaediscus postrugosus* (Reitlinger, 1949), near-axial sections, ×200.

23, Sample B-105, Echooka Formation, USNM 489246.

24, Sample B-130, USNM 489247.

27-36, *Asteroarchaediscus?* sp. A, axial sections, ×200. These specimens resemble *Asteroarchaediscus* in the occlusion of the tubular chamber but differ in the evolute, nearly planispiral coiling and narrowly discoidal shape.

27, 31, Sample B-56, USNM 489250, 54.

28, 30, Sample B-65, USNM 489251, 53.

29, Sample B-46, USNM 489252.

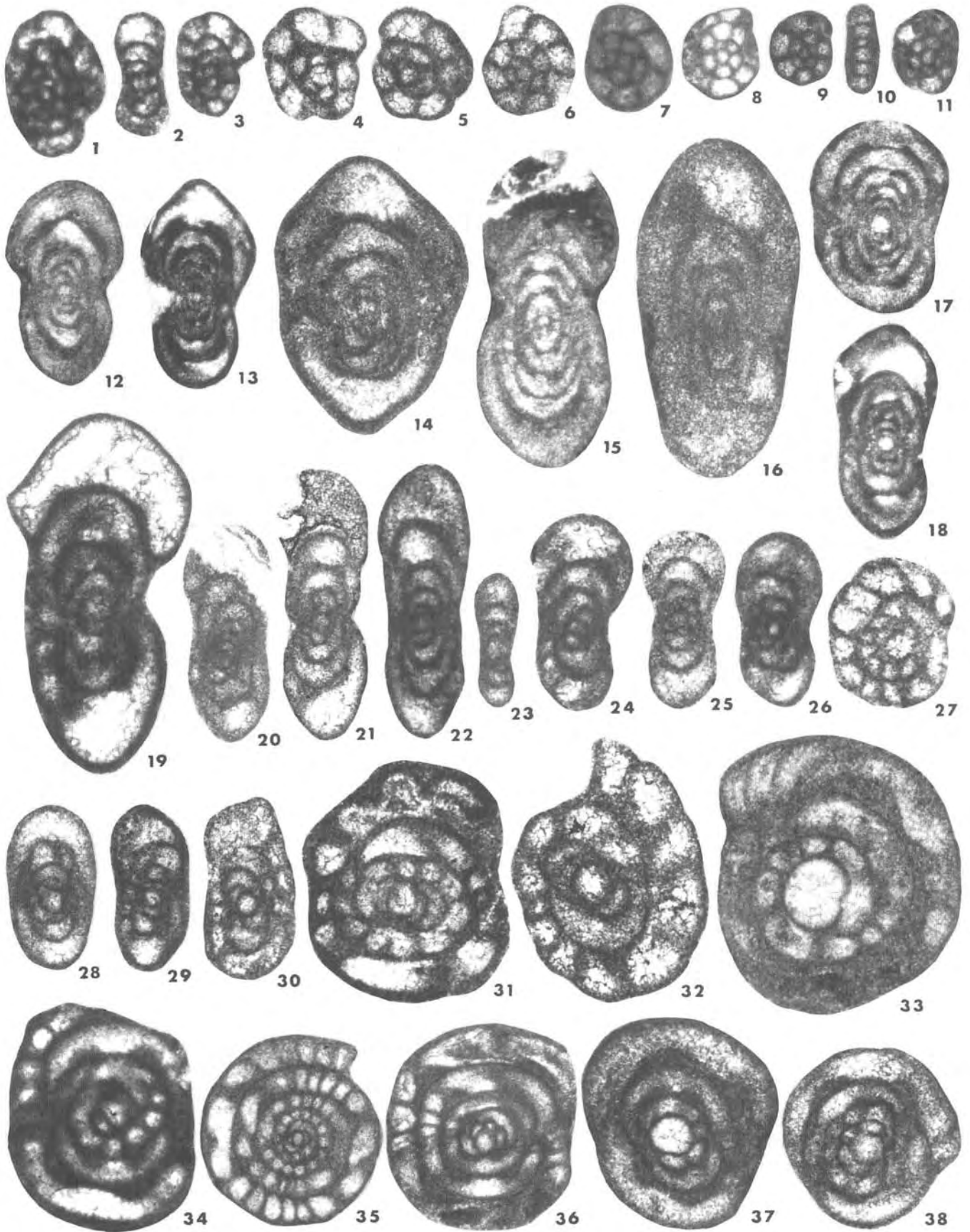
32, Sample B-63C, USNM 489255.

33, Sample B-35C, USNM 489256.

34, Sample B-55, USNM 489257.

35, Sample B-34, USNM 489258.

36, Sample B-52, USNM 489259.



pre-Echooka unconformity and partly accounts for the fewer parasequences at that location.

Siliciclastic beds of the Echooka Formation **unconformably** overlie the Wahoo Limestone. The basal meter of the Echooka near the western section contains early Late Permian (Wordian or **Capitanian**) conodonts that establish a hiatus of at least 40 million years at the unconformity.

### BIOSTRATIGRAPHY

Calcareous microfossils (Armstrong and others, 1970; **Mamet** and Armstrong, 1972, 1984; Armstrong and **Mamet**, 1977) and conodonts (**Krumhardt** and others, 1996) have been used as the primary biostratigraphic controls for the Lisburne Group in the northeast Brooks Range. The absence of many key taxa and the diachroneity in the ranges of taxa between Alaska and other areas due to migration have made it difficult to precisely correlate the Lisburne Group to strata beyond northern Alaska.

### CALCAREOUS MICROFOSSILS

Most Carboniferous foraminifers apparently originated in the central Eurasian Tethys (**Mamet** and Skipp, 1970) and, during the Late Mississippian to Middle Pennsylvanian, migrated westward across Arctic North America to reach southern Canada and the conterminous United States (Armstrong and **Mamet**, 1977; Groves, 1988). Foraminiferal diversity dropped markedly from Eurasia to North America probably owing to changing climatic and geographic conditions along the migration pathway (Ross and Ross, 1985). The Arctic region, however, retained many elements common to the Tethys, leading Ross (1967) to combine those areas into a Eurasian-Arctic Realm and group the rest of North America and South America into a Midcontinent-Andean Realm. **Mamet** (in **Mamet** and Belford, 1968, and in Armstrong and **Mamet**, 1977) relegated the Arctic faunas to a Taimyr-Alaska Realm transitional between the prolific Tethyan and relatively impoverished, phylogenetically incomplete North Ameri-

Figure 7. Foraminifers from the western Sadlerochit Mountains composite section (thin sections). Explanation of sample designations: A, lower part of section (fig. 2A), from Alapah Limestone; B, upper part of section (fig. 2B), from Wahoo Limestone except as noted; stratigraphic position of sample shown in figure 2. All illustrated specimens are repositied in the U.S. National Museum (USNM), Washington, D.C.

1-3, *Endostaffella* spp., ×100.

1, Sagittal section, sample A-71C, USNM 489260.

2, 3, Axial and sagittal sections, sample A-44C, USNM 489261, 62.

4, 5, "*Priscella*" sp., sagittal sections, ×100.

4, Sample B-26C, USNM 489263.

5, Sample B-46, USNM 489264.

6-11, *Mediocris breviscula* (Ganelina, 1951), sagittal sections except as noted, ×100.

6, Sample A-42, USNM 489265.

7, Sample B-34, USNM 489266.

8, Sample A-102C, USNM 489267.

9, Sample B-65, USNM 489268.

10, Axial section, sample B-56, USNM 489269.

11, Sample B-5C, Alapah Limestone, USNM 489270.

12-15, 17, 18, *Pseudoendothyra* spp., axial sections, ×50 except as noted.

12, 13, Sample B-142, USNM 489271, 72.

14, Sample B-137, ×100, USNM 489273.

15, Sample B-126, USNM 489274.

17, Sample B-134, USNM 489276.

18, Sample B-58, USNM 489277.

16, *Pseudoendothyra circuli* (Thompson, 1945), axial section, sample B-129, ×100, USNM 489275.

19, *Eostaffella* cf. *E. infulaeformis* (Ganelina, 1951), slightly

oblique-axial section, sample B-111, ×100, USNM 489278.

20, "*Millerella*" *designata* Zeller, 1953, axial section, sample B-46, ×100, USNM 489279.

21, *Millerella marblensis* Thompson, 1942, axial section, sample B-69, ×100, USNM 489280.

22, *Millerella pressa* Thompson, 1944, axial section, sample B-83C, ×100, USNM 489281.

23, *Novella?* sp., axial section, sample B-34, ×100, USNM 489282.

24-27, *Eostaffella?* *postmosquensis* Kireeva in Rauzer-Chernousova, Gryslova, Kireeva, Leontovich, Safonova and Chernova, 1951, (?= "*Millerella*" *tortula* Zeller, 1953), axial sections except as noted, ×100.

24, Sample B-71C, USNM 489283.

25, Sample B-148C, USNM 489284.

26, Sample B-84, USNM 489285.

27, Sagittal section, sample B-111, USNM 489286.

28-30, *Plectostaffella jakhensis* Reitlinger, 1971, ×100.

28, Axial section, sample B-136, USNM 489287.

29, Oblique-axial section, sample B-88, USNM 489288.

30, Oblique-sagittal section, sample B-150, USNM 489289.

31, 32, *Pseudostaffella* (*Semistaffella*) sp., sagittal sections, ×100.

31, Sample B-137, USNM 489290.

32, Sample B-133C, USNM 489291.

33, 37, 38, *Eoschubertella* spp., ×100.

33, Sagittal section, sample B-142, USNM 489292.

37, Axial section, sample B-135C, USNM 489296.

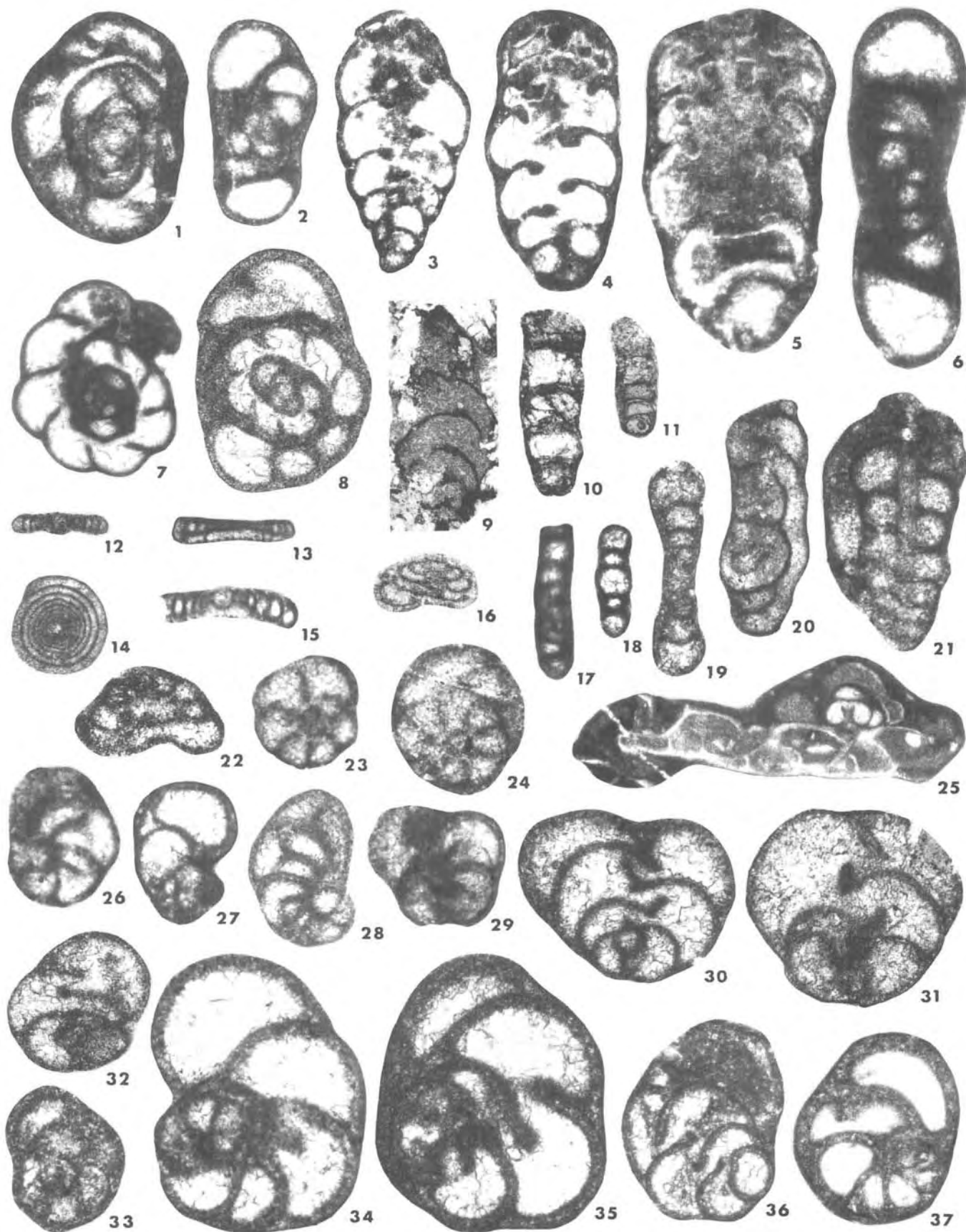
38, Axial section, sample B-136, USNM 489297.

34-36, *Pseudostaffella* (*Pseudostaffella*) spp.

34, Axial section, sample B-132, ×100, USNM 489293.

35, Sagittal section, sample B-130, ×50, USNM 489294.

36, Axial section, sample B-137, ×50, USNM 489295.



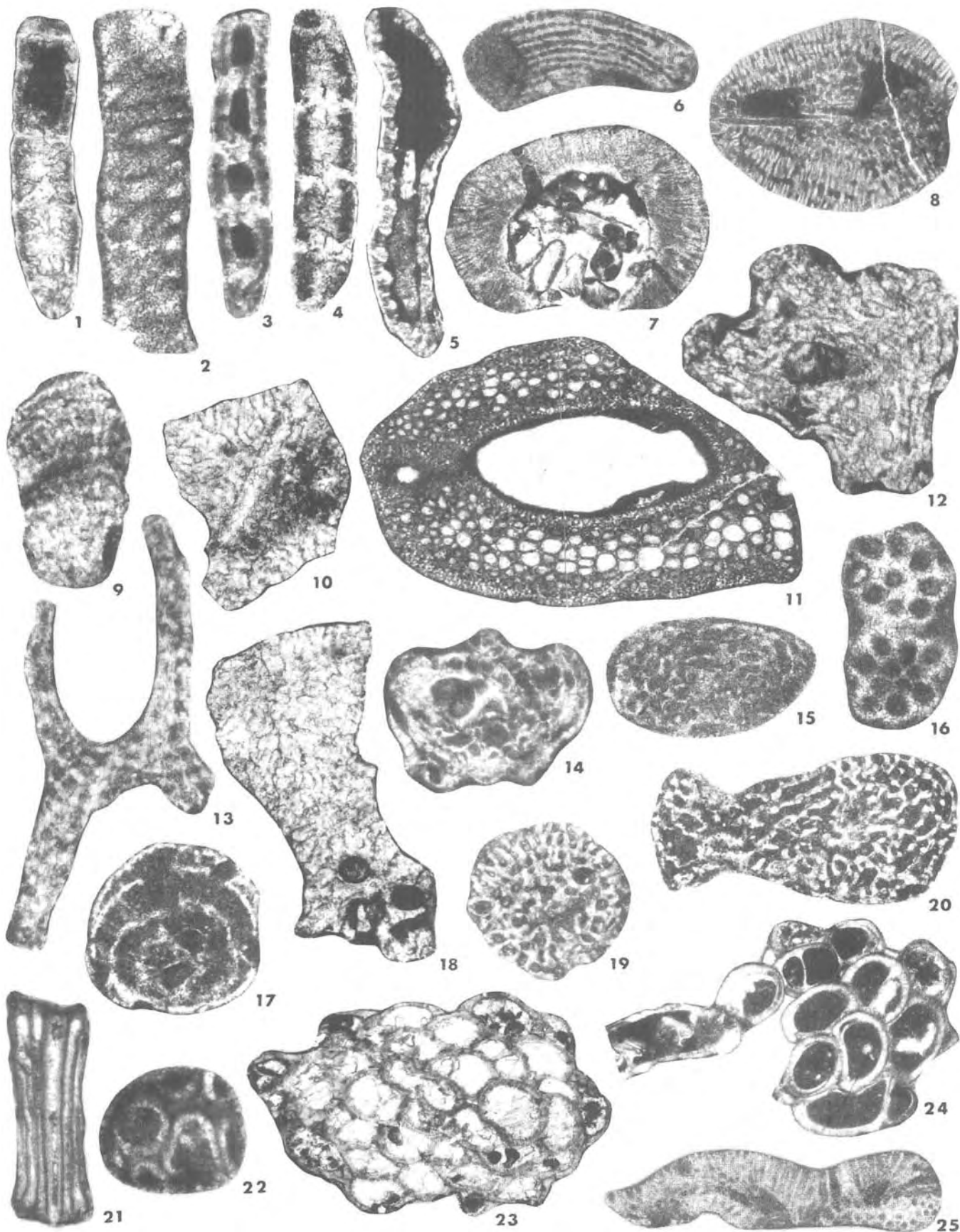
can Realms. Eurasian elements that "filtered" through the Arctic into the North American Realm provided a cosmopolitan assemblage for correlation across the Northern Hemisphere.

The close relationship between Canadian Arctic and Eurasian foraminiferan faunas has recently been confirmed in papers describing Early to Middle Pennsylvanian assemblages from the Sverdrup basin (Groves and others, 1994; Rui and others, 1996). Similarly, the Lisburne Group in the Sadlerochit Mountains contains a number of Eurasian foraminifers that, as in Arctic Canada, are never or rarely encountered in **sub-Arctic** North America. These taxa include *Asteroarchaediscus postrugosus*, *Endotaxis brazhnikovae*, *Howchinia* sp., *Kasachstanodiscus kischkinensis*, *Koskino-*

*bigenerina* sp., *Neoarchaediscus borealis*, *Novella?* sp., *Planospirodiscus absirnilis*, *Plectostaffella jakhensis*, and *Pseudostaffella (Semistaffella)* sp. During the middle Carboniferous, the Arctic clearly was the primary gateway for passage of Eurasian faunas into the rest of North America, and, conversely, it was a route for dispersion of typical North American forms into other regions. Bidirectional migration through the Arctic resulted in the nearly cosmopolitan distribution of biostratigraphically useful taxa. In North America, however, many of these taxa are immigrants and their appearances are younger than in Eurasia, where they appeared in evolutionary continuity with their ancestors. The challenge for high-resolution **biostratigraphy** between the Lisburne and coeval **sub-Arctic** North American strata is to gauge correctly the magnitude of

Figure 8. Foraminifers from the western Sadlerochit Mountains composite section (thin sections). Explanation of sample designations: A, lower part of section (fig. 2A), from Alapah Limestone; B, upper part of section (fig. 2B), from Wahoo Limestone except as noted; stratigraphic position of sample shown in figure 2. All illustrated specimens are repositied in the U.S. National Museum (USNM), Washington, D.C.

- 1, *Skippella?* sp., sagittal section, sample A-15,  $\times 100$ , USNM 489298.
- 2, *Globoendothyra?* sp., near axial section, sample A-10,  $\times 100$ , USNM 489299.
- 3-5, Palaeotextulariidae, oblique-longitudinal sections.
  - 3, *Consobrinella* sp., sample B-57C,  $\times 50$ , USNM 489300.
  - 4, *Koskinobigenerina* sp., sample B-57C,  $\times 40$ , USNM 489301.
  - 5, *Climacammina* sp., sample B-128,  $\times 50$ , USNM 489302.
- 6, *Planoendothyra* sp., axial section, sample B-83C,  $\times 100$ , USNM 489303.
- 7, *Endothyra excellens* (Zeller, 1953), near sagittal section, sample B-83C,  $\times 50$ , USNM 489304.
- 8, *Endothyra* sp., oblique-sagittal section, sample B-125C,  $\times 100$ , USNM 489305.
- 9, Indeterminate Protonodosariidae, oblique-longitudinal section, sample B-154, Echooka Formation,  $\times 100$ , USNM 489306.
- 10, 11, *Protonodosaria* spp., oblique-longitudinal sections, Echooka Formation,  $\times 100$ .
  - 10, Sample B-153, USNM 489307.
  - 11, Sample B-152, USNM 489308.
- 12, 14, *Turrispiroides* sp., axial and sagittal sections, respectively, sample B-63C,  $\times 100$ , USNM 489309, 11.
- 13, 15, *Monotaxinoides* spp.,  $\times 100$ .
  - 13, Near axial section, sample B-34, USNM 489310.
  - 15, Axial section, sample B-116C, USNM 489312.
- 16, *Howchinia* sp., tangential-axial section, sample B-34,  $\times 100$ , USNM 489313.
- 17-19, Pseudoammodiscidae,  $\times 100$ .
  - 17, *Brunsia* sp., axial section, sample A-35C, USNM 489314.
  - 18, *Pseudoammodiscus priscus* (Rauzer-Chernousova, 1948), axial section, sample A-44C, USNM 489315.
  - 19, *P. volgensis* (Rauzer-Chernousova, 1948), axial section, sample B-12C, USNM 489316.
- 20, Calcitornellin/calcivertellin encrusting foraminifer, sample B-88,  $\times 100$ , USNM 489317.
- 21, *Trepeilopsis* sp., longitudinal section, sample B-24C,  $\times 100$ , USNM 489318.
- 22-24, *Endotaxis brazhnikovae* Bogush and Yuferev, 1966,  $\times 100$ .
  - 22, Tangential-axial section, sample B-23, USNM 489319.
  - 23, Tangential-sagittal section, sample B-18, USNM 489320.
  - 24, Tangential-sagittal section, sample B-24C, USNM 489321.
- 25, *Palaeonubecularia* sp. encrusting bryozoan, sample B-83C,  $\times 50$ , USNM 489322.
- 26, *Biseriella parva* (Chernysheva, 1948), near sagittal section, sample B-34,  $\times 100$ , USNM 489323.
- 27-33, *Globivalvulina* of the group *G. bulloides* (Brady, 1876),  $\times 100$ .
  - 27-29, 32, 33, *Globivalvulina* cf. *G. bulloides*. 27, Near sagittal section, sample B-5C, Alapah Limestone, USNM 489324.
  - 28, Sagittal section, sample B-57C, USNM 489325.
  - 29, Tangential-axial section, sample B-45C, USNM 489326.
  - 32, Tangential-axial section, sample B-34, USNM 489329.
  - 33, Sagittal section, sample B-25, USNM 489330.
- 30.31, *Globivalvulina bulloides* (= *G. moderata* Reitlinger, 1949), tangential-axial sections.
  - 30, Sample B-60, USNM 489327.
  - 31, Sample B-70, USNM 489328.
- 34-36, *Globivalvulina granulosa* Reitlinger, 1950.
  - 34, Sagittal section, sample B-111,  $\times 100$ , USNM 489331.
  - 35, Oblique-axial section, sample B-110,  $\times 100$ , USNM 489332.
  - 36, Tangential-axial section, sample B-70,  $\times 50$ , USNM 489333.
- 37, *Globivalvulina* sp. aff. *G. granulosa* Reitlinger, 1950, sagittal section, sample B-142,  $\times 50$ , USNM 489334. Wall thickness in last chambers is 45-55  $\mu$ m.





diachroneity in key microfossil appearances. Were they geologically instantaneous or significantly delayed? The evidence suggests a mixture of both.

The foraminiferal succession across the North Slope, however, is generally consistent and can provide a fairly reliable scheme for local Mississippian and Pennsylvanian correlation. The WSM succession (fig. 3) is representative of the distribution expected in northeastern Alaska.

#### MISSISSIPPIAN

##### (ALAPAH LIMESTONE AND PART OF THE LOWER MEMBER OF THE WAHOO LIMESTONE)

Calcareous microfossil distribution in the Alapah Limestone in the western section is erratic because of poor exposures and inhospitable paleoenvironments ranging from cyclical, very high energy shoals and restricted lagoons in the lower part of the formation to thick, sabkha-type dolomites in the upper part. We have not studied the calcareous microfossils of the Alapah in the eastern section. Armstrong and Mamet (1977) show the distribution of selected calcareous foraminifers in the Lisburne Group at Sunset Pass, about 1 km west of our eastern section. Their biostratigraphy, however, is based on only a few taxa identified to the generic level. No detailed stratigraphic sequence of fora-

minifers is illustrated, thereby making comparison to our western section imprecise.

The lower part of the Alapah Limestone in the WSM section contains a meager calcareous microfossil assemblage that is tentatively correlated to the Meramecian, based on the occurrences of *Koninckopora minuta?* (incertae sedis) and *Skippella?* sp. (fig. 3). *Koninckopora* begins in the Osagean and in Eurasia extends into the lower Chesterian (=upper Visean, V3c). In North America, its disappearance is operationally considered to be within the Meramecian because its last definite occurrence is within the St. Louis Limestone and equivalents in the Midcontinent (Baxter and Brenckle, 1982) and because the genus occurs only rarely within the lowermost Chesterian of the Cordillera (Sando and others, 1969; Petryk and others, 1970). *Skippella*, a genus closely related in age and morphology to *Euendothyranopsis*, is not known to occur above the Meramecian (Armstrong and Mamet, 1977), but the Sadlerochit Mountains form (fig. 8:1) does not show all the attributes necessary for a positive identification; it may be a juvenile. Without a more diverse assemblage, a precise correlation for these specimens is not possible. Our unpublished collections from the base of the Alapah at Clarence River in the eastern Arctic National Wildlife Refuge (ANWR), about 170 km east of the WSM section (fig. 1), contain a

Figure 9. Algae and incertae sedis from the western Sadlerochit Mountains composite section (thin sections). All specimens are algae except figures 21-24, which are incertae sedis. Explanation of sample designations: A, lower part of section (fig. 2A), from Alapah Limestone; B, upper part of section (fig. 2B), from Wahoo Limestone except as noted; stratigraphic position of sample shown in figure 2. All illustrated specimens are deposited in the U.S. National Museum (USNM), Washington, D.C.

1, 4, *Donezella lutugini* Maslov, 1929, longitudinal sections.

1, Sample B-126,  $\times 80$ , USNM 489335.

4, Sample B-138C,  $\times 80$ , USNM 489338.

2, *Epimastoporella* sp., sample B-124,  $\times 100$ , USNM 489336.

3, *Donezella* sp., longitudinal section, sample B-132,  $\times 50$ , USNM 489337.

5, *Beresella* sp., longitudinal section, sample B-136,  $\times 50$ , USNM 489339.

6, *Fourstonella* sp., sample A-44C,  $\times 100$ , USNM 489340.

7, *Orthrosiphonoides* sp., sample B-118,  $\times 25$ , USNM 489341.

8, *Epistacheoides connorensis* Mamet and Rudloff, 1972, sample A-62C,  $\times 25$ , USNM 489342.

9, 13, *Masloviporidium delicatum* (Berchenko, 1982) emend. Groves and Mamet, 1985,  $\times 100$ .

9, Sample A-71C, USNM 489343.

13, Sample A-49, USNM 489347.

10, 18, "*Komia*" sp. A,  $\times 50$ . The blocky calcification of these specimens resembles that of the ungdarellin red alga *Komia*, but the thallus apparently encrusts around a central support

unlike the free-standing thallus of true *Komia*.

10, Sample B-58, USNM 489344.

18, Sample B-100C, USNM 489352.

11, *Archaeolithophyllum missouriense* Johnson, 1956, sample B-137,  $\times 25$ , USNM 489345.

12, *Berestovia filaris* Berchenko, 1982, sample B-136,  $\times 50$ , USNM 489346.

14, *Asphaltinella* sp., sample B-102,  $\times 50$ , USNM 489348.

15, *Stacheoides tenuis* Petryk and Mamet, 1972, sample B-49,  $\times 100$ , USNM 489349.

16, Indeterminate Dasycladaceae, sample B-143,  $\times 100$ , USNM 489350.

17, *Stacheia* sp., sample B-60,  $\times 100$ , USNM 489351.

19, *Aoujgalia variabilis* Termier and Termier, 1950, sample B-46,  $\times 50$ , USNM 489353.

20, *Stacheoides meandriformis* Mamet and Rudloff, 1972, sample B-25,  $\times 25$ , USNM 489354.

21, *Tubisalebra calamiformis* Bogush and Brenckle, 1982, longitudinal section, sample A-69C,  $\times 50$ , USNM 489355.

22, *Koninckopora minuta?* Weyer, 1968, abraded allochem, sample A-9C,  $\times 100$ , USNM 489356.

23, *Asphaltinoides macadami* (Brenckle and Groves, 1987), sample A-69C,  $\times 25$ , USNM 489357.

24, *Asphaltina cordillerensis* Mamet in Petryk and Mamet, 1972, sample B-27,  $\times 25$ , USNM 489358.

25, *Richella incrustata* Mamet and Roux in Mamet and others, 1987, sample B-126,  $\times 40$ , USNM 489359.

Meramecian *Eoendothyranopsis*-*Globoendothyra* fauna along with *Skippella* and *Koninckopora*. These occurrences lend some credence to a Meramecian assignment for the base of the Alapah in the WSM section.

The Chesterian foraminiferal sequence in the Alapah and lower member of the Wahoo generally agrees well with that found in other parts of North America (fig. 3). The appearance of *Asteroarchaediscidae* (*Asteroarchaediscus baschkiricus*, in particular) is characteristic of the lower Chesterian followed by *Biseriella parva*, *Eostaffella? postmosquensis* (?=*Millerella* "tortula"), and eosigmoilinids (*Eosigmoilina robertsoni* and *Brenckleina rugosa*). This succession has been reported in central and western North America (for example, Sando and others, 1969; Mamet and others, 1971; Mamet, 1975; Baxter and Brenckle, 1982; Brenckle, 1991), except that *Biseriella* has not been definitely found in the Chesterian of the Midcontinent. *Biseriella* of the group *B. parva* definitely starts in the upper half of the Alapah and is followed by its descendant form, *Globivalvulina* of the group *G. bulloides* near the top of the formation (fig. 3).

Calcareous microfossils become more plentiful in the lower member of the Wahoo Limestone because of more favorable depositional environments, but they do not attain the diversity and abundance seen higher in the section. The bryozoan-pelmatozoan packstone and grainstone that make up most of the lower member were probably deposited lower on the shelf than most other rocks in the Wahoo. The beds have relatively abundant *Asphaltina* and aoujgaliacean

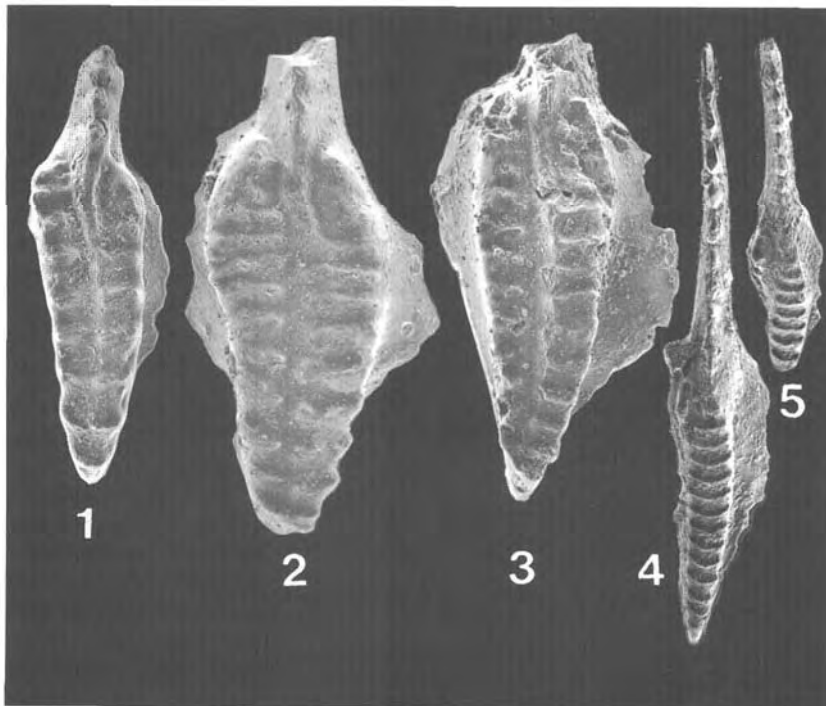
red algae that exploited the available light spectrum in this slightly deeper water zone.

#### PENNSYLVANIAN

##### (UPPER PART OF LOWER MEMBER AND UPPER MEMBER OF WAHOO LIMESTONE)

The Mississippian-Pennsylvanian boundary is within the upper part of the lower member of the Wahoo Limestone (figs. 3-5). This boundary, which coincides with the proposed international Mid-Carboniferous boundary, is defined by the appearance of the conodont *Declinognathodus noduliferus* subsp. and auxiliary guide fossils, including the foraminifers *Globivalvulina* sp. D (= *G. bulloides* Brady, 1876 = *G. moderata* Reitlinger, 1949), *Millerella marblensis*, and *M. pressa* (Lane, Bouckaert, and others, 1985). This foraminiferal definition of the boundary follows the criteria of Mamet (1975). In North America the boundary is best understood in terms of the microfossil succession at Arrow Canyon, Nevada, the candidate section for the Mid-Carboniferous boundary stratotype. At this locality, eosigmoilinid foraminifers disappear less than 0.5 m above the first *D. noduliferus*. *Globivalvulina bulloides* appears 2 m higher, followed by *M. pressa* and *M. marblensis* 6-7 m above that (Lane, Baesemann, and others, 1985; Brenckle and others, in press).

*Millerella marblensis*/*M. pressa*, which originated in the Midcontinent-Andean Realm, are unreliable markers elsewhere because of their rarity. Although they are present



**Figure 10.** Important conodont species limited thus far to the western Sadlerochit Mountains section (scanning electron micrographs). Virtually all other conodont taxa identified in both the eastern and western sections are illustrated in Krumhardt and others (1996). Stratigraphic position of samples shown in figure 2B; all specimens from Wahoo Limestone. All illustrated specimens are deposited in the U.S. National Museum (USNM), Washington, D.C.

1-5, Upper views of Pa elements,  $\times 100$ .

- 1, *Declinognathodus noduliferus* *inaequalis* (Higgins), sample B-85C, USNM 489360.
- 2, 3, *Declinognathodus noduliferus* *lateralis* (Higgins and Bouckaert), sample B-89C, USNM 489361, 62.
- 4, 5, *Idiognathoides pacificus* Savage and Barkeley, adult and juvenile specimens, sample B-89C, USNM 489363, 64.

in Alaska, millerellin faunas there are mostly related to *M. carbonica* (Armstrong and Mamet, 1977) that came from Eurasia. *Globivalvulina*, on the other hand, is abundant in the Lisburne Group and seemingly should be the taxon of choice for a foraminiferal-based definition of the Mississippian-Pennsylvanian boundary. This genus evolved from the morphologically similar species, *Biseriella parva*, through development of a granular clear layer (*diaphanotheca*) within the test wall. Because of its shape and coiling pattern, it is difficult to discern meaningful morphologic differences in unoriented thin sections, and *Globivalvulina* is best differentiated by wall thickness and structure. The first *Globivalvulina* is the species *G. bulloides*, which has a relatively thin wall (10–20 µm) and rudimentary clear layer. *Globivalvulina granulosa* evolved from *G. bulloides* later in the **Morrowan** through development of a more prominent diaphanotheca, thickening of the wall (20–40 µm) and larger size. Thin-walled, diaphanotheca-bearing specimens first appear in the western section near the top of the Alapah Limestone (fig. 2B, sample 5C; fig. 3) and within the lower member of the Wahoo Limestone well below the appearance of *Declinognathodus noduliferus* (fig. 2B, sample 47C). These specimens are identified as *Globivalvulina* of the group *G. bulloides* (figs. 8:27, 29, 32, 33) because their size is smaller than typical *G. bulloides*, although the wall thickness and structure are similar. It is not known if these smaller specimens are stratigraphically important or represent an ecophenotypic response to the restricted environment of the upper part of the Alapah and the bryozoan-pelmatozoan-dominated open-marine environment of the lower member of the Wahoo. In the eastern section, representatives of the *G. bulloides* group occur in the lowest sample analyzed for calcareous microfossils, 43 m above the base of the lower member of the Wahoo and 13 m below the Mississippian-Pennsylvanian boundary. In the western section, larger *G. bulloides* (fig. 8:30) appear in the lower part of the upper member of the Wahoo (fig. 2B, sample 57C) within the range of the eosigmoilinids that disappear above sample 65 (fig. 2B).

*Globivalvulina* overlaps the upper range of *Brenckleina rugosa* in the Cordillera (Skipp and others, 1985) but is unknown there below *Declinognathodus noduliferus*. The extended range in Alaska was puzzling at first because *Globivalvulina* appears with its precursor in both regions and its first occurrence would be expected to be similar. Recent foraminiferal work on Mid-Carboniferous boundary faunas suggests that the discrepancies are related to biogeographical distribution. Thin-walled *Globivalvulina* have now been reported beneath *D. noduliferus* in France (Perret, 1993), Algeria (Mamet and others, 1995), Ukraine (Vdovenko and others, 1990), and Japan (Katsumi Ueno, *Inst. Geoscience, Univ. Tsukuba, Ibaraki, Japan*, written commun., October 1995). These occurrences indicate that *Globivalvulina* developed initially in Eurasia during the late Chesterian and migrated into the North American–

Andean Realm early in the Pennsylvanian. The reliability of the genus as a worldwide indicator of the Mississippian-Pennsylvanian boundary is doubtful.

The appearance of *Palaeonubecularia* (= thick-walled "Pseudoglomospira" of Brenckle and others, 1982; Skipp and others, 1985) was proposed also as a possible indicator for the Mississippian-Pennsylvanian boundary. It occurs in the **Morrowan** in the WSM section and questionably in the Chesterian (fig. 3), although it is known definitely from the Chesterian in collections at Clarence River, eastern ANWR (Amoco Corporation, unpub. data). Its Pennsylvanian appearance in **sub-Arctic** North America is most likely a diachronous migration event from Eurasia. *Palaeonubecularia* was described originally from the Middle Pennsylvanian in eastern Europe (Reitlinger, 1950), and similar morphologic forms have been described under the names *Pseudolituotuba* (Vdovenko, 1971) and *Vostokovella* (Pronina, 1972) from the Mississippian in Eurasia. These three genera may be the same and have a combined range through much of the Carboniferous.

At the WSM section, eosigmoilinids and *Paraarchaediscus* disappear at the same level within the lower part of the upper member of the Wahoo Limestone directly below the incoming of *Globivalvulina granulosa*, the descendant of *G. bulloides* (fig. 3). The disappearance of *Paraarchaediscus*, a worldwide event in the Early Pennsylvanian, marks the end of archaediscids with a two-layered wall. Their morphology is reiterated by the *Pseudovidalinidae* beginning in the Middle Pennsylvanian (Brenckle and Wahlman, 1994).

Calcareous microfossils have not been used widely in the Midcontinent and Cordillera to subdivide the **Morrowan**. However, in those areas, the nonevolutionary appearance of the fusulinid genera *Pseudostaffella* (*Pseudostaffella*) and *Eoschubertella* is used to define the **Morrowan-Atokan** boundary (Mamet, 1975; Groves, 1986). Groves (1988) showed that *Pseudostaffella* (*Pseudostaffella*) evolved in Eurasia through the lineage *Plectostaffella*-*Pseudostaffella* (*Semistaffella*)-*Pseudostaffella* (*Pseudostaffella*), a succession that is also known in Arctic Canada (Groves and others, 1994), in the Wahoo Limestone in the WSM section, and elsewhere on the North Slope. Because only the end member of that lineage is represented in **sub-Arctic** North America and because the first pseudostaffellins in that region seem more advanced than the first ones appearing in the Tethys, Groves (1988) postulated that the group reached the North American–Andean Realm later. In that case, a *Pseudostaffella*-based **Morrowan-Atokan** boundary is diachronous between Arctic Alaska and the **Cordillera-Midcontinent**. The amount of diachroneity cannot be judged biostratigraphically because conodonts are less reliable than the foraminifers in this part of the section and there are no detailed successions of other fossil groups with which to compare in the upper member of the Wahoo. For now, the appearance of *Pseudostaffella* remains the most practical

way to correlate the base of the Atokan between the two regions.

In our sections, *Plectostaffella* appears in the upper member of the Wahoo Limestone, followed 15 to 35 m higher by the primitive fusulinids *Pseudostaffella* (*Pseudostaffella*), *Pseudostaffella* (*Semistaffella*), and *Eoschubertella*. The stratigraphic interval around the appearance of *Pseudostaffella* shows a pronounced increase in *Pseudoendothyra* specimens and a diminution of archaeodiscaceans. Armstrong and Mamet (1975) also noted abundant *Pseudoendothyra* at approximately the same level in eastern ANWR. At the top of this acme interval appear beds composed almost exclusively of densely packed thalli of the green alga *Donezella* (fig. 3; figs. 9:1, 3, 4). These so-called bafflestones (Mamet and de Batz, 1989), remnants of algal gardens, produce a lithology unique to the open-platform environment of the uppermost Wahoo. Up to that level, *Donezella* is a minor constituent in the upper member. Gruzlovic (1991) documented the absence of *Donezella* buildups within the Wahoo in the Plunge Creek section, northern Franklin Mountains (fig. 1), due to its more seaward position on the carbonate ramp.

In the ESM section, *Pseudostaffella* and *Eoschubertella* first appear 101 and 105 m, respectively, above the base of the upper member and with conodonts of the *Rhachistognathus minutus* Fauna (fig. 5). We consider *Pseudostaffella* a more reliable guide to the base of the Atokan in northern Alaska than the first appearance of *I. incurvus*? (a rare species in the eastern section) as proposed by Krumhardt and others (1996). The Morrowan-Atokan boundary, therefore, lies 75 m below the first diagnostic Atokan conodont and about halfway through the upper member in the eastern section.

*Pseudostaffella* and *Eoschubertella* first appear at 71 m and 76 m, respectively, above the base of the upper member in the western section, with conodonts of the *Idiognathodus* Fauna. In this section, only the upper 17 m of the Wahoo Limestone are Atokan.

No biostratigraphically significant calcareous microfossils were found between the entry of *Pseudostaffella* or *Eoschubertella* and the top of the Wahoo Limestone in the eastern and western sections that could be used for interregional correlation of that interval. The uppermost part of the Wahoo, in the eastern Sadlerochit Mountains and in the subsurface to the north, contains *Osagia* deposits (Armstrong, 1972; Armstrong and Mamet, 1974; Mamet and de Batz, 1989). These oncolitic, algal-foraminiferal clasts are thought to indicate very shallow water, restricted conditions. Their appearance near the top of the Wahoo in the eastern section indicates a final regressive phase of deposition; this phase may not have reached the western section or, more likely, the *Osagia* beds were deposited in the west but were later removed by erosion along the pre-Echooka Formation unconformity. Siliciclastic beds of the Echooka Formation disconformably overlie the Wahoo.

In the WSM section, these beds contain a poor assemblage of protonodosariid foraminifers (figs. 8:10, 11) that merely indicate an undifferentiated Late Pennsylvanian-Permian age.

#### CONODONTS

The conodont zonation proposed by Lane and Straka (1974) and later revised by Lane (1977) and Baesemann and Lane (1985) for uppermost Mississippian and Pennsylvanian (Morrowan and lower Atokan) rocks in North America is not applicable to the Lisburne Group of northeast Alaska because many index species are absent or appear earlier or later in northeast Alaska than in other areas of North America. The latest Chesterian *muricatus* Zone was defined by the first appearance of *Rhachistognathus muricatus* below the occurrence of either *Declinognathodus noduliferus* or *R. primus* (Lane and Straka, 1974; Baesemann and Lane, 1985). Baesemann and Lane (1985) subdivided the *muricatus* Zone into lower and upper subzones. The lower subzone was defined by the range of the zonal indicator below the appearance of *Adetognathus lautus* and the upper subzone by the overlapping ranges of *R. muricatus* and *A. lautus* below the appearance of *Declinognathodus noduliferus* or *R. primus*. In the Lisburne Group of northeast Alaska, *R. muricatus* consistently appears below *A. lautus* (Krumhardt and others, 1996), but the stratigraphic interval of the *muricatus* Zone appears to be remarkably thick, reaching 250 m in the Romanzof Mountains (Krumhardt and others, 1996, app. 1). Calcareous microfossils, however, suggest that the sequence of *R. muricatus* followed by *A. lautus* in the western Sadlerochit Mountains appears considerably earlier than in the western conterminous United States, and that *R. muricatus* ranges through the Chesterian and possibly into the late Meramecian in northeastern Alaska. Conodont faunas from the southern Appalachian basin confirm the extended range of *R. muricatus* at least through the Chesterian outside of Alaska (Huggins, 1983; Hassler and Stock, 1993; U.S. Geological Survey unpublished conodont collections). Consequently, we use an informal *lautus* Fauna for the interval represented by the overlapping ranges of *A. lautus* and *R. muricatus* below the range of *Declinognathodus noduliferus* (fig. 5) and abandon the *muricatus* Zone in northeast Alaska.

The conodont *Declinognathodus noduliferus* (Ellison and Graves) is more reliable than calcareous microfossils for positioning the Mississippian-Pennsylvanian boundary within the Lisburne Group. This boundary is defined by the appearance of *D. noduliferus* subsp. in evolutionary succession with its presumed precursor, *Gnathodus girtyi simplex* Dunn. This succession is well developed in the lower member of the Wahoo Limestone in the ESM section (Krumhardt and others, 1996). Above the level of the *noduliferus-primus* Zone, conodont zonal indices are absent to extremely rare in the Lisburne of northeast Alaska.

Consequently, we have used the informal faunal units of Krumhardt and others (1996) for most of the **Morrowan** and **Atokan** part of the Lisburne (fig. 5). The *noduliferus-primus* Zone extends to the first appearance of *R. minutus*, the name-bearer of the *minutus* Fauna. A lower subdivision of the *minutus* Fauna is recognized by the overlapping ranges of *R. minutus*, *R. muricatus*, and *R. websteri* below the first occurrence of *Idiognathodus* spp. (Krumhardt and others, 1996), and the *Idiognathodus* Fauna extends to the top of the Lisburne Group in northeast Alaska.

Krumhardt and others (1996) used the first appearance of *Idiognathodus incurvus?* as a guide to the base of the Atokan in the ESM section based on the work of Grayson and others (1989) in the conterminous United States. *Idiognathodus incurvus* is not a reliable indicator for the base of the Atokan in northeastern Alaska because of its rarity, and it is likely that its appearance in the eastern section is probably well above its level of origination. Instead, we use the first appearance of the foraminifer *Pseudostaffella* to approximate the Morrowan-Atokan boundary.

#### MISSISSIPPIAN

##### (ALAPAH LIMESTONE AND PART OF THE LOWER MEMBER OF THE WAHOO LIMESTONE)

Conodont species diversity and abundance is relatively low throughout the Alapah Limestone in both eastern and western Sadlerochit Mountains sections. Collections from the lower part of the Alapah in the western section are dominated by *Cavusgnathus unicornis*, *Kladognathus* sp., and *Syncladognathus geminus*, in order of decreasing abundance; gnathodids and rhachistognathids are rare. The conodont assemblages confirm the shallow-water, somewhat restricted depositional setting determined from micro-lithofacies criteria. Collections from the middle and upper parts of the Alapah contain chiefly *C. unicornis*, *Kladognathus* sp., *Hindeodus minutus*, and *Adetognathus lautus*, in order of decreasing abundance; gnathodids and rhachistognathids remain rare.

*Syncladognathus geminus* with *Cavusgnathus unicornis* place the lower 60 m of the Alapah Limestone in the western section in the late Meramecian to early Chesterian. Calcareous microfossils (see above) suggest placement of the lower 40 m in the Meramecian (fig. 3); *Rhachistognathus muricatus* also occurs in the lower 40 m. Its presence in the WSM section with *Syncladognathus geminus* and *Gnathodus texanus?* and with calcareous microfossils of probable Meramecian age extends its Mississippian range considerably downward in Alaska. It was previously thought to appear in the latest Chesterian (Baesemann and Lane, 1985; Krumhardt and others, 1996). The appearance of *Adetognathus lautus*, followed by *Hindeodus minutus* more than halfway through the Alapah (fig. 4), suggests a late Chesterian age for much of the formation.

A comparison of the conodont biostratigraphy of the Alapah Limestone in the eastern and western sections is preliminary because only a few conodont samples were taken from the formation in the eastern section. However, in both sections the predominant conodont species include *Cavusgnathus unicornis*, *Adetognathus lautus*, and *Kladognathus* sp. *Rhachistognathus muricatus* and *Gnathodus girtyi girtyi* are relatively rare and appear stratigraphically low, near the Meramecian-Chesterian boundary.

Conodont collections from the Mississippian part of the lower member of the Wahoo Limestone in the WSM section chiefly contain, in order of decreasing abundance, *Cavusgnathus unicornis*, *Kladognathus* sp., *Hindeodus minutus*, and *Gnathodus girtyi* subsp. *Adetognathus tyththus* occurs in low numbers throughout the lower member (fig. 4). This species is known to range from the upper Chesterian **Kinkaid** Limestone in the Illinois basin (Brown and others, 1990) into lowermost **Morrowan** strata in the northeast Brooks Range (Krumhardt and others, 1996). Its occurrence with Mississippian forms such as *C. unicornis* or *Kladognathus* sp. indicates a late (probably very late) Chesterian age for the lower 50 m of the member in the western section. Assemblages from the Mississippian part of the lower member in the ESM section chiefly contain, in order of decreasing abundance, *Cavusgnathus unicornis*, *Kladognathus* sp., *Gnathodus girtyi* subsp., and *Hindeodus minutus*. *Adetognathus tyththus* appears 22 m above the base of the lower member (fig. 4). Lacking evidence to the contrary, it seems reasonable that the lower 22 m of the member are also late Chesterian in age. Although the predominant conodonts in the Mississippian part of the lower member are the same in both our sections, *Gnathodus girtyi* subsp. is more abundant and *Hindeodus minutus* less abundant in the eastern section. The presence of *Lochriea commutata*, *Gnathodus bilineatus*, and greater numbers of *Gnathodus girtyi* subsp. (fig. 4) in the eastern section compared with the absence of *L. commutata* and *G. bilineatus* in the western section suggest that this part of the lower member formed in slightly deeper water open-marine conditions in the eastern section than in the western section.

#### PENNSYLVANIAN

##### (UPPER PART OF LOWER MEMBER AND UPPER MEMBER OF WAHOO LIMESTONE)

Conodont collections from the Pennsylvanian part of the lower member of the Wahoo Limestone in the ESM section are dominated by *Declinognathodus noduliferus* subsp., *Adetognathus tyththus*, and *Rhachistognathus muricatus*, in order of decreasing abundance. In the WSM section, this part of the lower member is only 4 m thick (versus 14 m in the ESM section) and produces low numbers of primarily *D. n. japonicus* and *R. muricatus*; the former marks the base of the Pennsylvanian in the eastern

and western sections. Additionally, *Gnathodus bilineatus* (possibly redeposited) and *Hindeodus minutus* occur in both sections. *Declinognathodus noduliferus inaequalis* was found only in the western section and may indicate that the base of the Pennsylvanian formed in somewhat deeper water open-marine conditions in the western section than to the east.

Conodonts are about twice as abundant in the upper member of the Wahoo Limestone in the ESM section compared to the WSM section. As elsewhere in the northeast Brooks Range, conodont zonal indices are absent to extremely rare in the upper member. Consequently, above the level of the *noduliferus-primus* Zone, the informal faunal units of Krumhardt and others (1996) are used (fig. 5).

Collections from the upper member of the Wahoo Limestone in the western section primarily include *Rhachistognathus* spp., *Adetognathus lautus*, and *Declinognathodus noduliferus* subsp., in order of decreasing abundance. The *noduliferus-primus* Zone extends to 17 m above the base of the member. The top of the succeeding lower *minutus* Fauna coincides with the last occurrence of *R. websteri* at 39 m above the base of the upper member (fig. 4). The *minutus* Fauna persists for another 31 m, at which level the first *Idiognathodus* appears, marking the base of the *Idiognathodus* Fauna that continues to the top of the formation (fig. 5).

Conodont assemblages from the upper member in the eastern section contain, in order of decreasing abundance, chiefly *Rhachistognathus* spp., *Declinognathodus noduliferus* subsp., *Adetognathus lautus* and, in its upper half, *Idiognathodus* spp. The *noduliferus-primus* Zone is followed by the *minutus* Fauna, which coincides with the beginning of well-developed shoal-water facies. The *Idiognathodus* Fauna characterizes the upper 85 m of the member (fig. 5).

In both study sections, deposition of the upper member began during the *noduliferus-primus* Zone. The upper limit of the succeeding *minutus* Fauna is at 107 m above the base of the member in the eastern section compared to 70 m in the western section. The highest biostratigraphic interval in the Wahoo, the *Idiognathodus* Fauna, extends for 85 m in the eastern section in comparison to just 18 m in the western section (fig. 5).

The predominant conodont species in the upper member are the same in both sections, except for *Idiognathodus* spp. *Gnathodus defectus*, commonly reported in uppermost Mississippian and lowermost Pennsylvanian rocks in the conterminous western United States (Dunn, 1970; Morrow and Webster, 1992), is rare and restricted to the lower *minutus* Fauna in both sections (fig. 4). Other relatively rare species are restricted to one or the other of the sections. *Diplognathodus? ellesmerensis?*, *Idiognathodus incurvus?*, and *Idiognathoides sinuatus* (1 to 3 specimens each) were only noted in the eastern section. *Declinognathodus noduliferus inaequalis* (17 specimens distributed in three collections; fig. 10:1), *D. n. lateralis* (5 specimens

in one collection; figs. 10:2, 3), and *Idiognathoides pacificus* (4 specimens in one collection; figs. 10:4, 5) were only found in the western section.

A 4-m interval containing common *Declinognathodus noduliferus inaequalis* and rare *D. n. lateralis* begins 36 m above the base of the upper member in the WSM section (fig. 2B, samples 85C and 89C). Both conodont samples were collected at the presumed top of parasequence boundaries and are from superficially coated grainstone and bryozoan-pelmatozoan-oolitic grainstone that lie below glauconitic bryozoan-pelmatozoan packstone-grainstone and wackestone. We suspect that both samples include part of the base (deepest water part) of the succeeding parasequence, and that *D. n. inaequalis* and *D. n. lateralis* were derived from those levels. The morphology of these species suggests an open-marine, somewhat deeper water environment than the shoal-water environment represented by oolitic grainstone. Higher in the section, a glauconitic, bioturbated, bryozoan-pelmatozoan packstone from the lower part of a parasequence produced the only specimens of *Idiognathoides pacificus* (fig. 2B, sample 122C), a very rare species in the Lisburne Group of the northeast Brooks Range. We believe it too represents an open-marine, possibly deeper water depositional setting than is characteristic of the Lisburne in the Sadlerochit Mountains. These data suggest that at least some parts of the upper member in the western section formed under deeper water conditions than have yet been documented in the eastern section.

Conodonts are rare and poorly preserved in the overlying Echooka Formation. A collection at 1 m above the base of the Echooka about 5 km east-southeast of the western section (USGS collection 29874-PC; sample collected by I.L. Tailleux, U.S. Geological Survey) produced two incomplete *Mesogondolella* Pa elements having the short vertical cusp and general posterior outline of *Mesogondolella phosphoriensis* (Youngquist, Hawley and Miller) (Heinz Kozur, oral commun., March 1996). Accordingly, this collection dates the base of the Echooka Formation as early Late Permian (=Wordian or Capitanian) and, at this locality, establishes a hiatus of at least 40 million years separating the Lisburne Group and Echooka Formation.

## CONCLUSIONS

Our investigations of the Lisburne Group in northeast Alaska have shown that although the group is generally fossiliferous, biostratigraphically reliable fossils are few for other than local or regional correlation. Many species that have been used for correlation in sub-Arctic North America and Eurasia are either absent or appear earlier or later in northeast Alaska.

The Alapah Limestone contains mainly low-diversity microfossil assemblages of chiefly long-ranging species that do not permit a refined biostratigraphy. *Skippella?* sp. and

*Koninckopora minuta?* help position the Meramecian-Chesterian boundary in the Sadlerochit Mountains sections. *Adetognathus lautus* with *Cavusgnathus unicornis* are diagnostic for the Chesterian, and *C. unicornis* with the *Biseriella parva* group and joined later by the *Globivalvulina bulloides* group indicate the middle to late Chesterian. The overlying Wahoo Limestone consists of many vertically stacked, lithologically similar parasequences that formed in shallowing-upward cycles. Fossil assemblages in the Wahoo are somewhat more diverse and slightly more biostratigraphically rewarding than those in the Alapah. *Cavusgnathus unicornis* with *Brenckleina rugosa* and *Adetognathus tythus* likely indicate a very late Chesterian age for the lower beds of the Wahoo. Higher in the formation, *Declinognathodus noduliferus* and *Pseudostaffella* spp. or *Eoschubertella* spp. appear to be the most reliable fossils for local and regional correlation of the base of the **Morrowan** and Atokan, respectively (figs. 3-5). Of secondary importance are *Adetognathus tythus* and *Brenckleina rugosa* that appear to be short ranging across the Mississippian-Pennsylvanian boundary.

Comparison of the lithostratigraphy and microfossil assemblages in the eastern and western Sadlerochit Mountains sections shows the following: (1) Deposition of the Alapah Limestone began earlier and the entire formation formed under more restricted conditions in the western section. (2) The Mississippian-Pennsylvanian boundary is at approximately the same stratigraphic level, 50-56 m above the base of the lower member of the Wahoo Limestone, and is marked by a chert-rich interval in both sections. (3) The Pennsylvanian part of the lower member and the entire upper member are much thinner in the western section, suggesting slower deposition and (or) more erosion along intraformational unconformities and along the pre-Echooka Formation **unconformity** in the west. Glauconite in the WSM section may indicate slower deposition at that locality. Much of the Atokan part of the Wahoo, including the *Osagi*-rich beds that are so prevalent in the upper part of the formation in the eastern Sadlerochit Mountains and the subsurface of northern ANWR, was likely eroded at the western section prior to deposition of the Echooka Formation. The recognition of only 15 parasequences in the western section in comparison with 24 in the eastern section also supports greater erosion and (or) nondeposition in the west. (4) The restriction of some cosmopolitan conodont species and glauconite to the western section suggests that at least part of the Wahoo was deposited in somewhat deeper water and (or) more open-marine conditions in the western section.

The difference in fossil ranges between the North Slope and other areas make precise correlation of the Lisburne Group difficult outside of northeastern Alaska. Nevertheless, the Lisburne microfossil succession is generally consistent along depositional strike across the eastern North Slope from Prudhoe Bay through ANWR and can provide

a fairly reliable scheme for local Mississippian-Pennsylvanian correlation.

**Acknowledgments.**—Baesemann and Brenckle thank C.E. Bartberger, Amoco Corporation, for his help in describing and collecting the western Sadlerochit Mountains sections near the Katakaturuk River and for his discussions of regional depositional environments. They also thank Amoco Corporation for supporting the Lisburne Group field work on the North Slope and for giving them permission to publish this report. Gruzlovic is grateful to Amoco Corporation for the opportunity to work as a summer intern completing a microlithofacies analysis of core data from Prudhoe Bay and outcrop data from the western Sadlerochit Mountains; he is particularly indebted to P.L. Brenckle and J.F. Baesemann. Krumhardt acknowledges the Geophysical Institute, University of Alaska Fairbanks, for enabling her to work on this study with Harris during parts of February 1995 and 1996, in the harsh winter climate of southern Florida.

## REFERENCES CITED

- Armstrong, A.K., 1972, Pennsylvanian carbonates, paleoecology, and rugose colonial corals, north flank, eastern Brooks Range, arctic Alaska: U.S. Geological Survey Professional Paper 747, 21 p.
- Armstrong, A.K., and Mamet, B.L., 1974, Carboniferous biostratigraphy, Prudhoe Bay State 1 to northeast Brooks Range, Arctic Alaska: American Association of Petroleum Geologists Bulletin, v. 58, no. 4, p. 646-660.
- , 1975, Carboniferous biostratigraphy, northeastern Brooks Range, arctic Alaska: U.S. Geological Survey Professional Paper 884, 29 p.
- , 1977, Carboniferous microfacies, microfossils, and corals, Lisburne Group, arctic Alaska: U.S. Geological Survey Professional Paper 849, 144 p.
- Armstrong, A.K., Mamet, B.L., and Dutro, J.T., Jr., 1970, Foraminiferal zonation and carbonate facies of Carboniferous (Mississippian and Pennsylvanian) Lisburne Group, central and eastern Brooks Range, Arctic Alaska: American Association of Petroleum Geologists Bulletin, v. 54, no. 5, p. 687-698.
- Baesemann, J.F., and Lane, H.R., 1985, Taxonomy of the genus *Rhachistognathus* Dunn (Conodonta: Late Mississippian to Early Pennsylvanian), in Lane, H.R., and Ziegler, Willi, eds., *Toward a boundary in the middle of the Carboniferous: Stratigraphy and paleontology*: Courier Forschungsinstitut Senckenberg, no. 74, p. 93-135.
- Baxter, J.W., and Brenckle, P.L., 1982, Preliminary statement on Mississippian calcareous foraminiferal successions of the Midcontinent (U.S.A.) and their correlation to western Europe: *Newsletters on Stratigraphy*, v. 11, p. 136-153.
- Brady, H.B., 1876, A monograph of Carboniferous and Permian Foraminifera (the genus *Fusulina* excepted): London, Palaeontographical Society, 166 p.
- Brenckle, P.L., 1991 [1990], Foraminiferal division of the Lower Carboniferous/Mississippian in North America, in Brenckle,

- P.L., and Manger, W.L., eds., International correlation and division of the Carboniferous System: Courier Forschungs-institut Senckenberg, no. 130, p. 65-78.
- Brenckle, P.L., Baesemann, J.F., Lane, H.R., West, R.R., Webster, G.D., Langenheim, R.L., Brand, U., and Richards, B.C., in press, Arrow Canyon, the Mid-Carboniferous boundary stratotype: 13th International Congress on Carboniferous-Permian Stratigraphy and Geology, Cracow, 1995, *Compte Rendu*.
- Brenckle, P.L., Groves, J.R., and Skipp, B.A., 1982, A Mississippian/Pennsylvanian (Mid-Carboniferous) boundary in North America based on calcareous Foraminifera, in Ramsbottom, W.H.C., Saunders, W.B., and Owens, B., eds., *Biostratigraphic data for a Mid-Carboniferous boundary: IUGS Subcommittee on Carboniferous Stratigraphy, Biennial Meeting, Leeds, 1981*, p. 42-51.
- Brenckle, P.L., and Wahlman, G.P., 1994, *Conilia*, a new Upper Paleozoic pseudovidalinid foraminifer: *Mémoires de l'Institut Géologique de l'Université de Louvain*, v. 35, p. 169-176.
- Brown, L.M., Rexroad, C.B., Beard, John, and Williams, David, 1990, Phylogenetic and zonal implications of *Cavusgnathus tythus* n. sp. (Conodonts) from the Kinkaid Limestone (Upper Mississippian) of western Kentucky, U.S.A.: *Geologica et Palaeontologica*, no. 24, p. 77-87.
- Carlson, R.C., 1990, Cement stratigraphy in the Wahoo Formation, Sadlerochit Mountains, Alaska [abs.]: *American Association of Petroleum Geologists Bulletin*, v. 74, no. 5, p. 625.
- Dunn, D.L., 1970, Conodont zonation near the Mississippian-Pennsylvanian boundary in western United States: *Geological Society of America Bulletin*, v. 81, p. 2959-2974.
- Grayson, R.C., Jr., Merrill, G.K., and Lambert, L.L., 1989, Phylogenetic basis for species recognition within the conodont genus *Idiognathodus*: Applicability to correlation and boundary placement, in Boardman, D.R., II, and three others, eds., *Middle and Late Pennsylvanian chronostratigraphic boundaries in north-central Texas: Glacial-eustatic events, biostratigraphy, and paleoecology: Lubbock, Tex., Texas Tech University Studies in Geology 2*, p. 75-94.
- Groves, J.R., 1986, Foraminiferal characterization of the Morrowan-Atokan (lower Middle Pennsylvanian) boundary: *Geological Society of America Bulletin*, v. 97, p. 346-353.
- 1988, Calcareous foraminifers from the Bashkirian stratotype (middle Carboniferous, south Urals) and their significance for intercontinental correlations and the evolution of the Fusulinidae: *Journal of Paleontology*, v. 62, p. 368-399.
- Groves, J.R., Nassichuk, W.W., Rui, L., and Pinard, Sylvie, 1994, Middle Carboniferous Fusulinacean biostratigraphy, northern Ellesmere Island (Sverdrup Basin, Canadian Arctic Archipelago): *Geological Survey of Canada Bulletin 469*, 55 p.
- Gruzlovic, P.D., 1991, Stratigraphic evolution and lateral facies changes across a carbonate ramp and their effect on parasequences of the Carboniferous Lisburne Group: Fairbanks, University of Alaska Fairbanks, M.S. thesis, 201 p.
- Hassler, S.E., and Stock, C.W., 1993, Conodont biostratigraphy of the Tuscumbia Limestone, Pride Mountain Formation, and Monteagle Limestone, in Pashin, J.C., ed., *New perspectives on the Mississippian System of Alabama*, Guidebook: Tuscaloosa, Ala., Alabama Geological Society, p. 51-59.
- Huggins, J.H., 1983, Meramecian conodonts and biostratigraphy of the (Upper Mississippian) Greenbrier Limestone (Hurricane Ridge and Greendale synclines), southwestern Virginia and southern West Virginia: Blacksburg, Va., Virginia Polytechnic Institute and State University, M.S. thesis, 304 p.
- Jameson, Jeremy, 1994, Models of porosity formation and their impact on reservoir description, Lisburne field, Prudhoe Bay, Alaska: *AAPG Bulletin*, v. 78, no. 11, p. 1651-1678.
- Krumhardt, A.P., Harris, A.G., and Watts, K.F., 1996, Lithostratigraphy, microlithofacies, and conodont biostratigraphy and biofacies of the Carboniferous Wahoo Limestone, northeast Brooks Range, Alaska: *U.S. Geological Survey Professional Paper 1568*, 71 p.
- Lane, H.R., 1977, *Morrowan* (Early Pennsylvanian) conodonts of northwestern Arkansas and northeastern Oklahoma, in Sutherland, P.K., and Manger, W.L., eds., *Upper Chesterian-Morrowan stratigraphy and the Mississippian-Pennsylvanian boundary in northeastern Oklahoma and northwestern Arkansas: Oklahoma Geological Survey Guidebook 18*, p. 177-180.
- Lane, H.R., Baesemann, J.F., Brenckle, P.L., and West, R.R., 1985, Arrow Canyon, Nevada: A potential Mid-Carboniferous boundary stratotype: *10th International Congress of Carboniferous Stratigraphy and Geology, Madrid, 1983, Compte Rendu*, v. 4, p. 429-440.
- Lane, H.R., Bouckaert, J., and twelve others, 1985, Proposal for an international Mid-Carboniferous boundary: *10th International Congress of Carboniferous Stratigraphy and Geology, Madrid, 1983, Compte Rendu*, v. 4, p. 323-339.
- Lane, H.R., and Straka, J.J., II, 1974, Late Mississippian and Early Pennsylvanian conodonts, Arkansas and Oklahoma: *Geological Society of America Special Paper 152*, 144 p.
- Mamet, B.L., 1975, Carboniferous Foraminifera and algae of the Amsden Formation (Mississippian and Pennsylvanian) of Wyoming: *U.S. Geological Survey Professional Paper 848-B*, 18 p.
- Mamet, B.L., and Armstrong, A.K., 1972, Lisburne Group, Franklin and Romanzof Mountains, northeastern Alaska, in *Geological Survey Research 1972: U.S. Geological Survey Professional Paper 800-C*, p. C127-C144.
- 1984, The Mississippian-Pennsylvanian boundary in the northeastern Brooks Range, Arctic Alaska: *Neuvikme Congrks International de Stratigraphie et de Géologie du Carbonifère: Carbondale, Ill., Southern Illinois University Press*, p. 428-436.
- Mamet, B.L., and Belford, D.J., 1968, Carboniferous Foraminifera, Bonaparte Gulf Basin, northwestern Australia: *Micro-paleontology*, v. 14, no. 3, p. 339-347.
- Mamet, B.L., and de Batz, Renaud, 1989, Carboniferous microflora, Lisburne Group, Sadlerochit Mountains, Alaska: *11th International Congress of Carboniferous Stratigraphy and Geology, Beijing, 1987, Compte Rendu*, v. 3, p. 50-60.
- Mamet, B.L., Madi, A., Bourque, P.A., and Sebbar, A., 1995, *Foraminifères Carbonifères du Grand Erg occidental, Bassin de Béchar, Algérie*: *Bulletin de la Société belge de la Géologie*, v. 103, nos. 1-2, p. 51-61.
- Mamet, B.L., and Skipp, B.A., 1970, Lower Carboniferous calcareous Foraminifera: Preliminary zonation and stratigraphic implications for the Mississippian of North America:



- 6th International Congress of Carboniferous Stratigraphy and Geology, Sheffield, 1967, *Compte Rendu*, v. 3, p. 1129-1146.
- Mamet, B.L., Skipp, B.A., Sando, W.J., and Maple, W.J.**, 1971, Biostratigraphy of Upper Mississippian and associated Carboniferous rocks in south-central Idaho: *American Association of Petroleum Geologists Bulletin*, v. 55, p. 20-33.
- Morrow, J.R., and Webster, G.D., 1992, New stratigraphic, petrographic, and biostratigraphic data on the proposed Mississippian-Pennsylvanian boundary stratotype, Granite Mountain, west-central Utah, in Sutherland, P.K., and Manger, W.L., eds., *Recent advances in Middle Carboniferous biostratigraphy—A symposium: Oklahoma Geological Survey Circular 94*, p. 55-67.
- Perret, M-F., 1993, Recherches micropaléontologiques et biostratigraphiques (conodontes-foraminifères) dans le Carbonifère pyrénéen: *Strata, Series 2*, v. 21, 597 p.
- Petryk, A.A., Mamet, B.L., and Macqueen, R.W.**, 1970, Preliminary foraminiferal zonation, Rundle Group and uppermost Banff Formation (Lower Carboniferous), southwestern Alberta: *Bulletin of Canadian Petroleum Geology*, v. 18, p. 84-103.
- Pronina, T.V., 1972, New representatives of middle Paleozoic Astorhizida of the Urals, in *New species of fossil plants and invertebrates of the Soviet Union: Akademiya Nauk SSSR, Izdatel'stvo "Nauka," Moscow*, p. 10-11 [in Russian].
- Reitlinger, E.A., 1949, Smaller foraminifers in the lower part of the Middle Carboniferous of the Middle Urals and Prikama: *Izvestiya Akademii Nauk SSSR, Seriya Geologicheskaya*, no. 6, p. 149-164 [in Russian].
- 1950, Foraminifers from Middle Carboniferous deposits in the central part of the Russian Platform (exclusive of the Family Fusulinidae): *Akademiya Nauk SSSR, Trudy Instituta Geologicheskikh Nauk, Geologicheskaya Seriya 47*, publication 126, 126 p. [in Russian].
- Ross, C.A., 1967, Development of fusulinid (Foraminiferida) faunal realms: *Journal of Paleontology*, v. 41, p. 1341-1354.
- Ross, C.A., and Ross, J.R.P., 1985, Carboniferous and Early Permian biogeography: *Geology*, v. 13, p. 27-30.
- Rui, L., Nassichuk, W.W., and Thorsteinsson, R., 1996, Middle Carboniferous fusulinaceans from the Canyon Fiord Formation, northwestern Melville Island (**Sverdrup** Basin, Canadian Arctic Archipelago): *Journal of Foraminiferal Research*, v. 26, p. 27-52.
- Sando, W.J., **Mamet, B.L.**, and Dutro, J.T., Jr., 1969, Carboniferous megafaunal and microfaunal zonation in the northern Cordillera of the United States: *U.S. Geological Survey Professional Paper 613-E*, 29 p.
- Skipp, B.A., Baesemann, J.F., and Brenckle, P.L., 1985, A reference area for the Mississippian-Pennsylvanian (**Mid-Carboniferous**) boundary in east-central Idaho, U.S.A.: **10th International Congress of Carboniferous Stratigraphy and Geology, Madrid, 1983, Compte Rendu**, v. 4, p. 403-428.
- Vdovenko, M.V., 1971, New foraminiferal genus from **Visean** strata of the Greater **Donbase**: *Dopovidi Akademii Nauk Ukrain'skoi RSR*, v. 10, p. 877-879 [in Russian].
- Vdovenko, M.V., Aisenberg, D. Ye., Nemirovskaya, T.I., and Poletaev, V.I., 1990, An overview of Lower Carboniferous biozones of the Russian Platform: *Journal of Foraminiferal Research*, v. 20, no. 3, p. 184-194.
- Watts, K.F., Harris, A.G., Carlson, R.C., Eckstein, M.K., Gruzlovic, P.D., Imm, T.A., Krumhardt, A.P., Lasota, D.K., Morgan, S.K., Enos, P., Goldstein, R., Dumoulin, J.A., and **Mamet, B.L.**, 1994, Analysis of reservoir heterogeneities due to shallowing-upward cycles in carbonate rocks of the Carboniferous Wahoo Limestone of northeastern Alaska: *Department of Energy Report, Contract DE-AC22-89BC14471*, 433 p.

Reviewers: **Kenneth J. Bird and John R. Groves**

# Lower Mississippian (Kinderhookian) Biostratigraphy and Lithostratigraphy of the Western Endicott Mountains, Brooks Range, Alaska

By Charles G. Mull, Anita G. Harris, and John L. Carter

## ABSTRACT

Geologic mapping in the western Endicott Mountains of the Brooks Range orogenic belt has delineated two distinctive facies of Lower Mississippian (Kinderhookian) rocks in the Endicott Mountains allochthon that were juxtaposed by thrusting during the Early Cretaceous. A distinctive reddish-brown-weathering siltstone unit that is as much as 215 m thick overlies the Upper Devonian to Lower Mississippian(?) Kanayut Conglomerate in part of the western Endicott Mountains. This unit contrasts markedly with the chiefly black Kayak Shale that typically overlies the Kanayut in the Key Creek sequence of the Endicott Mountains allochthon elsewhere in the Endicott Mountains.

The distinctive siltstone unit is here named the Isikut Member of the Kayak Shale and is one of the characteristic features of a stratigraphic assemblage that is herein formally designated the Aniak River sequence of the Endicott Mountains allochthon and that contrasts markedly with the Key Creek sequence. The Kanayut Conglomerate and Noatak Sandstone that underlie the Isikut in the Aniak River sequence are less than 400 m thick and are much thinner than the Kanayut and Noatak in other sequences of the Endicott Mountains allochthon in the central and eastern Endicott Mountains. Regional mapping shows that the Aniak River sequence is telescoped by thrusting over the Key Creek sequence. In the Howard Pass quadrangle, the Aniak River sequence and the Isikut Member of the Kayak trend about N. 70° W. and form the southern flank of the mountains from the vicinity of Howard Pass west to Feniak Lake. West of the Ipnarik River, the Aniak River sequence converges with the west-trending mountain front and forms most of the high mountain peaks at the western end of the Endicott Mountains. The structural juxtaposition of the Aniak River and Key Creek sequences is well exposed in the Safari Creek window, where Mississippian to Lower Cretaceous rocks of the Key Creek sequence underlie a thrust fault at the base of the Kanayut Conglomerate and Noatak Sandstone of the Aniak River sequence. The Isikut is particularly prominent on the northern side of the moun-

tains in the vicinity of Story Creek, where it hosts a zinc-lead-silver mineral occurrence that is marked by notable vein-breccia surface mineralization.

Conodont and brachiopod faunas from the Isikut Member of the Kayak Shale and overlying Kinderhookian units in the Aniak River sequence are similar to but more biostratigraphically diagnostic than faunas from Kinderhookian units in the Key Creek sequence. These faunas indicate that the Isikut Member is at least partly coeval with the lower part of the Kayak Shale elsewhere in the western Endicott Mountains and with the lower part of the Utokuk Formation of the Lisburne Group in the De Long Mountains. The conodonts in the Isikut Member are more abundant and diverse than in the Kayak Shale of the Key Creek sequence, indicating that the Isikut shallow-water environments provided a wider range of favorable habitats for conodonts than did the muddier Kayak Shale.

## INTRODUCTION

The discovery of a number of zinc-lead-silver occurrences in the central and western Brooks Range during the exploration of the National Petroleum Reserve in Alaska (NPRA) in the late 1970's (Theobald and Barton, 1978; Jansons, 1982) resulted in the need for more detailed evaluation of the mineral potential of the area.

In the Endicott Mountains of the central Brooks Range (fig. 1), the zinc-lead-silver mineral occurrences are numerous and are in Upper Devonian and Lower Mississippian rocks of the Endicott Group, which includes, in ascending order, the Hunt Fork Shale, Noatak Sandstone, Kanayut Conglomerate, and Kayak Shale (Tailleur and others, 1967). The most notable mineral occurrence, at Story Creek near the western end of the Endicott Mountains, lies near the top of the Endicott Group in a stratigraphic position that regionally is occupied by the Kayak Shale.

The Kayak Shale is a significant marker unit along a strike length of over 700 km in the Brooks Range. Along the northern flank of the Endicott Mountains, the Kayak

Shale is present as a nearly continuous belt overlying the Kanayut Conglomerate in lowland areas north of the mountain front, and it occurs in other discontinuous areas within the mountains. It is overlain by various formations of the **Lisburne** Group. The Kayak is also widespread in the Philip Smith, Romanzof, and British Mountains of the northeastern Brooks Range in northeastern Alaska and the northern Yukon Territory of Canada (fig. 1), where it overlies the **Kekiktuk** Conglomerate, which is a basal Mississippian clastic unit that overlies a major regional angular unconformity. The Kayak is also present in some of the allochthons in the thrust belt and thus had a significant north-south extent prior to structural telescoping that occurred during the Brookian orogeny.

Throughout most of its outcrop belt, the Kayak Shale characteristically consists of black shale containing yellowish-brown-weathering, bioclastic limestone beds in the upper part and relatively thin siltstone and very fine grained sandstone beds in the lower part. In the western Endicott Mountains, the stratigraphic position of the Kayak Shale is dominated by a conspicuous reddish-brown-weathering siltstone and sandstone unit (fig. 2) that is absent elsewhere in the Endicott Mountains. This unit is of particular interest because it hosts sphalerite-galena vein breccias in the Story Creek area. Recognition of this distinctive mappable unit may be a guide for future mineral exploration in the western Endicott Mountains.

In order to delineate the stratigraphic and structural controls on mineral occurrences in the area, detailed geologic mapping and stratigraphic studies of the western Endicott Mountains were conducted by the Alaska Division of Geological and Geophysical Surveys (ADGGS) during 1991-93 in collaboration with the U.S. Geological Survey (USGS), in support of the U.S. Bureau of Mines mineral evaluation of the area. Funding for the mapping by the ADGGS was provided by the U.S. Bureau of Mines; personnel from ADGGS, USGS, and University of Alaska Fairbanks participated in the mapping and stratigraphic studies.

## PREVIOUS STUDIES

Studies in the western Endicott Mountains began during the exploration of Naval Petroleum Reserve #4 (NPR-4) from 1946 to 1952. Reconnaissance traverses of the major rivers were carried out by a number of USGS geologists and resulted in several preliminary reports and maps in which the regional stratigraphic framework was established. Detailed mapping of the Etivluk River region north of the area studied in detail in our report (Tailleur and others, 1966) documented the regional structural style and recognized juxtaposed allochthonous facies. Chapman and others (1964) published a generalized geologic map of the

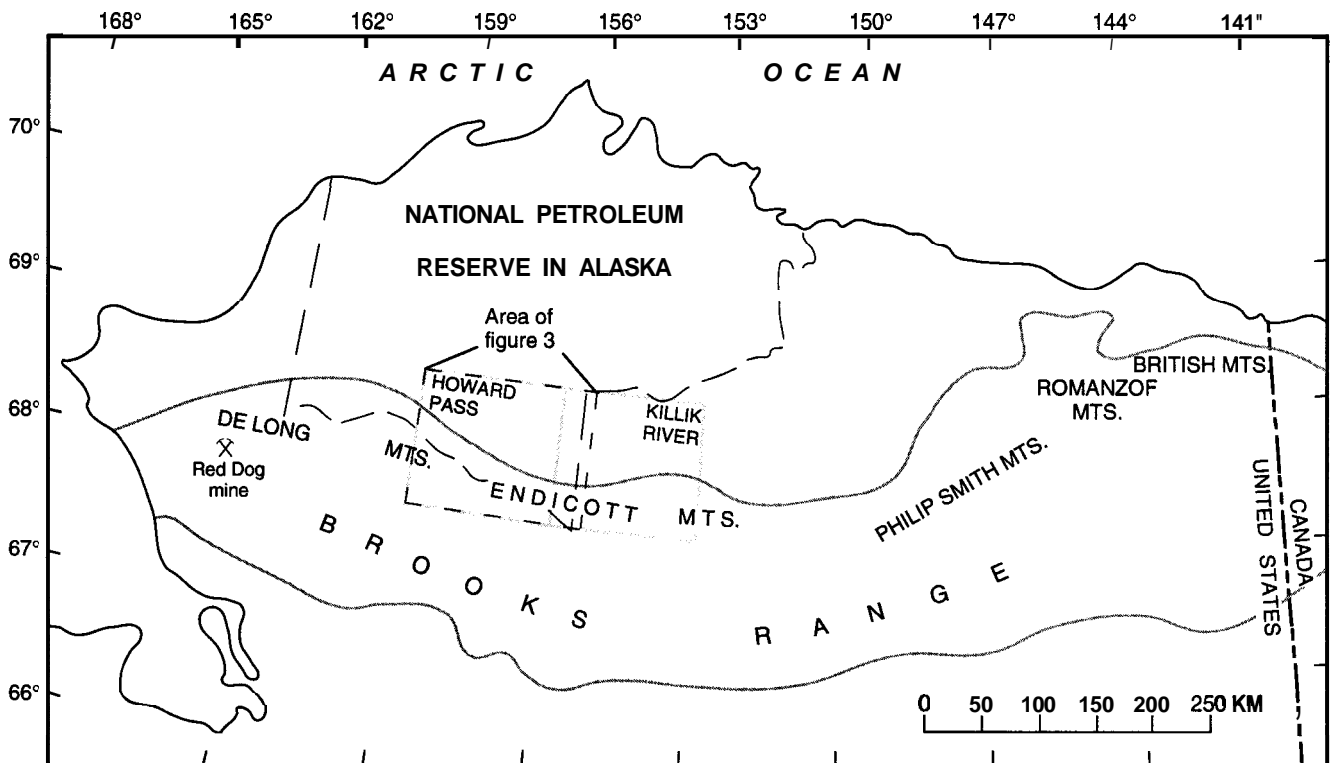


Figure 1. Index map of northern Alaska.

western Endicott Mountains and a description of its stratigraphy based on studies in the Killik-Etivluk region.

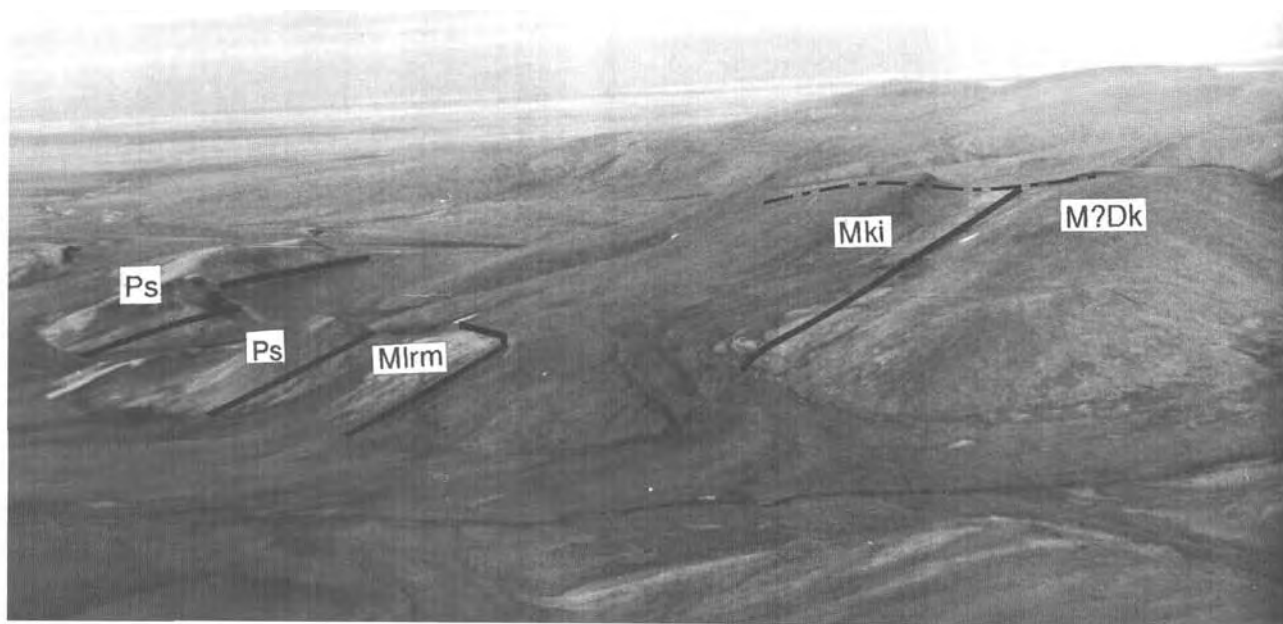
Renewed interest in the hydrocarbon potential of the NPRA (formerly NPR-4), from 1977 to 1982, resulted in additional regional studies of the stratigraphy and structure of the central and western Brooks Range that included recognition of new stratigraphic units. These units included the Kuna Formation, which overlies the Kayak Shale in the western Endicott Mountains (Mull and others, 1982) and is the host rock for the major zinc-lead ore deposit at Red Dog in the western De Long Mountains. Recent geologic maps of the Killik River quadrangle (Mull and others, 1996), and the western Endicott Mountains in the Howard Pass quadrangle (Mull and Werdon, 1994) incorporate much of the modern nomenclature.

Using geochemical studies conducted by the USGS (Theobald and Barton, 1978; Kelley and others, 1992; Kelley and Mull, 1995), the U.S. Bureau of Mines (Jansons and Baggs, 1980; Jansons and Parke, 1981; Jansons, 1982; Meyer and Kurtak, 1992) and the USGS (Duttweiler, 1987) identified a number of mineral occurrences in the western Endicott Mountains. The zinc-lead-silver occurrence near Story Creek was mapped and described by Ellersieck and others (1982; U.S. Geological Survey, unpub. data). Geochemical studies and evaluation of the mineral potential of the Killik River quadrangle by Kelley and Mull (1995) discuss some of the geochemistry and stratigraphy of the Kayak Shale in the area immediately east of the area

of our present study. Detailed biostratigraphic and lithologic studies of the Lisburne Group in the Howard Pass quadrangle and the western part of the Killik River quadrangle (Dumoulin and Harris, 1993; Dumoulin and others, 1993) were carried out as part of the USGS Alaska Mineral Resource Assessment Program (AMRAP). Detailed study of the geochemistry and genesis of several mineral deposits in the Kanayut Conglomerate and related rocks in the area is in progress by Melanie B. Werdon as part of a University of Alaska Fairbanks Ph.D. dissertation.

## GEOLOGIC SETTING

The Endicott Mountains and the foothills of the central Brooks Range thrust-and-fold belt are composed of a series of allochthons that consist dominantly of sedimentary rocks of Devonian to Early Cretaceous (Neocomian) age. Each allochthon is characterized by a distinctive stratigraphic assemblage that is of regional extent and contrasts markedly with the generally coeval stratigraphic assemblages of adjacent allochthons (Mayfield and others, 1988; Mull and others, 1996). The allochthons represent parts of formerly continuous sedimentary basins that were juxtaposed by multiple stages of north-vergent thrusting and folding during the Late Jurassic to Tertiary Brookian orogeny (Moore and others, 1994).



**Figure 2.** View to west showing conspicuous reddish-brown-weathering siltstone and sandstone unit, Isikut Member of Kayak Shale, at reference section in the Aniuk River area on the southern side of the western Endicott Mountains. Abbreviations: M?Dk, Kanayut Conglomerate; Mki, Isikut Member of Kayak Shale; Mlrm, Rough Mountain Creek unit of Lisburne Group; Ps, Siksikpuk Formation. Dashed line shows location of measured reference section.

The northern part of the Endicott Mountains is underlain by the Endicott Mountains allochthon (Mull and others, 1987)<sup>1</sup>, the structurally lowest of the formally named allochthons in the central Brooks Range (fig. 3A). This allochthon contains an Upper Devonian to Lower Cretaceous sedimentary section that is probably as much as 4 km thick. In the northern Endicott Mountains, the allochthon consists mostly of the Kanayut Conglomerate, Noatak Sandstone, and Hunt Fork Shale of the Endicott Group, which were deposited chiefly in a deltaic setting during the Late Devonian (Nilsen and Moore, 1984). These rocks form mountains that range up to 2,500 m elevation in the east, and decrease to about 1,500 m in the western Endicott Mountains. During the Early Mississippian, this coarse clastic succession was succeeded by shallow-water marine, fine-grained deposits of the Kayak Shale (Bowsher and Duro, 1957), the uppermost unit in the Endicott Group. Overlying the Kayak is the Lisburne Group (Lower Mississippian to Lower Pennsylvanian), which in the eastern Endicott Mountains is characterized dominantly by thick platform carbonate rocks (Armstrong and Mamet, 1978). This stratigraphic succession is referred to as the Killik River sequence of the Endicott Mountains allochthon (Mull and Werdon, 1994; Mull and others, 1996). In the western Endicott Mountains, the Kayak is overlain by black sooty shale, carbonate, and chert of the Kuna Formation (Mull and others, 1982), which is a basinal facies correlative with the platform carbonate rocks of the Lisburne Group farther east; this stratigraphic succession constitutes the Key Creek sequence (Mayfield and others, 1988; fig. 3). The Permian Siksikpuk Formation overlies the Carboniferous rocks of both the Killik River and Key Creek sequences.

In most of its outcrop belt, the Kayak Shale characteristically consists of about 80 percent black shale containing scattered reddish-brown-weathering concretions. Typically, the upper part of the Kayak contains conspicuous, relatively thin beds of yellowish-brown-weathering, bioclastic limestone; the basal part of the Kayak commonly contains thin siltstone and very fine grained sandstone beds that comprise less than 10 percent of the formation. The Kayak is generally a recessive unit that, in many places, is nearly buried by talus from the overlying, resistant Lisburne Group. In areas where it is overlain by the nonresistant Kuna Formation, the Kayak forms broad partly vegetated slopes with areas of weathered shale rubble; it is commonly well exposed only in stream cuts.

Because the Kayak Shale is an incompetent unit, it frequently forms a zone of structural detachment. Consequently, many exposures of the formation are characterized by intense folding so that its true stratigraphic thickness is

difficult to determine. Measurement of composite sections is also difficult because of the lack of distinctive marker beds, but the formation has an estimated thickness of as much as 300 m (Mull and others, 1996).

## ENDICOTT GROUP IN THE WESTERN ENDICOTT MOUNTAINS

The Key Creek sequence constitutes about half of the Endicott Mountains allochthon in the western Endicott Mountains. Dominantly coarse-grained clastic rocks of the Hunt Fork Shale, Noatak Sandstone, and Kanayut Conglomerate of the Endicott Group underlie most of the mountain areas, and are thought to range in age from Late Devonian to Early Mississippian(?) at the top of the Kanayut (Nilsen and Moore, 1984). The overlying Kayak Shale (uppermost formation of the Endicott Group) is exposed discontinuously along most of the northern front of the mountains from the Killik River west to the upper headwaters of Tukuto Creek in the central part of the Howard Pass quadrangle (fig. 3A). The Kayak Shale is also exposed in structural windows at the head of Safari Creek and at the headwaters of a tributary of the Aniuk River (fig. 3A). In the scattered streamcut exposures in this area, the Kayak consists dominantly of the characteristic black shale with scattered bioclastic limestone beds. West of the Etivluk River, volcanoclastic rocks are also present in this unit. In most of the western Endicott Mountains, the Kayak is stratigraphically overlain by a thin, light-gray, bioclastic limestone unit informally named the Rough Mountain Creek unit by Dumoulin and Harris (this volume), which separates the Kayak Shale from the Kuna Formation. The lithostratigraphy and biostratigraphy of the Rough Mountain Creek unit are discussed in detail by Dumoulin and Harris (this volume).

At Isikut Mountain east of Howard Pass, and elsewhere on the south side of the Endicott Mountains west of Howard Pass, the Kanayut is overlain by a conspicuous reddish-brown-weathering unit that consists chiefly of thin-bedded siltstone and fine-grained sandstone that forms low resistant rubble-covered *cuervas*, hogbacks, or ridges (fig. 2). The upper part of this unit is overlain by typical black Kayak Shale; light-gray, bioclastic limestone of the Rough Mountain Creek unit (Dumoulin and Harris, this volume); and the Kuna Formation. The dominant lithology, topographic expression, and weathering character of this siltstone unit contrast markedly with the Kayak Shale elsewhere in the Brooks Range. The unit is mapped westward from Isikut Mountain along the southern flank of the western Endicott Mountains to the headwaters of a northern tributary of the Aniuk River. It is also present along most of the northern flank of the mountains from the Ipnarik River west to the head of Makpik Creek, north of Feniak Lake (fig. 3A; Mull and Werdon, 1994). It is particularly **promi-**

---

<sup>1</sup> Also known as the Brooks Range allochthon in the DeLong Mountains of the western Brooks Range (Martin, 1970; Mayfield and others, 1988; Durnoulin and Harris, 1993; Dumoulin and others, 1993).

ment in the Safari Creek–Story Creek area, where it underlies a broad plateau that forms the northern flank of the mountains. Extrusive(?) volcanic rocks are also present locally within this unit on the northern flank of the mountains.

Mapping in the western Endicott Mountains indicates that the siltstone unit and underlying rocks are part of a stratigraphic sequence that forms extensive thrust sheets within the Endicott Mountains allochthon. The combined Kanayut Conglomerate and Noatak Sandstone in this stratigraphic sequence are <400 m thick and are notably finer grained than the Kanayut Conglomerate and Noatak Sandstone in the eastern Endicott Mountains, which are >1,500 m thick.

Because the distinctive siltstone unit, the Kanayut, and the Noatak constitute a stratigraphic sequence that has identifiable features of regional extent in the western Endicott Mountains, it is differentiated as the Aniak River sequence (Mull and Werdon, 1994) to distinguish it from the Key Creek sequence, which contains the black shale that is characteristic of the Kayak Shale elsewhere in the Endicott Mountains allochthon. Regional mapping shows that the thrust sheets containing the Aniak River sequence trend northwest from the upper Nigu River area and converge with the west-trending mountain front in the vicinity of the upper Ipnarik River. The thrust juxtaposition of the contrasting facies of the Aniak River and Key Creek sequences is particularly well exposed in the Safari Creek window at the headwaters of Safari Creek and in the headwaters of a northern fork of the Aniak River (fig. 3A). In some areas west of the headwaters of Safari Creek, an area of interbedded black shale and siltstone appears to be transitional between the two dominant facies and is mapped as the Key Creek sequence. The Aniak River sequence trends southeast from the Howard Pass and western Killik River quadrangle, but its lateral extent into adjacent quadrangles is unknown. The lithostratigraphy and biostratigraphy of the **Kinderhookian** strata that distinguish the Key Creek and Aniak River sequences are discussed in detail below.

## KINDERHOOKIAN STRATA OF THE KEY CREEK SEQUENCE

The Mississippian part of the Key Creek sequence in the western Endicott Mountains includes, in ascending order, the uppermost Kanayut Conglomerate, Kayak Shale, and the Rough Mountain Creek unit (Dumoulin and Harris, this volume) and most of the Kuna Formation (fig. 4). Exposures of these rocks are generally poor, widely scattered, and commonly structurally complicated. The Kayak consists of mainly black shale with interbedded limestone and shale at the top and a relatively thin interval of sandstone

and siltstone at the base termed the basal sandstone member of the Kayak by **Bowsher** and Dutro (1957). No stratigraphic sections of the Kayak Shale and the overlying Rough Mountain Creek unit have been measured in the Key Creek sequence; the thickness for the Kayak Shale shown in figure 4 is estimated. The general stratigraphic positions of fossil collections shown on figure 4 were determined from field relationships. The Mississippian part of the Key Creek sequence in the western Endicott Mountains is overlain by siliceous shale and chert of the Permian Siksikpuk Formation.

Conodont and (or) brachiopod data for both the Kayak Shale and overlying Rough Mountain Creek unit are given in table 1, and the approximate locations of fossil collections are shown on figure 3B. Harris and Carter analyzed the conodonts and brachiopods, respectively. Additional biostratigraphic data for the limestone and shale member of the Kayak Shale and the Rough Mountain Creek unit are given by Dumoulin and Harris (this volume). The sandstone member of the Kayak contains rare, poorly preserved conodonts of probable Kinderhookian age. The succeeding shale member is also poorly productive of conodonts, but the presence of *Pseudopolygnathus marginatus* indicates a **Kinderhookian** age. Conodonts are locally abundant in the limestones of the overlying limestone and shale member of the Kayak. Double-row bispathodids dominate the collections and suggest a relatively shallow-water depositional environment (figs. 5C-G, K). *Hindeodus crassidentatus* in the limestone and shale member of the Kayak and a poorly preserved siphonodellid in the overlying Rough Mountain Creek unit of the Lisburne Group restrict this part of the sequence to the middle to late **Kinderhookian** (figs. 5A, I, J). A brachiopod collection (table 1, loc. 93JS02C) from the limestone and shale member, however, helps further limit its age. This collection includes *?Podtscheremia albertensis?*; **spiriferids** of this type have their lower limit in the upper Kinderhookian. The Kayak specimens of *?P. albertensis*, however, are too poorly preserved to permit a definitive taxonomic assignment. Consequently, the limestone and shale member of the Kayak and the overlying Rough Mountain Creek unit are questionably assigned to the late **Kinderhookian**.

The Kuna Formation overlies the Rough Mountain Creek unit; its type section is in the Key Creek sequence, at the headwaters of Safari Creek (fig. 3B). In this area, according to Dumoulin and others (1994), conodonts in the lower part of the Kuna are middle Osagean in age (Upper **typicus Subzone** and lower part of the succeeding *anchoralis-latus* Zone), and those from 6 m below the contact of the Kuna with the overlying Permian Siksikpuk Formation indicate a middle to late Osagean age. In the De Long Mountains, however, strata assigned to the uppermost part of the Kuna contain radiolarians of Late Mississippian to early Middle Pennsylvanian age (Dumoulin and others, 1993).

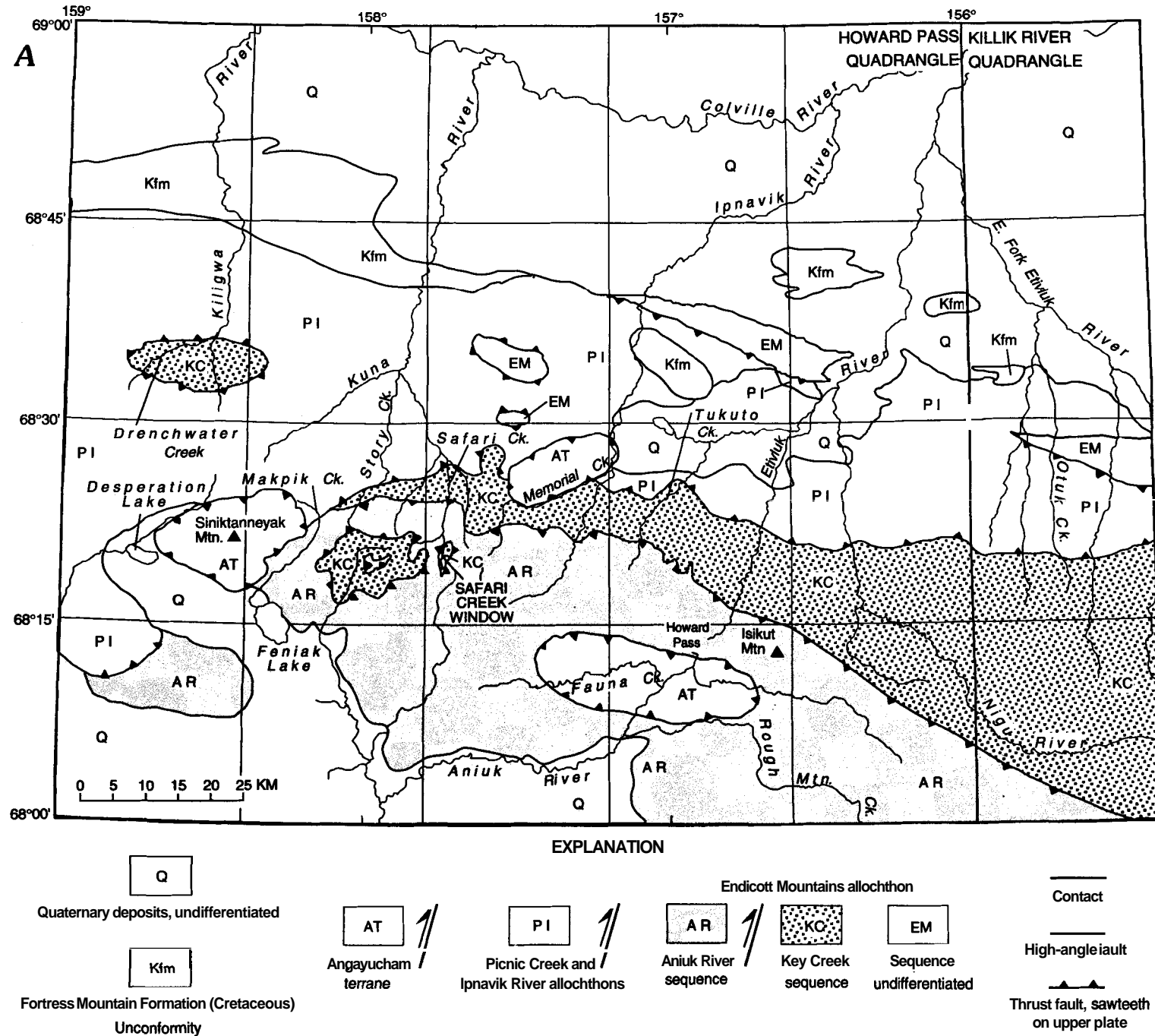


Figure 3. Maps of the western Endicott Mountains: **A**, Index map showing generalized distribution of allochthons and stratigraphic sequences in the Endicott Mountains allochthon. **B**, Location of conodont and brachiopod collections from Lower Mississippian rocks of the Aniuk River and Key Creek sequences of the Endicott Mountains allochthon. See table 1 for lithologic description, fauna, and age assignment.





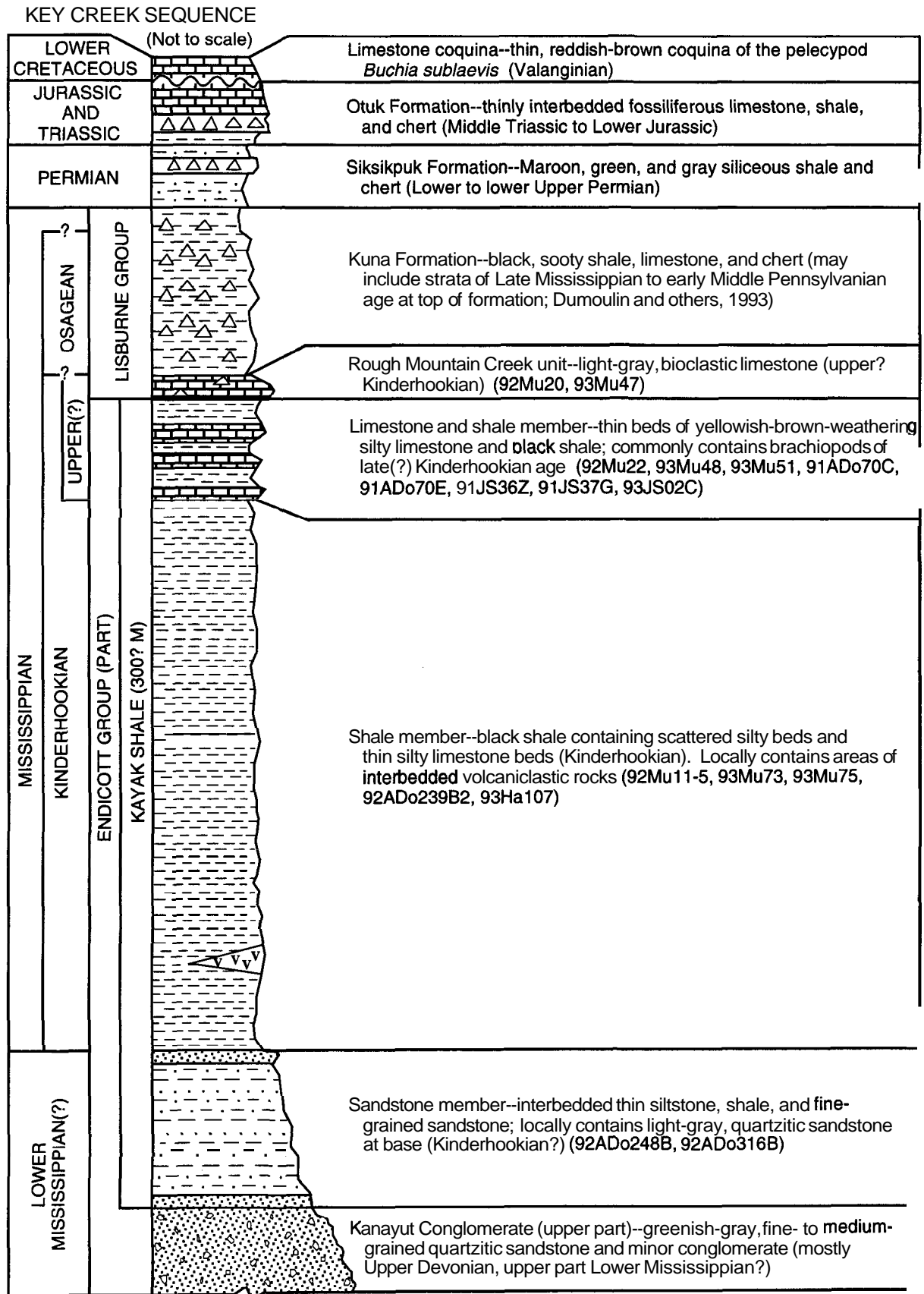


Figure 4. Stratigraphy of the upper part of the Key Creek sequence of the Endicott Mountains allochthon in the western Endicott Mountains, showing generalized lithologies and approximate locations of fossil collections from the Kayak Shale and Rough Mountain Creek unit of the Lisburne Group.

**Table 1. Paleontologic data for the Kayak Shale (Endicott Group) and overlying Rough Mountain Creek unit (Lisburne Group), western Endicott Mountains, Howard Pass quadrangle**

[Letters in locality number refer to collector: **ADo**, J.H. Dover; **Ha**, E. Harris; **JS**, J.M. Schmidt; **Mu**, C.G. Mull; and **TM**, T.E. Moore. Lithologies are field descriptions. Abbreviations for conodont genera: **B.**, *Bispathodus*; **H.**, *Hindeodus*; **Pat.**, *Patrognathus*; **Po.**, *Polygnathus*; **Ps.** *Pseudopolygnathus*; **S.**, *Siphonodella*. **R.**, rare (<5 specimens); **C.**, common (5-20 specimens); **A.**, abundant (21-100 specimens), **VA.**, very abundant (>100 specimens); **\***, biostratigraphically important **taxon**. CAI, color alteration index. Location of samples shown on fig. **3B**]

SEQUENCE AND STRATIGRAPHIC UNIT	LOC. NO. (USGS COLLN. NO.), QUAD., LAT. N./ LONG. W.	LITHOLOGY AND SAMPLE WEIGHT	CONODONTS AND (OR) BRACHIOPODS	CONODONT BIOFACIES	AGE AND CAI	REMARKS
KEY CREEK: Rough Mountain Creek unit of Lisburne Group	92Mu20 (32214-PC), B-2, 68°22'36"/ 157°08'39"	Light-gray crinoidal limestone interbedded with black chert and sooty shale. 6.2 kg	<b>Conodonts:</b> <i>B. aculeatus</i> (Branson and Mehl) (R) <i>Ps.</i> aff. <i>Ps. marginatus</i> (Branson and Mehl) (C) <i>Pseudopolygnathus</i> sp. indet. (R) <i>Siphonodella</i> sp. indet. of middle to late Kinderhookian morphotype (R)*	Indeterminate (too few conodonts); postmortem transport from or within relatively shallow to middle shelf, normal-marine depositional environment.	middle to late Kinderhookian 3-3.5	Upper Tukuto Creek, NE1/4 NW1/4 sec. 19, T. 12 S., R. 22 W. Appears to overlie a long, probably structurally complicated section of Kayak Shale which, in turn, overlies and is interbedded with volcanic rocks.
	93Mu47 (33319-PC), B-1, 68°18'53"/ 156°12'00"	Light-gray-weathering, black, partly sooty limestone. 5.8 kg	<b>Conodonts:</b> <i>B. aculeatus plumulus</i> (Rhodes, Austin, and Druce) (A) <i>B. ac. plumulus, nodosus</i> morphotype (R) <i>Ps.</i> sp. indet. (R)	Bispathodid biofacies; relatively shallow and moderately high energy normal-marine depositional environment.	Kinderhookian 3	Divide between Nigu and Etivluk Rivers; NE1/4 sec. 15, T. 34 N., R. 10 E. Relatively thin limestone interval overlies long section of red-brown-weathering silty shale that appears transitional between Isikut Member of Kayak Shale and typical Kayak.
KEY CREEK: Kayak Shale-- limestone and shale member	91JS36Z (31754-PC), B-4, 68°19'/ 158°04 5'	Tan-weathering, dark-gray, fine-grained sandy limestone containing skeletal debris. 7.6 kg	<b>Conodonts:</b> <i>B. aculeatus plumulus</i> (R) <i>Po. inornatus</i> E.R. Branson (R)	Indeterminate (too few conodonts); postmortem transport from normal-marine environment.	Kinderhookian 3-3.5	Upper Aniuk River area; NE1/4 sec. 25, T. 34 N., R. 3 E. Limestone overlies(?) about 10 m of volcanoclastic rocks and underlies spiculitic chert interpreted as Kuna Formation.
	91JS37G (31755-PC), B-4, 68°17.7'/ 157°58 5'	Tan-weathering, medium-gray, crinoidal packstone-wackestone. 6.6 kg	<b>Conodonts:</b> <i>B. aculeatus plumulus</i> (C) <i>H. aff. H. crassidentatus</i> (Branson and Mehl) (R)*	Indeterminate (too few conodonts); postmortem transport from bispathodid biofacies, from a relatively shallow water normal-marine environment.	middle to late Kinderhookian 3.5-4	Upper Aniuk River area. Limestone overlies black silty argillite containing 50% silt/sand flasers and laminae and some climbing ripples.
	92Mu22 (32210-PC), B-3, 68°21'46"/ 157°37'11"	Yellowish-brown-weathering, silty limestone. 5.3 kg	<b>Conodonts:</b> <i>B. aculeatus plumulus</i> (A) <i>B. ac. plumulus, nodosus</i> morphotype (R) <i>B. aculeatus</i> (C) <i>B. aff. B. stabilis</i> (Branson and Mehl) (R) <i>Po. communis communis</i> Branson and Mehl (R)	Postmortem winnow within bispathodid biofacies; relatively shallow water, normal-marine depositional environment.	Kinderhookian 3.5	Upper Memorial Creek; SW1/4 NW1/4 sec. 30, T. 12 S., R. 24 W. Grades into underlying shale member of Kayak Shale; very near contact of Kayak Shale with Rough Mountain Creek unit.
	93Mu48 (32211-PC), B-2, 68°20'25"/ 156°39'14"	Yellow-brown-weathering, silty limestone. 3.9 kg	<b>Conodonts:</b> 7 indet. bar, blade, and platform fragments	Indeterminate.	Post-Ordovician Paleozoic 3.5	East side of Etivluk River; SW1/4 sec. 7, T. 34 N., R. 10 E.

Table 1. Continued.

KEY CREEK: Kayak Shale-- limestone and shale member	93Mu51 (32212-PC), B-2, 68°23'34"/ 156°54'27"	Yellow-brown- weathering limestone interbedded with sooty black shale. 5.4 kg	Conodonts: <i>B. aculeatus plumulus</i> (C) <i>B. ac. plumulus, nodosus</i> morphotype (R) <i>B. aculeatus</i> (Branson and Mehl) (C) <i>H. crassidentatus</i> (R)* <i>Ps. marginatus</i> (R)	Bispathodid biofacies; relatively shallow water, normal-marine depositional environment.	middle to late Kinderhookian 3.5	East of Tukuto Creek; N1/2 sec. 18, T. 11 S., R. 21 W.
	91ADo70C (31748-PC), B-3 68°23.0'/ 157°40.5'	Medium-dark-gray, slightly <b>orangish-gray</b> - weathering, skeletal packstone--containing crinoids, solitary corals, brachiopods, and gastropods in bed 1 m thick. 4.7 kg	Conodonts: <i>B. aculeatus plumulus</i> (VA) <i>B. stabilis</i> (C) <i>H. crassidentatus</i> (R)* <i>Po. inornatus</i> (R) <i>Po. longiposticus</i> Branson and Mehl (R)	Bispathodid: normal-marine, relatively shallow water depositional environment. Conodonts are large, indicating a lag concentrate.	middle to late Kinderhookian -3	Headwaters of Safari Creek; sec. 26, T. 12 S., R. 25 W.
	91ADo70E (31747-PC), B-3, 68°23.0'/ 157°40.5'	Like 91ADo70C but in bed 2 m thick. 9.7 kg	Conodonts: <i>B. aculeatus plumulus</i> (VA) <i>B. ac. plumulus, nodosus</i> morphotype (R) <i>B. stabilis</i> (C) <i>H. crassidentatus</i> (C)*			Same locale as 91ADo70C but about 20 m stratigraphically or structurally higher.
	93JS02C (32218-PC), B-2, 68°22.25'/ 156°55.63'	Orange-weathering, gray, fossiliferous limestone 1 m thick containing crinoid <b>columnals</b> and other fossil debris; lies below 3 m of mixed black shale, <b>dark</b> - olive-gray calcareous shale, and nonspiculitic black mudstone. 5.5 kg	Conodonts: <i>B. aculeatus aculeatus</i> (R) <i>B. ac. plumulus</i> (R) <i>B. aculeatus</i> (R) <i>Po. longiposticus</i> (R) Brachiopods: <i>Eomartinopsis</i> sp.* <i>Punctospirifer</i> sp. <i>Actinoconchus</i> sp. <i>?Podtscheremia albertensis</i> (Warren)?* <i>Macropotamorhynchus</i> sp.	Indeterminate (too few conodonts); postmortem transport from or within bispathodid <b>biofacies</b> -- normal-marine, relatively shallow-water depositional environment.	Conodonts are Kinderhookian; brachiopods are late(?) Kinderhookian to possibly early Osagean 3 or 4	East of Tukuto Creek; sec. 25, T. 12 S., R. 22 W.
KEY CREEK: Kayak Shale-- shale member	92Mu11-5 (33253-PC), B-2, 68°18'53"/ 156°55'12"	Black shale containing limy beds. 6.1 kg	Conodonts: <i>B. stabilis</i> or <i>B. utahensis</i> (Sandberg and Gutschick) (R)	Indeterminate; too few conodonts.	<b>Kinderhookian</b> 2 or 3 (conodonts mostly covered by organic matter)	North of Howard Pass; W1/2 sec. 24, T. 34 N., R. 8 E.
	93Mu73 (32217-PC), B-4, 68°18.55'/ 158°05.68'	<b>Reddish-brown</b> - weathering, silty, thin- bedded limestone. 4.3 kg	Conodonts: <i>Polygnathus?</i> sp. indet. (R)	Indeterminate (too few conodonts).	Devonian to Early Mississippian; probably Kinderhookian 3 or 4	Headwaters of Aniak River; SW1/4 sec. 25, T. 34 N., R. 3 E.
	93Mu75, B-4, 68°19.22'/ 158°03.6'	Yellow-brown- weathering, silty, thin- bedded limestone. 4.6 kg	Conodonts: BARREN			Headwaters of Aniak River; NE1/4 sec. 30, T. 34 N., R. 4 E.
	92ADo239B2 (32209-PC), B-4, 68°18'16"/ 157°51'09"	1-1.5-foot-thick bed of orange-weathering, platy, fossiliferous (including crinoids, brachiopods, and gastropods) limy, sandstone. 6.8 kg	Conodonts: <i>B. aculeatus plumulus</i> (R) <i>B. aculeatus</i> (R) <i>B. aff. B. stabilis</i> (R) <i>Po. aff. Po. inornatus</i> (R) <i>Ps. marginatus</i> (R) <i>Ps. sp. indet.</i> (R)	Indeterminate (too few conodonts); normal-marine, shallow- to middle-shelf depositional environment.	Kinderhookian -3.5	Headwaters of Aniak River; SE1/4 NW1/4 sec. 25, T. 34 N., R. 4 W.
	93Ha107 B-2, 68°21'19"/ 156°54'34"	Greenish-black, <b>micaceous</b> siltstone containing flattened, indeterminate bivalved mollusks.			Indeterminate	East of Tukuto Creek.

Table 1. Continued.

SEQUENCE AND STRATIGRAPHIC UNIT	LOC. NO. (USGS COLLN. NO.), QUAD., LAT. N./LONG. W.	LITHOLOGY AND SAMPLE WEIGHT	CONODONTS AND (OR) BRACHIOPODS	CONODONT BIOFACIES	AGE AND CAI	REMARKS
KEY CREEK: Kayak Shale--sandstone member	92ADo248B (32207-PC), B-4, 68°20'21"/157°52'58"	Orange-weathering, sandy limestone containing brachiopods. 5.4 kg	<u>Conodonts</u> : <i>B. aff. B. aculeatus</i> (R)	Indeterminate (too few conodonts).	late Famennian to Kinderhookian, probably Kinderhookian 3 or 4	Headwaters of Aniuk River; NE1/4 sec. 23, T. 34 N., R. 4 W.
	92ADo316B (32208-PC), B-4, 68°20'13"/157°52'06"	2.5-ft bed of orange-weathering, fossiliferous (chiefly crinoidal) limy sandstone. 9.0 kg	<u>Conodonts</u> : <i>Pseudopolygnathus</i> sp. indet. (R)	Indeterminate (too few conodonts).	late Famennian to Kinderhookian, probably Kinderhookian 3 or 4	Same locale as 92ADo248B and probably stratigraphically lower.
ANIUK RIVER: Rough Mountain Creek unit of Lisburne Group	92Mu5-1 (31779-PC), A-2, 68°10'48"/156°39'54"	Gray, crinoidal limestone. 4.4 kg	<u>Conodonts</u> : <i>B. aculeatus plumulus</i> (R) <i>Po. communis communis</i> (R) <i>Po. inornatus</i> (R) <i>S.</i> sp. indet. of post- <i>S. sulcata</i> morphotype (R)*	Indeterminate (too few conodonts). Normal-marine, middle-shelf or deeper water depositional environment.	middle to late Kinderhookian 4	Isikut Mountain area; NW1/4NE1/4 sec. 7, T. 32 N., R. 10 E. Overtuned sequence of Rough Mountain Creek unit and Kuna Formation.
	92Mu5-2 (32204-PC), A-2, 68°10'31"/156°39'54"	Coarse-grained limestone. 6.7 kg	<u>Conodonts</u> : <i>B. aculeatus plumulus</i> (C) <i>B. aculeatus</i> (R) <i>B. stabilis</i> ? (R) <i>H. crassidentatus</i> (C)* <i>Po. communis communis</i> (R) <i>Ps.</i> sp. indet. (R)	Bispathoidid-hindeoidid; normal-marine, shallow- to middle-shelf depositional environment.	middle to late Kinderhookian 3.5	Isikut Mountain area. 92Mu5-2 is in thrust sheet that structurally overlies 92Mu5-1.
	92Mu10-2 (32205-PC), A-2, 68°06'59"/156°47'28"	Gray crinoidal limestone. 7.6 kg	<u>Conodonts</u> : <i>B. aculeatus plumulus</i> (R) <i>B. ac. plumulus, nodosus</i> morphotype (R) <i>B. aculeatus</i> (R) <i>B. stabilis</i> (R) <i>Po. communis communis</i> (A) <i>Ps. marginatus</i> (C) <i>Po.</i> sp. indet. and <i>Ps.</i> sp. indet. (A) <i>S. crenulata</i> (Cooper) (R)* <i>S.</i> sp. indet. (R)	Polygnathid-pseudopolygnathid biofacies: normal-marine, middle-shelf to slope depositional environment.	Lower <i>S. crenulata</i> Zone into Upper <i>S. crenulata</i> - <i>S. isosticha</i> Zone (=upper 113 of Kinderhookian but not very latest Kinderhookian) 3.5-4	Rough Mountain Creek; W1/2SW1/4 sec. 34, T. 32 N., R. 9 E.
	92Mu12-2 (32206-PC), A-2, 68°13'31"/157°01'58"	Light-gray, crinoidal limestone. 9.1 kg	<u>Conodonts</u> : <i>B. aculeatus plumulus</i> (R) <i>B. aculeatus</i> (C) <i>B. aff. B. stabilis</i> (R) <i>Ps. marginatus</i> (R)	Indeterminate (too few conodonts); normal-marine, shallow- to middle-shelf depositional environment.	Kinderhookian 3.5	Howard Pass area; SE1/4 SW1/4 sec. 21, T. 33 N., R. 8 E.
	93Mu63-1 (32202-PC), B-3, 68°15'43"/157°20'11"	Light-gray, crinoidal, cherty limestone in 3-m-thick interval with two thin chert beds. 6.1 kg	<u>Conodonts</u> : <i>B. aculeatus plumulus</i> (A) <i>B. ac. plumulus, nodosus</i> morphotype (R) <i>Ps.</i> sp. indet. (R)	Bispathoidid biofacies; normal-marine, relatively high-energy depositional environment.	Kinderhookian 3.5	Northern tributary of Fauna Creek; center sec. 18, T. 33 N., R. 7 E.

Table 1. Continued.

ANIUK RIVER: Rough Mountain Creek unit of Lisburne Group	93Mu65-1 (32203-PC), A-3, 68°11'53"/157°40'09"	Light-gray, light-gray- to yellowish-brown-weathering, partly cherty, crinoidal limestone. 5.8 kg	<b>Conodonts:</b> <i>B. aculeatus plumulus</i> (R) <i>B. ac. plumulus, nodosus</i> morphotype (R) <i>B. aculeatus</i> (A) <i>Po. communis</i> (A) <i>Po. sp. indet.</i> (R) <b>Brachiopods:</b> <i>Unispirifer</i> sp.	Postmortem transport within or from the bispathodid-polygnathid biofacies; shallow- to at least middle-shelf depositional environment.	Conodonts indicate Kinderhookian; brachiopods indicate Early Carboniferous 3.5-4	Aniuk River measured section, about 300 m above base; SW1/4 sec. 35, T. 33 N., R. 5 E. Gradationally overlies Isikut Member of Kayak Shale (93Mu65).
ANIUK RIVER: Kayak Shale-- limestone and shale member	92Mu10-1 (32199-PC), A-2, 68°07'14"/156°47'13"	Fine-grained silty limestone. 4.5 kg	<b>Conodonts:</b> <i>B. aculeatus plumulus</i> (R) <i>H. crassidentatus</i> (R)* <i>Po. aff. Po. inornatus</i> (R) <i>Po. sp. indet.</i> (R) <i>Ps. sp. indet.</i> (R)	Indeterminate (too few conodonts); normal-marine, probably middle-shelf depositional environment, near relatively high energy regime.	middle to late Kinderhookian 3	Rough Mountain Creek. Thrust fault repeat of 91Mu10-3.
	92Mu10-3 (31780-PC), A-2, 68°06'53"/156°47'32"	Fine-grained silty limestone. 4.5 kg	<b>Conodonts:</b> <i>B. aculeatus plumulus</i> (C) <i>B. ac. plumulus, nodosus</i> morphotype (R) <i>H. crassidentatus</i> (A) <i>Po. inornatus</i> (A) <i>Po. longiposticus?</i> (R) <i>Ps. sp. indet.</i> (R)	Postmortem transport from or within the polygnathid-hindeodid biofacies; normal-marine, probably middle-shelf depositional environment, near relatively high energy regime.	middle to late Kinderhookian 4	Rough Mountain Creek. Same stratigraphic interval as 92Mu10-1.
	93Mu63 (32201-PC), B-3, 68°15'15"/157°19'52"	Thin-bedded (beds 10 cm thick), silty limestone containing crinoidal debris. 5.1 kg	<b>Conodonts:</b> <i>B. aculeatus plumulus</i> (C) <i>B. ac. plumulus, nodosus</i> morphotype (R) <i>B. aculeatus</i> (A) <i>B. stabilis</i> (R) <i>H. aff. H. crassidentatus</i> (R)* <i>Po. aff. Po. inornatus</i> (R) Brachiopods: <i>Ovatia prolata</i> Carter <i>Piloricilla desmetensis</i> Carter* <i>Pustula morrocreekensis</i> Carter* <i>Seminucella parva</i> Carter* <i>Spinocarinifera parviformis</i> (Girty)	Postmortem transport within or from the bispathodid biofacies--the collection is probably a winnow derived from a normal-marine shelf depositional environment.	Conodonts indicate middle to late Kinderhookian; brachiopods indicate late Kinderhookian ( <i>Calvustrigis rutherfordi</i> Zone) 3.5	North tributary of Fauna Creek; S1/2 sec. 18, T. 33 N., R. 7 E.
	93Mu63-2 (32200-PC), B-3, 68°15'35"/157°19'51"	Yellowish-brown-weathering, dark-gray, fine-grained crinoidal limestone. 6.3 kg	<b>Conodonts:</b> <i>B. aculeatus plumulus</i> (C) <i>B. stabilis</i> (R) <i>Po. communis communis</i> (R) <i>Po. aff. Po. inornatus</i> (R) <i>Po. sp.</i> (R) <i>Ps. aff. Ps. marginatus</i> (R)	Indeterminate (too few conodonts); normal-marine, shallow- to middle-shelf depositional environment.	Kinderhookian 3.5	North tributary of Fauna Creek; NE1/4 sec. 19, T. 33 N., R. 7 E. Several meters below 93Mu63-1.
	93Mu80 (32213-PC), B-4, 68°19'05"/158°15'45"	Thin beds of silty limestone and black shale. 7.2 kg	<b>Conodonts:</b> <i>B. aculeatus</i> (R)	Indeterminate (too few conodonts).	Kinderhookian 3 or 4	Makpik Creek; S1/2 sec. 19, T. 34 N., R. 3 E.
ANIUK RIVER: Kayak Shale-- shale member	93TM37K (32193-PC), A-3, 68°12'/157°41'35"	Algal limestone within reddish- or orangish-brown-weathering, thin-bedded siltstone and silty shale; -30-50 m above 93Mu65. 11.5 kg	<b>Conodonts:</b> double-rowed <i>B. sp. indet.</i> (R) <i>H. aff. H. crassidentatus</i> (A)* <i>Po. inornatus</i> (R) <i>Ps. marginatus</i> and <i>Ps. orthoconstrictus</i> (Thomas) (VA)	Pseudopolygnathid biofacies: above to slightly below wave base, normal-marine shelf depositional environment.	Kinderhookian, very probably middle to late Kinderhookian 3.5	Uppermost bed of Aniuk River reference section at 224 m. This bed is separated from overlying thrust fault by about 500 m of shale.

Table 1. Continued.

SEQUENCE AND STRATI-GRAPHIC UNIT	LOC. NO. (USGS COLLN. NO.), QUAD., LAT. N./ LONG. W.	LITHOLOGY AND SAMPLE WEIGHT	CONODONTS AND (OR) BRACHIOPODS	CONODONT BIOFACIES	AGE AND CAI	REMARKS
ANIUK RIVER: Kayak Shale--Isikut Member	84Sta04 (29639-PC), B-4, 68°23.0'/ 157°55.8'	Fine-grained sandstone to siltstone (>5 ft. thick) containing slightly calcareous and pyritic layers with crinoid columnals. 5 kg	<b>Conodonts:</b> <i>B. aculeatus aculeatus</i> (C) <i>B. ac. plumulus, nodosus</i> morphotype (R) <i>H.?</i> sp. indet. (R) <i>Po. communis</i> (A)	Postmortem transport within or from the polygnathid biofacies; normal-marine, shallow- to middle-shelf depositional environment.	middle to late Kinderhookian 3.5	Story Creek Zn-Pb prospect; sec. 23, T. 12 S., R. 26 W.
	92Mu26, B-4, 68°24.9'/ 157°51.3'	Reddish-brown-weathering, limy siltstone containing scattered small crinoid columnals. 6.0 kg	<b>Conodonts:</b> BARREN			From ridge crest -1 km east of west fork of Safari Creek; NW1/4 sec. 19, T. 12 S., R. 25 W.
	93Mu65 (32192-PC), A-3 68°12'06"/ 157°41'29"	Reddish-brown, very silty, thin-bedded limestone interbedded with siltstone; -50 m above contact with Kanayut Conglomerate. 6.5 kg	<b>Conodonts:</b> <i>Po. communis</i> (R) <b>Brachiopods</b> <i>Composita immatura</i> (Girty) <i>Ovatia</i> sp. <i>Punctospirifer</i> sp. <i>?Spinocarinfera</i> sp. <i>Syringothyris</i> sp. Indet. orthotetid	Indeterminate (too few conodonts).	Conodonts indicate Famennian through Kinderhookian; brachiopods indicate Early Carboniferous, probably Kinderhookian -3.5	Aniuk River reference section, about 157 m above base; SW1/4 sec. 34, T. 33 N., R. 3 E.
	93Mu78-1, B-4, 68°21'40"/ 158°04'48"	Red-brown-weathering, thin-bedded, partly crinoidal, silty limestone. 4.1 kg	<b>Conodonts:</b> BARREN <b>Brachiopods:</b> <i>Calvustrigis rutherfordi</i> (Warren)* <i>Coledium</i> sp. <i>Schellwienella</i> sp. <i>Trigonoglossa</i> sp. Indet. small chonetid		late Kinderhookian ( <i>Calvustrigis rutherfordi</i> Zone)	Story Creek area; S1/2 sec. 30, T. 12 S., R. 26 W.
	93Ha109, B-3, 68°19'30"/ 157°13' 11"	Reddish-brown-weathering limestone containing crinoids and brachiopods.	<b>Brachiopods:</b> <i>Calvustrigis rutherfordi</i> (Warren)*		late Kinderhookian ( <i>Calvustrigis rutherfordi</i> Zone)	Upper Tukuto Creek area.
	93Ha110, B-3, 68°20'39"/ 157°11'09"	Fine-grained, micaceous sandstone and siltstone with thin limestone containing fossil hash.	<b>Brachiopods:</b> <i>Calvustrigis rutherfordi</i> (Warren)*			Indeterminate internal molds of snails and bivalves also noted.
	93Ha136 (32194-PC), B-3, 68°15'20"/ 157°20'00"	Orange-weathering, silty limestone within siltstone. 4.3 kg	<b>Conodonts:</b> <i>Ps. aff. Ps. nodomarginatus</i> (R) <i>B. ac. plumulus, nodosus</i> morphotype (R) <i>B. aff. B. ac. plumulus</i> (R) <i>H. crassidentatus</i> (R)* <i>Po. communis</i> (R) <b>Brachiopods</b> <i>Punctospirifer</i> sp. Indet. rhynchonellid Indet. terebratulid	Indeterminate (too few conodonts); probably shallow- to middle-shelf, normal-marine depositional environment.	Conodonts indicate middle to late Kinderhookian; brachiopods indicate Carboniferous 3.5-4	North tributary of Fauna Creek; center sec. 18, T. 33 N., R. 7 E.

Table 1. Continued.

ANIUK RIVER: Kayak Shale--Isikut Member	93Ha143, A-3, 68°13'23"/157°20'23"	Orange-weathering, fossiliferous, silty limestone bed containing brachiopods.	<b>Brachiopods</b> Indet. rhynchonellid Indet. productid		post-Silurian Paleozoic	North tributary of Fauna Creek.
	92TM17A (32195-PC), A-2, 68°11'21"/156°33'08"	Red-brown-weathering, sandy limestone containing abundant macrofossils interbedded with thin-bedded, micaceous, fine- and very fine grained sandstone. 5.9 kg	<b>Conodonts:</b> <i>B. aculeatus anteposicornis</i> (Scott) (R) <i>B. ac. aculeatus</i> (C) <i>B. ac. plumulus</i> (R) <i>B. ac. plumulus, nodosus</i> morphotype (R) <i>B. ac.</i> subsp. indet. (C) <i>B.</i> aff. <i>B. stabilis</i> (C) <i>Pat. variabilis</i> Rhodes, Austin, and Druce (C) <i>Po. communis communis</i> (A) <i>Ps. marginatus</i> (R) <i>Ps.</i> cf. <i>Ps. multistriatus</i> Mehl and Thomas (R)	Bispathodid biofacies; relatively high-energy, shallow-water normal-marine depositional environment.	Kinderhookian 3.5-4	Isikut Mountain; sec. 5, T. 32 N., R. 10 E. Unit depositionally overlies Kanayut Conglomerate. A conodont-rich sample.
	92TM29A (32196-PC), A-2, 68°14'/157°00'42"	Red-brown-weathering, argillaceous limestone in thin-bedded siltstone and very fine grained sandstone containing fossils and shallow-water sedimentary features. 12.0 kg	<b>Conodonts:</b> <i>B. aculeatus plumulus</i> (R) <i>B. aculeatus</i> (C) <i>Par. variabilis</i> (R)	Indeterminate (too few conodonts); all conodonts are fragments, indicating derivation from or deposition within a high-energy regime, probably in shallow-water.	Kinderhookian 4	Unit depositionally overlies Kanayut Conglomerate; sec. 21, T. 33 N., R. 8 E.
	93TM35L (32198-PC), A-2, 68°10'55'/156°38'05"	Reddish-brown-weathering, bioclastic limestone. 7.9 kg	<b>Conodonts:</b> <i>B. aculeatus aculeatus</i> (R) <i>Pat. variabilis</i> (VA) <i>Po. communis communis</i> , chiefly fragments (C) <i>Ps. orthoconstrictus</i> (C) <i>Ps.</i> sp. indet. (A) <b>Brachiopods:</b> Indet. orthotetid	<b>Postmortem</b> transport from or within the patrognathid biofacies. Within or adjacent to a high-energy, shoal-water depositional environment.	Kinderhookian 4	Isikut Mountain type section, 81.5 m above base; center of boundary between secs. 5 and 8, T. 32 N., R. 10 E.
	93TM35I, A-2, 68°10'55'/156°38'05"	Reddish-brown, silty limestone.	<b>Brachiopods:</b> Indet. orthotetid		Paleozoic	Isikut Mountain type section; float from 50 m above base of section.
	93TM35F, A-2, 68°10'55'/156°38'05"	Reddish-brown, silty limestone.	<b>Brachiopods:</b> Indet. chonetid Indet. productid		post-Silurian Paleozoic	Isikut Mountain type section; float from 45 m above base of section.

Table 1. Continued.

SEQUENCE AND STRATI-GRAPHIC UNIT	LOC. NO. (USGS COLLN. NO.), QUAD., LAT. N./ LONG. W.	LITHOLOGY AND SAMPLE WEIGHT	CONODONTS AND (OR) BRACHIOPODS	CONODONT BIOFACIES	AGE AND CAI	REMARKS
ANIUK RIVER: Kayak Shale--Isikut Member	93TM35C (32197-PC), A-2, 68°10'55"/ 156°38'05"	Reddish-brown-weathering, silty limestone. 5.5 kg	Conodonts: <i>B. aculeatus aculeatus</i> (A) <i>B. ac. plumulus</i> (R) <i>B. ac. aculeatus, nodosus</i> morphotype (R) <i>B. ac.</i> subsp. indet. (C) <i>Par. variabilis</i> (R) <i>Po. communis communis</i> (A) <i>Ps. cf. Ps. multistriatus</i> (R) Brachiopods: Indet. orthotetid	Postmortem transport from or within the bispathodid biofacies. Shallow-water, normal-marine, relatively high energy depositional environment. All conodonts are incomplete.	Conodonts indicate Kinderhookian 4	Isikut Mountain type section, 21 m above base. Sample represents tempestitelike deposits; center boundary between secs. 5 and 8, T. 32 N., R. 10 E.
	93TM37E, A-3, 68°12'06"/ 157°41'29"	Reddish-brown-weathering, silty limestone.	Brachiopods: <i>Actinoconchus</i> n. sp. <i>Macropotamorhynchus</i> sp. <i>Punctospirifer</i> sp. <i>?Spinocarinifera</i> sp. Indet. spiriferid		Kinderhookian to Osagean	Aniuk River reference section; float about 125 m above base of section.
	93JS03B, B-3, 68°20.33'/ 157°13.5'	Orange- to red-brown-weathering, sideritic, fossiliferous limestone containing bryozoans, brachiopods, and crinoid ossicles. 4.2 kg	Conodonts: BARREN			Upper Tukuto Creek area; sec. 15, T. 34 N., R. 7 E.
	93JS03E, B-3, 68°20.5'/ 157°13'	Red-weathering, sideritic limestone containing fossil hash of crinoid ossicles and brachiopods that forms layers 5-50 mm thick within siltstone. 4.5 kg	Conodonts: 1 M element of Late Devonian-Mississippian morphotype	Indeterminate: all other conodonts from this sample are indeterminate, nonabraded, fractured fragments that suggest a high-energy depositional environment and rather rapid burial.	Late Devonian-Mississippian 4	



## KINDERHOOKIAN STRATA OF THE ANIUK RIVER SEQUENCE

The base of the Kayak Shale in the Aniak River sequence is a reddish-brown-weathering siltstone and fine-grained sandstone unit that contains scattered thin, silty, fossiliferous limestone beds and occupies the stratigraphic position of part of the Kayak Shale. These strata contain sedimentary features that are characteristic of shallow-water depositional environments (including ripple marks and small-scale cross-laminations) and form a distinctive mappable unit in the western end of the Endicott Mountains that contrasts markedly with the characteristic Kayak Shale in the Key Creek sequence of the Endicott Mountains allochthon (compare figs. 4 and 6). This unit is here named the Isikut Member of the Kayak Shale. Relatively continuous sections of the Isikut were measured by T.E. Moore, K.E. Adams, and R.K. Crowder on the south side of Isikut Mountain (field nos. in the series 93TM35, lat 68°10' 55" N., long 156°38' 05" W.), which we define as the type locality of the Isikut, and on the east side of the upper Aniak River (field nos. in the series 93TM37, lat 68°12' 06" N., long 157°41' 29" W.), which we define as a reference section (fig. 2). The Isikut Member grades upward into black shale, typical of the Kayak, which contains a few bioclastic limestone beds at the top. The Kayak is overlain by the Rough Mountain Creek unit of the Lisburne Group followed by the Kuna Formation, as in the Key Creek sequence. This succession is capped by greenish-gray, siliceous shale and chert of the Permian Siksikpuk Formation (fig. 6).

Conodonts from many localities in the Isikut Member of the Kayak Shale through the Rough Mountain Creek unit of the Lisburne Group are chiefly middle to late **Kinderhookian** in age (table 1). One collection from the Rough Mountain Creek unit (table 1, loc. 92Mu10-2) contains *Siphonodella crenulata* (Cooper) (fig. 5L). This species indicates a late but not latest **Kinderhookian** age and demonstrates that the Kayak and at least part of the Rough Mountain Creek do not extend to the top of the isosticha-Upper crenulata Zone (the highest **Kinderhookian** conodont zone). Brachiopods from the Isikut and higher parts of the Kayak, however, restrict the age of at least the upper part of the Isikut Member, and all units in the sequence below the Kuna Formation, to the late **Kinderhookian**. Three brachiopod collections from the Isikut, none from measured sections, indicate the *Calvustrigis rutherfordi* Zone and include the zonal name bearer (table 1, locs. 93Mu78-1, 93Ha109, and 93Ha110; figs. 7s-v). Until now, *C. rutherfordi* (Warren) has only been reported from the "middle" member of the Banff Formation and its equivalents in westernmost Alberta, Canada (Carter, 1987), where the interval of the *C. rutherfordi* Zone yields conodonts of the late **Kinderhookian** isosticha-Upper crenulata Zone (Savoy and Harris, 1993; L.E. Savoy and A.G. Harris, unpub.

USGS conodont collections). Another brachiopod assemblage from the overlying limestone and shale member of the Kayak also indicates the *C. rutherfordi* Zone (table 1, loc. 93Mu63). Although *C. rutherfordi* is not present in this collection, other species restricted to the zone do occur, including *Piloricilla desmetensis* Carter, *Pustula morrocreekensis* Carter, and *Seminucella parva* Carter (figs. 7c-h, m-r).

The Isikut Member contains many of the same conodonts that occur in other parts of the Kayak, with some exceptions. *Patrognathus variabilis*, a species characteristic of very shallow water, generally high energy environments such as oolite shoals (Austin, 1976), is rare to very abundant in four collections from the Isikut, two from its type area (figs. 5Y-AA).

Conodont and brachiopod faunas from the Isikut Member of the Kayak Shale and overlying **Kinderhookian** units in the Aniak River sequence are similar to but more biostratigraphically diagnostic than faunas from **Kinderhookian** units in the Key Creek sequence. The Isikut faunas indicate that the member is at least partly coeval with the Kayak Shale elsewhere in the western Endicott Mountains.

Conodonts are more abundant and assemblages are considerably more diverse in the Isikut Member of the Kayak Shale than in the correlative sandstone and succeeding shale members of the Kayak in the Key Creek sequence. This observation suggests that a wider range of favorable environments were present during the **Kinderhookian** in the depositional area of the Isikut. The Isikut probably formed chiefly in shallow-water environments that were less muddy than correlative Kayak depositional sites in the Key Creek sequence. Although biostratigraphically diagnostic brachiopods are present in the Isikut in the Aniak sequence, none were identified in fossil collections from the lower part of the Kayak in the Key Creek sequence.

The limestone and shale member of the Kayak yields the same conodont species assemblage in both the Key Creek and Aniak River sequences, although conodonts are more abundant in the Aniak River sequence. Brachiopod collections indicate a late **Kinderhookian** age for the member in both sequences (table 1, samples 93JS02C and 93Mu63). Brachiopods were not collected from the overlying Rough Mountain Creek unit in either sequence, but conodonts are more abundant and diverse in the Aniak River sequence than in the Key Creek sequence, suggesting that the unit formed in a more hospitable, possibly slightly deeper shelf setting in the Aniak River sequence.

## DISCUSSION

Two contrasting stratigraphic sequences, the Key Creek and Aniak River sequences, are structurally juxtaposed in the western Endicott Mountains. The Aniak River sequence is characterized by the **Kinderhookian** Isikut Member of

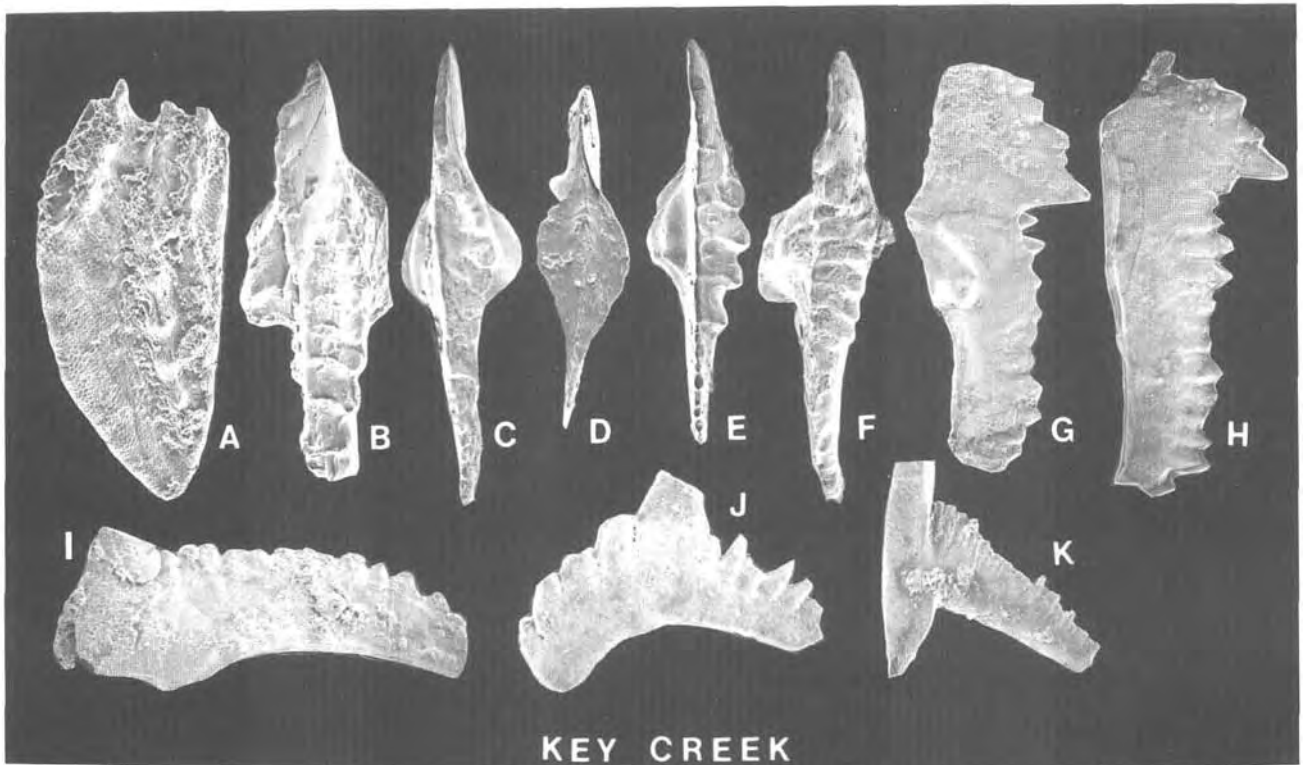
the Kayak Shale, which consists of distinctive reddish-brown-weathering siltstone that contrasts markedly with the characteristic black shale of the Kayak in the Key Creek sequence. Conodont faunas from both the Kayak Shale of the Key Creek sequence and the Isikut Member of the Kayak Shale of the Aniuk River sequence are middle to late **Kinderhookian** in age. Three brachiopod collections from the Isikut, however, indicate that at least part of the Isikut Member is late Kinderhookian in age. These data suggest that the Isikut may be coeval with much of the Kayak in the Key Creek sequence. In addition, the Isikut is **lithologically** similar to and at least partly coeval with the lower part of the Utukok Formation of the Lisburne Group in other sequences and allochthons in the De Long Mountains and Maiyumerak Mountains (for example, Sable and Dutro, 1961; Dutro, 1987; Dumoulin and Harris, 1992 and this volume). Poorly exposed rocks similar to the Isikut are also reported in the Endicott Mountains allochthon in the western Brooks Range south of Red Dog mine (Inyo Ellersieck, oral commun., 1996).

Numerous small zinc-lead mineral occurrences in the Endicott Group are present in both the upper part of the Kanayut Conglomerate and in the overlying Kayak Shale in the western Endicott Mountains. The most significant mineral occurrence in the Endicott Group consists of sphalerite and galena in vein breccias in the Isikut Member of the Kayak near Story Creek, where the Isikut is late **Kinderhookian** in age (table 1, loc. 93Mu78-1).

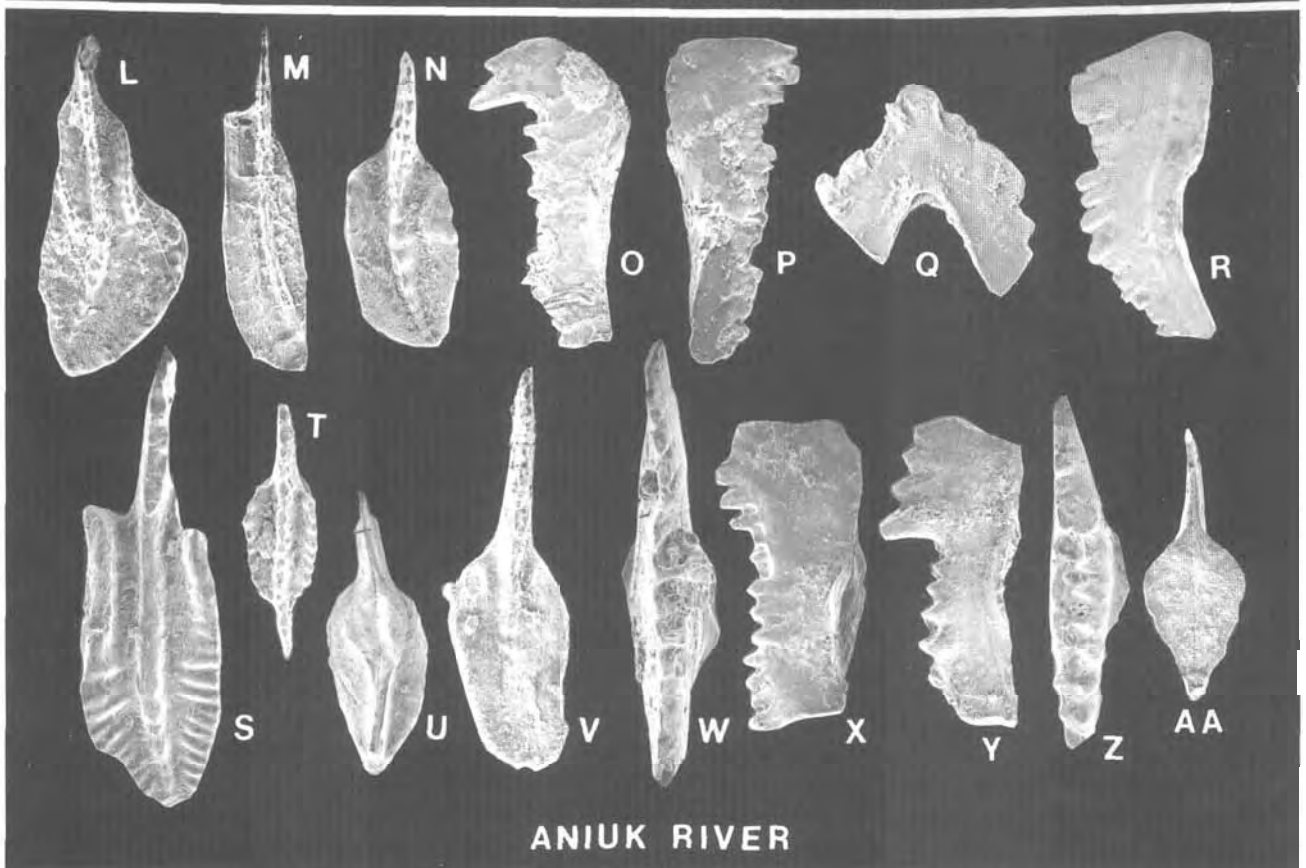
In addition to the occurrence of the Isikut Member of the Kayak Shale, the Aniuk River sequence is also characterized by a relatively thin section (<400 m) of the Kanayut Conglomerate and Noatak Sandstone of the Endicott Group. This thin section of Endicott Group **clastic** rocks contrasts markedly with the much thicker and coarser grained sections of Kanayut and Noatak in the Killik River sequence of the Endicott Mountains allochthon in the eastern Endicott Mountains, which are more than 3,000 m thick (Nilsen and Moore, 1984). The thrust juxtaposition of these contrasting facies is indicative of significant shortening within the Endicott Mountains allochthon.

Although no complete sections of the Kanayut Conglomerate and Noatak Sandstone in the Key Creek sequence of the Endicott Mountains allochthon have been measured, reconnaissance mapping and scattered stratigraphic studies suggest that the Endicott Group in the Key Creek sequence in the western Endicott Mountains is thicker than in the Aniuk River sequence but significantly thinner than in the Killik River sequence to the east. The comparatively thin Kanayut and Noatak section in the Aniuk River sequence suggests that it was deposited in a relatively distal part of the Endicott Group deltaic wedge, in contrast to the more proximal setting characteristic of the Kanayut in its type area to the east. The prominent siltstone and sandstone facies of the overlying Isikut Member of the Kayak Shale in the Aniuk River sequence, however, is anomalous in this scenario because it contrasts with the dominantly shalier facies of the Kayak to the east and appears to have been deposited in a relatively proximal setting. The implications of the Isikut Member for modeling Late Devonian and Early Mississippian deposition and tectonics in the western Endicott Mountains have yet to be assessed.

**Acknowledgments.**—Several geologists from both the U.S. Geological Survey and the Alaska Division of Geological and Geophysical Surveys made significant contributions to this study. R.R. Reifensstuhl, E.E. Harris, T.E. Moore, J.H. Dover, and J.M. Schmidt participated in the 1:63,360-scale mapping that delineated the distribution of the Isikut Member of the Kayak Shale and collected macrofossil and (or) conodont samples; Moore, K.E. Adams, and R.K. Crowder measured and described sections of the Isikut and underlying Kanayut Conglomerate and Noatak Sandstone; J.A. Dumoulin provided stratigraphic data for the limestone and shale member of the Kayak and the overlying Rough Mountain Creek unit. Some of the mapping would not have been completed without the contribution of Ken Butters of **TransAlaska Helicopters**, who was invariably a congenial and helpful field chauffeur in spite of sometimes difficult weather.



KEY CREEK



ANIUK RIVER

Figure 5. Kinderhookian conodonts from the Key Creek and Aniuk River sequences of the Endicott Mountains allochthon, western Endicott Mountains (scanning electron micrographs; all specimens Pa elements except as noted; illustrated specimens are repositied in the U.S. National Museum (USNM), Washington, D.C.). See figure 3B for location of collection and table 1 for faunal assemblage, biofacies, and lithostratigraphic data and USGS collection numbers.

A-K, Key Creek sequence.

A, B, Upper views, Rough Mountain Creek unit of Lisburne Group.

A, *Siphonodella* sp. indet. of middle to late Kinderhookian morphotype,  $\times 100$ , USNM 489646, loc. 92Mu20.

B, *Bispathodus aculeatus plumulus* (Rhodes, Austin, and Druce), *nodosus* morphotype,  $\times 50$ , USNM 489647, loc. 93Mu47.

C-K, Limestone and shale member of Kayak Shale.

C, D, K, *Bispathodus aculeatus plumulus* (Rhodes, Austin, and Dmce).

C, D, Upper and lower views,  $\times 40$  and  $\times 75$ , USNM 489648, 49, locs. 93Mu51 and 92Mu22.

K, M element, lateral view,  $\times 50$ , USNM 489656, same loc. as D.

E-G, *Bispathodus aculeatus plumulus* (Rhodes, Austin, and Druce), *nodosus* morphotype.

E, Upper view,  $\times 50$ , USNM 489650, same loc. as D.

F, Upper view,  $\times 30$ , USNM 489651, loc. 91ADo70E.

G, Inner lateral view,  $\times 40$ , USNM 489652, same loc. as C.

H, *Bispathodus stabilis* (Branson and Mehl), outer lateral view,  $\times 40$ , USNM 489653, loc. 91ADo70C.

I, J, *Hindeodus crassidentatus* (Branson and Mehl), Pa and Pb elements, lateral views,  $\times 40$ , USNM 489654, 55, same loc. as F.

L-AA, Aniuk River sequence.

L-Q, Rough Mountain Creek unit of Lisburne Group.

L, *Siphonodella crenulata* (Cooper), upper view,  $\times 50$ , USNM 489657, loc. 92Mu10-2.

M, *Siphonodella* sp. indet. of post-*S. sulcata* morphotype, juvenile element, upper view,  $\times 100$ , USNM 489658, loc. 92Mu5-1.

N, *Polygnathus communis* Branson and Mehl, Pa element, upper view,  $\times 50$ , USNM 489659, loc. 92Mu65-1.

O, *Bispathodus aculeatus plumulus* (Rhodes, Austin, and Dmce), outer lateral view,  $\times 50$ , USNM 489660, loc. 92Mu5-2.

P, *Bispathodus stabilis* (Branson and Mehl)?, inner lateral view,  $\times 75$ , USNM 489661, same loc. as O.

Q, *Hindeodus crassidentatus* (Branson and Mehl), Sa element, posterior view,  $\times 100$ , USNM 489662, same loc. as O.

R, S, Limestone and shale member of Kayak Shale, loc. 92Mu10-3.

R, *Hindeodus crassidentatus* (Branson and Mehl), outer lateral view,  $\times 50$ , USNM 489663.

S, *Polygnathus inornatus* E.R. Branson, upper view,  $\times 50$ , USNM 489664.

T, U, Shale member of Kayak Shale.

T, U, *Pseudopolygnathus orthoconstrictus* (Thomas), upper and lower views,  $\times 50$ , USNM 489665, 66, loc. 92TM37K.

V-AA, Isikut Member of Kayak Shale.

V, *Polygnathus communis* Branson and Mehl, upper view,  $\times 40$ , USNM 489667, loc. 84Sta04.

W-AA, loc. 92TM17A

*Bispathodus aculeatus anteposicornis* (Scott), upper view,  $\times 40$ , USNM 489668.

X, *Bispathodus aculeatus aculeatus* (Branson and Mehl), outer lateral view,  $\times 40$ , USNM 489669.

Y-AA, *Patrognathus variabilis* Rhodes, Austin, and Druce, lateral, upper, and lower views of three specimens,  $\times 50$ , USNM 48970-72.

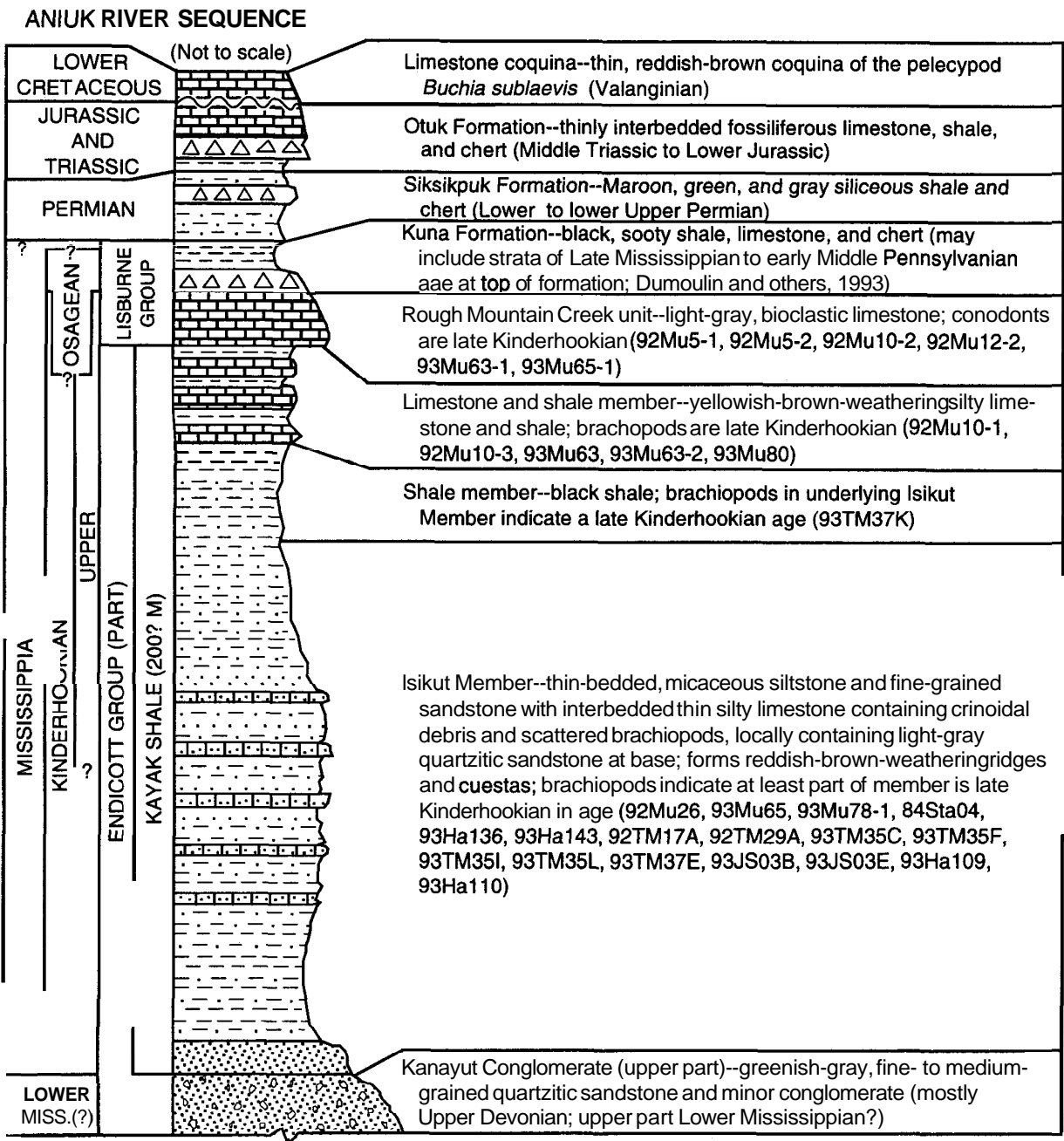
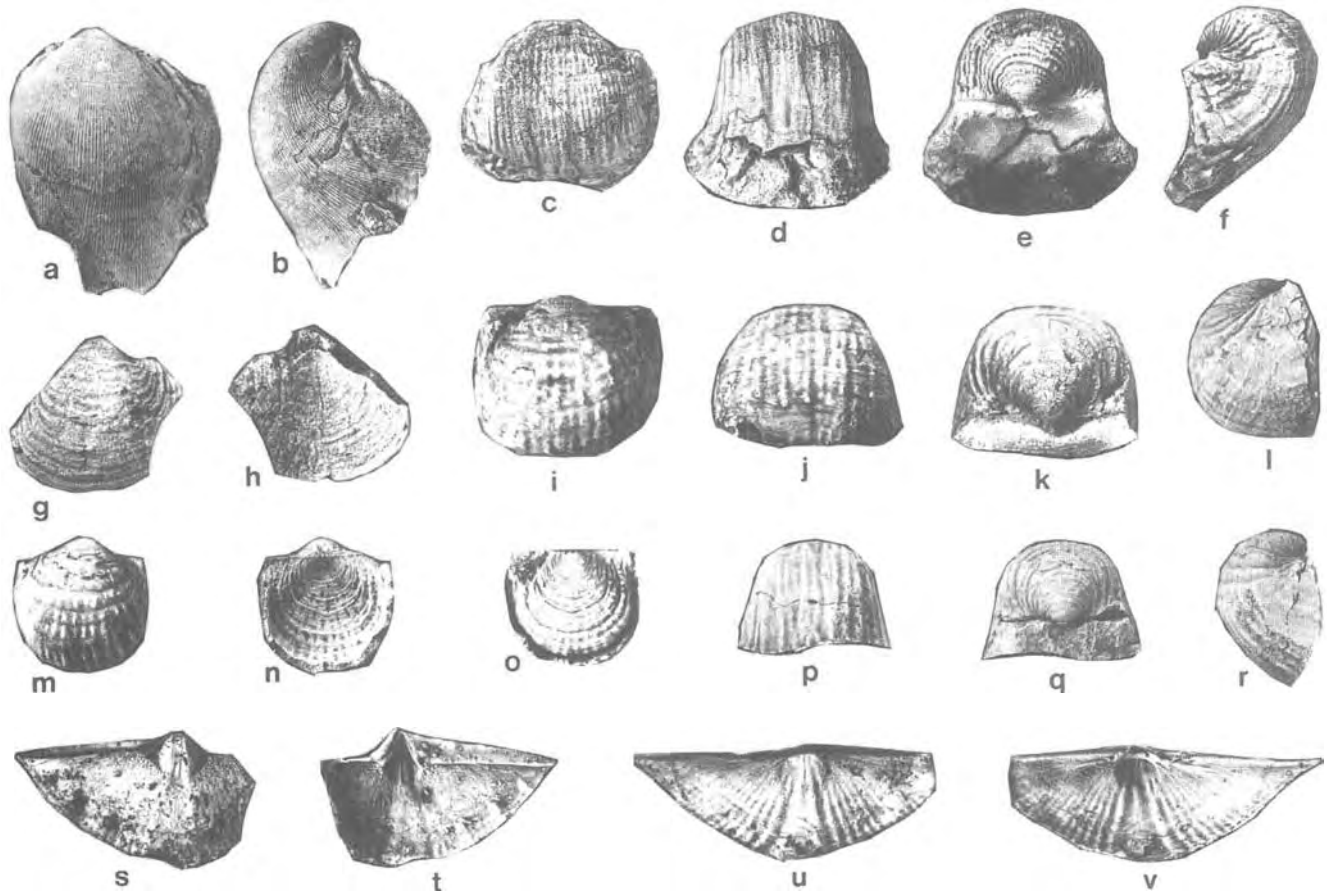


Figure 6. Stratigraphy of the upper part of the Aniuk River sequence of the Endicott Mountains allochthon in the western Endicott Mountains, showing generalized lithologies and approximate location of fossil collections from the Isikut Member of the Kayak Shale, and the Rough Mountain Creek unit of the Lisburne Group.



**Figure 7.** Brachiopods from the Kayak Shale, Aniak River sequence, Endicott Mountains allochthon, western Endicott Mountains. Illustrated specimens reposit in the Carnegie Museum of Natural History, Pittsburgh, Pa. (CM).

a-r, Limestone and shale member, loc. 93Mu63.

a, b, *Ovatia prolata* Carter, ventral and lateral views of natural mold of dorsal exterior, x1, CM 36054.

c-f, *Piloricilla desmetensis* Carter, ventral, anterior, posterior, and lateral views of ventral valve, x1, CM 36055.

g, h, *Pustula morroceekensis* Carter, ventral and dorsal views, x1, CM 36056.

i-l, *Spinocariniifera parviformis* (Girty), ventral, anterior, posterior, and lateral views of ventral valve, x2, CM 36057.

m-r, *Seminucella parva* Carter, ventral, dorsal, mold of dorsal exterior, anterior, posterior, and lateral views of complete specimen, x2, CM 36058.

s-v, Isikut Member, *Calvustrigis rutherfordi* (Warren), x1, loc. 93Mu78-1.

s, t, Natural mold and latex cast of ventral valve interior, CM 36059.

u, v, natural mold and latex cast of dorsal valve interior, CM 36060.

## REFERENCES CITED

- Armstrong, A.K., and Mamet, B.L., 1978, Microfacies of the Carboniferous Lisburne Group, Endicott Mountains, arctic Alaska. *in* Stelck, C.R., and Chatterton, B.D.E., eds., *Western and Arctic Canadian biostratigraphy*: Geological Association of Canada Special Paper 18, p. 333-394.
- Austin, R.L., 1976, Evidence from Great Britain and Ireland concerning West European Dinantian conodont paleoecology, *in* Barnes, C.R., ed., *Conodont paleoecology*: Geological Association of Canada Special Paper 15, p. 201-224.
- Bowsher, A.L., and Dutro, J.T., Jr., 1957, The Paleozoic section in the Shainin Lake area, central Brooks Range, Alaska: U.S. Geological Survey Professional Paper 303-A, 39 p.
- Chapman, R.M., Detterman, R.L., and Mangus, M.D., 1964, Geology of the Killik-Etivluk Rivers region, Alaska: U.S. Geological Survey Professional Paper 303-F, p. 325-407, 2 map sheets, scale 1:125,000.
- Carter, J.L., 1987, Lower Carboniferous brachiopods from the Banff Formation of western Alberta: Geological Survey of Canada Bulletin 378, 183 p.
- Dumoulin, J.A., and Harris, A.G., 1992, Devonian-Mississippian carbonate sequence in the Maiyumerak Mountains, western Brooks Range, Alaska: U.S. Geological Survey Open-File Report 92-3, 83 p.

- 1993, Lithofacies and conodonts of Carboniferous strata in the Ivotuk Hills, western Brooks Range, Alaska, in **Dusel-Bacon, Cynthia, and Till, A.B.**, eds., *Geologic studies in Alaska by the U.S. Geological Survey, 1992: U.S. Geological Survey Bulletin 2068*, p. 31-47.
- Dumoulin, J.A., Hams, A.G., and Schmidt, J.M., 1993, Deep-water lithofacies and conodont faunas of the Lisburne Group, west-central Brooks Range, Alaska, in **Dusel-Bacon, Cynthia, and Till, A.B.**, eds., *Geologic studies in Alaska by the U.S. Geological Survey, 1992: U.S. Geological Survey Bulletin 2068*, p. 12-30.
- 1994, Deep-water facies of the Lisburne Group, west-central Brooks Range, Alaska, in **Thurston, D.K., and Fujita, Kazuya**, eds., 1992 Proceedings of the International Conference on Arctic Margins: Anchorage, Alaska, U.S. Minerals Management Service Outer Continental Shelf Study MMS 94-0040, p. 77-82.
- Dutro, J.T., Jr., 1987, Revised megafossil biostratigraphic zonation for the Carboniferous of northern Alaska, in **Tailleur, I.L., and Weimer, Paul**, eds., *Alaskan North Slope geology: Bakersfield, Calif., Pacific Section, Society of Economic Paleontologists and Mineralogists, Book 50*, p. 359-364.
- Duttweiler, K.A., 1987, Use of factor analysis in locating base metal mineralization in the Killik River quadrangle, Alaska, in **Hamilton, T.D., and Galloway, J.P.**, eds., *Geologic studies in Alaska by the U.S. Geological Survey, 1986: U.S. Geological Survey Circular 998*, p. 27-30.
- Ellersieck, **Inyo**, Jansons, Uldis, Mayfield, C.F., and Tailleir, I.L., 1982, The Story Creek and Whoopee Creek lead-zinc-silver occurrences, western Brooks Range, Alaska, in **Coonrad, W.L.**, ed., *The United States Geological Survey in Alaska: Accomplishments during 1980: U.S. Geological Survey Circular 844*, p. 35-38.
- Jansons, Uldis, 1982, Zinc-lead occurrences in and near the National Petroleum Reserve in Alaska: U.S. Bureau of Mines Mineral Lands Assessment Report MLA 121-82, 55 p.
- Jansons, Uldis, and Baggs, D.W., 1980, Mineral investigations of the Misheguk Mountain and Howard Pass quadrangles, Alaska: U.S. Bureau of Mines Open-File Report 38-80, 76 p.
- Jansons, Uldis, and Parke, M.A., 1981, 1978 Mineral investigations in the Misheguk Mountain and Howard Pass quadrangles, Alaska: U.S. Bureau of Mines Open-File Report 26-81, 195 p.
- Kelley, K.D., Borden, J.C., Bailey, E.A., Fey, D.L., Motooka, J.M., and Roushey, B.H., 1992, Geochemically anomalous areas in the west-central part of the Howard Pass quadrangle, National Petroleum Reserve, Brooks Range, Alaska, in **Evans, D.C., and Dusel-Bacon, Cynthia**, eds., *Geologic studies in Alaska by the U.S. Geological Survey, 1991: U.S. Geological Survey Bulletin 2041*, p. 60-69.
- Kelley, K.D., and Mull, C.G., 1995, Maps showing areas of potential for mineral resources in the Killik River 1° × 3° quadrangle, Brooks Range, Alaska: U.S. Geological Survey Miscellaneous Field Studies Map MF-2225-A, scale 1:250,000.
- Martin, A.J., 1970, Structure and tectonic history of the western Brooks Range, De Long Mountains and Lisburne Hills, northern Alaska: *Geological Society of America Bulletin*, v. 81, no. 12, p. 3605-3621.
- Mayfield, C.F., Tailleir, I.L., and Ellersieck, **Inyo**, 1988, Stratigraphy, structure, and palinspastic synthesis of the western Brooks Range, northwestern Alaska, in **Gryc, George**, ed., *Geology and exploration of the National Petroleum Reserve in Alaska, 1974 to 1982: U.S. Geological Survey Professional Paper 1399*, p. 143-186.
- Meyer, M.P., and Kurtak, J.M., 1992, Results of the 1991 U.S. Bureau of Mines Colville mining district study: U.S. Bureau of Mines Open-File Report 75-92, 101 p.
- Moore, T.E., Wallace, W.K., Bird, K.J., Karl, S.M., Mull, C.G., and **Dillon, J.T.**, 1994, Geology of northern Alaska, in **Plafker, George, and Berg, H.C.**, eds., *The geology of Alaska: Boulder, Colo., Geological Society of America, The Geology of North America*, v. G-1, p. 49-140.
- Mull, C.G., Moore, T.E., Harris, E.E., and Tailleir, I.L., 1996, Geologic map of the Killik River quadrangle, central Brooks Range, Alaska: U.S. Geological Survey Open-File Map 94-679, 1 sheet, scale 1:125,000.
- Mull, C.G., Roeder, D.H., Tailleir, I.L., Pessel, G.H., Grantz, Arthur, and May, S.D., 1987, Geologic sections and maps across Brooks Range and Arctic Slope to **Beaufort Sea**, Alaska: *Geological Society of America Map and Chart Series MC 28S*, scale 1:500,000.
- Mull, C.G., Tailleir, I.L., Mayfield, C.F., Ellersieck, **Inyo**, and Curtis, S.M., 1982, New upper Paleozoic and lower Mesozoic stratigraphic units, central and western Brooks Range, Alaska: *American Association of Petroleum Geologists Bulletin*, v. 66, no. 3, p. 348-362.
- Mull, **C.G.**, and Weldon, M.B., 1994, Generalized geologic map of the western Endicott Mountains, central Brooks Range, Alaska: Alaska Division of Geological and Geophysical Surveys Public-Data File Map 94-55, 1 sheet, scale 1:250,000.
- Nilsen T.N.**, and Moore, T.E., 1984, Stratigraphic nomenclature for the Upper Devonian and Lower Mississippian(?) Kanayut Conglomerate, Brooks Range, Alaska: U.S. Geological Survey Bulletin 1529-A, 64 p.
- Sable, E.G., and Dutro, J.T., Jr., 1961, New Devonian and Mississippian formations in De Long Mountains, northern Alaska: *American Association of Petroleum Geologists Bulletin*, v. 45, p. 585-593.
- Savoy, **L.E.**, and Hams, A.G., 1993, Conodont biofacies and taphonomy along a carbonate ramp to black shale basin (latest Devonian and earliest Carboniferous), southernmost Canadian Cordillera and adjacent Montana: *Canadian Journal of Earth Sciences*, v. 30, p. 2404-2422.
- Tailleir, I.L., **Brosgé, W.P.**, and Reiser, H.N., 1967, Palinspastic analysis of Devonian rocks in northwestern Alaska, in **Oswald, D.H.**, ed., *International Symposium on the Devonian System, Calgary, Alberta, Canada, Alberta Society of Petroleum Geologists*, v. 2., p. 1345-1361.
- Tailleir, I.L., Kent, B.H., and Reiser, H.N., 1966, Outcrop geologic maps of the Nuka-Etivluk regions, northern Alaska: U.S. Geological Survey Open-File Report OF 66-128, scale 1:63,360, 7 sheets.
- Theobald, P.K., and Barton, H.N., 1978, Basic data for the geochemical evaluation of National Petroleum Reserve, Alaska: U.S. Geological Survey Open-File Report 78-70D, 15 p.

# Kinderhookian (Lower Mississippian) Calcareous Rocks of the Howard Pass Quadrangle, West-Central Brooks Range

By Julie A. Dumoulin and Anita G. Harris

## ABSTRACT

Calcareous rocks of **Kinderhookian** (early Early Mississippian) age are widely distributed across the Howard Pass quadrangle in the western Brooks Range. Most occur in the lower part of the Lisburne Group (herein called the Rough Mountain Creek unit) and the upper part of the Endicott Group (Kayak Shale) in two sequences (Key Creek and Aniak River) of the Endicott Mountains allochthon. **Kinderhookian** strata are also found in the Kelly River allochthon (Utukok Formation?) and in sections of uncertain stratigraphic affinity and structural level spatially associated with mafic volcanic rocks.

Predominant **Kinderhookian** lithologies in the Lisburne Group are skeletal supportstone (rich in pelmatozoans, bryozoans, and brachiopods) and lesser spiculite; skeletal supportstone and calcarenite are the chief calcareous rock types in the Kayak Shale. Conodont and brachiopod faunas indicate that all of the Rough Mountain Creek unit and much of the Kayak Shale in the study area are of late **Kinderhookian** age. Lithologic and paleontologic data suggest that **Kinderhookian** strata in the Howard Pass quadrangle were deposited largely in inner- and middle-shelf settings with normal marine salinity and locally high energy. Overall, calcareous beds in the Rough Mountain Creek unit accumulated in a wider range of environments, less subject to siliciclastic input, than did calcareous beds in the Kayak, and **Kinderhookian** beds of both units in the Key Creek sequence formed in less diverse, somewhat shallower environments than correlative rocks in the Aniak River sequence. Lithofacies patterns and contact relations imply that decreased siliciclastic influx, perhaps accompanied by relative sea-level rise, initiated deposition of the Rough Mountain Creek unit; relative sea-level rise and concurrent circulatory restriction most likely ended its deposition.

**Kinderhookian** calcareous rocks in the Howard Pass quadrangle have several implications for middle Paleozoic paleogeography of the western Brooks Range. First, sequences of the Endicott Mountains allochthon that contain the Rough Mountain Creek unit contrast sharply with other

sequences included in this allochthon that contain thicker and younger Carboniferous platform carbonate successions. These differences in stratigraphic succession suggest significant shortening within the Endicott Mountains allochthon. Second, **Kinderhookian** calcareous rocks in the Howard Pass quadrangle may have been a secondary source for carbonate turbidites of the Rim Butte unit (Ipnavik allochthon).

## INTRODUCTION

Mississippian strata throughout the Brooks Range in northern Alaska record a major shift in depositional regimes, from the siliciclastic fluvio-deltaic setting of the Endicott Group to the carbonate platform and associated deeper water environments of the Lisburne Group. Across most of the range, the first phases of Carboniferous carbonate production occurred during Osagean or Merarncian (late Early or early Late Mississippian) time (Armstrong and Mamet, 1977; Dumoulin and others, 1993, in press). Several thrust sheets within the Howard Pass quadrangle in the western Brooks Range (figs. 1, 2), however, contain calcareous rocks of **Kinderhookian** (early Early Mississippian) age that represent early, relatively short-lived episodes of neritic carbonate deposition. In this paper we describe the lithofacies, biofacies, and depositional environments of **Kinderhookian** calcareous rocks in the Howard Pass quadrangle and consider the implications of these rocks for middle Paleozoic paleogeographic reconstructions of the Brooks Range.

## STRATIGRAPHY AND GEOLOGIC SETTING

The calcareous rocks considered in this paper crop out within the foreland fold-and-thrust belt of the Brooks Range and represent both the upper part of the Endicott Group (chiefly upper part of the Kayak Shale) and the lower part of the Lisburne Group. The lower Lisburne Group strata, previously unnamed, are herein informally referred to as



the Rough Mountain Creek unit. Some **Kinderhookian** calcareous rocks described below are poorly exposed and (or) structurally complex and are of uncertain stratigraphic affinity.

In the structural framework of **Mayfield** and others (1988), **Kinderhookian** calcareous rocks are found in several different structural units (allochthons). The allochthons are distinguished on the basis of inferred structural level and differences in lithologic succession; differences are most pronounced in Carboniferous facies. Distinctive, coeval stratigraphic successions within a single allochthon are called sequences.

Most of the rocks discussed in this paper are assigned by Mull and others (this volume) to the Key Creek and Aniuk River sequences (Mull and Werdon, 1994) of the Endicott Mountains allochthon (Mull and others, 1987b; equivalent to the Brooks Range allochthon of **Mayfield** and others, 1988). **Kinderhookian** calcareous strata are also found in sequences considered by **Mayfield** and others (1988) to be part of the Picnic Creek and Kelly River allochthons, and in sequences of uncertain affinity in thrust contact with mafic volcanic rocks at Memorial Creek and in the **Pupik** Hills. The distribution of allochthons in the study area is shown in figure 2.

## PREVIOUS WORK AND METHODS

**Kinderhookian** calcareous rocks of the Howard Pass quadrangle have received little prior attention. Gray-weathering limestone in the lower part of the Lisburne Group, herein assigned to the Rough Mountain Creek unit, was first mentioned by Mull and others (1982, p. 349, 353) as a "discontinuous unnamed limestone" underlying the Kuna Formation. **Mayfield** and others (1988, p. 153) called this unit "Kogruk Formation or micritic limestone" and briefly described it in their discussion of the Key Creek sequence. Mull and Werdon (1994) referred to these rocks as "Kuna Formation, limestone facies" in the Key Creek sequence and "basal limestone of Kuna Formation" in the Aniuk River sequence and showed their distribution in the western Endicott Mountains. Conodont collections and age determinations from the Kayak Shale at several localities in the Howard Pass quadrangle are listed in Dumoulin and others (1993). Lower Mississippian biostratigraphy and lithostratigraphy of the western Endicott Mountains, with special emphasis on the Kayak Shale in the Howard Pass quadrangle, is discussed by Mull and others (this volume).

**Kinderhookian** calcareous rocks were examined at 18 localities across the Howard Pass quadrangle (fig. 2), and

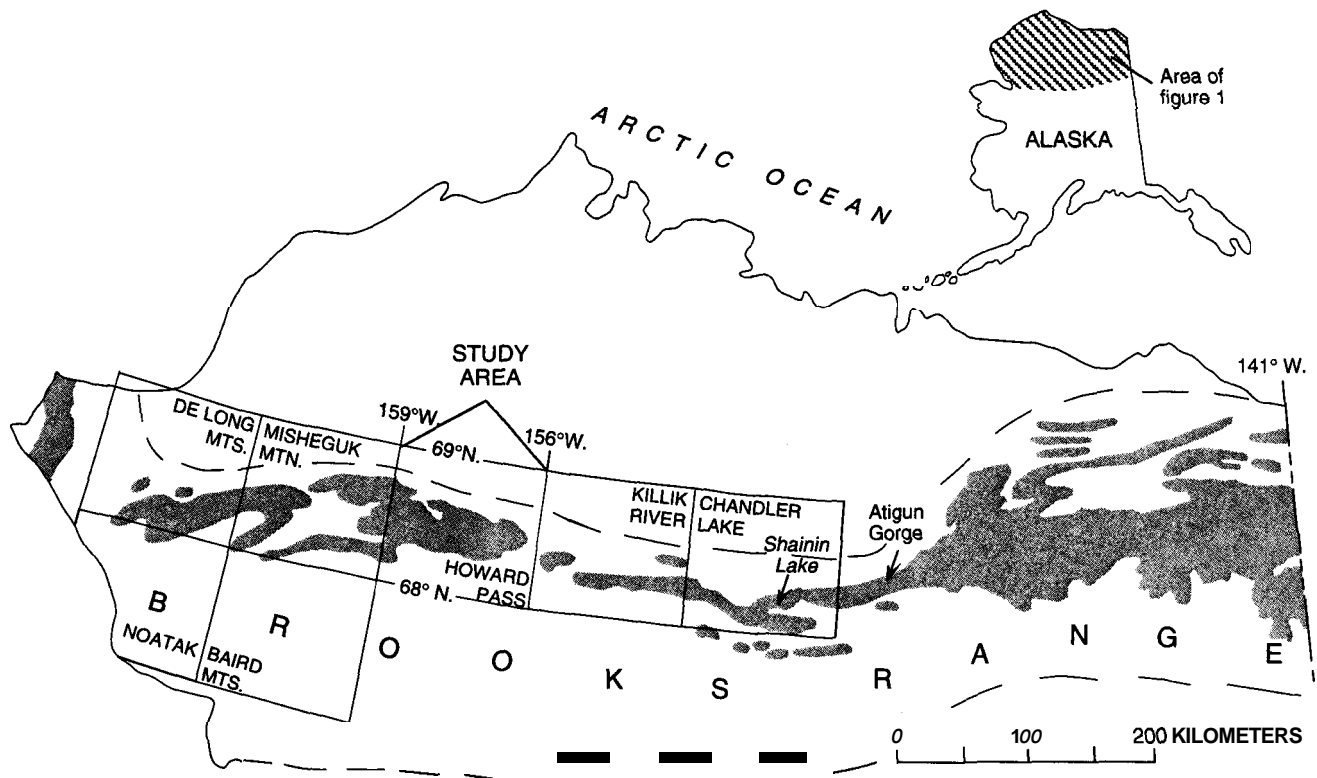


Figure 1. Distribution of the Lisburne Group (shaded) in northern Alaska (generalized from Armstrong and Mamet, 1978) and location of quadrangles and localities mentioned in the text.

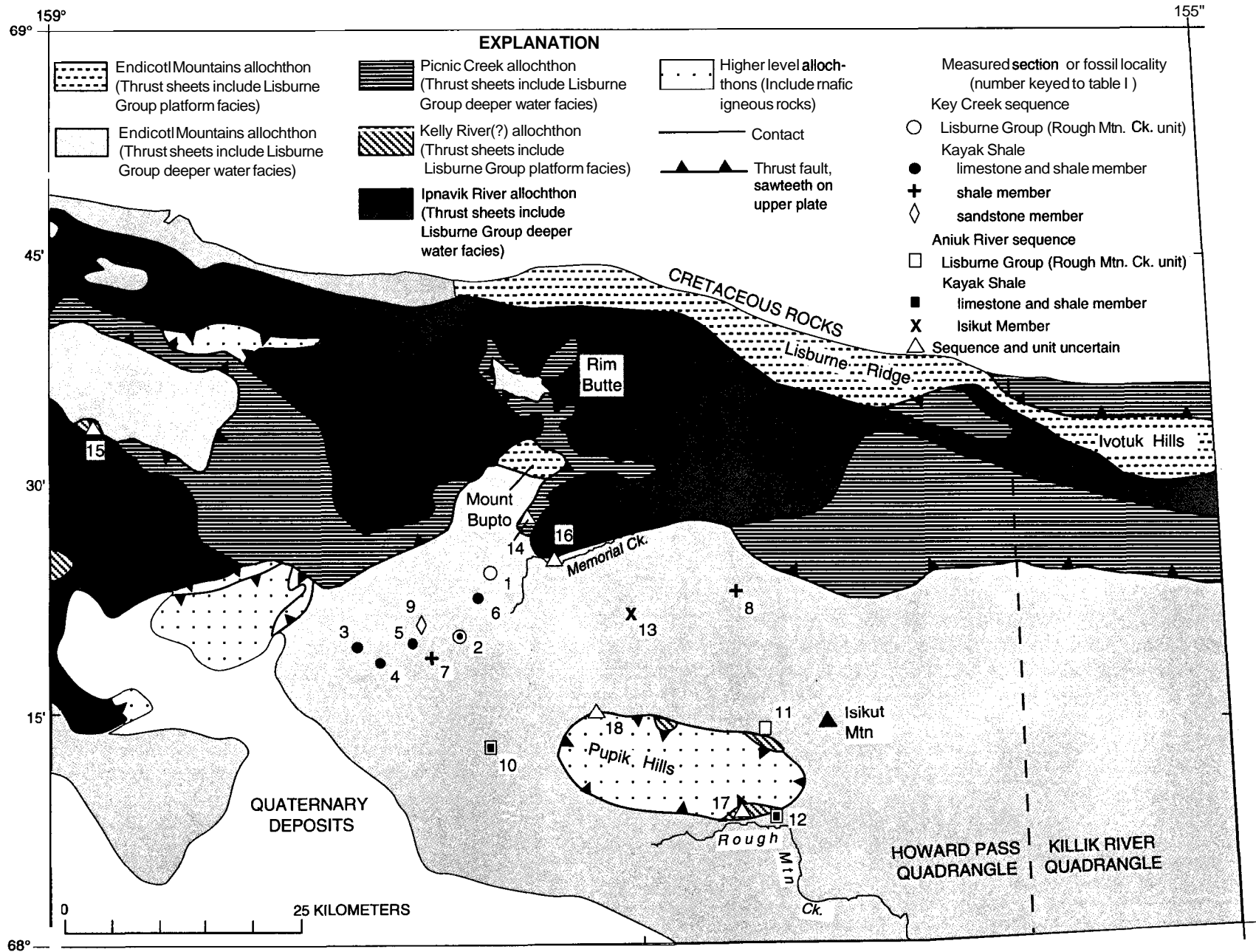


Figure 2. Location of measured sections and lithologic and fossil collections in Kinderhookian rocks of the Howard Pass quadrangle. See table I for geographic coordinates, key faunal components, and lithologies for numbered localities. Distribution of allochthons slightly modified from Mayfield and others (1988); allochthons may include thrust sheets of other allochthons too small to show at the scale of this map. Key Creek and Aniuk River sequences as used by Mull and Werdon (1994) and Mull and others (this volume); Isikut Member of Kayak Shale defined by Mull and others (this volume).

sections were measured at two good exposures (fig. 2, locs. 2 and 12). Petrographic descriptions are derived from field observations and examination of 120 thin sections. Limestones are classified after **Dunham** (1962). Nomenclature for mixed calcareous-quartz sediments has not yet been standardized; descriptions below use the conventions of **Dumoulin and Harris** (1992), in which quartzarenite contains more than 80 percent quartz exclusive of chert, grainstone contains less than 10 percent noncarbonate **detr**ital grains, and calcarenite refers to sediments of intermediate composition. Interpretations of depositional environments follow models in **Wilson** (1975) and **Scholle and others** (1983). Age and biofacies determinations are based on 23 productive conodont samples (table 1; see also **Mull and others**, this volume, table 1, for additional conodont and brachiopod data). Samples analyzed for this study contain conodonts with color alteration indices of 1.5-4 (mostly 3-4), indicating that the host rocks reached temperatures of at least 50-200°C (**Epstein and others**, 1977).

In order to facilitate comparisons between our study and the work of **Mull and others** (this volume), we have organized our data using the same framework of allochthons and sequences employed by these authors.

## ENDICOTT MOUNTAINS ALLOCHTHON

All sequences interpreted as part of the **Endicott** Mountains allochthon (**Mull and others**, 1987b) include extensive thick exposures of Upper Devonian and Lower Mississippian coarse **clastic** rocks—the Noatak Sandstone and Kanayut Conglomerate—overlain by the finer grained Kayak Shale. In the Key Creek sequence, the Kayak consists chiefly of black shale and mudstone, whereas in the Aniak River sequence (**Mull and Werdon**, 1994) the Kayak includes abundant reddish-brown-weathering siltstone, the Isikut Member of **Mull and others** (this volume, figs. 4, 6). In both sequences, the upper part of the Kayak Shale contains subordinate, generally orange-weathering, calcareous beds that underlie a relatively thin succession of the Lisburne Group. The Lisburne consists of gray limestone (Rough Mountain Creek unit) overlain by black siliceous **mudstone** and lesser black shale and dolostone (Kuna Formation of **Mull and others**, 1982).

### KEY CREEK SEQUENCE

Calcareous rocks of Kinderhookian age in the Key Creek sequence (see **Mull and others**, this volume, fig. 4) were examined at several localities in the central Howard Pass quadrangle, mainly southwest of Mount Bupto (fig. 2, locs. 1-9). The best exposures are at locality 2, 1 km southwest of the type section of the Kuna Formation (**Mull and others**, 1982) (figs. 3, 4).

## LITHOFACIES

### ROUGH MOUNTAIN CREEK UNIT

Sections of the Rough Mountain Creek unit at localities 1 and 2 (figs. 2, 3) are 8-17 m thick and consist chiefly of light- to medium-dark-gray limestone in even to undulatory, 0.5- to 40- (mostly 3- to 20-) cm-thick beds (fig. 5A). Most outcrops are lens- or mound-shaped and 30-100 m in lateral extent (fig. 4). Black fissile shale and blocky **mudstone** make up as much as 10 percent of some sections, chiefly as millimeter- to centimeter-thick partings and lenses but locally in intervals as much as 1 m thick; they are found largely in the upper few meters of the unit. Black to dark-gray, locally light-gray to tan chert and partially silicified limestone are found in all sections as nodules, stringers, and discontinuous beds 3-40 cm thick. Chert content varies greatly from bed to bed and from outcrop to outcrop. Some sections contain less than 5 percent chert, whereas others contain as much as 60 percent; 3-m-thick intervals in some exposures are 80-90 percent chert (fig. 5C). **Pelmat**ozoans, bryozoans, and brachiopods are abundant in outcrop; solitary and colonial corals are rare. We place the contact of the Rough Mountain Creek unit with the overlying Kuna Formation at the base of the first extensive (>1 m thick) interval of black shale and (or) mudstone.

Most Rough Mountain Creek limestones are moderately well to very poorly sorted, medium- to very coarse grained skeletal grainstones or packstones (fig. 5B). In many samples, grainstone and packstone are interlayered on a millimeter to centimeter scale or, less commonly, irregularly mixed, probably by bioturbation. Some beds are crudely graded, and some contain irregular laminae of brown, noncalcareous mud. **Pelmat**ozoan grains are abundant and form 60-80 percent of most samples, but bryozoan debris locally predominates. In some samples, grainier **pelmat**ozoan-rich layers alternate with muddier bryozoan-rich zones. Articulated **pelmat**ozoan ossicles and elongate fenestrate bryozoan fronds occur locally. Subordinate components of these limestones include brachiopods and ostracodes (often whole). Many bioclasts are partially pyritized; some are **micritized** or rimmed with microborings. A few samples contain about 1 percent quartz silt and (or) intraclasts, 1-2 mm long, of brown mud or micrite. Minor small rhombs of euhedral dolomite, generally 30-600  $\mu\text{m}$  in diameter, are disseminated in the muddier parts of many samples.

Rocks rich in sponge spicules are the second major constituent of the Rough Mountain Creek unit. Many of these rocks contain layers, a few millimeters to 5 cm thick, of **pelmat**ozoan and (or) bryozoan supportstone as described above, intercalated with spiculitic mudstone, wackestone, or packstone; spiculitic layers contain 10-40 percent spicules and few other bioclasts (fig. 5D). In chert-rich sections, spiculitic rocks make up the chert; spicules are siliceous and interlayers of nonspiculitic supportstone are

chiefly or completely replaced by silica, with generally excellent preservation of the original texture. In chert-poor sections, spicules are calcareous and interlayers of skeletal supportstone are not silicified. Both siliceous and calcareous spicules range from 12 to 200  $\mu\text{m}$  in diameter and reach 1 mm in length. Skeletal supportstone interlayers differ from similar layers not associated with spiculite in containing more brachiopods, as well as a few gastropods and possible foraminifers and algae. Spiculitic rocks in the Key Creek sequence are most abundant in the lower half of the Rough Mountain Creek unit.

#### KAYAK SHALE

The uppermost, limestone and shale member of the Kayak Shale was sampled at two localities in the Howard Pass B-3 quadrangle, and a section was measured at locality 2 (figs. 2, 3). Four poor exposures in the B-4 and B-2 quadrangles (fig. 2, locs. 3-5, 7) that probably represent the upper member of the Kayak were also examined, as were several samples described by Mull and others (this volume) as calcareous layers from lower members of the Kayak.

The limestone and shale member is at least 28 m thick (fig. 3). It is distinguished from the overlying Rough Mountain Creek unit by a sharp increase in the amount of intercalated shale and **mudstone** and by a change in the weathering color of limestone layers from gray to orange or tan. The section at locality 2 is 80-85 percent poorly exposed black to dark-gray fissile shale and mudstone; 5-15 percent orange-weathering, medium- to dark-gray, calcareous siltstone and sandstone; 0-10 percent laterally discontinuous beds of orange-weathering, medium-gray to black limestone; and 3-10 percent red- to **brown-weathering**, rounded to lensoid concretions, which are found in shale, siltstone, and sandstone and are 10-65 cm in maximum diameter.

Limestone intervals, generally 50 cm to 2 m thick, consist of irregular, 1- to 7-cm beds with wavy **millimeter-scale** partings (fig. 5E). These rocks are poorly sorted, coarse- to very coarse grained pelmatozoan supportstones with locally abundant brachiopods and subordinate bryozoans, gastropods, algae, and solitary corals (fig. 5F). Rocks rich in bryozoans or sponge spicules, common in the Rough Mountain Creek unit, are absent from this unit. A few percent detrital quartz silt and sand, generally concentrated into discrete thin laminae, is found in most samples (fig. 5F), and phosphatic clasts, bioclasts, and steinkerns occur locally. Euhedral rhombs of iron-rich dolomite ( $\pm$ siderite?), disseminated through most samples in abundances of 5-10 percent or more, produce the characteristic **orange-weathering** color of these rocks.

Very fine to fine-grained, well-sorted, calcite-cemented calcarenite in 0.5-4-cm beds forms intervals up to 2 m

thick that are intercalated with supportstone and (or) siliciclastic beds. These rocks are 10-80 percent calcareous material, as much as 30 percent iron-rich dolomite, and 20-60 percent noncarbonate grains. Calcareous grains are chiefly single crystals or crystal aggregates of calcite but include some pelmatozoan fragments and ostracodes. Iron-rich dolomite occurs as silt- and sand-sized red-rimmed rhombs. Noncarbonate grains are mainly angular **monocrystalline** quartz, lesser chert, phyllite, white mica, and chlorite, and rare tourmaline and zircon.

Concretions in both shale and calcarenite beds consist of tiny (4-60  $\mu\text{m}$ ) rhombs of yellow- to red-brown **iron-rich** dolomite, locally concentrated into clusters as much as 250  $\mu\text{m}$  across that display sweeping uniform extinction. Concretions in calcarenite contain as much as 10 percent silt and sand, chiefly quartz and lesser chert and feldspar.

Calcareous layers in the lower members of the Kayak Shale are similar to those described above from the limestone and shale member. Orange-weathering, brownish-gray limy beds 30-50 cm thick make up about 5 percent of the shale member at locality 8 (fig. 2) and consist of pelmatozoan **wacke/packstone** with subordinate brachiopods, ostracodes, and bryozoans. Orange-weathering, poorly sorted, very fine to fine-grained calcarenite intervals 30-75 cm thick form 5-10 percent of the basal sandstone member at locality 9 (fig. 2). Calcareous clasts (15-80 percent) are chiefly **brachiopods**, bryozoans, and pelmatozoans; other constituents include dolomite, monocrystalline quartz, and lesser chert, phyllite, white mica, and chlorite. Ferruginous dolomite rhombs are locally abundant in calcareous beds of both the shale and the sandstone members.

#### AGE AND BIOFACIES

A combination of conodont and brachiopod data suggest a late **Kinderhookian** age for both the Rough Mountain Creek unit and the upper part of the Kayak Shale in the Key Creek sequence. Conodont collections reported in this paper indicate a **Kinderhookian** age for these units (table 1). However, some samples from both units listed in Mull and others (this volume, table 1) yield conodont faunas of middle to late **Kinderhookian** age. In addition, a sample from the limestone and shale member of the Kayak (fig. 2, loc. 7) contains Kinderhookian conodonts and brachiopods of possible late **Kinderhookian** or early Osagean age. The presence of both of these faunas indicates a possible late **Kinderhookian** age for this sample and suggests that overlying parts of the Kayak and the Rough Mountain Creek unit can be no older than late **Kinderhookian**.

Conodonts from several calcareous lithologies in the Rough Mountain Creek unit and the Kayak Shale (table 1; see also Mull and others, this volume, table 1) yield biofacies data. Assemblages from pelmatozoan supportstone in both units represent bispathodid biofacies, or postmortem

Table 1. Conodont and lithologic data for selected Kinderhookian calcareous rocks, Howard Pass quadrangle, western Brooks Range

[Allochthon and (or) sequence: EMA, Endicott Mountains allochthon, sequence undetermined; EMA-KC, Key Creek sequence; EMA-AR, Aniak River sequence; KRA-K, Kelly River allochthon, Kelly sequence. Map number indicates locality shown on fig. 2. Letters in locality number refer to collector: ABS, S. Bie; AD, J.A. Dumoulin; ADo, J.H. Dover; ARM, R.T. Miyaka; JS, J.M. Schmidt. Lithology describes conodont sample only; compositional modifiers listed in order of decreasing abundance. Abbreviations for conodont genera: B., Bispathodus; H., Hindeodus; Pat., Patrognathus; Po., *Polygnathus*; Ps., Pseudopolygnathus; Si., Siphonodella; Syn., *Syncladognathus*. R, rare (<5 specimens); C, common (5-20 specimens); A, abundant (21-100 specimens); VA, very abundant (>100 specimens); \*, biostratigraphically important **taxon**. CAI, conodont color alteration index]

MAP NO., FIELD NO. (USGS COLLN. NO.), LAT. N./LONG. W.	ALLOCHTHON, SEQUENCE, AND STRAT. UNIT	LITHOLOGY AND SAMPLE WEIGHT	CONODONT FAUNA	CONODONT BIOFACIES	AGE AND CAI	REMARKS
1 91AD9F (31743-PC), 68°23'30"/ 157°39'15"	EMA-KC: Rough Mountain Creek unit of Lisburne Group	Pelmatozoan packgrainstone 7.7 kg	B. aculeatus <i>plumulus</i> (Rhodes, Austin, and Druce), nodosus morphotype (C)	Indeterminate (too few conodonts)	Kinderhookian 2-2.5	Assigned to Kayak Shale by Dumoulin and others (1993); B. aculeatus plumulus from this collection illustrated by these authors (fig. 5F).
2 92AD55-0 (32449-PC), 68°19'36"/ 157°45'15"		Pelmatozoan-bryozoan grainstone 9.4 kg	<i>Po. inornatus</i> E.R. Branson (R)	Indeterminate (too few conodonts)	Kinderhookian 4	About 1 km SW. of type section of the Kuna Formation. Near or at top of Rough Mountain Creek unit (see fig. 3).
92AD55-22 (32450-PC)	EMA-KC: Kayak Shale-- limestone and shale member	Pelmatozoan-bryozoan packgrainstone with locally abundant detrital <b>quartz</b> 9.3 kg	B. ac. <i>plumulus</i> , nodosus morphotype (R) B. stabilis (Branson and Mehl) or B. utahensis Sandberg and Gutschick (R) Ps. <i>orthoconstrictus</i> (Thomas)? (R)	Indeterminate (too few conodonts); postmortem transport from relatively shallow water, normal-marine depositional environment	Kinderhookian 4	About 12 m below contact with Rough Mountain Creek unit (see fig. 3).
92AD72-5 (32461-PC), 68°19'30"/ 157°44'55"	EMA-KC: Rough Mountain Creek unit of Lisburne Group	Partly silicified skeletal <b>pack/grainstone</b> interlayered with siliceous <b>spiculite</b> 11.9 kg	B. <i>stabilis</i> or B. <i>utahensis</i> (C) Po. <i>inornatus</i> E.R. Branson (A) Po. <i>longiposticus</i> Branson and Mehl (R)	Polygnathid; high-energy, relatively shallow water shelf depositional environment	Kinderhookian 4	From chert-rich outcrop 0.3 km SE. of 92AD55, about 5 m below top of Rough Mountain Creek unit.
92AD73G (32462-PC), 68°19'38"/ 157°45'05"		Pelmatozoan-bryozoan <b>grainstone</b> 9.5 kg	<i>Po. inornatus</i> (R) <i>Po. longiposticus</i> (R)	Indeterminate (too few conodonts)	Kinderhookian 4	Structural repeat of section at 92AD55 located 0.2 km to NE.; sample from about 6 m below top of Rough Mountain Creek unit.
3 91JS36Z (31754-PC), 68°19'/ 158°04.5'	EMA-KC: Kayak Shale-- limestone and shale member	<b>Skeletal grainstone</b> 7.6 kg	Conodont data in Mull and others (this volume, table 1)		Kinderhookian 3-3.5	Limestone stratigraphically overlies about 10 m of <b>volcaniclastic</b> rocks (in Kayak Shale?) and underlies <b>spiculitic chert</b> (Kuna Formation).
4 91JS37G (31755-PC), 68°17.7'/ 157°58.5'		Pelmatozoan packstone 6.6 kg	Conodont data in Mull and others (this volume, table 1)		middle to late Kinderhookian 3.5-4	Overlies black silty <b>argillite</b> containing 50% <b>sil/sand flasers</b> and laminae and some climbing ripples (Kayak Shale).

Table 1. Continued.

5 91JS38A (31756-PC), 68°19'40"/ 157°52'38"	EMA-KC: Kayak Shale-- limestone and shale member	Very fine grained calcareenite and calcareous siltstone 11.5 kg	<i>B. aff. B. ac. plumulus</i> (R) <i>Polygnathus</i> sp. indet. (R)	Indeterminate (too few conodonts)	Kinderhookian 3.5-4	Assigned to Kayak Shale by Dumoulin and others (1993, table 1).
6 91ADo70C, E (31748, 47-PC), 68°23.0'/ 157°40.5'		Pelmatozoan <b>pack/grainstone</b> , locally dolomitic 4.7 kg, 9.7 kg	Conodont data in Mull and others (this volume, table 1)		middle to late Kinderhookian ~3	91ADo70E about 20 m structurally (and stratigraphically?) above 91ADo70C.
7 93JS02C (32218-PC), 68° 22.25'/ 156°55.63'		Pelmatozoan grainstone 5.5 kg	Conodont and brachiopod data in Mull and others (this volume, table 1)		middle to late Kinderhookian, possibly late Kinderhookian 3 or 4	
8 92ADo239B2 (32209-PC), 68°18'16"/ 157°51'09"	EMA-KC: Kayak Shale-- shale member	Dolomitic pelmatozoan wackelpackstone 6.8 kg	Conodont data in Mull and others (this volume, table 1)		Kinderhookian ~3.5	
9 92ADo248B (32207-PC), 68°20'21"/ 157°52'58"	EMA-KC: Kayak Shale-- sandstone member	Calcareenite with diverse <b>bioclasts</b> , dolomite, and lesser quartz 5.4 kg	Conodont data in Mull and others (this volume, table 1)		Probably Kinderhookian 3 or 4	Probably stratigraphically lower than 92ADo248B.
92ADo316B (32208-PC), 68°20'13"/ 157°52'06"		Quartzose calcarenite 9.0 kg	Conodont data in Mull and others (this volume, table 1)			
For additional localities and paleontologic data for Key Creek sequence stratigraphic units, see Mull and others (this volume, table 1): Rough Mountain Creek unit (92Mu20, 93Mu47); Kayak Shale, limestone and shale member (92Mu22, 93Mu51)						
10 92AD24G (32429-PC), 68°12'37"/ 157°39'55"	EMA-AR: Rough Mountain Creek unit of Lisburne Group	Pelmatozoan-bryozoan grainstone 7.5 kg	<i>B. ac. plumulus, nodosus</i> morphotype (R) <i>B. ac. plumulus</i> (C) <i>Po. scobiniformis</i> E.R. Branson (R) <i>Ps.</i> sp. indet. (C)	Indeterminate (too few conodonts); normal-marine depositional environment	Kinderhookian 4	About 2 m below contact with Kuna Formation.
92AD24N (32430-PC)	EMA-AR: Kayak Shale-- limestone and shale member	Interlayered skeletal packstone and muddy quartz siltstone 7.0 kg	<i>B. ac. plumulus, nodosus</i> morphotype (R) <i>B. ac. plumulus</i> (R)			About 5 m below top of Kayak Shale.
11 92AD18A (32423-PC), 68°12'45"/ 156°10'50"	EMA-AR: Rough Mountain Creek unit	Pelmatozoan-bryozoan grainstone 5.6 kg	<i>B. ac. plumulus, nodosus</i> morphotype (A) <i>H. crassidentatus</i> (Branson and Mehl) (R)*	Bispathoid; normal-marine, relatively high energy depositional environment	middle to late Kinderhookian ~2.5	Several meters below contact with Kuna Formation.

Table 1. Continued.

MAP NO., FIELD NO. (USGS COLLN. NO.), LAT. N./ LONG. W.	ALLOCH- THON, SEQUENCE, AND STRAT. UNIT	LITHOLOGY AND SAMPLE WEIGHT	CONODONT FAUNA	CONODONT BIOFACIES	AGE AND CAI	REMARKS
12 92AD63A-12.6 (32455-PC), 68°07'41"/ 156°47'05"	EMA-AR: Rough Mountain Creek unit	Skeletal wackepackstone 10.1 kg	<i>Po. communis carina</i> Hass (R) <i>Ps. orthoconstrictus</i> (R) <i>Ps. sp. indet.</i> (R)	Indeterminate (too few conodonts)	Kinderhookian 4	About 3 m below contact with Kuna Formation (see fig. 6).
92AD63A-2.5 (32454-PC) 68°07'41"/ 156°47'05"		Interlayered pelmatozoan- bryozoan packstone and grainstone 11.1 kg	<i>B. ac. plumulus</i> (R) <i>B. stabilis</i> (C) [fig. 9I] <i>H. crassidentatus</i> (R)* <i>Po. communis carina</i> (A) <i>Po. communis communis</i> Branson and Mehl (C) <i>Ps. spp.</i> and <i>Ps. n. sp.?</i> (C) [fig. 9H] <i>Si. aff. Si. crenulata</i> (Cooper) (C)* [fig. 9E] <i>Si. isosticha</i> (Cooper) (R)* [fig. 9F] <i>Si. cf. Si. isosticha</i> (Cooper) (C)* [fig. 9G] <i>Si. sp. indet.</i> (C)	Polygnathid; outer-shelf to slope depositional environment	lower part of <i>Si. isosticha</i> -Upper <i>Si. crenulata</i> Zone (late, but not latest Kinderhookian) 4	12.5 m below contact with Kuna Formation (see fig. 6).
92AD64-6 (32456-PC), 68°07'38"/ 156°47'10"	EMA-AR: Kayak Shale-- limestone and shale member	Pelmatozoan grainstone 9.8 kg	<i>B. ac. aculeatus</i> (R) <i>H. crassidentatus</i> (C)* <i>Po. inornatus</i> (C) <i>Ps. sp. indet.</i> (R) <i>Syn. geminus</i> (Hinde) (C)* [fig. 9B]	Mixed biofacies; postmortem hydraulic mixing of species from a variety of shallow- to middle-shelf depositional environments	middle to late Kinderhookian 4	At least 11 m below contact with Rough Mountain Creek unit (see fig. 6). 92Mu10-1 (Mull and others, this volume, table 1) from same locale as 92AD64-6.
92AD65-4 (32457-PC), 68°07'35"/ 156°47'15"	EMA-AR: Rough Mountain Creek unit	Pelmatozoan-bryozoan grainstone 7.7 kg	<i>B. ac. aculeatus</i> (R) <i>B. stabilis</i> (R) <i>H. crassidentatus</i> (C)* <i>Po. communis carina</i> (A) <i>Ps. n. sp.</i> (C)	Polygnathid; shelf depositional environment	middle to late Kinderhookian 4	92AD65, 66 underlie and structurally repeat section at 92AD63, 64. 65-4 is about 4 m below contact with Kuna Formation. 92Mu10-2 (Mull and others, this volume, table 1) from same locale as 92AD65-4.
92AD66-1 (32458-PC), 68°07'32"/ 156°47'18"	EMA-AR: Kayak Shale-- limestone and shale member	Skeletal pack/grainstone 11.0 kg	<i>B. ac. plumulus</i> (R) <i>B. ac. plumulus, nodosus</i> morphotype (R) <i>B. stabilis</i> (C) <i>H. crassidentatus</i> (C)* <i>Po. inornatus</i> (C) <i>Syn. geminus</i> (C)* [figs. 9A, C, D]	Postmortem transport within or from the polygnathid- bispathodid biofacies; shelf (probably middle) depositional environment	middle to late Kinderhookian 4	At least 6 m below top of Kayak Shale. 92Mu10-3 (Mull and others, this volume, table 1) from same locale as 92AD66.
92AD66B (32459-PC), 68°07'25"/ 156°47'18"		Brachiopod pack/grainstone with locally abundant peloids and quartz silt 11.0 kg	<i>B. spp. indet.</i> (R) <i>H. crassidentatus</i> (C)* <i>Po. inornatus</i> and <i>Po. longiposticus</i> (C) <i>Ps. sp. indet.</i> (R)	Postmortem transport within or from the hindeodid- polygnathid biofacies; shelf depositional environment	middle to late Kinderhookian 4	A few meters below 92AD66D.
92AD66D (32460-PC), 68°07'27"/ 156°47'21"		Skeletal pack/grainstone 10.0 kg	<i>B. stabilis</i> (R) <i>H. crassidentatus</i> (R)* <i>Po. inornatus</i> (C)	Polygnathid; high-energy, relatively shallow water depositional environment	middle to late Kinderhookian 4	About 10 m below 92AD66-1. Nearly all conodonts fractured and somewhat deformed; abundant indeterminate fragments.

Table 1. Continued.

13 93JS03B, 68°20.33'/ 157°13.5'	EMA-AR: Kayak Shale– Isikut Member	Calcarenites with subequal amounts of dolomite, quartz, and chert 4.2 kg	Barren			From lower part of Isikut Member; probably stratigraphically higher than 93JS03E.
93JS03E, 68°20.5'/ 157°13'		Calcarenites with abundant bioclasts and lesser quartz 4.5 kg	Conodont data in Mull and others (this volume, table 1)		Late Devonian- Mississippian 4	Several m above contact with underlying Kanayut Conglomerate.
For additional localities and paleontologic data for Aniak River sequence stratigraphic units, see Mull and others (this volume, table 1): Rough Mountain Creek unit (92Mu5-1, 92Mu5-2, 92Mu12-2, 92Mu63-1); Kayak Shale, limestone and shale member (93Mu63, 93Mu63-2)						
14 92AD46A (32446-PC), 68°27'08"/ 157°31'02"	EMA(?): Rough Mountain Creek unit of Lisburne Group	Cross-bedded pelmatozoan packstone 11.8 kg	<i>B. ac. plumulus</i> (R) <i>Si. aff. Si. obsoleta</i> Hass (R)*	Indeterminate (too few conodonts)	middle to late (but not latest) Kinderhookian 1.5	92AD46 structurally underlies 92ADo78, 79; 46A is 0.5 m below base of Kuna Formation. Mayfield and others (1988) included these rocks in the Picnic sequence of the Picnic Creek allochthon.
92ADo78B (33320-PC), 68°26'48"/ 157°30'00"	EMA(?): Kayak Shale(?)	Quartzose calcarenite with minor bioclasts and rare glauconite 5.3 kg	<i>B. aculeatus</i> subsp. indet. (R) <i>B. stabilis</i> (A) <i>Po. communis cornmunis</i> (A) <i>Ps. marginatus</i> (Branson and Mehl) and <i>Ps. orthoconstrictus</i> (A) <i>Si. sulcata</i> (Huddle) (C)* [figs. 9J-L]	Bispathodid-polygnathid biofacies; shallow- to middle- shelf, normal-marine depositional environment	early to middle Kinderhookian ( <i>Si. sulcata</i> Zone into lowest part of the Lower <i>Si. crenulata</i> Zone) 2	92ADo78B is ~75 m stratigraphically below 92ADo79A.
92ADo79A (32216-PC), 68°26'50"/ 157°31'00"		Skeletal packstone with rare glauconite 11.8 kg	<i>B. aculeatus</i> subsp. indet. (C) <i>H. crassidentatus</i> (C)* <i>Po. cotmunnis cornmunis</i> (R) <i>Ps. marginatus</i> and <i>Ps. orthoconstrictus</i> and forms transitional between them (A) <i>Ps. sp. indet</i> (A)	Pseudopolygnathid-hindeodid biofacies: shallow- to middle- shelf, normal-marine depositional environment	middle to late Kinderhookian 2	
15 92AD57E (32451-PC), 68°33'43"/ 158°51'45"	KRA-K: Utukok Formation(?) of Lisburne Group	Dolomitic pelmatozoan wackepackstone 9.8 kg	<i>B. stabilis</i> or <i>B. utahensis</i> (R) <i>Po. cornmunis communis</i> (C) [figs. 9R, S] <i>Po. inornatus</i> (C) <i>Po. symmetricus</i> E.R. Branson (R) <i>Si. obsoleta</i> (VA)* [figs. 9T-AA]	Siphonodellid; outer-shelf or deeper water depositional environment	middle to early late Kinder- hookian (Upper <i>Si. duplicata</i> Zone to lower part <i>Si. isosticha</i> - Upper <i>Si. crenulata</i> Zone 2 or 3	Outcrop shown in figure 10B.
16 92AD37D (32443-PC), 68°24'00"/ 157°27'10"	ALLOCH- THON UNCERTAIN: Kayak Shale(?)	Pelmatozoan grainstone 9.0 kg	<i>H. crassidentatus?</i> (C)* <i>Po. inornatus</i> (C) [fig. 9Q] <i>Po. longiposticus</i> (R)	Polygnathid; relatively high energy, shallow-water depositional environment	middle to late Kinderhookian 3	Macrofossils from this locale (USGS colln. 12773-PC) suggest a Kinderhookian, possibly late Kinderhookian age (J.T. Dutro, Jr., written commun. to I.L. Tailleux, 1966).
17 92ABS196A (32468-PC), 68°08'04"/ 156°53'20"		Peloidal pack/grainstone 7.8 kg	<i>Po. cornmunis?</i> (R) <i>Po. inornatus</i> (R) <i>Po. spp. indet.</i> (C) <i>Si. sp. indet.</i> of middle to late Kinderhookian morphotype (C)*	Postmortem transport from polygnathid biofacies toward siphonodellid biofacies; middle-shelf or deeper water depositional environment	middle to late Kinderhookian 2.5-3	About 20 m structurally below contact with basalt.
92ABS196B		Calcareous siltstone 6.9 kg	Barren			About 5 m below 92ABS196A.
18 92ARM69A (32472-PC) 68°13'50"/ 157°20'40"		Fossiliferous limestone 7.0 kg	<i>Po. communis communis</i> (C) <i>Po. symmetricus</i> (C) <i>Syn. geminus</i> (C)* [figs. 9M, N] <u>Redeposited Devonian conodonts:</u> Icriodontid coniform elements (C) [figs. 9O, P]	Polygnathid; normal-marine shelf depositional environment	middle to late Kinderhookian 3	Contains redeposited Devonian coniform elements. On the basis of regional mapping, C.G. Mull believes these rocks are part of the Isikut Member (written commun., 1996).



transport from that biofacies, and indicate a shallow-water, intermittently high energy depositional environment with normal-marine salinity. A single sample of thinly interlayered siliceous spiculite and skeletal supportstone in the Rough Mountain Creek unit produced robust conodonts (polygnathid biofacies) that also indicate a shallow-water, high-energy regime. Samples of bryozoan-rich supportstone from the Rough Mountain Creek unit and of calcarenite from the Kayak Shale did not yield enough conodonts to delimit the biofacies.

DEPOSITIONAL ENVIRONMENT

ROUGH MOUNTAIN CREEK UNIT

Lithologic and faunal data from the Rough Mountain Creek unit indicate that deposition took place in relatively shallow shelf settings intermittently and (or) locally characterized by high-energy conditions. The moundlike shape and irregular distribution of outcrops suggest that the unit formed as discrete buildups, possibly capping local topographic highs.

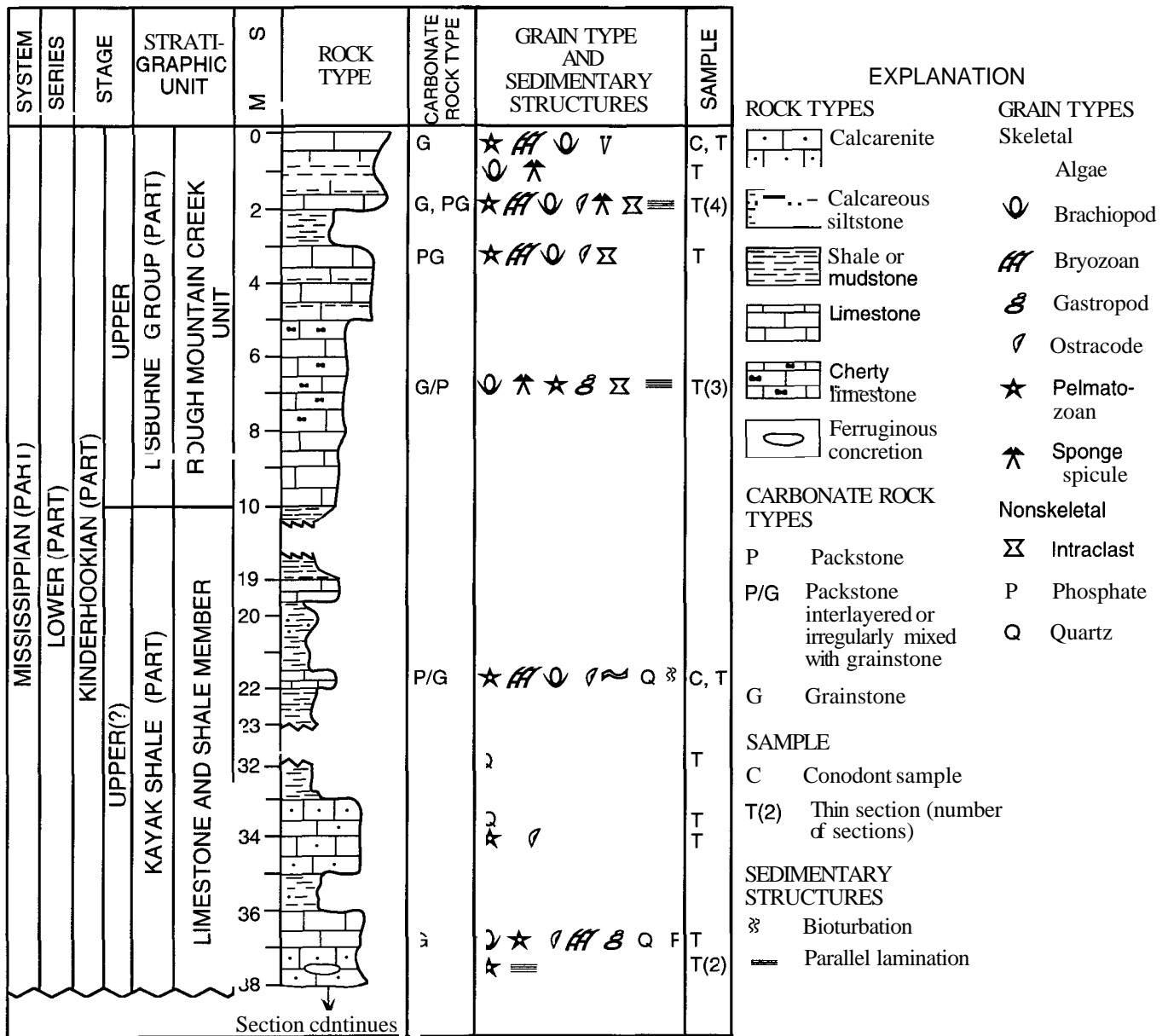


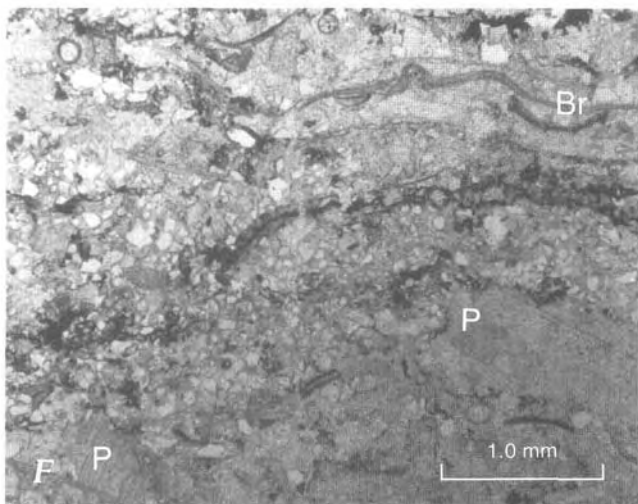
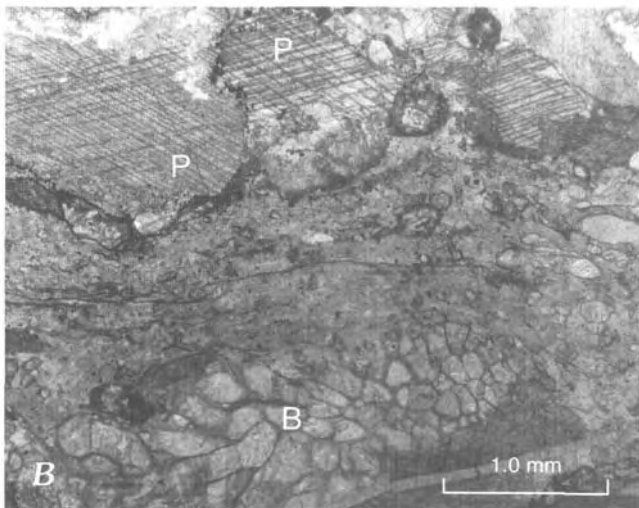
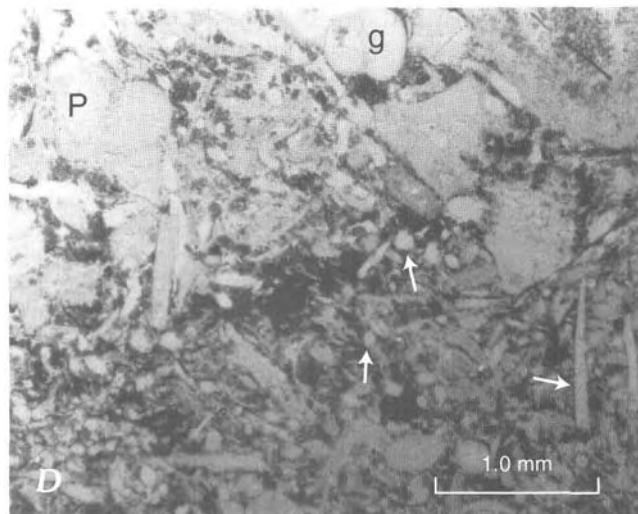
Figure 3. Measured section, upper part of Kayak Shale and lower part of Lisburne Group, Key Creek sequence (fig. 2, loc. 2). See table 1 for conodont analyses (samples 92AD55-0, -22).

Grain-supported texture, found throughout the unit, demonstrates that most deposition took place above wave base. True shoal conditions were probably not achieved, however, because these limestones contain considerable carbonate mud and some articulated bioclasts and are gen-

erally poorly sorted with little if any evidence of grain rounding or abrasion. Well-layered and (or) crudely graded beds most likely accumulated when storm surges brought grain-rich pulses into quieter, muddier environments. Bioturbation reworked and partially homogenized these



**Figure 4.** Kinderhookian rocks in the Key Creek sequence. **A,** View (toward west) of locality 2, figure 2 (arrow); Mlr, Rough Mountain Creek unit; Mk, Kayak Shale. **B,** Closer view of Kinderhookian section at locality 2; note discontinuous nature of Rough Mountain Creek unit (arrows) overlying poorly exposed Kayak Shale. Outcrop on left contains considerably more chert than does that on the right.



deposits, but it was not sufficient to obliterate all compositional layering. Muddy rip-up clasts and conodont assemblages that show signs of postmortem transport further evince the contribution of storm processes to this unit.

Faunal evidence corroborates the interpretation of a shallow-water, open-marine setting for the Rough Mountain Creek unit. The megafauna consists chiefly of normal-marine biota (pelmatozoans, bryozoans, and brachiopods); elements tolerant of high or variable salinity (gastropods, algae, foraminifers) are rare. Bored and micritized bioclasts—a subordinate but ubiquitous component of Rough Mountain Creek limestones—form most frequently in shallow-water (photic zone) conditions (Bathurst, 1976). Conodont biofacies in these rocks also indicate deposition in open, relatively shallow and locally agitated water.

Sponge spicules in the Lisburne Group are found in both deep- and shallow-water settings (Armstrong and Mamet, 1977), but the biotic associates and locally robust size of these spicules suggest a shallow-water environment. Elsewhere in the Brooks Range (for example, Shainin Lake; fig. 1), Carboniferous sponge spicules are particularly abundant in muddy sediments formed during initial phases of neritic carbonate production (J.A. Dumoulin, unpub. data). Spiculitic rocks in the Rough Mountain Creek unit appear to have accumulated in a similar manner.

#### KAYAK SHALE

Calcareous layers are increasingly common upward within the Kayak Shale but are everywhere thinner and less abundant than in the Rough Mountain Creek unit. Skeletal supportstones in the Kayak formed chiefly in minor, meter-scale carbonate buildups that were quickly smothered by renewed siliciclastic influx. Calcarenes are largely storm-generated mixtures of calcareous material eroded from these buildups and siliciclastic detritus. Mega- and microfaunas of the Kayak are similar to those of the Rough Mountain

Creek unit. The greater abundance of forms such as corals, gastropods, and calcareous algae in the Kayak, and the relative rarity of bryozoans and sponge spicules, suggest deposition in shallower and (or) more agitated water.

#### SUMMARY

Initiation and demise of **Kinderhookian** carbonate production in the study area reflect changes in sediment dispersal, circulation, and (or) sea level. Faunal and sedimentologic evidence indicates that both the Rough Mountain Creek unit and the underlying Kayak Shale formed in similar shallow-water shelf settings. Rise in relative sea level (that is, rise in absolute sea level and (or) subsidence of the shelf) may have accompanied the shift to predominantly carbonate accumulation, but decreased availability of siliciclastic sediment, perhaps tectonically induced, was most likely the chief cause. Intercalation of limestone and siliciclastics throughout the upper member of the Kayak suggests that the shift was gradual.

The contact between the Rough Mountain Creek unit and the overlying Kuna Formation, however, is sharp and implies an abrupt end to neritic carbonate deposition. The Kuna formed in a deeper water (sub-photic zone) setting characterized by anoxic to dysaerobic bottom conditions (Dumoulin and others, 1993). Relative sea-level rise and concomitant changes in circulation patterns probably extinguished Rough Mountain Creek carbonate production. This rise may have been in part eustatic—global sea level increased markedly during the late Kinderhookian (Ross and Ross, 1988)—but neritic carbonate deposition continued without obvious disruption in some parts of northern Alaska (for example, sequences of the Kelly River allochthon; Dumoulin and Harris, 1992) throughout the Early Mississippian. Thus, if Kinderhookian sea-level rise in the study area was sufficient to terminate carbonate production, it was most likely because the effect of this rise was intensified by tectonic subsidence. Development of one or more rift basins in northern Alaska during Late **Devonian–Carboniferous** time has been proposed by numerous workers (Moore and others, 1994) and may have played a role in the sudden demise of the Rough Mountain Creek unit.

#### ANIUK RIVER SEQUENCE

**Kinderhookian** calcareous rocks in the Aniak River sequence (Mull and others, this volume; fig. 6) were studied at several localities in the southeastern Howard Pass quadrangle (fig. 2, locs. 10–13). The best exposed and most complete section is on the north side of Rough Mountain Creek (fig. 2, loc. 12), where we recognize two successive thrust sheets that repeat the Kayak Shale and overlying Lisburne Group (figs. 6, 7).

◀ **Figure 5.** Sedimentary features of Kinderhookian rocks in the Key Creek sequence. **A–D**, Rough Mountain Creek unit; **E–F**, Kayak Shale. **A**, Even to slightly undulatory beds of skeletal packstone and grainstone, 5 m below top of section at locality 2 (fig. 2). **B**, Photomicrograph of pelmatozoan grainstone overlying muddy bryozoan packstone (fig. 2, loc. 1); P, pelmatozoan fragment; B, bryozoan fragment. **C**, Chert-rich outcrop at locality 2 (fig. 2). **D**, Photomicrograph of skeletal supportstone overlying muddy spiculite (fig. 2, loc. 1); P, pelmatozoan fragment; g, gastropod; arrows indicate siliceous sponge spicules in longitudinal and cross sections. **E**, Thin beds of skeletal supportstone, 22 m below top of section at locality 2 (fig. 2). **F**, Photomicrograph of skeletal supportstone shown in **E**; note locally abundant, angular quartz silt. P, pelmatozoan fragment; Br, brachiopod.

LITHOFACIES

ROUGH MOUNTAIN CREEK UNIT

At locality 12 (fig. 2), the Rough Mountain Creek unit is about 15 m thick in both the upper and lower thrust sheets. Elsewhere, the unit is exposed chiefly as rubble and

is of uncertain thickness. We estimate a total thickness of about 10 m at locality 11, and 35 m at locality 10 (fig. 2).

The Rough Mountain Creek unit in the Aniak River sequence is similar to correlative sections in the Key Creek sequence. In the Aniak River sequence, the unit consists chiefly of light- to medium-dark-gray-weathering, light- to

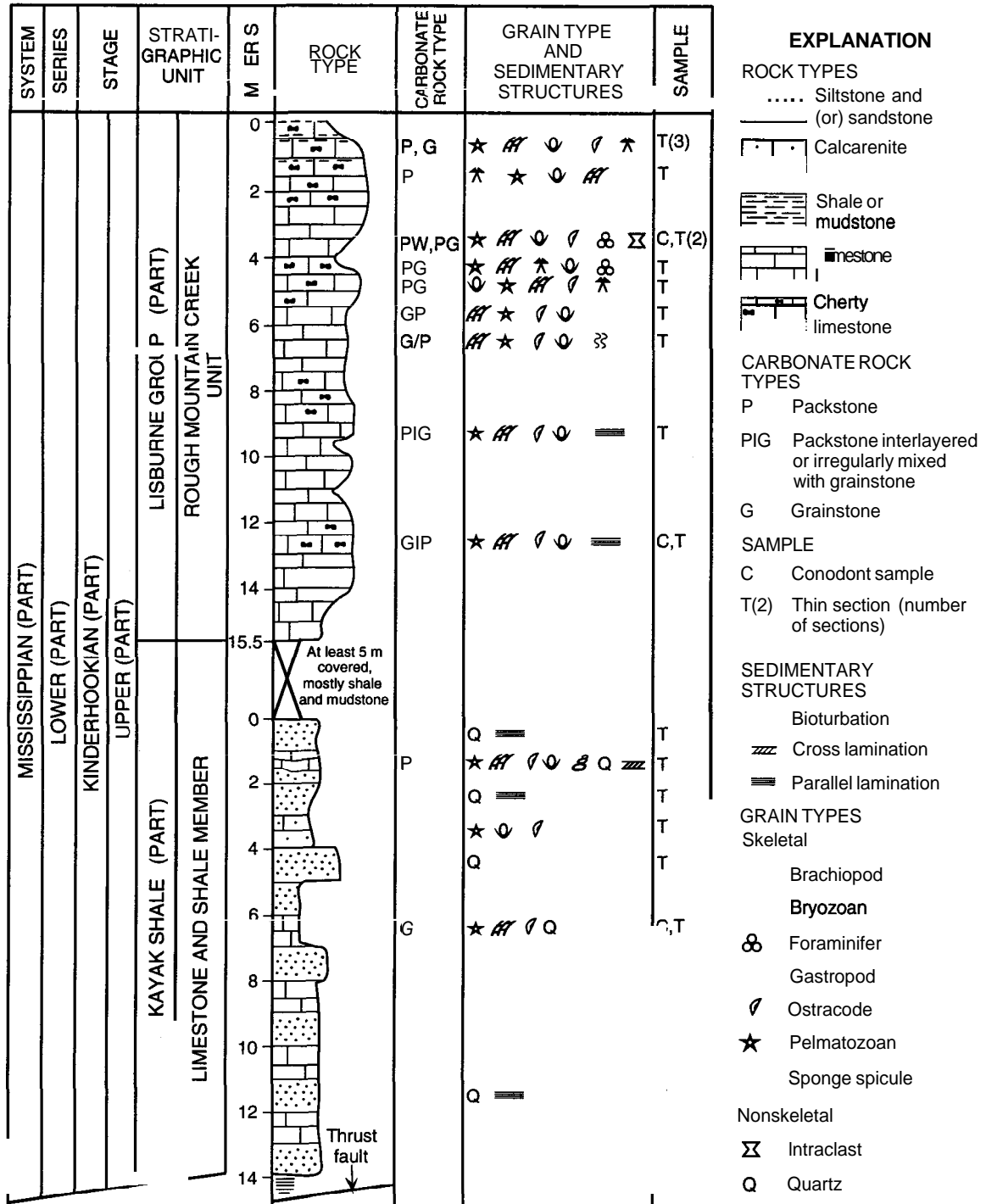


Figure 6. Measured section, upper part of Kayak Shale and lower part of Lisburne Group, Aniak River sequence, upper thrust sheet (fig. 2, loc. 12). See table 1 for conodont analyses (samples 92AD63A-2.5, 12.6, and 92AD64-6).

dark-gray limestone in irregular to undulatory, thin to thick (0.5-35 cm) beds with faint wavy laminae (fig. 8A). Most sections contain partings and beds (to 50 cm thick) of medium-gray to black, noncalcareous shale and (or) mudstone that increase upward from a few to about 10 percent (fig. 8A). Chert was noted only at the Rough Mountain Creek locality, where black (locally bluish or tan) bands, nodules, and lenses 5-20 cm thick make up 5-40 percent of less than half the section.

Limestones are mostly supportstones rich in pelmatozoans and (or) bryozoans, like those described above from the Key Creek sequence. Partial silicification, chiefly of pelmatozoans and brachiopods, is widespread in the Aniuk River supportstones. As in the Key Creek sequence, chert is rich in siliceous sponge spicules. Rocks with abundant calcareous spicules were not found in the Aniuk River sequence.

#### KAYAK SHALE

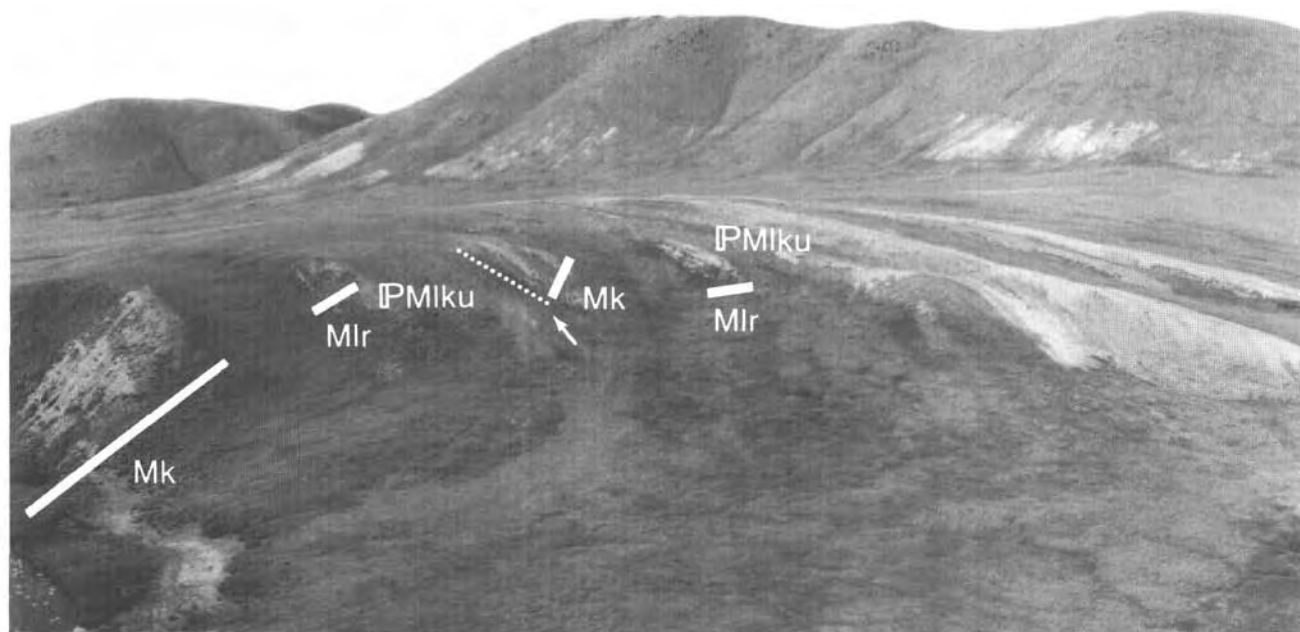
The limestone and shale member of the Kayak Shale was examined at two localities in the Aniuk River sequence (fig. 2, locs. 10, 12). At least 5 m of poorly exposed, black, noncalcareous shale and mudstone make up the uppermost part of the member and overlie 5-14 m of well-exposed noncalcareous siltstone (10-60 percent), calcarenite (10-60 percent), limestone (5-40 percent), and black, noncalcareous shale (<5-30 percent). These lithologies are generally intercalated on a scale of 0.5-1 m, although shale intervals may

be only a few centimeters thick. Concretions like those in the Key Creek sequence were not observed.

Orange-weathering, light- to medium-gray limestone forms locally lensoid or undulatory beds, 1.5-10 cm thick, which may contain millimeter-scale, low-angle cross laminae (fig. 8B). These rocks are pelmatozoan supportstones, much like those described above from the Kayak Shale in the Key Creek sequence; some contain rounded clasts of black shale as much as 2 mm long.

Yellow-brown- to orange-weathering, brownish-gray calcarenite in centimeter-thick undulatory beds is also similar to rocks described above from the Key Creek sequence (fig. 8C). Aniuk River calcarenite has well-developed cross- and parallel-laminae, locally disrupted by bioturbation. Composition is similar to, but more diverse than, that of calcarenite in the Key Creek sequence. Calcareous grains include brachiopods, bryozoans, gastropods, algae, and peloids, as well as pelmatozoans and ostracodes. Noncarbonate grains, mostly monocrystalline quartz, make up more than 80 percent of some samples. Aniuk River calcarenite contains sedimentary lithic grains, plagioclase, and possible biotite, in addition to all the noncalcareous grain types noted in correlative Key Creek sequence calcarenite.

Olive-gray- to light-gray-weathering, medium-gray, noncalcareous siltstone to fine-grained sandstone, not found in the Key Creek sequence, forms parallel-laminated, 1- to 3-cm-thick beds (fig. 8B). Grains are angular to subrounded and generally well sorted. Composition is similar to the



**Figure 7.** Kinderhookian rocks at Rough Mountain Creek (fig. 2, loc. 12); arrow and dotted line indicate base of upper thrust sheet. IPMIku, Kuna Formation (includes younger rocks); Mlr, Rough Mountain Creek unit; Mk, Kayak Shale.

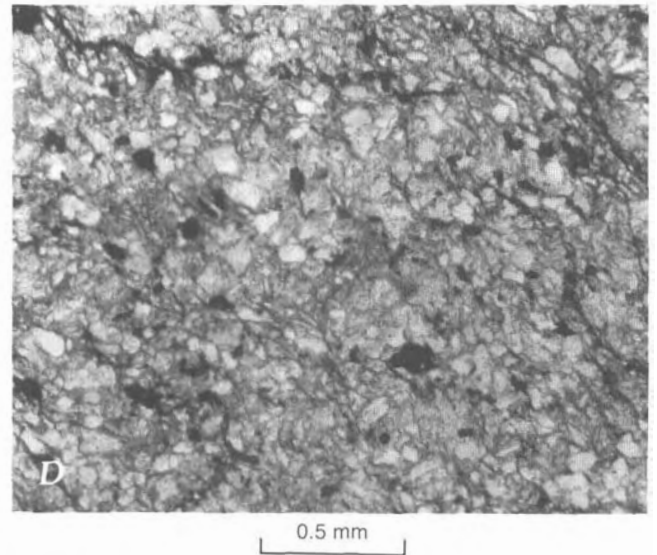
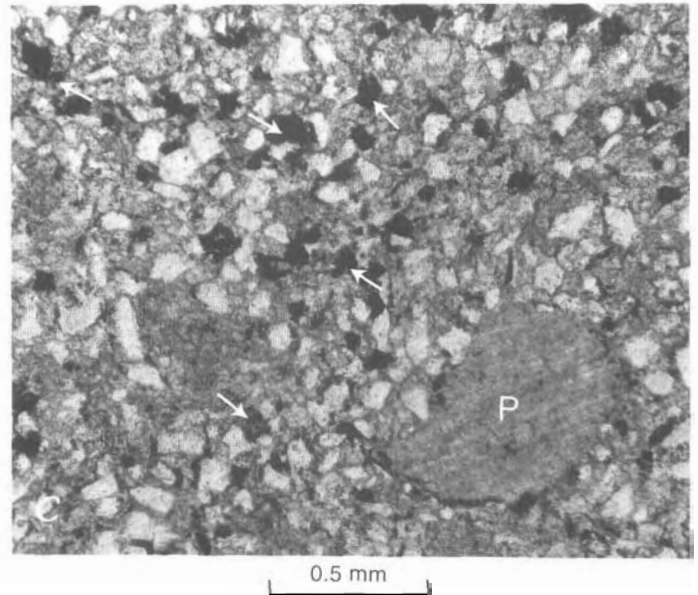
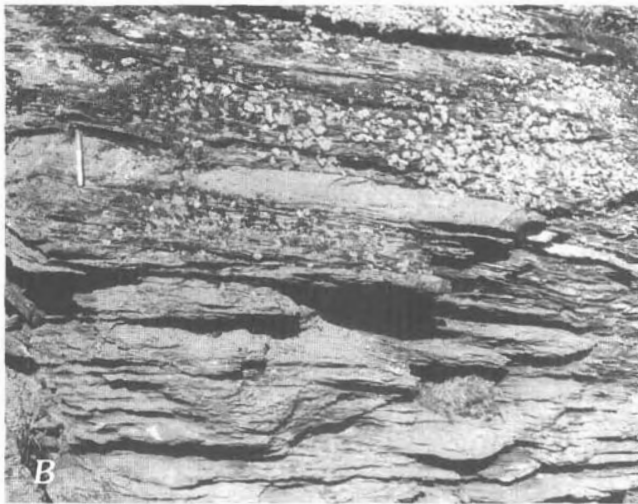
noncarbonate fraction of the calcarenite beds but includes abundant phyllosilicate pseudomatrix instead of calcite cement (fig. 8D).

Two samples from calcareous layers in the Isikut Member of the Kayak Shale were analyzed in thin section. Both are from the lower part of the member at locality 13 (fig. 2), where orange-weathering, limy layers a few millimeters to 5 cm thick make up less than 5 percent of the section and contain locally abundant pelmatozoans, brachiopods, and bryozoans. The layers consist of very fine to fine-grained, quartzose, dolomitic calcarenite like that described

above from the basal member of the Kayak in the Key Creek sequence.

#### AGE AND BIOFACIES

Comparison of conodont- and megafossil-based age determinations suggests that, as in the Key Creek sequence, both the Rough Mountain Creek unit and much (perhaps most) of the Kayak Shale in the Aniak River sequence are of late **Kinderhookian** age. Most samples from the Rough



**Figure 8.** Sedimentary features of Kinderhookian rocks in the Aniak River sequence at Rough Mountain Creek (fig. 2, loc. 12). **A**, Rough Mountain Creek unit; **B-D**, Kayak Shale. **A**, Thin, nodular beds of skeletal supportstone with partings of black, noncalcareous shale, 5 m below top of section, upper thrust sheet. **B**, Intercalated skeletal grainstone (bed with pen on it) and noncalcareous siltstone, base of section, lower thrust sheet. **C**, Calcarenite, 11 m above base of section, upper thrust sheet; contains abundant quartz (white grains), ferruginous dolomite rhombs (arrows), calcareous bioclasts such as pelmatozoan fragments (P), and calcite cement. **D**, Noncalcareous sandstone, 11.5 m above base of section in upper thrust sheet; chiefly quartz and phyllosilicate pseudomatrix.

Mountain Creek unit (table 1; see also Mull and others, this volume, table 1) produced conodonts of middle to late Kinderhookian age, but limestone near the base of the Rough Mountain Creek section yielded assemblages diagnostic of late, but not latest, Kinderhookian age (lower part of *Siphonodella isosticha*-Upper *Si. crenulata* Zone). Conodonts from the Kayak also chiefly indicate a middle to late Kinderhookian age, but brachiopods from one sample of the limestone and shale member, as well as several from the Isikut Member, denote the *Calvustrigis rutherfordi* Zone of late Kinderhookian age (Mull and others, this volume, table 1). These data thus suggest that most of the Kayak Shale and all of the overlying Rough Mountain Creek unit were deposited during the late Kinderhookian.

Conodont collections from the Aniuk River sequence represent a wider range of biofacies than do correlative samples from the Key Creek sequence (table 1). Finely interlayered packstone and grainstone 2.5 m above the base of the Rough Mountain Creek unit (fig. 2 and table 1, loc. 12, upper thrust sheet—sample 92AD63A-2.5) produce polygnathid biofacies conodonts, including some siphonodellids (figs. 9E-G); the species association and taphonomy suggest deposition on the outer shelf or slope. A collection from roughly the same stratigraphic position at this locality, but from the lower thrust sheet (92Mu10-2; Mull and others, this volume, table 1) contains conodonts of similar biofacies (polygnathid-pseudopolygnathid and rare siphonodellids) and environmental implications (middle shelf to slope).

Assemblages from the upper part of the Rough Mountain Creek unit indicate shallower depositional environments. Bryozoan-rich supportstone from the upper half of the unit at locality 11 (fig. 2, table 1) yielded bispathodid biofacies conodonts, chiefly *Bispathodus aculeatus plumulus*, nodosus morphotype, that suggest a high-energy, shallow-water depositional setting with normal-marine salinity. Coarse-grained, locally cherty crinoidal limestone from several localities (Mull and others, this volume) produced conodonts of bispathodid and related biofacies that imply shallow- to middle-shelf, locally high energy environments.

Conodonts from the Kayak Shale denote shallow- to mid-shelf, locally high energy depositional regimes much like those inferred for the upper part of the Rough Mountain Creek unit. Diagnostic samples from the limestone and shale member, obtained from skeletal supportstone, represent polygnathid and related biofacies. Calcarenite beds in the Isikut Member at locality 13 (fig. 2) yielded conodonts that are fragmented and fractured but not abraded, suggesting rapid burial in a high-energy environment. Other samples from this member reported in Mull and others (this volume) also denote a shallow- and (or) middle-shelf depositional setting. Particularly noteworthy are samples such as 93TM35L (USGS colln. 32198-PC), which contain conodonts representative of postmortem transport from or within

the patrogathid biofacies. These assemblages indicate very shallow water within or adjacent to a high-energy shoal.

## DEPOSITIONAL ENVIRONMENT

### ROUGH MOUNTAIN CREEK UNIT

Kinderhookian rocks of the Aniuk River sequence formed in depositional settings like those proposed for correlative strata in the Key Creek sequence. The Rough Mountain Creek unit is generally thicker in the Aniuk River sequence, indicating that carbonate production occurred over a longer time span and (or) in more optimal environments. Lithologic and faunal evidence denote shallow-water, inner- to middle-shelf settings for most of the unit, but conodont biofacies suggest that, at least locally, the basal beds formed in somewhat deeper, possibly outer-shelf to slope settings. The presence of these basal, deeper water beds implies that the transition from Kayak Shale to Rough Mountain Creek unit in this sequence was at least in part a response to a relative rise in sea level.

### KAYAK SHALE

Paleontologic and sedimentologic data suggest inner- to middle-shelf depositional environments for the Kayak Shale in the Aniuk River sequence. The upper member of the Kayak includes abundant siltstone and sandstone; the chiefly noncalcareous and diverse composition of these beds implies accumulation close to the siliciclastic source. Siltstone is, of course, even more abundant in the Isikut Member. Fragmented, but unabraded, conodonts from calcarenite in this member (table 1, loc. 13) support an interpretation of these beds as rapidly formed storm deposits. Other calcareous intervals, particularly those that contain conodonts of the patrogathid biofacies, probably accumulated in high-energy, near-shore shoals.

## COMPARISONS

The Rough Mountain Creek unit is distinguished from calcareous intervals in the underlying Kayak Shale by a number of features (tables 2, 3). In the Rough Mountain Creek unit, calcareous beds are chiefly limestone, weather gray, may contain notable amounts of chert, and are exposed in continuous intervals at least 8 m thick. In the Kayak Shale, calcareous beds consist both of limestone and abundant calcarenite, weather tan or orange (because of disseminated ferruginous dolomite), do not contain chert, and form intervals only 0.5-2 m thick. Bryozoan-rich supportstones and layers rich in sponge spicules are common in the Rough Mountain Creek unit but are absent from the Kayak. In summary, calcareous beds in the Kayak were deposited in a more limited range of environments subjected to a greater and more continuous siliciclastic influx

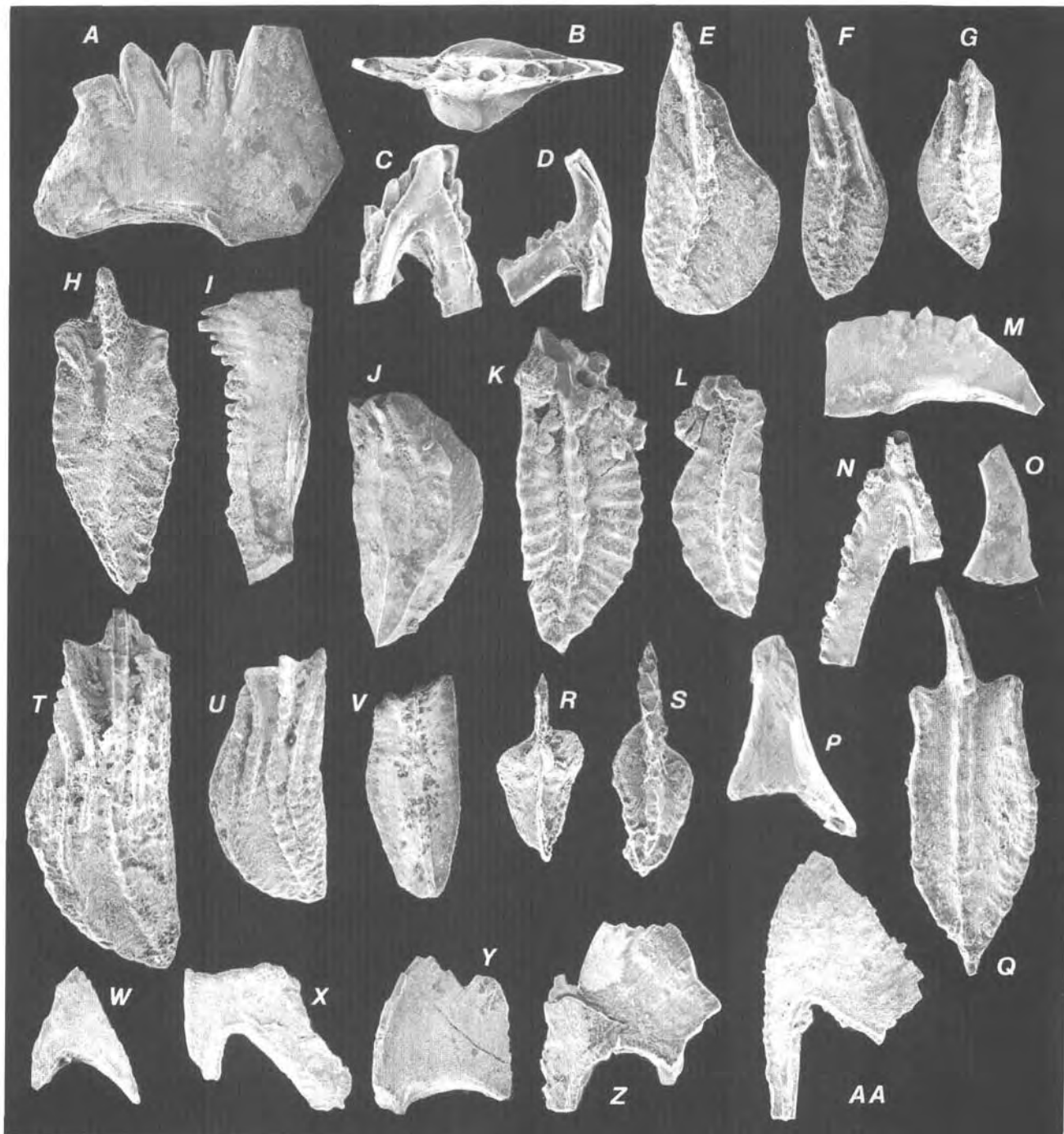


than were calcareous beds in the Rough Mountain Creek unit.

Some distinctions may also be made between Kinderhookian strata in the Key Creek sequence and in the Aniak River sequence (tables 2, 3). Exposures of the Rough Mountain Creek unit in the Key Creek sequence are somewhat thinner, more obviously mound shaped, contain more chert, and were deposited in a less diverse, generally shallower range of settings than correlative strata in the Aniak

River sequence. In particular, the basal part of the Rough Mountain Creek unit at locality 12 (fig. 2) accumulated in an outer-shelf to slope environment; no evidence of this depositional regime has been found in coeval beds in the Key Creek sequence.

The limestone and shale member of the Kayak Shale also differs somewhat between the two sequences. In the Key Creek sequence, the member contains more shale, less siltstone and sandstone, and slightly thicker calcareous in-



tervals than in the Aniak River sequence. Aniak River exposures include noncalcareous siltstone and sandstone not noted in the Key Creek, but they do not contain orange-weathering concretions. Calcareous beds in the Aniak River sequence contain more cross- and parallel-lamination and, like the overlying Rough Mountain Creek unit, appear to have formed in a more diverse suite of depositional environments.

## OTHER SEQUENCES

Kinderhookian conodonts have also been recovered from calcareous beds in several successions that, according to Mayfield and others (1988), are not part of the Endicott Mountains allochthon. These rocks are described below, along with our best estimates of their stratigraphic and structural positions.

### PICNIC SEQUENCE(?)

At locality 14 (fig. 2), about 5 km south of Mount Bupto, two thrust sheets that contain Kinderhookian rocks have been assigned to the Picnic sequence of the Picnic Creek allochthon (Mayfield and others, 1988). The lower thrust sheet contains 10 m of gray pelmatozoan limestone

beneath poorly exposed black chert and siliceous mudstone; we interpret these rocks as the Rough Mountain Creek unit and Kuna Formation of the Lisburne Group, respectively. Thrust above this section is an interbedded succession of uncertain affinity made up of about 150 m of limestone, calcarenite, quartz-rich sandstone, and mudstone that we assign to the Kayak Shale(?).

The Rough Mountain Creek unit at this locality forms several mound-shaped outcrops, 25-40 m long, of light-gray-weathering, medium-dark-gray limestone in even to undulatory, locally cross-laminated beds 2-25 cm thick. A few 5x50 cm, black chert nodules mark the base of the section, and millimeter-thick muddy partings were observed near the top. The limestone is pelmatozoan packstone and grainstone, locally interlayered on a millimeter to centimeter scale; some coarse grainstone layers are quite well sorted and contain broken and somewhat abraded grains. Minor constituents of these supportstones include bryozoans, brachiopods, rounded intraclasts of dark noncalcareous mud, a few percent angular quartz silt, and rare grains of glauconite.

The Kayak Shale(?) in the upper thrust plate consists of a calcareous, better exposed upper unit and a quartzose, rubbly lower unit, each about 75 m thick. The upper unit is yellowish-brown-weathering, gray, fossiliferous limestone and calcarenite (50 percent), dark argillite and mudstone

◀ **Figure 9.** Kinderhookian conodonts from calcareous rocks in the Howard Pass quadrangle (scanning electron micrographs; illustrated specimens are deposited in the U.S. National Museum, USNM, Washington, D.C.). See figure 2 for collection locations and table 1 for faunal and lithologic data.

A-I, Endicott Mountains allochthon, Aniak River sequence; loc. 12: A-D, limestone and shale member of the Kayak Shale; E-I, Rough Mountain Creek unit of the Lisburne Group.

A-D, *Syncladognathus geminus* (Hinde), ×75.

A, C, D, Lateral views of Pa, Sb, and Sc elements, USNM 489776-78, sample 92AD66-1 (USGS colln. 32458-PC).

B, Upper view of Pa element, USNM 489779, sample 92AD64-6 (USGS colln. 32456-PC).

E-I, Sample 92AD63A-2.5 (USGS colln. 32454-PC).

E, *Siphonodella crenulata* (Cooper), juvenile Pa element, upper view, ×50, USNM 489780.

F, *Siphonodella isosticha* (Cooper), Pa element, upper view, ×50, USNM 489781.

G, *Siphonodella* cf. *Si. isosticha* (Cooper), Pa element, upper view, ×50, USNM 489782.

H, *Pseudopolygnathus* n. sp.?, Pa element, upper view, ×50, USNM 489783. Lower side has expanded pit that extends as a posteriorly narrowing pseudokeel; resembles *Siphonodella sulcata* (Huddle) but *Pseudopolygnathus* n. sp.? has a flatter platform that widens anteriorly.

I, *Bispathodus stabilis* (Branson and Mehl), Pa element, inner lateral view, ×40, USNM 489784.

J-L, Endicott Mountains allochthon(?), Kayak Shale(?); loc. 14, sample 92ADo78B (USGS colln. 33320-PC). *Siphonodella sulcata* (Huddle), Pa elements, lower and upper views; J and L ×50 and K ×40, USNM 489785-87.

M-P, Allochthon uncertain, Kayak Shale(?); loc. 18, sample 92ARM69A (USGS colln. 32472-PC).

M, N, *Syncladognathus geminus* (Hinde), Pa element, outer lateral view, ×50 and S element, lateral view, ×100, USNM 489788, 89.

O, P, Redeposited Devonian icriodontid coniform elements, lateral views, ×100, USNM 489790, 91.

Q, Allochthon uncertain, Kayak Shale(?); loc. 16, sample 92AD37D (USGS colln. 32443-PC). *Polygnathus inornatus* E.R. Branson, Pa element, upper view, ×50, USNM 489792.

R-AA, Kelly River allochthon, Kelly sequence, Utukok Formation(?) of Lisburne Group; loc. 15, sample 92AD57E (USGS colln. 32451-PC).

R, S, *Polygnathus communis communis* Branson and Mehl, Pa elements, lower and upper views, ×75, USNM 489793, 94.

T-AA, *Siphonodella obsoleta* Hass, ×50. Although all elements of the siphonodellid apparatus are present in this sample and the CAI value is low, dolomitization of the host rock adversely altered their texture.

T-V, Pa elements, upper and lower views, USNM 489795-97. W, X, Melements, inner and outer lateral views, USNM 489798, 99.

Y-AA, Sa, Sb, and Sc elements, lateral views, USNM 489800-02.

Table 2. Comparison of lithologic and biostratigraphic data from Rough Mountain Creek unit and Utukok Formation(?), Howard Pass quadrangle, western Brooks Range

[Map number indicates locality shown on fig. 2. CAI, conodont color alteration index. Includes some conodont data from Mull and others (this volume). Abbreviations for skeletal and nonskeletal grain types: A, algae; BRA, brachiopod; BRY, bryozoan; C, coral; CH, chert; CO, coated grain; D, dolomite; E, epidote; F, feldspar; FO, foraminifer; G, gastropod; GL, glauconite; I, shaly or micritic intraclast; O, ostracode; P, phosphate; PE, pelmatozoan; PEL, peloids; PHY, phyllite; Q, quartz; SP, sponge spicule; T, tourmaline; W, white mica. Grain types are listed in approximate order of decreasing abundance]

STRATIGRAPHIC UNIT	Rough Mountain Creek unit	Rough Mountain Creek unit	Rough Mountain Creek unit	Utukok Formation(?)
ALLOCHTHON, SEQUENCE	Endicott Mountains Key Creek	Endicott Mountains Aniak River	Endicott Mountains(?) Aniak River(?)	Kelly River Kelly
MAP NO.	1, 2	10-12	14	15
THICKNESS (m)	8-17	10-35	About 10	At least 80
LITHOLOGIES	Limestone with locally abundant replacement chert and minor black shale and <b>mudstone</b>	Limestone with locally abundant replacement chert and minor black shale and <b>mudstone</b>	Limestone with minor chert nodules and <b>mm-thick</b> muddy partings	Limestone, locally dolomitized and (or) silicified; lesser calcarenite
CALCAREOUS ROCK TYPES AND INCLUDED GRAIN TYPES	Pelmatozoan and (or) bryozoan supportstone (PE, BRY, BRA, O, C, Q, I, D) Siliceous or calcareous spiculite with interlayers of skeletal supportstone (SP, PE, BRY, BRA, O, G, FO?, A?)	Pelmatozoan and (or) bryozoan supportstone (PE, BRY, BRA, O, C, FO, Q, I, D, P, G?, A?) Siliceous spiculite with interlayers of silicified skeletal supportstone (SP, PE, BRY, BRA, FO, D)	Pelmatozoan supportstone (PE, BRY, BRA, I, Q, GL)	Skeletal wackestone and packstone (PE, BRY, BRA, D) Skeletal <b>grainstone</b> (PE, O, BRA, PEL) Calcarenite (Q, PE, BRA, I, CO, CH, F, W, PHY, FO, T, E)
AGE, FAUNA, AND CAI	middle to late <b>Kinderhookian</b> Conodonts 2-4	late (but not latest) Kinderhookian Conodonts ~2.5-4	middle to late (but not latest) Kinderhookian Conodonts 1.5	middle to early late Kinderhookian Conodonts 2 or 3
BIOFACIES	Polygnathid, bispathodid	Polygnathid, bispathodid	Indeterminate	Siphonodellid
DEPOSITIONAL SETTING	Relatively shallow water, locally and (or) intermittently high energy shelf	Chiefly inner to middle shelf; locally outer shelf to slope	Shallow-water, relatively high energy shelf	Outer shelf or deeper

(40 percent), and gray-green to grayish-brown quartz-rich sandstone (10 percent), chiefly in **slabby** beds 1-5 cm thick. The lower unit is cream-colored, quartz-rich siltstone and sandstone with only minor calcareous layers.

Limestone sampled near the top of the upper unit is very poorly sorted skeletal packstone containing pelmatozoans, brachiopods, ostracodes, gastropods, notable and diverse algae (including probable dasycladacean and girvanellid forms), a few percent angular quartz silt, and rare glauconite. Some skeletal grains are micritized or have bored rims. Very fine to fine-grained calcarenite and noncalcareous sandstone were sampled near the base of the upper unit. Calcarenite weathers dark yellowish brown and contains 5-20 percent calcareous bioclasts (chiefly pelmatozoans and brachiopods), as much as 20 percent ferruginous dolomite, abundant quartz, and calcite cement. Minor constituents include chert, white mica, phosphate, and glauconite. Noncalcareous sandstone weathers pale yellowish brown and consists mostly of quartz, phyllosilicate-rich pseudomatrix, and at least 5 percent feldspar.

Conodonts indicate that the Rough Mountain Creek unit and the calcareous upper unit of the Kayak Shale(?) are of **Kinderhookian** age (table 1, loc. 14). Pelmatozoan packstone 0.5 m below the top of the Rough Mountain Creek unit yielded a middle to late (but not latest) Kinderhookian fauna. Packstone near the top of the Kayak(?) also produced middle to late Kinderhookian conodonts, and a collection of early to middle Kinderhookian age was obtained from calcarenite near the base of the upper unit. This last sample is the oldest definitively dated in this study and possibly the oldest Kinderhookian assemblage known from the study area (including those reported by Mull and others, this volume). Conodonts from both thrust plates at locality 14 have the lowest CAIs (1.5 and 2; table 1) of any Kinderhookian collections in the Howard Pass quadrangle.

Lithofacies and conodont biofacies of the rocks at locality 14 indicate a depositional setting much like that outlined for Kinderhookian strata elsewhere in the study area. Sedimentary structures and carbonate textures in the Rough Mountain Creek unit denote a shallow-water, relatively **high**

**Table 3.** Comparison of lithologic and biostratigraphic data from Kayak Shale and Kayak Shale(?), Howard Pass quadrangle, western Brooks Range

[Map number indicates locality shown on fig. 2. CAI, conodont color alteration index. Includes some conodont data from Mull and others (this volume). Abbreviations for skeletal and nonskeletal grain types: A, algae; B, biotite; BRA, brachiopod; BRY, bryozoan; C, coral; CC, calcite crystal or crystal aggregate; CH, chert; CHL, chlorite; D, dolomite; F, feldspar; G, gastropod; GL, glauconite; I, shaly or micritic intraclast; O, ostracode; P, phosphate; PE, pelmatozoan; PEL, peloid; PHY, phyllite; PL, plagioclase; Q, quartz; SL, sedimentary lithic grain; T, tourmaline; W, white mica; Z, zircon. Grain types are listed in approximate order of decreasing abundance]

STRATIGRAPHIC UNIT	Kayak Shale--limestone and shale member	Kayak Shale--limestone and shale member	Kayak Shale(?)--upper unit	Kayak Shale(?)
ALLOCHTHON, SEQUENCE	Endicott Mountains Key Creek	Endicott Mountains Aniuk River	Endicott Mountains(?) Aniuk River(?)	Uncertain--spatially associated with volcanic rocks
MAP NO.	2-7	10, 12	14	16-18
THICKNESS (m)	At least 28	At least 19	About 75	5-10
LITHOLOGIES	Mostly black shale and mudstone; lesser calcarenite, limestone, and dolomite concretions	Mostly black shale and mudstone, noncalcareous siltstone and fine-grained sandstone, and calcarenite; lesser limestone	Mostly limestone, calcarenite, dark argillite and mudstone; lesser quartzose sandstone	Mostly limestone; lesser calcarenite, noncalcareous siltstone and fine-grained sandstone, and shale
CALCAREOUS ROCK TYPES AND INCLUDED GRAIN TYPES	Pelmatozoan supportstone (PE, BRA, BRY, G, A, C, D, Q, P) Calcarenite (CC, Q, D, PE, O, CH, PHY, W, CHL, T, Z)	Pelmatozoan supportstone (PE, BRA, BRY, O, Q, D, I, G?, A?) Calcarenite (Q, PE, BRA, D, BRY, O, CH, G, A, PEL, PHY, W, CHL, SL, PL, T, Z, B?)	Skeletal packstone (PE, BRA, O, G, A, Q, GL) Calcarenite (Q, PE, BRA, D, CH, W, P, GL)	Skeletal supportstone (PE, BRA, O, BRY, PEL, Q, G, P) Peloidal supportstone (PEL, PE, BR, O) Calcarenite (Q, F, CC, D, CH, PHY, SL, CHL, W, T, Z)
AGE, FAUNA, AND CAI	middle to late (possibly late) Kinderhookian; Conodonts and brachiopods 3-4	late Kinderhookian ( <i>Calvustrigis rutherfordi</i> Zone) Conodonts and brachiopods 3-4	middle to late Kinderhookian near top of unit; early to middle Kinderhookian near base Conodonts 2	middle to late Kinderhookian Conodonts 2.5-3 Redeposited Devonian conodonts at loc. 18
CONODONT BIOFACIES	Bispathodid	Polygnathid, polygnathid-bispathodid, hindeodid-polygnathid, bispathodid	Bispathodid-polygnathid, pseudopolygnathid-hindeodid	Polygnathid
DEPOSITIONAL SETTING	Normal-marine, relatively shallow water, intermittently high energy shelf	Locally high energy, inner to middle shelf	Normal-marine, relatively high energy, inner to middle shelf	Locally high energy, normal-marine, middle shelf (locally deeper?)

energy environment. Conodonts from the upper unit of the Kayak Shale(?) represent the pseudopolygnathid-hindeodid and bispathodid-polygnathid biofacies, which suggest a shallow- to middle-shelf, normal-marine depositional regime; lithofacies data support this interpretation. The presence of glauconite in rocks of both thrust sheets suggests low rates of sedimentation (Wilson, 1975).

The rocks in both thrust sheets at locality 14 are unlike coeval strata, such as the Kurupa Sandstone of Mull and others (1987a), that are exposed in the Picnic Creek allochthon. The succession at locality 14 is most similar to Kinderhookian sections in the Aniuk River sequence of the Endicott Mountains allochthon (tables 2, 3).

### KELLY SEQUENCE

Limestone of Kinderhookian age crops out in the westernmost part of the Howard Pass quadrangle, on the

north flank of the De Long Mountains (fig. 2, loc. 15; table 2); Mayfield and others (1988) include these rocks in the Kelly sequence of the Kelly River allochthon. At this locality, about 80 m of very light to medium-dark-gray limestone underlain by several meters of orange-weathering, medium-gray calcarenite are in thrust contact with Devonian limestone to the south (fig. 10A) and with Cretaceous siliciclastic rocks to the north (C.G. Mull, written commun., 1990).

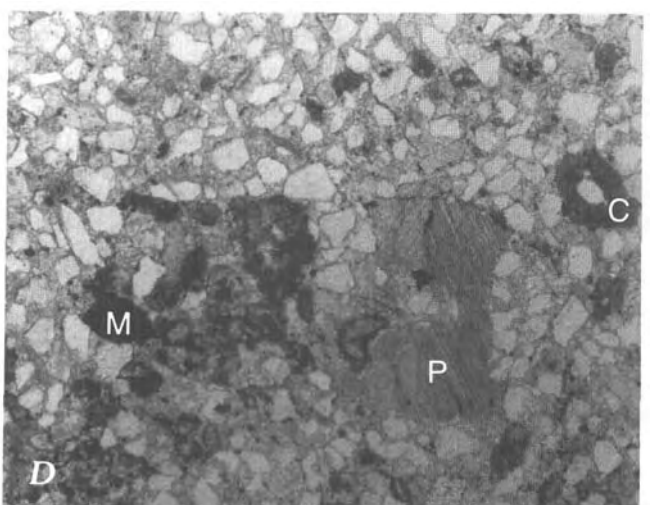
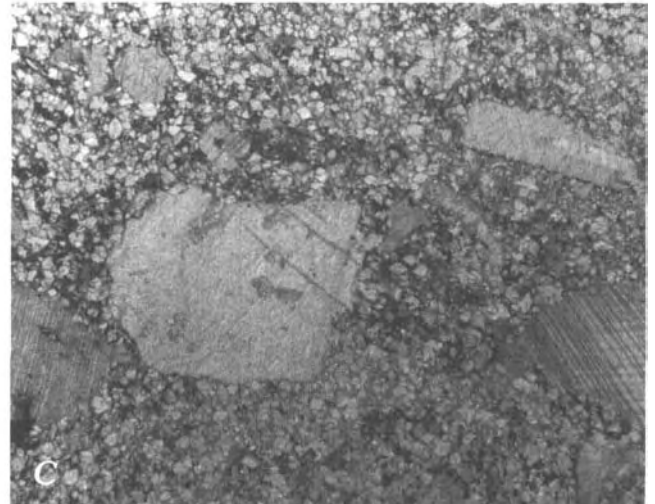
The Mississippian limestone forms platy- to flaggy-weathering thin beds (0.5-10 cm) with subordinate zones of thick to massive beds (>30 cm). Thin-bedded intervals are mostly skeletal wackestone and packstone (fig. 10B). Skeletal grainstone makes up most of the thicker bedded zones, as well as thicker (>5 cm) beds within the thin-bedded intervals. Thinner, muddier beds are preferentially dolomitized and richer in chert; bands and nodules of light-gray to black chert and partially silicified limestone make up about 5-15 percent of the total section.

Skeletal **pack/wackestones** contain abundant pelmatozoan debris and lesser bryozoans (mainly encrusting forms) and brachiopods; some crinoid ossicles and brachiopod valves are still articulated (fig. 10B). Bioclasts are commonly concentrated into millimeter-thick layers and lenses. The muddy matrix of most samples is largely replaced by euhedral dolomite rhombs (fig. 10C), and some skeletal grains are completely or partially silicified. Grainstones consist chiefly of pelmatozoan fragments with subordinate ostracodes, brachiopods, and peloids.

Calcarenite forms **slabby**, centimeter-thick beds and is fine to very fine grained and poorly sorted. Some beds are chiefly calcite-cemented, angular quartz, with subordinate

grains of chert, feldspar, white mica, phyllite, tourmaline, and epidote. Other beds contain these constituents as well as abundant calcareous grains, including pelmatozoan ossicles (some with micritized rims), brachiopods, echinoid spines, foraminifers, and notable micritic intraclasts and coated grains (fig. 10D).

Pelmatozoan **wacke/packstone** 50 m above the base of the limestone section yields conodonts of middle to early late Kinderhookian age (Upper *Si. duplicata* Zone to lower part of *Si. isosticha*-Upper *Si. crenulata* Zone). These conodonts represent the siphonodellid biofacies and suggest a depositional environment of outer shelf or deeper. Mud-supported textures, notable articulated bioclasts, and com-



**Figure 10.** Kinderhookian rocks in the Kelly sequence (fig. 2, loc. 15). A, View (toward north) of Kinderhookian limestone (center); Devonian limestone in lower left. B, Dolomitic skeletal wackestone that yielded middle to early late Kinderhookian conodonts; note abundant articulated crinoid ossicles on bedding surfaces. C, Photomicrograph of skeletal wackestone shown in B; pelmatozoan fragments float in a matrix of lime mud largely replaced by finely crystalline dolomite. D, Photomicrograph of calcarenite underlying Kinderhookian limestone; the sample contains abundant quartz, calcite cement, skeletal grains such as pelmatozoan fragments (P), and lesser coated grains (C) and micritic clasts (M).

plete siphonodellid apparatuses (figs. 9T-AA) in these rocks support this interpretation; grain-supported layers were probably introduced into a predominantly quiet, below-wave-base setting by storms and (or) turbidity flows.

We provisionally correlate the rocks at locality 15 with the lower part of the Utukok Formation of the Lisburne Group (Sable and Dutro, 1961; Dumoulin and Harris, 1992); this unit is widely exposed west of the study area, chiefly in sequences of the Kelly River allochthon. The Utukok is characterized by intervals of limestone tens to hundreds of meters thick intercalated with quartzose calcarenite and other siliciclastic lithologies. The lower part of the formation is known to be Kinderhookian, largely on the basis of conodonts, at a number of localities west and southwest of the study area (Dumoulin and Harris, 1992).

### UNCERTAIN AFFINITY

**Kinderhookian** calcareous strata are spatially associated with volcanic rocks at several localities in the study area. The stratigraphic unit and structural level (allochthon) represented by these calcareous rocks is uncertain. At Memorial Creek (fig. 2, loc. 16), 5-10 m of intercalated limestone, siliciclastic strata, and dark-gray, noncalcareous shale are thrust beneath basalts of uncertain age. Orange- to yellow-brown-weathering, medium-gray limestone makes up about two-thirds of the calcareous section and forms irregular, nodular beds, 2- to 5- (rarely, 10-) cm thick, locally separated by partings of gray shale. These beds are poorly sorted grainstone and grain/packstone made up chiefly of pelmatozoan fragments, lesser brachiopods, ostracodes, and bryozoans, rare peloids, and a few percent quartz silt. Some bioclasts are micritized.

Orange- to yellow-brown-weathering, greenish-gray, locally calcareous siltstone to fine-grained sandstone forms planar, 2- to 12-cm-thick beds with local wispy parallel laminae. Grains are angular to rounded quartz (about 80 percent), notable feldspar (5-10 percent), and minor chert, phyllite, mudstone, chlorite, white mica, tourmaline, and zircon. Some beds contain no carbonate; others are calcite cemented and include minor dolomite as well as probable calcareous clasts that are difficult to differentiate from cement.

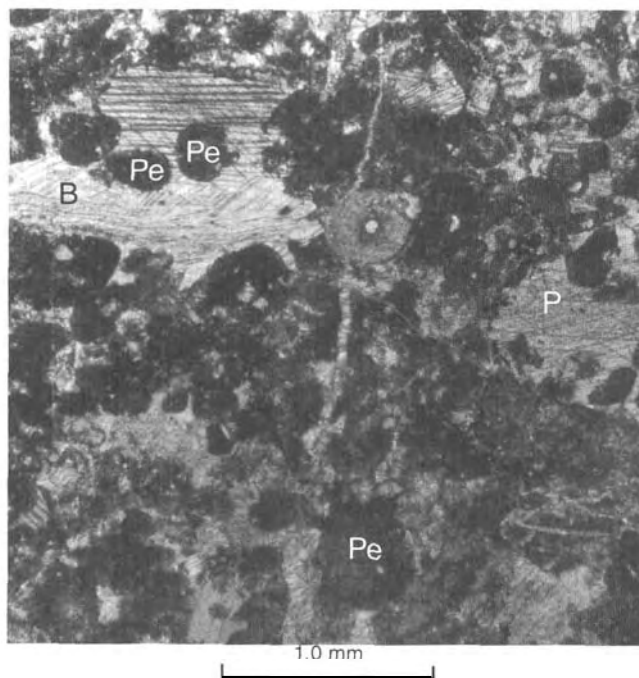
Nodular-bedded limestone near the top of this section contains conodonts of middle to late **Kinderhookian** age. This assemblage represents the polygnathid biofacies and indicates a moderately high energy, shallow-water, depositional environment with normal-marine salinity. Nodular limestone beds with shale partings and a stenohaline fauna are typical of a middle-shelf setting (Scholle and others, 1983; Dumoulin and Harris, 1992).

Calcareous rocks of Kinderhookian age are also found in thrust contact beneath mafic volcanic rocks in the Pupik Hills. At locality 17 (fig. 2), rubble of very light to light-

gray-weathering, medium-gray limestone and yellow-brown to gray, finely parallel- and cross-laminated, locally bioturbated calcareous siltstone crop out a few tens of meters structurally below basalt. The limestone is peloidal grain/packstone with rare pelmatozoans, brachiopods, and ostracodes; the irregular shape and relatively coarse (>200  $\mu\text{m}$ ) grain size of many of the peloids suggest that they are micritized skeletal grains (fig. 11). The calcareous siltstone is much like that described above from Memorial Creek. Conodonts of middle to late Kinderhookian age were obtained from the peloidal limestone; the assemblage formed by postmortem transport from the polygnathid toward the siphonodellid biofacies and suggests a depositional setting of middle shelf or deeper.

About 5 m of orange-weathering, gray limestone intercalated with shale is exposed in the northwestern Pupik Hills at locality 18 (fig. 2). The limestone contains locally abundant brachiopods, pelmatozoans, and bryozoans, as well as phosphatized fragments and steinkerns of gastropods and ostracodes and rare ichthyoliths. A conodont assemblage of middle to late Kinderhookian age, which includes some redeposited Devonian coniform elements, was recovered from these rocks. The assemblage represents the polygnathid biofacies and indicates a shelf depositional environment.

Thus, Kinderhookian strata structurally associated with mafic volcanic rocks in the study area consist of relatively thin intervals of fossiliferous limestone intercalated with calcarenite and (or) shale and were probably deposited in a middle-shelf setting. This association is most like the Kayak



**Figure 11.** Photomicrograph of peloidal grainstone of Kinderhookian age, east side of the Pupik Hills (fig. 2, loc. 17). B, brachiopod; P, pelmatozoan fragment; Pe, peloid.

Shale, but exposures are too limited and (or) too little studied to be confidently assigned to any particular allochthon or sequence (table 3). Several features of these rocks are unusual and have not been found in other Kayak sections in the study area. These features include the abundance of detrital feldspar in the Memorial Creek section, and the presence of abundant micritized bioclasts and of reworked Devonian conodonts at the Pupik Hills localities. Notable detrital feldspar is a distinctive component of Devonian and Carboniferous limestones in sequences of the Nuka Ridge allochthon (Mayfield and others, 1988), and feldspathic calcareous sandstone is reported from Kayak Shale in this allochthon in the Noatak quadrangle (Mayfield and others, 1987). Reworked Devonian conodonts in **Kinderhookian** strata in the Pupik Hills suggest that this section may originally have been underlain by Devonian carbonate rocks, which in turn implies an affinity with sequences of the Kelly River allochthon. Further study may allow more precise correlation of these distinctive Kinderhookian rocks.

## REGIONAL CORRELATION

As noted above, calcareous rocks of Osagean and younger Mississippian age are thicker and more widespread throughout the Brooks Range than are those of **Kinderhookian** age. However, basal Lisburne Group and Kayak Shale sections of definite **Kinderhookian** age are known from several localities in the western and central Brooks Range and can be compared with **Kinderhookian** calcareous rocks in the Howard Pass quadrangle.

### LISBURNE GROUP

**Kinderhookian** strata assigned to the Lisburne Group crop out chiefly in the western Brooks Range in the lower part of the Utukok Formation but have also been reported from the Atigun Gorge area in the central Brooks Range (fig. 1). The Utukok ranges in thickness from less than 30 to more than 1,000 m and consists of intercalated calcareous and siliciclastic rocks (mainly limestone, calcarenite, quartzarenite, and shale); the Utukok is recognized mainly in sequences of the Kelly River allochthon (Curtis and others, 1984; Sable and Dutro, 1961).

Faunas of **Kinderhookian** age, mostly conodonts, have been recovered from the Utukok Formation in the Baird Mountains, De Long Mountains, Misheguk Mountain, and Noatak quadrangles (fig. 1; Mayfield and others, 1984, 1987, 1990; Dumoulin and Harris, 1992), but detailed information on **Kinderhookian** lithofacies and biofacies is available only from the Baird Mountains (Dumoulin and Harris, 1992). In this area, the Utukok is at least 180 m thick; the lower third of the formation contains robust polygnathid conodonts of probable **Kinderhookian** age. These basal strata

are nodular-bedded skeletal **wacke/packstone**, with lesser interbeds of **quartzose** calcarenite and shale, deposited in a moderate-energy, middle-shelf environment.

**Kinderhookian** limestone also occurs in the lower Lisburne Group in the central Brooks Range, near Atigun Gorge (fig. 1), in strata generally included in the Endicott Mountains allochthon (e.g., Mull and others, 1987b). The Lisburne in this area is about 650 m thick and largely Osagean through Chesterian in age (Dumoulin and others, in press). Gray, slightly argillaceous(?) limestone at the base of the Lisburne about 25 km southwest of the gorge, however, produced **Kinderhookian**, chiefly bispathodid conodonts (92TM105B; T.E. Moore, U.S. Geological Survey, written commun., 1996; A.G. Harris, unpub. data). These beds are poorly sorted, coarse-grained, **pelmatozoan-bryozoan grain/packstone** (J.A. Dumoulin, unpub. data). Lithologically similar strata at the base of the Lisburne about 18 km to the northeast yielded conodonts of comparable biofacies, but probable Osagean age, and formed in a shallow-water shelf setting (Dumoulin and others, in press).

Elsewhere in the central Brooks Range, the age of the base of the Lisburne Group is generally considered to be Osagean but is typically poorly constrained. Armstrong and Mamet (1977, fig. 3) show the basal age as uncertain at all four of their central Brooks Range Lisburne sections. Lithofacies of these basal rocks, however, where known in detail, are unlike those of **Kinderhookian** strata in the Howard Pass quadrangle. At Shainin Lake (fig. 1), for example, definitively Osagean rocks are found about 80 m above the base of the section (J.A. Dumoulin and A.G. Harris, unpub. data). Basal Lisburne strata at this locality are undated but consist of argillaceous bryozoan wackestone and packstone, a facies rare or absent in Howard Pass **Kinderhookian** rocks.

### KAYAK SHALE

Calcareous strata of **Kinderhookian** age are also found in the Kayak Shale in both the western and central Brooks Range. West of the Howard Pass quadrangle, the Kayak has not been studied in detail. Late **Kinderhookian** conodonts were collected from at least one Kayak section in the De Long Mountains quadrangle in rocks of the Ipnavik River allochthon (Mayfield and others, 1990); no information is available on the lithofacies or biofacies of these rocks.

In the central Brooks Range, the type section of the Kayak Shale is at Shainin Lake (fig. 1; Bowsher and Dutro, 1957) in a thrust sheet of the Endicott Mountains allochthon (Mull and others, 1987b). The section is about 290 m thick; two calcareous members separated by at least 40 m of black shale make up the upper quarter of the formation (Bowsher and Dutro, 1957). The lower, argillaceous limestone member is as much as 24 m thick (Bowsher and Dutro, 1957) and consists of locally spiculitic bryozoan wackestone, in-

terbedded with black shale, which thickens and coarsens upward into bryozoan-pelmatozoan grainstone (J.A. Dumoulin, unpub. data). Conodonts from the base and top of the member are **Kinderhookian**; the upper collection represents the polygnathid biofacies and denotes a moderately shallow water, moderate-energy depositional environment with normal marine salinity (A.G. Harris, unpub. data). The upper, red limestone member is 5.5 m of coarse- to very coarse grained, moderately well sorted pelmatozoan grainstone; it contains common bryozoans and brachiopods, and Kinderhookian bispathodid conodonts suggestive of a middle-shelf, high-energy setting (J.A. Dumoulin and A.G. Harris, unpub. data).

At Atigun Gorge (fig. 1), the Kayak Shale is at least 210 m thick; less than 4 percent of the section is limestone (Dumoulin and others, in press). Two 4-m intervals of orange-weathering skeletal packstone and grainstone are separated by 152 m of shale. Bioclasts in these limestones are chiefly pelmatozoans and bryozoans, with minor brachiopods and sponge spicules. Conodonts from the lower limestone are definitively Kinderhookian; those from the upper limestone are late Kinderhookian or younger. Both collections represent the polygnathid biofacies and indicate deposition in high- to moderate-energy, moderately shallow water with normal-marine salinity. The limestones are interpreted as biostromes formed in large part by storm processes.

## DISCUSSION

The data reviewed above indicate that Kinderhookian calcareous strata included in the Kayak Shale are relatively widely distributed and are found in sequences of the Endicott Mountains, Picnic Creek(?), and Ipnarik River allochthons, as well as sequences of uncertain affinity associated with mafic volcanic rocks. Kinderhookian rocks assigned to the Lisburne Group, however, occur chiefly in three distinct types of succession. (1) In the Howard Pass quadrangle, Lisburne strata of Kinderhookian age are found mainly in the Endicott Mountains allochthon, where they constitute an anomalously thin, shallow-water section abruptly succeeded by black, fine-grained **siliciclastic** rocks of the Kuna Formation. These **Kinderhookian** sections represent early, short-lived establishment of **neritic** carbonate production that was extinguished, probably by relative sea-level rise, by at least early middle Osagean time (Dumoulin and others, 1994). (2) West of the Howard Pass quadrangle, Kinderhookian limestone included in the Lisburne has been identified mainly in sequences of the Kelly River allochthon. These sequences record shallow-water, chiefly carbonate accumulation that persisted from at least Middle Devonian through early Late Mississippian time (Dumoulin and Harris, 1992). (3) East of the Howard Pass quadrangle, Lisburne strata of Kinderhookian age are rare and form the base of thick, long-lived carbonate platform sequences in

the Endicott Mountains allochthon. Most **Kinderhookian** calcareous rocks throughout the Brooks Range were deposited in moderately shallow, locally or intermittently agitated water, although the lower argillaceous limestone member of the Kayak at Shainin Lake and some parts of the Utukok Formation in the western Brooks Range accumulated in quieter, possibly deeper water.

These distribution and lithofacies patterns have two implications for paleogeographic reconstruction of the western Brooks Range. First, sequences in the Howard Pass quadrangle that contain the Rough Mountain Creek unit differ sharply in lithofacies succession from other sequences, also included in the Endicott Mountains allochthon, that comprise thick successions of chiefly Osagean through Chesterian carbonate platform rocks. Such sequences are exposed in the study area at Mount Bupto and Lisburne Ridge (fig. 2) and in the western Killik River quadrangle in the Ivtuk Hills (fig. 2) (Dumoulin and others, 1993; Dumoulin and Harris, 1993; A.G. Harris, unpub. data). The abrupt juxtaposition of these contrasting lithofacies supports the suggestion, based on facies relations in the central Brooks Range, that there has been significant shortening within the Endicott Mountains allochthon (for example, Dumoulin and others, in press; Moore and others, 1989).

A second implication of our study is that Kinderhookian calcareous rocks in the Howard Pass quadrangle may represent a secondary source for chiefly Osagean carbonate turbidites of the Rim Butte unit (Dumoulin and others, 1993). These turbidites, widely distributed throughout the study area in sequences of the Ipnarik River allochthon, contain reworked **Kinderhookian** conodonts of uncertain provenance. Thrust sheets of the Kelly River allochthon contain rocks (Utukok Formation) that seem, on the basis of age, lithofacies, and biofacies, most likely to have produced the turbidites in the Rim Butte unit (Dumoulin and others, 1993), but these rocks are exposed chiefly west of the Howard Pass quadrangle. Kinderhookian strata in the study area, particularly the Rough Mountain Creek unit in the Aniuk River sequence, do not match as well in all aspects but do contain at least some of the conodonts (for example, *Siphonodella*) redeposited in the Rim Butte turbidites. In the paleogeographic reconstruction of **Mayfield** and others (1988), an epicontinental basin separated rocks of the Endicott Mountains and Ipnarik River allochthons during middle Paleozoic time, but this basin may not have formed until the Late Mississippian (Dumoulin and Harris, 1992). Thus, **Kinderhookian** calcareous rocks of the Howard Pass quadrangle may have provided an additional source for the Rim Butte turbidites.

Acknowledgments.—We thank S. Bie, J.H. Dover, R.T. Miyaoka, and J.M. Schmidt for collecting some samples examined in this study, and T.E. Moore for the loan of **Kinderhookian** limestone samples from the Atigun Gorge area.



## REFERENCES CITED

- Armstrong, A.K., and Mamet, B.L., 1977, Carboniferous microfacies, microfossils, and corals, Lisburne Group, arctic Alaska: U.S. Geological Survey Professional Paper 849, 144 p.
- 1978, Microfacies of the Carboniferous Lisburne Group, Endicott Mountains, Arctic Alaska, *in* Stelck, C.R., and Chatterton, B.D.E., eds., Western and Arctic Canadian biostratigraphy: Geological Association of Canada Special Paper 18, p. 333-394.
- Bathurst, R.G.C., 1976, Carbonate sediments and their diagenesis, *in* Developments in sedimentology, v. 12: New York, Elsevier, 658 p.
- Bowsher, A.L., and Dutro, J.T., Jr., 1957, The Paleozoic section in the Shainin Lake area, central Brooks Range, Alaska: U.S. Geological Survey Professional Paper 303-A, 39 p.
- Curtis, S.M., Ellersieck, Inyo, Mayfield, C.F., and TAILLEUR, I.L., 1984, Reconnaissance geologic map of southwestern Misheguk Mountain quadrangle, Alaska: U.S. Geological Survey Miscellaneous Investigations Map 1-1502, 2 sheets, scale 1:63,360.
- Dumoulin, J.A., and Harris, A.G., 1992, Devonian-Mississippian carbonate sequence in the Maiyumerak Mountains, western Brooks Range, Alaska: U.S. Geological Survey Open-File Report 92-3, 83 p.
- 1993, Lithofacies and conodonts of Carboniferous strata in the Ivotuk Hills, western Brooks Range, Alaska, *in* Dusel-Bacon, Cynthia, and Till, A.B., eds., Geologic studies in Alaska by the U.S. Geological Survey, 1992: U.S. Geological Survey Bulletin 2068, p. 31-47.
- Dumoulin, J.A., Harris, A.G., and Schmidt, J.M., 1993, Deep-water lithofacies and conodont faunas of the Lisburne Group, western Brooks Range, Alaska, *in* Dusel-Bacon, Cynthia, and Till, A.B., eds., Geologic studies in Alaska by the U.S. Geological Survey, 1992: U.S. Geological Survey Bulletin 2068, p. 12-30.
- 1994, Deep-water facies of the Lisburne Group, west-central Brooks Range, Alaska, *in* Thurston, D.K., and Fujita, Kazuya, eds., 1992 Proceedings of the International Conference on Arctic Margins: Anchorage, Alaska, U.S. Minerals Management Service Outer Continental Shelf Study MMS 94-0040, p. 77-82.
- Dumoulin, J.A., Watts, K.F., and Hams, A.G., in press, Stratigraphic contrasts and tectonic relationships between Carboniferous successions in the Trans-Alaska Crustal Transect corridor and adjacent areas, northern Alaska: Journal of Geophysical Research.
- Dunham, R.J., 1962, Classification of carbonate rocks according to depositional texture, *in* Ham, W.E., ed., Classification of carbonate rocks: American Association of Petroleum Geologists Memoir 1, p. 108-121.
- Epstein, A.G., Epstein, J.B., and Harris, L.D., 1977, Conodont color alteration—An index to organic metamorphism: U.S. Geological Survey Professional Paper 995, 27 p.
- Mayfield, C.F., Curtis, S.M., Ellersieck, Inyo, and TAILLEUR, I.L., 1984, Reconnaissance geologic map of southeastern Misheguk Mountain quadrangle, Alaska: U.S. Geological Survey Miscellaneous Investigations Map I-1503, 2 sheets, scale 1:63,360.
- 1990, Reconnaissance geologic map of the De Long Mountains A-3 and B-3 quadrangles and parts of the A-4 and B-4 quadrangles, Alaska: U.S. Geological Survey Miscellaneous Investigations Map I-1929, 2 sheets, scale 1:63,360.
- Mayfield, C.F., Ellersieck, Inyo, and TAILLEUR, I.L., 1987, Reconnaissance geologic map of the Noatak C5, D5, D6, and D7 quadrangles, Alaska: U.S. Geological Survey Miscellaneous Investigations Map I-1814, 1 sheet, scale 1:63,360.
- Mayfield, C.F., TAILLEUR, I.L., and Ellersieck, Inyo, 1988, Stratigraphy, structure, and palinspastic synthesis of the western Brooks Range, *in* Gryc, George, ed., Geology and exploration of the National Petroleum Reserve in Alaska, 1974-1982: U.S. Geological Survey Professional Paper 1399, p. 143-186.
- Moore, T.E., Nilsen, T.H., and Brosgé, W.P., 1989, Sedimentology of the Kanayut Conglomerate, *in* Mull, C.G., and Adams, K.E., eds., Dalton Highway, Yukon River to Prudhoe Bay, Alaska, Bedrock geology of the eastern Koyukuk basin, central Brooks Range, and eastcentral Arctic Slope, Guidebook 7, v. 2, Fairbanks, Alaska, Alaska Division of Geological and Geophysical Surveys, p. 267-276.
- Moore, T.E., Wallace, W.K., Bird, K.J., Karl, S.M., Mull, C.G., and Dillon, J.T., 1994, Geology of northern Alaska, *in* Plafker, George, and Berg, H.C., eds., The geology of Alaska: Boulder, Colo., Geological Society of America, The Geology of North America, v. G-1, p. 49-140.
- Mull, C.G., Crowder, R.K., Adams, K.E., Siok, J.P., Bodnar, D.A., Harris, E.E., Alexander, R.A., and Solie, D.N., 1987a, Stratigraphy and structural setting of the Picnic Creek allochthon, Killik River quadrangle, central Brooks Range, Alaska: a summary, *in* TAILLEUR, I.L., and Weimer, Paul, eds., Alaskan North Slope geology: Bakersfield, Calif., Pacific Section, Society of Economic Paleontologists and Mineralogists, Book 50, p. 649-662.
- Mull, C.G., Roeder, D.H., TAILLEUR, I.L., Pessel, G.H., Grantz, Arthur, and May, S.D., 1987b, Geologic sections and maps across Brooks Range and Arctic Slope to Beaufort Sea, Alaska: Geologic Society of America Map and Chart Series MC 28S, scale 1:500,000.
- Mull, C.G., TAILLEUR, I.L., Mayfield, C.F., Ellersieck, Inyo, and Curtis, S.M., 1982, New upper Paleozoic and lower Mesozoic stratigraphic units, central and western Brooks Range, Alaska: American Association of Petroleum Geologists Bulletin, v. 66, no. 3, p. 348-362.
- Mull, C.G., and Werdon, M.B., 1994, Generalized geologic map of the western Endicott Mountains, central Brooks Range, Alaska: Alaska Division of Geological and Geophysical Surveys Public-Data File Map 94-55, 1 sheet, scale 1:250,000.
- Ross, C.A., and Ross, J.R.P., 1988, Late Paleozoic transgressive-regressive deposition, *in* Wilgus, C.K., Hastings, B.S., Posamentier, H., Van Wagoner, J., Ross, C.A., and Kendall, C.G. St. C., eds., Sea-level changes: an integrated approach: Society of Economic Paleontologists and Mineralogists Special Publication 42, p. 227-247.
- Sable, E.G., and Dutro, J.T., Jr., 1961, New Devonian and Mississippian formations in the De Long Mountains, northern Alaska: American Association of Petroleum Geologists Bulletin, v. 45, p. 585-593.
- Scholle, P.A., Bebout, D.G., and Moore, C.H., eds., 1983, Carbonate depositional environments: American Association of Petroleum Geologists Memoir 33, 708 p.
- Wilson, J.L., 1975, Carbonate facies in geologic history: New York, Springer-Verlag, 471 p.

Reviewers: C.G. Mull and J.M. Schmidt

# Late Middle Cambrian Trilobites of Siberian Aspect from the Farewell Terrane, Southwestern Alaska

By James M. St. John and Loren E. Babcock

## ABSTRACT

An unnamed limestone unit in the platform facies of the White Mountain sequence of the Farewell terrane, southwestern Alaska, contains a rich assemblage of trilobites indicative of a late Middle Cambrian age. Newly identified trilobites seem to represent taxa low in the *Ptychagnostus punctuosus* Interval-zone that are equivalent to part of the Mayan Stage of Siberia. Twenty-eight species, some in open nomenclature, were identified, including five new species.

The platform facies of the White Mountain sequence of the Farewell terrane contains Proterozoic and Paleozoic sedimentary rocks. Based mostly on stratigraphic evidence, the Farewell terrane has been interpreted as native to Laurentia. However, many trilobite species and nearly all genera in upper Middle Cambrian strata are of Siberian biogeographic aspect; other species and genera are widespread in their distribution. Taxa characteristic of Laurentian open-shelf lithofacies have not been observed. Late Middle Cambrian trilobites from southwestern Alaska were evidently dispersed between present-day Siberia and Alaska, perhaps in cool water below a thermocline. Biogeographic information supports the possibility that Siberia was close to the Innuitian margin of Laurentia during the Middle Cambrian.

## INTRODUCTION

This paper documents some late Middle Cambrian trilobites from a limestone bed in an unnamed carbonate-siliciclastic unit in the platform facies of the White Mountain sequence of the Farewell terrane (previously referred to as the Nixon Fork terrane or subterrane; for example, Patton, 1978; Jones and others, 1987; Babcock and others, 1993) in southwestern Alaska. The unnamed Middle Cambrian unit contains two trilobite-rich beds that together yield some of the most diverse Cambrian trilobite assemblages known from Laurentia (the North American–Greenland paleocontinent). Taxa present in the succession have important implications for interpreting the tectonostratigraphic and paleogeographic history of the entire Farewell terrane. The

trilobites have been mentioned previously (Palmer and others, 1985; Babcock and Blodgett, 1992; Babcock and others, 1993, 1994; St. John and Babcock, 1994; Jacobson and others, 1996) and described in an unpublished report (St. John, 1994). Specimens are from limestone deposited in an inferred deep-shelf environment (see Babcock and others, 1993, 1995; St. John, 1994; St. John and Babcock, 1994) of a tectonostratigraphic terrane interpreted as native to Laurentia (Blodgett and Clough, 1985). However, most of the trilobite species and genera are not of Laurentian biogeographic aspect. Some taxa were widespread in the Middle Cambrian, but most have closest biogeographic affinities with taxa previously described from Siberia. This suggests that some species dispersed between Siberia and the Innuitian margin of Laurentia, probably in cool water (<10°C) below a marine thermocline. The close similarity of southwestern Alaskan and Siberian faunas supports the hypothesis that the Innuitian margin of Laurentia and Siberia were relatively close during the late Middle Cambrian.

## STUDY AREA AND STRATIGRAPHY

### STUDY AREA

Trilobites studied here are from a limestone bed in an unnamed unit that crops out in the Holitna basin in the Farewell terrane, southwestern Alaska (fig. 1). Trilobite-bearing beds are found in a small cliff (approximately 4.5 m high) in the NW<sup>1</sup>/<sub>4</sub>, sec. 27, T. 11 N., R. 42 W. of the Sleetmute A-2 quadrangle (1:63,360-scale series; fig. 2). Fossils are preserved in wackestone that is mostly light gray in color but is locally reddish or yellowish. Although fossils are distributed throughout the wackestone at this locality, trilobites are concentrated in the upper 40-cm-thick limestone bed. Some specimens were collected in 1984 by Sohio (now British Petroleum) geologists, and others were collected in 1984 by R.B. Blodgett (formerly of the U.S. Geological Survey).

Rocks interpreted as equivalent to those in the Holitna basin are exposed in the vicinity of Lone Mountain (fig. 1), southeast of McGrath, Alaska (McGrath C-4 and B-4

quadrangles, 1:63,360-scale series), where Proterozoic to lower Paleozoic stratigraphic relationships are clearer (Babcock and others, 1993, 1994). However, fossils from the Lone Mountain area have been highly altered by meta-

morphism and stylolitization. For these reasons, only the trilobites from the Holitna basin are described in this report, but inferred stratigraphic relationships are based principally on sections in the Lone Mountain area.

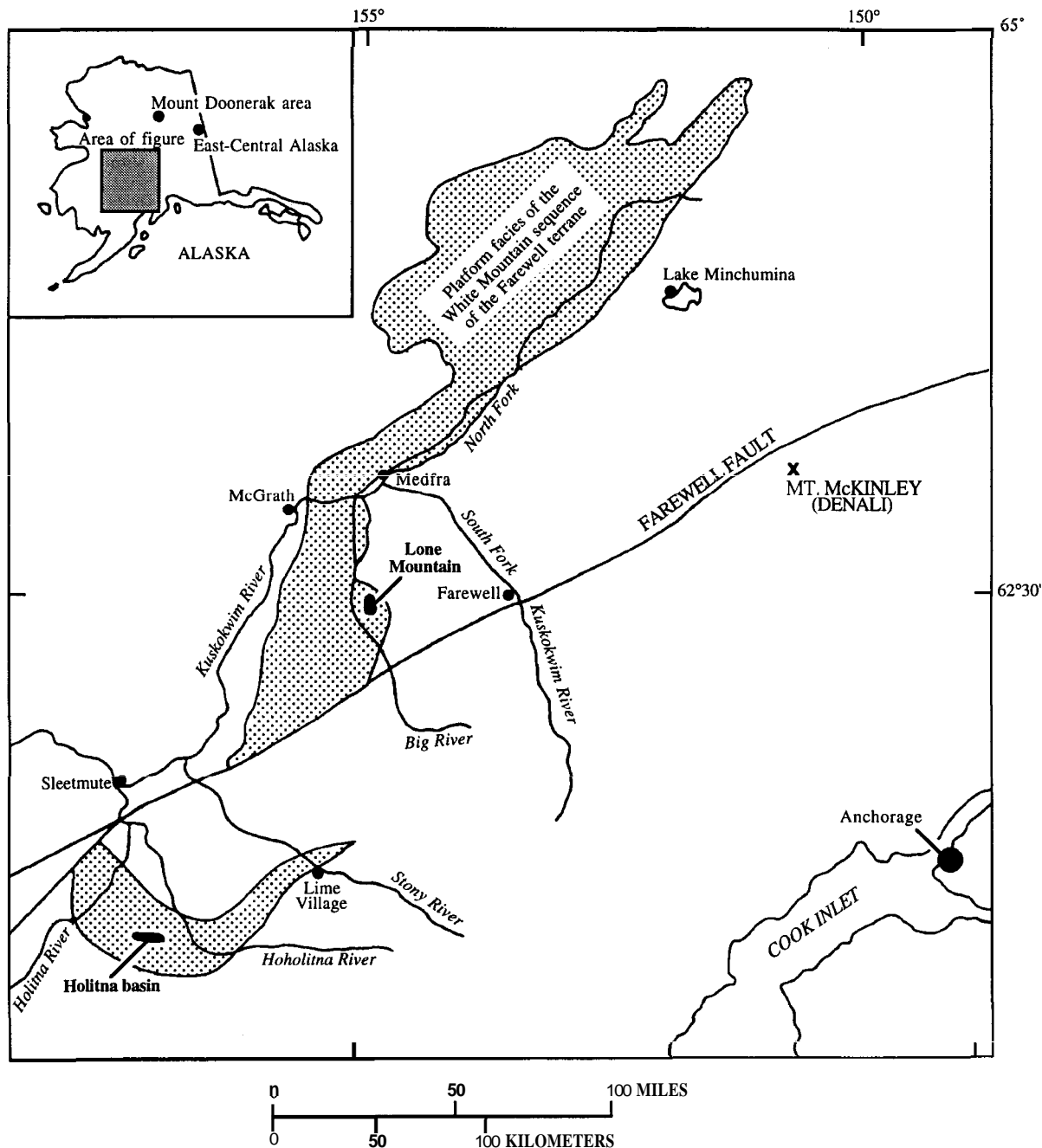
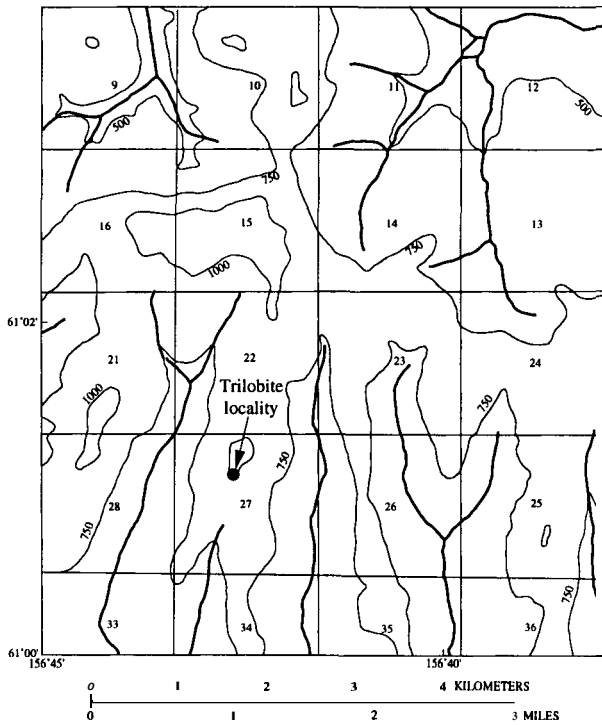


Figure 1. Index map of southwestern and west-central Alaska showing location of the platform facies of the White Mountain sequence of the Farewell terrane (modified from Jacobson and others, 1996). Map areas discussed in text: Holitna basin, area of Proterozoic and lower Paleozoic sedimentary-rock exposures in an east-west-trending anticlinorium in the Sleetmute A-2 quadrangle; and Lone Mountain, area of Proterozoic and lower Paleozoic sedimentary-rock exposures in the vicinity of Lone Mountain, McGrath B-4 and C-4 quadrangles.

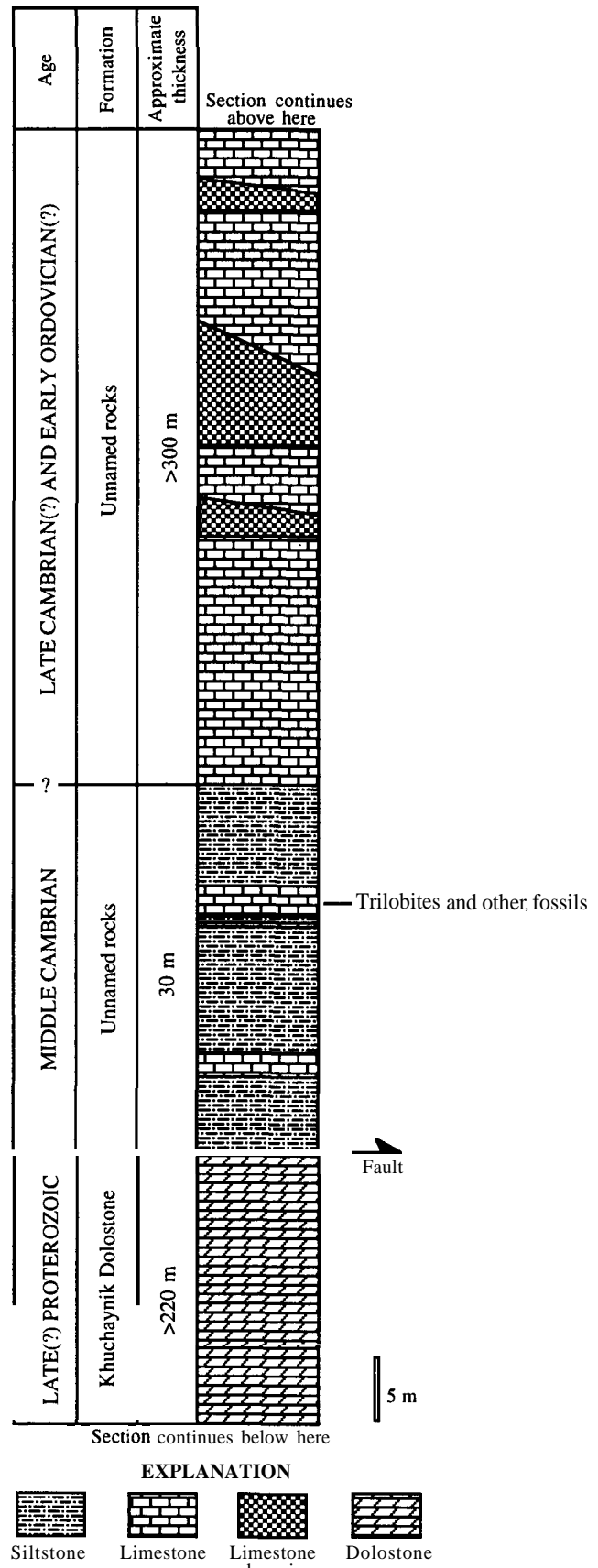
**PHYSICAL STRATIGRAPHY**

Middle Cambrian rocks from the Holitna basin and Lone Mountain areas (fig. 3) are part of a Proterozoic to Paleozoic succession of shelf carbonate and siliciclastic rocks that exceeds 950 m in thickness (Babcock and others, 1993, 1994, 1995; St. John 1994; Jacobson and others, 1996). The Proterozoic units are in fault contact with spo-



**Figure 2.** Index map of trilobite locality in the Holitna basin (see fig. 1; from U.S. Geological Survey, 1954, Sleetmute A-2 quadrangle, 1:63,360-scale series; contour interval is 250 ft, or 82.5 m).

**Figure 3.** Generalized Proterozoic and Cambrian-Ordovician stratigraphy in the platform facies of the White Mountain sequence of the Farewell terrane. Trilobites mentioned here are from the upper limestone bed in the Middle Cambrian interval of the section (after Jacobson and others, 1996). Trilobites and other fossils of somewhat older age within the Middle Cambrian (see Palmer and others, 1985) are also present in the lower limestone bed depicted on the stratigraphic column but were not identified for this paper. The approximate positions of thick carbonate breccia beds present in strata overlying the Middle Cambrian deposits are included in this columnar section for reference because these prominent ridge-forming carbonate breccias are visible during low-flying helicopter reconnaissance flights and aid in orienting geologists to the positions of the trilobite-bearing Middle Cambrian limestones.



radically exposed Middle Cambrian rocks consisting of light-brown, thinly bedded, quartzitic siltstones and two ridge-forming, trilobite-bearing wackestones. The upper wackestone is interbedded with siltstone near the base (fig. 3). A thick section of black, unfossiliferous, platy lime mudstones (Upper Cambrian to Lower Ordovician(?); Jacobson and others, 1996) conformably overlies the Middle Cambrian rocks. Several thick, ridge-forming carbonate breccia beds occur near the base of the black, platy lime **mudstone** unit (fig. 3). These carbonate breccia beds are inferred to have been deposited in relatively deep water, perhaps in a slope or basinal environment similar to that known from the Mount Doonerak area in north-central Alaska (fig. 1; Julian, 1989; Dumoulin and Harris, 1994), and elsewhere in Laurentia (for example, Jacobson and others, 1996, and references therein).

#### TECTONOSTRATIGRAPHIC TERRANE DEFINITION

The platform facies of the White Mountain sequence of the Farewell terrane (Decker and others, 1994) refers to rocks previously mapped as parts of the Nixon Fork, Dillinger, East Fork, and Minchumina terranes by Jones and others (1987). The platform facies consists primarily of a thick succession of lower Paleozoic carbonate rocks overlain by upper Paleozoic and Mesozoic quartz-carbonate terrigenous deposits (Patton, 1978). In addition to Paleozoic and Mesozoic rocks, Late(?) Proterozoic age rocks were recently identified in part of the succession (Babcock and others, 1994; Jacobson and others, 1996). Within the White Mountain sequence, shallow-water platform rocks of early to middle Paleozoic age grade laterally to the east into deeper water basinal lithofacies (Blodgett, 1983a; Bundtzen and Gilbert, 1983; Gilbert and Bundtzen, 1983; Blodgett and Clough, 1985; Blodgett and Gilbert, 1992a, b; Decker and others, 1994).

The provenance of rocks in the Farewell terrane has been the subject of changing interpretation. In an early interpretation, Coney and others (1980) considered the terrane to be exotic to North America because of its perceived position beyond the Paleozoic Cordilleran passive margin of Laurentia and its proximity to other terranes considered to be exotic. More recently, numerous workers interpreted the terrane as native to Laurentia (Potter and others, 1980; Plumley and others, 1981; Plumley and Coe, 1983; Blodgett, 1983a, 1983b; Churkin and Whitney, 1983; Gemuts and others, 1983; Potter, 1984; Vance-Plumley and others, 1984; Blodgett and Clough, 1985; Rohr and Blodgett, 1985; Potter and Blodgett, 1992; Babcock and others, 1993), based on paleomagnetic, paleontologic, stratigraphic, and structural data. Stratigraphic evidence indicates that the Farewell terrane was an extension of continental Laurentia that was disrupted by major transform faults (Blodgett and Clough, 1985). According to present coordinates, platform facies occur to the northwest and basinal facies to the southeast.

#### BIOSTRATIGRAPHY

Trilobites described here probably represent the lower part of the upper Middle Cambrian *Ptychagnostus punctuosus* Interval-zone or, less likely, both the upper Middle Cambrian *P. atavus* and the *P. punctuosus* Interval-zones of Robison (1984). Correlation of the fauna is based primarily on agnostoid trilobites and, to a lesser extent, on other trilobites (table 1). Agnostoids are the most useful trilobites for global biostratigraphic correlation of the Middle Cambrian (Robison, 1984), but such key agnostoid genera as *Ptychagnostus* and *Lejopyge* are not present in the Alaskan collections. Most of the non-agnostoid (libristomate and corynexochoid) genera are long ranging, which limits their value for biostratigraphy.

The biostratigraphic distributions of trilobite genera and species recorded here are summarized in table 1. Almost all the taxa have been recorded from strata of the *Ptychagnostus punctuosus* Interval-zone of Robison (1984), but most are also present in the *P. atavus* Interval-zone. Such rare taxa as *Juraspis*, *Tchaispis*, *Hartshillia clivosa*, and *Bailiaspis picta* have imperfectly known paleogeographic and biostratigraphic ranges in eastern Siberia. *Megagnostus? laevis*, *Juraspis schabanovi*, and *Tchaispis* n. sp. occur near the *P. atavus*-*P. punctuosus* Interval-zone boundary in eastern Siberia. Preference for a *P. punctuosus* Interval-zone assignment for the Alaskan collections is based on the presence of *Megagnostus? resecta*, which is found only in the *P. punctuosus* Interval-zone in Sweden, Denmark, and Spain. The zonal interpretation is further supported by correlation with a similar fauna from the lower *Centropleura oriens* Zone (=lower *Anomocarioides limbataeformis* Zone of Egorova and others, 1982) of Siberia (Shabanov and others, 1967), which seems to be equivalent to the *P. punctuosus* Interval-zone. Together, range data for trilobite species from Siberia (Egorova and others, 1982) and Alaska suggest a modified correlation scheme for comparing upper Middle Cambrian strata of Siberia with strata from elsewhere (fig. 4).

#### BIOGEOGRAPHY

Paleobiogeographic distributions of trilobites (figs. 5-7) from the platform facies of the White Mountain sequence of the Farewell terrane are summarized in table 2. The agnostoid trilobites (*Linguagnostus*, *Peronopsis*, *Megagnostus*, and *Peratagnostus*) have widespread distributions. Of the other trilobites, nearly all previously identified species are known from Siberia (table 2), where they are present in outer-shelf lithofacies (Korobov, 1973; Egorova and others, 1982). Three species are also known from the paleocontinent Baltica (present-day Scandinavia), and at least one species is present in peri-Gondwanan terranes (present-day Spain, England, and eastern Newfound-

Table 1. Biostratigraphic distribution of trilobite genera and species reported here from an unnamed upper Middle Cambrian limestone unit in the Holitna basin, Sleetmute A-2 quadrangle, southwestern Alaska

[Biostratigraphic range extensions into the *Ptychagnostus punctuosus* Interval-zone are here documented for *Proampyx difformis*, *Bailiaspis picta*, *Hartshillia clivosa*, *Tchaispis* n. sp., and *Granularaspis*.]

Taxa	Agnostoid Interval-zones (Robison, 1984)			
	<i>Ptychagnostus gibbus</i> Interval-zone	<i>Ptychagnostus atavus</i> Interval-zone	<i>Ptychagnostus punctuosus</i> Interval-zone	<i>Lejopyge laevigata</i> Interval-zone
<i>Linguagnostus gronwalli</i>		X	X	
<i>Peronopsis</i>	X	X	X	X
<i>Megagnostus? laevis</i>		X	X	
<i>Megagnostus? resecta</i>			X	
<i>Peratagnostus cicer</i>		X	X	X
<i>Proampyx acuminatus</i>		X	X	X
<i>Proampyx difformis</i>				X
<i>Juraspis schabanovi</i>			X	
<i>Bailiaspis picta</i>		X		
<i>Dasometopus breviceps</i>			X	X
<i>Hartshillia clivosa</i>	X?			
<i>Tchaispis korobovi</i>		X		
<i>Corynexochus perforatus</i>	X	X	X	
<i>Kootenia</i>	X	X	X	
<i>Anopolenus henrici</i>	X	X	X	
<i>Paradoxides</i>	X	X	X	X
<i>Solenopleura</i>	X	X	X	X
<i>Parasolenopleura</i>	X	X	X	X

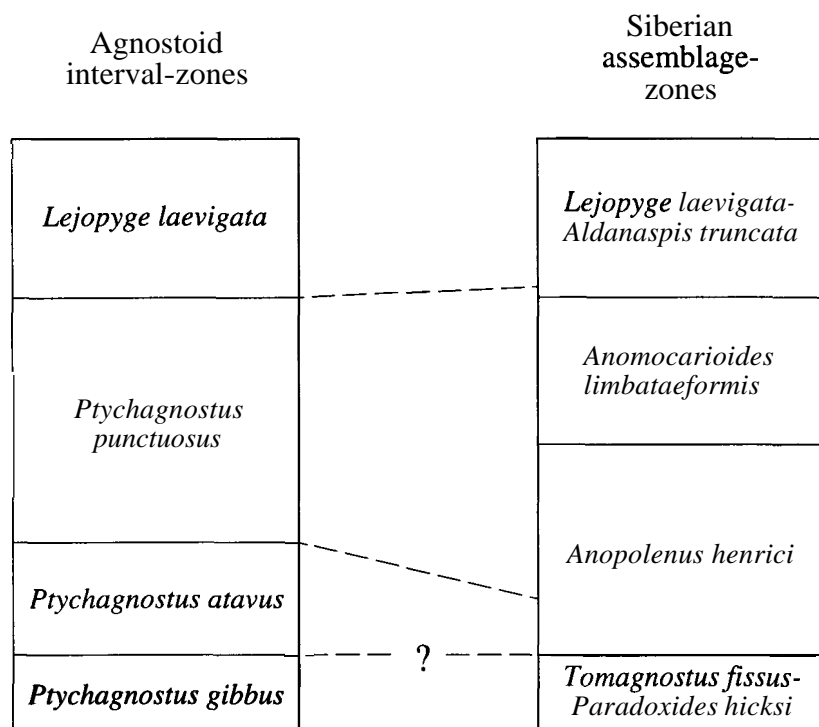


Figure 4. Proposed biostratigraphic correlation between Siberia (where trilobite assemblage zones are used) and elsewhere (using agnostoid interval-zones of Robison, 1984). Correlation is based on a comparison of the first appearances of key agnostoid species in Siberia (according to Egorova and others, 1982) and their appearances worldwide relative to Robison's (1984) interval-zones.



A



C



E



H



J



K



B



D



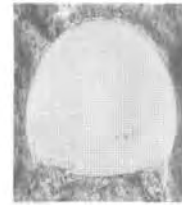
F



I



G



O



L



M



N



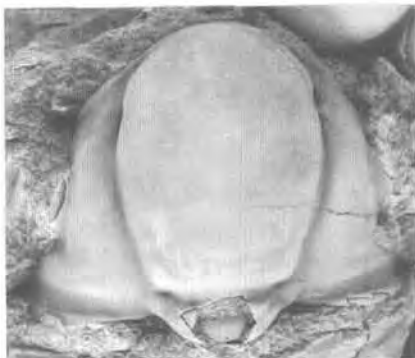
P



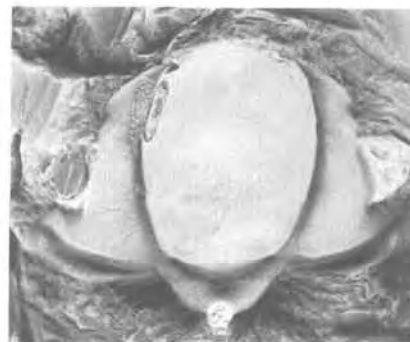
Q



R



S



T



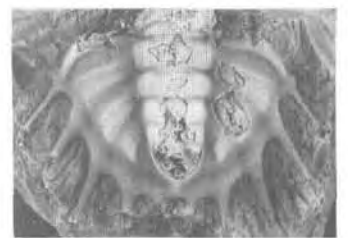
U



V



W



X

land). Other trilobites identified only to genus level have a Siberian or Baltic biogeographic aspect (*Solenopleura* and *Parasolenopleura*), were widespread (*Paradoxides*), or were pantropical (*Kootenia*) during the Middle Cambrian. The co-occurrence of cool-water (for example, *Paradoxides* and *Solenopleura*) and pantropical (for example, *Kootenia*) trilobite taxa is common in environments that had open-ocean access when those areas were in low paleolatitudes (for example, Babcock, 1994b). This co-occurrence is difficult to explain but may be the result of some pantropical genera such as *Kootenia* containing both cool-water-adapted species and warm-water-adapted species. However, the possibility that some species were rather eurytopic with respect to water temperature cannot be ruled out.

Biogeographic evidence suggests that the unnamed unit of the Farewell terrane was deposited in an area influenced by cool water, probably below the thermocline. Dispersal of trilobites of extra-Laurentian aspect in cool-water marine environments accounts for their presence in a native Laurentian terrane (see Babcock, 1994a, b; St. John and Babcock, 1994). This explanation has been used to account for the presence of putative cool-water trilobites of extra-Laurentian aspect in other Middle or Upper Cambrian, autochthonous Laurentian rocks from North Greenland (Babcock and Robison, 1989; Babcock, 1990; Babcock, 1994a, b) and Nevada (Cook and Taylor, 1975; Taylor and Cook, 1976; Taylor, 1976; Babcock, 1990). Importantly, a Middle Cambrian trilobite assemblage from an autochthonous terrane in the Mount Doonerak area of north-central Alaska (Dutro and others, 1984) also includes taxa having either a Siberian aspect or widespread distribution, but Middle Cambrian faunas from autochthonous Laurentian

rocks of east-central Alaska (Palmer, 1968) have biogeographic affinities with shallow-water, open-shelf lithofacies of Laurentia. Biogeographic distributions of Middle Cambrian Alaskan trilobites thus provide additional evidence for the existence of a permanent thermocline during the Middle Cambrian (see Babcock, 1994a, b).

The seemingly anomalous absence of some cosmopolitan open-shelf agnostoid taxa, such as *Ptychagnostus* and *Hypagnostus*, from the Farewell terrane may be explained by paleogeography. An embayment created adjacent to the peninsular extension of the Farewell terrane (see Blodgett and Clough, 1985) during the Middle Cambrian may have been restrictive enough to prevent water masses from delivering many open-shelf agnostoid taxa to the area that is now the Holitna basin.

The large number of trilobite taxa shared between inferred cool-water lithofacies of the Farewell terrane and Siberia suggests that Siberia may have been relatively close to the southwest Alaskan sector of the Innuitian margin of Laurentia during the late Middle Cambrian (fig. 8). Close proximity of these two areas during the Paleozoic was previously suggested by Hoffman (1991) and Condie and Rosen (1994). The hypothesis is also supported by other paleobiogeographic evidence from the Farewell terrane (Blodgett, 1983a, b; Potter, 1984; Blodgett and Gilbert, 1992b) and from a native Laurentian terrane in the Mount Doonerak area of the central Brooks Range (Dutro and others, 1984). Other regional geological data further support the hypothesis that Siberia was either a rift partner with the Cordilleran margin of Laurentia during the Late Proterozoic to early Paleozoic (Sears and Price, 1978) or was positioned close to the Innuitian margin of Laurentia (Hoffman, 1991; Condie and Rosen, 1994).

Acknowledgments.— We thank A.R. Palmer (Institute for Cambrian Studies) for sparking our initial interest in this project and for preparing and identifying many specimens. An earlier version of this paper (St. John, 1994) was reviewed by S.M. Bergstrom (The Ohio State University) and W.C. James (formerly of The Ohio State University, now with the Ohio Environmental Protection Agency). R.B. Blodgett (formerly of the U.S. Geological Survey) arranged field logistics, collected much of the material, and provided locality information. Raymond Sullivan (San Francisco State University) also collected some of the study material. Bill Beebe (Area Forester, McGrath Branch of the Alaska Department of Natural Resources, Division of Forestry) provided helicopter support for some of the field work. Tom Gray (The Ohio State University) printed some of the photographs. This work was supported by a grant from the National Geographic Society and a Seed Grant from The Ohio State University to Babcock, and by grants from Sigma Xi and the Friends of Orton Hall fund of The Ohio State University to St. John.

◀ Figure 5. Upper Middle Cambrian trilobites from a limestone bed in the platform facies of the White Mountain sequence of the Farewell terrane, Sleetmute A-2 quadrangle, Alaska; all specimens are testaceous unless otherwise noted and are located at The Ohio State University. A-D, *Linguagnostus* groenwalli Kobayashi: A, cephalon; B, pygidium; C, cephalon; D, pygidium; all  $\times 6$ . E-I, *Megagnostus? laevis* Pokrovskaya: E, cephalon; F, pygidium; G, pygidium (same specimen as in F) in lateral view; H, cephalon; I, cephalon (same specimen as in H) in lateral view; all  $\times 5$ . J, K, *Peratagnostus* cicer Tullberg: J, cephalon; K, pygidium; both  $\times 6$ . L, *Peronopsis* sp., broken pygidium,  $\times 5$ . M, N, *Megagnostus? resecta* Gronwall: M, cephalon; N, pygidium; both  $\times 4$ . O, undetermined agnostoid 1, cephalon,  $\times 6$ . P, undetermined agnostoid 2, broken cephalon,  $\times 5$ . Q, undetermined agnostoid 3, broken cephalon?,  $\times 5$ . R, *Kootenia?* sp., pygidium,  $\times 2$ . S-X, *Kootenia* n. sp.: S, cephalon,  $\times 2$ ; T, cephalon,  $\times 3$ ; U, labrum,  $\times 3$ ; V, pygidium,  $\times 2$ ; W, pygidium, latex cast of external mold,  $\times 3$ ; X, pygidium,  $\times 2$ .

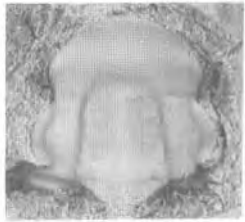


Figure 6. (p. 277) Upper Middle Cambrian trilobites from a limestone bed in the platform facies of the White Mountain sequence of the Farewell terrane, Sleetmute A-2 quadrangle, Alaska; all specimens are testaceous unless otherwise noted and are located at The Ohio State University. A, B, *Proampyx difformis* Angelin: A, cranidium; B, cranidium, latex cast of external mold; both  $\times 3$ ; C, D, *Proampyx acuminatus* Angelin: C, cranidium, latex cast of external mold; D, cranidium; both  $\times 3$ . E, *Proampyx?* sp., pygidium,  $\times 3$ . F, *Proampyx?* sp., pygidium,  $\times 3$ . G-K, *Juraspis* n. sp.: G, cranidium, latex cast of external mold; H, cranidium; I, pygidium, latex cast of external mold; J, pygidium; K, partly exfoliated librigena; all  $\times 3$ . L, *Juraspis schabanovi* Egorova in Egorova and Shabanov; dorsal shield having some sclerites displaced,  $\times 3$ . M, N, *Hartshillia clivosa* Lazarenko: M, cephalon; N, cephalon (same specimen as in M) in lateral view; both  $\times 3$ . O, *Juraspis?* sp., incomplete exoskeleton,  $\times 2$ . P-Q, *Dasometopus breviceps* Angelin: P, cephalon,  $\times 4$ ; Q, cephalon, latex cast of external mold,  $\times 3$ . R-U, *Tchiaspis* n. sp.: R, incomplete cephalon, latex cast of external mold,  $\sim 1.25\times$ ; S, cephalon,  $\times 2$ ; T, cephalon (same specimen as in S) in frontal view,  $\times 2$ ; U, incomplete cephalon,  $\sim 1.25\times$ . V, *Bailiaspis picta* Korobov: V, cephalon,  $\sim 1.25\times$ ; W, cephalon,  $\times 1.5$ . X, Y, *Bailiaspis* sp.: X, incomplete

Table 2. Biogeographic distribution of trilobite genera (G) and species (s) reported from an unnamed upper Middle Cambrian limestone unit in the Holitna basin, Sleetmute A-2 quadrangle, southwestern Alaska.

[Abbreviations: CR, Canadian Rocky Mountains; AP, Appalachia; EN, eastern Newfoundland; GB, Great Basin; NG, North Greenland; AU, Australia; AN, Antarctica; SC, South China; SB, Siberia; SD, Scandinavia; UK, England south of the Caledonian suture; BO, Bohemia; WE, western Europe (Spain and France); AK, eastern and central Alaska; NA, northern Africa (Morocco).]

Taxa	CR	AP	EN	GB	NG	AU	AN	SC	SB	SD	UK	BOWE	AK	NA
<i>Linguagnostus gronwalli</i>	-	-	-	-	s	G?	-	G	s	s	G	-	-	-
<i>Peronopsis</i> sp.	G	G	G	G	G	G	G	G	G	G	G	G	G	G
<i>Megagnostus? laevis</i>		G	G?	-	G	G	-	-	s	G	G	-	G	-
<i>Megagnostus? resecta</i>	-	G	G?	-	G	G	-	-	G	s	G	-	s	-
<i>Peratagnostus cicer</i>	-	s	s	-	s	G	-	s	s	s	-	-	-	G
<i>Proampyx acuminatus</i>	-	-	-	-	-	-	-	-	s	s	-	-	-	-
<i>Proampyx difformis</i>	-	-	-	-	-	-	-	-	s?	s	-	-	-	-
<i>Juraspis schabanovi</i>	-	-	-	-	-	-	-	-	s	-	-	-	-	-
<i>Bailiaspis picta</i>	-	-	G	-	-	-	-	-	s	G	G	-	G	-
<i>Dasometopus breviceps</i>	-	-	-	-	G	-	-	-	s	s	-	-	-	-
<i>Hartshillia clivosa</i>	-	-	G	-	G	-	-	-	s	-	G	-	-	-
<i>Tchiaspis</i> n.sp.	-	-	-	-	-	-	-	-	s	-	-	-	-	-
<i>Corynexochus perforatus</i>	G	-	G	G	G?	G	-	G	s	G	G	-	G	G
<i>Kootenia</i> n.sp.	G	G	-	G	G	G	G	G	G	G	G	-	-	G
<i>Granularaspis</i> n.sp.	-	-	-	-	-	-	-	-	G	-	-	-	-	-
<i>Anopolenus henrici</i>	-	-	s	-	-	-	-	-	s	-	s	-	-	-
<i>Paradoxides</i> n.sp.	-	G	G	-	-	-	-	-	G	G	G	G	G	G
<i>Solenopleura</i> sp.	?	G	-	-	G	?	G	-	G	G	G	G	G	-
<i>Parasolenopleura</i> sp.	-	-	-	-	G	-	-	-	-	-	G	-	G	-



A



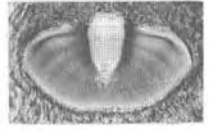
B



C



D



E



F



G



L



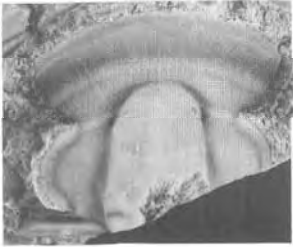
K



M



N



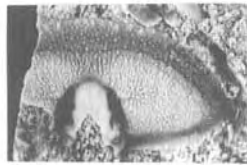
H



I



J



P



R



O



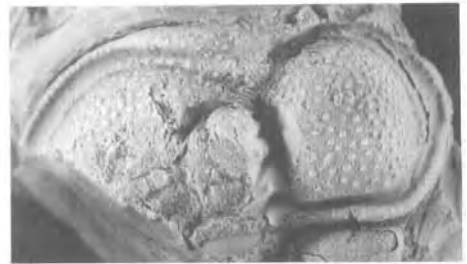
V



W



Q



S



X



Y



U



T



*A*



*B*



*C*



*D*



*E*



*F*



*G*



*H*



*J*



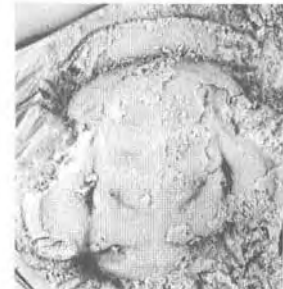
*I*



*K*



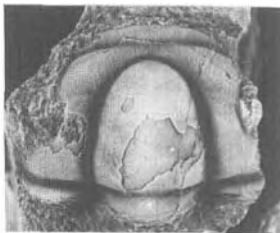
*L*



*M*



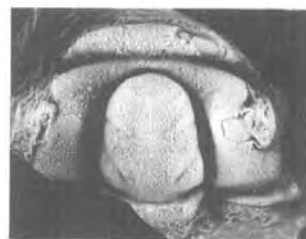
*N*



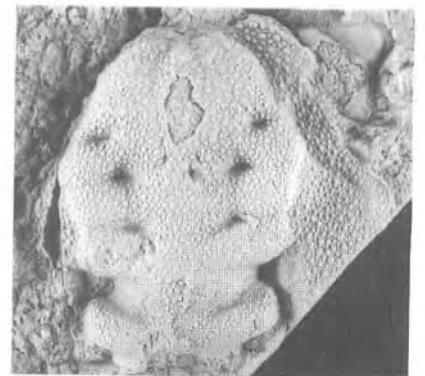
*O*



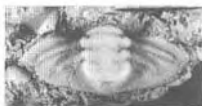
*P*



*S*



*U*



*Q*

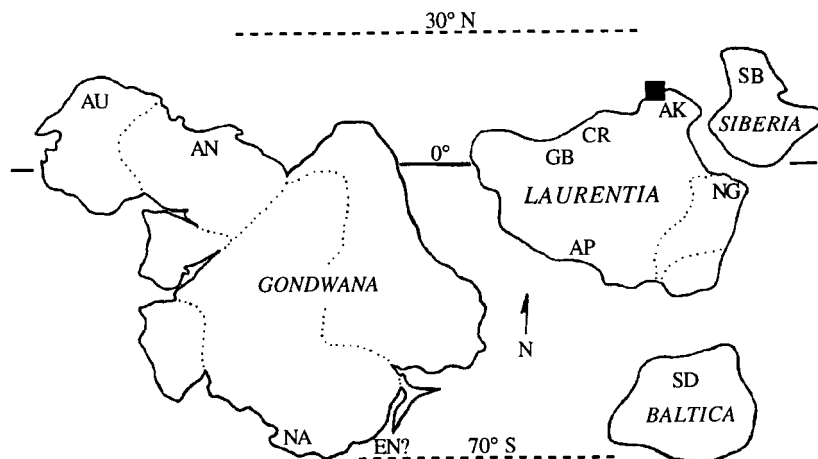


*R*



*T*

**Figure 7.** (p. 278) Upper Middle Cambrian trilobites from a limestone bed in the platform facies of the White Mountain sequence of the Farewell terrane, Sleetmute A-2 quadrangle, Alaska; all specimens are testaceous unless otherwise noted and are located at The Ohio State University. A-I, *Paradoxides* n. sp.: A, cranium,  $\times 1.25$ ; B, broken labrum,  $\times 1.5$ ; C, broken librigena,  $\times 1.25$ ; D, cranium,  $\times 1.5$ ; E, pygidium, latex cast of external mold,  $\times 2.5$ ; F, pygidium,  $\times 3$ ; G, broken anterior thoracic segment,  $\times 1.25$ ; H, broken posterior thoracic segment,  $\times 1.25$ ; I, malformed (teratologic?) pygidium showing lateral asymmetry and anomalous small spine on the right side,  $\times 2$ . J, *Anopolenus henrici* Salter, cranium,  $\times 1.5$ . K, *Corynexochus* cf. *C. perforatus* Lermontova, broken cranium,  $\times 7$ . L, M, undetermined polymeroid 1: L, broken cranium; M, broken cranium; both  $\times 3$ . N, undetermined polymeroid 2, incomplete librigena having long genal spine,  $\times 1$ . O-Q, *Parasolenopleura* sp.: O, broken cranium,  $\times 3$ ; P, cranium,  $\times 4$ ; Q, pygidium,  $\times 2$ . R-T, *Solenopleura* sp.: R, broken thoracic segment on same slab as specimen in T,  $\times 4$ ; S, broken cranium,  $\times 2$ ; T, pygidium,  $\times 4$ . U, *Granularaspis* n. sp., broken cranium,  $\times 1.5$ .



**Figure 8.** Paleogeographic map showing hypothesized relative positions of paleocontinents and other major tectonic blocks in the late Middle Cambrian. The map is hybridized from some published sources (mostly the  $-500$ -Ma reconstruction in Hoffman, 1991, and the Middle Cambrian reconstruction in Scotese and McKerrow, 1990) and inferences from biogeographic distributions of trilobites discussed in this paper. Dotted lines indicate margins of some major, present-day geographic features and are given for reference only. Black square indicates inferred paleogeographic position of the platform facies of the White Mountain sequence during the Middle Cambrian based on information in Plafker and Berg (1994). Approximate positions of most biogeographic regions discussed elsewhere in this paper are shown by two-letter abbreviations (see table 2). During the Middle Cambrian, most landmasses are inferred to have been located between  $30^{\circ}\text{N}$ . and  $70^{\circ}\text{S}$ . latitude; those positions are indicated for reference.

## REFERENCES CITED

- Babcock, L.E., 1990, Biogeography, phylogenetics, and systematics of some Middle Cambrian trilobites from open-shelf to basinal lithofacies of North Greenland and Nevada: Lawrence, Kans., University of Kansas, Ph.D. dissertation, 222 p.
- 1994a, Systematics and phylogenetics of polymeroid trilobites from the Henson Gletscher and Kap Stanton Formations (Middle Cambrian), North Greenland: *Grønlands geologiske Undersøgelse Bulletin*, v. 169, p. 79-127.
- 1994b, Biogeography and biofacies patterns of Middle Cambrian polymeroid trilobites from central North Greenland: palaeogeographic and palaeoceanographic implications: *Grønlands geologiske Undersøgelse Bulletin*, v. 169, p. 129-147.
- Babcock, L.E., and Blodgett, R.B., 1992, Biogeographic and paleogeographic significance of Middle Cambrian trilobites of Siberian aspect from southwestern Alaska [abs.]: *Geological Society of America Abstracts with Programs*, v. 24, no. 5, p. 4.
- Babcock, L.E., Blodgett, R.B., and St. John, James, 1993, Proterozoic and Cambrian stratigraphy and paleontology of the Nixon Fork terrane, southwestern Alaska, in Ortega-Gutiérrez, Fernando, Coney, P.J., Centano-Garcia, Elena, and Gómez-Caballero, Arturo, eds., *Proceedings of the First Circum-Pacific and Circum-Atlantic Terrane Conference: Universidad Nacional Autónoma de Mexico, Guanajuato, Mexico*, p. 5-7.
- 1994, New Late(?) Proterozoic-age formations in the vicinity of Lone Mountain, McGrath quadrangle, west-central Alaska, in Till, A.B., and Moore, T.E., eds., *Geologic studies in Alaska by the U.S. Geological Survey, 1993: U.S. Geological Survey Bulletin 2107*, p. 143-155.
- Babcock, L.E., and Robison, R.A., 1989, Paleobiogeographic significance of Middle Cambrian trilobites from North Greenland [abs.]: *Geological Society of America Abstracts with Programs*, v. 21, no. 6, p. A340.
- Babcock, L.E., St. John, James, Jacobson, S.R., Askin, R.A., and Blodgett, R.B., 1995, Neoproterozoic to early Paleozoic geologic history of the Nixon Fork subterrane of the Farewell terrane, Alaska [abs.]: *Geological Society of America Abstracts with Programs*, v. 27, no. 5, p. 2-3.
- Blodgett, R.B., 1983a, Paleobiogeographic affinities of Devonian fossils from the Nixon Fork terrane, southwestern Alaska, in Stevens, C.H., ed., *Pre-Jurassic rocks in western North American suspect terranes: Los Angeles, Calif., Pacific Section, Society of Economic Paleontologists and Mineralogists*, p. 125-130.

- 1983b, Paleobiogeographic affinities of Devonian fossils from the Nixon Fork terrane, southwestern Alaska [abs.]: Geological Society of America Abstracts with Programs, v. 15, no. 5, p. 428.
- Blodgett, R.B., and Clough, J.G., 1985, The Nixon Fork terrane—part of an in-situ peninsular extension of the Paleozoic North American continent [abs.]: Geological Society of America Abstracts with Programs, v. 17, no. 6, p. 342.
- Blodgett, R.B., and Gilbert, W.G., 1992a, Paleogeographic relations of lower and middle Paleozoic strata of southwest and west-central Alaska [abs.]: Geological Society of America Abstracts with Programs, v. 24, no. 5, p. 8.
- 1992b, Upper Devonian shallow-marine siliciclastic strata and associated fauna and flora, Lime Hills D-4 quadrangle, southwest Alaska, in Bradley, D.C., and Dusel-Bacon, C., eds., *Geologic studies in Alaska by the U.S. Geological Survey, 1991*: U.S. Geological Survey Bulletin 2041, p. 106-115.
- Bundtzen, T.K., and Gilbert, W.G., 1983, Outline of geology and mineral resources of the upper Kuskokwim region, Alaska: *Journal of the Alaska Geological Society*, v. 3, p. 101-117.
- Churkin, Michael, Jr., and Whitney, J.W., 1983, Craton fragments in Alaska and the Yukon [abs.]: Geological Society of America Abstracts with Programs, v. 15, no. 5, p. 429.
- Condie, K.C., and Rosen, O.M., 1994, Laurentia-Siberia connection revisited: *Geology*, v. 22, p. 168-170.
- Coney, P.J., Jones, D.L., and Monger, J.W.H., 1980, Cordilleran suspect terranes: *Nature*, v. 288, p. 329-333.
- Cook, H.E., and Taylor, M.E., 1975, Early Paleozoic continental margin sedimentation, trilobite biofacies, and the thermocline, western United States: *Geology*, v. 3, p. 559-562.
- Decker, John, Bergman, S.C., Blodgett, R.B., Box, S.E., Bundtzen, T.K., Clough, J.G., Coonrad, W.L., Gilbert, W.G., Miller, M.L., Murphy, J.M., Robinson, M.S., and Wallace, W.K., 1994, Geology of southwestern Alaska, in Plafker, George, and Berg, H.C., eds., *The geology of Alaska: Boulder, Colo., Geological Society of America, The Geology of North America*, v. G1, p. 285-310.
- Dumoulin, J.A., and Harris, A.G., 1994, Depositional framework and regional correlation of pre-Carboniferous metacarbonate rocks of the Snowden Mountain area, central Brooks Range, northern Alaska: U.S. Geological Survey Professional Paper 1545, 66 p.
- Dutro, J. T., Jr., Palmer, A.R., Repetski, J.E., and Brosgé, W.P., 1984, Middle Cambrian fossils from the Doonerak anticlinorium, central Brooks Range, Alaska: *Journal of Paleontology*, v. 58, p. 1364-1371.
- Egorova, L.I., Shabanov, Y.Y., Pegel, T.V., Savitsky [Savitskiy], V.E., Suchoy, S.S., and Chernysheva [Tchernysheva], N.E., 1982, Mayskiy yarusa stratotipicheskoy mestnosti (sredniy kembriy yugo-vostoka Sibirskoy platformy): *Trudy Mezhdovedstvennyy Stratigraficheskoy Komitet SSSR*, v. 8, 146 p. [The stratotype locality of the Mayan Stage (Middle Cambrian of the south-eastern Siberian Platform).] [In Russian]
- Gemuts, I., Puchner, C.C., and Steffel, C.I., 1983, Regional geology and tectonic history of western Alaska: *Journal of the Alaska Geological Society*, v. 3, p. 67-85.
- Gilbert, W.G., and Bundtzen, T.K., 1983, Paleozoic stratigraphy of the Farewell area, southwest Alaska Range, Alaska [abs.]: Alaska Geological Society Symposium, *New Developments in the Paleozoic Geology of Alaska and the Yukon*, Anchorage, Alaska, 1983, Program and Abstracts, p. 10-11.
- Hoffman, P.F., 1991, Did the breakout of Laurentia turn Gondwanaland inside-out?: *Science*, v. 252, p. 1409-1412.
- Jacobson, S.R., Blodgett, R.B., and Babcock, L.E., 1996, Organic matter and thermal maturation of lower Paleozoic rocks from the Nixon Fork subterrane of the Farewell terrane, west-central and southwestern Alaska, in Moore, T.E., and Dumoulin, J.A., eds., *Geologic studies in Alaska by the U.S. Geological Survey, 1994*: U.S. Geological Survey Bulletin 2152, p. 81-87.
- Jones, D.L., Silberling, N.J., Coney, P.J., and Plafker, George, 1987, Lithotectonic terrane map of Alaska (west of the 141st meridian): U.S. Geological Survey Miscellaneous Field Studies Map MF-1874-A, 1 sheet, scale 1:250,000.
- Julian, F.E., 1989, Structure and stratigraphy of lower Paleozoic rocks, Doonerak window, central Brooks Range, Alaska: Houston, Tex., Rice University, Ph.D. dissertation, 128 p. [Not seen; cited, Dumoulin and Harris, 1994, p. 48.]
- Korobov, M.N., 1973, Trilobity semeystva Conocoryphidae i ikh znachenie dlya stratigrafii kembriyskikh otlozheniy: *Trudy Geologicheskogo Instituta*, v. 211, 176 p. [Trilobites of the family Conocoryphidae and their importance for the stratigraphy of Cambrian deposits.] [In Russian]
- Palmer, A.R., 1968, Cambrian trilobites of east-central Alaska: U.S. Geological Survey Professional Paper 559-B, 115 p.
- Palmer, A.R., Egbert, R.M., Sullivan, Raymond, and Knoth, J.S., 1985, Cambrian trilobites with Siberian affinities, southwestem Alaska [abs.]: *American Association of Petroleum Geologists Bulletin*, v. 69, p. 295.
- Patton, W.W., 1978, Juxtaposed continental and oceanic-island arc terranes in the Medfra quadrangle, west-central Alaska, in Johnson, K.M., *The United States Geological Survey in Alaska: Accomplishments during 1977*: U.S. Geological Survey Circular 772-B, p. 38-39.
- Plafker, George, and Berg, H.C., 1994, Overview of the geology and tectonic evolution of Alaska, in Plafker, George, and Berg, H.C., eds., *The geology of Alaska: Boulder, Colo., Geological Society of America, The Geology of North America*, v. G1, p. 989-1021.
- Plumley, P.W., and Coe, R.S., 1983, Paleomagnetic data from Paleozoic rocks of the Nixon Fork terrane, Alaska and their tectonic implications [abs.]: Geological Society of America Abstracts with Programs, v. 15, no. 5, p. 428.
- Plumley, P.W., Coe, R.S., and Patton, W.W., 1981, Paleomagnetic study of the Nixon Fork terrane, west-central Alaska [abs.]: Geological Society of America Abstracts with Programs, v. 13, no. 7, p. 530.
- Potter, A.W., 1984, Paleobiogeographical relations of Late Ordovician brachiopods from the York and Nixon Fork terranes, Alaska [abs.]: Geological Society of America Abstracts with Programs, v. 16, no. 6, p. 626.
- Potter, A.W., and Blodgett, R.B., 1992, Paleobiogeographic relations of Ordovician brachiopods from the Nixon Fork terrane, west-central Alaska [abs.]: Geological Society of America Abstracts with Programs, v. 24, no. 5, p. 76.
- Potter, A.W., Gilbert, W.G., Ormiston, A.R., and Blodgett, R.B., 1980, Middle and Upper Ordovician brachiopods from Alaska and northern California and their paleogeographic implica-

- tions [abs.]: Geological Society of America Abstracts with Programs, v. **12**, p. **147**.
- Robison, R.A., 1984**, Cambrian Agnostida of North America and Greenland, part 1, Ptychagnostidae: University of Kansas Paleontological Contributions, Paper **109**, **59** p.
- Rohr, D.M., and Blodgett, R.B., **1985**, Upper Ordovician Gastropoda from west-central Alaska: Journal of Paleontology, v. **59**, p. **667-673**.
- St. John, J.M., **1994**, Systematics and biogeography of some upper Middle Cambrian trilobites from the Holitna basin, southwestern Alaska: Columbus, Ohio, The Ohio State University, **M.S.** thesis, **90** p.
- St. John, James, and Babcock, L.E., **1994**, Biogeographic and paleogeographic implications of Middle Cambrian trilobites of extra-Laurentian aspect from a native **terrane** in southwestern Alaska [abs.]: Geological Society of America Abstracts with Programs, v. **26**, no. **5**, p. **63**.
- Scotese, C.R., and McKerrow, W.S., **1990**, Revised world maps and introduction, in McKerrow, W.S., and Scotese, C.R., eds., Palaeozoic palaeogeography and biogeography: Geological Society Memoir, no. **12**, p. **1-21**.
- Sears, J.W., and Price, R.A., **1978**, The Siberian connection: a case for Precambrian separation of the North American and Siberian cratons: Geology, v. **6**, p. **267-270**.
- Shabanov, Y.Y., Savitskiy, V.E., and Chernysheva [Tchemysheva], N.E., **1967**, Biostratigrafiya Mayskogo yarusa Igarskogo rayona: Trudy Sibirskogo Nauchno-Issledovatel'skogo Instituta Geologii, Geofiziki i Mineralnogo Syrya (SNIIGGIMS), v. **55**, p. **59-65**. [Biostratigraphy of the Mayan Stage in the **Igarka** region.] [In Russian]
- Taylor, M.E., **1976**, Indigenous and redeposited trilobites from Late Cambrian basinal environments: Journal of Paleontology, v. **50**, p. **668-700**.
- Taylor, M.E., and Cook, H.E., **1976**, Continental shelf and slope facies in the Upper Cambrian and lowest Ordovician of Nevada: **Brigham** Young University Geology Studies, v. **23**, no. **2**, p. **181-214**.
- Vance-Plumley, Peggy, Plumley, P.W., Coe, R.S., and Reid, Jane, **1984**, Preliminary paleomagnetic results from three Ordovician carbonate sections in the **McGrath** quadrangle, central Alaska [abs.]: Eos (American Geophysical Union Transactions), v. **65**, no. **45**, p. **866**.
- Reviewers: **Marti** Miller, A.R. Palmer, and R.A. **Robison**

# Apatite Fission-Track Thermotectonic History of Crystalline Rocks in the Northern Saint Elias Mountains, Alaska

By Paul B. O'Sullivan, George Plafker, and John M. Murphy

## ABSTRACT

Apatite fission-track data for 13 crystalline rock samples indicate rapid regional Neogene denudation within the northern Saint Elias Mountains in Alaska. All samples but one record rapid Pliocene and early Pleistocene cooling ( $4.5\text{--}1.3$  Ma) in all major structural blocks. The one exception is from a diorite block in *mélange* of the coastal foothills that yields a late Miocene age ( $9.5\pm 2.3$  Ma). Calculated denudation rates for the group of 12 young samples average from 1.5 to 1.9 **km/Ma**, and the rates are fairly uniform over most of the area sampled. Exposure of these samples at the surface today requires about 4.5-8 km of denudation since the samples began cooling below paleotemperatures of about  $110^{\circ}\text{C}$ . Continued rapid denudation of the region is indicated by local Holocene marine terraces, by coseismic uplift of shorelines, and by extreme topographic relief in an alpine environment that is characterized by high erosion rates.

## INTRODUCTION

The purpose of this study was to obtain rocks suitable for apatite fission-track dating and to relate these data to the thermotectonic history of the northern Saint Elias Mountains and the adjacent foothills and lowlands in Alaska. Fission tracks in apatite grains preserve a record of the thermal history of the host rock below temperatures of approximately  $110^{\circ}\text{C}$ , making them ideal for testing models of denudation of upper-crustal rocks (Naeser, 1979; Gleadow and others, 1986). Quantitative laboratory and natural annealing studies have shown that for geologic time intervals on the order of  $10^6\text{--}10^8$  yr, fission-track ages and the lengths of confined tracks are reduced when apatite is subjected to temperatures between approximately 60 and  $110^{\circ}\text{C}$  (Gleadow and others, 1986). The length reduction of confined tracks in apatite results in reduction of the fission-track age. Thus, the fission-track age, combined with the length distribution of the confined tracks, directly reflects

the thermal history of the host rock below  $110^{\circ}\text{C}$  (Gleadow and others, 1986).

The northern Saint Elias Mountains and the adjacent foothills are of particular interest for fission-track studies because the topography, geology, and historic earthquake data all indicate late Cenozoic tectonic uplift in this region. Furthermore, this region is an ideal location for fission-track denudation studies because of a fortuitous combination of high topographic relief, an abundance of apatite-bearing crystalline rocks, availability of thermal data and samples from deep exploratory wells along the coastal lowlands, and a good regional geologic framework (Plafker and others, 1994a; G. Plafker, unpub. data) within which to interpret the fission-track data.

In this paper we present the data and interpretations of 13 fission-track analyses of apatite from crystalline rocks from the Yakutat and Mount Saint Elias 1:250,000 scale quadrangles of the northern Saint Elias Mountains in Alaska (fig. 1). Sample location, elevation, crystallization age, and lithology are given in table 1; the fission-track analytical data are presented in table 2. The time scale used throughout this manuscript was that of Harland and others (1990).

Samples were collected during a U.S. Geological Survey regional geologic mapping and mineral resource assessment project from 1967 to 1969 and during subsequent field work between 1978 and 1989. The fission-track samples used in this study had been previously dated by K-Ar or U-Pb methods or were from intrusive bodies of known age. All the fission-track samples are from granitoid rocks of intermediate composition except for one (#2) which is a granulitic quartzofeldspathic schist. The K-Ar and U-Pb dates provide protolith crystallization ages of the samples, whereas the apatite analyses provide data on denudation rates above a depth that corresponds to the annealing temperature of about  $110^{\circ}\text{C}$ . The samples analyzed for fission tracks represent all of the major lithotectonic blocks in the area with the exception of the Mount Cook block, and were chosen to provide the broadest possible geographic distribution and the maximum range in elevations.

## PREVIOUS WORK

The field relations, petrology, and isotopic ages of the samples collected in 1967-69 are given in Hudson and others (1977a, b). Data on the 1978-89 samples, as well as a summary of the regional geologic setting and tectonic evolution, were presented by Plafker and others (1994a, and references therein). Ages of all the K-Ar samples in the study area have been compiled by Wilson and others (1994).

There are no other published apatite fission-track studies in the Alaska segment of the Saint Elias Mountains. To the north, in the Mount Logan region of Canada (fig. 1), fission-track analyses were made from samples collected in vertical profiles of the mountain (Parrish, 1981; O'Sullivan and others, 1995; O'Sullivan and Cume, 1996). These studies found apatite fission-track ages that range from about 40 Ma at the top (>6,000 m) to about 4 Ma at the base of the mountain (<1,000 m) and zircon fission-track ages of about 43 Ma throughout the section. Interpretation of these data suggests that Mount Logan experienced three periods of rapid cooling during the middle Eocene, middle Miocene, and Pliocene as the result of episodes of kilometer-scale denudation (O'Sullivan and others, 1995; O'Sullivan and Currie, 1996).

## GEOGRAPHIC SETTING

The northern Saint Elias Mountains are high, rugged mountain ranges that contain extensive icefields and glaciers and include some of the most dramatic topographic relief in the world, ranging from sea level to 6 km (fig. 1). In Alaska, these mountains include Mount Saint Elias (5,489 m), the third highest peak on the North American continent, and in the vicinity of the international boundary with Canada, many other peaks and ridges that rise above 4,000 m. Mount Logan (6,050 m), the second highest peak in North America, lies just north of our study area in Canada. On the south side of the mountain range is a rugged "foothills" belt as much as 50 km wide in which local relief on the ridges and peaks ranges from several hundred meters to 2,000 m.

The larger glaciers and ice fields in the high central part of the mountains have surface elevations between 1,500 m and 2,600 m. Glaciers on the south side of the range drain southward across the "foothills" into Malaspina Glacier and Yakutat Bay and across the coastal lowland southeast of Yakutat Bay to the Gulf of Alaska. Because glaciers that drain to the south extend nearly to the coast, rivers in the area are short with the exception of the Alsek River, which crosses the range in the southern part of the area. **Outwash** deposited by these energetic glacial streams, together with glacial moraine and beach deposits, comprise a lowland of variable width along much of the coast.

## TECTONIC SETTING

The Yakutat-Saint Elias area lies near a complex junction between the northwest-trending Fairweather-Queen Charlotte dextral transform fault and a belt of east- to north-east-trending folds, thrust faults, and oblique thrust faults that characterizes the extension of the Aleutian convergence zone across the continental shelf to the transform boundary (fig. 2). South of the study area, the Pacific plate is moving to the northwest at a rate of 5.2 cm/yr with respect to the North American plate (DeMets and others, 1990). This direction is at a slight oblique angle to the northwest-trending Fairweather-Queen Charlotte dextral fault system and at an angle of up to 30° to major structures west of Yakutat Bay, which trend dominantly east-west to northeast.

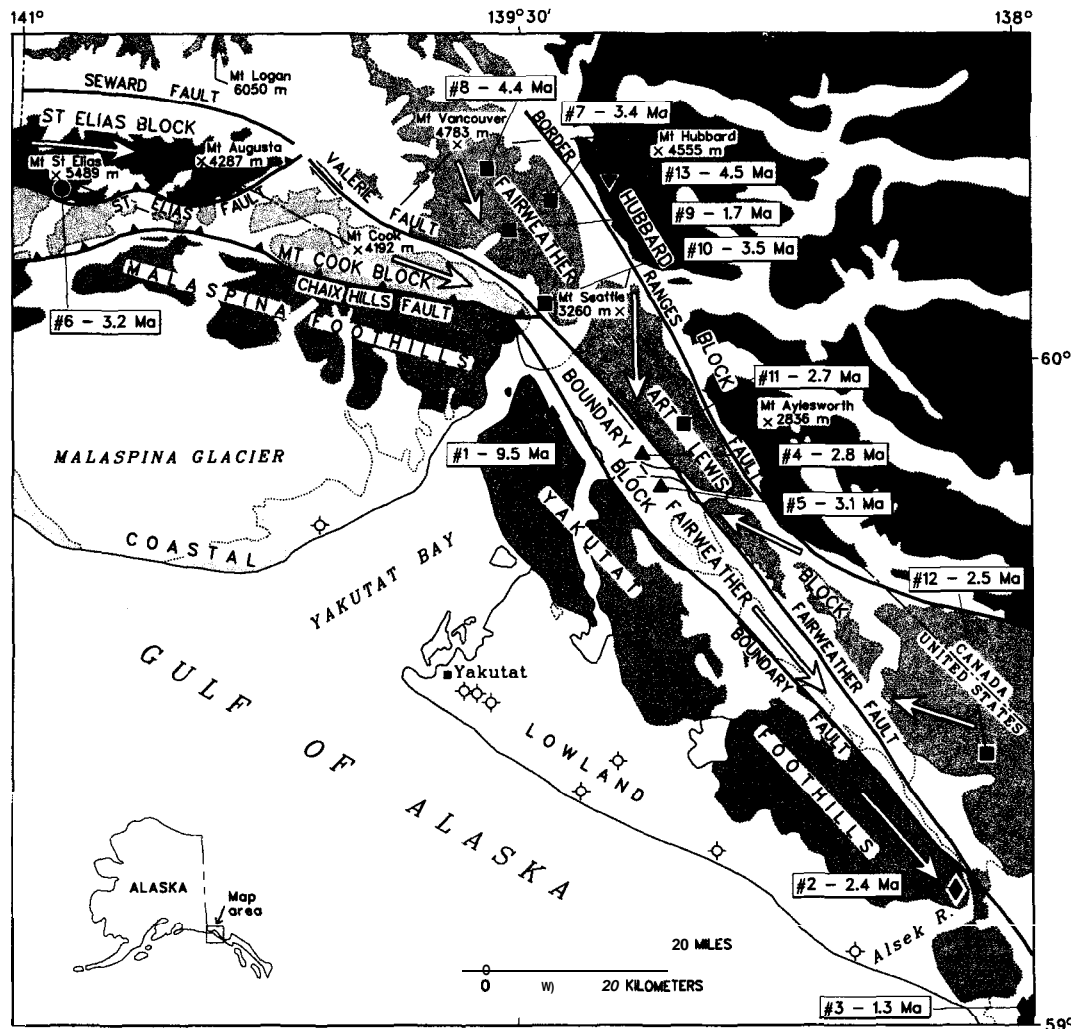
The allochthonous Yakutat terrane is bounded on the north by the Fairweather and Chugach-Saint Elias faults and is tightly coupled to the Pacific plate (Lahr and Plafker, 1980). Geologic evidence suggests that for the past 100,000 yr, strike-slip motion on the Fairweather fault has kept pace with the Pacific plate motion (Plafker and others, 1978). Total Neogene displacement on the Fairweather-Queen Charlotte transform system is on the order of 600 km (Plafker and others, 1994a). Seismologic data for the Saint Elias earthquake of 28 February 1979 ( $M_s=7.1$ ) and its aftershocks indicate southeastward displacement of the upper plate at the interface with the underthrusting combined Pacific plate and Yakutat terrane in a focal region that includes much of the mountain belt west of Yakutat Bay; depth of the interface in this area is poorly constrained at about 15 km (Lahr and others, 1979; Stephens and others, 1980; Perez and Jacob, 1980). Thus, the combined Yakutat terrane and Pacific plate are actively underthrusting the region north of the Chugach-Saint Elias fault, and compressive shortening is taken up in a broad belt of late Cenozoic folds and dip-slip to dextral-oblique thrusts to the south. Partly as a consequence of this underthrusting and crustal thickening, the Yakutat-Saint Elias area has experienced tectonic deformation, uplift, and deep erosion since middle to late Miocene time (Plafker and others, 1994a, and references therein).

Five major faults or systems of faults divide the study area into six large tectonic blocks (fig. 1). From northeast to southwest these structural boundaries are the (1) Border Ranges fault, (2) Seward-Valerie-Fairweather faults, (3) Saint Elias fault, (4) Chaix Hills fault, and (5) Boundary fault. In part, these faults coincide with boundaries of the major tectonostratigraphic terranes (fig. 2). Thus, the Border Ranges fault juxtaposes the undifferentiated Wrangellia and Alexander terranes (Wrangellia composite terrane) on the north against the Chugach terrane to the south, and the Seward-Valerie-Fairweather fault system juxtaposes the Chugach terrane against the Yakutat terrane to the south



(Plafker and others, 1994a). The Yakutat terrane is interpreted as a segment of the Chugach terrane that is overlain by a distinctive Tertiary sequence and was displaced some 600 km northward along the Fairweather fault from the continental margin of southeastern Alaska south of Chatham Strait (Plafker and others, 1994a). Some of these faults, and all of the major faults that define terrane boundaries, are inferred to extend to considerable depths, possibly to the base of the continental crust. Of these, only the Fairweather fault is known to be historically active, although there has been post-Pliocene displacement on the Chaix Hills fault and probable post-Oligocene displacement on the Chugach–Saint Elias fault (Plafker and others, 1994b, and references therein).

The Fairweather fault experienced dextral displacements of between 1 and 4 m along its entire onshore length in 1958 during a 7.9 magnitude earthquake (Plafker and others, 1994b). A series of very large earthquakes in 1899–90 resulted in widespread coseismic tectonic uplift of as much as 14.4 m along the shores of Yakutat Bay and along the outer coast as much as 150 km west of Yakutat Bay (Tarr and Martin, 1912). Although the causative faults have not been definitively identified, dislocation models of the vertical shoreline deformation are most compatible with slip on at least three north- to northeast-dipping thrust faults or blind thrusts that deform the shorelines of Yakutat Bay south of the Chaix Hills and Boundary faults (Plafker and Thatcher, 1982; Plafker and others, 1994b).



**Figure 1.** Map of study area showing locations, map numbers (see tables 1 and 2), and fission-track ages of 13 fission-track samples. Major structural blocks are distinguished by differences in shading. The solid sample location symbols (diamonds, triangles, circles, squares, and inverted triangles) differ for each of the structural blocks. Open arrows indicate general direction of increasing metamorphic gradient within structural blocks. Open circles with barbs in the coastal lowland indicate locations of dry petroleum exploration wells. Geology modified from Hudson and others (1977b) and Plafker and others (1994a). See tables 1 and 2 for sample data.

Table 1. Data for apatite fission-track samples from the northern Saint Elias Mountains in Alaska

<sup>1</sup> Map number	<sup>2</sup> Fission-track sample number	Quadrangle	<sup>3</sup> K-Ar/U-Pb age (Ma)	Elevation (ft/m)	Fission-track age (Ma)	Lithology
<b>South of the Boundary fault</b>						
1	68APR72B2/ 63APR196	Yakutat D-4	160±3.5 (h)	2,6501808	9.5k2.3	Quartz diorite
2	68APS57F	Yakutat A-1	4.1±0.12 (b), 3.8k0.15 (b) (re-run)	2,4001732	2.4k0.6	Quartzofeldspathic biotite schist
3	68APR77D	Yakutat A-1	48.2±6 (b)	1,8751571	1.3±0.3	Biotite adamellite
<b>Between Boundary fault and Fairweather fault</b>						
4	67APR42A	Yakutat D-4	51.1±3 (h)	2,0251617	2.8k0.4	Diorite
5	67APR42B	Yakutat D-3	42.7±2 (b), 48.4±2 (m)	2,3351712	3.1k0.8	Adamellite
<b>Mount Saint Elias</b>						
6	69APR54A (re-run)	St. Elias B-8	54.1±1.7 (h)	11,000±1,500/ 3,353±457	3.2±0.5	Quartz diorite
<b>Between Fairweather fault and Border Ranges fault</b>						
7	81APR5	St. Elias B-4	50.9±3.9 (b)	7,65012,332	3.4i1.3	Foliated hornblende diorite
8	69APR32A	St. Elias B-5	46.8±1 (m) 44.6±1 (b)	8,20012,499	4.4±1.0	Granodiorite
9	69APR40A2	St. Elias A-5	30.6±1 (b)	5,00011,524	1.7k0.4	Granodiorite?
10	67APR78A	St. Elias A-4	20.9±3 (m) 18.5±1 (h)	3,0251922	3.5±1.2	Tonalite
11	80APR49A	Yakutat D-3	36.2±1.4 (b), 37.1k1.4 (b)	4,10011,250	2.7±0.7	Biotite muscovite tonalite
12	78APR8 67APR94C (re-run)	Yakutat B-1	34.7±1.0 (z) 23.1k2.0 (b)	2,0001600	2.5k0.7	Granite
<b>North of Border Ranges fault</b>						
13	69APR31B	St. Elias B-4	279±8 (h)	6,00011,829	4.5k0.9	Hornblende diorite (altered)

<sup>1</sup> Locations shown on figure 1<sup>2</sup> Where two numbers are shown, the isotopic age and fission-track ages were determined on different closely-spaced samples from the same pluton<sup>3</sup> All are K-Ar analyses except for U-Pb zircon age given for sample #12 (78APR8). Dated mineral phases shown in parentheses as follows: b-biotite, m-muscovite, h-hornblende, z-zircon. The K-Ar ages have been compiled by Wilson and others (1994); the U-Pb zircon age is by T. W. Stern (U.S.G.S., written commun., 1979).<sup>4</sup> See table 2 for analytical data

## GEOLOGIC SETTING OF THE ANALYZED SAMPLES

The Hubbard block north of the Border Ranges fault consists of early and middle Paleozoic volcanic-arc and oceanic-plateau rocks of the Wrangellia composite terrane. The bedded rocks are intruded and metamorphosed to greenschist facies by alkalic Middle Pennsylvanian plutons,

large foliated quartz diorite and tonalite plutons of Late Jurassic age, and smaller nonfoliated plutons of mid-Cretaceous and Tertiary age. The only fission-track sample (#13) from this block is an altered hornblende diorite from a large pluton that has a K-Ar age of 279±8 Ma.

The Fairweather-Art Lewis block between the Border Ranges fault and the Seward-Valerie-Fairweather faults consists of an accretionary complex of Cretaceous flysch

Table 2. Fission-track analytical results for the northern Saint Elias Mountains in Alaska

Standard and induced track densities measured on mica external detectors ( $g=0.5$ ), and fossil-track densities on internal mineral surfaces. Parentheses show number of tracks counted. Ages for apatite samples calculated using  $\zeta=379.2/3$  for dosimeter glass CN5 (analyst P. O'Sullivan).

Map number (fig. 1)	Number of grains	Standard track density ( $\times 10^6 \text{ cm}^{-2}$ )	Fossil track density ( $\times 10^5 \text{ cm}^{-2}$ )	Induced track density ( $\times 10^6 \text{ cm}^{-2}$ )	Chi square probability (Percent)	Fission-track age (Ma)	Uranium (ppm)	Mean track length ( $\mu\text{m}$ )	Standard deviation ( $\mu\text{m}$ )
1	25	1.449 (5654)	32.81 (18)	94.98 (521)	95.8	$9.5 \pm 2.3$	8.2	$14.3 \pm 0.2$ (17)	0.77
2	25	1.449 (5654)	23.46 (16)	2.713 (1850)	83.6	$2.4 \pm 0.6$	23.4	$14.0 \pm 0.3$ (33)	1.21
3	25	1.449 (5654)	21.62 (14)	4.567 (2958)	82.8	$1.3 \pm 0.3$	39.4	$13.9 \pm 0.2$ (44)	1.10
4	25	1.449 (5654)	87.02 (44)	8.546 (4321)	8.1	$2.8 \pm 0.4$	73.7	$14.0 \pm 0.3$ (22)	1.26
5	25	1.449 (5654)	25.13 (14)	2.206 (1229)	85.2	$3.1 \pm 0.8$	19.0	$14.1 \pm 0.3$ (17)	1.27
6	25	1.449 (5654)	33.99 (37)	2.907 (3164)	86.4	$3.2 \pm 0.5$	25.1	$14.1 \pm 0.2$ (81)	1.19
7	18	1.449 (5654)	35.04 (7)	2.838 (567)	94.9	$3.4 \pm 1.3$	24.5	$14.5 \pm 0.3$ (6)	0.87
8	25	1.449 (5654)	35.29 (22)	2.186 (1363)	83.2	$4.4 \pm 1.0$	18.9	$14.0 \pm 0.3$ (21)	1.27
9	25	1.449 (5654)	22.53 (18)	3.639 (2908)	88.1	$1.7 \pm 0.4$	31.4	$14.1 \pm 0.2$ (45)	1.17
10	25	1.449 (5654)	824.2 (8)	65.52 (636)	3.1	$3.5 \pm 1.2^1$	5.7	$13.8 \pm 0.2$ (16)	1.25
11	25	1.449 (5654)	27.47 (17)	2.7991 (1727)	99.3	$2.7 \pm 0.7$	24.1	$14.4 \pm 0.2$ (26)	1.20
12	25	1.449 (5654)	21.89 (13)	2.413 (1433)	77.1	$2.5 \pm 0.7$	20.8	$14.1 \pm 0.3$ (10)	0.98
13	25	1.449 (5654)	30.97 (24)	1.871 (1450)	58.6	$4.5 \pm 0.9$	16.1	$13.5 \pm 0.2$ (62)	1.27

<sup>1</sup> Central age, used where pooled data fail  $\chi^2$  test at <5 percent. Errors quoted at  $\pm 1\sigma$ .

and mafic volcanic rocks (Chugach terrane) that have been highly deformed and variably metamorphosed from greenschist to amphibolite grade. Intrusive rocks within this sequence include widespread felsic stocks, sills, and dikes of dominantly Paleogene age. All six fission-track samples from this block (#7-12) are from small- to moderate-sized plutons of intermediate composition that have **K-Ar** ages between about 20 to 50 Ma (Wilson and others, 1994). One fission-track sample (#12) from a granite in the southern part of the block has a conventional U-Pb age of 35 Ma (T.W. Stem, U.S.G.S., written commun., 1979); a sample from a nearby locality in the same pluton has a **K-Ar** age of 23.1 Ma. The U-Pb age likely dates the time of intrusion, whereas the **K-Ar** age probably represents a reset age due to local intrusive activity between approximately 17 and 23 Ma.

The Saint Elias block between the Seward and Saint Elias faults consists of epidote amphibolite and amphibolite-facies metavolcanic rocks and pelitic schist with a distinctive east-west structural grain. The metamorphic rocks are intruded by Paleogene plutons and undated gabbro. This block may be a sliver of the Chugach terrane that was

transferred to the south side of the Fairweather fault and subsequently displaced some 200 km to the northwest by dextral slip along the fault (Plafker and others, 1994a). The one fission-track sample from this block (#6) is from a small felsic intrusive exposed on the sheer south face of Mount Saint Elias between about 3,000 and 3,800 m as determined by helicopter altimeter. The sample analyzed is one of several felsic plutonic rocks that were collected from float on Libbey Glacier at the base of the south face; three of the samples collected yielded **K-Ar** ages that range from 35 to 56 Ma.

The Boundary-Fairweather block is a sliver of probable Yakutat terrane flysch and melange that has been variably metamorphosed between greenschist and amphibolite facies by emplacement of extensive Paleogene plutons. Two closely spaced fission-track samples (#4, 5) are from large plutons of intermediate composition in this block. **K-Ar** ages of the samples are 51.1 Ma and 42.7-48.4 Ma, respectively.

The Malaspina-Yakutat Foothills segment of the Yakutat terrane that lies south of the Chaix Hills and Boundary faults has a basement of allochthonous Cretaceous flysch

and *mélange* intruded by Paleogene plutons and small mafic bodies of Miocene age. Metamorphic grade is dominantly lower zeolite facies except in one area north of Alsek River, where rocks reach amphibolite grade in a structural high. Basement rocks are overlain by a Tertiary sequence that includes more than 12,000 m of Eocene and younger continental, paralic, and marine, predominantly clastic sediments that are locally intruded by mafic plugs and dikes of probable Miocene age. One fission-track sample east of Yakutat Bay is from a quartz diorite block in *mélange* (#1); although an isotopic age was not determined for this sample, a nearby sample from the same block has a K-Ar age of 160 Ma, and this is assumed to be the minimum protolith age for the entire block. The sample west of Alsek River (#2) is a quartzofeldspathic schist in an area of anomalously high metamorphic grade that has K-Ar ages of only 3.8-4.1 Ma. The sample east of Alsek River (#3) is from a large adamellite pluton that has a K-Ar age of 48 Ma.

### LONG-TERM DIFFERENTIAL UPLIFT AND TILTING INDICATED BY METAMORPHIC FACIES UNITS

Metamorphic rocks in the Yakutat–Saint Elias area underwent a penetrative deformation in Late Cretaceous to early Tertiary time (about 58-67 Ma). Subsequent deformation in the Miocene (17-23 Ma) was accompanied by emplacement of small epizonal igneous intrusions and by local thermal recrystallization (Hudson and others, 1977b).

Mapped metamorphic facies show many discontinuities across major faults that are suggestive of postmetamorphic differential uplift between crustal blocks (Hudson and others, 1977b). Furthermore, regional metamorphic gradients within blocks indicate that (1) the Saint Elias, Mount Cook, and Boundary–Fairweather blocks are tilted downward to the west or northwest parallel to their general structural grains; (2) the Fairweather–ArtLewis block is tilted downward to the northwest and southeast, flanking a high located northeast of Yakutat Bay; and (3) the foothills south of the Boundary fault are locally tilted steeply downward to the northwest, away from a thermally recrystallized area north of the Alsek River (fig. 1) that has yielded anomalously young K-Ar ages of about 4 Ma on metamorphic biotite (table 1; #2).

### FISSION-TRACK METHODOLOGY

Fission-track analyses were carried out in the laboratories of the School of Earth Sciences at La Trobe University, Melbourne, Australia. Apatite concentrates were separated using conventional magnetic and heavy-liquid techniques. Apatite samples were irradiated in the X-7 facility of the HIFAR reactor, Lucas Heights, New South Wales, Australia, following the procedures outlined by Green (1986). The external detector method (Gleadow, 1981) was used exclusively throughout this study. Fission-track ages were calculated using the zeta calibration method and the standard fission-track age equation (Naeser, 1979;

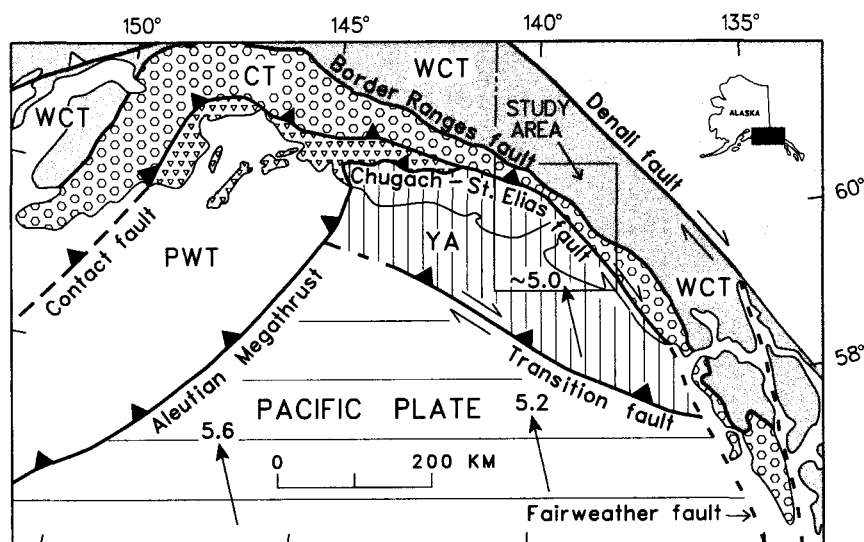


Figure 2. Map showing regional tectonic setting of the study area. Geology after Plafker and others (1994a); arrows and numerals indicate relative-motion vectors, in centimeters, of the Yakutat terrane (Lahr and Plafker, 1980) and the Pacific plate (DeMets and others, 1990). Abbreviations: WCT, Wrangellia composite terrane; CT, Chugach terrane; PWT, Prince William terrane and younger accreted rocks; YA, Yakutat terrane.

Hurford and Green, 1982). Errors were calculated using the techniques of Green (1981). The  $\chi^2$  statistic is used to detect the probability that all age grains analyzed belong to a single population of ages (Galbraith, 1981). A probability of <5 percent is evidence of an asymmetric spread of single-grain ages. In instances where a spread in ages is found, the "conventional analysis" (Green, 1981), based purely on Poissonian variation, is not valid and the "central age" (Galbraith and Laslett, 1993), which is essentially a weighted-mean age, is reported. Confined fission-tracks were measured following the recommendations of Laslett and others (1982).

In this study, apatite fission-track data were interpreted using the understanding of apatite fission-track system response described by Green and others (1989). This understanding is based on an empirical kinetic description of laboratory annealing data of Durango apatite (Green and others, 1986). When fission-tracks form in apatite, they have a fairly constant mean length of about 16  $\mu\text{m}$  (Gleadow and others, 1986). Following their formation, fission tracks in apatite progressively shorten (anneal) at a rate that depends primarily on temperature (Gleadow and others, 1986). Therefore, increased annealing results in shorter tracks, reduced track density, and a reduction in the fission-track age (Gleadow and others, 1986). Total annealing results in the reduction of the fission-track age to zero. Because new tracks continuously form throughout geologic time, the distribution of track lengths in an apatite grain reflects the integrated thermal history of the grains host rock (Green and others, 1989). In detail, the rate of annealing depends on the chemical composition; fission-tracks in chlorine-rich apatites are slightly more resistant to annealing than fission-tracks in fluorine-rich apatites (Green and others, 1986). Thermal-history interpretations are based on a quantitative treatment of annealing achieved by computer modeling (Green and others, 1989) of track shortening and age evolution through likely thermal histories for an average apatite composition ( $\text{Cl}/(\text{Cl} + \text{F}) \approx 0.1$ ), while making appropriate adjustments for the actual Cl composition likely in each sample. This model by Laslett and others (1987) for annealing of fission tracks in apatite gives predictions that are consistent with geologic constraints on annealing behavior, as explained by Green and others (1989). Predictions based on this composition should slightly overestimate the actual amount of annealing, although in thermal histories resulting from continuous cooling, as in this study, compositional effects play a relatively minor role (Green and others, 1989).

## DISCUSSION

In an attempt to constrain the denudation history of the northern Saint Elias Mountains in Alaska, we have determined fission-track ages and measured confined track lengths

for 13 apatite samples (fig. 1, table 2; all fission-track errors listed as  $\pm 1\sigma$  unless otherwise discussed). The apatite fission-track ages we determined (between  $9.5 \pm 2.3$  and  $1.3 \pm 0.3$  Ma) are all significantly less than the emplacement and metamorphic ages of these samples (table 1), and the mean track lengths are all very long (between  $14.5 \pm 0.3$  and  $13.5 \pm 0.2$   $\mu\text{m}$ ), with narrow track-length distributions (standard deviations between 0.77 and 1.27  $\mu\text{m}$ ; table 2). Applying the track-annealing model of Laslett and others (1987) to the fission-track data suggests that all 13 samples were exposed to paleotemperatures  $> 110^\circ\text{C}$ , which resulted in total resetting of the apatite fission-track ages, prior to rapid cooling to paleotemperatures  $< 50^\circ\text{C}$  during the late Cenozoic at the time suggested by each apatite age.

The 10 samples in the region north of the Yakutat Foothills range in age from 1.7 to 4.5 Ma. Of these, the oldest samples, (#8, 13), are located toward the northern limit of this region, suggesting the possibility of slight downward-to-the-north tilting resulting in increased denudation to the south. Furthermore, the fission-track age of our most inland sample (#13) is identical to those obtained for the lowest samples from the southern base of the Logan massif, north of the study area, at roughly the same elevation (O'Sullivan and others, 1995; O'Sullivan and Currie, 1996). This result could reflect generally uniform late Neogene rates of cooling and denudation over a broad inland part of the northern Saint Elias Mountains.

The general lack of correlation between the fission-track uplift data and the metamorphic gradients (except near the Alsek River in the southeastern Yakutat Foothills) reflects a long and complex postmetamorphic history that is not evident in most of the Neogene fission-track record. Within the Yakutat Foothills, fission-track ages that decrease from about 9.5 Ma (#1) near Yakutat Bay to 2.4 Ma (#2) just north of Alsek River to 1.3 Ma (#3) south of Alsek River suggest that the northwestern part of the Yakutat Foothills has relatively less denudation than the area farther southeast. This is in accord with the generally low-grade laumontite-facies metamorphism in upper Mesozoic rocks that comprise the Yakutat and Malaspina Foothills in the vicinity of Yakutat Bay and with the absence of metamorphism in Tertiary sedimentary rocks penetrated by wells drilled for petroleum on the coastal lowland (fig. 1) and offshore (Plafker, 1987).

The two samples in the southeastern part of the Yakutat Foothills were selected to test the possibility of local anomalously high uplift rates in the vicinity of Alsek River relative to areas farther north. Such uplift is suggested by steep metamorphic gradients mapped in the field that decrease northwestward and by exceptionally young K-Ar ages of 3.8-4.1 Ma that were obtained from metamorphic biotite in schistose Cretaceous rocks (#2) near Alsek River. The fission-track ages of 2.4 Ma for this same schist sample and of 1.3 Ma for a granitic sample from a pluton just south of the Alsek River (#3) are compatible with the field evidence

for extremely rapid cooling and exhumation in this part of the foothills belt.

Our limited data do not indicate any abrupt changes in ages across the major faults except possibly between sample #1 (9.5 Ma) and the nearest samples north of the Boundary fault, which have ages of about 3 Ma (#4, 5). Because of the marked difference in protolith age and chemistry of sample #1 (Jurassic diorite) relative to samples northeast of the Boundary fault (Tertiary granodiorite to granite), direct comparisons of the fission-track ages may not be valid without additional information on the compositions of the apatite in these rocks. However, because the data suggest that all the rocks analyzed have experienced continuous cooling from paleotemperatures high enough to totally reset the apatite fission-track ages, any differences in apatite chemistry between samples would play a relatively minor role (for example, Green and others, 1989).

To determine the rate of denudation throughout the region, we make the simplifying assumption that there are no structural breaks across which there are large Neogene vertical displacements. This assumption seems to be valid, since there does not seem to be a strong correlation between sample age and elevation within each structural block, nor are there any obvious differences in ages across individual faults. When the fission-track age and elevation data are regressed together (except sample #1), the resulting curve yields a rough estimate of when and how fast cooling occurred over the area (fig. 3). Such a curve has a slope of 1.9 km/Ma, which is an approximation of the regional uplift rate. Furthermore, since there is no break in slope at high elevations on figure 3 that would be indicative of the base of the partial-annealing zone, the onset of cooling of the samples from paleotemperatures exceeding about  $110\pm 10^{\circ}\text{C}$  can only be constrained beginning at 4.5 Ma (#13), the oldest sample excluding sample #1. Using a denudation rate of about 1.9 km/Ma, the predicted depth at which fission-track ages should now be zero is about 4 km below sea level (curve A, fig. 3). This value also matches the depth of total annealing in a thermal regime with a geothermal gradient of about  $25^{\circ}\text{C}/\text{km}$ , which is the maximum gradient based on thermal data from wells drilled for petroleum on the adjacent continental shelf (Flett, 1992). If a lower gradient of  $20^{\circ}\text{C}/\text{km}$  is used, then the amounts of denudation increase by 20 percent. As a test of general validity, a regression of ages of samples #7, 8, and 9 from relatively near each other (at the scale of sampling) yields a denudation rate of only 0.39 km/Ma, which would yield 0-Ma fission-track ages above sea level (about 900 m; plot not shown). It is clear that this regression is not reasonable, as surface temperatures are far too low for significant apatite annealing. If, however, all samples from the same block (Fairweather-Art Lewis block) are regressed (#7-12) a denudation rate of 1.5 km/Ma is obtained, which is closer to the rate obtained for all the ages (except #1) from the region. In this case, modern zero ages would be expected at depths

below sea level exceeding about 3 km, and an age of about 4.4 Ma would be expected at about 3,500-m elevation (curve B, fig. 3). However, a predicted geothermal gradient of about  $37^{\circ}\text{C}/\text{km}$  would be necessary for this scenario to be correct, and such a gradient appears to be unreasonably high for the region based on the data in Flett (1992).

In general terms, the estimated denudation rate from regression of all fission-track ages (except #1) is consistent with cooling in an assumed regional geothermal gradient of about  $25^{\circ}\text{C}/\text{km}$  because such a model yields similar depths at which samples began recording "age" (that is, 4-km depth and about  $110^{\circ}\text{C}$ ). Using a sea-level datum, the samples studied here must have been uplifted 4 km plus an additional amount equal to their surface elevation. This means that a sample now at 1,500-m elevation was exhumed from depths exceeding about 5.5 km since the time given by its fission-track age. For example, sample #9, with a measured age of  $1.7\pm 0.4$  Ma and a predicted age (from the regression curve) of about 3 Ma, has been uplifted and exhumed by approximately 5.5 km since about 3 Ma, at an average rate of 1.8 km/Ma.

Assuming that the scenario above for cooling of the samples is correct, uplift and denudation began in the area prior to 4.5 Ma, (predicted age of highest sample, #6). Because much of the cooling associated with the onset of fission-track length retention occurred early in the recent history of each sample (that is, during the first 2 km of uplift and denudation and hence cooling from  $110^{\circ}\text{C}$  to less than  $50^{\circ}\text{C}$ ), past and present denudation rates are probably similar. Thus, much of the modern surface elevation of samples must have been achieved late in each samples uplift and exhumation history. This implies that rapid uplift in the region is continuing today, as is also suggested by the generally high elevations and relief throughout the region, by Pliocene marine sedimentary rocks at elevations as high as 1,800 m, and by historic coseismic coastal uplift during the 1899 Yakutat Bay earthquake (Plafker and others, 1994a, b).

## SUMMARY

The following interpretations of the fission-track ages depend in part on the validity of assumed rapid cooling from about  $110^{\circ}\text{C}$ , on a regional geothermal gradient of about  $20\text{-}25^{\circ}\text{C}/\text{km}$ , and on roughly uniform cooling and denudation over the entire study area.

1. All fission-track samples, except #1, passed through the apatite partial annealing zone (about  $110^{\circ}\text{C}$  to about  $50^{\circ}\text{C}$ ) at 4.5-1.3 Ma. These data, together with topographic, geologic, and historic earthquake data, suggest young and ongoing uplift of much of the Yakutat-Saint Elias region. This cooling episode appears to overlap the youngest part of the cooling and denudation history for Mount Logan

north of the study area (O'Sullivan and others, 1995; O'Sullivan and Currie, 1996).

2. There is no clear-cut relationship between fission-track age and location of samples relative to the major faults and terrane boundaries. The one possible exception is between sample #1 and samples #4 and #5 across the northern part of the Boundary fault. This lack of a relationship between fission-track age and location suggests that the structural blocks north of the Boundary fault cooled relatively uniformly over most of the study area.

3. There is no strong correlation between fission-track age and elevation, although the ages suggest a possible slight increase in age with elevation (fig. 3 except for sample #1). The cause of the data scatter cannot be determined with this reconnaissance data set.

4. The denudation rate for all samples, except #1, is interpreted to be approximately 1.5 to 1.9 km/Ma. Vertical profiles of fission-track data are needed to determine details of the denudation history at specific localities within the study area.

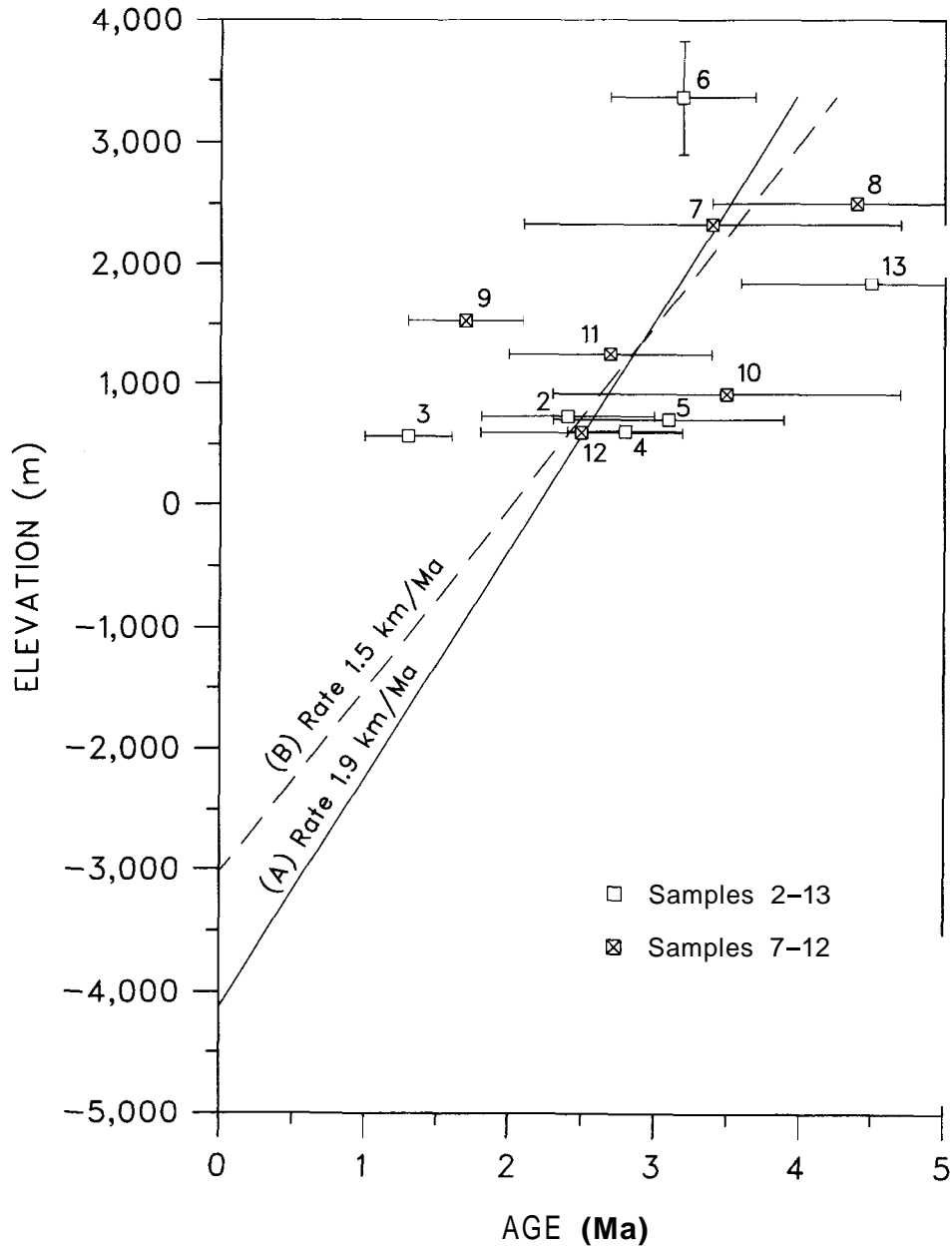


Figure 3. Linear regressions of fission-track age versus elevation for samples #2-13 (curve A) and for samples #7-12 in the Fairweather-Art Lewis block only (curve B). Sample symbols and numbers are the same as in figure 1; sample data are given in tables 1 and 2.

5. Ages of samples #1-3 south of the Boundary fault are compatible with local denudation north of Alsek River and tilt downward toward the northwest, which was previously inferred from metamorphic gradients (Hudson and others, 1977b). Elsewhere, the metamorphic gradients show no correlation with apatite age, as might be expected for rocks that reflect a much longer history than is recorded by the fission-track data.

6. At locality #2 near Alsek River, the close coincidence between 3.8-4.1 Ma biotite **K-Ar** ages from schist that most likely has a Late Cretaceous protolith and apatite fission-track ages of 2.4 Ma suggests the possibility of a previously unsuspected Pliocene(?) thermal event that reset the biotite **K-Ar** ages. This inferred thermal event must have been of limited areal extent because it did not reset **K-Ar** ages of intrusive rocks at nearby sample localities (#3, 12).

In conclusion, our reconnaissance fission-track study provides evidence of widespread young denudation in the northern Saint Elias Mountains of Alaska that we interpret as driven by collision of the Yakutat terrane with the southern margin of Alaska. However, the details of this denudation history cannot be deduced from the available data.

Acknowledgments. — Samples used for this study were collected between 1963 and 1981 during field studies funded by the U. S. Geological Survey. The fission-track analyses were made possible with support for sample irradiations supplied through a grant to the La Trobe University Fission-Track Research Group from the Australian Institute of Nuclear Science and Engineering.

## REFERENCES CITED

- DeMets, C., Gordon, R.G., Argus, D.F., and Stein, S., 1990, Current plate motions: *Geophysical Journal International*, v. 101, no. 2, p. 425-478.
- Flett, T.O., 1992, Temperature gradients, in Turner, R.F., ed., *Geologic report for the Gulf of Alaska planning area: Minerals Management Service OCS Report MMS 92-0065*, 302 p.
- Galbraith, R.F., 1981, On statistical models for fission track counts: *Mathematical Geology*, v. 13, p. 471-488.
- Galbraith, R.F., and Laslett, G.M., 1993, Statistical models for mixed fission track ages: *Nuclear Tracks*, no. 21, p. 459-470.
- Gleadow, A.J.W., 1981, Fission track dating methods: what are the real alternatives?: *Nuclear Tracks*, no. 5, p. 3-14.
- Gleadow, A.J.W., Duddy, I.R., Green, P.F., and Lovering J.F., 1986, Confined fission track lengths in apatite—a diagnostic tool for thermal history analysis: *Contributions to Mineral Petrology*, v. 94, p. 405-415.
- Green, P.F., 1981, A new look at statistics in fission track dating: *Nuclear Tracks*, no. 5, p. 77-86.
- 1986, On the thermo-tectonic evolution of northern England: Evidence from fission track analysis: *Geology*, v. 5, p. 493-506.
- Green, P.F., Duddy, I.R., Gleadow, A.J.W., Tingate, P.T., and Laslett, G.M., 1986, Thermal annealing of fission tracks in apatite—1, a qualitative description: *Chemical Geology (Isotope Geoscience Section)*, v. 59, p. 237-253.
- Green, P.F., Duddy, I.R., Laslett, G.M., Hegarty, K.A., Gleadow, A.J.W., and Lovering, J.F., 1989, Thermal annealing of fission tracks in apatite—4, Qualitative modeling techniques and extensions to geological timescales: *Chemical Geology (Isotope Geoscience Section)*, v. 79, p. 155-182.
- Harland, W.B., Annstrong, R.L., Cox, A.V., Craig, L.E., Smith, A.G., and Smith, D.G., 1990, *A geologic time scale 1989*: Cambridge, England, Cambridge University Press, 263 p.
- Hudson, Travis, Plafker, George, and Lanphere, M.A., 1977a, Intrusive rocks of the Yakutat-Saint Elias area, south-central Alaska: *U.S. Geological Survey Journal of Research*, v. 5, no. 2, p. 155-172.
- Hudson, Travis, Plafker, George, and Turner, D.L., 1977b, Metamorphic rocks of the Yakutat-Saint Elias area, south-central Alaska: *U.S. Geological Survey Journal of Research*, v. 5, no. 2, p. 173-184.
- Hurford, A.J., and Green, P.F., 1982, A users guide to fission-track dating calibration: *Earth and Planetary Science Letters*, v. 59, p. 343-354.
- Lahr, J.C., and Plafker, George, 1980, Holocene Pacific-North American plate interaction in southern Alaska: implications for the Yakataga seismic gap: *Geology*, v. 8, p. 483-486.
- Lahr, J.C., Plafker, George, Stephens, C.D., Fogelman, K.A., and Blackford, M.E., 1979, Interim report on the Saint Elias earthquake of 18 February 1979: *U.S. Geological Survey Open-File Report 79-670*, 35 p.
- Laslett, G.M., Kendall, W.S., Gleadow, A.J.W., and Duddy, I.R., 1982, Bias in measurement of fission-track length distributions: *Nuclear Tracks*, no. 6, p. 79-85.
- Laslett, G.M., Green, P.F., Duddy, I.R., and Gleadow, A.J.W., 1987, Thermal modeling of fission tracks in apatite—2, A quantitative analysis: *Chemical Geology, (Isotope Geoscience Section)*, v. 65, p. 1-13.
- Naeser, C.W., 1979, Fission track dating and geologic annealing of fission tracks, in Jager, E., and Hunziker, J.C., eds., *Lectures in isotope geology*: New York, Springer-Verlag, New York, p. 154-169.
- O'Sullivan, P.B., and Currie, L.D., 1996, Tectonic implications of multiple episodes of Middle to Late Cenozoic denudation of Mt Logan, Yukon Territory, Canada: *Earth and Planetary Science Letters*, v. 144, p. 251-262.
- O'Sullivan, P.B., Currie, L.D., Holdsworth, G., and Parrish, R.R., 1995, Multiple episodes of middle to late Cenozoic uplift and erosion of Mount Logan, Y.T., Canada, evidence from apatite fission track analyses [abs.]: *Geological Society of America Abstracts with Programs*, v. 27, no. 5, p. 69.
- Pamsh, R.R., 1981, Uplift rates of Mount Logan, Y.T. and British Columbias central Coast Ranges using fission track dating methods: *Eos (American Geophysical Union Transactions)*, v. 62, no. 6, p. 60.
- Perez, O.J., and Jacob, K.H., 1980, Saint Elias, Alaska, earthquake of February 28, 1979: tectonic setting and precursory seismic pattern: *Bulletin of the Seismological Society of America*, v. 70, no. 5, p. 1595-1606.



- Plafker, George, 1987, Regional geology and petroleum potential of the northern Gulf of Alaska continental margin, in Scholl, D.W., Grantz, Arthur, and Vedder, J.G., eds., Chapter 11, Geology and resource potential of the continental margin of western North America and adjacent ocean basins—Beaufort Sea to Baja California, v. 6 of Circum-Pacific Council for Energy and Mineral Resources Earth Science Series: Houston, Tex., Circum-Pacific Council for Energy and Mineral Resources, p. 229-268.
- Plafker, George, Gilpin, L.M., and Lahr, J.C., 1994b, Neotectonic map of Alaska, in Plafker, George, and Berg, H.C., eds., The geology of Alaska: Boulder, Colo., Geological Society of America, The Geology of North America, v. G-1, pl. 12, 1 sheet with text, scale 1:2,500,000.
- Plafker, George, Hudson, Travis, Bmns, T. R., and Rubin, Meyer, 1978, Late Quaternary offsets along the Fairweather fault and crustal plate interactions in southern Alaska: Canadian Journal of Earth Sciences, v. 15, no. 5, p. 805-816.
- Plafker, George, Moore, J.C., and Winkler, G.R., 1994a, Geology of the southern Alaska margin, in Plafker, George and Berg, H.C., eds., The geology of Alaska: Boulder, Colo., Geological Society of America, The Geology of North America, v. G-1, p. 389-449.
- Plafker, George, and Thatcher, Wayne, 1982, Geological and geophysical evaluation of the mechanisms of the great 1899-1900 Yakutat Bay, Alaska, earthquakes [abs.]: Program and Abstracts, American Geophysical Union Conference on Fault Behavior and the Earthquake Generating Process, Snowbird, Utah, Oct. 11-15, 1982.
- Stephens, C.D., Lahr, J.C., Fogleman, K.A. and Homer, R.B., 1980, The St Elias, Alaska, earthquake of February 28, 1979: regional recording of aftershocks and short term, pre-earthquake seismicity: Bulletin of the Seismological Society of America, v. 70, no. 5, p. 1607-1633.
- Tarr, R.S., and Martin, Lawrence, 1912, The earthquakes at Yakutat Bay, Alaska, with a preface by G. K. Gilbert: U.S. Geological Survey Professional Paper 69, 135 p.
- Wilson, F.H., Shew, N., and Dubois, G.D., 1994, Map and table showing isotopic age data in Alaska, in Plafker, George and Berg, H.C., eds., The geology of Alaska: Boulder, Colo., Geological Society of America, The Geology of North America, v. G1, pl. 8, 1 sheet with tables, scale 1:2,500,000.

Reviewers: T.E. Moore and Andrei Sarna-Wojcicki

# Paleomagnetic Results from Devonian and Permian Rocks at Saginaw Bay, Kuiu Island, Southeastern Alaska

By Sherman Gromme and John W. Hillhouse

## ABSTRACT

Paleomagnetic directions have been determined for unfossiliferous Paleozoic red arkose and siltstone at Saginaw Bay on Kuiu Island, southeastern Alaska. At least three components of natural remanent magnetization were isolated in these rocks, the younger two of which are inferred to be Permian and Cretaceous or Tertiary in age, respectively. The highest temperature and hence oldest component is similar to the paleomagnetic directions reported by other researchers in the lithologically similar Karheen Formation, 130 km to the south near Craig on Prince of Wales Island. Consequently, the previous suggestion by others of a correlation of the **redbeds** at Saginaw Bay with the Lower Devonian Karheen Formation is confirmed by our data, and structural continuity is thereby established across this part of the Craig subterrane of the Alexander terrane. The oldest overprint is similar to primary paleomagnetic directions isolated in two igneous rock units of the Permian Halleck Formation. The reversed magnetic polarity of the Halleck Formation samples is consistent with results reported by others from Pennsylvanian and Permian rocks of the Alexander terrane, thereby supporting the inference that the Alexander terrane was in the northern hemisphere during the Pennsylvanian and Permian time of constant reversed geomagnetic polarity.

## INTRODUCTION

An exceptionally complete and mostly **unmetamorphosed** stratigraphic sequence of rocks ranging in age from Silurian through Tertiary on northern Kuiu and Kupreanof Islands in southeastern Alaska has been described by Muffler (1967). Paleozoic and early Mesozoic rocks in this area were a key part of the original definition of the Alexander tectonostratigraphic terrane (Berg and others, 1980). Two paleomagnetic studies have been conducted in the Triassic Hound Island Volcanics (Hillhouse and Gromme, 1980; Haeussler and others, 1992a), the latter of which provided definite evidence that the Alexander **terrane** (fig. 1) was displaced from the North American craton

during Triassic time and was subsequently accreted to the craton. More recently, paleomagnetic evidence from the gravitationally layered ultramafic intrusions of Duke Island (fig. 1) has demonstrated that the paleolatitude of the Alexander terrane was more than  $25^{\circ}$  south of its present location in mid-Cretaceous time (Bogue and others, 1995). Plate-tectonic northward transport of the Alexander terrane and inboard (or eastward) terranes with respect to the North American craton was complete by mid-Eocene time (Irving and others, 1996; see also references cited in Bogue and others, 1995). Little is known of the pre-Triassic movement history of the Alexander terrane; the most convincing paleomagnetic data are from the Devonian Karheen Formation in its type area (Bazard and others, 1995) and from other Devonian rocks on and adjacent to Prince of Wales Island in the vicinity of Craig (Van der Voo and others, 1980) (fig. 1).

During the 1979 and 1982 field seasons the authors made an extensive paleomagnetic collection from most of the least metamorphosed bedded rocks in southeastern Alaska, ranging in age from Silurian through Cretaceous. Owing to pervasive magnetic overprinting and, in the carbonate rocks typical of the Permian, probable lack of any primary remanent magnetization, these collections yielded little useful data. In the Saginaw Bay and Keku Strait areas described by Muffler (1967) (indicated respectively by S and H in fig. 1), we concentrated on the abundant Permian rocks but also sampled as much of the rest of the stratigraphic section below the Hound Island Volcanics as possible, in all of which no evidence of metamorphism had been reported. Muffler (1967) described a nonfossiliferous sequence of red arkose and subordinate red siltstone that occurs in a small area on the west shore of Saginaw Bay. These **redbeds** are in apparent structural conformity with Silurian bedded rocks above and below them, but the lower contacts of the **redbeds** are all faults and the upper contact is concealed by salt water. Because of the absence of fossils, Muffler (1967) assigned a provisional Late Silurian age to the red arkose unit based on surmised stratigraphic position, but he also stated that the arkose might be an allochthonous fault block. No fossils were found during a subsequent reexamination of this area (D.A. Brew, U.S.

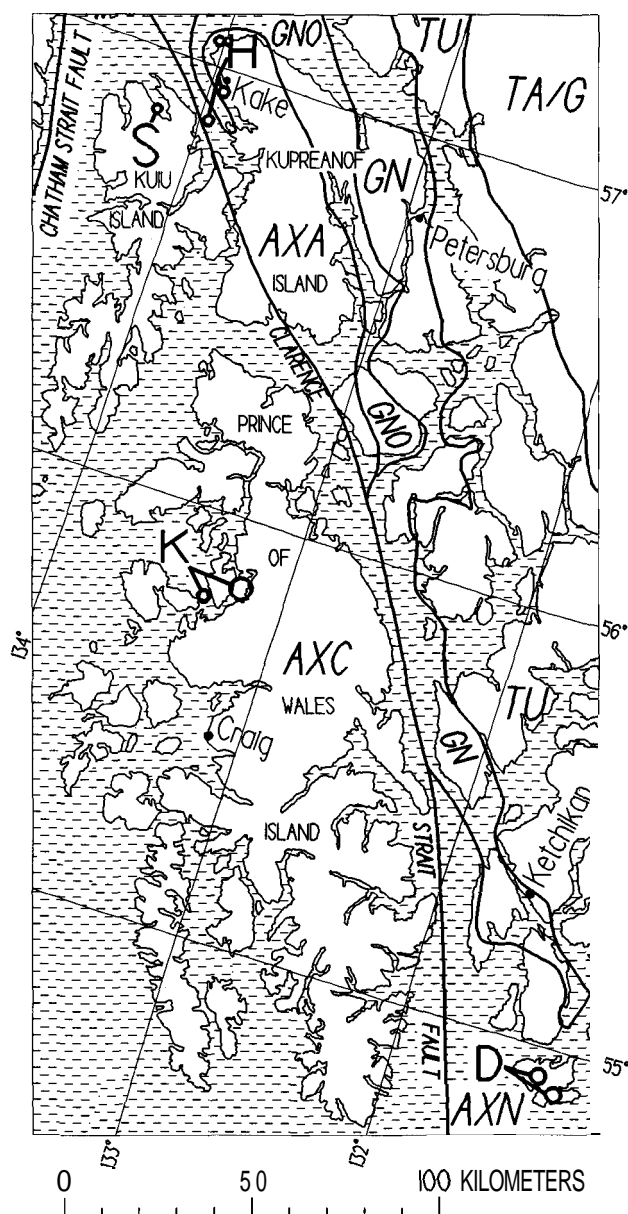


Figure 1. Index map of southernmost part of southeastern Alaska, showing geologic terrane boundaries (after Berg and others, 1980; Silberling and others, 1994). Major faults and other terrane boundaries shown as heavy solid lines. Terrane labels as follows: **AXC**, Craig subterrane of Alexander terrane; **AXA**, Admiralty subterrane of Alexander terrane; **AXN**, Annette subterrane of Alexander terrane; **GN**, Gravina-Nutzotin belt; **GNO**, Gravina-Nutzotin belt overlapping older terranes; **TU**, Taku terrane; **TA/G**, Tracy Am terrane and granitic rocks of the coast plutonic complex. Paleomagnetic study areas shown as open circles: **H**, Keku Strait and Hound Island Volcanics (Haessler and others, 1992a); **K**, Karheen Formation (Bazard and others, 1995); **D**, Duke Island, showing location of ultramafic intrusions (Bogue and others, 1995); **S**, Saginaw Bay (this study).

Geological Survey, written commun., 1982), but a provisional lithologic correlation was suggested by Brew and others (1984) with part of the Early Devonian Karheen Formation that occurs 130 km to the south (indicated by **K** in fig. 1).

The Karheen Formation was first described by Eberlein and Churkin (1970) as consisting of a heterogeneous sequence of clastic rocks, red colored in part, consisting mostly of sandstone but also including some siltstone and conglomerate and minor amounts of limestone. On the basis of megafossils, Eberlein and Churkin (1970) stated that the possible age range of the Karheen Formation was Late Silurian to Early Devonian, but they also indicated that the graptolites, corals, stromatoporoids, and crinoids collected by them were of Early Devonian age. This age assignment was not changed by Eberlein and others (1983). Subsequently, analyses of conodont collections have further restricted the age of the Karheen Formation to middle Early Devonian (Bazard and others, 1995, and references cited therein). Ovenshine (1975) added much detail to the lithologic description of the Karheen, interpreting it as partly of intertidal or near-tidal origin because of the presence of mudcracks, ripple marks, festoon cross-bedding, red color, and other sedimentary features. Eberlein and Churkin (1970) and Ovenshine (1975) characterized the Karheen Formation as a clastic wedge coarsening to the southwest or south. The paleogeographic significance of the Karheen clastic wedge has been discussed and elaborated by Gehrels and Saleeby (1987a) and Gehrels and others (1996), who showed on the basis of analyses of detrital zircons that the source area consisted at least partly of Precambrian rocks much older than any pre-Karheen rocks of the Alexander terrane. Gehrels and others (1996) concluded that the pre-Paleozoic cratonal part of the provenance of the Karheen Formation lay to the southwest in present-day coordinates; in other words, the older part of the Karheen provenance was not part of the North American craton. This conclusion supports the earlier interpretation of paleomagnetic data by Van der Voo and others (1980) and Bazard and others (1995) as demonstrating that the rocks of the Alexander terrane originated far from their present position in relation to the North American craton.

Because of the apparent abundance of hematite in the red arkoses and siltstones at Saginaw Bay, we made an extensive paleomagnetic collection from them. Initial laboratory results were unpromising, showing only a complex magnetic overprint, but the recent publication by Bazard and others (1995) of excellent paleomagnetic results from the Karheen Formation stimulated more extensive analysis of our data. We found that the **redbeds** in Saginaw Bay have the same direction of primary magnetization as the Karheen Formation, supporting the lithologic correlation and consequent assignment of Devonian age.

Table 1. Paleomagnetic directions.

[N, number of specimens. *I*, *D*: inclination and declination in degrees.  $\alpha_{95}$ : radius of cone of 95-percent confidence (Fisher, 1953).  $\alpha_{MAX}$ ,  $\alpha_{MIN}$ : radii of ellipse of 95-percent confidence (Onstott, 1980).  $I_P$ ,  $D_P$ : inclination and declination of pole to plane of  $\alpha_{MAX}$ .]

Entry <sup>1</sup>	N	I	D	$\alpha_{95}$	$\alpha_{MAX}$	$\alpha_{MIN}$	$I_P$	$D_P$
<b>Redbeds</b> of Devonian Karheen Formation at Saginaw Bag								
1	53	50.4	66.8	7.1				
2	45	45.5	73.6	6.6				
3	25	24.6	60.9		12.7	6.0	64.0	261.2
4	25	25.6	249.0		17.3	5.7	64.4	69.6
5		80.0	329.5					
6		62.3	341.4	10.1				
7	15	38.7	77.5	4.6				
8	4	33.9	61.7	20.9				
9	4	22.1	38.5	20.0				
10	15	-22.5	79.2	4.6				
11	4	-17.3	57.8	20.9				
12	4	-2.6	36.2	20.0				
Permian Halleck Formation at <b>Saginaw Bay</b>								
13	8	-27.4	70.2	10.8				
14	4	-19.7	82.9	39.9				
15	6	-5.7	88.8	6.1				
16	8	-41.7	89.9	10.8				
17	4	-28.9	96.6	39.9				
18	6	-38.5	75.8	6.1				

<sup>1</sup>Description of entries:

1. Mean of all natural remanent magnetization (NRM) directions before structural correction.
2. Mean of selected NRM directions before structural correction, omitting data affected by post-Permian subordinate magnetic overprint.
3. Least-squares intersection (Kirschvink, 1980) of thermal demagnetization planes before structural correction.
4. Least-squares intersection of thermal demagnetization planes after structural correction.
5. Predicted Cretaceous field direction (van Fossen and Kent, 1992) assuming no post-Cretaceous displacement of Alexander terrane.
6. Cretaceous field direction predicted from results from Duke Island (Bogue and others, 1995).
7. Mean of best-fit thermal demagnetization lines for site I before structural correction.
8. As for entry 7: site **IIb**.
9. As for entry 7: site **IIc**.
- 10–12. As for entries 7–9, but after structural correction.
13. Mean of best-fit thermal demagnetization lines for a basaltic sill in the Halleck Formation before structural correction.
14. As for entry 13, for reheated limestone directly overlying the sill in the Halleck Formation.
15. As for entry 13, for pillow lava in the Halleck Formation.
- 16–18. As for entries 13–15, but after structural correction.

## FIELD AND LABORATORY METHODS

Two localities were sampled on the west shore of Saginaw Bay (site I at lat  $56^{\circ}51'44''$  N., long  $134^{\circ}11'13''$  W., and site II at lat  $56^{\circ}51'32''$  N., long  $134^{\circ}10'54''$  W.); at these localities oriented cores were obtained from four different structural blocks as follows: site I, 20 cores, strike  $358^{\circ}$ , dip  $62^{\circ}$  E.; site IIa, 12 cores, strike  $290.5^{\circ}$ , dip  $50^{\circ}$  N.; site IIb, 14 cores, strike  $304^{\circ}$ , dip  $56^{\circ}$  NE., site IIc, 10 cores, strike  $279^{\circ}$ , dip  $28^{\circ}$  E. The cores were obtained with a gasoline-powered portable diamond drill and were oriented with a magnetic compass and clinometer. Magnetic azimuths were checked by backsighting.

The rocks we sampled are interbedded reddish and orange siltstone and sandstone; the finer grained material tends to be redder. Minor calcite veins as much as 1 cm thick are present. At site IIa we observed felsic porphyry dikes about 5 m away from the first oriented cores; more complete descriptions of these dikes, which have not been dated, are given by Muffler (1967) and Brew and others (1984).

Laboratory measurements were made with a commercial three-axis superconducting magnetometer. Preliminary alternating-field demagnetizations were done with a commercial 400-Hz tumbling demagnetizer, but the results were not promising and will not be discussed further. Progress-

sive thermal demagnetizations were done in air with a laboratory-built nonmagnetic oven in which the residual magnetic field is less than 3 nT. Principal-component analysis (Kirschvink, 1980) was used to separate the different components of remanent magnetization in the **stepwise** thermal demagnetization data. Of the total of 56 oriented cores, specimens from 33 of them were thermally demagnetized, distributed as follows: site I, 15; site IIa, 6; site IIb, 6; site IIc, 6. This distribution of data among four sites with differing structural attitudes is expected to yield an effective fold or tilt test for magnetic stability. This test is fundamental to the technique of paleomagnetism and is considered to have a positive result when the angular dispersion of paleomagnetic directions decreases significantly after the data from various sampling sites are corrected for their respective structural attitudes. Traces of primary magnetization were found in only 25 of the 33 cores so treated, but all four sites (separate structural blocks) are represented in the final results.

## PALEOMAGNETIC RESULTS

A summary of our results is presented in table 1. The directions of natural remanent magnetization (NRM) be-

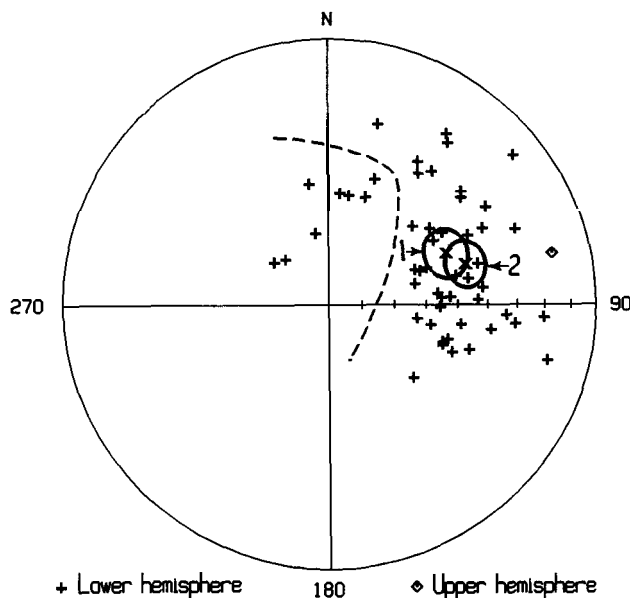


Figure 2. Equal-area projection of NRM directions in Devonian redbeds, before structural correction. Dashed line separates directions in specimens magnetically overprinted by adjacent dikes (left) from directions in specimens dominated by another overprint of different age (right). Two averages are shown with associated circles of 95-percent confidence: 1, average of all measurements; 2, average excluding specimens overprinted by local dikes (entries 1 and 2 in table 1).

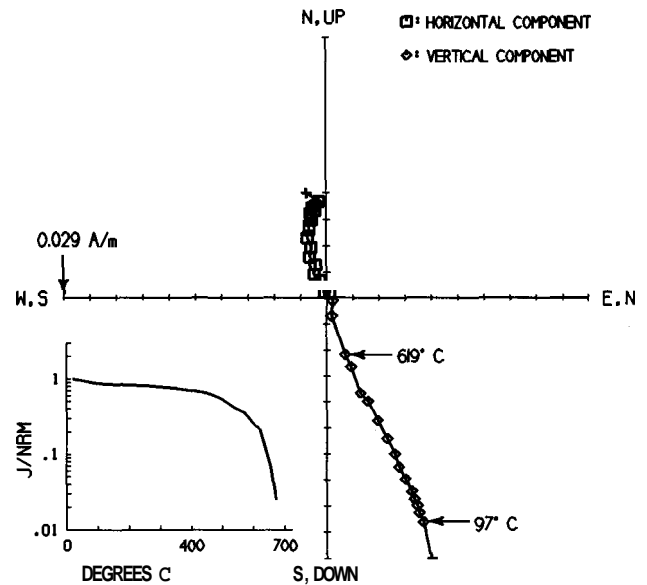
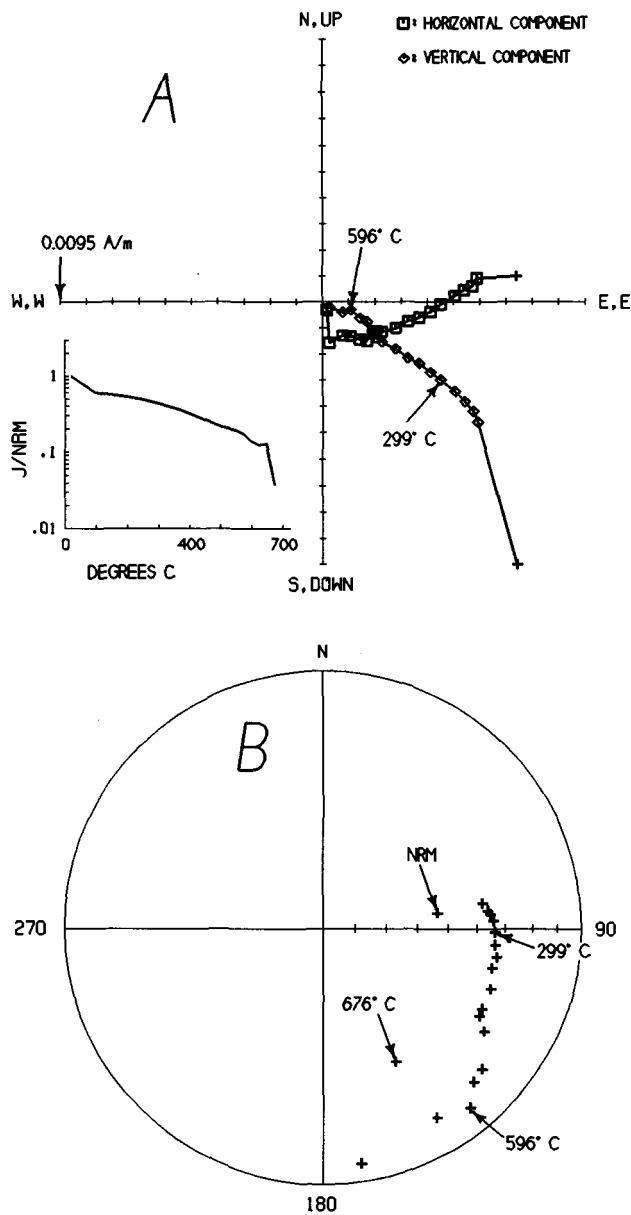


Figure 3. Vector component diagram showing thermal demagnetization (before structural correction) of a specimen carrying mainly a magnetic overprint caused by adjacent dikes. Scale is 0.0029 A/m per division. Inset shows decay of NRM with increasing temperature; units are magnetization intensity (J) normalized to initial value (NRM) and plotted on a logarithmic scale. Note that magnetization decays univectorially to the origin, and that most of NRM is thermally unblocked only at high temperature.

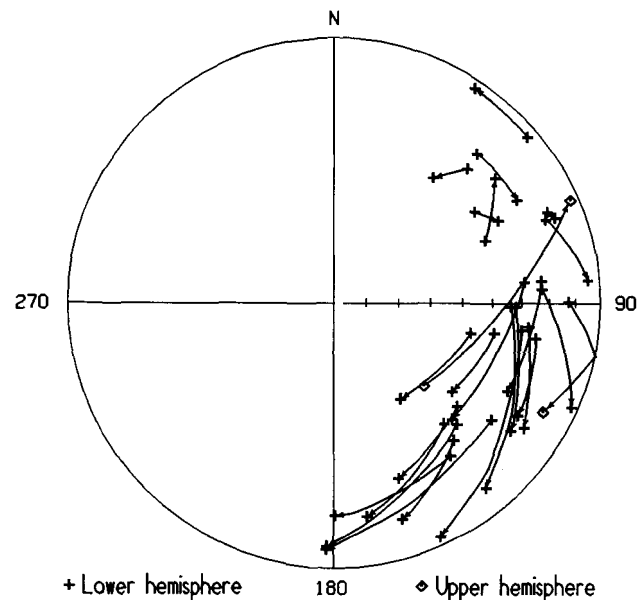
fore structural correction are shown in figure 2. Making the structural corrections (untilting the beds to horizontal around the strikes) caused the distribution of NRM directions to



**Figure 4.** Vector component diagram (A) and equal-area projection (B) showing thermal demagnetization (before structural correction) of a specimen carrying a combination of unipolar dominant overprint magnetization and original Devonian magnetization. Scale of vector diagram is 0.00095 A/m per division. Inset in A shows decay with temperature of NRM; units are magnetization intensity (J) normalized to initial value (NRM) and plotted on a logarithmic scale. Note that decay of magnetization is not univectorial and does not approach the vector origin; the 676° point in B represents laboratory artifact, as all NRM is erased by this heating step. Points from 299° through 596° are used to define the line and plane fit by least-squares to the demagnetization trajectory.

diverge; the Fisher (1953) concentration parameter for the four sites decreases from 15 to 2, signifying a strongly negative result of the fold test. Some of the NRM directions are directed northward and steeply down, and the proximity of the specimens carrying these directions to the porphyry dikes at site IIa indicates probable remagnetization by the dikes. Based on NRM direction and core location, we have divided the data into two populations as indicated in figure 2 and have calculated mean directions for the total population and for the subpopulation that appears negligibly affected by the dikes. The two means do not differ significantly, but the subpopulation does not have an elongate, or "streaked," distribution and therefore appears to represent one postfolding remagnetization. The mean of the subpopulation of NRM directions does not, however, represent any post-Silurian geomagnetic field direction that might be inferred for this part of southeastern Alaska, contingent on our poor knowledge of its pre-Cretaceous plate-tectonic history. Two of the questions arising from our new data are the age and cause of this dominant paleomagnetic overprint, because a somewhat similar overprint direction, characterized by normal polarity, easterly declination, and steep inclination, is ubiquitous in the pre-Cretaceous rocks we have sampled throughout southeastern Alaska, has been illustrated by Van der Voo and others (1980), and has also been discussed by Haeussler and others (1992a).

Progressive thermal demagnetization results from one of the cores nearest to the porphyry dikes are shown in



**Figure 5.** Equal-area projection showing least-squares planes fit to thermal demagnetization trajectories of all specimens unaffected by local magnetic overprint, before structural correction. Arrows indicate direction of change in magnetization directions with increasing temperature of demagnetization.

figure 3. The magnetization decays nearly univectorially toward the origin of the vector diagram and is stable to nearly the Curie temperature of hematite ( $675^{\circ}\text{C}$ ). This is clear evidence that remagnetization by the dikes was complete, supporting our subdivision of the NRM data.

In figure 4 we show progressive thermal demagnetization results for a core from site I that was apparently unaffected by the thermal event represented by the porphyry dikes but that clearly carries two earlier components of NRM. The lower temperature component is the dominant overprint (labeled 2 in figure 2), while at the highest temperatures no stable endpoint is reached. Nonetheless, in this example (which is typical of our best thermal demagnetization data) the great-circle distribution of directions is appropriate for least-squares analysis of intersecting best-fit planes (Kirschvink, 1980). We were able to fit plausible planes to 25 of the 33 sets of thermal demagnetization data. The arc segments fitted are illustrated in figure 5; segments corresponding to some of the cores are shorter than would provide optimal definition of their corresponding planes. Only 2 of the 25 planes are defined by arc lengths less than  $10^{\circ}$ , however, and the common intersection of the best-fit planes has good significance, both before and after structural correction. The best-fit planes after structural correc-

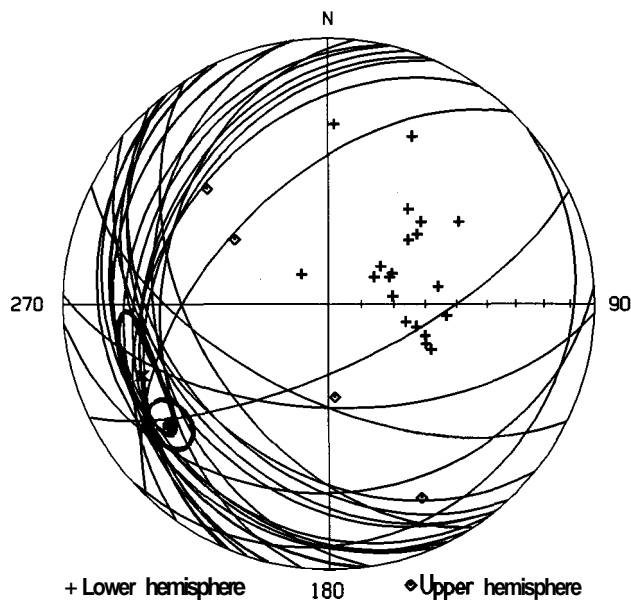


Figure 6. Equal-area projection showing common intersection of planes fit to thermal demagnetization trajectories, after structural correction. Planes are shown in lower hemisphere; plus and diamond symbols are poles to planes. "X" denotes locus of best-fit common intersection (Kirschvink, 1980), and surrounding ellipse represents bivariate 95-percent confidence interval (Onstott, 1980) as shown in table 1. Asterisk denotes magnetization direction in type Karheen Formation, with circle of 95-percent confidence (Bazard and others, 1995).

tion are shown in figure 6. Here the poles to the planes form only a fair girdle, but there are enough data that application of bivariate Bingham statistics (Onstott, 1980) to the best-fit pole to the girdle produces a gratifyingly small confidence ellipse centered on the mean common intersection of the planes (see entry 4 of table 1). Because this common intersection is pointed toward by the higher temperature ends of nearly all of the individual fitted segments (arrowheads, fig. 5), we conclude that the common intersection after structural correction represents the primary NRM direction even though none of the individual thermal demagnetization trajectories comes close to reaching it.

Bazard and others (1995) reported a mean primary NRM direction in 29 sites in the type area of the Karheen Formation (Eberlein and Churkin, 1970). These data from the Karheen Formation represent both geomagnetic polarities and pass both the fold test and the consistency-of-reversals test. We have added the mean direction given by them (declination  $232.7^{\circ}$ , inclination  $25.6^{\circ}$ , 95-percent confidence radius 7.1") to figure 6, and observe that it does not differ significantly from our inferred result for the Saginaw Bay redbeds (declination  $249.0^{\circ}$ , inclination  $25.6^{\circ}$ , with bivariate 95-percent confidence radii  $17.3^{\circ}$  and  $5.7^{\circ}$ ). We conclude that the redbeds at Saginaw Bay are part of the Karheen Formation, as surmised by Brew and others (1984). Moreover, within the intrinsic limits of accuracy of the paleomagnetic data, this concordance demonstrates existence of structural integrity across the part of the Craig subterrane of the Alexander terrane between localities K and S in figure 1.

Before structural correction, the poles to the planes fitted to the thermal demagnetization data form a somewhat better girdle than that shown in figure 6, and the ellipse of 95-percent confidence around the mean common intersection of the planes is correspondingly slightly smaller (entry 3, table 1). This intersection may represent the dominant overprint magnetization, which would therefore have been acquired after the sites had attained their contrasting structural attitudes and would ordinarily be referred to as "postfolding remagnetization." Use of the method of intersecting demagnetization planes for estimating mean directions in this way precludes use of the customary paleomagnetic fold test as described above because the mean of all the intersections of the best-fit planes is only an inferential representation of the original magnetization directions themselves. The mean intersections before and after structural correction are both well determined and are  $51^{\circ}$  of arc apart irrespective of polarity (calculated from entries 3 and 4 of table 1). Because these attributes imply that two separate magnetization directions have been estimated and that the magnetizations must have been acquired at quite different times, the results constitute a reasonable substitute for a positive conventional fold test (see Hillhouse and Gromme, 1988, for more extensive discussion of this method).

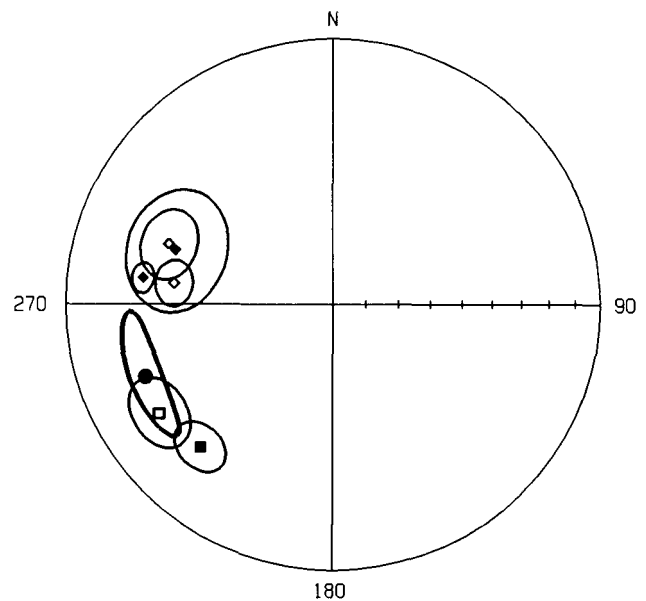
## DEVONIAN DATA FOR ALEXANDER TERRANE

Paleomagnetic data for Alexander Terrane rocks of Ordovician through Carboniferous age in the area around Craig have been published by Van der Voo and others (1980). Bazard and others (1995) state that one of the Devonian formations sampled by Van der Voo and others (the Wadleigh Limestone) is dominated by secondary magnetizations. We have reexamined the published data for the Wadleigh and concur that for one of the sites (site 4 in table 1 of Van der Voo and others, 1980) primary magnetization was probably not isolated. The other two Wadleigh sites of Van der Voo and others (1980), however, together with their Port Refugio Formation and Coronados Volcanics data, form a well-clustered set of four site-mean directions, two with reversed polarity and two with normal polarity, that are close to antipodal after structural correction and hence are unlikely to represent postfolding secondary magnetization. We show these previously published Devonian data in figure 7 for comparison with the Karheen Formation results.

The age of folding of the Paleozoic rocks in the area of Craig is not well known according to Bazard and others (1995) and Van der Voo and others (1980), but Gehrels and Saleeby (1987a,b) show results of comprehensive investigations of the Alexander terrane including the part of Prince of Wales Island south of the vicinity of Craig (fig. 1). A regional unconformity separates Upper Triassic strata from Lower Permian and older rocks (Gehrels and Saleeby, 1987b), so any hypothetical pre-folding and post-Devonian bipolar remagnetization would seem necessarily to have occurred prior to the Pennsylvanian-Permian superchron of constant reversed geomagnetic polarity. Evidence of igneous activity of this age is not present in the area of Prince of Wales Island (Eberlein and Churkin, 1970; Eberlein and others, 1983; Gehrels and Saleeby, 1987a), so existence of a bipolar post-Devonian predeformation remagnetization is unlikely.

The Devonian paleomagnetic data of Van der Voo and others (1980) have similar inclinations to those in the Karheen Formation, but the declinations of the 1980 data are of the order of  $50^\circ$  clockwise from the Karheen declinations (fig. 7). Bazard and others' (1995) Karheen sites are located about 30 km north of the Devonian sites of Van der Voo and others (1980), which are all located in the vicinity of Craig (fig. 1), so the declination difference could conceivably have a tectonic origin. Eberlein and others (1983) have shown on their map an inferred concealed throughgoing fault that separates these two areas. Nonetheless, a tectonic explanation seems unlikely in light of the widespread structural coherence of much of Prince of Wales Island and Kuiu Island evidenced by the paleomagnetic concordance of the two Karheen sampling areas that are

separated by 130 km. For bipolar regional remagnetization to have affected the Wadleigh, Port Refugio, and Coronados sampling sites (Van der Voo and others, 1980) but not the Karheen sites (Bazard and others, 1995) is also unlikely in view of the small separation (30 km) between the two areas. A third, ad hoc explanation for the declination difference would be relatively rapid apparent polar wander due to plate motion, which is possible because the Karheen Formation is Lower Devonian, whereas the Wadleigh Limestone, Coronados Volcanics, and Port Refugio Formation are all Middle and (or) Upper Devonian (Eberlein and Churkin, 1970; Van der Voo and others, 1980). This question cannot be resolved by the data available at present, but we note that Devonian paleomagnetic latitudes calculated for the Karheen Formation, Wadleigh Limestone, Port Refugio Formation, and Coronados Volcanics range from  $14^\circ$  to  $23^\circ$ , either north or south of the paleoequator (Van



- ◇ ● Middle and Upper Devonian (Van der Voo and others, 1980)
- ● Karheen Formation (Bazard and others, 1995)
- Karheen Formation (this study)

Figure 7. Equal-area projection showing comparison of inferred primary magnetization direction in Saginaw Bay red beds (table 1) with published paleomagnetic results from Devonian rocks in the vicinity of Craig. Directions are in the lower hemisphere; solid symbols denote normal polarity, and open symbols denote reversed magnetization projected through the origin. Upper Devonian rocks sampled are aquagene tuffs in the Port Refugio Formation and sandy and silty limestone in the Wadleigh Limestone; Middle Devonian data are from volcanoclastic rocks of the Coronados Volcanics (Van der Voo and others, 1980). The Karheen Formation is middle Lower Devonian (Bazard and others, 1995).



der Voo and others, 1980; Bazard and others, 1995). Within their respective formal uncertainties, these paleolatitudes are mutually consistent.

## POST-DEVONIAN SECONDARY MAGNETIZATIONS

We now turn to an attempt to identify the ages and causes of the two components of overprint magnetization in the **redbeds** at Saginaw Bay. Because the effect occurs only over a restricted area, we consider the remagnetization associated with the porphyry dikes to be subordinate in importance. In figure 8 we compare the direction of the dominant overprint, as estimated from the common intersection of best-fit planes before structural correction, with the mean NRM direction for specimens unaffected by the porphyry dikes. The two mean directions are similar, although not

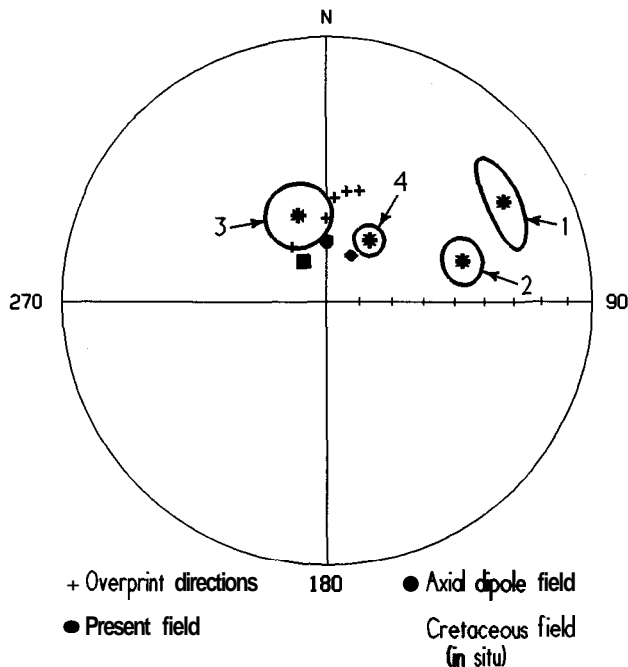


Figure 8. Equal-area projection on lower hemisphere showing evidence for ages of secondary magnetizations. Four directions are shown as asterisks with associated ellipses or circles of 95-percent confidence: 1, dominant postdeformational overprint direction from figure 7 and table 1; 2, average NRM direction of selected specimens as in figure 2 and table 1; 3, predicted Cretaceous field direction assuming the Alexander terrane was located 3,000 km to the south at that time (Bogue and others, 1995) (entry 6 in table 1); 4, Cretaceous overprint direction in Keku Strait (Haeussler and others, 1992a). In situ predicted Cretaceous field direction is derived from cratonic reference pole of van Fossen and Kent (1992) (entry 5 in table 1). Plus symbols are paleomagnetic directions in specimens overprinted by adjacent dikes; these are the best-fit lines for univectorial thermal demagnetization trajectories as in figure 3 and are the subordinate overprint.

identical. The fact that the thermal demagnetization trajectories represented in figure 5 nearly all move away from this common intersection (entry 3 of table 1) means that it represents a lower temperature component and hence is conventionally presumed to be younger, as is implicit in the analysis described above. These overprint directions are all in the lower hemisphere—that is, they have positive inclinations—which implies that they all represent one geomagnetic polarity. Thermal "pulses" or events that cause such pervasive remagnetization are likely to be of such long duration as to span many geomagnetic polarity reversals during most parts of geologic time, especially if the thermal events are visibly represented by coeval plutonic rocks. The only two post-Devonian times during which this was not so are in the Carboniferous-Permian superchron of constant reversed polarity and in the Cretaceous long normal superchron (Harland and others, 1990). Ancient pervasive unipolar paleomagnetic overprints are likely to have been produced during one of these two times.

Haeussler and others (1992a) found two post-Triassic magnetic overprint directions in the Triassic Hound Island Volcanics in Keku Strait (H in fig. 1). The older of these has a northeast and steeply downward direction and was assigned a maximum age of  $108 \pm 11$  Ma by interpretation of a large amount of complex data acquired by the  $^{40}\text{Ar}/^{39}\text{Ar}$  step-heating method using sericite and biotite (Haeussler and others, 1992a). The younger overprint was ascribed to heating by local gabbro intrusions that were dated at  $23 \pm 2$  Ma (using the same  $^{40}\text{Ar}/^{39}\text{Ar}$  method with plagioclase) and have typical Tertiary normal and reversed directions (Haeussler and others, 1992b). Other radiometric ages in this area have been presented by Douglass and others (1989): a K-Ar date of  $107 \pm 3$  Ma was obtained on hornblende from a granitic intrusion on the north end of Kupreanof Island, 10 km northeast of Kake (fig. 1). Two K-Ar dates were obtained from silicic intrusions on the northwestern corner of Kuiu Island 20 km southwest of our Saginaw Bay locality (fig. 1); these ages are  $24 \pm 1$  Ma (biotite in granite) and  $20 \pm 1$  Ma (hornblende in monzodiorite). Igneous rocks of these two age groups (Late Cretaceous and mid-Tertiary) are parts of the well-established Muir-Chichagof Belt II plutonic province (Brew and Morrell, 1983) and the Kupreanof-Etolin volcanic-plutonic belt (Brew, 1994), respectively. Thus, one interpretation of the bimodal NRM directions shown in figure 2 could be that they represent local Tertiary and regional Cretaceous overprints. We caution, however, that the age of the porphyry dikes at site IIa is unknown and that they are felsic in composition (Brew and others, 1984), whereas the Tertiary volcanism in the immediate vicinity is mafic in composition (Muffler, 1967; Haeussler and others, 1992a).

In figure 8 we have shown separately the paleomagnetic directions (determined by thermal demagnetization) at site IIa that we believe originated from reheating by the

nearby dikes. Because these directions are linearly distributed ("streaked"), we have not computed a mean; the magnetizations likely retain variable but small remnants of the dominant regional overprint. For comparison we show the present geomagnetic field direction, the axial geocentric dipole field direction (which can be considered to be typical of the latter part of Tertiary time if both polarities are considered), and the Cretaceous field direction calculated from the reference paleomagnetic pole for the North American craton given by van Fossen and Kent (1992). From these three reference fields it is not possible to identify an age for this overprint (which is quite different in direction from the dominant one). Butler and others (1993) have done extensive and thorough thermal demagnetization of many specimens from a variety of Devonian and Carboniferous formations in the general vicinity of Craig (fig. 1), and reported that the average direction of the secondary magnetizations that they isolated is within about 4° of parallel to the present geomagnetic field. In contrast, the results we show in figure 8 are unrelated to the present field direction at Saginaw Bay.

Use of the Cretaceous field direction calculated directly from the cratonic reference pole is not very useful because of the well-demonstrated 3,000 km northward movement of the westernmost Cordillera between mid-Cretaceous and mid-Eocene times (Bogue and others, 1995; Irving and others, 1996). Therefore, we include in figure 8 a field direction (data point 3) with confidence interval calculated directly from the paleomagnetic direction in the 110-Ma gravitationally layered **ultramafic** intrusions of Duke Island, 270 km to the southeast (Bogue and others, 1995) (D, fig. 1). Validity of this calculation rests on the assumptions that no large-magnitude post-Cretaceous displacement occurred on the Clarence Strait Fault that separates the Craig and Annette subterrane of the Alexander terrane, and moreover that Duke Island was not significantly rotated with respect to our Saginaw Bay locality. These assumptions seem acceptable because the direction calculated from the Duke Island data differs mainly in inclination from the craton reference, as would be predicted from simple northward transport of the Alexander terrane. This field direction transferred from Duke Island differs greatly from both the dominant overprint direction and from the selected mean NRM direction, and therefore if the dominant overprint is Cretaceous in age as we have suggested above, it is necessary to invoke post-Cretaceous westward tilting of at least our sampling area at Saginaw Bay. For site I this would mean that the beds were in an overturned position (by about 30°) when they were remagnetized and were subsequently partially restored to their present attitude. This is an improbable aspect of our hypothetical Cretaceous age assignment for the dominant overprint. Moreover, from the data illustrated in figure 8 it is not possible to choose between Tertiary or Cretaceous age to assign to the porphyry

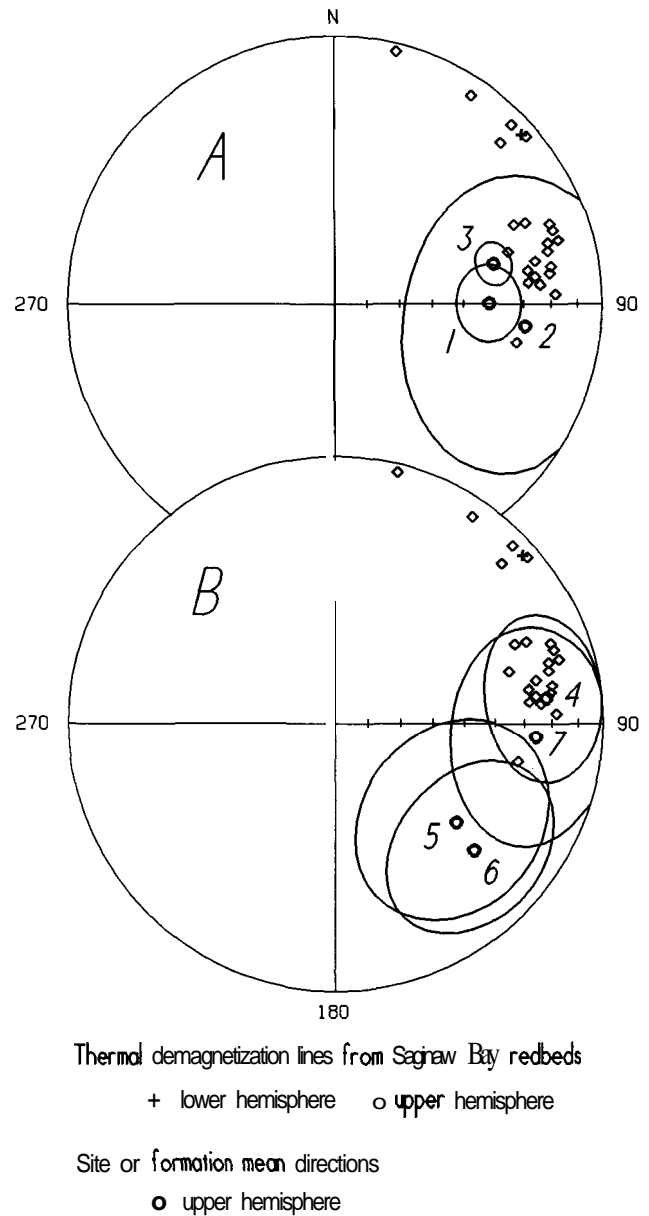


Figure 9. Equal-area projections comparing individual best-fit lines for overprint thermal demagnetization trajectories from three sites in the redbeds at Saginaw Bay after structural correction, with Permian and Carboniferous paleomagnetic data. A, comparison with preliminary thermal demagnetization data (averages of best-fit lines) from three sites in the Permian Halleck Formation at Saginaw Bay (entries 16-18 in table 1): 1, basaltic sill (8 specimens); 2, thin limestone reheated by the same sill (4 specimens); 3, pillow lava (6 specimens). B, comparison with selected results from Carboniferous rocks in the vicinity of Craig (Van der Voo and others, 1980): 4, white limestone in the Pennsylvanian Ladrone Limestone; 5, mudstone in the Pennsylvanian Klawak Formation; 6, limestone in the Klawak Formation; 7, all sites in the Mississippian Peratrovich Formation combined. Circles are 95-percent confidence cones centered on mean directions.

dikes that caused the local but complete remagnetization that we have termed the "subordinate overprint."

The question of regional tilting of the rocks subsequent to Cretaceous remagnetization was discussed at length by Haeussler and others (1992a). They concluded that the Cretaceous overprint direction they observed in Keku Strait (declination =  $35^\circ$ , inclination =  $67^\circ$ ,  $\alpha_{95} = 5^\circ$ ; shown as 4 in fig. 8) implies westward tilting of about  $20''$  around an axis trending  $339^\circ$ , and that this axis parallels the major structural trends in southeastern Alaska, but they also pointed out that no specific geologic or petrologic evidence could be found in support of such regional tilting. The pervasive paleomagnetic overprints that we have consistently observed in the Permian rocks we sampled in eastern Saginaw Bay and western Keku Strait, as well as other pre-Cretaceous rocks elsewhere in southeastern Alaska, are closely similar in direction to that reported by Haeussler and others (1992a) but are not parallel to the dominant overprint we have identified in our Karheen Formation samples (fig. 8), and so we seek another explanation for this overprint.

## PERMIAN PALEOMAGNETIC RESULTS

Permian mafic igneous rocks occur widely in the Saginaw Bay–Keku Strait area; they include andesitic flows in the Cannery Formation and basaltic volcanics in the Halleck Formation (Muffler, 1967). We sampled several volcanic units in the Halleck Formation, of which about half were paleomagnetically unstable. For comparison with the dominant overprint, we show in figure 9 preliminary results from three rock units in the Halleck Formation located at lat  $56^\circ 52' 40''$  N., long  $134^\circ 9' 2''$  W. in Saginaw Bay, 3 km northeast from our sampling sites in the Karheen **redbeds** (see also table 1). The results in figure 9 are structurally corrected and represent thermal demagnetization of a total of 18 specimens. Because there are only two independent structural attitudes for these three sites and because geomagnetic secular variation has not been averaged by such limited data, a fold test that can be evaluated statistically cannot be made. The angle between the mean directions for the two igneous rock units (which have different structural attitudes; compare entries 13 and 15 with entries 16 and 18 in table 1) decreases from  $28''$  to  $11''$  when the structural correction is made, however, which constitutes a qualitatively positive result of a minimal fold test.

In order to extend the comparison we have also obtained best-fit unconstrained lines ("free" lines in the sense of Kirschvink, 1980) to selected thermal demagnetization data from the Saginaw Bay **redbeds**, as illustrated by the example in figure 4, these lines do not trend toward the origin, but their site-mean directions (entries 7, 8, and 9 in table 1) are similar to the NRM directions shown in figure

2. In other words, these least-squares lines represent removal of the dominant secondary magnetization. For site **IIa**, no sufficiently collinear points exist in the thermal demagnetization data to define any lines, but 15 reasonable lines were obtained for site I, 4 for site **IIb**, and 4 of poor linearity for site **IIc**. The directions of the individual best-fit lines after structural correction are shown in both parts of figure 9. By making the comparison in this way (after structural correction) we are ignoring the significance of the negative fold test for the selected NRM directions, and this problem shows up in the distribution of the **redbed** data in figure 9. While most of the Devonian **redbed** data in figure 9A are close to the Permian results, 6 of the 23 directions have northeast declinations, significantly different from the Permian results. These 6 points are among the 8 from sites **IIb** and **IIc**, and we can only explain the divergence by stating that the best collinearity of points fit to lines was obtained for site I. In other words, the data for sites **IIb** and **IIc** represent more than one component of magnetization that are not resolved by the best-fit lines. With this reservation, it is clear from the comparison in figure 9A that the dominant secondary magnetization in these Devonian **redbeds** was acquired during Permian time.

To carry the comparison another step, we show in figure 9B four selected sets of paleomagnetic directions from Carboniferous rocks in the vicinity of Craig, published by Van der Voo and others (1980). We have selected these data as they appear to us to be least affected by the secondary magnetizations found by Butler and others (1993) in their reexamination of the paleomagnetism of the Paleozoic rocks in the vicinity of Craig. The 95-percent confidence circles for the Carboniferous mean directions are large, but two of the four enclose the site I group of thermal demagnetization lines from the Devonian **redbeds**. The differences among the Carboniferous data are not statistically significant and moreover cannot be explained by apparent polar wander. If we assume, however, that the shift in paleomagnetic direction at Prince of Wales Island that would be predicted from Carboniferous-Permian apparent polar wander was not large relative to these uncertainties, then the similarity between the Carboniferous directions and the thermally demagnetized overprint directions in figure 9B supports our conclusion that the dominant remagnetization is Permian in age.

## CONCLUSIONS

Three components of natural remanent magnetization (NRM) have been isolated in nonfossiliferous Paleozoic red arkose and siltstone exposed on the west shore of Saginaw Bay on northern Kuiu Island. The youngest component is either Tertiary or Cretaceous in age, has normal

polarity, is subordinate in distribution, and was likely caused by igneous activity represented by either the Kupreanof-Etolin volcanic-plutonic belt described by Brew (1994) or the Muir-Chichagof Belt II plutonic province defined by Brew and Morrell (1983). The next oldest component of NRM is inferred to be Permian but predeformation in age because of its coincidence after structural correction with paleomagnetic directions in igneous rocks of the Permian Halleck Formation at Saginaw Bay. **This** component has reversed polarity and is the dominant magnetic overprint. The third magnetization, inferred to be the oldest because it has the highest thermal retention (highest unblocking temperatures, near the Curie temperature of hematite), could only be isolated by finding the least-squares intersection of all the thermal demagnetization trajectories as corrected for tectonic dips. This oldest magnetization is closely coincident with that isolated by Bazard and others (1995) in the Lower Devonian Karheen Formation, 130 km to the south near Craig. We conclude that these **redbeds**, first tentatively assigned to the Silurian by Muffler (1967), are part of the Lower Devonian Karheen Formation, thus **confirming** the surmise of Brew and others (1984). Because of the near-coincidence of paleomagnetic declinations, structural unity appears to have existed since Devonian time across this restricted portion of the Craig subterrane of the Alexander terrane (fig. 1).

The paleomagnetic inclinations in the Karheen Formation correspond to a paleolatitude of about 14°, either north or south of the Devonian equator. The paleogeographic implications of this paleolatitude have been dealt with by Bazard and others (1995), who concluded that combining the paleomagnetic directions with **paleontological-provincial** inferences based on fauna in the underlying Silurian Heceta Limestone leads to placement of the Alexander terrane adjacent to the Scandinavian part of Baltica, in the Devonian southern hemisphere. Gehrels and others (1996) have combined the paleomagnetic data with evidence of provenance of Precambrian **detrital** zircons in rocks of the Alexander terrane to conclude that the terrane could have been adjacent to either the ancient Pacific margin of Australia-Antarctica or to that of Baltica during Late Silurian and Early Devonian time. We add that the paleolatitudes for other Devonian rocks in the vicinity of Craig, published earlier by Van der Voo and others (1980), support such paleogeographic reconstructions. Moreover, the reversed polarity we find in two igneous rock units in the Permian Halleck Formation, together with the almost completely reversed magnetization in the Pennsylvanian rocks of the Craig area reported by Van der Voo and others (1980), corroborate the reversed polarity inferred from a study of the Permian Pybus Formation in Keku Strait reported by Haeussler and others (1992a), who pointed out that this result implies that the Alexander terrane was in the northern hemisphere during the time of Pennsylvanian-Permian reversed geomagnetic polarity.

## REFERENCES CITED

- Bazard, D.R., Butler, R.F., Gehrels, G.E., and Soja, C.M., 1995, Early Devonian paleomagnetic data from the Lower Devonian Karheen Formation suggest Laurentia-Baltica connection for the Alexander terrane: *Geology*, v. 23, p. 707-710.
- Berg, H.C., Jones, D.L., and Coney, P.J., 1980, Map showing pre-Cenozoic tectonostratigraphic terranes of southeastern Alaska and adjacent areas: U.S. Geological Survey Open-File Report 78-1085, rev. 1980, 2 sheets, scale 1:1,000,000.
- Bogue, S.W., Gromme, Sherman, and Hillhouse, J.W., 1995, Paleomagnetism, magnetic anisotropy, and mid-Cretaceous paleolatitude of the Duke Island (Alaska) ultramafic complex: *Tectonics*, v. 14, p. 1,133-1,152.
- Brew, D.A., 1994, Latest Mesozoic and Cenozoic magmatism in southeastern Alaska, in Plafker, George, and Berg, H.C., eds., *The geology of Alaska: Boulder, Colo., Geological Society of America, The Geology of North America*, v. G-1, p. 621-656.
- Brew, D.A., and Morrell, R.P., 1983, Intrusive rocks and plutonic belts of southeastern Alaska, U.S.A., in Roddick, J.A., ed., *Circum-Pacific plutonic terranes: Geological Society of America Memoir 159*, p. 171-193.
- Brew, D.A., Ovenshine, A.T., Karl, S.M., and Hunt, S.J., 1984, Preliminary reconnaissance geologic map of the Petersburg and parts of the Port Alexander and Sumdum 1:250,000 quadrangles, southeastern Alaska: U.S. Geological Survey Open-File Report 84-405, 43 p., 2 sheets, scale 1:250,000.
- Butler, R.F., Gehrels, G.E., and Bazard, D.R., 1993, Secondary magnetizations in Paleozoic strata of the Alexander terrane, southeast Alaska [abs.]: *Eos (American Geophysical Union Transactions) Supplement*, October, p. 205.
- Douglass, S.L., Webster, J.H., Burrell, P.D., Lanphere, M.A., and Brew, D.A., 1989, Major-element chemistry, radiometric ages, and locations of samples from the Petersburg and parts of the Port Alexander and Sumdum quadrangles, southeastern Alaska: U.S. Geological Survey Open-File Report 89-527, 66 p., 1 sheet, scale 1:250,000.
- Eberlein, G.D., and Churkin, Michael, Jr., 1970, Paleozoic stratigraphy in the northwest coastal area of Prince of Wales Island, southeastern Alaska: U.S. Geological Survey Bulletin 1284, 67 p.
- Eberlein, G.D., Churkin, Michael, Jr., Carter, Claire, Berg, H.C., and Ovenshine, A.T., 1983, Geology of the Craig quadrangle, Alaska: U.S. Geological Survey Open-File Report 83-91, 52 p., 4 sheets, scale 1:250,000.
- Fisher, R.A., 1953, Dispersion on a sphere: *Proceedings of the Royal Society of London, Series A*, v. 217, p. 295-305.
- Gehrels, G.E., Butler, R.F., and Bazard, D.K., 1996, Detrital zircon geochronology of the Alexander terrane, southeastern Alaska: *Geological Society of America Bulletin*, v. 108, p. 722-734.
- Gehrels, G.E., and Saleeby, J.B., 1987a, Geology of southern Prince of Wales Island, southeastern Alaska: *Geological Society of America Bulletin*, v. 98, p. 123-137.
- 1987b, Geologic framework, tectonic evolution, and displacement history of the Alexander terrane: *Tectonics*, v. 6, p. 151-173.
- Haeussler, P.J., Coe, R.S., and Onstott, T.C., 1992a, **Paleomag-**

- netism** of the Hound Island Volcanics: revisited: *Journal of Geophysical Research*, v. 97, p. 19,617-19,639.
- Haeussler, P.J., Coe, R.S., and **Renne**, Paul, 1992b, **Paleomagnetism** and geochronology of 23 Ma gabbroic intrusions in the Keku Strait, Alaska, and implications for the Alexander terrane: *Journal of Geophysical Research*, v. 97, p. 19,641-19,649.
- Harland, W.B., Armstrong, R.L., Cox, A.V., Craig, L.E., Smith, A.G., and Smith, D.G., 1990, A geologic time scale 1989: Cambridge, England, Cambridge University Press, 263 p.
- Hillhouse, J.W., and Gromme, Sherman, 1980, Paleomagnetism of the Triassic Hound Island Volcanics, Alexander terrane, southeastern Alaska: *Journal of Geophysical Research*, v. 85, p. 2,594-2,602.
- 1988, Early Cretaceous paleolatitude of the **Yukon-Koyukuk** province, Alaska: *Journal of Geophysical Research*, v. 93, p. 11,735-11,752.
- Irving, Edward, Wynne, P.J., Thorkelson, D.J., and Schiarizza, P., 1996, Large (1000 to 4000 km) northward movements in the northern Cordillera 85 to 45 Ma: *Journal of Geophysical Research*, v. 101, p. 17,901-17,916.
- Kirschvink**, J.L., 1980, The least-squares line and plane and the analysis of paleomagnetic data: *Geophysical Journal of the Royal Astronomical Society*, v. 62, p. 699-718.
- Muffler, L.J.P. 1967, Stratigraphy of the Keku Islets and neighboring parts of **Kuiu** and Kupreanof Islands, southeastern Alaska: U.S. Geological Survey Bulletin 1241-C, 52 p.
- Onstott, T.C., 1980, Application of the Bingham distribution function in paleomagnetic studies: *Journal of Geophysical Research*, v. 85, p. 1,500-1,510.
- Ovenshine, A.T., 1975, Tidal origin of parts of the Karheen Formation (Lower Devonian), southeastern Alaska, in Ginsburg, R.N., ed., Tidal deposits, a **casebook** of recent examples and fossil counterparts: New York, Springer-Verlag, p. 127-133.
- Silberling, N.J., Jones, D.L., Monger, J.W.H., Coney, P.J., Berg, H.C., and Plafker, George, 1994, Lithotectonic terrane map of Alaska and adjacent parts of Canada, in Plafker, George and Berg, H.C., eds., *The geology of Alaska: Boulder, Colo., Geological Society of America, The Geology of North America*, v. **G-1**, pl. 3.
- Van der Voo, Rob, Jones, Meridee, Gromme, Sherman, Eberlein, G.D., and **Churkin**, Michael, Jr., 1980, Paleozoic **paleomagnetism** and northward drift of the Alexander terrane, southeastern Alaska: *Journal of Geophysical Research*, v. 85, p. 5,281-5,296.
- van Fossen, M.C., and Kent, D.V., 1992, Paleomagnetism of 122 Ma plutons in New England and the **mid-Cretaceous** field in North America: true polar wander or large-scale differential mantle motion?: *Journal of Geophysical Research*, v. 97, p. 19,651-19,661.

Reviewers: Peter J. Haeussler and Jon T. Hagstrum

# Description and Regional Setting of the Silver Bay Segment of the Sitka Fault Zone, Southeastern Alaska, and Evidence for Possible Sinistral Separation

By David A. Brew

## ABSTRACT

The Silver Bay segment is part of the regional 200-km-long high-angle Sitka fault zone, a zone that has had an important role in the tectonic and metallogenic history of the northwestern part of southeastern Alaska. The Silver Bay segment contains kilometer-scale slivers of a distinctive highly altered dioritic rock of inferred Jurassic age that are separated about 20 km sinistrally from Wrangellia terrane intrusive rocks of inferred Jurassic age. That separation may be the remnant of a larger **post-Jurassic** separation that has been cancelled in part by dextral movements of late Tertiary age. The inferred sinistral separation contrasts with the dominant dextral separation of most of the major faults in the region. The Silver Bay segment is about 40 km long and is a fault zone about 0.4-2.0 km wide that includes different numbers of strands at different places, gouge units, slices of the relatively undeformed Cretaceous and other rocks that border the segment, and horses of serpentinite, Triassic(?) metacarbonate, and distinctive Jurassic(?) diorite. The history of tectonic movements in the vicinity of the Silver Bay segment involves several events: (1) mid-Cretaceous compression of Chugach terrane (Kelp Bay Group) rocks against Wrangellia terrane rocks to the east on the Border Ranges fault; (2) coeval and perhaps later collapse of the Sitka Graywacke flysch prism against the Kelp Bay Group rocks to the east; and (3) subsequent long-lived but probably intermittent Tertiary transcurrent movements on faults approximately parallel to the Chugach-Wrangellia terrane boundary and to the offshore Fairweather-Queen Charlotte fault.

## INTRODUCTION

The Silver Bay segment is part of the 200-km-long Sitka fault zone as defined by Loney and others (1975, p. 71). Plate 3 of that report shows the main parts of the Sitka fault zone: the Islas Bay, Neva Strait, and Patterson Bay faults. The Silver Bay segment of the Sitka fault zone pro-

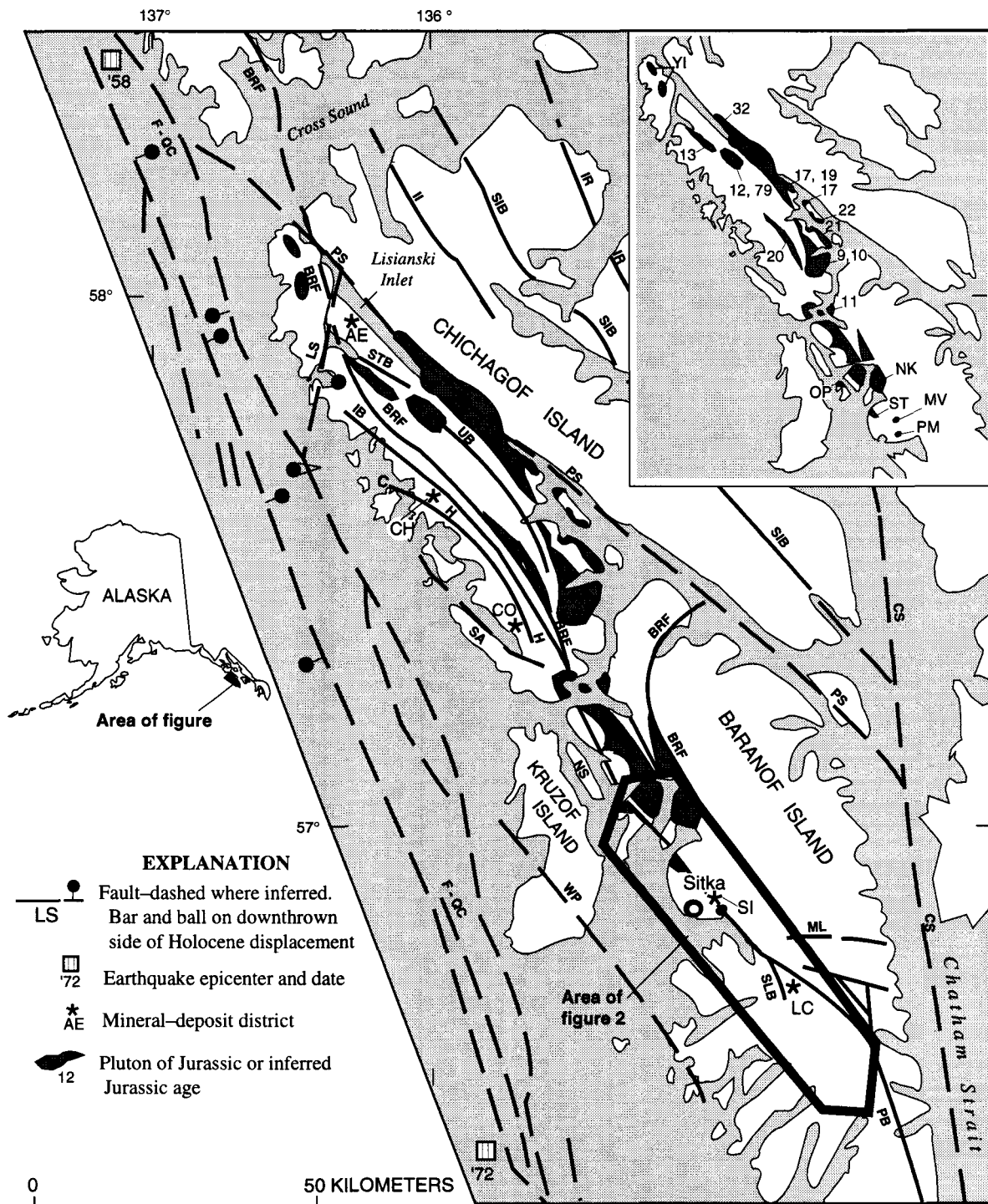
vides the best and most readily accessible exposures of this major fault and was therefore selected for the study reported here. This article describes the geologic features in and around the Silver Bay segment together with its regional setting; in addition, it is speculated that the distribution of distinctive dioritic horses along the fault indicates sinistral separation of about 20 km.

The Sitka fault zone is one of several major fault zones in northern southeastern Alaska (Loney and others, 1975; Brew and others, 1991c). It is a high-angle fault zone that has had an important role in the tectonic and metallogenic history of the northwestern part of southeastern Alaska. The Sitka fault zone extends from about **Yakobi** Island on the north to the east coast of **Baranof** Island on the south and has three major segments: (1) an unnamed wide zone in western Chichagof Island, referred to here as the west Chichagof fault system, which has the Islas Bay fault as a major component; (2) the Neva Strait fault; and (3) the Patterson Bay fault (fig. 1). The Sitka fault zone is (1) located close to the original site of the tectonic boundary between the flysch and the **mélange** facies of the Chugach lithotectonic terrane; (2) a localizing factor, together with a family of 50-Ma granitic plutons, of significant low-sulfide gold-quartz deposits (fig. 1)—namely, the Apex-El Nido, Chichagof, Cobol, Sitka, and Lucky Chance districts (Twenhofel and Sainsbury, 1958; Rossman, 1959; Brew and others, 1991a; Taylor and others, 1994); (3) related to past and perhaps the present regime of transcurrent continental-margin tectonics; (4) locally coincident with the Border Ranges fault, which separates the Chugach and Wrangellia lithotectonic terranes, because of young movements on the Sitka fault; and (5) a localizing factor, together with the currently active outboard Fairweather-Queen Charlotte fault, in the development of the Holocene-age Mount Edgecumbe volcanic field on nearby **Kruzof** Island (Riehle and others, 1992).

The most conclusive evidence of the separation in the Sitka fault zone is 8 km of dextral offset of 50-Ma, **pre-30-Ma** age plutonic units along its southern extension, the Patterson fault (Loney and others, 1975, p. 72). There is

also one place on southern Chichagof Island where offset Cretaceous-age geologic units allow estimation of 10 km of overall dextral displacement (see below; Loney and others, 1975; Johnson and Karl, 1985). However, near Sitka, the fault zone is the host of kilometer-scale slivers of a distinctive highly altered dioritic rock of inferred Jurassic

age that suggest a maximum of about 20 km of sinistral separation from similar Jurassic plutonic rocks in the Wrangellia terrane. That separation may be the remnant of a larger post-Jurassic separation (Hart, 1995) that has been cancelled in part by dextral movements of late Tertiary age. Alternatively, the separation could be a relict from an



original distribution of small dioritic stocks or from dioritic blocks having been incorporated in the Kelp Bay *mélange*. Regionally, there are significant numbers of plutons of Jurassic and inferred Jurassic age in the Alexander terrane in addition to those rocks in the Wrangellia terrane (fig. 1). At present the Sitka fault zone is aseismic (Geological Survey of Canada, 1994), and there is no evidence of offset of Holocene deposits. However, Rossman (1959, p. 195, 196) and Plafker and others (1994) used geomorphic features interpreted to be fault scarps to suggest the possibility of recent offsets on northern Chichagof Island.

## GENERAL FEATURES OF THE SITKA AND RELATED FAULT ZONES

The Sitka fault zone is on western Chichagof and **Baranof** Islands between the offshore Queen Charlotte fault (fig. 1; Carlson and others, 1979) and the inboard Peril Strait and **Chatham** Strait faults (fig. 1; Ovenshine and Brew, 1972; Loney and others, 1975; Sonnevil, 1981; Hudson and others, 1982). The **Fairweather–Queen** Charlotte fault is currently among the most active in the Pacific region and currently has about 4 **cm/yr** right-lateral movement

(Page, 1969; Plafker and others, 1976) and has had an estimated total of 600 km of right-lateral Neogene movement (Plafker, 1987, p. 256). The Peril Strait fault connects the Fairweather–Queen Charlotte fault with the **Chatham** Strait fault and does not offset Holocene units, nor is it seismically active (Geological Survey of Canada, 1994). It records at least 40 km of right-lateral movement since the middle Cretaceous (Loney and others, 1975, p. 71). The **Chatham** Strait fault is seismically active at its northern end (Brew and others, 1995), which is north of the area shown on figure 1; it is a major regional fault and in southeastern Alaska records about 150–180 km of right-lateral separation since middle Tertiary time (Ovenshine and Brew, 1972; Sonnevil, 1981; Hudson and others, 1982). Seismic activity still farther north, on the **Shakwak** segment of the Denali system, currently appears to be transferred westward to the Fairweather–Queen Charlotte fault by way of a poorly understood seismic zone in northern Glacier Bay (Homer, 1990; Brew and others, 1995). As noted above, the Sitka fault zone itself is aseismic (Geological Survey of Canada, 1994).

The history of tectonic movements in the vicinity of the Sitka fault zone involves several events, two of which predate the fault movements just described. The first is mid-Cretaceous compression of Chugach terrane (Kelp Bay Group) rocks against Wrangellia terrane rocks to the east on the Border Ranges fault; the second is the coeval and perhaps later collapse of the Sitka Graywacke flysch prism against the Kelp Bay Group rocks to the east. The subsequent history involves long-lived but probably intermittent Tertiary transcurrent movements on faults approximately parallel to the Chugach–Wrangellia terrane boundary and to the offshore Fairweather–Queen Charlotte fault. A Border Ranges fault-related event is interpreted to have been post-Early Cretaceous and **pre-50-Ma** because the Chugach terrane *mélange* is as young as Valanginian (Plafker and others, 1976; Plafker and Berg, 1994) and the Border Ranges fault is intruded and stitched by a 50-Ma pluton about 140 km to the north on western Chichagof Island. This event may be dated more exactly by the middle Cretaceous age of metamorphic minerals in the *mélange* on western Chichagof Island (Decker and others, 1980). The collapse of the Sitka Graywacke flysch prism is inferred to have occurred within the same period but to have persisted somewhat longer. These interpretations could be refined if the precise age of the Cretaceous Sitka Graywacke were known; Loney and others (1975) discussed the **then**-available evidence (which is still the only available evidence) and interpreted the unit's age to be Cretaceous. The possible age correlations were also discussed by Brew and **Morrell (1979b)**, who concluded that no more accurate age could be supported for the rocks in the Sitka region. The subsequent transcurrent movements were between 50 Ma and 25 Ma based on displaced plutons (Loney and

---

Figure 1. Sketch map of Chichagof and **Baranof** Islands and of southeastern Gulf of Alaska, showing the Sitka fault zone, other faults and lineaments, the seaward extension of the **Fairweather–Queen** Charlotte fault system, the distribution of distinctive dioritic bodies of inferred Jurassic age, and selected mineral-deposit locations. Modified from Loney and others, 1975; Carlson and others, 1979; Johnson and Karl, 1985; and Karl and others, 1988, 1990. Fault abbreviations as follows: BRF, Border Ranges; C, Chichagof; CS, **Chatham** Strait; F-QC, Fairweather–Queen Charlotte; H, Hirst; **IB**, **Islas** Bay; **II**, Idaho Inlet; IR, Indian River; LS, **Lisianski** Strait; ML, Medveje Lake; NS, Neva Strait; PB, Patterson Bay; PS, Peril Strait; SA, Slocum Arm; SIB, Sitkoh Bay; SLB, Silver Bay; STB, Stag Bay; UB, Ushk Bay; WP, Windy Passage. The Sitka fault zone includes the West Chichagof fault system (which consists of C, IB, H, SA, STB, UB, NS, PB, and SLB). Most of these faults are younger than the BRF (Border Ranges fault) and have locally modified it; the **BRF** location is modified from Johnson and Karl (1985) and Karl and others (1990). Mineral-deposit districts shown by black asterisks are as follows: AE, Apex–El Nido; CH, Chichagof; CO, Cobol; LC, Lucky Chance; and SI, Sitka. Metaplutonic bodies interpreted here to be "ugly diorite" (term from Karl and others, 1988) of inferred Jurassic age are shown as black areas and are labeled with the Loney and others (1975) numbers: 12, 13, 15, 20, and with MV, Mount Verstovia; NK, Nakwasina Sound; OP, Olga Point; PM, Pulp Mill at Silver Bay; ST, Starrigavan Bay; and YI, **Yakobi** Island. Plutons of known Jurassic age plutons are labeled with the Loney and others (1975) numbers: 9, 10, 11, 17, 19, 21, 32, 22, and 79 for sake of completeness. The contacts of many of the bodies identified with the Loney and others (1975) numbers have been modified by Johnson and Karl (1985).



others, 1967, 1975), but both earlier movements and later movements are considered possible. The speculative sinistral displacement discussed in this article could have occurred as part of any of these episodes, or conceivably even earlier.

The Sitka fault zone appears simple regionally, but it is complicated in detail (Loney and others, 1975, p. 71-72; Johnson and Karl, 1985). Between Lisianski Strait and the north end of Neva Strait (LS and NS on fig. 1), the broad West Chichagof fault system includes the Stag Bay, Ushk Bay, Islas Bay (also known as Sea Level), Hirst, Chichagof, and Slocum Arm faults, as well as a number of smaller unnamed faults. Along Neva Strait south to about Nakwasina Sound (NK on fig. 1) the Neva Strait fault has a single major trace bounded by wide zones of cataclasis and some minor strands. About 10 km north of Sitka, the Neva Strait fault splits into at two major, but closely adjacent, strands that are the northern expression of the Silver Bay segment. At and north of Silver Bay itself, the Silver Bay segment is a 0.4- to 1.0-km-wide zone with sharp bounding faults (figs. 2, 3). South of Silver Bay, the segment connects to the Patterson Bay fault (fig. 1) through a complex of en echelon faults and cataclastic zones marked by lineaments. The original mapping (Berg and Hinckley, 1963; Loney and others, 1975) did not fully portray the scale or intensity of deformation in this particular part of the Sitka fault zone. The well-developed lineaments on central Baranof Island are shown in figure 2 to indicate their lack of correspondence to any faults. Brew and others (1963) established that only a very few of those lineaments are faults; instead, most are related to bedding, foliation, and joints.

At the northern end of the Sitka fault zone near Lisianski Strait and Yakobi Island, which is close to the juncture of the Peril Strait and Fairweather-Queen Charlotte faults in Cross Sound (fig. 1), the well defined faults of the zone appear to die out (Loney and others, 1975; Johnson and Karl, 1985). At its southern end, the Patterson Bay fault is interpreted to join the Chatham Strait fault (Loney and others, 1975).

## GEOLOGIC RELATIONS IN AND ALONG THE SITKA FAULT ZONE

The specific geologic relations in and along all of the Sitka fault zone provide the framework for the detailed description of the Silver Bay segment; those relations are therefore described briefly here. The Sitka fault zone cuts a variety of units and varies in its relation to the nearby Border Ranges fault, which is the boundary between the Chugach lithotectonic terrane to the west and the Wrangellia terrane to the east (Plafker and others, 1976). The Chugach terrane consists of the *mélange-facies* Kelp Bay Group and

the accretionary flysch prism Sitka Graywacke. At the northern end of the Sitka fault zone, in the West Chichagof fault system (fig. 1), several individual strands are sharply defined (Loney and others, 1975; Johnson and Karl, 1985) and the system is only about 5 km from and is parallel to the Border Ranges fault. One of the two northern strands terminates against the Mirror Harbor gabbroic body of probable 40- to 43-Ma age (Brew, 1994). The other terminates against the Lisianski Strait fault, which is a north-northeast-trending feature with about 2 km of possible post-50-Ma right-lateral separation on the trace of the Border Ranges fault (Johnson and Karl, 1985) that may be due to a combination of right-lateral and southeast-side-down displacement. Apparently, the movement on the West Chichagof fault system either died out or, more likely, was transferred to the Fairweather-Queen Charlotte fault by way of the Lisianski Strait fault. The rocks in and to the west of the West Chichagof fault zone consist of Kelp Bay Group *mélange*, Sitka Graywacke, and large kilometer-scale slivers of highly altered diorite of Jurassic(?) age that is referred to familiarly as the "ugly diorite" (Karl and others, 1988); the "ugly diorite" and other Jurassic plutonic rocks are also present in the Wrangellia and Alexander terranes to the northeast (fig. 1). To the east are the same units and a tectonic collage containing a variety of small-fault-bounded blocks that is part of the Kelp Bay Group as defined by Karl and others (1982).

About 20 km to the south of Lisianski Strait, near the Chichagof gold camp (CH on fig. 1), there is an echelon southwestward stepping of the faults of the West Chichagof zone, and most strands are in the Sitka Graywacke. These strands, together with other smaller strands, merge into the Slocum Arm fault (which is the northwestern extension of the Neva Strait fault) about another 40 km to the southeast. At that point, rocks of the Kelp Bay Group are on both sides of the Sitka fault zone, and the Border Ranges fault is less than 2 km distant from the zone. It is in this area that the 10 km of dextral separation is estimated from Loney and others (1975) to be present on the Slocum Arm fault.

Along the Neva Strait fault (fig. 1), most of the rocks to the west belong to the Kelp Bay Group and Sitka Graywacke (Loney and others, 1975), but a small sliver of Jurassic(?) dioritic rock like that common in the Wrangellia terrane is also exposed (fig. 2) (Karl and others, 1988, 1990). Rocks to the east are the Kelp Bay Group and a Jurassic-age Wrangellia terrane pluton (Loney and others, 1975; Brew and others, 1988; Karl and others, 1990). To the south is the fault segment referred to here as the Silver Bay segment, which is described in detail below. At its southern end, the Silver Bay segment is mostly within rocks of the Kelp Bay Group (Loney and others, 1975; Karl and others, 1982) and passes through a poorly understood series of en echelon branches into the Patterson Bay fault.

Along the Patterson Bay fault (fig. 1), rocks to the west are mostly low-metamorphic-grade Sitka Graywacke

and undivided Kelp Bay Group (Loney and others, 1975; Loney and Brew, 1987; Brew and others, 1992). Rocks to the east were mapped as belonging to the Kelp Bay Group by Loney and others (1975), but the stratigraphic assign-

ment of these latter rocks is not entirely clear (Brew and Morrell, 1979a). At its southern end the Patterson Bay fault is interpreted to merge with the Chatham Strait fault (Loney and others, 1975).

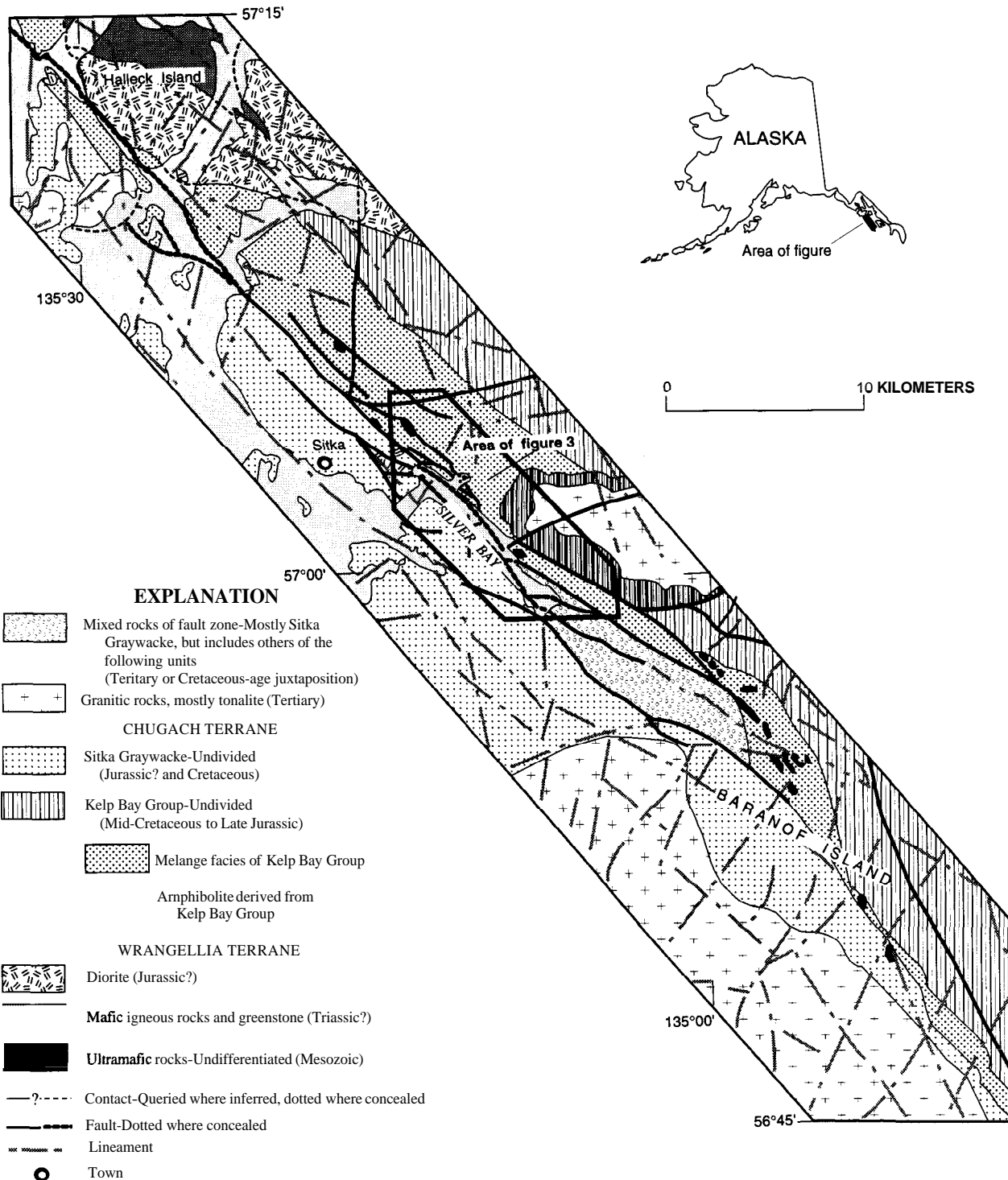


Figure 2. Sketch map of the Sitka area, showing map units adjacent to the Silver Bay fault, its traces, and other fault segments and lineaments. Modified from Loney and others (1975), Karl and others (1990), and from unpublished lineament maps by D.A. Brew. Surficial deposits not shown. Base map compiled from Sitka and Port Alexander 1:250,000-scale topographic maps.

### SILVER BAY SEGMENT DESCRIPTION AND INTERPRETATION

The Silver Bay segment is the southern part of the Neva Strait fault part of the Sitka fault zone as defined by Loney and others (1975, p. 71-72, pl. 2). The present study

was undertaken primarily to provide detailed information on this major fault zone, which is relatively accessible on shorelines and by roads and trails; in contrast, most major faults in southeastern Alaska are either concealed by water or are in very difficult terrain. The detailed mapping for this study was done intermittently, a few days at a time, from 1981 to 1992. The study draws on earlier work by

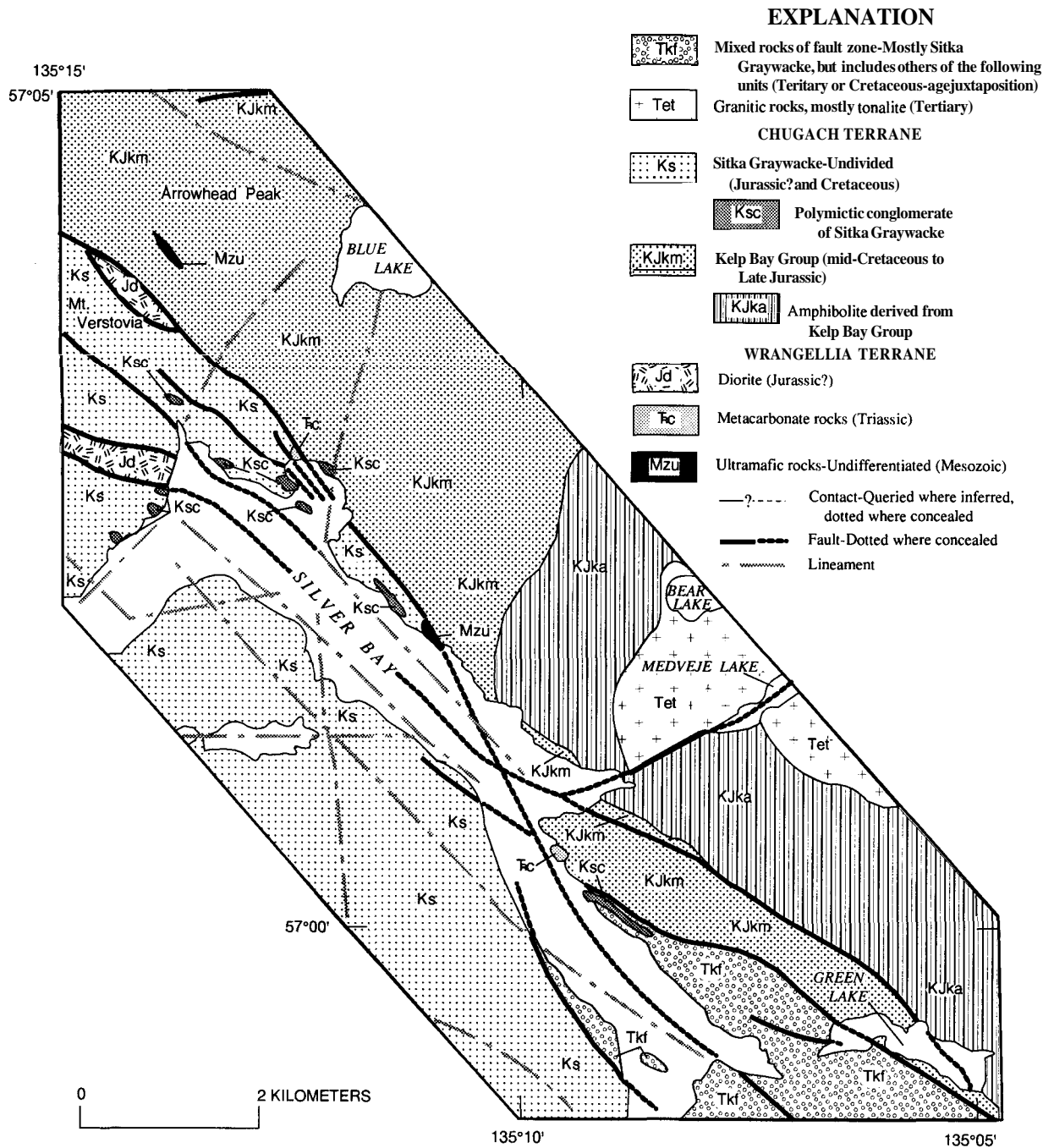


Figure 3. Sketch map of the Silver Bay fault at Silver Bay, showing fault traces, lineaments, and detailed map units. Based on unpublished mapping by H.C. Berg and D.W. Hinckley, 1960; H.C. Berg, 1961; D.A. Brew, 1981-1982; and modified in part from Loney and others (1975) and Karl and others (1990). Surficial deposits not shown. Base map compiled from Port Alexander D-4 and Sitka A-4 1:63,360-scale topographic maps.

Berg and Hinckley (1963), Loney and others (1975), and Karl and others (1990), and it incorporates some preliminary findings of the recent study of Haeussler and others (1994).

The detailed mapping of the Silver Bay segment provides a perspective on the complexity of all of the major Chichagof and **Baranof** Island faults and fault zones that has not been available from previous reconnaissance studies. The Silver Bay segment extends from about 20 km north of Sitka south to the Patterson Bay fault (fig. 1); it is a fault zone (fig. 3) about 40 km long and 0.4–2.0 km wide that includes different numbers of strands at different places, gouge units, slices of the less deformed Cretaceous and other rocks that border the segment, and horses of serpentinite, metacarbonate, and distinctive Jurassic(?) diorite. The four kilometer-scale dioritic horses may have been derived from units exposed on and near Halleck Island (fig. 2), about 20 km north of Silver Bay. They are indicated by "OP", "ST", MV, and "PM" on figure 1 and by the units with the symbol "Jd" on figure 3. The horses suggest that the main sense of movement on the fault is sinistral. This suggestion contrasts with the dextral separation of about 10 km estimated for the Slocum Arm fault (Loney and others, 1975, pl. 1) and 8 km of right-lateral separation on the Patterson Bay fault (Loney and others, 1975, p. 72; Brew and others, 1991b). All of these separations, except the last noted, probably resulted from the most recent movements of late Tertiary or Holocene(?) age, and the inferred 20 km of sinistral separation may be the remnant of an older and larger separation that has been reduced by younger dextral movements. Two alternative explanations for the distribution of the diorite slices have been proposed: G. Plafker (U.S. Geological Survey, written commun., 1996) suggested that the slices were originally olistostromal blocks in the Kelp Bay Group **mélange** rather than being fault blocks derived from now-exposed plutons. The source or provenance of the olistostromal blocks would presumably be the same Jurassic-age plutons noted above. The other alternative explanation is that the slices are fault-modified stocks that are more or less in their original locations.

The wide variety of rock types and units in the Silver Bay fault segment, the fact that some of the rocks now in the segment were metamorphosed before their incorporation in the zone and their original character thus obscured local cross-faulting, and the absence of exposure except along roads, trails, and shorelines all complicate the mapping of the fault. The fault strands have been mapped in the highland areas by a combination of field observations and interpretation of topography, aerial-photo features, and side-looking-aperture-radar images. Some of the complexities readily discernible from detailed mapping (figs. 2, 3) are that (1) no single major strand continues for more than several kilometers; (2) major strands are offset from each other by less than 1 km; (3) major strands generally under-

lie the major waterways; (4) the number of strands increases from two about 15 km north of Sitka to a maximum of five near the mouth of Silver Bay, then decreases to three at the head of the bay; (5) slices near the sides of the fault zone are comprised mostly of rocks adjacent to the fault; (6) serpentinite lenses occur along some strands but are small and local; and (7) structural strikes in rocks within each slice tend to parallel the adjoining strands. The two major slices in the northern part of the fault are described in more detail below.

The fault slices noted in point (5) above are so abundant and so narrow near the head of Silver Bay that they are classified as a separate fault-bounded map unit (**TKf** on fig. 3). The individual slices consist of lozenges and horses of graywacke, slate, and argillite like that in the Sitka Graywacke bounding the fault segment.

A variety of types and orientations of shear-sense indicators would be expected in the fault zone given its complex history. There could be indicators associated with the compression of the Chugach terrane Kelp Bay Group rocks against Wrangellia **terrane** rocks to the east on the Border Ranges fault in the mid-Cretaceous (Loney and others, 1975, p. 64, 66; Haeussler and others, 1996). These include the coeval and perhaps later collapse of the Sitka Graywacke flysch prism against Kelp Bay Group rocks to the east, and one or more of the subsequent and probably intermittent transcurrent movements on the Border Ranges fault and on related parallel faults. Only two areas are reported to have shear-sense indicators on the Border Ranges fault or other faults on Chichagof and **Baranof** Islands: (1) Pavlis and others (1989) and Roeske and others (1992) determined a dextral sense in the Border Ranges fault zone in Glacier Bay about 230 km north of Sitka and interpreted that movement to have been post-Early Cretaceous. (2) Haeussler and others (1994) reported a strong subhorizontal preferred orientation of cobbles in Sitka Graywacke conglomerates in the Silver Bay fault zone and subhorizontal dextral slickenlines on young fault surfaces; the former are interpreted here to have resulted from the stress regime during the deformation of the flysch prism, and the latter are interpreted to indicate at least part of the later transcurrent movement regime. Structural studies by Davis (1996) indicate a transtensional origin during the deformation of the flysch prism. In the present study, the Jurassic(?) dioritic rocks in the fault slices north of Sitka and near the mouth of Silver Bay were examined for shear-sense indicators; a poorly developed S-C fabric involving deformed phenocrysts exists in dioritoid enclaves at both localities, but no unambiguous **kinematic** interpretation could be made. There are, therefore, no reported indicators with a sinistral sense, and few reported with a dextral sense, anywhere in the region.

Two cross-sectional exposures of the Silver Bay fault segment near Sitka demonstrate the complexity of the rocks in the zone. One is at Starrigavan Bay, about 10 km north of Sitka (ST on fig. 1), and one is at the north end of Silver

Bay (near PM on fig. 1; fig. 2). At Starrigavan Bay, highly deformed and altered Jurassic(?) diorite on the east is separated by a young gouge zone from Kelp Bay Group slaty argillite, argillite, metavolcanic rocks, and minor polymictic conglomerate to the west and by an inferred fault from similar mtlange with at least one block of Triassic-age carbonate to the east. This occurrence of metacarbonate is significant because it is the same age as larger carbonate blocks in the mtlange unit 70 km to the north and may be the same age as the metacarbonates within the Silver Bay segment at Silver Bay.

The diorite is now irregularly foliated, with the internal foliation of relict dioritoid blocks angularly discordant to the foliation in enclosing mylonitic matrix and to the overall trend of the young gouge zone. The diorite is best described as very fine to medium-grained chlorite-quartz-feldspar gneiss with a color index of about 15-50. The interpretation that it is a Jurassic(?) body is based on the similarity between the few, less deformed, small dioritoid enclaves that are present in this fault slice and the undeformed diorite in the dated Jurassic body about 4 km to the north on the northeastern side of the Border Ranges fault (figs. 1, 2; Loney and others, 1967, 1975). The gouge-zone contact of the diorite with the rocks to the west is mostly concealed beneath the unconsolidated deposits in a valley. An apparently similar gouge zone that developed in the Kelp Bay Group rocks to the west is within meters of the contact of Kelp Bay-affinity argillite and polymictic conglomerate of the Sitka Graywacke farther west, but this zone is largely covered by shoreline rip-rap.

The exposures at the northwest end of Silver Bay, near the Pulp Mill (PM on fig. 1), indicate that most of the rocks within the fault segment are from the Sitka Graywacke. These exposures have more fault strands than do the Starrigavan Bay exposures. However, as at Starrigavan Bay, the rocks to the northeast of the fault zone are assigned to the *mélange* facies of the Kelp Bay Group (fig. 3.) and consist of mixed phyllite, chert, graywacke, argillite, greenstone, and greenschist. At Herring Cove, which is near the mouth of Silver Bay, and on for about 5.5 km to the south-southeast (fig. 3), there are meter-scale blocks of unfossiliferous metacarbonate inferred on the basis of lithologic similarity to the fossiliferous block east of Starrigavan Bay (Karl and others, 1990) to be of Triassic age. Neither outcrop yielded any conodonts (A.G. Harris, U.S. Geological Survey, written commun., 1982; B.R. Wardlaw, U.S. Geological Survey, written commun., 1988).

Within the fault-sliced Sitka Graywacke is a large (figs. 2, 3) sliver of the highly altered diorite of inferred Jurassic age that is similar to the one at Starrigavan Bay. The least altered parts of the highly altered diorite are foliated, seriate, fine- to coarse-grained chlorite diorite with a color index of about 40. This is the southernmost outcrop of this "ugly diorite" rock type in the Chugach terrane in southeastern Alaska.

## SUMMARY

The Silver Bay fault segment is perhaps the best exposed of any southeastern Alaska fault. It is part of the 200-km-long Sitka fault zone, whose complicated history probably starts with the rheologic discontinuity between the outboard flysch and inboard mtlange facies of the Chugach lithotectonic terrane. That boundary was modified during collapse of the Chugach terrane against the Wrangellia terrane to the east; that fault, in turn, was modified by repeated intermittent transcurrent movement from Late Cretaceous to sometime during mid-Tertiary time. In its present form, the Silver Bay segment has multiple strands with somewhat different characteristics. It also contains intervening slices composed of diverse map units, including lenses of Jurassic(?) diorite and Triassic(?) metacarbonate that are interpreted to have been displaced from the Wrangellia terrane and lenses of serpentinite of uncertain origin. The youngest movements on the fault were dextral and transcurrent, as were probably most of the Late Cretaceous and early Tertiary movements, but the distribution of remnants of the Jurassic(?) diorite suggest the possibility that part of the transcurrent regime was sinistral.

## REFERENCES CITED

- Berg, H.C., and Hinckley, D.W., 1963, Reconnaissance geology of northern Baranof Island, Alaska: U.S. Geological Survey Bulletin 1141-0, 24 p.
- Brew, D.A., 1994, Latest Mesozoic and Cenozoic magmatism in southeastern Alaska, in Plafker, George, and Berg, H.C., eds., *The geology of Alaska: Boulder, Colo., Geological Society of America, The Geology of North America, v. G-1*, p. 621-656.
- Brew, D.A., Drew, L.J., Schmidt, J.M., Root, D.H., and Huber, D.F., 1991a, Undiscovered locatable mineral resources of the Tongass National Forest and adjacent areas, southeastern Alaska: U.S. Geological Survey Open-File Report 91-10, 370 p., 15 maps at 1:250,000, 1 map at 1:500,000, 11 figs.
- Brew, D.A., Hammarstrom, J.M., Himmelberg, G.H., Wooden, J.L., Loney, R.A., and Karl, S.M., 1991b, Crawfish Inlet pluton, Baranof Island, southeastern Alaska—A north-tilted Eocene body or an untilted enigma [abs.]: *Geological Society of America Abstracts with Programs*, v. 23, no. 2, p. 8.
- Brew, D.A., Himmelberg, G.R., Loney, R.A., and Ford, A.B., 1992, Distribution and characteristics of metamorphic belts in the south-eastern Alaska part of the North American Cordillera: *Journal of Metamorphic Geology*, v. 10, p. 465-482.
- Brew, D.A., Homer, R.B., and Barnes, D.F., 1995, Bedrock-geologic and geophysical research in Glacier Bay National Park and Preserve: unique opportunities of local to global significance, in Engstrom, D.R., ed., *Proceedings of the Third Glacier Bay Science Symposium, 1993: Anchorage, Alaska, U.S. National Park Service*, p. 5-14.
- Brew, D.A., Karl, S.M., Barnes, D.F., Jachens, R.C., Ford, A.B., and Homer, R.B., 1991c, A northern Cordilleran ocean-con-

- tinent transect: Sitka Sound to Atlin Lake, British Columbia: Canadian Journal of Earth Sciences, v. 28, no. 6, p. 840-853.
- Brew, D.A., Karl, S.M., and Miller, J.W., 1988, Megafossils (Buchia) indicate Late Jurassic age for part of Kelp Bay Group on **Baranof** Island, southeastern Alaska, in Galloway, J.P., and Hamilton, T.D., eds., Geologic studies in Alaska by the U.S. Geological Survey during 1987: U.S. Geological Survey Circular 1016, p. 147-149.
- Brew, D.A., Loney, R.A., Pomeroy, J.S., and Muffler, L.J.P., 1963, Structural influence on development of linear topographic features, southern **Baranof** Island, southeastern Alaska: U.S. Geological Survey Professional Paper 475-B, p. B-110 - B-113.
- Brew, D.A., and Morrell, R.P., 1979a, The Wrangell terrane ("Wrangellia") in southeastern Alaska: the **Tarr** Inlet suture zone with its northern and southern extensions, in Johnson, K.M., and Williams, J.R., eds., The United States Geological Survey in Alaska: Accomplishments during 1978: U.S. Geological Survey Circular 804-B, p. B121-B123.
- 1979b, Correlation of the Sitka Graywacke, unnamed rocks in the Fairweather Range, and Valdez Group, southeastern Alaska, in Johnson, K.M., and Williams, J.R., eds., The United States Geological Survey in Alaska: Accomplishments during 1978: U.S. Geological Survey Circular 804-B, p. B123-B125.
- Carlson, P.R., Plafker, G., **Brun**s, T.R., and Levy, W.P., 1979, Seaward extension of the Fairweather fault, in Johnson, K.M., and Williams, J.R., eds., The U.S. Geological Survey in Alaska: Accomplishments during 1978: U.S. Geological Survey Circular 804-B, p. B135-B139.
- Davis, J.S., 1996, Tectonic significance of constrictional finite strains in the Chugach accretionary complex, **Baranof** Island, S.E. Alaska [abs.]: Geological Society of America Abstracts with Programs, v. 28, no. 7, p. A-187.
- Decker, J.E., Wilson, F.H., and Turner, D.L., 1980, **Mid-Cretaceous** subduction event in southeastern Alaska [abs.]: Geological Society of America Abstracts with Programs, v. 12, no. 3, p. 103.
- Geological Survey of Canada, 1994, Canada—Seismicity: Geological Survey of Canada, National Atlas, 5th ed., one sheet, scale 1:7,500,000.
- Haeussler, P.J., Davis, J.S., Roeske, S.M., and Karl, S.M., 1994, Late Mesozoic and Cenozoic faulting at the leading edge of North America, Chichagof and **Baranof** Islands, southeastern Alaska [abs.]: Geological Society of America Abstracts with Programs, v. 26, no. 7, p. A-317.
- Haeussler, P.J., Karl, S.M., and Bradley, D.C., 1996, Oblique accretion of part of the Mesozoic **Kelp** Bay Group in southeastern Alaska [abs.]: Abstracts with Programs Geological Society of America, v.28, no. 7, p. A-437.
- Hart, C.J.R., 1995, Sinistral translation of accreted terranes: Yoyo tectonics in the Canadian Cordillera [abs.]: Final Program and Abstracts: Geological Association of Canada **Annual Meeting**, May 17-19, 1995, Victoria, B.C., p. A-43.
- Homer, R.B., 1990, Seismicity in the Glacier Bay region of southeast Alaska and adjacent areas of British Columbia, in **Milner**, A.M., and Wood, J.D., Jr., eds., Proceedings of the Second Glacier Bay Science Symposium, Sept. 19-22, 1988, Glacier Bay National Park, **Gustavus**, Alaska: Anchorage, Alaska, U.S. National Park Service, p. 6-11.
- Hudson, T., Plafker, G., and Dixon, **K.**, 1982, Horizontal offset history of the **Chatham** Strait fault, in Coonrad, W.L., ed., The United States Geological Survey in **Alaska—Accomplishments during 1980**: U.S. Geological Survey Circular **844**, p. 128-132.
- Johnson, B.R., and Karl, S.M., 1985, Geologic map of western Chichagof and **Yakobi** Islands, southeastern Alaska: U.S. Geological Survey Miscellaneous Geologic Investigations Map **I-1506**, scale 1:125,000, 1 sheet, 15 p. pamphlet.
- Karl, S.M., Brew, D.A., and **Wardlaw**, B.R., 1990, Significance of Triassic Marble at Nakwasina Sound, southeastern Alaska, in Dover, J.H., and Galloway, J.B., eds., Geologic studies in Alaska by the U.S. Geological Survey in 1989: U.S. Geological Survey Bulletin 1946, p. 21-28.
- Karl, S.M., Decker, J.E., and Johnson, B.R., 1982, Discrimination of Wrangellia and the Chugach terrane in the Kelp Bay Group on Chichagof and **Baranof** Islands, southeastern Alaska, in Coonrad, W.L., ed., The United States Geological Survey in Alaska—Accomplishments during 1980: U.S. Geological Survey Circular 844, p. 124-128.
- Karl, S.M., Johnson, B.R., and Lanphere, M.A., 1988, New K-Ar ages for plutons on western Chichagof Island and on **Yakobi** Island, in Galloway, J.P., and Hamilton, T.D., eds., Geologic studies in Alaska by the U.S. Geological Survey during 1987: U.S. Geological Survey Circular 1016, p. 164-168.
- Loney, R.A., and Brew, D.A., 1987, Regional **thermal** metamorphism and deformation of the Sitka Graywacke, southern **Baranof** Island, southeastern Alaska: U.S. Geological Survey Bulletin 1779, 17 p.
- Loney, R.A., Brew, D.A., and Lanphere, M.A., 1967, **Post-Paleozoic** radiometric ages and their relevance to fault movements, northern southeastern Alaska: Geological Society of America Bulletin, v. 78, p. 511-526.
- Loney, R.A., Brew, D.A., Muffler, L.J.P., and Pomeroy, J.S., 1975, Reconnaissance geology of Chichagof, **Baranof**, and **Kruzof** Islands, Alaska: U.S. Geological Survey Professional Paper 792, 105 p.
- Ovenshine, A.T., and Brew, D.A., 1972, Separation and history of the **Chatham** Strait fault, southeast Alaska, North America: 24th International Geological Congress, Section 3, p. 245-254.
- Page, R.A., 1969, Late Cenozoic movement on the Fairweather fault in southeastern Alaska: Geological Society of America Bulletin, v. 80, no. 9, p. 1873-1878.
- Pavlis, T.L., Roeske, S.M., Sisson, V.L., and Smart, K., 1989, Evidence for Cretaceous dextral strike-slip on the Border Ranges fault in Glacier Bay National Park, Alaska [abs.]: **Eos** (American Geophysical Union Transactions), v. 70, p. 1337.
- Plafker, George, 1987, Regional geology and petroleum potential of the northern Gulf of Alaska continental margin, in Scholl, D.W., Grantz, A., and Vedder, J.G., eds., Geology and resource potential of the continental margin of western North America and adjacent ocean basins: Houston, Tex., **Circum-Pacific Council for Energy and Mineral Resources**, Earth Science Series, v. 6, p. 229-268.
- Plafker, George, and Berg, H.C., 1994, Overview of the geology and tectonic evolution of Alaska, in **Plafker**, George, and Berg, H.C., eds., The geology of Alaska: Boulder, Colo.,

- Geological Society of America, *The Geology of North America*, v. **G-1**, p. 989-1021.
- Plafker, George, Gilpin, L.M., and Lahr, J.C., 1994, Neotectonic map of Alaska, in Plafker, George, and Berg, H.C., eds., *The geology of Alaska: Boulder, Colo., Geological Society of America, The Geology of North America*, v. **G-1**, pl. 12, scale 1:2,500,000.
- Plafker, George, Hudson, T., and Rubin, M., 1976, Late Holocene offset features along the Fairweather fault, in Cobb, E.H., ed., *The United States Geological Survey in Alaska—Accomplishments during 1975: U.S. Geological Survey Circular 733*, p. 57-58.
- Plafker, George, Jones, D.L., Hudson, T., and Berg, H.C., 1976, The Border Ranges fault system in the Saint Elias Mountains and the Alexander Archipelago, in Cobb, E.H., ed., *The United States Geological Survey in Alaska—Accomplishments during 1975: U.S. Geological Survey Circular 733*, p. 14-16.
- Riehle, J.R., Champion, D.E., Brew, D.A., and Lanphere, M.A., 1992, Pyroclastic deposits of the Mount Edgecumbe volcanic field, Alaska: evolution of a stratified magma chamber: *Journal of Volcanology and Geothermal Research*, v. 53, p.117-143.
- Roeske, S.M., Pavlis, T.L., Snee, L.W., and Sisson, V.B., 1992,  $^{40}\text{Ar}/^{39}\text{Ar}$  isotopic ages from the combined Wrangellia-Alexander terrane along the Border Ranges fault system in the eastern Chugach Mountains and Glacier Bay, Alaska, in Bradley, D.C., and Ford, A.B., eds., *Geologic studies in Alaska by the U.S. Geological Survey, 1990: U.S. Geological Survey Bulletin 1999*, p.180-195.
- Rossman, D.L., 1959, Geology and ore deposits of northwestern Chichagof Island, Alaska: *U.S. Geological Survey Bulletin 1058-E*, 79 p.
- Sonnevil, R.A., 1981, The Chilkat-Prince of Wales plutonic province, in Albert, N.R.D., and Hudson, T., eds., *The United States Geological Survey in Alaska—Accomplishments during 1979: U.S. Geological Survey Circular 823-B*, p. B112-B114.
- Taylor, C.D., Goldfarb, R.J., Snee, L.W., Gent, C.A., Karl, S.M., and Haeussler, P.J., 1994, New age data for gold deposits and granites, Chichagof Mining District, SE Alaska: evidence for a common origin [abs.]: *Geological Society of America Abstracts with Programs*, v. 26, no. 7, p. A-140.
- Twenhofel, W.S., and Sainsbury, C.L., 1958, Fault patterns in southeastern Alaska: *Geological Society of America Bulletin*, v. 69, p. 1431-1442.

Reviewers: R.A. Loney and G. Plafker

# U.S. Geological Survey Reports on Alaska Released in 1995\*

Compiled by John P. Galloway and Susan Toussaint

\*[Some reports dated earlier did not become available until 1995; they are included in this listing.]

## ABBREVIATIONS

**C1108** Carter, L.M.H., ed., Energy and environment—application of geosciences to decision-making: U.S. Geological Survey Circular 1108 (10th V.E. **McKelvey** Forum on Mineral and Energy Resources, 1995), 134 p.

- Ager, Thomas, 1995, Late Cenozoic climate history of Alaska and Yukon [abs.]: U.S. Geological Survey Open-File Report 95-247, p. 24.
- Ahlbrandt, T.S.**, 1995, Central and eastern North Slope of Alaska initiative [abs.]: U.S. Geological Survey Open-File Report 95-247, p. 60.
- Alcorn, M.G., and Dorava, J.M., 1995, Overview of environmental and hydrogeologic conditions at Anchorage Air Route Traffic Control Center, Alaska: U.S. Geological Survey Open-File Report 95-409, variously paged.
- Alcorn, M.G., and Dorava, J.M., 1995, Overview of environmental and hydrogeologic conditions at Deadhorse, Alaska: U.S. Geological Survey Open-File Report 95-437, variously paged.
- Alcorn, M.G., and Hogan, E.V., 1995, Overview of environmental and hydrogeologic conditions near Juneau, Alaska: U.S. Geological Survey Open-File Report 95-412, variously paged.
- Armstrong, A.K.**, and **Mamet, B.L.**, 1994, Evidence of climate change in the Lower and Middle Carboniferous shallow-water carbonate rocks of Arctic Alaska, New Mexico, and Arizona: U.S. Geological Survey Bulletin 2110, p. 52–58.
- Bailey, B.J., and Hogan, **E.V.**, 1995, Overview of environmental and hydrogeologic conditions near Kenai, Alaska: U.S. Geological Survey Open-File Report **95-410**, variously paged.
- Barnes, P.W., Kvenvolden, Keith, Reimnitz, Erk, and Carter, L.D., 1995, Arctic coastal erosion and the interaction of sea ice, permafrost and hydrates [abs.]: U.S. Geological Survey Open-File Report 95-247, p. 31.
- Barnes, P.W., and Reimnitz, Erk, 1995, Geologic and **climatic** implications of ice-rafted sediment in the Arctic [abs.]: U.S. Geological Survey Open-File Report 95-247, p. 32.
- Beavan, John, [1991], Crustal deformation measurements in the Shumagin seismic gap, Alaska: U.S. Geological Survey contract report, grant no. 14-08-0001-G1792, 6 p.
- 1992, Crustal deformation measurements in the Shumagin seismic gap, Alaska: U.S. Geological Survey contract report [number not given], 9 p.
- 1993, Crustal deformation measurements in the Shumagin seismic gap, Alaska: U.S. Geological Survey contract report, grant no. 14-08-0001-G1792, 11 p.
- Bird, K.J., Cole, Frances, Howell, D.G., and **Magoon, L.B.**, 1995, The future of oil and gas in northern Alaska, **C1108**, p. 45–47.
- Bird, K.J., and Howell, D.G., 1995, North Slope petroleum potential [abs.]: U.S. Geological Survey Open-File Report 95-247, p. 61.
- Brabets, T.P., 1995, Application of surface geophysical techniques in a study of the geomorphology of the lower Copper River, Alaska: U.S. Geological Survey **Water-Resources Investigations Report WRi 94-4165**, 47 p.
- Bradbury, J.P., and **Krebs, W.N.**, eds., 1995, Diatom genus **Actinocyclus** in the Western United States: U.S. Geological Survey Professional Paper 1543 A-B, 73 p.
- Bradley, Dwight, and others to be selected, 1995, Paleozoic tectonics of the Circum-Arctic (proposed research) [abs.]: U.S. Geological Survey Open-File Report 95-247, p. 53.
- Brew, D.A., compiler, 1995, Geologic map of the Craig, Dixon Entrance, and parts of the Ketchikan and Prince Rupert quadrangles, southeastern Alaska: U.S. Geological Survey Open-File Report 95-215, 1 sheet, scale 1:250,000.
- Brew, D.A., Drinkwater, J.L., Ford, A.B., and Himmelberg, G.R., 1995, The **Taku** transect and its granitic rocks, Coast Mountains complex, southeastern Alaska: U.S. Geological Survey Circular 1129, p. 29–30.
- Brew, D.A., Ford, A.B., Himmelberg, G.R., and Drinkwater, J.L., 1994, Coast Mountains complex of southeastern Alaska and adjacent regions: U.S. Geological Survey Bulletin 2135, p. 21–28.
- Brewer, M.C., 1995, Influence of active layer boundary conditions in the correlation of permafrost temperatures with air temperatures [abs.]: U.S. Geological Survey Open-File



- Report 95-247, p. 33.
- Brigham-Grette, J., Carter, L.D., Marincovich, L., Jr., Brouwers, E.M., and Hopkins, D.M., 1994, Warm Pliocene high sea-level records from Arctic Alaska and possible implications for Antarctic ice volume 2.8–2.2 Ma: U.S. Geological Survey Open-File Report 94-588, p. 5–6.
- Brocher, T.M., Allen, R.M., Stone, D.B., Wolf, L.W., and Galloway, B.K., 1995, Data report for onshore-offshore wide-angle seismic recordings in the Bering-Chukchi Sea, western Alaska and eastern Siberia: U.S. Geological Survey Open-File Report 95-650, 57 p.**
- Brouwers, E.M., 1994, Systematic paleontology of Quaternary Ostracode assemblages from the Gulf of Alaska, Part 3—Family Cytheruridae: U.S. Geological Survey Professional Paper 1510, 45 p., 24 pls.
- 1995, Late Pleistocene and Holocene climates, **Beaufort Sea** [abs.]: U.S. Geological Survey Open-File Report 95-247, p. 25.
- Campbell, W.J., and Josberger, E.G., 1995, Arctic and Antarctic sea ice studies [abs.]: U.S. Geological Survey Open-File Report 95-247, p. 34–35.
- Carter, D.L., 1995, Late Cenozoic Arctic climate change [abs.]: U.S. Geological Survey Open-File Report 95-247, p. 26.
- Claar, D.V., and Lilly, M.R., 1995, Ground-water and surface-water elevations in the Fairbanks International Airport area, Alaska, 1990–94: U.S. Geological Survey Open-File Report 95-382, 155 p., 2 pls.
- Clow, G.D., and Lachenbruch, A.H., 1995, Permafrost temperatures and the changing climate [abs.]: U.S. Geological Survey Open-File Report 95-247, p. 36–37.
- Collett, T.S., 1995, Resource potential of Arctic gas hydrates [abs.]: U.S. Geological Survey Open-File Report 95-247, p. 62.
- Collett, T.S., and Kvenvolden, K.A., 1995, Relation between permafrost-associated gas hydrates and global climate [abs.]: U.S. Geological Survey Open-File Report 95-247, p. 38.
- Cooper, Alan, Eittreim, Steve, **Marlow, Mike**, Scholl, Dave, and Grantz, Art, 1995, GLORIA side-scan surveys of polar basins [abs.]: U.S. Geological Survey Open-File Report 95-247, p. 39.
- Cooper, Alan, Scholl, David, and Grantz, Art, 1995, Polar shallow-drilling geologic-research program [abs.]: U.S. Geological Survey Open-File Report 95-247, p. 27.
- Cowan, E.A., Powell, R.D., Carlson, P.R., Kayen, R.E., Cai, Jinkui, Seramur, K.C., and Zellers, S.D., 1995, Cruise report: R/V Alpha Helix cruise-173 to western Prince William Sound, Yakutat Bay, and Glacier Bay National Park, northeastern Gulf of Alaska, August 17–September 3, 1993: U.S. Geological Survey Open-File Report 94-258, 176 p.**
- Cowan, J.R., 1995, Overview of environmental and hydrogeologic conditions at Bettles Field, Alaska: U.S. Geological Survey Open-File Report 95-343, variously paged.**
- 1995, Overview of environmental and hydrogeologic conditions at Chandalar Lake, Alaska: U.S. Geological Survey Open-File Report 95-348, 9 p.
- 1995, Overview of environmental and hydrogeologic conditions at Sand Point, Alaska: U.S. Geological Survey Open-File Report 95-408, 8 p.
- Crosson, R.S., and Creager, K.C., 1994, Annual technical report: 1992: earthquake hazard research in the Pacific Northwest and Alaska: U.S. Geological Survey contract report, grant no. 14-08-0001-G1803, 55 p.**
- Dickinson, K.A., Campbell, J.A., and Dula, W.F., Jr., 1995, Geology, geochemistry, and uranium favorability of Tertiary rocks in south-central Alaska: U.S. Geological Survey Bulletin 2098-A-B, 33 and 38 p. (Part A: Dickinson, K.A., Geology, geochemistry, and uranium favorability of the Tertiary Kenai Group in the Susitna Lowlands at the northern end of Cook Inlet basin, Alaska. Part B: Dickinson, K.A., Campbell, J.A., and Dula, W.F., Jr., 1995, Geology, geochemistry, and uranium favorability of Tertiary continental sedimentary rocks in the northwestern part of the Cook Inlet area, Alaska.)
- Dorava, J.M., 1995, Overview of environmental and hydrogeologic conditions at **Nome**, Alaska: U.S. Geological Survey Open-File Report 95-178, 12 p.
- 1995, Overview of environmental and hydrogeologic conditions at Unalakleet, Alaska: U.S. Geological Survey Open-File Report 95-347, variously paged.
- Dorava, J.M., and Hall, J.D., 1995, Overview of environmental and hydrogeologic conditions at Farewell, Alaska: U.S. Geological Survey Open-File Report 95-175, 13 p.
- 1995, Overview of environmental and hydrogeologic conditions at Puntilla Lake, Alaska: U.S. Geological Survey Open-File Report 95-177, 10 p.
- Dorava, J.M., and Hogan, E.V., 1995, Overview of environmental and hydrogeologic conditions at Bethel, Alaska: U.S. Geological Survey Open-File Report 95-173, variously paged.
- Dorava, J.M., and Murray, R.P., 1995, Overview of environmental and hydrogeologic conditions on Hinchinbrook Island, Alaska: U.S. Geological Survey Open-File Report 95-176, 12 p.
- Doukas, M.P., 1995, Compilation of sulfur dioxide and carbon dioxide emission-rate data from Cook Inlet volcanoes (Redoubt, Spurr, Iliamna, and Augustine), Alaska during the period from 1990 to 1994: U.S. Geological Survey Open-File Report 95-55, 15 p.
- Doukas, M.P., **McGimsey, R.G.**, and Dorava, J.M., 1995, 10 years of volcanic activity in Alaska: 1983 to 1992: A video (Pyre Peak, Akutan volcano, Bogoslof volcano, Westdahl volcano, Veniaminof volcano, Augustine volcano, Redoubt Volcano, Spurr volcano): U.S. Geological Survey Open-File Report 95-61-A, VHS videotape, 95-61-B, 13 p. text.
- Drinkwater, J.L., Brew, D.A., and Ford, A.B., 1995, Geology, petrography, and geochemistry of granitic rocks from the Coast Mountains complex near Juneau, southeastern Alaska: U.S. Geological Survey Open File Report 95-638, 119 p.
- Dumoulin, J.A., and Harris, A.G., 1994, Depositional framework and regional correlation of pre-Carboniferous metacarbonate rocks of the **Snowden** Mountain area, central Brooks Range, northern Alaska: U.S. Geological Survey Professional Paper 1545, 66 p., 3 pls.
- Eppinger, R.G., **McHugh, J.B.**, Briggs, P.H., **D'Angelo, W.M.**, Doughten, M.W., Fey, D.L., **Hageman, P.L.**, Knight, R.J., Meier, A.L., Motooka, C.L., Motooka, J.M., **O'Leary, R.M.**, Roushey, B.H., and Hopkins, R.T., 1995, Geochemical data for environmental studies at Nabesna and Kennecott,

- Alaska: water, leachates, stream-sediments, **heavy-mineral-concentrates**, and rocks: U.S. Geological Survey Open-File Report **95-645A**, 91p.
- Eppinger, R.G., **McHugh**, J.B., Briggs, P.H., **d'Angelo**, W.M., Doughten, M.W., Fey, D.L., **Hageman**, P.L., Hopkins, R.T., Knight, R.J., Meier, A.L., Motooka, **J.M.**, **O'Leary**, R.M., and Roushey, B.H., 1995, Geochemical data for environmental studies at Nabesna and Kennecott, Alaska: water, leachates, stream-sediments, heavy-mineral-concentrates, and rocks: U.S. Geological Survey Open-File Report **95-645A**, 91 p. and **95-645B**, diskette version.
- Ferrians**, O.J., Jr., 1995, Permafrost map of Alaska [abs.]: U.S. Geological Survey Open-File Report 95-247, p. 40.
- Fitzpatrick, Joan, **Landis**, Gary, Hinkley, Todd, and Rye, Robert, 1995, Recent climate history of southeastern Alaska from high-resolution ice core records [abs.]: U.S. Geological Survey Open-File Report 95-247, p. 28.
- Folger, H.A., Koch, R.D., Hopkins, R.T., Cieutat, B.A., Goldfarb, R.J., Nokleberg, W.J., and Hoffman, J.D., 1995, Analytical results and sample locality maps of **stream-sediment**, heavy-mineral-concentrate, and rock samples from the Gulkana quadrangle, south-central Alaska: U.S. Geological Survey Open-File Report 95-509, 105 p., 2 sheets, scale 1:250,000.
- Galloway, J.P., 1995, Radiocarbon dates for the Nushagak Peninsula, southwestern Alaska: U.S. Geological Survey Open-File Report 95-583, 8 p.
- Galloway, J. P., and Laney, J., 1994, Status of geologic mapping in Alaska; a digital bibliography: U.S. Geological Survey Open-File Report 94-675-A (text), 100 p. + **94-675-B** (1 diskette for IBM-compatible computers) + **94-675-C** (1 diskette for Macintosh computers).
- Gautier, D.L., **Dolton**, G.L., Takahashi, **K.I.**, and Varnes, K.L., eds., 1995, 1995 national assessment of United States oil and gas resources—results, methodology, and supporting data: U.S. Geological Survey Digital Data Series CD-ROM DDS-30. [Accompanies: U.S. Geological Survey, National Oil and Gas Resource Assessment Team, 1995, 1995 national assessment of United States oil and gas resources; Overview of the 1995 National assessment of potential additions to technically recoverable resources of oil and gas-onshore and State waters of the United States: U.S. Geological Survey Circular 1118, 20 p.
- George, S.L., 1995, Digital release of stream-sediment, **heavy-mineral-concentrate**, and other geochemical data collected in the **McCarthy** 1° × 3" quadrangle, Alaska: U.S. Geological Survey Open-File Report 95-623, 11 p.
- 1995, Digital release of stream-sediment, heavy-mineral-concentrate, soil, and other geochemical data collected in the Nabesna 1° × 3° quadrangle, Alaska: U.S. Geological Survey Open-File Report 95-625, 10 p. + 1 computer diskette.
- 1995, Digital release of stream-sediment, heavy-mineral-concentrate, and other geochemical data collected in the Circle 1° × 3° quadrangle, Alaska: U.S. Geological Survey Open-File Report 95-626, 12 p.
- 1995, Digital release of stream-sediment, heavy-mineral-concentrate, soil, and other geochemical data collected in the Big Delta 1° × 3° quadrangle, Alaska: U.S. Geological Survey Open-File Report 95-627, 10 p.
- Gilpin, L.M., Carver, G. A., and Hemphill-Haley, E., 1994, Paleoseismicity of the SW extent of the 1964 Alaskan earthquake rupture zone, eastern Aleutian Arc, Kodiak Islands, Alaska: U.S. Geological Survey Open-File Report 94-568, 70 p.
- Goldfarb, R.J., Borden, J.C., and Winkler, G.R., 1995, Geochemical survey of the Valdez 1" × 3" quadrangle, south-central Alaska: U.S. Geological Survey Bulletin, 77 p., 1 sheet, scale 1:250,000.
- Gray, J.E., 1994, Environmental geochemistry of mercury deposits in Alaska: U.S. Geological Survey Fact Sheet **94-072**.
- Haeussler, Peter, [1994], The next big earthquake in southern Alaska may come sooner than you think. Are you prepared?: U.S. Geological Survey, 24 p.
- Haeussler, P.J., and Plafker, G., 1995, Earthquakes in Alaska: U.S. Geological Survey Open-File Report **95-624**, 1 map, scale [ca. 1:4,200,000]
- Hamilton, T.D., 1995, The last interglacial in Alaska [abs.]: U.S. Geological Survey Open-File Report 95-247, p. 29.
- Hall, J.D., 1995, Overview of environmental and hydrogeologic conditions at Iliamna, Alaska: U.S. Geological Survey Open-File Report 95-346, variously paged.
- 1995, Overview of environmental and hydrogeologic conditions at Lake Minchumina and Skwentna, Alaska: U.S. Geological Survey Open-File Report 95-438, variously paged.
- Hanson, S.L., and **Perkins**, D.M., 1995, Seismic sources and recurrence rates as adopted by USGS staff for the production of the 1982 and 1990 probabilistic ground motion maps for Alaska and the conterminous United States: U.S. Geological Survey Open-File Report 95-257, 39 p. + 2 diskettes.
- Hawkins**, D.B., 1995, Environmental overview and hydrogeologic conditions at Federal Aviation Administration facilities near Fairbanks, Alaska: U.S. Geological Survey Open-File Report 95-172, 11 p.
- Heinrichs**, T.A., **Mayo**, L.R., Trabant, D.C., and March, R.S., 1995, Observations of the surge-type Black Rapids Glacier, Alaska, during a quiescent period, **1970-92**: U.S. Geological Survey Open-File Report 94-512, variously paged, 1 diskette.
- Himmelberg, G.R., and Loney, R.A., 1995, Characteristics and petrogenesis of Alaskan-type ultramafic-mafic intrusion, southeastern Alaska: U.S. Geological Survey Professional Paper **1564**, 47 p.
- Hogan, E.V., 1995, Overview of environmental and hydrogeologic conditions near Petersburg, Alaska: U.S. Geological Survey Open-File Report 95-342, variously paged.
- 1995, Overview of environmental and hydrogeologic conditions at Wrangell, Alaska: U.S. Geological Survey Open-File Report 95-344, variously paged.
- 1995, Overview of environmental and hydrogeologic conditions at Sitka, Alaska: U.S. Geological Survey Open-File Report 95-345, variously paged.
- Hogan, E.V., and Dorava, J.M., 1995, Overview of environmental and hydrogeologic conditions at seven Federal Aviation Administration facilities in interior Alaska: U.S. Geological Survey Open-File Report 95-341, variously paged.

- Hogan, E.V., and Nakanishi, A.S., 1995, Overview of environmental and hydrogeologic conditions near Kodiak, Alaska: U.S. Geological Survey Open-File Report 95-406, variously paged.
- Isaacs, C.M., Bird, K.J., Medrano, Marjorie, Keller, M.A., Piper, D.Z., and Gautier, D.L., 1995, Preliminary report on major and minor elements in cores from the Triassic Shublik Formation, Jurassic and Cretaceous Kingak Shale, and Cretaceous Pebble Shale Unit, Hue Shale, and Torok Formation, North Slope, Alaska: U.S. Geological Survey Open-File Report 95-236, 30 p.
- Keith, T.E.C., 1995, Geochemical data of fumarolically altered rocks, Valley of Ten Thousand Smokes, Alaska: U.S. Geological Survey Open-File Report 95-47, 20 p.
- ed., 1995, The 1992 eruptions of Crater Peak vent, Mount Spurr Volcano, Alaska: U.S. Geological Survey Bulletin 2139, 220 p.
- Kelley, J.S., Lane, L.S., Wrucke, C.T., Brosgé, W.P., and Taillieur, I.L., 1995, Brooks Range transect [abs.]: U.S. Geological Survey Open-File Report 95-247, p. 64.
- Kelley, K.D., 1995, Natural environmental effects of silver-lead-zinc-deposits in the Brooks Range, Alaska: U.S. Geological Survey Fact Sheet FS-092-95.
- Kelley, K.D., and Mull, C.G., 1995, The Alaska Mineral Resource Assessment Program—Background information to accompany geologic and mineral-resource maps of the Killik River 1° × 3" quadrangle, northern Alaska: U.S. Geological Survey Circular 1117, 15 p.
- 1995, Maps showing areas of potential for mineral resources in the Killik River 1° × 3" quadrangle, Alaska: U.S. Geological Survey Miscellaneous Field Studies Map MF-2225-A, 25 p., 1 sheet, scale 1:250,000.
- 1995, Geochemistry of minus-100-mesh and minus-80-mesh sediment samples from the Killik River 1° × 3" quadrangle, Alaska: U.S. Geological Survey Miscellaneous Field Studies Map MF-2225-B, 2 sheets, scale 1:250,000.
- Kelley, K.D., Mull, C.G., and Barton, H.N., 1995, Maps showing distribution of selected elements in minus-30-mesh stream sediment samples from the southern part of the Killik River 1° × 3" quadrangle, Alaska: U.S. Geological Survey Miscellaneous Field Studies Map MF-2225-C, 2 sheets, scale 1:250,000.
- 1995, Geochemistry and mineralogy of heavy-mineral concentrates from the southern part of the Killik River 1° × 3" quadrangle, Alaska: U.S. Geological Survey Miscellaneous Field Studies Map MF-2225-D, 2 sheets, scale 1:250,000.
- Kriegler, A.T., and Lilly, M.R., 1995, Water-elevation, stream-discharge, and ground-water quality data in the Alaska Railroad industrial area, Fairbanks, Alaska, May 1993 to May 1995: U.S. Geological Survey Open-File Report 95-364, 257 p., 1 pl.
- Kunk, M.J., 1995, <sup>40</sup>Ar/<sup>39</sup>Ar age-spectrum data for hornblende, plagioclase and biotite from tephros collected at Dan Creek and McCallum Creek, Alaska, and in the Klondike Placer District near Dawson, Yukon Territory, Canada: U.S. Geological Survey Open-File Report 95-217-A (paper copy), 52 p., 95-217-B, (3-1/2 inch diskette).
- Kvenvolden, K.A., 1995, Permafrost and gas hydrate as possible sources of methane [abs.]: U.S. Geological Survey Open-File Report 95-247, p. 42.
- Kvenvolden, K.A., and Carlson, P.R., 1995, Oil spills in Prince William Sound, Alaska, C1108, p. 105–107.
- Lachenbruch, A.H., 1994, Permafrost, the active layer, and changing climate: U.S. Geological Survey Open-File Report 94-694, 43 p. [Transcript with minor editorial changes of a plenary address to the Sixth International Conference on Permafrost, Beijing, July 6, 1993.]
- Landis, G.P., Fitzpatrick, J.J., and Everett, T., 1995, Analysis of firm gases collected at shallow depths in the Wrangell-St. Elias Range, Alaska, the CISP2 site, Greenland, and Taylor Dome site, East Antarctica: U.S. Geological Survey Open-File Report 95-222, variously paged.
- Lemke, K.J., May, B.A., and Vanderpool, A.M., 1995, Bibliography for Hayes, Spurr, Crater Peak, Redoubt, Iliamna, Augustine, Douglas, and Aniakchak Volcanoes, Alaska: U.S. Geological Survey Open-File Report 95-435, 33 p.
- Lemke, K.J., and Vanderpool, A.M., 1995, Overview of environmental and hydrogeologic conditions at Dutch Harbor, Alaska: U.S. Geological Survey Open-File Report 95-411, variously paged.
- Lorenson, T. D., and Kvenvolden, K. A., 1995, Methane in coastal sea water, sea ice, and bottom sediments, Beaufort Sea, Alaska: U.S. Geological Survey Open-File Report 95-70, 84 p.
- Lorenson, T.D., Kvenvolden, K.A., Barnes, P.W., Popp, B.N., Sansone, F.J., Rust, T.M., Lilley, M.D., and Olson, E.J., 1995, Maps showing isotopic composition of methane in seawater of the Alaskan Beaufort Sea, 1994: U.S. Geological Survey Open-File Report 95-669, 1 map.
- Markon, Carl, and Kirk, William, 1994, Development of a digital land cover data base for the Selawik National Wildlife Refuge: U.S. Geological Survey Open-File Report 94-627, variously paged.
- McGimsey, R.G., and Miller, T.P., 1995, Quick reference to Alaska's active volcanoes and listing of historical eruptions, 1760–1994: U.S. Geological Survey Open-File Report 95-520, 13 p.
- McGimsey, R.G., Neal, C.A., and Doukas, M.P., 1995, 1992 volcanic activity in Alaska: summary of events and response of the Alaska Volcano Observatory: U.S. Geological Survey Open-File Report 95-83, 26 p.
- Miller, J.W., Elder, W.P., and Determan, R.L., 1995, Mesozoic macrofossil locality map, checklists, and pre-Quaternary stratigraphic section of the Mt. Katmai and adjacent parts of the Afognak and Naknek quadrangles, Alaska Peninsula, Alaska: U.S. Geological Survey Miscellaneous Field Studies Map MF-2021-G, 3 sheets, scale 1:250,000.
- Miller, T.P., 1995, Alaska Volcano Observatory (Alaska volcanic hazards) [abs.]: U.S. Geological Survey Open-File Report 95-247, p. 45–46.
- Moll-Stalcup, E., Lanphere, M., and Brosgé, W., 1995, The age and composition of the Beaver volcanic field, northern Alaska: U.S. Geological Survey Open-File Report 95-666, 8 p.
- Molnia, B.F., 1995, Inventory of North American glaciers [abs.]: U.S. Geological Survey Open-File Report 95-247, p. 47.
- Nakanishi, A.S., 1995, Overview of environmental and hydrogeologic conditions at Merrill Field Airport, Anchorage, Alaska: U.S. Geological Survey Open-File Report 95-171,

- variously paged.
- 1995, Overview of environmental and hydrogeologic conditions on Fire Island, Anchorage, Alaska: U.S. Geological Survey Open-File Report 95-174, variously paged.
- Nakanishi, A.S., and Dorava, J.M., 1994, Overview of environmental and hydrogeologic conditions at Saint Marys, Alaska: U.S. Geological Survey Open-File Report 94-481, variously paged.
- 1994, Overview of environmental and hydrogeologic conditions at Galena, Alaska: U.S. Geological Survey Open-File Report 94-525, variously paged.
- 1994, Overview of environmental and hydrogeologic conditions at Fort Yukon, Alaska: U.S. Geological Survey Open-File Report 94-526, variously paged.
- 1994, Overview of environmental and hydrogeologic conditions at Tanana, Alaska: U.S. Geological Survey Open-File Report 94-527, variously paged.
- Neal, C. A., Doukas, M.P., and McGimsey, R.G., 1995, 1994 volcanic activity in Alaska: summary of events and response of the Alaska Volcano Observatory: U.S. Geological Survey Open-File Report 95-271, 18 p.
- Nelson, G.L., 1995, Overview of environmental and hydrogeologic conditions near Big Delta, Alaska: U.S. Geological Survey Open-File Report 95-180, 11 p.
- Nokleberg, W.J., Parfenov, L.M., Monger, J.W.H., Baranov, B.V., Byalobzhesky, S.G., Bundtzen, T.K., Feeney, T.D., Fujita, Kazuya, Gordey, S.P., Grantz, Arthur, Khanchuk, A.I., Natal'in, B.A., Natapov, L.M., Norton, I.O., Patton, W.W., Jr., Plafker, George, Scholl, D.W., Sokolov, S.D., Sosunov, G.M., Stone, D.B., Tabor, R.W., Tsukanov, N.V., Vallier, T.L., and Wakita, Koji, 1994, Circum-North Pacific tectonostratigraphic terrane map: U.S. Geological Survey Open-File Report 94-714, 221 p., 5 sheets, scale 1:10,000,000.
- Okal, E.A., and Stein, Seth, [1993], Constraints on tectonic deformation in the southern Alaska subduction zone from historical seismicity: U.S. Geological Survey contract report, grant no. 14-08-0001-G1952, 7 p.
- Page, R.A., and Haeussler, P.J., 1995, Earthquake information needs in south-central Alaska: U.S. Geological Survey Open-File Report 95-696, 8 p.
- Palcsak, B.B., and Dorava, J.M., 1994, Overview of environmental and hydrogeologic conditions at Dillingham, Alaska: U.S. Geological Survey Open-File Report 94-482, 19 p.
- Plafker, George, 1995, Neotectonics and earthquake risk in southern Alaska [abs.]: U.S. Geological Survey Open-File Report 95-247, p. 48.
- Plafker, G., and Rubin, M., 1994, Paleoseismic evidence for "yo-yo" tectonics above the eastern Aleutian subduction zone; coseismic uplift alternating with even larger interseismic submergence: U.S. Geological Survey Open-File Report 94-568, p. 155-157.
- Rice, W.A., and Hogan, E.V., 1995, Overview of environmental and hydrogeologic conditions at Cold Bay, Alaska: U.S. Geological Survey Open-File Report 95-179, variously paged.
- Richter, D.H., Rosenkrans, D.S., and Steigenvald, M.J., 1995, Guide to the volcanoes of the western Wrangell Mountains, Alaska—Wrangell–St. Elias National Park and Preserve: U.S. Geological Survey Bulletin 2072, 31 p.
- Rickman, R.L., 1995, Hydrologic and water-quality data for the lower Bradley River, Alaska, March 1993 to April 1994: U.S. Geological Survey Open-File Report 95-338, variously paged.
- Schneider, J.L., ed., 1994, 1994 annual report on Alaska's mineral resources: U.S. Geological Survey Circular 1113, 69 p.
- Switzer, J.C. and Porcella, R.L., compilers, 1995, Catalogue of U.S. Geological Survey strong-motion records, 1993: U.S. Geological Survey Circular 1121, 10 p.
- Taylor, D.J., and Zihlman, F.N., 1995, Geological and geophysical information from the National Petroleum Reserve Alaska on CD-ROM as a tool in support of geoscientific decision-making, C1108, p. 42-43.
- Tripp, R.B., King, H.D., and Light, T.D., 1995, Mineralogical maps showing the distribution of ore-related minerals in the minus-30-mesh, nonmagnetic heavy-mineral fraction of stream sediment, Healy quadrangle, Alaska: U.S. Geological Survey Miscellaneous Field Studies Map MF-2058-D, 2 sheets, scale 1:250,000.
- U.S. Geological Survey, 1994, Environmental geochemistry of mercury mines in Alaska: U.S. Geological Survey Fact Sheet no. 94-072, 1 leaf.
- U.S. Geological Survey, National Oil and Gas Resource Assessment Team, 1995, 1995 national assessment of United States oil and gas resources; overview of the 1995 National assessment of potential additions to technically recoverable resources of oil and gas—onshore and State waters of the United States: U.S. Geological Survey Circular 1118, 20 p.
- Waythomas, C.F., 1995, Surficial geologic map of northern Adak Island, Alaska: U.S. Geological Survey Open-File Report 95-128, 6 p., 1 sheet.
- Williams, R.S., Jr., coordinator, 1995, Final report of the Polar Research Program Strategies Workshop: U.S. Geological Survey Open-File Report 95-247, 72 p.
- Wilson, F.H., Detterman, R.L., Miller, J.W., and Case, J.E., 1995, Geologic map of the Port Moller, Stepovak Bay, and Simeonof Island quadrangles, Alaska Peninsula, Alaska: U.S. Geological Survey Miscellaneous Investigations Series Map I-2272, 2 sheets, scale 1:250,000.
- Wilson, F.H., Miller, T.P., Vallier, T.L., Scholl, D.W., and Veltre, Douglas, 1995, Geology, resource endowment, geologic hazards, and human prehistory of the Aleutian arc [abs.]: U.S. Geological Survey Open-File Report 95-247, p. 58.
- Yamaguchi, D.K., 1993, Killed-forest record of the great 1964 earthquake in Alaska, in Annual report: Collaborative research (U.S. Geological Survey and University of Colorado, Institute of Arctic and Alpine Research), agreement no. 14-08-0001-G2075, 26 p.

# Reports about Alaska in Non-USGS Publications Released in 1995 that Include USGS Authors

Compiled by John P. Galloway and Susan Toussaint

[Some reports dated 1994 did not become available until 1995; they are included in this listing. USGS authors are marked with asterisks (\*)]

## ABBREVIATIONS

GSA Geological Society of America Abstracts with Programs, v. 27, no. 6.  
GSA1 Geological Society of America Abstracts with Programs, v. 26, no. 7.  
Eos Eos (American Geophysical Union Transactions), v. 75, no. 44, suppl.

- Adams, D.D., Freeman, C.J., \*Goldfarb, R.J., \*Gent, C.A., and \*Snee, L.W., 1994, Age, fluid inclusion, and isotopic characteristics of mesothermal gold mineralization, Valdez Creek district, Alaska: 14th Biennial Interior Alaska Mining Conference, Program volume, p. 26.
- Adrain, J.M., Chatterton, B.D.E., and \*Blodgett, R.B., 1995, Silurian trilobites from southwestern Alaska: *Journal of Paleontology*, v. 69, no. 4, p. 723–736.
- \*Aleinikoff, J.N., \*Moore, T.E., \*Nokleberg, W.J., and \*Koch, R.D., 1995, Preliminary U-Pb ages from detrital zircons from the Arctic Alaska and Yukon-Tanana terranes, Alaska [abs.]: GSA, p. 2.
- Ambos, E.L., \*Mooney, W.D., and \*Fuis, G.S., 1995, Seismic refraction measurements within the Peninsular terrane, south central Alaska: *Journal of Geophysical Research*, v. 100, no. B3, p. 4079–4095.
- Andreassen, K., \*Hart, P.E., and \*Grantz, A., 1995, Seismic studies of a bottom-simulating reflection related to gas hydrate beneath the continental margin of the Beaufort Sea: *Journal of Geophysical Research*, v. 100, no. B7, p. 12,659–12,673.
- \*Atwater, B.F., 1994, Subduction-earthquake telltales beneath coastal lowlands [abs.]: GSA1, p. 239–240.
- Babcock, L.E., St. John, James, Jacobson, S.R., Askin, R.A., and \*Blodgett, R.B., 1995, Neoproterozoic to early Paleozoic geologic history of the Nixon Fork subterrane of the Farewell terrane, Alaska [abs.]: GSA, p. 2–3.
- \*Bailey, E.A., \*Gray, J.E., \*Miller, M.L., and Balen, M.D., 1995, Mercury accumulation in vegetation from the Red Devil and Cinnabar Creek mercury mines in southwestern Alaska [abs.]: GSA, p. 3.
- \*Barnes, D.A., Mariano, J., \*Morin, R.L., \*Roberts, C.W., and \*Jachens, R.C., 1994, Incomplete isostatic gravity map of Alaska, in Plafker, George, and Berg, H.C., eds., 1994, The geology of Alaska: Boulder, Colo., Geological Society of America, The Geology of North America, vol. G-1, pl. 9, 1 sheet, scale: 1:2,500,000.
- Barnett, D.E., Bowman, J.R. Pavlis, T.L., Rubenstone, J.R., \*Snee, L.W., and Onstott, T.C., 1994, Metamorphism and near-trench plutonism during initial accretion of the Cretaceous Alaskan forearc: *Journal of Geophysical Research*, v. 99, no. B12, p. 24,007–24,024.
- Baxter, M.E., and \*Blodgett, R.B., 1994, A new species of *Droharhynchia* (Brachiopoda) from the lower Middle Devonian (Eifelian) of west-central Alaska: *Journal of Paleontology*, v. 68, no. 6, p. 1235–1240.
- \*Belkin, H.E., [1995], Fluid inclusion systematics of epithermal mercury-antimony mineralization, southwestern Alaska [abs.]: *Fluid Inclusion Research*, v. 26, 1993, p. 12–13.
- \*Bird, K.J., \*Cole, Frances, \*Howell, D.G., and \*Magoon, L.B., 1995, The future of oil and gas in northern Alaska [abs.]: *American Association of Petroleum Geologists Bulletin*, v. 79, no. 4, p. 579.
- \*Blodgett, R.B., and Johnson, J.G., 1994, First recognition of the genus *Verneulia* Hall and Clark (Brachiopoda, Spiriferida) from North America (west-central) Alaska: *Journal of Paleontology*, v. 68, no. 6, p. 1240–1242.
- \*Blodgett, R.B., Savage, N.M., Pedder, A.E.H., and Rohr, D.M., 1995, Biostratigraphy of an Upper Lower Devonian (Emsian) limestone unit at "Reef Ridge", Medfra B-3 quadrangle, west-central Alaska [abs.]: GSA, p. 6–7.
- \*Blodgett, R.B., \*Weems, R.E., and \*Wilson, F.H., 1995, Upper Jurassic reptiles from the Naknek Formation, Alaska Peninsula; a glimpse into Alaska's own "Jurassic Park" [abs.]: GSA, p. 6.
- \*Bogue, S.W., \*Gromme, S., and \*Hillhouse, J.W., 1995, Paleomagnetism, magnetic anisotropy, and mid-Cretaceous paleolatitude of the Duke Island (Alaska) ultramafic com-

- plex: *Tectonics*, v. 14, no. 5, p. 1133–1152.
- Boyd, T.M., \*Engdahl, E.R., and \*Spence, William, 1995, Seismic cycles along the Aleutian arc: analysis of seismicity from 1957 through 1991: *Journal of Geophysical Research*, v. 100, no. B1, p. 621–644.
- \*Bradley, D., \*Haessler, P., \*Nelson, S., Kusky, T., Donley, D.T., and \*Goldfarb, R., 1995, Geologic effects of Paleogene ridge subduction, Kenai Peninsula, southern Alaska [abs.]: *GSA*, p. 7.
- Brigham-Grette, J., \*Carter, L.D., \*Marincovich, L., \*Brouwers, E., and Hopkins, D.M., 1994, Pliocene sea-level record from Arctic Alaska and possible implications for Antarctic ice volume 2.8–2.2 Ma [abs.]: *GSA*, p. 144.
- Bundtzen, T.K., and \*Miller, M.L., 1989, Geology and metallogeny of Cretaceous–early Tertiary volcanic and plutonic rocks of western Alaska [abs.], *in* International symposium: tectonics, energy and mineral resources of the North-West Pacific (abstracts): v. II (C. B. Borukayev, ed., and others): *Khabarovsk, Russian Far East Academy of Sciences, Institute of Tectonics and Geophysics*, p. 80.
- Bundtzen, T.K., \*Nokleberg, W. J., and \*Plafker, George, 1995, Metallogenic belts of mainland Alaska [abs.]: *Geological Association of Canada and Mineralogical Association of Canada, (GAC/MAC), Annual Meeting, Victoria '95, Victoria, British Columbia, Canada, 1995, Final program and abstracts*, v. 20, p. 12.
- \*Cady, J.W., 1995, Oceanic island arc terrane hidden beneath Brooks Range, Alaska [abs.]: *GSA*, p. 8.
- \*Carlson, P.R., \*Kvenvolden, K.A., \*Hostettler, F.D., \*Rapp, J.B., \*Threlkeld, C.N., and \*Warden, Augusta, 1995, Oil spills, 25 yrs apart, in Prince William Sound, Alaska [abs.]: *GSA*, p. 9.
- Chalmers, R.W., Measures, E.A., Rohr, D.M., and \*Blodgett, R.B., 1995, Depositional environments of an upper Lower Devonian (Emsian) limestone unit at "Reef Ridge", Medfra B-3 quadrangle, west-central Alaska [abs.]: *GSA*, p. 9.
- Cochran, O., Echelmeyer, K., Harrison, W., Nolan, M., \*Heinrichs, T., and \*Mayo, L., 1995, Patterns of motion, geometry and sediment production of Black Rapids Glacier, Alaska [abs.]: *GSA*, p. 10.
- \*Cole, Frances, \*Bird, K.J., \*Howell, D.G., \*Roure, François, \*Valin, Z.C., \*Pawlewicz, M.J., \*Robbins, S.L., and Toro, Jaime, 1995, Deformation and foreland basin sedimentation in the north-central Brooks Range, Alaska [abs.]: *American Association of Petroleum Geologists Bulletin*, v. 79, no. 4, p. 581–582.
- \*Cole, F., \*Howell, D.G., and \*Bird, K., 1994, Geometry and timing of deformation in the north-central Brooks Range, Alaska [abs.]: *Eos*, p. 646–647.
- \*Cole, Frances, \*Roure, François, \*Bird, K.J., \*Howell, D.G., and Toro, Jaime, 1995, Kinematic models for the north-central Brooks Range fold and thrust belt, Killik River quadrangle, Alaska [abs.]: *GSA*, p. 10.
- \*Collett, T.S., and \*Bird, K.J., 1993, Unfrozen, high-salinity intervals within ice-bearing permafrost, North Slope of Alaska: International Conference on Permafrost (6th, 1993, Beijing, China), *Proceedings*, v. 1, p. 94–99.
- Crowder, R.K., Mull, C.G. (Gil), and \*Adams, K.E., 1995, Lowstand depositional systems related to Early Cretaceous rifting of the Arctic Alaska plate: a new stratigraphic play on Alaska's North Slope [abs.]: *American Association of Petroleum Geologists Bulletin*, v. 79, no. 4, p. 582.
- \*Csejtey, Béla, Jr., \*Ford, A.B., \*Wrucke, C.T., \*Dutro, J.T., Jr., \*Harris, A.G., and Brease, P.F., 1995, Geologic correlations across the Denali fault in south-central Alaska: implications for Cenozoic fault displacement [abs.]: *GSA*, p. 12–13.
- \*Csejtey, Béla, Jr., \*Wrucke, C.T., \*Ford, A.B., and Brease, P.F., 1995, Differences in late Mesozoic and late Cenozoic tectonics of the central Alaska Range, Alaska: overthrusting versus high-angle faulting [abs.]: *GSA*, p. 13.
- \*Dinter, D.A., 1995, Grounding of shear- and pressure-thickened sea ice on the upper continental slope of north of Alaska during the late Wisconsin glacial [abs.]: *GSA*, p. 15.
- Donley, D.T., Kusky, T.M., and \*Bradley, D.C., 1995, Emplacement of Tertiary Nuka, Aialik, and related near-trench plutons, Chugach accretionary wedge, Alaska [abs.]: *GSA*, p. 15.
- Doser, D.I., Pelton, J.R., \*Page, R.A., and Veilleux, A., 1995, Body waveform modeling studies of south-central Alaskan earthquakes [abs.]: *Seismological Research Letters*, v. 66, no. 12, p. 30. [Seismological Society of America 90th annual meeting, 1995].
- \*Doukas, M.P., \*McGimsey, R.G., and \*Dorava, J.M., 1995, A video of 10 years of volcanic activity in Alaska: 1983 to 1992 [abs.]: *GSA*, p. 15.
- \*Dover, J.H., 1995, Internal structural styles and timing in "allochthons" of the Howard Pass quadrangle, west-central Brooks Range, Alaska [abs.]: *GSA*, p. 15.
- \*Dumoulin, J.A., Watts, K.F., and \*Harris, A.G., 1995, Lithofacies, conodont biostratigraphy, and regional correlation of the Lisburne Group at Shainin Lake and Atigun Gorge, central Brooks Range, northern Alaska [abs.]: *GSA*, p. 16.
- \*Dusel-Bacon, C., Hansen, V.L., and \*Scala, J.A., 1995, High-pressure amphibolite facies dynamic metamorphism and the Mesozoic tectonic evolution of an ancient continental margin, east-central Alaska: *Journal of Metamorphic Geology*, v. 13, no. 1, p. 9–24.
- \*Dusel-Bacon, Cynthia, \*Lanphere, M.A., Hansen, V.L., and \*Aleinikoff, J.N., 1995, Thermochronometric constraints on Mesozoic contraction and extension in the eastern Yukon-Tanana upland, Alaska [abs.]: *GSA*, p. 16.
- \*Flores, R.M., and \*Stanley, R.G., 1995, Tertiary Usibelli Group of Suntrana, Alaska: Fluctuating baselevel deposits in a fluvial pathway to Cook Inlet [abs.]: *GSA*, p. 18–19.
- \*Fuis, G.S., Levander, A.R., \*Lutter, W.J., Wissinger, E.S., \*Moore, T.E., and Christensen, N.I., 1995, Seismic images of the Brooks Range, Arctic Alaska, reveal crustal-scale duplexing: *Geology*, v. 23, no. 1, p. 65–68.
- \*Fuis, G.S., \*Lutter, W.J., \*Moore, T.E., Levander, A.R., and Wissinger, E.S., 1994, Interpretation of the deep structure of the Brooks Range, Arctic Alaska [abs.]: *Eos*, p. 646.
- \*Fuis, G.S., \*Moore, T.E., \*Brocher, T.M., \*Plafker, George, \*Fisher, M.E., Levander, A.R., and Wissinger, E.S., 1995, Deep structure and evolution of the north and south margins of Alaska through time and space [abs.]: *GSA*, p. 19.
- Galloway, B.K., Klemperer, S.L., \*Childs, J.R., and Bering-Chukchi Working Group, 1994, New seismic reflection profiles of the continental crust and Moho, Bering and Chukchi

- Seas transect, Alaska [abs.]: Eos, p. 642.
- \*Galloway, J.P., 1995, The U.S. Geological Survey Alaskan radiocarbon database: Current Research in the Pleistocene, v. 12, p. 80–82.
- \*Gamble, B.M., \*Richter, D.L., \*Lanphere, M.A., and \*Reed, B.L., 1995, Tertiary volcanic rocks, eastern Lime Hills quadrangle, Alaska [abs.]: GSA, p. 20.
- \*Gardner, C.A., Cashman, K.V., and \*Neal, C.A., 1995, Repeated volatile zonation in the tephra deposits from the 1992 eruption of Crater Peak, Alaska—magma chamber or magma transport processes? [abs.]: GSA, p. 20.
- \*Goldfarb, R.J., 1995, Review of "Geology of Alaska", George Plafker and H.C. Berg, eds., Geological Society of America, Geology of North America, v. 1, G-1, 1055 p.: Economic Geology, v. 90, p. 988.
- \*Goldfarb, R.J., Christie, T., Skinner, D., \*Haeussler, P., and \*Bradley, D., 1995, Gold deposits of Westland New Zealand southern Alaska—Products of the same tectonic processes? *in* Mauk, J., ed., PACRIM '95 Symposium volume, p. 239–244.
- \*Goldfarb, R.J., \*Snee, L.W., and \*Pickthorn, W.J., 1995, Orogenesis, high-T thermal events, and gold vein formation within metamorphic rocks of the Alaskan Cordillera [abs.]: Fluid Inclusion Research, v. 26, 1993, p. 58.
- \*Grantz, Arthur, \*Hart, P.E., \*Phillips, R.L., \*McCormick, Michael, \*Perkin, R.G., Jackson, Ruth, Gagnon, Alan, Li, Shusun, Byers, Carl, and Schwartz, K.R., 1994, Preliminary results of a binational research cruise in the western Arctic Ocean: Polar Geography and Geology, v. 18, no. 3, p. 187–210.
- \*Gray, J.E., 1995, Environmental geochemistry of mercury mines in Alaska: Alaska Geology, Newsletter of the Geological Society of Alaska, v. 25, no. 3, p. 1–5.
- \*Gray, J.E., \*Bailey, E.A., and \*Miller, M.L., 1995, Environmental effects downstream from mercury mines in southwestern Alaska [abs.]: GSA, p. 22.
- \*Grow, J.A., \*Miller, J.J., Mull, C.G. (Gil), and \*Bird, K.J., 1995, Seismic stratigraphy near the Tunalik well, North Slope, Alaska [abs.]: American Association of Petroleum Geologists Bulletin, v. 79, no. 4, p. 586.
- 1995, Seismic stratigraphy near the Tunalik well, North Slope, Alaska [abs.]: GSA, p. 23.
- \*Grybeck, D.J., 1995, A retrospective view of the role of earth science in the ANILCA decision [abs.]: GSA, p. 23.
- \*Haeussler, P.J., \*Bradley, D.C., \*Goldfarb, R.J., and \*Snee, L.W., 1995, A link between ridge subduction and turbidite-hosted gold mineralization in southern Alaska [abs.]: GSA, p. 21.
- \*Haeussler, P.J., \*Bradley, D.C., \*Goldfarb, R.J., \*Snee, L.W., and \*Taylor, C.D., 1995, Link between ridge subduction and gold mineralization in southern Alaska: Geology, v. 23, no. 11, p. 995–998.
- \*Hamilton, T.D., 1995, Diapiric extrusions of bluff sediments in the glacial Lake Noatak basin, northwestern Alaska [abs.]: GSA, p. 24.
- \*Hamilton, T.D., and \*Carter, L.D., 1995, Environmental setting for early humans in northern Alaska: 15–8 ka [abs.]: GSA, p. 23–24.
- \*Hampton, M.A., 1994, Classification of properties of Holocene sediment in Shelikof Strait, Alaska: Marine Georesources & Geotechnology, v. 12, no. 3, p. 237–257.
- \*Harris, A.G., \*Dumoulin, J.A., \*Repetski, J.E., and \*Carter, Claire, 1995, Correlation of Ordovician rocks across northern Alaska [abs.]: GSA, p. 24–25.
- 1995, Correlation of Ordovician rocks of northern Alaska, *in* Cooper, J.D., Droser, M.L., and Finney, S.C., eds., Ordovician odyssey: short papers for the Seventh International Symposium on the Ordovician System: Fullerton, Calif., The Pacific Section for Sedimentary Geology (SEPM), Book 77, p. 21–26.
- \*Harris, A.G., and Krumhardt, A.P., 1995, Conodont-based correlation of the upper Endicott and Lisburne Groups (Carboniferous), northeast Brooks Range, Alaska [abs.]: GSA, p. 25.
- Hart, W.K., Preece, S.J., Siebert, T.M., and \*Richter, D.H., 1995, Eruptive products and styles within the Skookum Creek Volcanic Center, Wrangell volcanic field, Alaska [abs.]: GSA, p. 25.
- Herzfeld, U.C., Roush, J.J., Lohuis, K., and \*Molnia, B.F., 1994, Surge crevasse patterns, ice surface roughness and ice velocity: an attempt at quantitative analysis of 1993 and 1994 observations on Bering Glacier, Alaska [abs.]: Eos, p. 63.
- Heslop, Kate, \*Dusel-Bacon, Cynthia, and Williams, I.S., 1995, Survival of zircon U-Pb isotopic systems through partial melting and high P-T dynamothermal metamorphism, Yukon-Tanana terrane, Alaska [abs.]: GSA, p. 26.
- Himmelberg, G.R., \*Brew, D.A., and \*Ford, A.B., 1995, Low-grade, M1 metamorphism of the Douglas Island Volcanics, western metamorphic belt near Juneau, Alaska, *in* Schiffman, P., and Day, H.W., eds., Low-grade metamorphism of mafic rocks: Geological Society of America Special Paper 296, p. 51–66.
- Jackson, H.R., \*Grantz, A., Reid, I., \*May, S.D., and \*Hart, P.E., 1995, Observations of anomalous oceanic crust in the Canada Basin, Arctic Ocean: Earth and Planetary Science Letters, v. 134, no. 1/2, p. 99–106.
- Jolly, A.D., \*Lahr, J.C., \*Power, J.A., \*Stihler, S.D., \*Ward, P.L., and \*McNutt, S.R., 1994, Velocity models for locations of shallow seismicity along the northeastern portion of the Aleutian volcanic arc [abs.]: Eos, p. 423–424.
- \*Kelley, J.S., and \*Brosge, W.P., 1995, Paleozoic basins and shelf deposits of the Central Brooks Range, possible analogs to basins under the Arctic coastal plain, northern Alaska [abs.]: American Association of Petroleum Geologists and Society of Economic Paleontologists and Mineralogists 1995 Annual Convention, p. 49.
- 1995, Geologic framework of a transect of the central Brooks Range: Regional relations and an alternative to the Endicott Mountains allochthon: American Association of Petroleum Geologists Bulletin, v. 79, no. 8, p. 1087–1116.
- \*Kelley, J.S., \*Wrucke, C.T., and Lane, L.S., 1995, Stratigraphy of pre-Mississippian rocks in the Clarence River area, northeastern Alaska and northwestern Yukon Territory [abs.]: GSA, p. 57.
- \*Kelley, J.S., \*Wrucke, C.T., Lane, L.S., and Foland, R.L., 1995, Franklinian rocks along the Alaska-Yukon border in the northeastern Brooks Range, implications for reflection seismic imaging under the Arctic coastal plain of the

- Arctic National Wildlife Refuge, Alaska [abs.]: American Association of Petroleum Geologists Bulletin, v. 79, no. 4, p. 590.
- Klemperer, S.L., on behalf of Bering-Chukchi Working Group [includes USGS], 1995, Preliminary results of deep seismic profiling offshore Alaska from the Aleutian basin to the Arctic Ocean [abs.]: GSA, p. 57.
- Kodosky, L.G., and \*Keith, T.E.C., 1995, Further insights into the geochemical evolution of fumarolic alteration, Valley of Ten Thousand Smokes, Alaska: Journal of Volcanology and Geothermal Research, v. 65, no. 314, p. 181–190.
- \*Kvenvolden, K.A., \*Carlson, P.R., \*Hostettler, F.D., \*Threlkeld, C.N., and \*Warden, A., 1995, Geochemical identification of oil products used in the historical development of Alaska [abs.]: GSA, p. 21.
- \*Kvenvolden, K.A., and \*Lorenson, T.D., 1995, A review of methane in permafrost near Fairbanks, Alaska [abs.]: GSA, p. 58.
- \*Kvenvolden, K.A., \*Lorenson, T.D. and Lilley, M.D., 1992, Methane in the Beaufort Sea on the continental shelf of Alaska: Eos (American Geophysical Union Transactions), v. 73, no. 43, suppl., p. 309.
- \*LaHusen, R.G., 1994, Real-time monitoring of lahars using ground vibrations [abs.]: GSA1, p. 377.
- Lane, L.S., Cecile, M.P., \*Kelley, J.S., \*Wrucke, C.T., and Hofmann, H.J., 1995, Paleogeographic implications of early Paleozoic shelf to basin transitions, northern Yukon and Alaska [abs.]: GSA, p. 58–59.
- \*Light, T.D., \*Schmidt, J.M., \*Peterson, D.P., \*Gamble, B.M., \*Grybeck, Donald, \*Miller, M.L., \*Wilson, F.H., \*Brew, D.A., and \*Nokleberg, W.J., 1995, Statewide assessment of the potential for undiscovered mineral resources in Alaska [abs.]: GSA, p. 61.
- \*Lorenson, T.D., \*Kvenvolden, K.A., \*Barnes, P.W., Popp, B.N., Sansone, F.J., Rust, T.M., Lilley, M.D., and Olson, E.J., 1995, Isotopic composition of methane in seawater of the Alaskan Beaufort Sea [abs.], in International Union of Geodesy and Geophysics, Geophysics and the Environment, general assembly, 21st, Boulder, Colo., 1995, Abstracts week B, p. B314.
- Mann, D.H. and \*Hamilton, T.D., 1995, Late Pleistocene and Holocene paleoenvironments of the North Pacific coast: Quaternary Science Reviews, v. 14, p. 449–471.
- Mathez, E.A., Duba, A.G., Peach, C.L., Léger, A., Shankland, T.J., and \*Plafker, George, 1995, Electrical conductivity and carbon in metamorphic rocks of the Yukon-Tanana terrane, Alaska: Journal of Geophysical Research, v. 100, no. B7, p. 10,187–10,196.
- McGeary, Susan, Diebold, J.B., Bangs, N.L., and Bond, Gerard, 1994, Preliminary results of the Pacific to Bering shelf seismic experiment [abs.]: Eos, p. 643.
- \*McGimsey, R.G., \*Richter, D.H., \*Waythomas, C.F., and Donaldson, J.A., 1995, Potential hazards from future eruptions of Mt. Churchill, Alaska [abs.]: GSA, p. 63.
- Miller, L.D., \*Goldfarb, R.J., \*Snee, L.W., \*Gent, C.A., and Kirkham, R.A., 1995, Structural geology, age, and mechanisms of gold vein formation at the Kensington and Jualin deposits, Berners Bay district, southeast Alaska: Economic Geology, v. 90, no. 2, p. 343–368.
- \*Miller, M.L., \*Bailey, E.A., \*Gray, J.E., and Balen, M.D., 1995, Mineral-environmental mercury studies and issues of public concern, Sleetmute quadrangle, southwest Alaska [abs.]: GSA, p. 64.
- \*Miller, T.P., and Kirianov, V. Yu., 1994, Timing of large Holocene volcanic events in the western Aleutian arc, Alaska [abs.]: Eos, p. 731.
- \*Molnia, B.F., 1995, Bering Glacier resumes its surge: Eos (American Geophysical Union Transactions), v. 76, no. 29, p. 291.
- \*Molnia, B.F., and Molnia, M.I., 1995, Comparison of spaceborne ERS-1 & SIR-C synthetic aperture radar (SAR) with airborne SAR of the Bering Glacier, Alaska [abs.]: GSA, p. 65.
- \*Molnia, B.F., and \*Post, Austin, 1995, Holocene history of Bering Glacier, Alaska: a prelude to the 1993–1994 surge: Physical Geography, v. 16, no. 2, p. 87–117.
- \*Moore, T.E., \*Fuis, G.S., O'Sullivan, P.B., and Murphy, J.M., 1994, Evidence of Laramide age deformation in the Brooks Range, Alaska [abs.]: GSA1, p. 383.
- \*Moore, T.E., \*Grantz, Arthur, and Roeske, S.M., 1994, Continent-ocean transition in Alaska: the tectonic assembly of eastern Denalia, in Speed, R.C., ed., Phanerozoic evolution of North American continent-ocean transitions: Boulder, Colo., Geological Society of America, Summary volume to accompany the Decade of North American Geology continent-ocean transect series, p. 399–441.
- \*Moore, T.E., Wallace, W.K., and \*Fuis, G.S., 1994, Shingled tectonic wedges in the central Brooks Range orogen [abs.]: Eos, p. 646.
- 1995, Northward-tapering orogenic wedge, central Brooks Range, Alaska [abs.]: GSA, p. 65.
- \*Mori, Jim, 1995, Volcano seismology, hazards assessment: Reviews of Geophysics, v. 33, suppl., pt. 1, p. 263–267. [Mentions Mt. Spurr and Redoubt Volcanoes.]
- Mull, C.G. (Gil), \*Moore, T.E., Werdon, M.B., and Crowder, R.K., 1995, How the central Brooks Range mountain-front and foothills came to be [abs.]: GSA, p. 66.
- \*Neal, C.A., \*McGimsey, R.G., Waythomas, C.F., \*Miller, T.P., and Nye, C.J., 1995, The last 3400 years at Aniakchak caldera, Alaska [abs.]: GSA, p. 67.
- \*Nelson, C.H., \*Phillips, R.L., \*McRea, James, Jr., \*Barber, J.H., Jr., \*McLaughlin, M.W., and \*Chin, J.L., 1994, Gray whale and Pacific walrus benthic feeding grounds and sea floor interaction in the Chukchi Sea: U.S. Minerals Management Service, OCS Study, MMS 93-0042, variously paged. [Technical report for Minerals Management Service / IA No. 14157.1]
- \*Nelson, S.W., Huber, Carol, and Davidson, Dean, 1995, U.S. Geological Survey mineral resource assessment activities in the Chugach National Forest and their application by the Forest Service [abs.]: GSA, p. 67–68.
- Newberry, R.J., Solie, D.N., Burns, L.E., Wiltse, M.A., \*Hammond, W.R., and Swainbank, R., 1995, Geophysical and geological evidence for pervasive, northeast-trending, left-lateral faults in eastern interior Alaska [abs.]: GSA, p. 68.
- \*Nokleberg, W.J., \*Foster, H.L., and \*Aleinikoff, J.N., 1995, Tectonic model for the Yukon-Tanana, Seventymile, Stikinia, and Wrangellia terranes along the Trans-Alaska



- Crustal Transect (TACT), east-central Alaska [abs.]: GSA, p. 69.
- \*Nokleberg, W.J., Monger, J.W.H., and Parfenov, L.M., 1995, Mesozoic and Cenozoic tectonics of the circum-north Pacific [abs.]: GSA, p. 68–69.
- 1995, Mesozoic and Cenozoic tectonics of the Circum-North Pacific [abs.]: Geological Association of Canada and Mineralogical Association of Canada, (GAC/MAC), annual meeting, Victoria '95, Victoria, British Columbia, Canada, 1995, Final program and abstracts, v. 20, p. 76.
- \*Nokleberg, W.J., \*Zierenberg, R.A., Lance, L.M., and \*Schmidt, J.M., 1989, Metallogensis of sedimentary-exhalative zinc-lead-silver deposits, northwestern Brooks Range, Alaska [abs.], in International symposium: tectonics, energy and mineral resources of the north-west Pacific (abstracts): v. II (C. B. Borukayev, ed., and others): Khabarovsk, Russian Far East Academy of Sciences, Institute of Tectonics and Geophysics, p. 95–97.
- Nye, C.J., \*Neal, C.A., \*Miller, T.P., and \*McGimsey, R.G., 1995, Extreme tholeiitic to calcalkaline transition at Aniakchak volcano, east-central Aleutian arc [abs.]: GSA, p. 69.
- Ort, M.H., Wohletz, K.H., \*McNeal, C.A., and McConnell, V.S., 1995, Mechanics of magma/water interactions, Ukinrek Maars, Alaska [abs.], in International Union of Geodesy and Geophysics, Geophysics and the Environment, general assembly, 21st, Boulder, Colo., 1995, Abstracts week A, p. A467.
- O'Sullivan, P.B., Murphy, J.M., Blythe, A.E., and \*Moore, T.E., 1994, Fission track evidence indicates that the present-day Brooks Range, Alaska, is a Cenozoic, not Early Cretaceous physiographic feature [abs.]: Eos, p. 646.
- \*Page, R.A., \*Plafker, George, and Pulpan, Hans, 1995, Earthquakes and block rotation in east-central Alaska [abs.]: GSA, p. 70.
- 1995, Block rotation in east-central Alaska: a framework for evaluating earthquake potential?: Geology, v. 23, no. 7, p. 629–632.
- Patrick, B. E., and \*Till, A. B., 1992, Cordilleran high pressure metamorphism in Northern Alaska: a consequence of island arc-continent collision [abs.]: 29th International Geological Congress, Abstracts, v. 1, p. 62.
- \*Patton, W.W., Jr., and \*Moll-Stalcup, E.J., 1995, Crustal composition and magmatic history of the central part of the Yukon-Koyukuk basin, Alaska [abs.]: GSA, p. 71.
- \*Plafker, G., 1989, Phanerozoic tectonic evolution of Alaska [abs.], in International symposium: tectonics, energy and mineral resources of the north-west Pacific (abstracts): v. II (C. B. Borukayev, ed., and others): Khabarovsk, Russian Far East Academy of Sciences, Institute of Tectonics and Geophysics, p. 44.
- \*Plumlee, G.S., \*Kelley, K.D., \*Goldfarb, R.J., \*Gray, J.E., \*Taylor, C.D., and \*Eppinger, R.G., 1995, Geological and geochemical controls on the composition of mine drainages and natural drainages in mineralized areas with specific examples from Alaska [abs.], in Alaska Miners Association, Juneau Branch, Conference, Juneau, Alaska, 1995, Abstracts of Professional Papers.
- 1995, The environmental geology and geochemistry of mineral deposits with applications to Alaska [abs.], in Alaska Miners Association, Juneau Branch, Conference, Juneau, Alaska, 1995, Abstracts of Professional Papers, p. 49–51.
- Popov, L.Y., \*Blodgett, R.B., and Anderson, A.V., 1994, First occurrence of the genus *Bicarinata* (Brachiopoda, Inarticulata) from the Middle Devonian in North America (Alaska): Journal of Paleontology, v. 68, no. 6, p. 1214–1218.
- \*Post, Austin, and Motyka, R.J., 1995, Taku and Le Conte Glaciers, Alaska: calving-speed control of late Holocene asynchronous advances and retreats: Physical Geography, v. 16, no. 1, p. 59–82.
- \*Power, J.A., and Jolly, A.D., 1994, Seismicity at 10- to 45-km depth associated with the 1992 eruptions of Crater Peak vent, Mount Spurr, Alaska [abs.]: Eos, p. 715.
- Richards, R.W., and \*Molnia, B.F., 1995, Medial moraine band of the Bering Glacier, southcentral Alaska [abs.]: Geological Society of America Abstracts with Programs, v. 27, no. 1, p. 77–78.
- \*Richter, D.H., Preece, S.J., \*McGimsey, R.G., and Westgate, J.A., 1995, Mount Churchill, Alaska: source of the late Holocene White River Ash: Canadian Journal of Earth Sciences, v. 32, no. 6, p. 741–748.
- Roeske, S.M., \*Dusel-Bacon, C., \*Aleinikoff, J.N., \*Snee, L.W., and \*Lanphere, M.A., 1995, Metamorphic and structural history of continental crust at a Mesozoic collisional margin, the Ruby terrane, central Alaska: Journal of Metamorphic Geology, v. 13, no. 1, p. 25–40.
- Roeske, S.M., \*Snee, L.W., Pavlis, T.L., and Sisson, V.B., 1995, Tectonic response of the Chugach accretionary complex to early Cenozoic oblique subduction [abs.]: GSA, p. 74.
- Rogers, J. A., and \*Stephens, C.D., 1995, SSAM: real-time seismic spectral amplitude measurement on a PC and its application to volcano monitoring: Bulletin of the Seismological Society of America, v. 85, no. 2, p. 632–639.
- Ryherd, T.J., \*Carter, Claire, and Churkin, Michael, Jr., 1995, Middle through Upper Ordovician graptolite biostratigraphy of the Deceit Formation, northern Seward Peninsula, Alaska [abs.]: GSA, p. 75.
- Sauber, Jeanne, Gipson, John, and \*Plafker, George, 1995, Predicted displacement field associated with glacial fluctuations in southern Alaska [abs.], in International Union of Geodesy and Geophysics, Geophysics and the Environment, general assembly, 21st, Boulder, Colo., 1995, Abstracts week A, p. A36.
- Sauber, Jeanne, \*Plafker, George, and Gipson, John, 1995, Geotectonic measurements used to estimate ice transfer during Bering Glacier surge: Eos (American Geophysical Union Transactions), v. 76, no. 29, p. 289–290.
- Savage, N.M., and \*Blodgett, R.B., 1995, A late Emsian *Amydrotaxis* (conodont) species from the Devonian of southwestern Alaska [abs.]: GSA, p. 76.
- 1995, A new species of the conodont *Amydrotaxis* from the Early Devonian of southwestern Alaska: Alaska Division of Geological and Geophysical Surveys Professional Report 117, p. 69–73.
- Savage, N.M., \*Blodgett, R.B., and Brease, P.F., 1995, Late Devonian (early Frasnian) conodonts and brachiopods from Denali National Park, south-central Alaska [abs.]: GSA, p. 76.
- Savage, N.M., Rohr, D.M., and \*Blodgett, R.B., 1995, Late

- Silurian conodonts from the Medfra B-4 quadrangle, west-central Alaska [abs.]: GSA, p. 76–77.
- \*Scholl, D.W., \*Stevenson, A.J., and \*Hart, P.E., 1995, Eocene formation of the Bering Sea basin linked to regional-scale tectonism of Alaska—implications for energy gas resources and the accumulation of massive hydrate deposits (VAMPs) [abs.]: American Association of Petroleum Geologists Bulletin, v. 79, no. 4, p. 596–597.
- Seramur, K.C., \*Kayen, R.E., Cowan, E.A. and Powell, R.D., 1994, Lithologic and geotechnical characteristics of grounding-line sediments at Muir Glacier: implications for interpretation of seismic reflection profiles [abs.]: GSA1, p. 474.
- Shelton, K.L., Underwood, M.B., and \*Howell, D.G., 1994, Regional stable isotope variations of calcite veins from Lisburne corridor, frontal Brooks Range, north-central Alaska: indicators of thermal maturity and hydrocarbon migration [abs.]: Eos, p. 647.
- Silberling, N.J., Jones, D.L., Monger, J.W.H., Coney, P.J., Berg, H.C., and \*Plafker, G., 1994, Lithotectonic terrane map of Alaska and adjacent parts of Canada, in Plafker, George, and Berg, H. C., eds., 1994, The geology of Alaska: Boulder, Colo., Geological Society of America, The Geology of North America, v. G-1, pl. 3, 1 sheet, scale 1:2,500,000.
- \*Stephens, C.D., \*Page, R.A., \*Lahr, J.C., and \*Fogleman, K.A., 1995, Crustal seismicity in the Anchorage region of Alaska [abs.]: GSA, p. 78–79.
- \*Stricker, G.D., \*Affolter, R.H., \*Tripp, R.B., and \*McHugh, J.B., 1995, Effects of discontinuous permafrost on groundwater flow and contaminant transport [abs.]: GSA, p. 80.
- \*Till, A.B., 1995, Multiple pulses of deformation in the metamorphic core of the Brooks Range—implications for tectonic evolution of the orogen [abs.]: GSA, p. 81.
- \*Till, A.B., and \*Harris, A.G., 1995, Evidence for post-Triassic emplacement of metamorphic rocks of the Yukon-Tanana terrane above Triassic marine sedimentary rocks in the Kantishna Hills, central Alaska Range, Alaska [abs.]: GSA, p. 81.
- \*Till, A.B., and \*Snee, L.W., 1995,  $^{40}\text{Ar}/^{39}\text{Ar}$  evidence that formation of blueschists in continental crust was synchronous with foreland fold and thrust belt deformation, western Brooks Range, Alaska: Journal of Metamorphic Geology, v. 13, no. 1, p. 41–60.
- \*Trabant, D.C., and \*Molnia, B.F., 1994, Ice speed, ice thickness, and proglacial-lake stage and turbidity trends at the surging Bering Glacier, Alaska [abs.]: Eos, p. 63.
- \*von Huene, R., Flueh, E., and the Kodiak Seis/Vent research group, GEOMAR, \*Fisher, Mike, and Jones, Kevin, 1994, Shipboard results from the Kodiak Seis cruise, Gulf of Alaska [abs.]: Eos, p. 597.
- \*Waite, R.B., \*Mastin, L.G., and \*Miller, T.P., 1994, Velocities and spin of hydromagmatic ballistics from Mt. Spurr (Alaska) 1992 [abs.]: IAVCEI, International Volcanological Congress, 1994, Ankara, Turkey, Abstracts: Ankara, Turkey, Middle East Technical University, Department of Geological Engineering, Special Publications no. 2, n.p.
- Wallace, W.K., \*Moore, T.E., and \*Plafker, George, 1994, Variations in structure from the Endicott Mountains allochthon to the parautochthon, north-central Brooks Range, Alaska [abs.]: Eos, p. 646.
- Watts, K.F., and \*Harris, A.G., 1995, Paleogeography and sequence stratigraphy of the Lisburne Group (Carboniferous) of northeastern Alaska [abs.]: GSA, p. 83.
- \*Waythomas, C.F., \*Miller, T.P., and Kirianov, V.Y., 1994, Post-glacial evolution of northern Adak Island, Alaska: American Quaternary Association, Program and Abstracts of the 13th Biennial meeting, 19–22 June, 1994, p. 179.
- Wiles, G.C., Calkin, P.E., and \*Post, Austin, 1995, Glacier fluctuations in the Kenai Fjords, Alaska, U.S.A.: an evaluation of controls on iceberg-calving glaciers: Arctic and Alpine Research, v. 27, no. 3, p. 234–245.
- \*Wilson, F.H., and \*Bickerstaff, D.P., 1995, Middle Tertiary volcanism on the Alaska Peninsula, the Meshik arc revisited [abs.]: GSA, p. 85.
- \*Wilson, F.H., \*Shew, N., and DuBois, G.D., 1994, Map and table showing isotopic age data in Alaska, in Plafker, George, and Berg, H. C., eds., 1994, The geology of Alaska: Boulder, Colo., Geological Society of America, The Geology of North America, v. G-1, pl. 8, 1 sheet, scale 1:2,500,000, with tables.
- Wissinger, E.S., Levander, A., \*Fuis, G.S., and \*Lutter, W.J., 1994, Crustal wedging in the Brooks Range, Alaska [abs.]: Eos, p. 646.